INVESTIGATION OF LONG TERM SAFE STORAGE OF CARBON DIOXIDE IN DEEP COAL SEAMS WITH ENHANCED METHANE RECOVERY

By

Ashani Savinda Ranathunga

BSc Eng. (Hons)

Supervised by:

Prof Ranjith Pathegama Gamage

A thesis submitted in the fulfilment of the requirements for the degree of Doctor of Philosophy

Department of Civil Engineering

Monash University

Melbourne, Australia

January 2017

Copyright notice

DEDICATION

This thesis is dedicated to my parents, my brother and my husband for their unconditional support to carry out this work.

This thesis is with publication, in accordance with section 17.2 of the Research Graduate Committee regulations (Doctorate)

General Declaration

Monash University

In accordance with Monash University Doctorate Regulation 17.2 Doctor of Philosophy and Research Master's regulations the following declarations are made:

I hereby declare this thesis contains no material which has been accepted for the award of any other degree or diploma at any university or equivalent institution and that, to the best of my knowledge and belief, this thesis contains no material previously published or written by another person, except where due reference is made in the text of the thesis.

Signature: [redacted]

Print Name: Ashani Savinda Ranathunga

Date: 25/01/2017

Thesis including published works declaration

I hereby declare that my published works contain no materials which have been accepted for the award of any other degree or diploma at any university or equivalent institution and that, to the best of my knowledge and belief, these published works contains no material previously published or written by another person, except where due reference is made in the text of the published works.

This thesis includes 5 original papers published in peer reviewed journals. The core theme of the thesis is investigation of long term safe storage of carbon dioxide in deep coal seams with enhanced methane recovery. The ideas, development and writing up of all the papers in the thesis were the principal responsibility of myself, the candidate, working within the Department of Civil Engineering, Monash University, under the supervision of Prof Ranjith Pathegama Gamage.

Chapter 5 (partially), 6 and 8 (partially) report my published works resulted during the studies undertaken for this degree and my contribution to the work involved the following:

[The inclusion of co-authors reflects the fact that the work came from active collaboration between researchers and acknowledges input into team-based research.]

Thesis Chapter	Publication title	Publication status	Nature and % of candidate's contribution	Co-author name(s) Nature and % of Co-author's contribution	Co-authors, Monash student
5	A macro-scale experimental study of sub and supercritical CO_2 flow behaviour in Victorian brown coal.	Published **Journal: Fuel**	Initiation, key ideas, literature review, conduct of experiments, data analysis and writing up: 85%	1. Ranjith PG – key ideas 5% 2. MSA Perera – reviewing the manuscript 3% 3. Y JU – key ideas 3% 4. V Vishal – key ideas 2% 5. PNK De Silva – key ideas 2%	No No No No No
6	Supercritical CO_2 saturation-induced mechanical property alterations in low rank coal: An experimental study	Published **Journal: Journal of Supercritical fluids**	Initiation, key ideas, literature review, conduct of experiments, data analysis and writing up: 85%	1. Ranjith PG – key ideas 8% 2. MSA Perera – reviewing the manuscript 5% 3. H Bui – key ideas 2%	No No No

6	Effect of coal rank on various fluid saturations creating mechanical property alterations using Australian coals	Published **Journal: Energies**	Initiation, key ideas, literature review, conduct of experiments, data analysis and writing up: 85%	1. Ranjith PG – key ideas 8% 2. MSA Perera – reviewing the manuscript 7%	No No
6	Influence of CO_2 adsorption on the strength and elastic modulus of low rank Australian coal under confining pressure.	Published **Journal: International Journal of Coal Geology**	Initiation, key ideas, literature review, conduct of experiments, data analysis and writing up: 85%	1. Ranjith PG – key ideas 8% 2. MSA Perera – reviewing the manuscript 7%	No No
8	An experimental investigation of applicability of CO_2 enhanced coal bed methane recovery technique to low rank coal	Published **Journal: Fuel**	Initiation, key ideas, literature review, conduct of experiments, data analysis and writing up: 85%	1. Ranjith PG – key ideas 8% 2. MSA Perera – reviewing the manuscript 5% 3. CH Wei – key ideas 2%	No No No

I have renumbered sections of published papers in order to generate a consistent presentation within the thesis.

Student signature: [redacted] **Date:** 25/01/2017

The undersigned hereby certify that the above declaration correctly reflects the nature and extent of the student's and co-authors' contributions to this work. In instances where I am not the responsible author I have consulted with the responsible author to agree on the respective contributions of the authors.

Main Supervisor signature: [redacted] **Date:** 25/01/2017

Thesis including unpublished works declaration

I hereby declare that my unpublished works contain no materials which have been accepted for the award of any other degree or diploma at any university or equivalent institution and that, to the best of my knowledge and belief, these unpublished published works contains no material previously published or written by another person, except where due reference is made in the text of the unpublished works.

This thesis includes 6 unpublished (under review) publications. The core theme of the thesis is to investigate the long term safe storage of carbon dioxide in deep coal seams with enhanced methane recovery. The ideas, development and writing up of all the papers in the thesis were the principal responsibility of myself, the candidate, working within the Department of Civil Engineering, Monash University, under the supervision of Prof Ranjith Pathegama Gamage.

Chapter 4, 5 (partially) and 7 (partially) report my unpublished works resulted during the studies undertaken for this degree and my contribution to the work involved the following:

[The inclusion of co-authors reflects the fact that the work came from active collaboration between researchers and acknowledges input into team-based research.]

Thesis Chapter	Publication title	Publication status	Nature and % of candidate's contribution	Co-author name(s) Nature and % of Co-author's contribution	Co-authors, Monash student
4	Super-critical carbon dioxide flow behaviour in low rank coal: A meso-scale experimental study	Under review **Journal: CO_2 Utilization**	Initiation, key ideas, literature review, conduct of experiments, data analysis and writing up: 85%	1. Ranjith PG – key ideas 8% 2. MSA Perera – reviewing the manuscript 7%	No No
4	Effect of effective stress and coal matrix swelling on coal flow behaviour during CO_2 sequestration	Under review **Journal: CO_2 Utilization**	Initiation, key ideas, literature review, conduct of experiments, data analysis and writing up: 85%	1. Ranjith PG – key ideas 8% 2. MSA Perera – reviewing the manuscript 7%	No No
4	The influence of CO_2 properties and reservoir depth on coal matrix swelling: A meso-scale experimental study using low rank coal	Under review **Journal: Energy and Fuels**	Initiation, key ideas, literature review, conduct of experiments, data analysis and writing up: 85%	1. Ranjith PG – key ideas 8% 2. MSA Perera – reviewing the manuscript 7%	No No

4	A review and model development for estimation of gas adsorption-induced coal matrix swelling	Under review **Journal: International Journal of Energy Research**	Initiation, key ideas, literature review, data analysis and writing up: 85%	1. Ranjith PG – key ideas 8% 2. MSA Perera – reviewing the manuscript 7%	No No
5	A laboratory-scale numerical study of CO_2 flow through coal under down-hole stress conditions: Application for CO_2 storage	Under review **Journal: Energy and Fuels**	Initiation, key ideas, literature review, data analysis and writing up: 85%	1. Ranjith PG – key ideas 8% 2. MSA Perera – reviewing the manuscript 7%	No No
7	Key factors controlling coal's strength property alterations during CO_2 enhanced coal bed methane production: A numerical study	Under review **Journal: Natural Gas Science and Engineering**	Initiation, key ideas, literature review, data analysis and writing up: 85%	1. Ranjith PG – key ideas 8% 2. MSA Perera – reviewing the manuscript 7%	No No

I have renumbered sections of unpublished papers in order to generate a consistent presentation within the thesis.

Student signature: [redacted] **Date:** 25/01/2017

The undersigned hereby certify that the above declaration correctly reflects the nature and extent of the student's and co-authors' contributions to this work. In instances where I am not the responsible author I have consulted with the responsible author to agree on the respective contributions of the authors.

Main Supervisor signature: [redacted] **Date:** 25/01/2017

Acknowledgement

I would like to acknowledge following people for their support and assistance throughout my PhD research work. This dissertation would have not been possible without their guidance and help.

First and foremost, I would like to gratefully acknowledge the enthusiastic supervision of Prof. Ranjith Pathegama for his guidance, inspiration and unconditional support all through my candidature. His ideas and concepts have had a remarkable influence on my research work. The excellent and friendly atmosphere provided by him was quite accommodating for me to carry out a smooth and rewarding research life. The motivations and encouragement received to produce quality research work was incredible and outstanding. I would also like to express my greatest gratitude to my co-supervisor Dr Ha Bui, who provided invaluable assistance and perceptive comments on my research.

Secondly, I would like to convey my sincere gratitude to Dr Samintha Perera, who is also my co-supervisor, for mentoring and guiding me all the way through my candidature at Monash University. I was fortunate enough to work with her during my candidature and the assistance I received especially in planning experimental work, numerical work, writing up technical papers and this dissertation is commendable. Her expertise knowledge on my research area, particularly CO_2 sequestration in deep coal seams was immensely helpful to carry out my research wok.

The administration staff of the Civil Engineering department of Monash University also need to be mentioned here for their support during the PhD candidature specially, Ms Jenny Manson, Ms Min Major and Mr Christopher Powell. More than 80% of my research work consisted of experimental work which required a lot of help from many individuals. Without the friendly and helpful technical staff at Civil Engineering Laboratory of Monash University, mainly, Mr Long Goh, Mr Zoltan Csaki, Mr Michael Leach, Mr Jeff Doddrell and Mr Alexander Benjamin, the experimentations would not have been successful. Their ideas and assistance, especially during the modifications of existing high pressure rock tri-axial set up for methane injections and using the macro-scale advanced core flooding set up were notable and grateful. The help and guidance received from the Monash Centre for Electron Microscopy (MCEM) staff, specially Dr Xia Feng, Dr Amelia Liu and Prof Peter Miller during micro-structural investigations also need to be appreciated. Another notable mention should be given to Dr Asadul Haque for his assistance and guidance for the X-ray CT scanning. Dr Alex McKnight is also greatly acknowledged for his assistance with proofreading the technical papers and this dissertation.

I was lucky enough to spend my PhD candidature with wonderful, cheerful and helpful group of colleagues at Monash University. I am thankful to Nadeesha, Shi shi, Dilanth, Tharaka, Ayal, Pabasara, Radhika, Chengpeng, Decheng, Xiaogang, Yunlong and Chathurika for their company throughout my PhD life. I also received the assistance from several undergraduate students, Coco, Hamish and Tanjuli during my experimental work and I am thankful for their corporation.

I also would like to acknowledge the Monash University for providing the opportunity to study in Monash and particularly the financial assistance that I have been offered.

At last but not least, my deepest appreciation is owed to my beloved parents (Somasiri and Swarna Ranathunga) and brother (Kenneth Ranathunga) for their unconditional support and guidance right way since childhood. Finally, I would like to acknowledge the practical and moral support I received from my loving husband (Dr Damith Chathuranga), and been patient and kind with my busy PhD life.

Thesis Synopsis

Enhanced coal bed methane recovery by carbon dioxide (CO_2-ECBM) has been identified as an economical coal bed methane production-enhancement technique, as this process has the ability to significantly enhance the coal bed methane production while sequestrating a considerable amount of CO_2 in deep coal seams. However, the suitable coal seams for CO_2 sequestration and ECBM processes are located in deep underground (> 800 m depth), where CO_2 is expected to be in at its highly chemically active super-critical state. According to current research findings, injection of CO_2 into deep coal seams causes both seam permeability and strength to be significantly reduced, and these reductions are considerably higher when the CO_2 is in super-critical condition. Furthermore, variations of coal seam properties also cause variations in the hydro-mechanical behaviour of coal during CO_2 injection. The permeability reduction causes the amount of injectable CO_2 in and producible methane (CH_4) from coal seams to become unpredictable and this strength reduction affects the long-term safety of the ECBM and CO_2 sequestration processes, as it may cause the injected CO_2 to back-migrate into the atmosphere sometime after injection. Therefore, the injection of massive amounts of CO_2 into deep coal seams to harvest maximum amounts of methane from the seam while reducing the anthropogenic CO_2 volume in the atmosphere has become a great challenge.

The main objective of this study is therefore to understand the effects of injecting gas properties and reservoir properties on coal flow and strength properties during CH_4 recovery through experimental (85%), numerical (10%) and analytical (5%) investigations.

Due to the lack of studies regarding the effect of coal rank on coal mass hydro-mechanical behaviour during CO_2 sequestration, low rank brown coal was mainly used for the experimental work. In addition, both natural and homogenous reconstituted specimens were used for the study to evaluate the influence of the heterogeneity of coal. The experimental work was conducted at (a) micro- (b) meso- and (c) macro-scale to determine the potential alterations to coal petro-physical properties with exposure to CO_2. The injecting gas properties (fluid types: CO_2, N_2 and water, and phase and pressure of CO_2) and coal seam properties (depth and temperature) were varied during the flow and strength studies and different saturation periods were incorporated during the strength studies to investigate the long-term effect of CO_2 on coal. The results were compared with the results for high rank coal in the research literature to determine the influence of carbon content on flow and strength alterations in coal. The following key findings were obtained from the experimental investigations.

CO_2 adsorption-induced coal matrix swelling is greater at higher CO_2 pressures, particularly for the super-critical phase of CO_2, regardless of reservoir depth or the maturity of the coal. Super-critical CO_2 has much lower permeability than sub-critical CO_2 in any coal type, and this influence of CO_2 phase condition increases with increasing carbon content. As expected, the permeability is reduced by around 25 to 80% with increasing depth for CO_2 permeation regardless of rank, and this influence of depth on permeability reduces with the phase transition from sub- to super-critical in any type of coal. Further, in comparison with the experimental permeability values for low rank coal and the permeability values for high rank coal reported in the literature, high rank coal exhibits a greater reduction in permeability than low rank coal due to sorption-induced strains, and the opposite is the case for stress-induced permeability. Interestingly, N_2 has the potential to reverse the CO_2 induced swelling areas to some extent in any coal type by up to around 30%, and this recovery ability can be increased by allowing sufficient time for N_2 flooding. Temperature has a positive effect on permeability at higher pore pressures, regardless of coal rank.

The strength results showed a reduction of around 40 to 80% of both strength and stiffness for super-critical CO_2 saturations of up to 10 MPa CO_2 saturation pressure in any coal type and a greater reduction in high rank coal, similar to the flow results. Interestingly, CO_2 adsorption-induced coal matrix alterations are largely completed with the initial interaction with CO_2, although considerable further coal matrix re-arrangement may occur at a slower rate. Water also causes a significant strength reduction in coal irrespective of coal rank, and interestingly, these reductions are higher for high rank coal. N_2 has the ability to enhance the strength of coal slightly in both low and high rank coals, and this enhancement is greater for low rank coals. Depth has a positive effect on coal strength during CO_2 sequestration. Both reconstituted and natural brown coal samples undergo similar variations with different fluid saturations, such as reductions of strength and stiffness for CO_2 and water saturations and increments of strength and stiffness for N_2 saturation.

The experimental results from both flow and strength studies were modelled using the COMSOL Multiphysics simulator and the results showed: (1) greater amounts of CO_2 can be sequestrated in coal seams even at greater depths and higher CO_2 pressures despite the flow reduction observed if sufficient time is allowed for CO_2 permeation and (2) the volume of coal subjected to plastic deformation increases with the increase in CO_2 saturation pressure contributing more ductile nature for the reservoir rock.

Next, the applicability of low rank coal seams as potential CO_2-ECBM sites was tested, and the results showed the ability of super-critical CO_2 to recover methane faster with 100% sweep efficiency. However, the shorter durations for CO_2 breakthrough under super-critical conditions result in quicker swelling, which may lead to lower CO_2 storage and CH_4 production ability in the long term.

A 3-D field-scale model was developed using the COMET3 simulator to investigate the optimum injection scenarios and seam conditions to optimize the CO_2-ECBM process. The results showed that long-term CH_4 production increases with the increment of injecting pressure and temperature and the reduction depth of injection. When the bed moisture content is higher than the critical moisture content, higher long-term CH_4 production was observed. Use of higher percentage of N_2 during N_2 and CO_2 co-injection can enhance the gas production, however, this leads for greater amount of N_2 leakages and lesser amount of CO_2 adsorption in long-term. Three injection wells at around 350 m spacing showed the maximum long-term (50 years) CH_4 production. However, a greater number of production wells improved methane production in the short-term, although production is limited in the long term.

In regard to the analytical work, an empirical relationship for gas adsorption-induced coal matrix swelling as a function of all the parameters (injecting gas properties and reservoir properties) was developed using basic statistics. The model can estimate the swelling of different coal types (> 75% fixed carbon content) under various gas sorptions with around ±1% accuracy compared to experimental observations.

Table of Contents

List of Publications

Following publications have resulted during the studies undertaken for this degree.

Book Chapters

1. **Ranathunga AS**, Perera MSA, Ranjith PG. Challenges and issues for CO_2 storage in deep coal seams. *Rock Mechanics and Engineering*, Volume 5: Chapter 3, Taylor and Francis group, CRC press, Balkema, Netherlands. (In press)

Peer-reviewed journal papers

1. **Ranathunga AS**, Perera MSA, Ranjith PG, Wei CH (2017). An experimental investigation of applicability of CO_2 enhanced coal bed methane recovery technique to low rank coal. *Fuel*, 189, 391-399.

2. **Ranathunga AS**, Perera MSA, Ranjith PG (2016). Influence of CO_2 adsorption on the strength and elastic modulus of low rank Australian coal under confining pressure. *International Journal of Coal Geology* 167, 148-156.

3. **Ranathunga AS**, Perera MSA, Ranjith PG, Bui H (2016). Supercritical CO_2 saturation-induced mechanical property alterations in low rank coal: An experimental study. *The Journal of Supercritical Fluids* 109, 134-140.

4. Perera MSA, **Ranathunga AS**, Ranjith PG (2016). Effect of coal rank on various fluid saturations creating mechanical property alterations using Australian coals. *Energies* 9(6), 440.

5. **Ranathunga AS**, Perera MSA, Ranjith PG, De Silva GPD (2016). A macro-scale view of the influence of effective stress on carbon dioxide flow behaviour in coal: An experimental study. *Geomechanics and Geophysics for Geo-Energy and Geo-Resources*, 1-16. [DOI: 10.1007/s40948-016-0042-2]

6. Zhang XG, Ranjith PG, Perera MS, **Ranathunga AS**, Haque A (2016). Gas Transportation and Enhanced Coalbed Methane Recovery Processes in Deep Coal Seams: A Review. *Energ Fuel* 30, 8832-8849.

7. Perera MSA, Ranjith PG, Rathnaweera TD, **Ranathunga AS**, Koay A, Choi X (2016). A Review of CO_2-Enhanced Oil Recovery with a Simulated Sensitivity Analysis. *Energies* 9, 481

8. **Ranathunga AS**, Perera MSA, Ranjith PG, Ju Y, Vishal V, De Silva PNK (2015). A macro-scale experimental study of sub and supercritical CO_2 flow behaviour in Victorian brown coal. *Fuel* 158: 864-873.

9. Perera MSA, Ranjith PG, **Ranathunga AS**, Koay A, Zhao J, Choi S (2015). Optimization of enhanced coal-bed methane recovery using numerical simulation. *Journal of Geophysics and Engineering* 12, 90.

10. **Ranathunga AS**, Perera MSA, Ranjith PG (2014). Deep coal seams as a greener energy source: a review. *Journal of Geophysics and Engineering*, 11,1-17.

11. **Ranathunga AS**, Perera MSA, Ranjith PG, Zhang XG (2017). Super-critical carbon dioxide flow behaviour in low rank coal: A meso-scale experimental study. *Journal of CO_2 Utilization* (under review).

12. **Ranathunga AS**, Perera MSA, Ranjith PG, Zhang XG (2017). The influence of CO_2 properties and reservoir depth on coal matrix swelling: A meso-scale experimental study using low rank coal. *Energ Fuel* (under review).

13. **Ranathunga AS**, Perera MSA, Ranjith PG (2017). A review and model development for estimation of gas adsorption-induced coal matrix swelling. *International Journal of Energy Research* (under review).

14. **Ranathunga AS**, Perera MSA, Ranjith PG (2017). Key factors controlling coal's strength property alterations during CO_2 enhanced coal bed methane production: A numerical study. *Journal of Natural Gas Science and Engineering* (under review).

15. **Ranathunga AS**, Perera MSA, Ranjith PG (2017). Effect of effective stress and coal matrix swelling on coal flow behaviour during CO_2 sequestration. *Journal of CO_2 Utilization* (under review).

16. **Ranathunga AS**, Perera MSA, Ranjith PG (2017). A laboratory-scale numerical study of CO_2 flow through coal under down-hole stress conditions: Application for CO_2 storage. *Energ Fuel* (under review).

17. Perera MSA, Ranjith PG, Rathnaweera TD, **Ranathunga AS**, Ze TM, Choi SK, Wu B (2017). Effects of reservoir and well properties on sand production during the extrusion of hydrocarbons from geological formations. *Energies* (under review).

18. Perera MSA, Ranjith PG, Rathnaweera TD, **Ranathunga AS**, Liu T, Wu B (2017). An experimental study to quantify sand production during oil recovery from conventional shallow geological formations. *Energy and Fuels* (under review).

19. Zhang XG, Ranjith PG, Perera MSA, **Ranathunga AS**. Effect of coal mass moisture content in adsorption of carbon dioxide, methane and nitrogen of low rank coal (in progress).

20. Zhang XG, Ranjith PG, Perera MSA, **Ranathunga AS**. Salinity-dependent strength characteristics of low rank coal: An experimental study (in progress).

Peer-reviewed conference papers

1. **Ranathunga AS**, Perera MSA, Ranjith PG. De Silva GPD (2016). A macro scale overview on coal mass permeability alterations occur upon CO_2 injection into Australian low rank coal, International conference on Geo-mechanics, Geo-energy and Geo-resources (IC3G 2016), Melbourne, Australia, 28-29 September, 2016; Paper no 92.

2. **Ranathunga AS**, Perera MSA, Ranjith PG, Haque RT (2016). An experimental study on behaviour of reconstituted low rank coal under different fluid saturations, ISRM International Symposium and EUROCK 2016, Cappadocia, Turkey, 29-31 August, 2016; Paper no 166.

3. **Ranathunga AS**, Perera MSA, Ranjith PG (2015). CO_2 sequestration in deep unmineable coal seams: A numerical study, International Conference on Geotechnical Engineering (ICEG 2015), Colombo, Sri Lanka, 10-11 August, 2015; Paper No. 168.

4. **Ranathunga AS**, Perera MSA, Ranjith PG (2014). An Experimental Study to Investigate Temperature Effect on Permeability of Victorian Brown Coal during CO_2 Sequestration, ISRM International Symposium and 8th Asian Rock Mechanics Symposium (ARMS8), Sapporo, Japan, 14-16 October, 2014; Paper No. ARMS8_PO-82.

Notations and abbreviations

Notations

$\emptyset_a$	porosity by adsorption
$\frac{\Delta\varepsilon_s}{\Delta p_s}$	strain caused by unit change by sorption pressure
CF_4	tetraflurometthane
CO_2	Carbon Dioxide
C_t	total reservoir gas content
D'	empirical curve fitting parameters
E_{CO_2}	elastic modulus of CO_2 adsorbed sample
E_F	analogous to Young's modulus but for the fracture
E_{intact}	elastic modulus of intact coal sample
F_a	axial load
L_0	sample length when t=0
L_t	sample length at time t
N_2	Nitrogen
P_E	curve fitting parameter
P_L	Langmuir pressure constant
P_c	confining pressure
P_d	downstream vessel pressure
P_{eff}	effective stress
P_i	injection pressure
P_o	downstream pressure
P_u	upstream vessel pressure
P_σ	curve fitting parameter
R_{vit}	Vitrinite reflectance
R_{xy}	correlation coefficient
S_{max}	maximum swelling of the coal
T_c	critical temperature
V_L	Langmuir volume constant
V_{abs}	volume of the absolute adsorption
V_d	volume of downstream pressure vessels
V_{des}	volume of gas desorbed from the matrix
V_{std}	mole volume of gas at standard temperature and pressure
V_u	volume of upstream pressure vessels
W_0	surface adsorption capacity of the substrate
W_{abs}	excess sorption

W_c	water content
b_{new}	new cleat width
b_{old}	initial cleat width
c_f	cleat compressibility
c_i	initial reservoir concentration
c_i	pressure difference between confining pressure and pore pressure
c_k	the differential swelling coefficient
c_m	matrix shrinkage compressibility
c_p	pore volume compressibility
c_r	grain compressibility
f_a	ratio of effective porosity
k'	empirical curve fitting parameters
k_0	initial permeability
k_{new}	permeability at pressure *p*
k_{old}	original reservoir permeability
l_m^*	change in the dimension of the coal matrix block in horizontal direction with pressure
p_{50}	Langmuir parameter for the swelling/shrinkage strain
α_s	volumetric welling/shrinkage coefficient
ε_v	volumetric swelling
ρ_L	van der Waals density of the gas
ρ_a	density of the adsorbed phase
ρ_g	gas density
ρ_s	sample density
σ_h^e	effective horizontal stress
σ_{CO_2}	strength of CO_2 adsorbed sample
σ_{intact}	strength of intact coal sample
φ_i	initial coal mass porosity
ΔE_{CO_2}	elastic modulus reduction due to CO_2 adsorption
ΔE_{max}	curve fitting parameter
ΔP_0	the step change of pressure in vessels at time = 0,
Δp_s	change in equivalent sorption pressures
$\Delta\sigma_{CO_2}$	strength reduction due to CO_2 adsorption
$\Delta\sigma_{max}$	curve fitting parameter
ΔS	change of the adsorbate mass
A	cross-section area of the sample
Ar	Argon
C	reservoir concentration

$C\%$	fixed carbon content
CH_4	Methane
D	a constant related to the affinity of the sorbent of the gas
K	bulk modulus
L	length of the sample
M	constrained axial modulus
Q	flow rate
R	gas constant
S	volumetric swelling
T	temperature
Xe	Xenon
a	gas storage capacity ratios of sample with upstream
b	gas storage capacity ratios of sample with downstream
f	fraction from 0 to 1
g	gravitational acceleration
k	permeability
n	exponent of pressure dependent permeability
p	pore pressure
t	time
α	effective stress parameter
$-\alpha$	slope of the pressure decay curve
β	adiabatic compressibility of the injecting fluid
ρ	gas density
φ	coal mass porosity
ϑ	Poisson's ratio

Abbreviations

AE	Acoustic Emission
ARI	Advanced Resource International
BTU	British Thermal Units
BV	Ball Valve
CBM	Coal Bed Methane
CCS	Carbon Capture and Storage
CSG	Coal Seam Gas
CT	Computed Tomography
CV	Check Valve
D-A	Dubnin-Astakhov
db	Dry basis
DEERL	Deep Earth Energy Research Laboratory
Dk	Dark
D-R	Dubnin-Radushkevich
EBSD	Electron Backscattered Electron Detector
ECBM	Enhanced Coal Bed Methane recovery
EDS	Energy Dispersive X-Ray Spectroscopy
EIA	Energy Information Administration
ESEM	Environmental Scanning Electron Microscopy
FEG	Field Emission Gun
FEM	Finite Element Analysis
FIB	Focused Ion Beam
Flex. Hose	Flexible Hose
GHG	Green House Gas
ICCP	International Committee for Coal Petrology
IEA	International Energy Agency
IPCC	International Panel on Climate Change
Lt	Light
LVDT	Linear Variable Differential Transformer
MCEM	Monash Centre for Electron Microscopy
M-d	Medium-Dark
MGC	Milli Gas Counter
M-l	Medium-Light

NV	Needle Valve
OHS	Occupational Health and Safety
Pa	Pale
PG	Pressure Gauge
PR	Pressure Regulator
PT	Pressure Transducer
RaaD	Resolution at a Distance
RC	Reconstituted Coal
RMSE	Root Mean Square Error
RTD	Temperature Probe
RV	Relief Valve
SDD	Silicon Drift Detector
SEM	Scanning Electron Microscope
STEM	Scanning Transmission Electron Microscopy
TCF	Trillion Cubic Feet
UCS	Unconfined Compressive Strength
UNFCCC	United Nations Framework Convention on Climate Change
VIF	Variance Inflation Factor
wb	wet basis
XMFIG	X-Ray Microscopy Facility for Imaging Geo-materials

Part 1: Chapters 1, 2 and 3 - Introduction, Literature review, and Materials, instrumentation and experimental methods

Part 1: Introduction, Literature review, and Materials, instrumentation and experimental methods

This section of the thesis consists of three chapters (Chapters 1, 2 and 3) including the Introduction, Literature review, and Materials, instrumentation and experimental methods. These chapters provide an overview of the research area addressed, including previous studies and existing gaps. How those gaps are addressed and the methodologies and procedures adopted are detailed next. A summary of the content of each chapter is presented below.

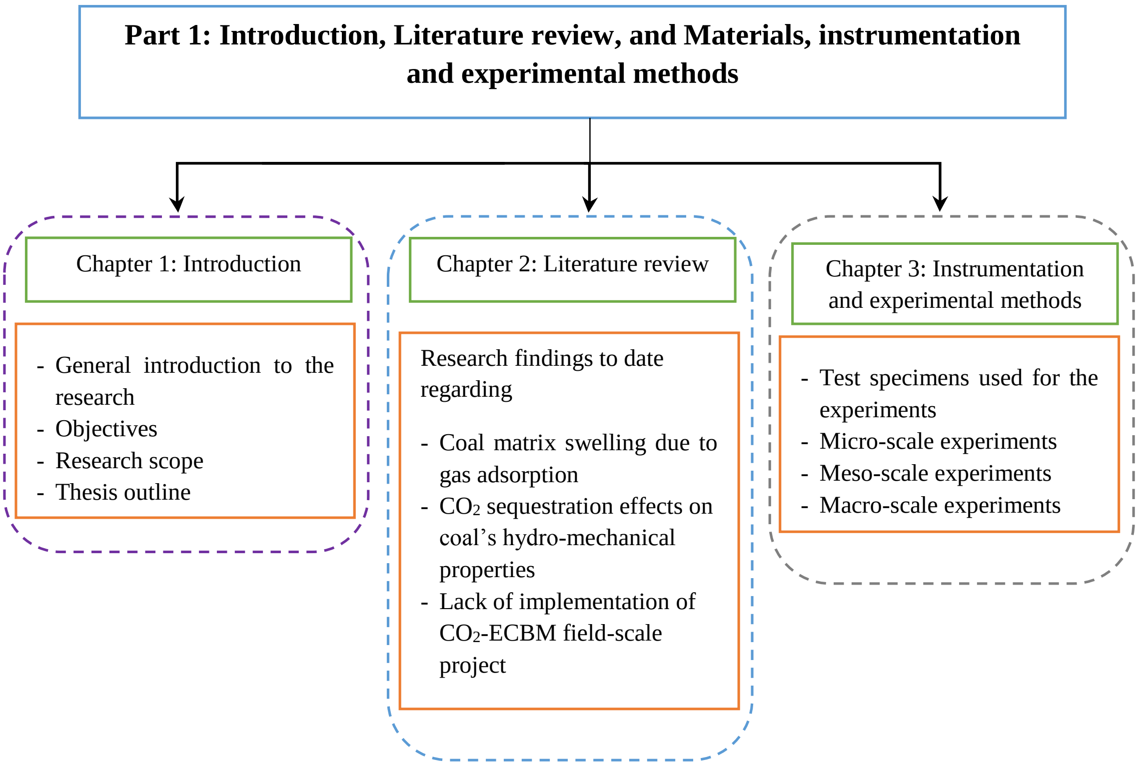

PART 1 - CHAPTER 1

Introduction

1. Introduction

1.1 Background

Energy consumption is rapidly increasing due to the ever-increasing population of the world (Figure 1.1). The present world energy demand is basically fulfilled by oil (35.7%), natural gas (25.6%), coal (19.3%), nuclear (9.9%), biofuels and waste (5.5%), hydro-power (2.3%) and others (geothermal, solar, wind, heat etc. 1.7%) (IEA, 2015). However, according to the EIA (2015), oil and coal resources, which are major contributors to the energy supply, will remain so for at least four to five decades, which indicates the importance of searching for new energy sources. In the last few decades, much attention has been given to natural gas production as a replacement for oil and coal and to overcome the environmental issues caused by them, such as global warming. As a result, natural gas production increased by around 35% from 1973 to 2014, with around 32% and 15% reductions in oil and coal energy production, respectively (IEA, 2015). Coal bed methane (CBM) is a natural gas which provides around 6 to 9% of the current natural gas production (EIA, 2016). CBM is formed during the coalification process and is trapped in the coal matrix. CBM consists mainly of methane (CH_4) (more than 90%) and is used as a low emission alternative for energy production (Figure 1.2).

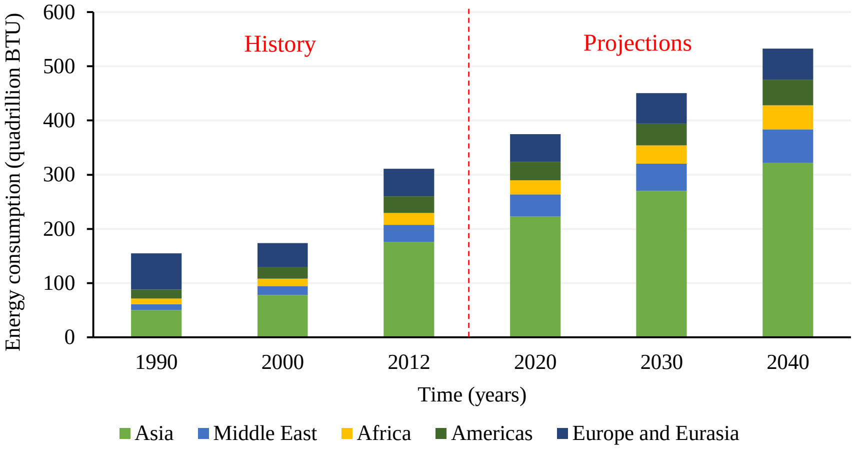

Figure 1.1. World energy consumption by region (EIA, 2016)

According to Gale and Freund (2001), around 200 m^3 of methane may be generated for each tonne of coal formed. Most of this methane is subsequently lost, but undisturbed deep coal seams may still contain up to 25 m^3 of methane per tonne of coal which is adsorbed in the coal. According to White et al. (2005), there are around 3010 to 7840 trillion cubic feet (Tcf) of international CBM resources of which around 510 Tcf is recoverable. In Australia, 310 to 410 Tcf of CBM resources are available, while around 60 Tcf are recoverable (White et al., 2005).

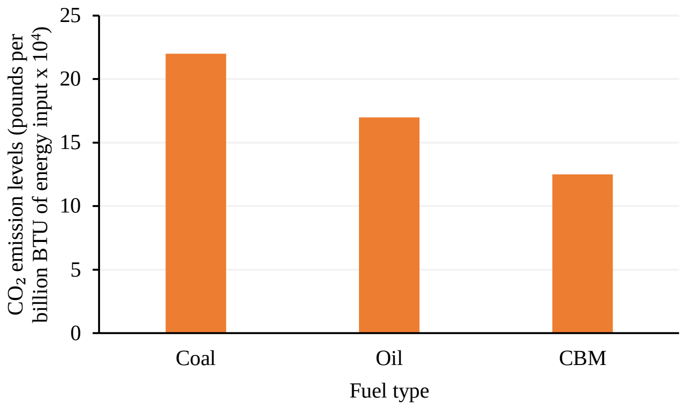

Figure 1.2. Carbon dioxide emission levels for different fuel types (EIA, 2015)

CBM is conventionally recovered by means of reservoir pressure depletion by reducing the partial pressure of the species adsorbed into the coal mass, which eventually reverses the physical adsorption potential (Metcalfe et al., 1991). This pressure depletion method is simple but inefficient, as it can recover less than 50% of the gas-in-place (Gale and Freund, 2001). Hence, a substantial amount of CH_4 in coal is left behind with the current operating method. Although hydraulic pressure is used to assist recovery, a sufficient number of wells must be drilled to achieve adequate gas recovery due to the low permeability of deep coal seams. As a consequence, methods such as enhanced coal-bed methane (ECBM) recovery are used in order to lessen the drawbacks of the reservoir pressure depletion method currently used in the industry.

1.2 Enhanced Coal Bed Methane (ECBM) recovery

Coal acts as a massive adsorbent bed (Puri et al., 1991) and this adsorbent bed can be regenerated not only by using pressure depletion, but also by inert gas stripping, as well as by displacement desorption (Ruthven, 1984). Inert gas stripping is accomplished by reducing the partial pressure by introducing a low-adsorbing gas at constant pressure. In displacement desorption, another gas with higher adsorption capacity is injected into the coal seam, which displaces the adsorbed gas in the coal seam. In general, the recovery of CH_4 using any of these methods is known as ECBM recovery, which can be achieved using several recovery agents, including N_2, CO_2 and flue gas (Syed et al., 2013). However, of the numerous patents documenting ECBM (Every and Luino Dell'Osso, 1977; Puri and Pendergraft, 1995; Puri and Stein, 1989; Seidle et al., 1997), most have focused on N_2 and CO_2 injection. CO_2 sequestration-induced methane recovery enhancement has drawn a good deal of attention due to the following advantages:

- CO_2 has a significantly higher affinity to adsorb into the coal matrix than CH_4 (Figure 1.3). Therefore, when CO_2 is injected into the coal seam, it improves the recovery of CH_4 by directly displacing the CH_4. In addition, CO_2 injection also causes the reduction of the effective partial pressure of the CH_4 (Stevens et al., 2001), which eventually causes the adsorbed CH_4 to be desorbed from the coal matrix.

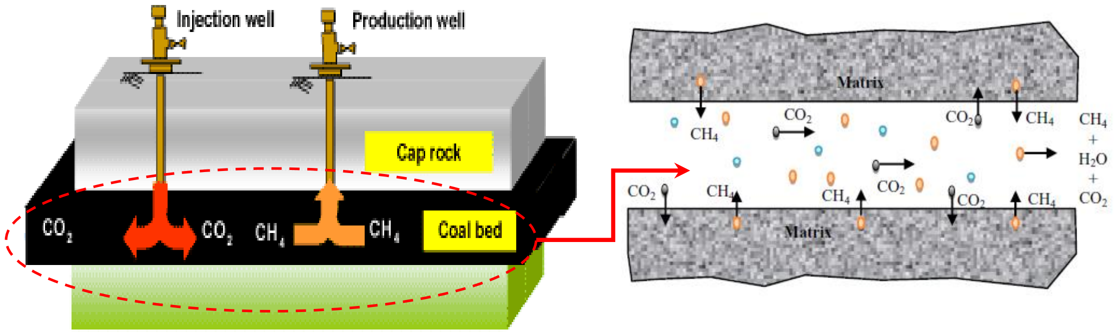

Figure 1.3. CO_2-enhanced coalbed methane mechanism

- 5-15 gigatons of CO_2 in the world can be sequestered in coal beds by the profits gained from CH_4 production through the ECBM recovery process (White et al., 2005).
- Suitable coal beds are adjacent to many large power plants so that the cost of CO_2 transportation is low (Stevens et al., 2001).
- Past studies have shown that around 98% of the CO_2 in coal seams exists in an adsorbed phase on the walls of the coal micro-pores, while the rest remain as free gas inside the cleats (Day et al., 2008). Therefore, CO_2 exists in a more stable form and remains stored within the seam, providing the seam is not disturbed (Gale and Freund, 2001), which decreases the risk of back-migration.
- The storage ability of CO_2 provides an additional advantage by reducing the anthropogenic CO_2 in the atmosphere, leading to a viable option for the mitigation of global warming (Perera and Ranjith, 2012).
- Coal has a large surface area on which the methane is adsorbed (20–200 m^2/g) (Gale and Freund, 2001) and large porosity values due to its dual pore system (White et al., 2005). Therefore, coal-bed methane reservoirs can store as much as five times the amount of CO_2 as that contained in conventional sandstone reservoirs (White et al., 2005).

These advantages highlight the importance of using CO_2 injection-induced methane recovery enhancement in deep unmineable coal seams.

1.3 Statement of problem and research significance

Although the CO_2-ECBM process has many advantages, it has some drawbacks due to the significant changes in the chemico-physical properties of coal after the injection of CO_2. Coal has a polymer-like network structure (see Figure 1.4) and is therefore often affected by the gas or solvent with which it is in contact. According to Perera and Ranjith (2012), large strains are induced between the surface of the pore walls and the adsorbed gas layer in the coal matrix during CO_2 adsorption into the coal matrix, which is commonly known as *coal matrix swelling*. This is a well-known fact and has been observed in large-scale field trials of CO_2 injection in the Allison unit in the San Juan basin and the Williston basin in North Dakota, USA, the Fenn Big Valley basin in Alberta, Canada, the Silesian basin in Poland and the Ishikari basin in Yubari, Japan (Perera et al., 2012).

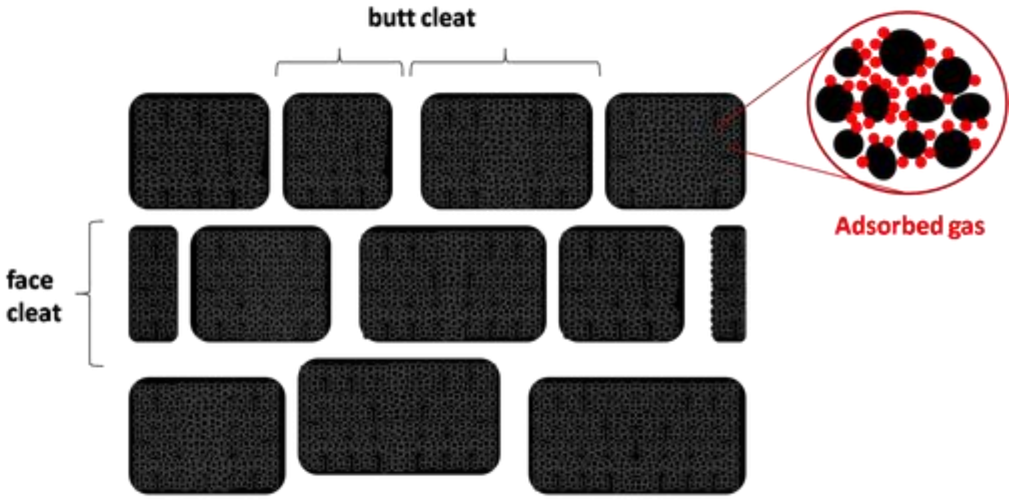

(a) Pore structure of a typical coal seam (created by the author using data from https://coalbedmethane.wordpress.com/tag/cleat/)

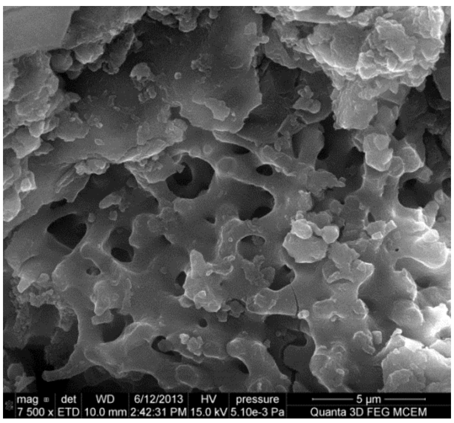

(b) Pore structure of brown coal (from Gippsland basin) *

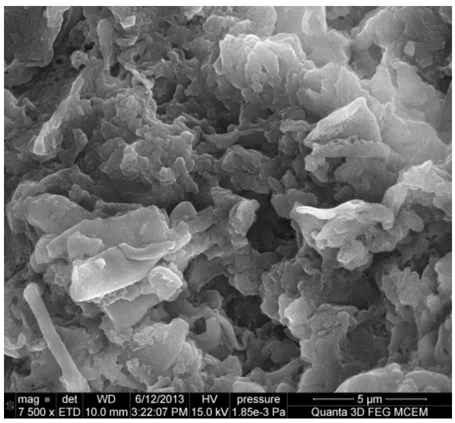

(c) Pore structure of black coal (from Sydney basin) *

Figure 1.4. Typical pore structure of coal (*Conditions used to obtain SEM images: scale 5 µm, probe current 15 kV and spot size 4.5 under low vacuum)

➢ *Influence of effective factors on CO_2 adsorption-induced coal matrix swelling*

This CO_2 adsorption-induced coal matrix swelling process is dependent on the properties of both the seam and the injected CO_2. According to previous studies, swelling exhibits an inverted-U shaped variation with coal rank, due to the corresponding variation of the coal mass properties such as moisture, carbon content and pore space (Perera et al., 2011b). Further, the temperature of a coal seam reduces the swelling with the reduced sorption capacities (Bae and Bhatia, 2006). In relation to injecting gas properties, CO_2 swells coal much more than CH_4 due to its greater adsorption capacity (Day et al., 2010). On the other hand, the extent of swelling is largely dependent on the pressure and the physical state of the injected CO_2, and super-critical CO_2 (above the critical point of CO_2: 31.8^0C and 7.38 MPa) creates much greater swelling than gas or liquid CO_2 due to its higher chemical potential (Day et al., 2008; Perera et al., 2011a). However, potential coal seams for CO_2 sequestration are available at extremely deep locations and there is a high possibility of phase change from gas/liquid to the super-critical state in the underground environment owing to changes in field conditions (De Silva, 2013). This confirms the likely occurrence of high swelling rates in deep coal seams with CO_2 injection.

Gaps to be addressed:

- Swelling studies on intact coal samples under different in situ stresses, especially on low rank coal are lacking.
- Different models have been proposed to predict swelling in coal with gas adsorption-induced swelling, however none of the models show the total effect of all the effective factors (adsorbing gas type, temperature, coal rank, moisture content, etc.) on the swelling behaviour of coal.

➢ *Influence of CO_2 adsorption-induced coal matrix swelling on coal flow properties*

The effectiveness of the CO_2-ECBM process in any coal seam is greatly influenced by the permeability of the CO_2 injected into the seam, which is dependent on a number of factors, as given below:

- Coal matrix swelling, which causes the internal coal seam pore space available for fluid/gas movement to be reduced.
- CO_2 injecting pressure and seam depth, both of which change the effective stress on the coal seam and eventually, the seam's pore connectivity space.
- Seam temperature, which creates thermal expansion in the seam and also leads to reduced sorption capacity with kinetic energy increment in injected CO_2 molecules.

Importantly, the injected CO_2 phase condition critically influences its flow behaviour in the seam, and super-critical CO_2, the form of CO_2 expected in deep coal seams, has significantly lower permeability than gas/ liquid CO_2, which causes unpredictable CO_2 injectivity into deep coal seams. The reduction of seam permeability over time after CO_2 injection is a common issue faced by many field-scale CO_2 sequestration projects. For example, there was around 50% reduction in CO_2 injectivity at the Allison unit CO_2 sequestration project in the San Juan basin, USA, during the first two years of injection (Reeves and Oudinot, 2005). Therefore, comprehensive studies are needed to understand super-critical CO_2 movement in the coal mass compared to that of sub-critical CO_2 by examining the swelling and permeability caused by different phases and pressures of CO_2 at different depths and temperatures.

Gaps to be addressed:

- In relation to permeability studies, very few studies have been conducted on low rank coals to identify the variation of coal permeability patterns with coal rank for sub-critical and super-critical CO_2 flows.
- Few studies have used macro-scale permeability tests which would help to examine the applicability of adsorption theories at a larger scale to permit accurate estimation of field CO_2 storage capacity.

➢ *Influence of CO_2 adsorption-induced coal matrix swelling on coal mechanical properties*

The secure storage of CO_2 injected in the seam is critically important in CO_2 geo-sequestration in deep coal seams in terms of environmental safety and health. It is important to prevent the upward migration of CO_2, as this has potential to cause distress and on occasion death, and lateral migration into aquifers and surrounding more permeable geologic strata. These factors are mainly dependent on the coal mass strength properties. However, the fact that CO_2 adsorption-induced swelling creates a weakening effect in deep coal seams is well known (Masoudian et al., 2014; Perera et al., 2013; Viete and Ranjith, 2006; Vishal et al., 2015). This strength reduction is greatly dependent on CO_2 phase and pressure, increases with increasing pressure, and super-critical CO_2 causes much greater strength reduction than gas/liquid (sub-critical) CO_2. Therefore, knowledge of the effects of both sub-critical and super-critical CO_2 adsorptions on coal strength is needed for the long-term safe storage of CO_2 in deep coal seams.

Gaps to be addressed:

- No study to date has concerned the effect of coal rank on strength with CO_2 movement in the coal matrix, particularly for super-critical CO_2, which is the expected phase condition of CO_2 in preferable coal seams for CO_2 ECBM.

- No study to date has considered the variation of the effect of different fluid saturations with coal rank.
- Except for several days or weeks (up to three weeks) of CO_2 saturation, no study has considered the effect of the duration of CO_2 adsorption on coal strength.

➢ *Effect of coal heterogeneity on investigation of CO_2 storage-induced coal mass behaviour*

Existing government policies, public perceptions, and strict rules on coal mining affect the implementation of CO_2 sequestration in deep coal seams. The current lack of knowledge related to coal seam CO_2 sequestration severely hampers the implementation of this process in potential coal seams around the world. The complex heterogeneous nature of coal, which creates location-dependent coal seam properties, is the main reason for the limited knowledge of coal CO_2 sequestration. Homogeneous samples with properties reproducible in the laboratory would provide significant advantages, especially in understanding the effects of various factors on the properties of coal (Jasinge 2010). Therefore, reconstituted homogenous specimens need to be developed and tested for the study of CO_2 adsorption-induced coal mass flow and strength behaviours.

Gaps to be addressed:

- No study to date has concerned the effect of super-critical CO_2 on flow and strength behaviour in reconstituted coal samples to confirm the use of these samples to represent natural coal samples while avoiding the heterogeneity effect.

➢ *Factors affecting methane recovery during CO_2 sequestration*

To harvest the maximum amount of methane from coal seams by sequestrating a large amount of CO_2, the methane production rates at production wells and CO_2 injection capacities are important. As explained earlier, the reduction of CO_2 injection and related methane production has been observed in several field-scale studies within a few years of injection (White et al., 2005). The reservoir properties, injecting gas properties and the injection and production well arrangements collectively affect the CO_2 injection and CBM production amounts (Masoudian, 2016). Therefore, it is necessary to determine the optimum conditions for the effective implementation of CO_2-ECBM in deep coal reservoirs.

Gaps to be addressed:

- Experimental investigations on the applicability of low rank coal as a possible catalyst for CO_2-ECBM studies are lacking.

- Although some experimental, numerical and field studies have been conducted on the ECBM process and production enhancement techniques, none to date has considered the influences of all the possible primary effective factors for the process, and it has therefore been difficult to obtain comprehensive knowledge of the subject.

1.4 Aims and specific objectives of the thesis

The main aim of this research work is to identify ideal injection strategies to find the optimum conditions to harvest methane (CH_4) from deep coal seams while storing maximum amounts of CO_2.

This will be achieved by achieving the following objectives:

1. Understand the effects of coal mass properties and injecting fluid properties on CO_2 flow behaviour in deep coal seams considering the structural changes in the coal matrix due to CO_2 adsorption;
2. Quantify the effects of the adsorption of super-critical CO_2 on the strength, deformation properties and swelling behaviour of coal at the pressures and temperatures expected for deep coal seam CO_2 sequestration;
3. Develop knowledge of the CO_2 migration and storage patterns expected for the sorptive exchange of CO_2 and CH_4 and investigate the optimum conditions to recover CH_4 while storing maximum amounts of CO_2 in deep coal seams.

1.5 Research Scope

Studies related to coal mass behaviour during CO_2 sequestration have been limited to high rank coal on the basis of the wide application of high rank coal in CO_2 sequestration and ECBM processes. The infrequent existence of brown coal at sufficient depths for feasible CO_2 sequestration has caused less attention being given to similar investigations for low rank coals such as brown coal. According to Garduno et al. (2003), the Jackson, Yegua and Wilcox formation in Texas has deep lignite formations (800 to 3800 ft from the standard sea level (SSL)) with CO_2-ECBM potential, and Hernandez et al. (2006) stated that the close proximity of many CO_2 point sources near these potential Texas low rank coals will generate attractive economic conditions. In the case of Victorian brown coal, Cooperative Research Centre for Greenhouse Gas Technologies (CO2CRC) studies carried out in 2005 showed the existence of possible brown coal CO_2 storage sites in the on- and off-shore Gippsland Basin at un-mineable depths (400 - 800 m) (Hooper et al., 2005; Jasinge, 2010). Given such possibilities, the present study was undertaken to find the storage potential and ECBM effectiveness of CO_2 in brown coal obtained from the Gippsland basin, Victoria, Australia.

The results obtained from these low rank coals were compared with the results of high rank coal reported in the research literature to evaluate the effect of coal rank on CO_2 adsorption-induced coal flow and strength behaviours to overcome one of the main drawbacks identified in the research gaps. Reconstituted samples were also prepared using powdered brown coal from the same origin and tested for super-critical CO_2 adsorption-related flow and strength variations for comparison with natural samples. Several macro-scale experiments representing a thin coal reservoir were also implemented to obtain the storage capacities of brown coal at different seam depths and under different CO_2 pressures. Micro-structural variations during different fluid saturations and different CO_2 pressures and durations were also incorporated to explain the results of the meso-scale and macro-scale experiments. Next, the applicability of low-rank brown coal as a potential catalyst for CO_2-ECBM projects was investigated by conducting a series of CO_2 core flooding tests on CH_4 saturated brown coal specimens. Due to limitations in the experimental apparatus, and the extensive time and high cost required to perform the tests, the test conditions used for laboratory scale tests are often restricted, which may fail to represent the actual field conditions. To eliminate these limitations, numerical simulations can be utilised to predict the probable behaviours of coal under high CO_2 pressures at great depths. Hence, both laboratory-scale flow and strength studies were modelled using the COMSOL Multiphysics simulator to predict the possible behaviour of deep coal seams under CO_2 sequestration. Finally, a comprehensive field-scale numerical model was performed using the COMET3 numerical simulator to obtain the optimum reservoir conditions, injecting gas properties and well arrangements to efficiently and effectively implement CO_2-ECBM projects in deep coal seams. Table 1.1 summarises the research scope and the work carried out to fulfil the study’s aim and objectives.

Table 1.1. Research Scope

No.	**Type of study**	**Title of research work**	**Scale**
01.	Experimental	Effect of CO_2 properties and reservoir depth on coal permeability	Meso & micro
02.	Experimental and empirical	Evaluate the individual effects of effective stress and sorption-induced strain on the evolution of coal permeability	Meso
03.	Experimental	Effect of temperature on coal permeability	Meso
04.	Experimental and empirical	Effect of CO_2 properties and reservoir depth on coal matrix swelling	Meso
05.	Model development	Estimation of gas adsorption-induced coal matrix swelling in different coal types	-
06.	Experimental	Effect of CO_2 properties on coal permeability and flow behaviour along the coal seam using reconstituted coal	Macro
07.	Experimental	Influence of effective stress on carbon dioxide flow behaviour and CO_2 storage capacity in coal using reconstituted coal	Macro

08.	Numerical	Predict the expected fluid flow along the coal seam and storage capacity variations in coal for various CO_2 properties under different down-hole stresses using reconstituted coal	Macro
09.	Experimental	Effect of CO_2 properties on coal strength	Meso & Micro
10.	Experimental	Effect of coal rank on various fluid saturations creating mechanical property alterations	Meso & Micro
11.	Experimental	Effect of CO_2 saturation time on coal strength	Meso & Micro
12.	Experimental	Influence of CO_2 adsorption on the strength and elastic modulus of coal under confining pressure	Meso
13.	Experimental	Behaviour of reconstituted coal samples after different fluid saturations under loading	Meso & Micro
14.	Numerical	Effect of effective factors on coal mass mechanical properties using reconstituted coal	Meso
15.	Experimental	Applicability of CO_2 enhanced coal bed methane recovery to low rank coal	Meso
16.	Numerical	Optimization of CO_2-enhanced coal bed methane recovery	Field

- Objective 1
- Objective 2
- Objective 3

1.6 Organisation of thesis

This thesis is presented in five parts which include nine chapters. A description of the five parts and their included chapters is provided in brief below.

1.6.1 Part 1: Introduction, Literature review, and Materials, instrumentation and experimental methods

Part 1 of this thesis comprises three chapters (Chapters 1, 2 and 3) which provide the background to the research area, a review of the major findings of previous studies pertaining to this research, major knowledge gaps and the objectives of this research to advance the understanding of the research area. The materials and instruments used for testing and the experimental methods are also explained in this chapter.

Chapter 1 – Introduction

A general introduction to the whole research program is included in this chapter. The chapter includes a brief description of the increasing energy demand, the potential of coal bed methane to fulfil this rising energy demand, coal bed methane recovery using CO_2 sequestration and its advantages, gaps in existing research, and specific objectives, followed by the research scope and the thesis outline.

Chapter 2 –Literature Review

This chapter consists of a critical review of the results of the most pertinent previous studies in the literature to date, and has seven main sections. The first section details the importance of CO_2 sequestration in coal seams and what happens when CO_2 is injected into coal seams. Next, coal matrix swelling is discussed, paying attention to the effect of effective factors (coal mass properties and injecting gas properties) on the swelling of coal. The alterations of flow and strength behaviours and the related previous findings are detailed in the fourth and fifth sections of the literature review. Then, existing CO_2-ECBM-related field-scale projects are listed with observations. Few field-scale projects on CO_2-ECBM have been implemented to date, and the reasons for the lack of implementation are discussed in the final section.

Chapter 3 – Materials, instrumentation and experimental methods

This chapter presents the experimental program adopted for the present research work. Three types of tests were conducted during the research, which consisted of micro-, meso- and macro-scale experiments. First, the materials used and how they were prepared for the tests are explained. Next, the instrumentation used, their capabilities and how they were utilised for the present study are described. Finally, a brief description of the experimental conditions and the methods used is presented.

1.6.2 Part 2: Investigation of variations of coal flow properties during carbon dioxide sequestration

Part 2 of the thesis is dedicated to a discussion of coal mass flow behaviour during CO_2 sequestration. This is presented with the aid of two major chapters of the thesis (Chapters 4 and 5), which consider laboratory testing, empirical and analytical model development, and numerical modelling. A brief summary of each chapter is provided below.

Chapter 4 – Meso-scale studies of coal flow properties during carbon dioxide sequestration using natural coal specimens

This chapter presents the outcomes of meso-scale studies conducted using natural brown coal to investigate flow property variation due to CO_2 sequestration and consists of five main sections. In the first section, a series of experimental core-flooding tests on low-rank brown coal from the Gippsland basin is detailed pertaining to the effect of reservoir depth and injecting gas properties. The results of these tests are presented in this chapter in the form of a submitted journal paper "*Super-critical carbon dioxide flow behaviour in low rank coal: A meso-scale experimental study*".

According to the findings in Section 1, both effective stress and the sorption-induced strain in coal mass cause the observed permeability variations with CO_2 permeation. For the effective application of the CO_2-ECBM process, identification of the influence of permeability alterations due to each parameter (effective stress and swelling) is needed. Therefore, the second section reports on a study conducted to differentiate the effect of effective stress and sorption-induced swelling on coal mass permeability by calibrating the adsorbing-gas permeabilities (CO_2) using the effective stress parameters for comparatively non-adsorbing gas permeabilities (N_2) for both low and high rank Australian coals. The results of these tests are presented in this chapter in the form of a submitted journal paper "*Effect of effective stress and coal matrix swelling on coal flow behaviour during CO_2 sequestration*".

The third section details a study conducted to investigate the effect of temperature on the permeability of coal. A series of tri-axial flow experiments was conducted on brown coal specimens from the Gippsland basin, Victoria. Both N_2 and CO_2 were injected to distinguish the structural changes which occur due to CO_2 permeation. The results of the experiments are discussed in detail, paying attention to the effects of temperature on the coal matrix.

The fourth section of this chapter reports the effects of sub-critical and super-critical CO_2 adsorption-induced swelling on the permeability of brown coal, which are the reasons for the permeability variations observed in the first section. This is covered by a submitted journal paper entitled "*The influence of CO_2 properties and reservoir depth on coal matrix swelling: A meso-scale experimental study using low rank coal*". This paper shows how the CO_2 adsorption-induced swelling effect varies with the phase condition of adsorbing CO_2 and illustrates how the effect varies under different injecting and confining pressure conditions.

The final section is the analytical component of the thesis, and provides a detailed description of the development of an empirical equation using basic statistics to predict the maximum swelling term in the D-R equation (one of the most widely-used gas adsorption equations which was modified to predict swelling of coal). In this case, the effects of both coal mass and injecting gas physical properties on maximum swelling variation were investigated and a descriptive model for the maximum swelling term was then developed as a function of all the effective factors. This section is a submitted journal paper entitled "*A review and model development for estimation of gas adsorption-induced coal matrix swelling*".

Chapter 5 – Macro-scale studies of coal flow properties during carbon dioxide sequestration using reconstituted coal

This chapter contains three sections which present the outcomes of macro-scale studies conducted using reconstituted brown coal for the investigation of flow property variation due to CO_2 sequestration. The first section of this chapter provides details of the reconstituted coal's permeability and testing. Further, reconstituted coal permeability is compared for both sub-critical and super-critical conditions. CO_2 flow behaviour along the coal sample is also studied with comparison to alternative N_2 permeation. This section is presented in the form a published journal paper entitled "*A macro-scale experimental study of sub- and super-critical CO_2 flow behaviour in Victorian brown coal*".

The second section of Chapter 5 examines the coal flow behaviour under different CO_2 phase conditions with respect to reservoir depth. Further, the variation of the storage capacity with CO_2 pressure and the reservoir depth is also presented.

The final section presents a laboratory-scale numerical model developed to predict the expected fluid flow along the coal seam and storage capacity variations in coal with various CO_2 properties under different down-hole stresses. This model was developed using the experimental results presented in Sections 1 and 2 and was extended for higher CO_2 pressures and reservoir depths to observe the flow behaviour of deep coal seams. The storage capacity was also modelled during this study and the results are presented in detail. This section is a submitted journal paper entitled "*A laboratory-scale numerical study of CO_2 flow through coal under down-hole stress conditions: Application for CO_2 storage*".

1.6.3 Part 3: Investigation of coal mechanical property variations during carbon dioxide sequestration

Part 3 of the thesis is dedicated to a discussion of coal mass strength variations during CO_2 sequestration. This is presented with the aid of two major chapters of the thesis (Chapters 6 and 7), which consider comprehensive laboratory tests and a numerical study. A brief summary of each chapter is provided below.

Chapter 6 - Investigation of coal mechanical property variations during carbon dioxide sequestration using natural coal

This chapter includes three main sections which detail the strength variations of coal during CO_2 sequestration using natural coal samples. Most of the experiments were conducted using Victorian brown coal (lignite) and black coal from the Sydney basin (bituminous) was also used for several studies to enable a comparison of the effect of coal rank on strength behaviours. The first section of this chapter refers to a strength study conducted to investigate the effects of sub-critical and super-critical CO_2 adsorption on the strength of low rank coals. A series of unconfined compressive strength (UCS) tests was conducted on natural brown coal samples under both sub- and super-critical CO_2 saturation conditions. This section is presented in the form a published journal paper entitled "*Super-critical CO_2 saturation-induced mechanical property alterations in low rank coal: An experimental study*".

The second section of this chapter describes a strength study conducted to investigate the effects of different saturation mediums, CO_2, N_2 and water, on the strength of both low and high rank coals. UCS tests were conducted on natural intact brown coal samples from the Gippsland basin and natural fractured black coal from the Sydney basin, which had been saturated in different mediums (CO_2, N_2, and water) under different saturation pressures. This section is presented in the form of a published journal paper entitled "*Effect of coal rank on various fluid saturation-created mechanical property alterations using Australian coals*".

The third and final section of this chapter investigates the effect of confining pressure (reservoir depth) on the strength variations observed during UCS tests. A series of tri-axial strength tests was conducted on low rank brown coal specimens for both sub- and super-critical CO_2 saturations. In addition, the effect of CO_2 exposure time on coal's mechanical properties was investigated under super-critical CO_2 saturation conditions, in order to determine the effect of long-term CO_2 injection on coal seam mechanical properties, as CO_2-ECBM is a long-term process. Brown coal was used to conduct the experiments upon CO_2 saturation for different time durations to observe the time effect. This section is presented in the form a published journal paper entitled "*Influence of CO_2 adsorption on the strength and elastic modulus of low rank Australian coal under confining pressure*".

Chapter 7 - Investigation of coal mechanical property variations during carbon dioxide sequestration using reconstituted coal

CO_2 storage in deep coal seams significantly alters the petro-physical properties of the coal masses and precise evaluation of such alterations is difficult due to the highly heterogeneous nature of coal. This indicates the importance of testing reconstituted coal samples. Therefore, the main focus of this chapter is to investigate the strength variations of coal samples during CO_2 injection using reconstituted specimens. Low rank brown coal was used to prepare the samples and the first section of the chapter details a series of UCS tests conducted for these samples with different fluid saturations (CO_2, N_2, and water). The results are compared with those for natural brown coal samples to evaluate the effect of the heterogeneity of coal on the results.

The last section of this chapter studies coal mass strength behaviour under deep underground conditions expected during CO_2 sequestration by developing numerical models extending the experimental results obtained in the first section of this chapter. The COMSOL Multiphysics numerical simulator was first used to simulate the uniaxial experimental results, and then to model the tri-axial behaviour of brown coal saturated under different CO_2 conditions. This section is a submitted journal paper entitled "*Key factors controlling coal's strength property alterations during CO_2 enhanced coal bed methane production: A numerical study*".

1.6.4 Part 4: Investigation of carbon dioxide sequestration-induced methane recovery enhancement

Part 4 consists of one chapter which details an experimental and numerical study conducted to determine the optimum conditions to harvest methane by storing CO_2.

Chapter 8 - Investigation of carbon dioxide sequestration-induced methane recovery enhancement

This chapter consists of two main sections. The first section focuses on an experimental study conducted to investigate the applicability of low rank coal seams for CO_2 sequestration-induced methane recovery enhancement projects. A series of CO_2 core flooding tests was carried out on methane-saturated meso-scale Victorian brown coal specimens. Different CO_2 injection pressures were selected, representing both sub- and super-critical CO_2, to observe how methane enhancement varies with CO_2 phase conditions. This section is presented in the form of a published journal paper entitled "*An experimental investigation of applicability of CO_2 enhanced coal bed methane recovery technique to low rank coal*".

The last section of this chapter details a field-scale numerical study performed using the COMET3 simulator to determine the most favourable conditions for CO_2-ECBM. All the possible effective factors relating to CO_2 storage and CH_4 production, such as coal seam properties, injecting gas properties and injection and production well arrangements in a typical low rank coal seam, were studied. The optimum conditions to efficiently and effectively implement CO_2-ECBM projects were identified and explained in this section.

1.6.5 Part 5: Conclusions and suggestions for future research

This part consists of only one chapter (Chapter 9), which discusses the overall conclusions of this study and provides some recommendations for future investigations.

Chapter 9 - Conclusions and suggestions for future research

The final chapter of the thesis presents the conclusions drawn from the experimental and numerical investigations and offers some recommendations for future research studies.

1.7 References

Bae, J.-S., Bhatia, S.K., 2006. High-Pressure Adsorption of Methane and Carbon Dioxide on Coal. *Energ Fuel* 20, 2599-2607.

Jasinge, D., 2010. An investigation of the effect of carbon dioxide sequestration on the behaviour of brown coal (*PhD thesis*) Monash University, Melbourne, Australia.

Ruthven, D.M., 1984. *Principles of adsorption and adsorption processes* John Wiley & Sons, NY, USA, pp. 336–375.

Day, S., Fry, R., Sakurovs, R., 2008. Swelling of Australian coals in supercritical CO_2. *International Journal of Coal Geology* 74, 41-52.

Day, S., Fry, R., Sakurovs, R., Weir, S., 2010. Swelling of Coals by Supercritical Gases and Its Relationship to Sorption. *Energ Fuel* 24, 2777-2783.

De Silva, P., 2013. A study of CO_2 storage capacity in sedimentary rocks (*PhD thesis*) Monash University, Melbourne, Australia.

Energy Information Administration, Washington, USA (2015), Annual Energy Outlook 2015 – with projections to 2040, [online] Available at: http://www.eia.gov/forecasts/aeo/pdf/0383(2015).pdf [Accessed 16 Sep. 2016].

Energy Information Administration, Washington, USA (2016). International Energy Outlook 2016-World energy demand and economic outlook - Energy Information Administration. [online]
Available at: https://www.eia.gov/outlooks/ieo/world.cfm [Accessed 16 Sep. 2016].

Every, R.L., Luino Dell'Osso, J., 1977. Method for removing methane from coal. U.S. Patent No. 4,043,395.

Gale, J., Freund, P., 2001. Coal-Bed Methane Enhancement with CO_2 Sequestration Worldwide Potential. Environmental Geosciences 8, 210-217.

Hernandez, G., Bello, R.O., McVay, D.A., Ayers, W.B., Rushing, J.A., Ruhl, S.K., Hoffmann, M.F., Ramazanova, R.I., 2006. Evaluation of the Technical and Economic Feasibility of CO_2 Sequestration and Enhanced Coalbed Methane Recovery in Texas Low-Rank Coals, Society of Petroleum Engineers (SPE) gas technology symposium, Calgary, Alberta, Canada, paper no 100584.

Hooper, B., Murray, L., Gibson-Poole, C., 2005. Latrobe Valley CO_2 Storage Assessment: Final Report. Cooperative Research Centre for Greenhouse Gas Technologies, Canberra CO2CRC Publication No. RPT05-0108.

International Energy Agency (IEA). Key World Energy Statistics, Paris. 2015, p. 5–9. (<https://www.iea.org/publications/freepublications/publication/KeyWorld_Statistics_2015.pdf>);

Garduno, J.L., Morand, H., Saugier, L., Ayers Jr, W., McVay, D.A., 2003. CO_2 sequestration potential of Texas low-rank coals Society of Petroleum Engineers (SPE) Annual Technical Conference and Exhibition, Denver, Colorado, 2003, paper no 84154.

Masoudian, M.S., 2016. Multiphysics of carbon dioxide sequestration in coalbeds: A review with a focus on geomechanical characteristics of coal. *Journal of Rock Mechanics and Geotechnical Engineering* 8, 93-112.

Masoudian, M.S., Airey, D.W., El-Zein, A., 2014. Experimental investigations on the effect of CO_2 on mechanics of coal. *International Journal of Coal Geology* 128–129, 12-23.

Perera, M.S.A., Ranjith, P.G., Choi, S.K., Airey, D., 2011a. The effects of sub-critical and super-critical carbon dioxide adsorption-induced coal matrix swelling on the permeability of naturally fractured black coal. *Energy* 36, 6442-6450.

Perera, M.S.A., Ranjith, P.G., Choi, S.K., Bouazza, A., Kodikara, J., Airey, D., 2011b. A review of coal properties pertinent to carbon dioxide sequestration in coal seams: with special reference to Victorian brown coals. *Environmental Earth Sciences* 64, 223-235.

Perera, M.S.A., Ranjith, P.G., Viete, D.R., 2013. Effects of gaseous and super-critical carbon dioxide saturation on the mechanical properties of bituminous coal from the Southern Sydney Basin. *Applied Energy* 110, 73-81.

Puri, R., Pendergraft, P.T., 1995. Method for producing methane-containing gaseous mixtures. US Patent 5,388,645.

Puri, R., Stein, M.H., 1989. Method of coalbed methane production. US Patent 4,883,122.

Puri, R., Yee, D., Buxton, T.S., Majahan, O., 1991. Method of increasing the permeability of a coal seam. U.S. Patent No. 5,014,788.

Metcalfe, R., Yee, D., Seidle, J., Puri, R., (1991). Review of research efforts in coalbed methane recovery, Society of Petroleum Engineers (SPE) Asia-Pacific Conference, Perth, Australia, pp. 727–740.

Perera, M.S.A., Ranjith, P.G., 2012. Carbon dioxide sequestration effects on coal's hydro-mechanical properties: a review. *Int J Energ Res* 36, 1015-1031.

Reeves, S., Oudinot, A., 2005. The Allison Unit CO_2-ECBM Pilot–A Reservoir and Economic Analysis, 2005 International Coalbed Methane Symposium, Paper, pp. 16-20.

Seidle, J.P., Yee, D., Puri, R., 1997. Method for recovering methane from a solid carbonaceous subterranean formation. *Journal of Cleaner Production* 5, 166-166.

Speight, J.G., 2012. *The Chemistry and Technology of coal*. Marcel Dekker, Inc., New York.

Stevens, S.H., Kuuskraa, V.A., Gale, J., Beecy, D., 2001. CO_2 injection and sequestration in depleted oil and gas fields and deep coal seams: worldwide potential and costs. *Environmental Geosciences* 8, 200-209.

Syed, A., Durucan, S., Shi, J.Q., Korre, A., 2013. Flue Gas Injection for CO_2 Storage and Enhanced Coalbed Methane Recovery: Mixed Gas Sorption and Swelling Characteristics of Coals. *Energy Procedia* 37, 6738-3745.

Viete, D.R., Ranjith, P.G., 2006. The effect of CO_2 on the geomechanical and permeability behaviour of brown coal: Implications for coal seam CO_2 sequestration. *International Journal of Coal Geology* 66, 204-216.

Vishal, V., Ranjith, P., Singh, T., 2015. An experimental investigation on behaviour of coal under fluid saturation, using acoustic emission. *Journal of Natural Gas Science and Engineering* 22, 428-436.

White, C.M., Smith, D.H., Jones, K.L., Goodman, A.L., Jikich, S.A., LaCount, R.B., DuBose, S.B., Ozdemir, E., Morsi, B.I., Schroeder, K.T., 2005. Sequestration of Carbon Dioxide in Coal with Enhanced Coalbed Methane Recovery: A Review. *Energ Fuel* 19, 659-724.

1.8 Chapter summary

This chapter provides a general overview of the research area addressed by this thesis. The importance of implementing CO_2-ECBM is highlighted at the beginning of this chapter and the importance of determining coal mass behaviour with the introduction of CO_2 into deep coal seams are then discussed. The statement of the research question is clearly defined, leading to the objectives of this research study. The main specific research aims are then presented with the scope of the research work. Finally, the structure of the thesis is presented. There are nine chapters in the thesis and the brief contents of each chapter are presented in this chapter.

PART 1 - CHAPTER 2

Literature Review

2. Literature Review

2.1 Overview

This chapter discusses the literature on the challenges and issues encountered while sequestrating CO_2 in deep coal seams for enhanced coal bed methane recovery (CO_2-ECBM).

First, the various methods of CO_2 storage and the advantages of CO_2-ECBM are discussed in detail. Next, the challenges in CO_2 sequestration in deep coal seams are identified and critically reviewed in different sections. The first is *Coal matrix swelling*, the most important and common challenge in storing CO_2 in the coal matrix which occurs due to the induction of a strain between the coal matrix and the adsorbing CO_2 layer. Coal matrix swelling leads to a re-arrangement in the coal mass physical structure that eventually affects the flow properties and the integrity of the coal mass. This is discussed in reviewing previous studies regarding the permeability and strength variations of the coal mass upon exposure to CO_2 with various effective factors, such as injecting gas properties (phase and pressure) and coal seam properties (coal rank, depth and temperature). Several field-scale CO_2-ECBM projects have been reported in the literature and these are summarised with their major outcomes. Considering the field-scale projects conducted to date, there has been a shortage of implementations, due to the complexities associated with the highly heterogeneous nature of coal, environmental and human health risks, current policies and regulations and public perceptions of CO_2 sequestration in deep coal seams and these are discussed next. Finally, the current issues associated with the implementation process are identified and recommendations are proposed.

A journal article and a book chapter have been produced based on Chapter 2 of the thesis and the details are given below.

Journal article:

Ranathunga AS, Perera MSA, Ranjith PG (2014). Deep coal seams as a greener energy source: a review. *Journal of Geophysics and Engineering*, 11,1-17.

Book chapter:

Ranathunga AS, Perera MSA, Ranjith PG. Challenges and issues for CO_2 storage in deep coal seams. *Rock Mechanics and Engineering*, Volume 5: Chapter 3, Taylor and Francis group, CRC press, Balkema, Netherlands. (In press)

2.2 Introduction

2.2.1 Greenhouse gas effects and global warming

Emissions of greenhouse gasses (GHGs) will increase the average global temperature by 1.1 to 6.4 ^{0}C by the end of the 21st century (Pachauri and Reisinger, 2007), and exceeding the current global average temperature by more than 2 ^{0}C will lead to serious consequences. Therefore, the International Panel on Climate Change (IPCC) has warned of the need for a 50-80% global GHG emissions reduction by 2050 (Pachauri and Reisinger, 2007).

Carbon dioxide (CO_2) is one of the most significant greenhouse gases, and the anthropogenic CO_2 content (the CO_2 generated due to human activities) in the atmosphere is critical. In particular, the burning of fossil fuels such as coal, oil and gas has caused a substantial increase in the concentration of CO_2 in the atmosphere (Borah et al., 2011; Pachauri and Reisinger, 2007; Perera and Ranjith, 2012; Ranathunga et al., 2014; Stangeland, 2007; White et al., 2005). According to Sundquist et al. (2008), this increase in atmospheric CO_2 concentration from around 280 to more than 380 ppm over the last 25 years has caused measurable global warming. The potential adverse impacts of global warming are sea-level rises, increased frequency and intensity of wildfires, floods, droughts, and tropical storms, changes in the amount, timing, and distribution of rain, snow, and run-off, and the disturbance of coastal marine and other ecosystems. Rising atmospheric CO_2 is also increasing the amount of CO_2 absorbed by seawater, causing the ocean to become more acidic, which potentially disruptively affects marine plankton and coral reefs (Sundquist et al., 2008).

At the 21st United Nations Framework Convention on Climate Change (UNFCCC), held in Marrakech and Paris in 2016, the participants, including Australia, agreed to commit to a maximum temperature rise of 2 ^{0}C above pre-industrial levels, and to consider lowering that maximum to 1.5 degrees in the near future (UNFCC, 2016). Therefore, it is imperative to investigate possible CO_2 mitigation options and to implement them as soon as possible.

Some possible CO_2 mitigation options are carbon dioxide capture and storage or sequestration (CCS), energy efficiency improvements, the switch to less carbon-intensive fuels, nuclear power, renewable energy sources, enhancement of biological sinks, and reduction of non-CO_2 greenhouse gas emissions (Stangeland, 2007; Sundquist et al., 2008; White et al., 2005). Of these methods, CCS has the potential to reduce overall mitigation costs and increase flexibility in achieving greenhouse gas emission reductions (Gale, 2004; Metz et al., 2005; Perera and Ranjith, 2012; White et al., 2005).

2.2.2 CO_2 storage

Before human-caused CO_2 emissions began the natural processes that make up the global "carbon cycle" (Figure 2.1), a near balance was maintained between the uptake of CO_2 and its release back to the atmosphere. However, existing CO_2 uptake mechanisms (sometimes called CO_2 or carbon "sinks") are insufficient to offset the accelerating pace of emissions related to human activities (Sundquist et al., 2008). According to Sundquist et al. (2008), annual carbon emissions from burning fossil fuels in the United States are about 1.6 Gigatons, whereas annual uptake amounts are only about 0.5 Gigatons, resulting in a net release of about 1.1 Gigatons per year. Hence, controlling atmospheric CO_2 will require deliberate mitigation with an approach that combines reducing emissions and increasing storage.

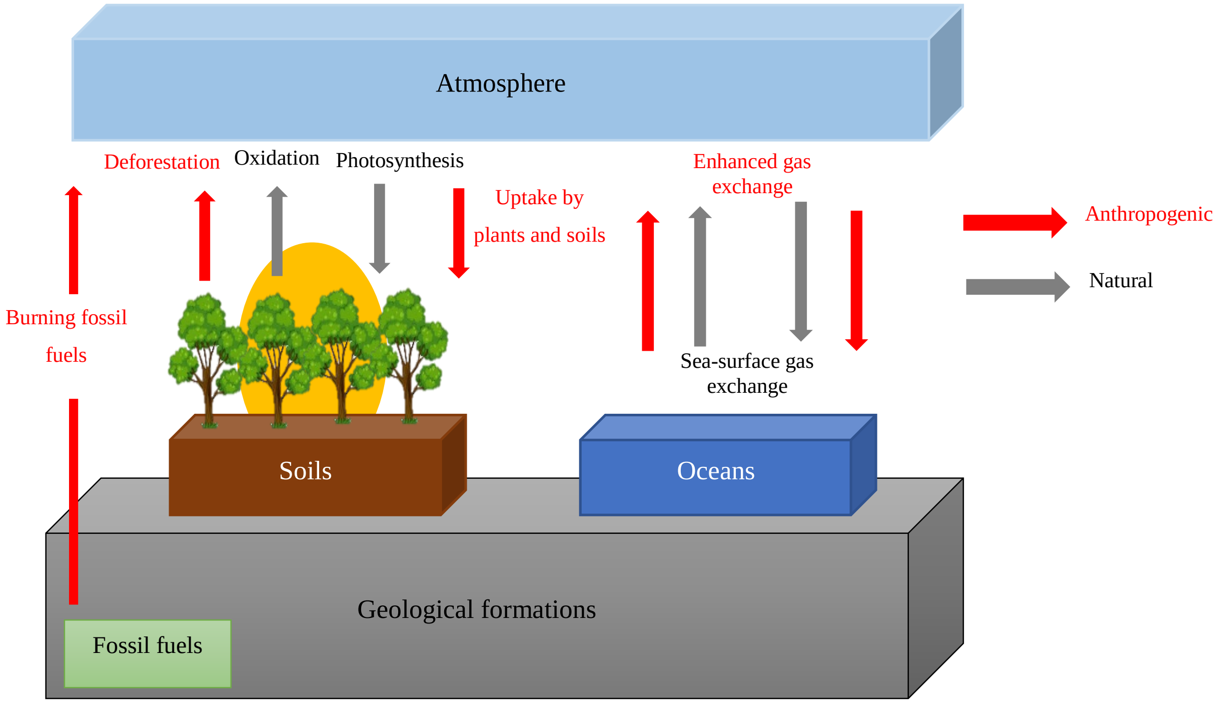

Figure 2.1. Global carbon cycle (created by author using data from Benson and Cole, 2008)

CCS basically means the removal of CO_2 directly from anthropogenic sources (capture) and its disposal in geological or oceanic media, either permanently (sequestration), or for geologically significant time periods (storage) (Benson and Cole, 2008). The term "carbon sequestration" is used to describe both natural and deliberate processes by which CO_2 is either removed from the atmosphere or diverted from emission sources and stored in the ocean, terrestrial environments (vegetation, soils, and sediments), and deep geological formations. With over 60% of worldwide emissions coming from point sources that are potentially amenable to CO_2 capture, the prospects for CCS to significantly reduce CO_2 emissions are great (Sundquist et al., 2008). Technical and economic assessments suggest that over the coming century, CCS may contribute up to 20% of CO_2 emission reductions, equivalent to the reductions expected from efficiency improvements and large-scale deployment of renewable energy resources (Benson and Cole, 2008; Metz et al., 2005). Therefore, CO_2 sequestration is a promising solution for the required outcomes of the UNFCCC.

To significantly reduce global emissions to pre-industrial levels, huge volumes of CO_2 must be sequestered. For example, a large coal-fired power plant emits about 8 million tons of CO_2 annually (Sundquist et al., 2008). At the pressures and temperatures expected for sequestration reservoirs, the volume required to sequester CO_2 as a super-critical fluid is about 10 million cubic meters (Mm^3) per year. According to existing studies (Bachu, 2003; Benson and Cole, 2008; Metz et al., 2005; Perera and Ranjith, 2012; White et al., 2005), there are various methods for sequestrating CO_2, mainly on-shore and off-shore.

2.2.2.1 Off-shore CO_2 sequestration

Injecting CO_2 into off-shore marine sediments is one potential approach to the sequestration of CO_2 (Figure 2.2), in which CO_2 is injected into off-shore sediments and stored deep beneath the ocean, avoiding the threats of direct ocean injection and effects on ocean ecology. There are several advantages in off-shore CO_2 sequestration compared to on-shore CO_2 sequestration. According to House et al. (2006), CO_2 is denser than seawater below 3000 m; therefore, off-shore reservoirs with suitable permeability in deep seawater make the cap rock less significant. Furthermore, marine sediments offer large storage potential. For example, the cretaceous sandstones of New Jersey have the capacity to store at least several hundred billion tons of CO_2, which is enough to dispose of all the CO_2 from power plants within 250 km of the coast near the reservoir for the next century (Schrag, 2009). Another advantage of off-shore CO_2 storage is the ability to manage pressure within the geologic formation by drilling additional wells to release pore fluid to the ocean, which avoids injected CO_2 back-migration to the atmosphere by the prevention of fractures (Archer and Brovkin, 2008). Moreover, the released pore fluid is similar to seawater, unlike the pore fluid released from on-shore CO_2 sequestration, and is more environmentally friendly (Vaughan and Lenton, 2011).

Although off-shore CO_2 sequestration acts as a large anthropogenic CO_2 storage pool, some researchers (Adams and Caldeira, 2008; Drange et al., 2001; Sabine and Tanhua, 2010) have found a number of challenges in this process. In relation to the lack of secure storage life, high operational and transportation costs (most off-shore sites are located far away from CO_2 trapping points) there are many environmental concerns, such as ocean acidification. Therefore, based on economic factors, the storage life and availability of sites, on-shore CO_2 sequestration has been identified as the most viable solution to the problem.

2.2.2.2 On-shore CO_2 sequestration

Another option to reduce anthropogenic CO_2 emissions to the atmosphere is to capture and store the CO_2 in porous rock media (sedimentary rocks) deep under the surface. Globally, the CO_2 storage capacity in saline aquifers is quite high, and recent estimates for the U.S. alone show a potential storage capacity of 2020 to 14,220 Gigatons of CO_2 ($GtCO_2$) (Orr, 2009). Depths below 800 to 1000 m, where the CO_2 density is high enough (500 to 700 kg/m^3) to limit the storage volume, are suitable for on-shore CO_2 sequestration. In this technique, the presence of low-permeability formations called cap rocks above the storage zone is crucial in order to prevent the back-migration of stored CO_2 into the atmosphere (Ranjith and Perera, 2012).

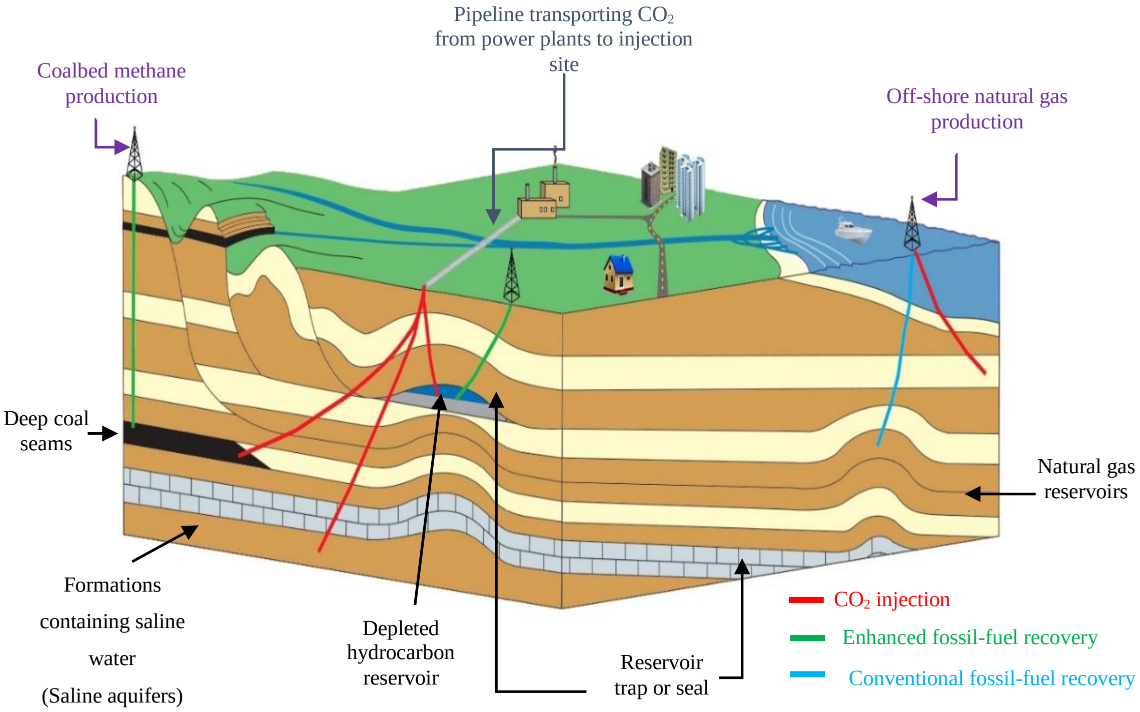

Figure 2.2. On-shore and off-shore CO_2 sequestration methods (created by author using data from Sundquist et al., 2008)

Oil and gas reservoirs are one potential choice for on-shore CO_2 sequestration (Figure 2.2). For example, for the purpose of enhanced oil recovery (EOR), around 30 megatons of CO_2 ($MtCO_2$) are injected into oil reservoirs in west Texas each year (Sundquist et al., 2008). The potential for fuel recovery to offset the sequestration cost and the already available underground and surface infrastructure (wells, equipment and pipelines) make this method attractive (Orr, 2009).

Injection of CO_2 into deep saline formations (Figure 2.2) is also being tested on a commercial scale. CO_2 is typically in its super-critical phase at sub-surface temperatures and pressures, which is denser than natural gas but less dense than brine or oil. The injected CO_2 interacts with the fluids and minerals present in the saline aquifers. CO_2 is relatively soluble in brine, and the resulting brine mixture is slightly denser than brine alone. Further, under typical sub-surface conditions, CO_2 is dissolved in brine at a proportion of 1:20 (CO_2: brine) by volume (Stevens et al., 2001). Once a larger volume of CO_2 is dissolved, the driving force for upward migration of CO_2 is eliminated, and the CO_2 is immobilized while it continues to dissolve slowly, which will continue for a time-scale of centuries (Bachu, 2000).

The Otway basin in Victoria, Australia is one such deep saline formation which is used as a pilot project site to demonstrate the geological storage of CO_2 by the Cooperative Research Centre for Greenhouse Gas Technologies (CO2CRC) (CO2CRC, 2016). This is the world's largest carbon capture and storage demonstration project with over 80,000 tonnes of CO_2 injected and stored in a variety of geological formations, and it has confirmed the safety and cost-effectiveness of CO_2 storage in saline aquifers (CO2CRC, 2016).

Deep un-mineable coal seams are also possible storage locations, with international coal bed methane resources of 3010–7840 trillion cubic feet (Orr, 2009). When CO_2 is injected into coal seams, it adsorbs into the coal matrix and then desorbs the methane (CH_4) developed during the coalification process, which migrates to the fractures and can be recovered. This process is known as enhanced coal bed methane (ECBM) recovery (Orr, 2009; Ranathunga et al., 2014; White et al., 2005). ECBM recovery is further discussed in the following sections.

2.2.3 CO_2 sequestration in deep coal seams

Coal is formed from the biodegradation of buried plants, and the process of forming coal from buried plants subjected to burial pressure and temperature is called the coalification process. Naturally-formed coal is composed of a solid matrix with well-defined networks of natural fracture systems called cleats, which form during the coalification process. Therefore, the more mature the coal mass, the more developed the cleat system. Depending on the degree of coalification, coal can be categorised into several ranks, mainly high rank (bituminous coal and anthracite – >80%) and low rank (lignite and sub-bituminous coal - <80%), and rank increases with increasing coal maturity. Coal is composed of carbon (50%-98%), hydrogen (3%-13%), oxygen and smaller amounts of other elements, and the composition is dependent on the coal rank (Table 2.1). For example, high rank coal has greater carbon content than low rank coal. Generally, coal can be separated into brown coal (lignite and sub-bituminous) and black coal (bituminous and anthracite), depending on the carbon content (Figure 2.3). According to Miedzińska et al. (2013), the characteristic surface morphology of a coal sample normally appears to be granular structure under the scanning electron microscopy (SEM). There are many slots and free spaces between the grains, with abundant storage of methane. Due to its chemical properties (atomic structure and carbon content), coal has a greater affinity to absorb CO_2 than other gases, such as methane (CH_4) and nitrogen (N_2). This provides the basis for the CO_2 sequestration process to be on-going (White et al., 2005).

Table 2.1. Chemical properties of different coal ranks (Durie, 2013)

Coal property / Coal rank	Carbon (*db %)	Volatile matter (*db %)	Moisture content (%)	Specific energy (*db kJ g^{-1})
Lignite	60-75	45-55	50-70	25-30
Sub-bituminous	75-80	40-45	25-30	28-32
Bituminous	80-90	20-40	5-10	30-35
Anthracite	90-95	5-7	2-5	35-38

Note: *db – dry basis

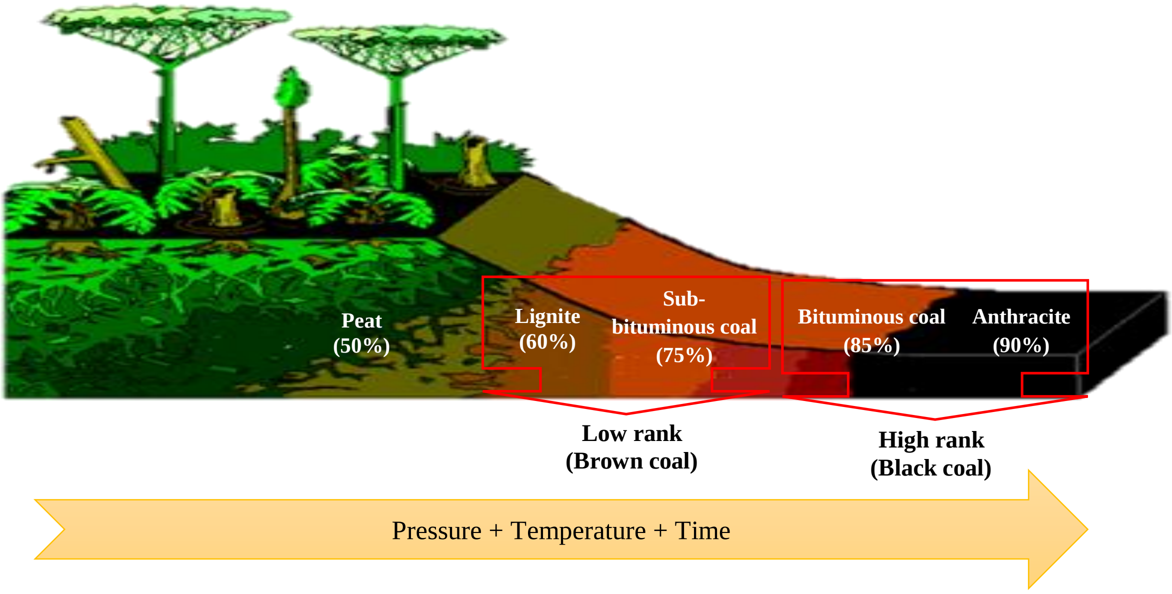

Figure 2.3. Coalification process of coal (created by the author using data from http://www.detectingdesign.com/fossilrecord.html)

2.2.4 How is CO_2 stored in deep coal seams?

According to Shi et al. (2014), gases are stored in coal beds by three mechanisms:

- physically adsorbed by compounds on the internal surfaces of coal
- adsorbed within the molecular structure; and
- within pores and natural structures.

Around 98% of CO_2 exists in an adsorbed phase on the walls of coal micro-pores, while the rest remains as free gas inside the cleats (Battistutta et al., 2010; Perera and Ranjith, 2012; Shi and Durucan, 2005; White et al., 2005). Therefore, CO_2 exists in a stable form in coal, which reduces the risk of back-migration (Shi and Durucan, 2005). Moreover, during the coalification process, a large amount of methane (CH_4) is formed. When CO_2 is injected into a coal seam, it improves the recovery of CH_4 by directly displacing the methane from the coal, or by lowering the effective partial pressure of the CH_4 (Harpalani and Schraufnagel, 1990). This phenomenon is known as enhanced coal bed methane (ECBM) recovery, which may eventually offset the cost of sequestration of CO_2. Figure 2.4 illustrates a schematic diagram of the ECBM process.

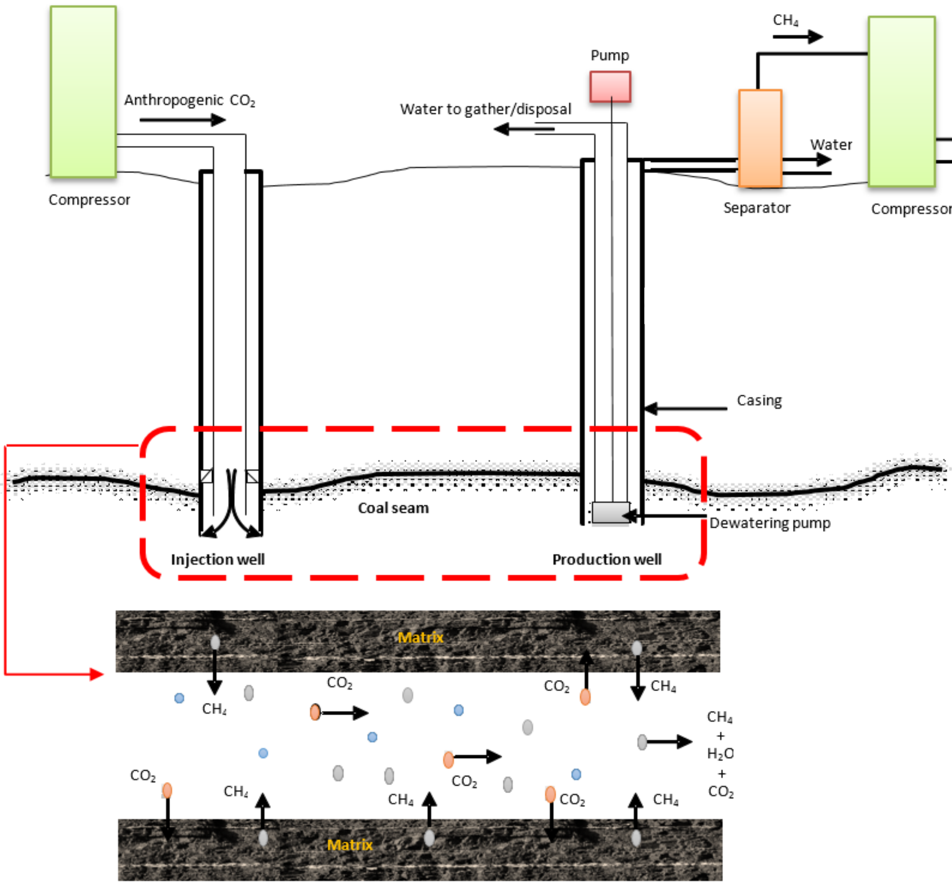

Figure 2.4. Enhanced coal-bed methane recovery process

Since coal has a larger surface area associated with the micro-pore structure compared with the conventional reservoirs of a given volume of rock, it can store a substantial amount of CO_2 within the pore spaces (Stevens et al., 2001). For example, the combined Bowen and Sidney basins in eastern Australia can store about 11.2 gigatons of CO_2 (Stevens et al., 2001). According to Harpalani and Schraufnagel (1990), 5-15 gigatons of CO_2 in the world can be sequestered in coal beds by the profits gained from CH_4 production through the ECBM recovery process. These details demonstrate the prospective importance of CO_2 sequestration in deep un-minable coal seams.

2.2.5 What happens when CO_2 is injected into coal seams?

As stated above, in coal beds, most gases exist in an adsorbed phase in the coal matrix and some as free gas in the fracture pore space. Generally, the coal mass natural cleat system formed during the coalification process governs gas movement through the coal matrix, unless a large joint exists (White et al., 2005). In the gas transport process in coal, first it moves through its natural cleat system and then adsorbs into the coal matrix along the cleat walls (White et al., 2005) (Figure 2.5). When the gas molecules reach the micro-pores in the coal matrix, they follow the diffusion process (Figure 2.5), as the mean flow path of the gas molecules is greater than the micro-pore diameter. In contrast, when the gas molecules reach the cleats, flow is controlled by the coal mass permeability (Darcy flow), as the mean flow path of the gas molecules is smaller than the cleat width. However, the diffusion process is quite a slow process, and it therefore takes much longer than the pressure-driven advection process in cleats.

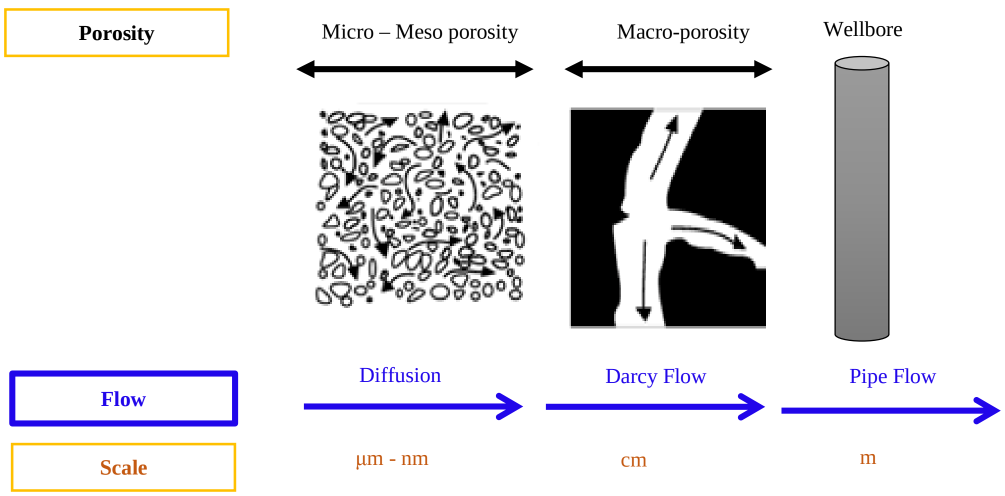

Figure 2.5. Gas transport process in coal (Bromhal et al., 2005)

According to existing research, both CO_2 storage and ECBM recovery are dependent on the coal mass and adsorbing gas properties, such as coal rank, moisture content, temperature, depth, existing gas composition and adsorbing gas pressure, gas type and phase, and injection and production well operations (Gilman and Beckie, 2000; Sawyer et al., 1990). Laboratory isotherm measurements demonstrate that medium- to high-rank coal can adsorb approximately twice as much CO_2 by volume as CH_4, and the common assumption is that, for higher rank coals, the ECBM process stores 2 moles of CO_2 for every mole of CH_4 desorbed (White et al., 2005). However, some researchers have determined that some low-rank coals may adsorb as much as 10 moles of CO_2 for every mole of CH_4 (Ranathunga et al., 2014). Vishal et al. (2013a) investigated the feasibility of CO_2 driven ECBM recovery in Indian coals (coal type - black coal) using a field-scale numerical model. These researchers found that approximately three times the volume of CO_2

can be sequestered in place of every volume of CH_4 for high-rank coals. Field applications and laboratory experiments have shown that this ratio may be even higher at depths greater than 800 m, where gaseous CO_2 changes to super-critical CO_2 (White et al., 2005) .

However, according to Viete and Ranjith (2006), the injection of CO_2 into coal causes its chemical and physical properties to be greatly changed, resulting in unpredictable amounts of injectable CO_2 and producible CH_4 in coal seams. There has been much research conducted on this process, which has revealed that a great degree of swelling is caused by CO_2 adsorption into the coal matrix that, in turn, can cause the permeability and the overall strength of the coal mass to be severely decreased (Fujioka et al., 2010; Jasinge, 2010; Wang et al., 2011).

2.3 Coal matrix swelling

Coal matrix swelling occurs due to the lowering of the surface energy of the coal with gas adsorption. The decreased surface energy has the effect of lessening the strength of the chemical bonding in the atomic structure of the matrix, resulting in a volumetric expansion (up to around 30% in confined environments), or swelling of the coal, leading to a highly non-covalently associated state (Larsen, 1997). As stated by Gibbs (1878), the surface energy of the coal mass can be given by Eq. [2.1]:

$$\Delta\gamma = -\frac{RT}{MS}\int_0^P x\, d(\ln P) \qquad [2.1]$$

where, $\Delta\gamma$ is change in surface energy, R is universal gas constant, T is temperature, M is molecular weight of CO_2, S is surface area of coal, x is the amount of adsorption (g [adsorbent]/g [coal]) and P is the CO_2 pressure. According to Eq. [2.1], because of the greater adsorption capacity of CO_2 (x) compared to CH_4 and N_2, the coal mass loses more surface energy and tends to swell significantly during CO_2 injection (Viete & Ranjith, 2006). According to Day et al. (2010), the amount of swelling in coal is directly related to the absolute adsorption capacity (Eq. [2.2]):

$$V_s = -0.0037 + 0.1596V_{abs} + 0.0101V_{abs}^2 \qquad [2.2]$$

where, V_s is the volumetric swelling percentage and V_{abs} is the volume of absolute adsorption. Meanwhile, there is a direct relationship between amount of matrix shrinkage and desorbed gas volume at the standard pressure (Harpalani and Chen, 1995) (Eqs. [2.3] and [2.4]).

$$\varepsilon_v = C\left(\frac{V_L p}{P_L+p}\right) \qquad [2.3]$$

$$V_{des} = \left(\frac{V_L p}{P_L+p}\right) \qquad [2.4]$$

where, ε_v is the volumetric strain of the coal matrix, C is a constant depending on the coal mass properties, p is the pore pressure, $V_{des}$is the volume of gas desorbed from the coal matrix, and P_L and V_L are Langmuir pressure and volume, respectively.

It should be noted that swelling does not occur isotopically throughout the coal structure, but rather occurs more readily in the organic regions (macerals), which causes compression of the inorganic regions (minerals) of the matrix (Day et al., 2010). This is due to the strength of the bonding within the minerals being much greater than that between the organic molecules within the coal matrix. According to Anggara et al. (2013, 2014) and Day et al. (2011), the degree of swelling is dependent on the moisture content (Figure 2.6), whereas the megascopic texture controls the swelling behaviour with respect to bedding orientation. It has been noted that the degree of swelling is greater in the direction perpendicular to the bedding plane of the coal matrix than parallel to the plane (Karacan, 2007) (Figure 2.7). This is caused by the heterogeneity of swelling between the organic and inorganic components within the coal matrix. As a result of this, and the inherent weaknesses found along bedding planes, it has been shown that cracks more readily develop along the face cleats, as opposed to across the bedding planes along the butt cleats (Anggara et al., 2014). As mentioned previously, swelling of the coal matrix breaks the natural balance of the structure, with direct influences on permeability and strength reduction, which are the key factors in the CO_2 sequestration process.

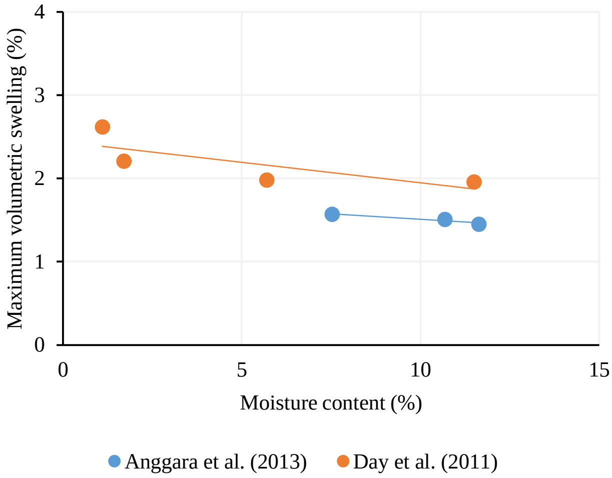

Figure 2.6. Variation of maximum volumetric swelling at different moisture contents (Anggara et al., 2013; Day et al., 2011)

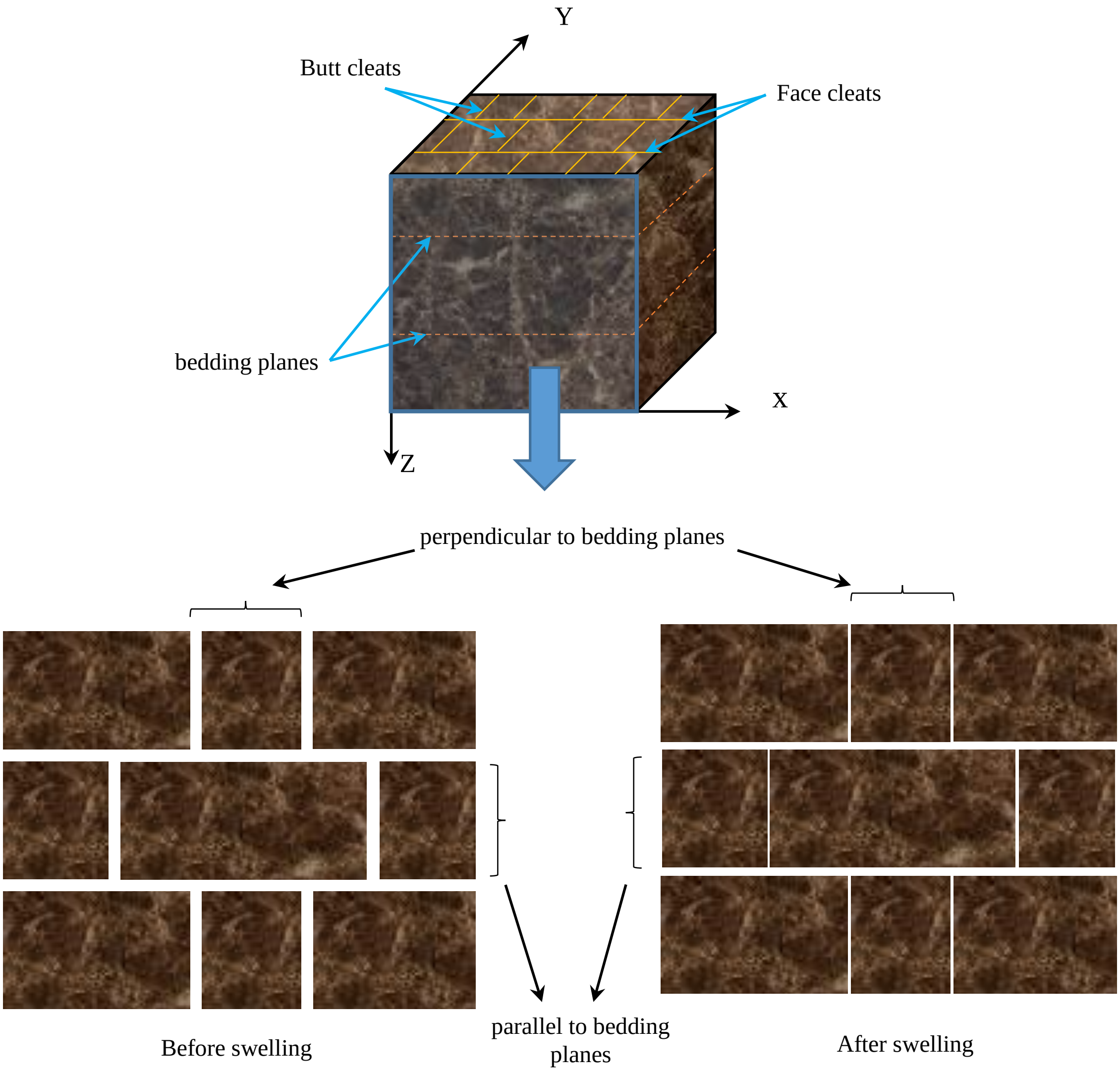

Figure 2.7. Heterogeneity of coal matrix swelling

2.3.1 Effective factors for CO_2 injection-induced coal matrix swelling

According to previous studies (Czapliński & Hołda, 1982; Day et al., 2010; Deevi & Suuberg, 1987; Jasinge et al., 2011; Majewska & Ziętek, 2007; Shi & Durucan, 2005), seam properties (coal rank and temperature) and injecting CO_2 properties (injecting CO_2 phase and pressure) are some effective factors for coal matrix swelling. These are therefore discussed in the following sections.

2.3.1.1 Seam properties

a) Coal rank

In general, the deeper the coal seam, the higher the rank, and this explains the effect of coal seam location on the CO_2 sequestration process. However, some contradictions can be seen in the research findings on the effect of coal rank on its swelling. For example, Reucroft & Sethuraman (1987) found that there is an inverse correlation between coal rank and matrix swelling; high- rank coal undergoes less swelling than lower-ranking coal under the same environmental conditions.

These results have been confirmed by Ceglarska-Stefańska & Czapliński (1993) (Figure 2.8(a)). This is thought to be due to the less mobile polymers present in high-ranking coal in contrast to low-ranking coal. This has the effect of preventing such a great deal of swelling at the molecular level, which transfers to less swelling at the macromolecular level (Ceglarska-Stefańska & Czapliński, 1993). However, Walker et al. (1988) observed the increment only for lignite to highly volatile bituminous coals, and any further increase of rank causes the swelling effect to be reduced with increasing rank in the anthracite region (Figure 2.8(a)).

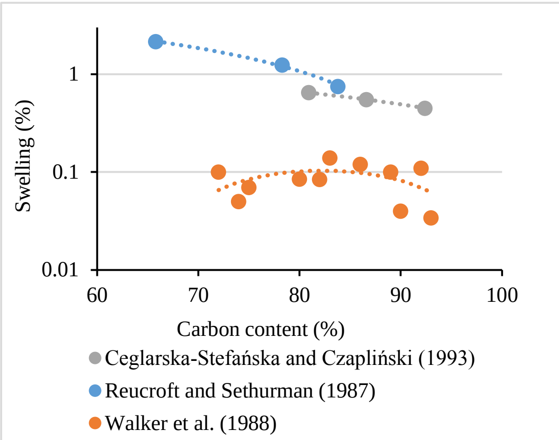

(a) Effect of coal rank

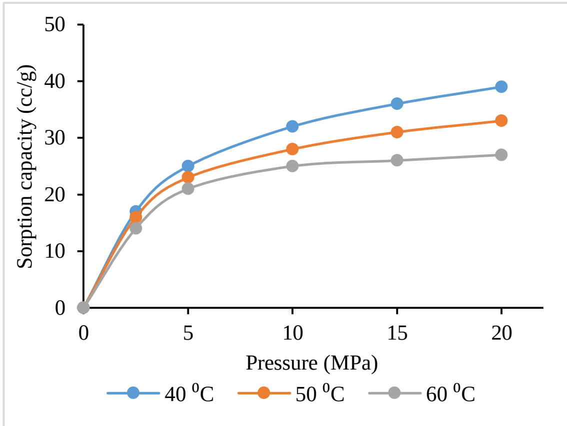

(b) Effect of temperature (Bae & Bhatia, 2006)

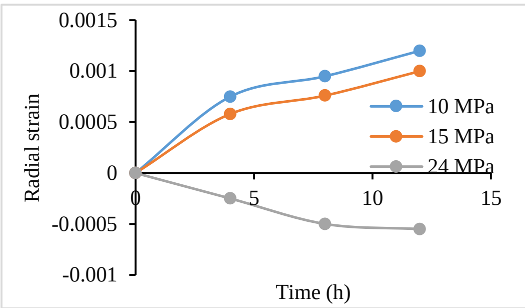

(i) For bituminous coal (Perera et al. (2011)

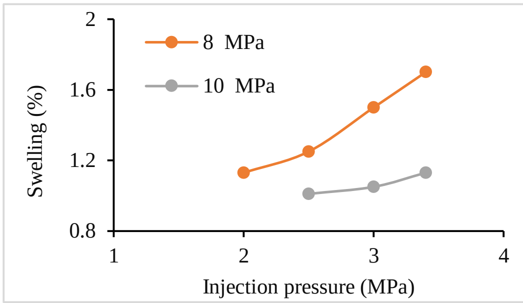

(ii) For brown coal (Jasinge et al. (2012)

(c) Effect of depth

Figure 2.8. Effect of seam properties on swelling

b) Temperature

With increased temperature, gas adsorption capacity is reduced (Ceglarska-Stefańska & Czapliński, 1993), because with the temperature increment, gas molecules are released from the adsorbed phase as their kinetic energy is accordingly increased. According to Perera & Ranjith (2012), Bae & Bhatia (2006) and Kronimus et al. (2008), super-critical CO_2 is more significantly subjected to the temperature effect than sub-critical CO_2 (Figure 2.8(b)). As discussed in the previous section, sorption capacity is directly proportional to the coal matrix swelling. Hence, similar behaviour can be suggested for the temperature effect on swelling (Perera & Ranjith, 2012).

According to the geothermal gradients, underground temperature proportionally increases with depth. Therefore, according to both of these influences (rank and temperature), the CO_2 sequestration-created swelling effect is clearly dependent on the location of the coal seam.

c) Depth (in situ stresses)

When the depth is increased, CO_2 permeability in coal seams is reduced, since the pore space available for gas movement shrinks considerably at greater depths, due to the higher confinement, resulting in higher tortuosity and consequently lower flow rate through the coal mass. This reduction of coal permeability for CO_2 causes less CO_2 adsorption into the coal matrix, resulting in less matrix swelling. This observation is irrelevant to coal rank, according to the studies by Jasinge et al. (2012) for brown coal (Figure 2.8(c)-(i)) and Perera et al. (2011b) (Figure 2.8 (c)-(ii)), for bituminous coal. These studies reported similar observations of less coal matrix swelling at higher confinements.

2.3.1.2 Injecting CO_2 properties

Beyond 7.38 MPa pressure and 31.8^{0}C temperature, CO_2 exists in its super-critical condition (Figure 2.9) (Perera et al. 2011a; Vishal et al. 2013b). It is known that the preferred coal seams for the ECBM production process are normally present beyond 1000 m from the ground surface, where the pressure and temperature are higher than the critical value of CO_2 (7.38 MPa and 31.8^{0}C), and CO_2 is therefore present in the super-critical state (Figure 2.9). Perera et al. (2011b) conducted a series of tri-axial experiments under sub-critical and super-critical CO_2 adsorption to investigate the CO_2 phase and pressure effect on coal swelling. They measured the radial strain increment in the coal samples during 15 hours of sub-critical and super-critical CO_2 adsorption, maintaining the system temperature above the critical temperature of CO_2 (31.8^{0}C) (Figure 2.10(a)). According to their results, both sub-critical (up to around 0.0015 radial strain) and super-critical CO_2 (up to around 0.0045 radial strain) adsorptions induce considerable swelling in coal, and the swelling created by super-critical CO_2 adsorption is more than three times greater than sub-critical CO_2 adsorption-induced swelling (Figure 2.10(a)). This is probably due to the highly chemically reactive nature of super-critical CO_2 compared to sub-critical CO_2. This implies that un-mineable coal seams are more vulnerable to the swelling effect. The effect of CO_2 pressure on coal swelling has also been studied by Day et al. (2010), Harpalani & Chen (1995) and Pan & Connell (2006), who have confirmed the increment of swelling with CO_2 pressure (Figure 2.10(b)). In addition, Day et al. (2010) (Figure 2.10(b)) and Pan & Connell (2006) (Figure 2.10(b)) described the behaviour at high pressures, where the swelling ratio may decrease after reaching a maximum swelling. Therefore, it is clear that not only gas injection pressure but also the adsorbing gas phase condition have a significant effect on coal matrix swelling.

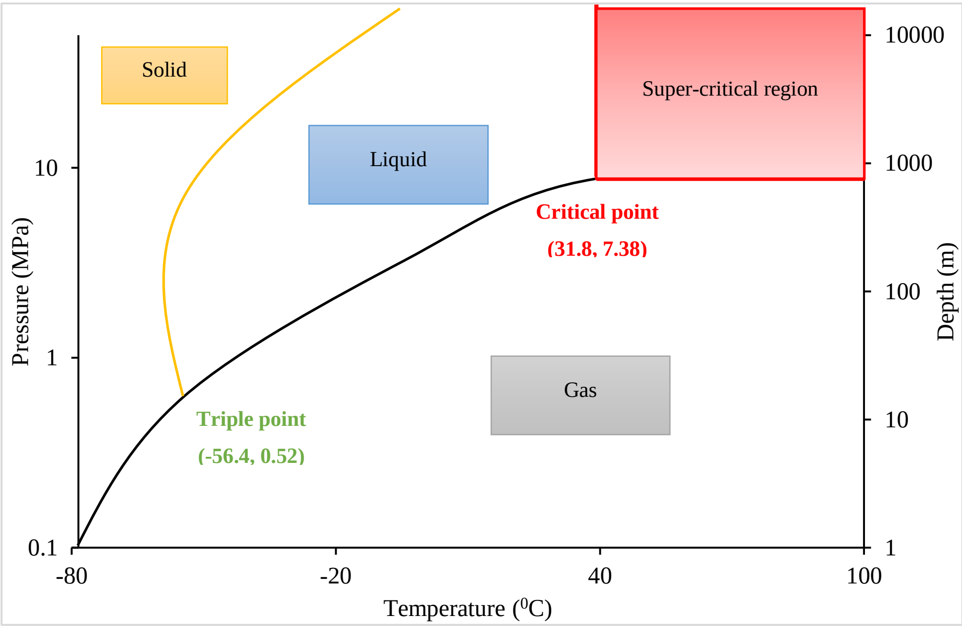

Figure 2.9. CO_2 phase diagram (Oldenburg, 2006)

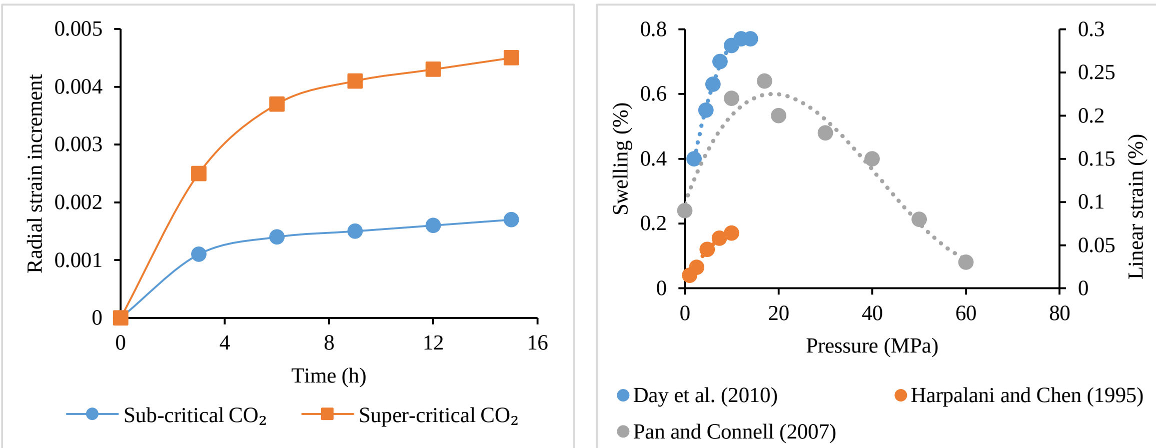

a) Radial strain increments during a 15 h swelling period

(b) Effect of CO_2 pressure

Figure 2.10. Coal swelling with CO_2 injection (Day et al., 2010; Harpalani & Chen, 1995; Pan & Connell, 2006; Perera et al., 2011(b))

2.4 CO_2 sequestration effect on deep coal-seam flow characteristics

Expansion of the coal matrix with swelling induced by CO_2 adsorption leads to the closure of cleats and fractures, as well as the reduction of the pore space available for gas movement, which eventually results in reduction of permeability. As the reduction of permeability directly obstructs the injection of CO_2, it is necessary to have a comprehensive understanding of the process, to enable better control of CO_2 injection.

2.4.1 Does CO_2 sequestration create unpredictable CO_2 injectivity?

Permeability is a term that provides a quantitative picture of the flow ability through any media. According to previous studies (Perera et al., 2011a; Perera & Ranjith 2012; White et al., 2005), the permeability of natural coal seams varies with coal mass properties such as coal rank (carbon content and cleat structure), temperature and confining pressure, and injecting gas properties, such as phase and pressure.

Importantly, CO_2 injection into a deep coal seam causes its permeability to be altered, mainly due to CO_2 adsorption-induced coal matrix swelling. Existing research studies clearly show the significant swelling created by CO_2 injection into deep coal seams and the corresponding reduction of coal mass pore spaces and eventually permeability (Viete & Ranjith, 2006; Perera et al., 2011b; Vishal et al., 2013b). According to Perera et al. (2011a), this permeability reduction (up to around 80%) increases with increasing CO_2 injection pressure and CO_2 phase transition from sub- to super-critical (Table 2.2). Moreover, as shown in Table 2.2, the temperature of the coal seam has a significant influence on the coal permeability alterations which occur with CO_2 injection, and CO_2 permeability in coal increases with increasing temperature only at higher CO_2 injection pressures (>10MPa). This is basically due to the fact that, with increasing temperature, the sorption capacity of and the swelling effect in coal are reduced, due to the increased kinetic movement of the CO_2 molecules (Bae and Bhatia 2006), resulting in increased coal permeability at higher temperatures. This indicates the importance of selecting a coal seam with appropriate physical properties to achieve effective CO_2 sequestration in coal.

In relation to the CO_2 sequestration process, Durucan & Shi (2009) found some permeability reduction in deep coal seams due to methane adsorption. They also found that this permeability reduction with methane adsorption is partially recovered when permeability enhancement occurs with methane desorption (coal matrix shrinkage) during the CO_2 sequestration process. However, CO_2 creates much higher swelling effects in coal compared to methane or many other types of gas, and the effect is greater than the coal mass shrinkage effect during CH_4 desorption (Ranathunga et al. 2014). Therefore, the CO_2 sequestration process causes coal seam permeability to be significantly reduced over time. Therefore, the CO_2 sequestration process will require permeability enhancement treatments over time.

Table 2.2. Effect of CO_2 injection on coal seam permeability during CO_2 sequestration

<table>
<tr><th>Effective factor</th><th>Key observation</th></tr>
<tr><td>Coal rank</td><td>- The CO_2 adsorption capacity is greater for high rank coal compared to low rank coal, which leads to greater matrix swelling for higher rank coal and relatively lower permeability compared to low rank coal (Saghafi et al., 2007).
- High-rank coal has a greater surface area compared to low rank coal due to its cleat structure developed during the coalification process, which leads to greater adsorption capacity.
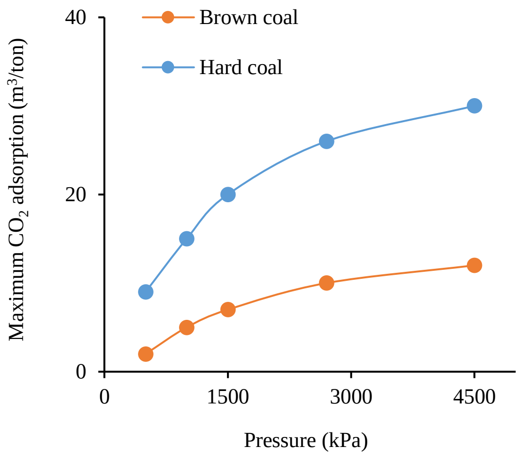

Variation of gas adsorption capacity in coal with pressure (Saghafi et al., 2007)</td></tr>
<tr><td>Temperature</td><td>- A significant increase in coal permeability can be observed with increasing temperature for higher CO_2 injection pressures (>10MPa), and an insignificant effect on permeability at low CO_2 injection pressures (<9 MPa) (Perera & Ranjith, 2012)
- Kinetic energy of gas molecules increases with increasing temperature. By the time the kinetic energy exceeds the intermolecular forces, the molecules tend to be released with random motion, which reduces the gas adsorption capacity in coal (Clarkson & Bustin, 1997).
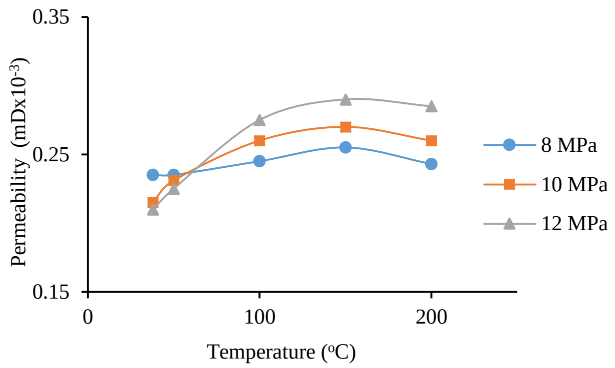

Temperature effects on CO_2 permeability at 20 MPa confinement (Perera & Ranjith, 2012)</td></tr>
<tr><td>Confining pressure</td><td>- Under the same experimental conditions, higher confining pressure induces lower permeability (Day et al., 2010; Perera et al., 2011a)
- The compressive force created by higher confinements at greater depths causes the pore space available for gas movement to shrink considerably, resulting in higher tortuosity and consequently lower flow rate through the coal mass (Perera et al., 2011a).</td></tr>
</table>

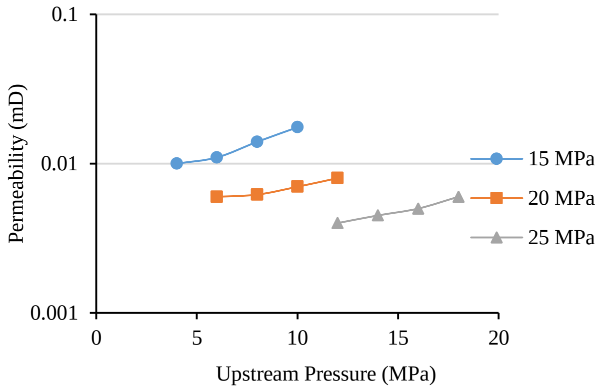

Permeability for CO_2 movement with confining pressure (Perera et al., 2011a)

CO_2 phase and pressure

- Permeability reduction increases with increasing CO_2 injection pressure and CO_2 phase transition from sub- to super-critical (Perera et al., 2011a; Shi & Durucan, 2005). CO_2 tends to change from sub-critical to super-critical in deep coal seams with high temperature and pressure (approximately 7.38 MPa and 31.8^{0}C) (Figure 2.9)
- A drastic increment in coal adsorption is observed after 7.38 MPa up to around 9 MPa, with an indication of CO_2 adsorption increase in super-critical state.
- The transformation of sub-critical to super-critical phase leads to different thermo-physical and transport properties, which may also influence the sorption capacity (Wang et al., 2011). The greater swelling effect, as well as the higher increment in its viscosity, contribute to the great decline in permeability (Jasinge et al. 2010)

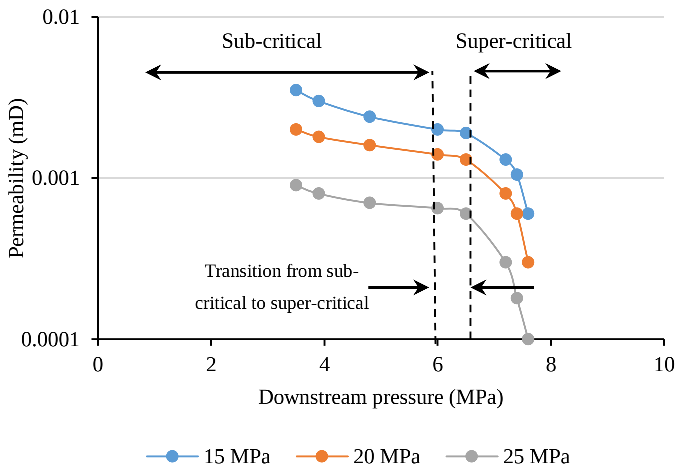

Permeability for CO_2 movement with injection pressure (Perera et al., 2011a)

2.4.2 Permeability models to predict coal permeability during CO_2 flow

A number of permeability models have been developed considering both the geomechanical effect and sorption-induced coal swelling. A brief review of the permeability models is presented in Table 2.3.

Table 2.3. A summary of permeability models

Reference	Model	Nomenclature
Gray (1987)	$\sigma_h^e - \sigma_{ho}^e = -\frac{\vartheta}{1-\vartheta}(p - p_o) + \frac{E}{(1-\vartheta)}\frac{\Delta\varepsilon_s}{\Delta p_s}\Delta p_s$ $k = k_i exp\{-3c_f[(\sigma_h^e - \sigma_{ho}^e) - (p - p_o)]\}$	σ_h^e – effective horizontal stress Δp_s – change in equivalent sorption pressures $\frac{\Delta\varepsilon_s}{\Delta p_s}$ – strain caused by unit change by sorption pressure ϑ – Poisson's ratio k – permeability k_0 – initial permeability c_f – cleat compressibility
Sawyer et al. (1990)	$\varphi = \varphi_i[1 + c_P(P - P_i)] - c_m(1 - \varphi_i)\left(\frac{\Delta P_i}{\Delta C_i}\right)(C - C_i)$ $\frac{k}{k_i} = \left(\frac{\varphi}{\varphi_i}\right)^n$	c_p - pore volume compressibility c_m - matrix shrinkage compressibility φ - coal mass porosity φ_i - initial coal mass porosity P - reservoir pressure P_i - initial reservoir pressure C - reservoir concentration C_i - initial reservoir concentration n – exponent of pressure dependent permeability
Pekot and Reeves (2002)	$\varphi = \varphi_i[1 + c_P(P - P_i)] - c_m(1 - \varphi_i)\left(\frac{\Delta P_i}{\Delta C_i}\right)[(C - C_i) + c_k(C_t - C)]$ $\frac{k}{k_i} = \left(\frac{\varphi}{\varphi_i}\right)^n$	c_k – the differential swelling coefficient C_t – total reservoir gas content
Seidle and Huitt (1995)	$\varphi = \varphi_i + \varphi_i\left[1 + \frac{2}{\varphi_i}\right]\varepsilon_l\left[\frac{Bp_i}{1 + Bp_i} - \frac{Bp}{1 + Bp}\right]$ $\frac{k}{k_i} = \left(\frac{\varphi}{\varphi_i}\right)^n$	ε_l – Langmuir volume B – A Langmuir constant p – pressure p_i – initial pressure
Harpalani and Chen (1995) and Ma (2011)	$\frac{k_{new}}{k_{old}} = \frac{\left(1 + \frac{2l_m^*\Delta p}{\varphi_i}\right)^3}{1 - l_m^*\Delta p}$ $l_m^*\Delta p = -1 + \sqrt{1 + \varepsilon_l\left[\frac{Bp_i}{1 + Bp_i} - \frac{Bp}{1 + Bp}\right] + \frac{1+\vartheta}{E}(P - P_i)}$	k_{new} – permeability at pressure p k_{old} – original reservoir permeability l_m^* - change in the dimension of the coal matrix block in horizontal direction with pressure E – Young's modulus
Levine (1996)	$\frac{b_{new}}{a} = \frac{b_{old}}{a} + \frac{1-2\vartheta}{E}(P - P_i) + \frac{\varepsilon_l p_{50}}{(p_{50} + p)^2}(P - P_i)$ $k = \frac{(1.013 \times 10^9)b_{new}^3}{12a}$	b_{new} – new cleat width a – cleat spacing b_{old} – initial cleat width p_{50} – Langmuir parameter for the swelling/shrinkage strain b/a – cleat porosity
Palmer and Mansoori (1996)	$\varphi = \varphi_i[1 + c_m(P - P_i)] + c_l\left[\frac{K}{M} - 1\right]\left[\frac{Bp}{1 + Bp} - \frac{Bp_i}{1 + Bp_i}\right]$ $c_m = \frac{g}{M} - \left[\frac{K}{M} + f - 1\right]c_r$ $\frac{k}{k_i} = \left(\frac{\varphi}{\varphi_i}\right)^n$ $M = \frac{E(1-\vartheta)}{(1+\vartheta)(1-2\vartheta)}, K = \frac{E}{3(1-2\vartheta)}$	c_l and B – Langmuir model parameters K – bulk modulus M – constrained axial modulus f – fraction from 0 to 1 c_r – grain compressibility g - a geometric term related to the orientation of the natural cleat system

Gilman and Beckie (2000)	$\Delta\sigma_x^e = \frac{\vartheta}{1-\vartheta}\Delta p + \frac{E}{1-\vartheta}\alpha_s \Delta S$ $\frac{k}{k_0} = exp\left(-\frac{3\Delta\sigma_x^e}{E_F}\right)$	E_F - Analogous to Young's modulus but for the fracture ΔS – change of the adsorbate mass α_s - volumetric welling/shrinkage coefficient
Shi and Durucan (2005)	$\sigma_h^e - \sigma_{ho}^e = -\frac{\vartheta}{1-\vartheta}(p-p_i) + \frac{E\varepsilon_s}{3(1-\vartheta)}$ $k = k_i exp\{-3c_f[(\sigma_h^e - \sigma_{ho}^e) - (p - p_o)]\}$	c_f - cleat compressibility ε_s – swelling strain
Cui and Bustin, (2005), Cui et al., (2007) and Jaeger et al. (2007)	$\varphi = \varphi_i + \frac{(1-2\vartheta)(1+\vartheta)}{E(1-\vartheta)}(p-p_i) - \frac{2(1-2\vartheta)}{3(1-\vartheta)}(\varepsilon_s - \varepsilon_{so})$ $\frac{k}{k_i} = \left(\frac{\varphi}{\varphi_i}\right)^n$	$\sigma - \sigma_0$ – change in mean stress
Robertson 2006	$\frac{k}{k_0} = exp\left\{3\left[c_f(p-p_i) + \frac{2}{\varphi_i}\left[\frac{1-2\vartheta}{E}(P-P_i) - \frac{\varepsilon_{max}P_L}{(P_L+P_0)}ln\left(\frac{P_L+P}{P_L+P_0}\right)\right]\right]\right\}$ $c_f = \frac{c_i}{\alpha(\sigma-\sigma_0)}\left[1-e^{-\alpha(\sigma-\sigma_0)}\right]$	ε_{max} and P_L – Langmuir parameters α – rate of decline of cleat compressibility
Liu and Rutqvist (2010)	$\frac{k_f}{k_{f0}} = \left[1 + \frac{(1-R_m)}{\varphi_{f0}}(\Delta\varepsilon_v - \Delta\varepsilon_s)\right]^3$	$\Delta\varepsilon_v$ – volumetric strain R_m – modulus reduction ratio (rock mass modulus/rock matrix modulus) Subscript *f* - fracture Subscript *c* - initial conditions
Connell et al. (2010a)	$k = k_0 exp\left\{3\left[C_{pc}^M\left(\frac{1}{3}(2\bar{p}_r + \bar{p}_z) - \bar{p}_p\right) - (1-\gamma)\bar{\varepsilon}_s\right]\right\}$	C_{pc}^M- cleat compressibility $\bar{p}_r$- radial confining pressure $\bar{p}_z$- axial confining pressure $\bar{\varepsilon}_s$ – sorption induced bulk modulus strain

2.5 CO_2 Sequestration Effect on Deep Coal Seam Mechanical Properties

Not only CO_2 injectivity into coal seams, but also the overall strength of these seams is altered by CO_2 injection, which is a greater threat in terms of long-term safety of the CO_2 storage process in deep coal seams, as it may cause the back-migration of injected CO_2 into the atmosphere. Therefore, it is of great importance to have a comprehensive understanding of the effect of CO_2 sequestration to achieve better control of coal mass integrity during and after CO_2 sequestration.

As proposed by Gibbs (1878) and Griffith (1921), material strength depends on the chemical potential of the adsorbate, and replacement of the existing adsorbate with one more chemically potent causes it to be weakened. CO_2 is clearly a more chemically potent gas than pre-adsorbed methane in coal seams (Gibbs, 1878; Griffith, 1921). This implies that the replacement of the CH_4 with CO_2 injection causes the coal seam strength to be reduced. The natural coal mass structure is a glassy, strained and cross-linked macro-molecular structure with high energy, which limits the freedom of coal molecules to move, resulting in a highly brittle structure (Larsen et al., 1997; Majewska & Ziętek, 2007; Goodman et al., 2005). When CO_2 is adsorbed, the coal mass polymer structure is rearranged (Figure 2.11) with the increment of free volume in the coal matrix and the ductile properties of the coal structure are enhanced, affecting the elastic modulus of the coal (Perera & Ranjith, 2012).

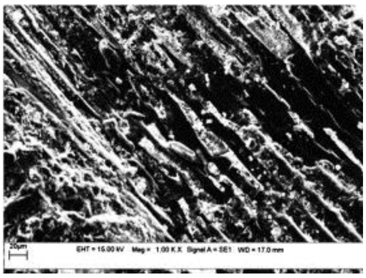

(a) Natural coal under 1k magnification

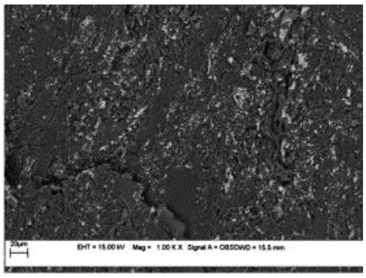

(b) CO_2 adsorbed coal under 1k magnification

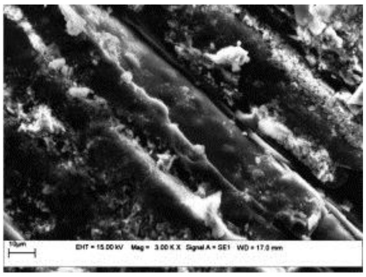

(c) Natural coal under 3k magnification

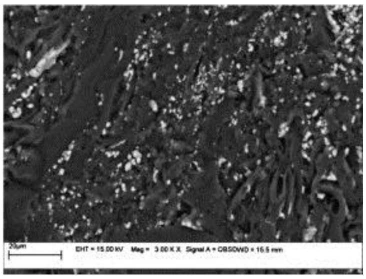

(d) CO_2 adsorbed coal under 3k magnification

Figure 2.11. Scanning Electron Microscopy (SEM) images of coal before and after CO_2 adsorption (Masoudian et al., 2014)

The reduction of coal strength with CO_2 injection into it is well known, and this strength reduction varies with seam location and injecting CO_2 properties (Aziz & Ming-Li, 1999; Czapliński & Hołda, 1982; Day et al., 2010; Jasinge et al., 2011; Perera & Ranjith, 2012). For example, CO_2 adsorption-induced strength reduction (up to around 80%) is greater for high rank coal located at greater depths, and increasing the injecting CO_2 pressure causes greater brittleness reduction (up to around 70%) in the coal seam (Perera et al., 2015). Table 2.3 illustrates the current findings on this issue.

Importantly, the CO_2 sequestration and ECBM processes typically target deep coal deposits, and at such locations CO_2 may not exist in a sub-critical phase, as it does under standard laboratory conditions, but instead exists in a super-critical state. Therefore, Karacan (2007) and Aziz & Ming-Li (1999) found that when CO_2 pressure increases, so too do the strength losses. These additional strength losses are due to the greater adsorptive potential and dissolution ability of super- over sub-critical CO_2. In this way, super-critical CO_2 is able to access more of the coal matrix than sub-critical CO_2, which can have more effects on coal seam integrity (Table 2.4).

Table 2.4. Effect of CO_2 injection on coal seam strength during CO_2 sequestration

<table>
<tr><th>Effective factor</th><th>Key observation</th></tr>
<tr><td>Adsorbing gas property</td><td>CO_2 (sub-critical) saturation decreases the strength of brown coal, while for N_2, the effect is the opposite. This is because N_2 is capable of replacing the existing CO_2 in the coal mass by reducing the partial pressure of the seam and consequently recovering the swelling areas to some extent (Kiyama et al., 2011).

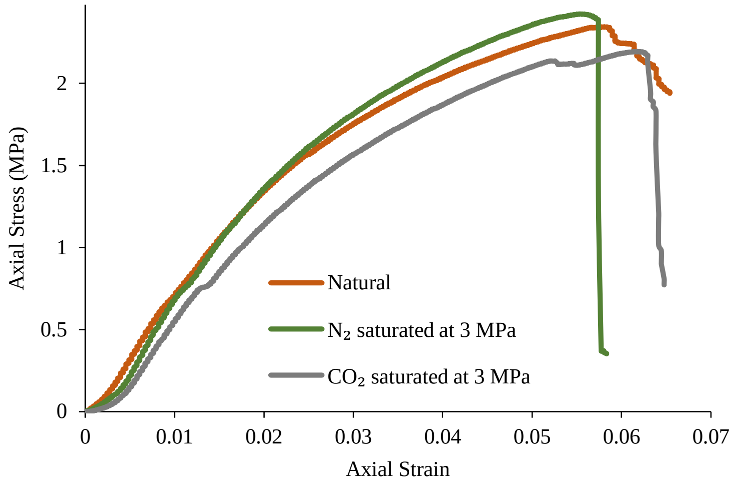

Axial stress vs. axial strain curves for different saturation mediums (Perera et al. 2011c)</td></tr>
<tr><td>Coal rank</td><td>CO_2 saturation causes up to 4.5 times greater strength reduction in bituminous coal compared to lignite as there is a greater surface area in high density coal. High rank coal seams located deep underground offer more loci for CO_2 adsorption due to their well-developed cleat system, causing more swelling than low rank coal (Ranjith & Perera, 2012).

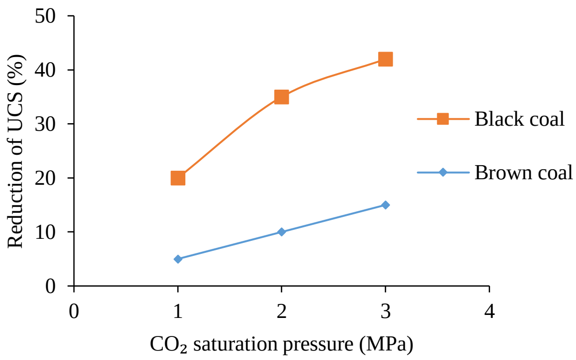

Comparison of UCS strength reduction in bituminous and lignite coal (Ranjith & Perera, 2012)</td></tr>
<tr><td>CO_2 pressure and phase</td><td>• There is a linearly increasing trend for strength reduction with increased injection pressure (Perera et al., 2013)
• The increasing injection pressure has a significant negative effect on cleat performance with greater adsorption-induced swelling (Perera et al., 2013)
• There is a greater strength reduction (approximately 40%) in super-critical CO_2 compared to normal gaseous CO_2 due to the greater adsorptive potential for super-critical CO_2 (Perera et al., 2013)</td></tr>
</table>

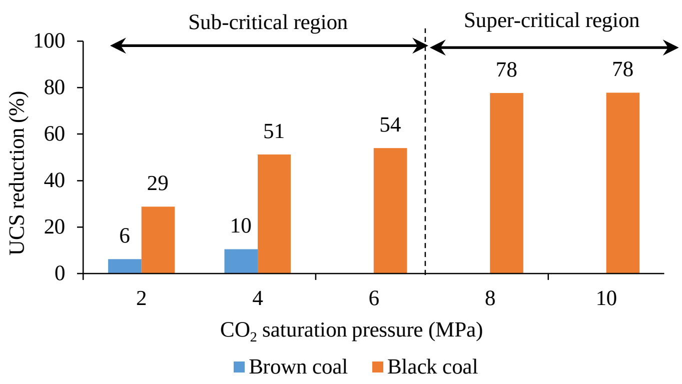

Effects of gaseous and super-critical CO_2 saturation on coal strength (Perera et al., 2011c;2013)

While this CO_2 adsorption-induced strength reduction and crack formation cause the injected CO_2 to be back-migrated into the atmosphere, there is an additional concern related to the potential for fault instability located between the deposited CO_2 and the surface, leading to potential damage to infrastructure. Therefore, a better understanding of coal mass behaviour is essential for the safe implementation of field-scale CO_2 sequestration.

Although CO_2 sequestration is a promising method to reduce and control the greenhouse gas effect through the geological storage of anthropogenic CO_2, it still remains in the experimental stage, as many aspects need to be studied before being put into practice to avoid the risks associated with this process. Most of the possible coal seams for CO_2 sequestration are thin (0.5–5 m), contain many faults, and are very low in permeability (0.001–0.005 Darcy) (Gale, 2004). Therefore, CO_2 adsorption-induced swelling in such seams may develop higher stresses in the top (overlying) and bottom (underlying) rock strata, which can create possible migration paths for injected CO_2 out of the coal mass through the faults generated.

2.6 Coal CO_2 Sequestration Field Projects

The USA, Canada, Poland, China, Australia, Japan and some other countries are using ECBM recovery via CO_2 sequestration at a field scale. Table 2.5 summarizes some of the main field-scale CO_2 sequestration projects in the world. In addition to Table 2.5, initial testing for CO_2 sequestration in China has confirmed a large potential resource for CO_2 sequestration. There are two potential settings for CO_2 storage within China's carboniferous coal deposits: the north-east China coal region and the Ordos basin in north-central China (Wong et al., 2007). Of these, the north-east China coal region is heavily industrialized, with numerous coal-fired power plants that could provide cheap CO_2 for injection. The Ordos basin in north-central China has superior reservoir quality, with minimal fracturing and higher permeability, and the potential for CO_2 sequestration is around 660 million tons in this basin (Stevens et al., 1999). In 2002, China initiated field-scale CO_2 sequestration with the collaboration of Canada, and during the first three years, the project was planned to perform three pilot micro-tests before the selection of a suitable location meeting the requirements for a full-scale pilot test (White et al., 2005). According to Wong et al. (2007), the first micro-pilot test at the south Qinshui basin, Shanxi Province, China was successful and the field data were well-matched using a tuned reservoir model. Further, a multi-well pilot project was designed and planned to proceed (Wong et al., 2007). However, most of the current field-scale CO_2 sequestration projects have faced the common issue of reduction of CO_2 injection capacity within 6 months to two years after initiation due to coal matrix swelling (refer to Table 2.5).

Table 2.5. Field-scale CO_2 sequestration projects around the world

CO_2 sequestration project	**Details of well configuration**	**Details of gas injection**	**Remarks**
Allison Unit **San Juan basin – USA** (Clarkson and Bustin, 1997; Reeves, 2001, 2002a; Reeves, 2002b; Reeves et al., 2002; Reeves & Oudinot, 2005; White et al., 2005)	Has 4 CO_2 injection wells and 9 CH_4 production wells, drilled at 320-acre spacing	• CO_2 was injected at a maximum injection pressure of 17 MPa • Over 6 ½ years, 6.4 Bcf of CO_2 was injected	• The first experimental CO_2-ECBM recovery pilot project in the world, started in 1995 and the rank is medium to low volatile bituminous coal. • Initially, significant reduction in injectivity was observed due to coal matrix swelling and effective stress increment. • Gas production caused the overall reduction of pressure and reservoir volume and caused CO_2 adsorbed near the injection wells to be desorbed and migrate further from the wells. This increased permeability by reversing the swelling areas close to injection wells.

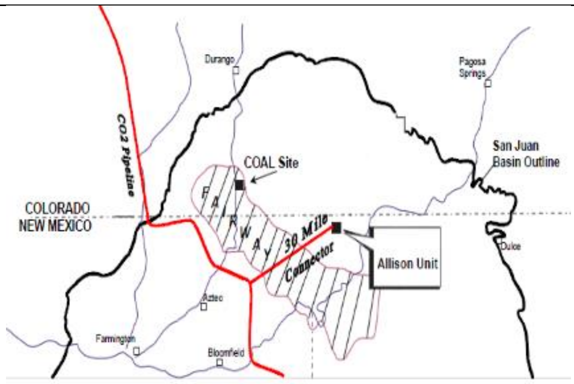

Allison Unit- San Juan basin, USA (Reeves, 2001)

Williston basin **North Dakota – USA** (Botnen et al., 2009; Perera & Ranjith, 2012; White et al., 2005)	Consists of five wells to around 340m depth	• Estimated CO_2 storage capacity is 10.3 TCU • Weakly developed cleat system was the main challenge for the injection of CO_2	• Second largest coal deposit in USA, consists of lignite coal deposit • 13 molecules of CO_2 can be sequestrated for each molecule of CH_4 • Due to coal mass swelling, 10-fold reduction was observed in first year

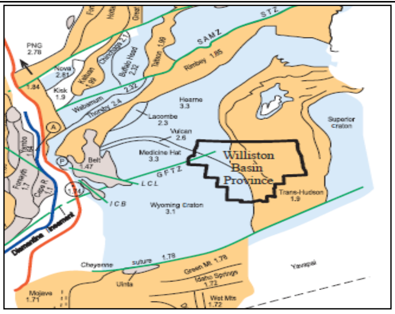		Williston basin, North Dakota – USA (Peterson & Schmoker, 1995)	
Fenn Big Valley basin Alberta – Canada (Mavor et al., 2004; Perera & Ranjith, 2012; White et al., 2005)	Consists of two wells	• Both CO_2 and flue gas were injected • In 1997, 12 tons of CO_2 was injected and after a short process of CH_4 production, around 15 tons of CO_2 was injected. • Since the absolute permeability of the coal seam was very low (1 mad) during the pure CO_2 period, flue gas (13% CO_2, 87% N_2) was injected into the same injection wells in 2000. • Pure N_2 was injected to enhance the CO_2 injection rate and the absolute permeability of the coal seam was increased up to around 13.8 mad • Since the absolute permeability was reduced (1 mad) after 9 days, a mixture of CO_2 and N_2 (47% CO_2, 53% N_2) was injected, which increased the absolute permeability up to 5.6 mad	• Consists of 500 TCU out of 700 TCU coal-bed methane resources in Canada • First pilot test of injecting flue gas in the world • Rank is highly volatile B-bituminous
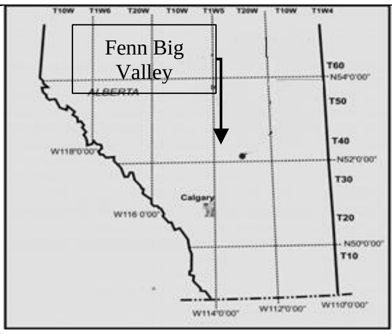		Fenn Big Valley basin Alberta – Canada (Gentzis et al., 2008)	
Dowson River site Southern Bowen basin Australia (Perera & Ranjith, 2012; Reeves & O'Neill, 1989)	Three major phases 1 Micro-pilot testing (one CO_2 injection well/ CH_4 production well) 2 Five-spot pilot testing (4 CO_2 injection wells and one CH_4 production well) 3 Nine-spot pattern field testing (16 CO_2 injection wells and 25 CH_4 production wells, drilled at 80-320-acre spacing	• During first phase CO_2 was injected followed by a soak period, to allow the CO_2 to be adsorbed into coal • During second phase, both pure CO_2 and a mixture of CO_2 and N_2 were injected	• Estimated CBM resource base is 178 Tscf • The coals are high-volatile bituminous A and B • The timing of the demonstration is 4.3 years • If the project were to be successful, phase 3 would become a commercial operation

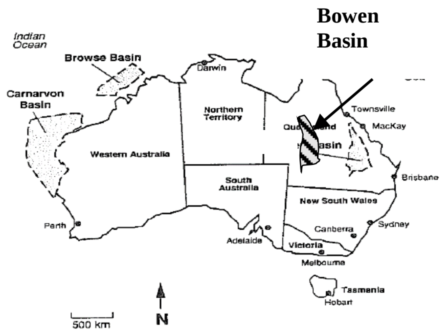		Location of Southern Bowen basin, Australia (Source: Reeves & O'Neill, 1989)	
Silesian basin, Poland (Reduction of CO_2 Emissions by Means of CO_2 Storage in the Silesian Coal Basin of Poland – RECOPL) (Perera & Ranjith, 2012; Reeves & Taillefert, 2002; White et al., 2005)	One CO_2 injection well and one CH_4 production well located 105 m from each other	• During first 6 months of CO_2 injection in 2004, permeability was reduced from 10-100 (CO_2 injection capacity - 1 ton/day) from the initial permeability (CO_2 injection capacity - 20 ton/day) • In mid-2005, a hydraulic fracture was created and CO_2 injection capacity increased up to 15 tons/day	• Small-scale project • 93% of the injected CO_2 was stored and 55-70% enhancement of CH_4 production was observed in the field tests
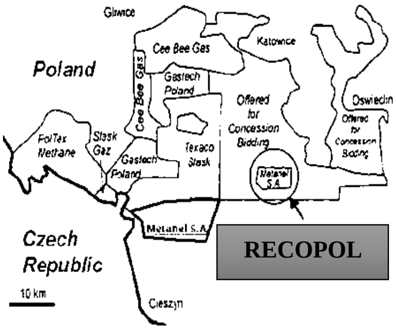		Location of Silesian basin, Poland (Reeves & Taillefert, 2002)	
Ishikari basin Yubari – Japan (Fujioka et al., 2010; Perera & Ranjith, 2012; White et al., 2005)	Two CO_2 injection wells and one CH_4 production well	• During the first year, without any gas production, a total of around 35.7 metric tons of CO_2 was injected at a rate of 2.3 tons/day, which reduced to 11 metric tons in the second year • Due to decrease of effective pressure close to the injection well, CO_2 injection was increased from 1.6 tons/day to 3.5 tons/day • N_2 injection in 2005 enhanced the CO_2 injection by up to 6.6 tons/day and gradually dropped again to the initial rate, and was then again increased because of effective stress variation.	• Small-scale project • Injection pressure was maintained at 15 MPa, which was slightly less than the cleat opening pressure of 15.8 MPa • A total of 480 tons of CO_2 was injected between 2004-2006

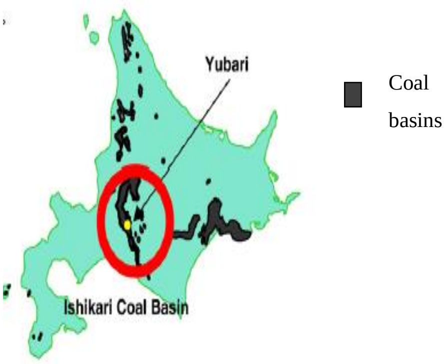

Location of Ishikari coal basin, Japan (Fujioka et al., 2010)

Interestingly, this matrix swelling-created CO_2 injectivity reduction has sometimes been recovered by the reduced effective stress close to the CO_2 injection well, and as a result considerable CO_2 injection capacity enhancements have been recorded (Fujioka et al., 2010; White et al., 2005). However, the combined influence has mostly had a negative effect on CO_2 sequestration and coal seam gas production. Therefore, various coal seam permeability enhancement techniques, including inert gas (N_2) injection and hydro fracturing, have been performed in the field.

Of these projects, the Ishikari basin and Fenn Big Valley basin projects have injected pure N_2 (Mavor et al., 2004; White et al., 2005; Fujioka et al., 2010) and the Fenn Big Valley basin and Southern Bowen basin have injected a mixture of N_2 and CO_2 (flue gas) (Reeves & O'Neill, 1989; Mavor et al., 2004; White et al., 2005; Syed et al., 2013) into the coal seam to recover the CO_2 adsorption-induced swelled areas in the coal matrix to some extent. Although injecting an inert gas like N_2 (Mavor et al., 2004; White et al., 2005; Fujioka et al., 2010) or a mixture of CO_2 and N_2 (Reeves & O'Neill, 1989; Mavor et al., 2004; White et al., 2005) can increase coal seam permeability by a substantial amount, the increase is not sufficient for an economical CO_2 sequestration project. Therefore, more advanced approaches, such as hydro fracturing, have been required to enhance coal seam permeability to achieve an acceptable CO_2 injection capacity in the field (Ruehl, 1968; Mazza et al., 1981; Puri et al., 1991; Reeves & Taillefert, 2002).

Hydro fracturing techniques have already been tested in some field-scale projects, including the Silesian basin (Reeves & Taillefert, 2002; White et al., 2005). However, there are some disadvantages to the hydro fracturing process, since the creation of hydraulic fractures may cause the coal seam to be weakened, and this may enhance the risk of injected CO_2 back-migration into the atmosphere. Therefore, creating hydro-fractures in coal seams, where they have already been weakened due to super-critical CO_2 injection, is a great challenge and no extensive study has been conducted on this to date. Therefore, a far-reaching study is required, using comprehensive experiments representing in situ conditions and advanced numerical modelling approaches, before putting hydro fracturing into practice.

2.7 What causes the lack of CO_2 sequestration implementation?

Basically, CO_2 sequestration in deep coal seams can be divided into two general sub-systems: operational and in situ. The operational sub-system includes components such as CO_2 capture, transportation, and injection. Once CO_2 is injected into coal beds, it enters an in situ sub-system. Past technological innovations and experiences have provided the tools and proficiency to handle and control CO_2 in the operational sub-system with adequate certainty and safety; however, in the in situ sub-system knowledge is currently lacking, particularly of the environmental and human health risks. Furthermore, public perceptions, the economics of CO_2 sequestration and policy barriers are other challenges which discourage the use of CO_2-ECBM projects, in spite of their multiple advantages (Bae & Bhatia, 2006; Holloway, 2005; Howard, 2002).

2.7.1 Complexity associated with coal heterogeneity

Some characteristics are required for effective and safe CO_2 sequestration in coal seams. These include i) sufficient capacity for storing large volumes of CO_2, ii) adequate CO_2 injectivity (permeability of at least 1–5 mD), iii) a minimally faulted and/or folded reservoir, and iv) a reservoir well confined with an overlying seal to prevent leakage of injected CO_2 into the atmosphere (Bachu, 2007; Gale & Freund, 2001). However, the satisfaction of all of these criteria is challenging and is made complex by the highly heterogeneous nature of coal. As discussed in Sections 2.4 and 2.5, the behaviour of CO_2 permeability and coal seam strength vary with seam and injecting CO_2 properties (coal rank, temperature, confining pressure, CO_2 phase and pressure). This leads to unpredictable CO_2 injectivity and coal seam integrity. In addition, the heterogeneous nature of coal increases the uncertainty in determining the properties representative of the whole seam (Day et al., 2008; Ozdemir & Schroeder, 2009; Renzik et al., 1978; Robertson, 2005; Saghafi et al., 2007; Wang, 2007). Furthermore, there may be significant variations in properties within the same core sample or between different core samples obtained from the same coal seam. Therefore, the heterogeneous nature of coal has been a key hurdle to the confirmation of the effects of in situ coal properties on coal's behaviour.

According to De Silva & Ranjith (2013) and Jasinge et al. (2011), homogenous reconstituted coal samples with reproducible properties can be used to overcome this problem. Figure 2.12 shows the variation of permeability with effective stress for reconstituted and natural samples of brown coal. The figure depicts very similar permeability behaviour of CO_2 in the natural specimen and the reconstituted specimen (Jasinge et al., 2011). Therefore, reconstituted coal samples can be used to avoid the complexities associated with coal heterogeneity. However, thorough investigation of the coal mass structure and its characteristics for different localities is crucial for the safe execution of field-scale CO_2-ECBM.

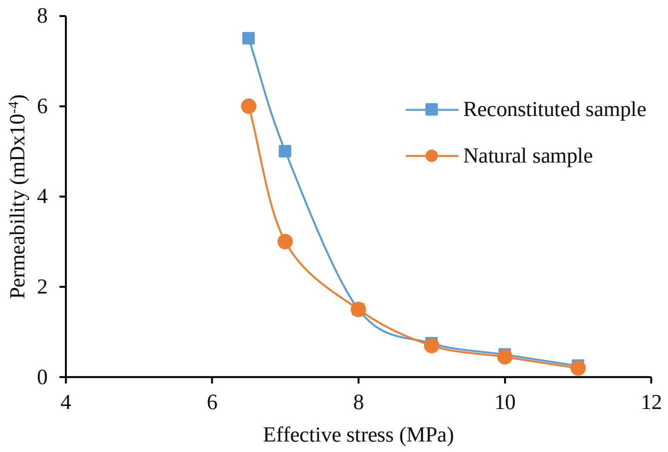

Figure 2.12. Permeability behaviour with effective stress for natural and reconstituted coal samples (Jasinge et al., 2011)

2.7.2 Environmental and human health risks

The question of whether safe and stable storage of CO_2 in the sub-surface can be assured is probably the most important issue facing the underground storage of CO_2 at present, because this is likely to have a high impact on public acceptability. To protect the environment and the health and safety of the public, monitoring and verification of geologically-sequestered CO_2 is essential. Moreover, it is essential to satisfy the expected regulatory demands and to lessen any uncertainties associated with the long-term safety and security of projects (White et al., 2005). In situ pressure gauges, chemical tracers, isotropic ratios, geophysical methods, visual inspection and the production response by nearby wells are some methods used for the detection of movement of stored CO_2 (Hall et al., 1994). However, due to the limitations and uncertainties associated with those methods, there are complexities in fulfilling the monitoring process, such as (i) uncertainties due to wellbore storage effects in using pressure gauges, (ii) the adsorptive nature of coal may irreversibly sorb the compounds added as chemical tracers, and (iii) the precision of measurements using geophysical methods (Chikatamarla et al., 2004; White et al., 2005).

2.7.3 Policy, regulation and public perceptions of CO_2 sequestration using ECBM

For the operation of CO_2 sequestration in a safe and secure manner, the formation and application of sound regulatory and legal frameworks are essential. Public perceptions, policies, regulations and international conventions exist which may offer assistance or barriers to CO_2 capture and storage using ECBM recovery.

2.7.3.1 Policies, regulations and international agreements

The use of CO_2 sequestration will add to the cost of fossil fuel energy with some exceptions. Worldwide disposition of CO_2 sequestration could be encouraged by policies that address the added cost of CO_2 storage, not only in developed countries but also in countries where access to affordable energy is a key development priority. Some national governments have provided limited early inducements for CO_2 sequestration projects, while the United Nations Framework Convention on Climate Change (UNFCCC) and its Kyoto Protocol could both be used to encourage CO_2 storage. For example, the UNFCCC has accepted Norway's national inventory of greenhouse gas emissions, under which CO_2 from the Sleipner gas field which has been geologically stored does not contribute to Norway's emissions (Kheshgi et al., 2006). To date, no CO_2 sequestration projects have been submitted for approval under the Clean Development Mechanism of the Kyoto Protocol (Kheshgi et al., 2006). Within the European Union (EU) emissions trading system, CO_2 stored in geological formations can be deducted from member states' inventories, based on the provisional monitoring guidelines of member states, until succeeded by permanent EU monitoring guidelines (Kheshgi et al., 2006). In the long term, the effective application of CO_2 storage will rely on economically efficient approaches to address the additional costs.

An effective legal and regulatory framework would facilitate good CO_2 sequestration practices without forming unintended barriers to the deployment of CO_2 sequestration. An expanded use of coal CO_2 sequestration would be accompanied by reductions in costs, improvements in technology, and improved understanding of risks and their management. A regulatory framework that encourages good practice and incorporates the evolving understanding of risk and its management could promote these improvements.

2.7.3.2 Public perceptions

Public acceptance and support is of great importance for coal CO_2 sequestration. At this stage, the public is largely unaware of coal CO_2 sequestration. Many public survey results confirm this lack of awareness of the public about CO_2 storage in coal seams. For example, less than 4% were aware about carbon capture and storage in coal seams in a survey conducted in the United States of 1200 people in 2003 (Shackely et al., 2004). In a survey conducted in Japan in 2004, 22% were aware of CO_2-ECBM out of 1006 responses (Curry et al., 2005). The Netherlands and the United Kingdom have also conducted surveys on public perceptions of CO_2-ECBM and found that many people (>50%) were concerned about the risk of leakage and accidents, and impacts on the environment, ecosystem, and human health (Curry et al., 2005; Gough et al., 2006). Early experience will leave a legacy for coal CO_2 sequestration in terms of public perceptions of it. Clear assessment of the merits of coal CO_2 sequestration and the competing technologies is a prerequisite for informed decisions. This would enable the merits of each option to be weighed in the context of a broad range of priorities, including the long-term risks of climate change.

2.8 Conclusions and Suggestions

2.8.1 Conclusions

- With the process of industrialization and modernization, carbon dioxide emissions are becoming a major concern directly leading to global warming. Various approaches have been proposed to address the problem by significantly reducing the amount of greenhouse gas (CO_2) in the atmosphere, including the use of renewable fuels, energy-efficient technology and carbon sequestration. Of these feasible methods, carbon dioxide sequestration in deep un-mineable coal seams is recognised as one of the most promising methods, based on cost and safety considerations.
- CO_2 sequestration involves the capture of CO_2 released from anthropogenic sources and its secure storage in deep underground locations off- or on-shore. However, in terms of safety, reliability and cost, on-shore sequestration is more effective than off-shore sequestration. Of the various potential CO_2 storage sinks deep underground (e.g. depleted oil and gas fields, saline aquifers, shale beds, and coal mines), CO_2 storage in deep coal seams offers unique advantages, and the offsetting of CO_2 sequestration costs by the production of a valuable energy product like methane (coal seam gas) is critical. This process is known as enhanced coal bed methane (ECBM) recovery.
- However, adsorption of the injected CO_2 into the coal mass causes it to swell, leading to significant alterations in its internal rock mass structure, resulting in major modifications to CO_2 injectivity and coal mass integrity. This CO_2 adsorption-induced coal matrix swelling is dependent on both seam (coal rank, temperature and confining pressure) and injected CO_2 properties (CO_2 phase and pressure), and the swelling reduces with increasing temperature due to the reduced sorption capacity. On the other hand, the amount of swelling is largely dependent on the pressure and the physical state of the injected CO_2, and super-critical CO_2 creates a much greater swelling effect than sub-critical CO_2, due to its greater chemical potential. Furthermore, high-pressure injection of CO_2 causes the swelling process to be enhanced due to the higher flow ability of the injected CO_2 under reduced effective stress conditions (difference of confining pressure and injection pressure) at increased injection pressures. However, potential coal seams for CO_2 sequestration are available at extremely deep locations and there is a high possibility of phase change from sub- to super-critical state in the underground environment owing to changes in field conditions. This confirms the likely existence of high swelling rates in deep coal seams with CO_2 injection.

- The effectiveness of the CO_2 storage process in any coal seam is greatly influenced by the flow ability of the injected CO_2 through the seam, which is dependent on a number of factors, including coal rank, seam temperature, seam depth (confining pressure) and CO_2 injecting pressure and phase. Importantly, the injected CO_2 phase condition critically influences its flow behaviour in the seam. In the super-critical state, the expected form of the CO_2 in deep coal seams, CO_2 has significantly lower permeability than sub-critical CO_2, which causes unpredictable CO_2 injectivity into deep coal seams.
- Secure storage of injected CO_2 in the seam is critically important in CO_2 geo-sequestration in deep coal seams in terms of environmental health and safety. It is important to prevent the back-migration of $CO_{2,}$ as this has potential to cause mine outbursts and lateral migration into aquifers and surrounding more permeable geologic strata. These factors are mainly dependent on the coal mass strength properties. However, it is well known that CO_2 adsorption-induced swelling causes weakening in deep coal seams. This strength reduction is greatly dependent on injecting CO_2 phase and pressure, and it increases with increasing pressure. In addition, super-critical CO_2 creates much greater strength reduction than sub-critical CO_2. High rank coal seams located deep underground are subjected to greater strength reduction with CO_2 injection, as they offer more loci for CO_2 adsorption.
- Reduction of seam permeability over time after CO_2 injection is a common issue faced by many field-scale CO_2 sequestration projects. For example, there was around 50% reduction in CO_2 injectivity at the Allison unit CO_2 sequestration project in the San Juan basin, USA, during the first two years of injection.
- Existing government policies, public perceptions, and strict rules on coal mining affect the implementation of CO_2 sequestration in deep coal seams. The lack of knowledge related to coal seam CO_2 sequestration has severely affected the implementation of this process in potential coal seams around the world. The complex heterogeneous nature of coal, which causes location-dependent coal seam properties, is one reason for the delay in the adoption of coal CO_2 sequestration.

2.8.2 Recommendations

- Extensive laboratory tests on different type of coals, in particular lignite, sub-bituminous, bituminous and anthracite can be used to obtain a greater understanding of CO_2 sequestration in the coal mass in a controlled environment. These results can be used to support reservoir studies and then be extended to other advanced studies (risk assessment studies, economic optimization studies, project-screening models etc.).

- Numerous studies have been conducted on CO_2 sequestration in coal seams. However, knowledge regarding enhanced methane production remains limited. Therefore, more attention to enhanced methane production-related coal seam alterations is required.
- More demonstration projects of CO_2 storage in deep coal seams are required to increase knowledge of CO_2 sequestration-induced flow and mechanical property changes.
- A detailed monitoring system (near-surface monitoring and seam monitoring) is essential for CO_2 sequestration projects, to ensure the integrity of CO_2 storage and CH_4 production and to avoid possible hazards related to CO_2 back-migration into the atmosphere. This would lead to greater confidence and improved public perceptions.

2.9 References

Adams, E. E., & Caldeira, K. (2008). Ocean storage of CO_2. *Elements, 4*(5), 319-324.

Anggara, F., Sasaki, K., Sugai, Y., (2013). Swelling Measurements of a Low Rank Coal in Supercritical CO_2. International Journal of Geosciences 4, 863-870.

Anggara, F., Sasaki, K., Rodrigues, S., & Sugai, Y. (2014). The effect of megascopic texture on swelling of a low rank coal in supercritical carbon dioxide. *International Journal of Coal Geology*, *125*, 45-56.

Archer, D., & Brovkin, V. (2008). The millennial atmospheric lifetime of anthropogenic CO_2. *Climatic Change*, *90*(3), 283-297.

Aziz, N. I., & Ming-Li, W. (1999). The effect of sorbed gas on the strength of coal – an experimental study. *Geotechnical & Geological Engineering, 17*(3-4), 387-402.

Bachu, S. (2000). Sequestration of CO_2 in geological media: criteria and approach for site selection in response to climate change. *Energy Conversion and Management*, *41*(9), 953-970.

Bachu, S. (2003). Screening and ranking of sedimentary basins for sequestration of CO_2 in geological media in response to climate change. *Environmental Geology, 44*(3), 277-289.

Bachu, S. (2007). Carbon dioxide storage capacity in uneconomic coal beds in Alberta, Canada: Methodology, potential and site identification. *International Journal of Greenhouse Gas Control, 1*(3), 374-385.

Bae, J.-S., & Bhatia, S. K. (2006). High-Pressure Adsorption of Methane and Carbon Dioxide on Coal. *Energy & Fuels, 20*(6), 2599-2607.

Battistutta, E., van Hemert, P., Lutynski, M., Bruining, H., & Wolf, K.-H. (2010). Swelling and sorption experiments on methane, nitrogen and carbon dioxide on dry Selar Cornish coal. *International Journal of Coal Geology, 84*(1), 39-48.

Benson, S. M., & Cole, D. R. (2008). CO_2 sequestration in deep sedimentary formations. *Elements, 4*(5), 325-331.

Borah, R. C., Ghosh, P., & Rao, P. G. (2011). A review on devolatilization of coal in fluidized bed. *International Journal of Energy Research, 35*(11), 929-963.

Bromhal, G. S., Sams, W. N., Jikich, S., Ertekin, T., & Smith, D. H. (2005). Simulation of CO_2 sequestration in coal beds: The effects of sorption isotherms. *Chemical Geology, 217*(3), 201-211.

Chikatamarla, L., Cui, X., & Bustin, R. M. (2004). *Implications of volumetric swelling/shrinkage of coal in sequestration of acid gases.* Paper presented at the Coalbed Methane Symposium, Tuscaloosa, AL, Paper no. 0435.

Clarkson, C. R., & Bustin, R. M. (1997). Variation in permeability with lithotype and maceral composition of Cretaceous coals of the Canadian Cordillera. *International Journal of Coal Geology, 33*(2), 135-151.

CO2CRC. (2016). The Otway Research Facility - CO2CRC. [online] Available at: http://www.co2crc.com.au/otway-research-facility/.

Connell, L.D., Lu, M., Pan, Z., (2010). An analytical coal permeability model for tri-axial strain and stress conditions. *International Journal of Coal Geology* 84 (2), 103–114.

Cui, X., Bustin, R.M., (2005). Volumetric strain associated with methane desorption and its impact on coalbed gas production from deep coal seams. *AAPG Bulletin* 89 (9), 1181–1202.

Cui, X., Bustin, R.M., Chikatamarla, L., (2007). Adsorption-induced coal swelling and stress, implications for methane production and acid gas sequestration into coal seams. *Journal of Geophysical Research-Solid Earth* 112, B10202.

Curry, T.E., Reiner, D.M., Ansolabehere, S., Herzog, H.J., (2005). How aware is the public of carbon capture and storage? MIT Laboratory for Energy and the Environment, Cambridge, U.S.A

Czapliński, A., & Hołda, S. (1982). Changes in mechanical properties of coal due to sorption of carbon dioxide vapour. *Fuel, 61*(12), 1281-1282.

Day, S., Duffy, G., Sakurovs, R., & Weir, S. (2008). Effect of coal properties on CO_2 sorption capacity under supercritical conditions. *International Journal of Greenhouse Gas Control, 2*(3), 342-352.

Day, S., Fry, R., Sakurovs, R., & Weir, S. (2010). Swelling of Coals by Supercritical Gases and Its Relationship to Sorption. *Energy & Fuels, 24*(4), 2777-2783.

De Silva, G. P. D., Ranjith, P. G., & Perera, M. S. A. (2015). Geochemical aspects of CO_2 sequestration in deep saline aquifers: A review. *Fuel, 155*, 128-143.

De Silva, P., & Ranjith, P.G. (2013). Advanced core flooding apparatus to estimate permeability and storage dynamics of CO_2 in large coal specimens. *Fuel, 104*, 417-425.

Drange, H., Alendal, G., & Johannessen, O. M. (2001). Ocean release of fossil fuel CO_2: A case study. *Geophysical Research Letters, 28*(13), 2637-2640.

Durie, R. (2013). *The science of Victorian brown coal: structure, properties and consequences for utilization*: Butterworth-Heinemann. Oxford, pp 103.

Durucan, S., & Shi, J.-Q. (2009). Improving the CO_2 well injectivity and enhanced coalbed methane production performance in coal seams. *International Journal of Coal Geology, 77*(1–2), 214-221.

Fujioka, M., Yamaguchi, S., & Nako, M. (2010). CO_2-ECBM field tests in the Ishikari Coal Basin of Japan. *International Journal of Coal Geology, 82*(3), 287-298.

Gale, J. (2004). Geological storage of CO_2: What do we know, where are the gaps and what more needs to be done? *Energy, 29*(9), 1329-1338.

Gentzis, T., Goodarzi, F., Cheung, F., & Laggoun-Défarge, F. (2008). Coalbed methane producibility from the Mannville coals in Alberta, Canada: A comparison of two areas. *International Journal of Coal Geology, 74*(3), 237-249.

Gibbs, J. W. (1878). On the equilibrium of heterogeneous substances. *American Journal of Science*(96), 441-458.

Gilman, A., & Beckie, R. (2000). Flow of coal-bed methane to a gallery. *Transport in Porous Media, 41*(1), 1-16.

Goodman, A., Favors, R., Hill, M., & Larsen, J. W. (2005). Structure changes in Pittsburgh No. 8 coal caused by sorption of CO_2 gas. *Energy & Fuels, 19*(4), 1759-1760.

Gough, C., Shackley, S., Holloway, S., Bentham, M., Bulatov, I., McLachlan, C., Klemes, J., Purdy, R., Cockerill, T., (2006). An integrated assessment of carbon dioxide capture and storage in the UK, In: 8th International Conference on Greenhouse Gas Control Technologies [Proceedings]/ [edited by Greenhouse Gas Control Technologies. Trondheim, Norway: GHGT8. Greenhouse Gas Control Technologies, Technical report 87.

Gray, I., (1987). Reservoir engineering in coal seams, part 1—the physical process of gas storage and movement in coal seams. *SPE Reservoir Engineering* 2 (1), 28–34.

Griffith, A. A. (1921). The Phenomena of Rupture and Flow in Solids. *Philosophical Transactions of the Royal Society of London. Series A, Containing Papers of a Mathematical or Physical Character, 221*, 163-198.

Hall, F., Chunhe, Z., Gasem, K., Robinson Jr, R., & Dan, Y. (1994). *Adsorption of Pure Methane Nitrogen and Carbon Dioxide and Their Binary Mixtures on Wet Fruitland Coal.* Paper presented at the SPE Eastern Regional Meeting.

Harpalani, S., & Schraufnagel, A. (1990). Measurement of parameters impacting methane recovery from coal seams. *International Journal of Mining and Geological Engineering, 8*(4), 369-384.

Harpalani, S., Chen, G., (1995). Estimation of changes in fracture porosity of coal with gas emission. Fuel 74 (10), 1491–1498.

Holloway, S. (2005). Underground sequestration of carbon dioxide—a viable greenhouse gas mitigation option. *Energy, 30*(11–12), 2318-2333.

House, K. Z., Schrag, D. P., Harvey, C. F., & Lackner, K. S. (2006). Permanent carbon dioxide storage in deep-sea sediments. *Proceedings of the National Academy of Sciences, 103*(33), 12291-12295.

Howard, H. (2002). *Carbon sequestration via mineral carbonation: overview and assessment*: MIT Laboratory for Energy and the Environment.

Jaeger, J.C., Cook, N.G.W., Zimmerman, R.W., (2007). Fundamentals of Rock Mechanics, 4th edition. Blackwell Publishing, Malden, MA.

Jasinge, D., Ranjith, P. G., & Choi, S. K. (2011). Effects of effective stress changes on permeability of Latrobe Valley brown coal. *Fuel, 90*(3), 1292-1300.

Jasinge, D., Ranjith, P., Choi, S.-K., Kodikara, J., Arthur, M., & Li, H. (2009). Mechanical properties of reconstituted Australian black coal. *Journal of Geotechnical and Geoenvironmental Engineering, 135*(7), 980-985.

Jasinge, D., Ranjith, P., Choi, X., & Fernando, J. (2012). Investigation of the influence of coal swelling on permeability characteristics using natural brown coal and reconstituted brown coal specimens. *Energy, 39*(1), 303-309.

Karacan, C. Ö. (2007). Swelling-induced volumetric strains internal to a stressed coal associated with CO_2 sorption. *International Journal of Coal Geology, 72*(3), 209-220.

Kheshgi, H., Stileman, T., Cappelen, F., Crookshank, S., Heilbrunn, A., Lee, A., Mikus, T., Robson, W., Senior, B., (2006). Carbon Dioxide Capture and Geological Storage: Contributing to Climate Change Solutions. SPE International Health, Safety & Environment Conference, Abu Dhabi, UAE, Paper no. SPE-98583-MS.

Kiyama, T., Nishimoto, S., Fujioka, M., Xue, Z., Ishijima, Y., Pan, Z., & Connell, L. D. (2011). Coal swelling strain and permeability change with injecting liquid/supercritical CO_2 and N_2 at stress-constrained conditions. *International Journal of Coal Geology, 85*(1), 56-64.

Kronimus, A., Busch, A., Alles, S., Juch, D., Jurisch, A., & Littke, R. (2008). A preliminary evaluation of the CO_2 storage potential in unminable coal seams of the Münster Cretaceous Basin, Germany. *International Journal of Greenhouse Gas Control, 2*(3), 329-341.

Larsen, J. W., Flowers, R. A., Hall, P. J., & Carlson, G. (1997). Structural rearrangement of strained coals. *Energy & Fuels, 11*(5), 998-1002.

Levine, J.R., (1996). Model study of the influence of matrix shrinkage on absolute permeability of coal bed reservoirs. Geological Society, London, Special Publications 109 (1), 197–212.

Liu, H.-H., Rutqvist, J., (2010). A new coal-permeability model, internal swelling stress and fracture–matrix interaction. *Transport in Porous Media* 82 (1), 157–171.

Ma, Q., Harpalani, S., Liu, S., (2011). A simplified permeability model for coalbed methane reservoirs based on matchstick strain and constant volume theory. *International Journal of Coal Geology* 85 (1), 43–48.

Majewska, Z., & Ziętek, J. (2007). Changes of acoustic emission and strain in hard coal during gas sorption–desorption cycles. *International Journal of Coal Geology, 70*(4), 305-312.

Masoudian, M.S., Airey, D.W., El-Zein, A., (2014). Experimental investigations on the effect of CO_2 on mechanics of coal. *International Journal of Coal Geology* 128–129, 12-23.

Mavor, M., Gunter, W., & Robinson, J. (2004). *Alberta multiwell micro-pilot testing for CBM properties, enhanced methane recovery and CO_2 storage potential.* Paper presented at the SPE Annual Technical Conference and Exhibition.

Mazza, R. L., Dahl, H. D., & Umphrey, R. W. (1981). Pretreatment for fracturing coal seams: U.S. Patent No. 4,283,089.

Metz, B., Davidson, O., De Coninck, H., Loos, M., & Meyer, L. (2005). *Carbon dioxide capture and storage*: IPCC Geneva, Switzerland.

Miedzińska, D., Niezgoda, T., Małek, E., & Zasada, D. (2013). Study on coal microstructure for porosity levels assessment. *Bulletin of the Polish Academy of Sciences: Technical Sciences, 61*(2), 499-505.

Oldenburg, C. M. (2006). Geologic carbon sequestration: CO_2 transport in depleted gas reservoirs *Gas Transport in Porous Media* (pp. 419-426): Springer, Netherlands.

Orr, F. M. (2009). Onshore geologic storage of CO_2. *Science, 325*(5948), 1656-1658.

Ozdemir, E., & Schroeder, K. (2009). Effect of moisture on adsorption isotherms and adsorption capacities of CO_2 on coals. *Energy & Fuels, 23*(5), 2821-2831.

Pachauri, R., & Reisinger, A. (2007). Climate change 2007: synthesis report. Contribution of working groups I. II and III to the Fourth Assessment Report of the Intergovernmental Panel on Climate Change, IPCC, Geneva, Switzerland.

Palmer, I., Mansoori, J., (1996). How permeability depends on stress and pore pressure in coalbeds, a new model. SPE Annual Technical Conference and Exhibition. Denver, Colorado, Paper no.

Pan, Z., & Connell, L. D. (2007). A theoretical model for gas adsorption-induced coal swelling. *International Journal of Coal Geology, 69*(4), 243-252.

Pekot, L.J., Reeves, S.R., (2002). Modelling coal matrix shrinkage and differential swelling with CO_2 injection for enhanced coalbed methane recovery and carbon sequestration applications. Topical report, Contract No. DE-FC26-00NT40924, U.S. DOE, Washington, DC. 14–17 pp.

Perera, M. S. A., & Ranjith, P. G. (2012). Carbon dioxide sequestration effects on coal's hydro-mechanical properties: a review. *International Journal of Energy Research, 36*(10), 1015-1031.

Perera, M. S. A., Ranjith, P. G., & Peter, M. (2011). Effects of saturation medium and pressure on strength parameters of Latrobe Valley brown coal: Carbon dioxide, water and nitrogen saturations. *Energy, 36*(12), 6941-6947.

Perera, M. S. A., Ranjith, P. G., & Viete, D. R. (2013). Effects of gaseous and super-critical carbon dioxide saturation on the mechanical properties of bituminous coal from the Southern Sydney Basin. *Applied Energy, 110*(0), 73-81.

Perera, M. S. A., Ranjith, P. G., Airey, D. W., & Choi, S. K. (2011). Sub- and super-critical carbon dioxide flow behavior in naturally fractured black coal: An experimental study. *Fuel, 90*(11), 3390-3397.

Perera, M. S. A., Ranjith, P. G., Choi, S. K., & Airey, D. (2011). The effects of sub-critical and super-critical carbon dioxide adsorption-induced coal matrix swelling on the permeability of naturally fractured black coal. *Energy, 36*(11), 6442-6450.

Perera, M., Ranjith, P., Viete, D., & Choi, S. (2012). Parameters influencing the flow performance of natural cleat systems in deep coal seams experiencing carbon dioxide injection and sequestration. *International Journal of Coal Geology, 104*, 96-106.

Peterson, J. A., & and Schmoker, J. W. (1995). *Geologic report, Williston Basin Province* [Online]. Available from: http://pubs.usgs.gov/dds/dds-069/dds-069-w/contents/REPORTS/069_W_CH_062.pdf. [Accessed on 26th March 2015].

Puri, R., Yee, D., Buxton, T. S., & Majahan, O. (1991). Method of increasing the permeability of a coal seam: U.S. Patent No. 5,014,788.

Ranathunga, A. S., Perera, M. S. A., & Ranjith, P. G. (2014). Deep coal seams as a greener energy source: a review. *Journal of Geophysics and Engineering, 11*(6), 063001.

Ranjith, P.G., & Perera, M. (2012). Effects of cleat performance on strength reduction of coal in CO_2 sequestration. *Energy*, 45, 1069-1075.

Reeves, S. (2001). *Geological Sequestration of CO_2 in Deep, Unmineable Coalbeds: An Integrated Research and Commerical-Scale Field Demonstration Project.* Paper presented at the SPE Annual Technical Conference and Exhibition.

Reeves, S. (2002). *Coal-Seq project update: field studies of ECBM recovery/CO_2 sequestration in coal seams.* Paper presented at the Proceedings of the 6th International Conference on Greenhouse Gas Control Technologies

Reeves, S. (2002). Field studies of enhanced methane recovery and CO_2 sequestration in coal seams. *World Oil, 223*(12), 56-60.

Reeves, S., & O'Neill, P. (1989). *Preliminary results from the broad meadow pilot, project Bowen basin Australia.* Proceedings, 1989 Coalbed Methane Symposium, University of Alabama School of Mines and Energy Development and Gas Research Institute, Tuscaloosa, AL, pp 273-91.

Reeves, S., & Oudinot, A. (2005). *The Allison Unit CO_2-ECBM Pilot–A Reservoir and Economic Analysis.* Paper presented at the 2005 International Coalbed Methane Symposium, Tuscaloosa, AL, Paper no 0522.

Reeves, S., & Taillefert, A. (2002). Reservoir Modeling for the Design of the RECOPOL CO_2 Sequestration Project, Poland *Topical Report*, DOE Contract No. DE-FC26-00NT40924 (February).

Reeves, S., Clarkson, C., & Erickson, D. (2002). Selected field practices for ECBM recovery and CO_2 sequestration in coals based on experience gained at the Allison and Tiffany Units, San Juan Basin *Topical Report*, DOE Contract No. DE-FC26-00NT40924 (September).

Reucroft, P. J., & Sethuraman, A. R. (1987). Effect of pressure on carbon dioxide induced coal swelling. *Energy & Fuels, 1*(1), 72-75.

Robertson, E.P., Christiansen, R.L., (2005). Measuring and Modeling Sorption-Induced Coal Strain, 4th Annual DOE/NETL Conference on Carbon Capture and Sequestration, Alexandria, Virginia, pp. 2-5.

Robertson, E.P., Christiansen, R.L., (2006). A permeability model for coal and other fractured, sorptive-elastic media. SPE Eastern Regional Meeting. Society of Petroleum Engineers, Canton, Ohio, USA.

Ruehl, W. (1968). Method of degassing and fracturing coal seams: U.S. Patent No. 3,384,416.

Sabine, C. L., & Tanhua, T. (2010). Estimation of anthropogenic CO_2 inventories in the ocean. *Annual Review of MarineSscience, 2*, 175-198.

Saghafi, A., Faiz, M., & Roberts, D. (2007). CO_2 storage and gas diffusivity properties of coals from Sydney Basin, Australia. *International Journal of Coal Geology, 70*(1), 240-254.

Sawyer, W., Paul, G., & Schraufnagel, R. (1990). Development and application of a 3D coalbed simulator. *CIM/SPE*, 90-119.

Sawyer, W.K., Paul, G.W., Schraufnagel, R.A., 1990. Development and application of a 3D coalbed simulator. International Technical Meeting Hosted Jointly by the Petroleum Society of CIM and the Society of Petroleum Engineers. Calgary, Alberta, Canada. CIM/SPE 90-1119.

Schrag, D. P. (2009). Storage of carbon dioxide in offshore sediments. *Science, 325*(5948), 1658-1659.

Sean, P. D., & Pitman, M. D. (2012). *The Fossil Record* [Online]. Available from: http://www.detectingdesign.com/fossilrecord.html [accessed on 05/03/2014]

Seidle, J.R., Huitt, L.G., (1995). Experimental measurement of coal matrix shrinkage due to gas desorption and implications for cleat permeability increases. International Meeting on Petroleum Engineering. Society of Petroleum Engineers, Inc, Beijing, China, Paper no. SPE-30010-MS.

Shackley, S., McLachlan, C., Gough, C., (2004). The public perception of carbon dioxide capture and storage in the UK: results from focus groups and a survey. *Climate Policy* 4, 377-398.

Shi, J. Q., & Durucan, S. (2005). CO_2 Storage in Deep Unminable Coal Seams. *Oil & Gas Science and Technology, 60*(3), 547-558

Shi, J. Q., Durucan, S., & Shimada, S. (2014). How gas adsorption and swelling affects permeability of coal: A new modelling approach for analysing laboratory test data. *International Journal of Coal Geology, 128*, 134-142.

Shi, J.Q., Durucan, S., (2005). A model for changes in coalbed permeability during primary and enhanced methane recovery. *SPE Reservoir Evaluation and Engineering* 8 (4), 291–299.

Stangeland, A. (2007). A model for the CO_2 capture potential. *International Journal of Greenhouse Gas Control, 1*(4), 418-429.

Stevens, S. H., Kuuskraa, V. A., Gale, J., & Beecy, D. (2001). CO_2 injection and sequestration in depleted oil and gas fields and deep coal seams: worldwide potential and costs. *Environmental Geosciences, 8*(3), 200-209.

Stevens, S. H., Kuuskraa, V. A., Spector, D., & Riemer, P. (1999). CO_2 sequestration in deep coal seams: pilot results and worldwide potential. Greenhouse Gas Control Technologies, 175-180.

Sundquist, E.T., Burruss, R., Faulkner, S., Gleason, R., Harden, J., Kharaka, Y., Tieszen, L., Waldrop, M. (2008). *Carbon sequestration to mitigate climate change*: US Department of the Interior, US Geological Survey (https://pubs.usgs.gov/fs/2008/3097/pdf/CarbonFS.pdf)

Syed, A., Durucan, S., Shi, J. Q., & Korre, A. (2013). Flue Gas Injection for CO_2 Storage and Enhanced Coalbed Methane Recovery: Mixed Gas Sorption and Swelling Characteristics of Coals. *Energy Procedia, 37*, 6738-3745.

Vaughan, N. E., & Lenton, T. M. (2011). A review of climate geoengineering proposals. *Climatic Change, 109*(3-4), 745-790.

Viete, D. R., & Ranjith, P. G. (2006). The effect of CO_2 on the geomechanical and permeability behaviour of brown coal: Implications for coal seam CO_2 sequestration. *International Journal of Coal Geology, 66*(3), 204-216.

Vishal, V., Ranjith, P., & Singh, T. (2013b). CO_2 permeability of Indian bituminous coals: Implications for carbon sequestration. *International Journal of Coal Geology, 105*, 36-47.

Vishal, V., Singh, L., Pradhan, S., Singh, T., Ranjith, P., (2013a). Numerical modeling of Gondwana coal seams in India as coalbed methane reservoirs substituted for carbon dioxide sequestration. *Energy* 49, 384-394.

UNFCC (2016). The Paris Agreement - main page. [online] Unfccc.int. Available from: http://unfccc.int/paris_agreement/items/9485.php [accessed on 16/12/2016]

Wang, G. X., Zhang, X., Wei, X., Fu, X., Jiang, B., & Qin, Y. (2011). A review on transport of coal seam gas and its impact on coalbed methane recovery. *Frontiers of Chemical Science and Engineering*, *5*(2), 139-161.

Wang, X. (2007). Influence of coal quality factors on seam permeability associated with coalbed methane production (*PhD thesis*). University of New South Wales, Australia.

White, C.M., Smith, D.H., Jones, K.L., Goodman, A.L., Jikich, S.A., LaCount, R.B., DuBose, S.B., Ozdemir, E., Morsi, B.I., Schroeder, K.T. (2005). Sequestration of Carbon Dioxide in Coal with Enhanced Coalbed Methane Recovery: A Review. *Energy & Fuels*, *19*(3), 659-724.

Wong, S., Law, D., Deng, X., Robinson, J., Kadatz, B., Gunter, W.D., Jianping, Y., Sanli, F., Zhiqiang F. (2007). Enhanced coalbed methane and CO_2 storage in anthracitic coals—Micro-pilot test at South Qinshui, Shanxi, China. *International Journal of Greenhouse Gas Control*, *1*(2), 215-222.

2.10 Chapter summary

CO_2-ECBM has been identified as an economical coal bed methane production-enhancement technique, as this process has the ability to significantly enhance coal bed methane production, while sequestrating considerable amounts of CO_2 in deep coal seams. However, suitable coal seams for CO_2 sequestration and ECBM are located deep underground (> 800 m depths), where CO_2 is expected to be in its highly chemically active super-critical state. According to existing research, the injection of CO_2 into deep coal seams causes the induction of strain between the coal matrix and the adsorbing CO_2 layer, commonly known as *coal matrix swelling*. This swelling causes both seam permeability and strength to be significantly reduced and these reductions are considerably greater for super-critical CO_2. The permeability reduction causes the amount of injectable CO_2 and producible methane (CH_4) in coal seam to become unpredictable. In addition, the strength reduction affects the long-term safety of the ECBM and CO_2 sequestration processes, as it may cause the injected CO_2 to back-migrate into the atmosphere. Therefore, the injection of massive amounts of CO_2 into deep coal seams to harvest maximum amounts of methane from the seam while reducing the volume of anthropogenic CO_2 in the atmosphere has become a great challenge. Many studies have been conducted to date to investigate the effects of CO_2 storage in deep coal seams, both experimentally and numerically. However, the complexities associated with greater coal heterogeneity have resulted in difficulties in quantitatively and qualitatively validating the findings from the experimental work. Furthermore, environmental and human health risks, policies, regulations and public perceptions have made implementation of CO_2-ECBM challenging. Extensive laboratory tests on different types of coals can be used to obtain a clearer view of the effects of CO_2 sequestration in the coal mass in a controlled environment. These results can be used to support reservoir studies and then be extended to other advanced studies (risk assessment studies, economic optimization studies, project-screening models etc.).

PART 1 - CHAPTER 3

Materials, Instrumentation and Experimental Methods

3. Materials, Instrumentation and Experimental methods

3.1 Overview

The comprehensive research program developed to achieve the research objectives stated in Chapter 1 is shown in Figure 3.1.

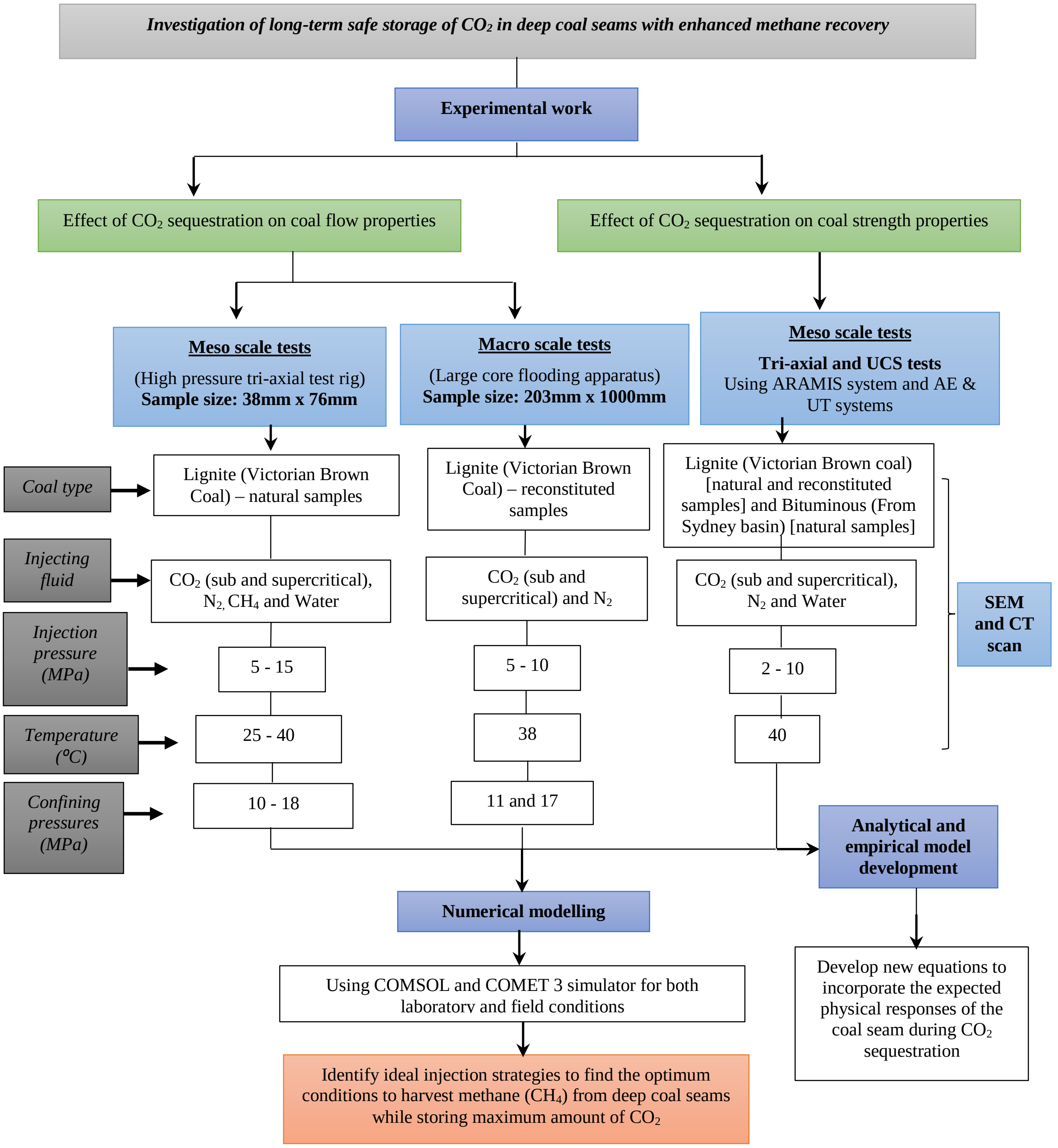

Figure 3.1. Detailed research plan

This chapter discusses the materials, instrumentation and experimental procedures adopted to complete the research plan shown in Figure 3.1. The first section highlights the materials used for the tests. For the present study, micro-, meso- and macro-scale studies were conducted to obtain an overview of the coal matrix changes during CO_2 sequestration. Further, coupled hydro-mechanical tests were conducted to investigate both the flow and mechanical properties of the coal mass during exposure to CO_2 for effective methane production and long-term safe storage of CO_2. The instrumentation, sample preparation and experimental procedures used for the testing of coal specimens are detailed next in this chapter under three main sections: micro-scale, meso-scale and macro-scale tests. Finally, the methods used for experimental permeability calculations are explained.

3.2 Test specimens used for the present research

3.2.1 Origin of materials

As observed in Chapter 2, many CO_2-ECBM studies have been conducted on high-rank coal specimens, but much less attention has been given to low-rank coal such as brown coal because of the scarcity of brown coal seams at depths suitable for CO_2 sequestration. As mentioned in Chapter 1, according to Garduno et al. (2003), the Jackson, Yegua and Wilcox formation in Texas has deep lignite formations (800 to 3800 ft from standard sea level (SSL)) with CO_2-ECBM potential. In the case of Australia, Hooper et al. (2005) and Jasinge (2010) stated that there are possible brown coal storage sites on- and off-shore of the Gippsland basin at 400 - 800 m depths. Further, the CO_2 produced from the coal power stations situated in Gippsland can be easily stored in the coal beds, which is advantageous and economical (Hooper et al., 2005). Hence, investigation of the possibility of using these brown coal seams for CO_2-ECBM is needed. Therefore, brown coal samples originating from the Hazelwood open-cut coal mine at Morwell, Gippsland, Victoria, Australia (Figure 3.2) were used for the present work to conduct the experiments. Figure 3.2 shows the location of the coal specimens obtained and an as-received coal block.

The Gippsland basin covers around 40,000 km^2 in south-eastern Australia and around 1/5 of the basin is on-shore while the rest of the basin is off-shore (Durie, 2013). The Gippsland basin first developed as a rift basin in Lower Cretaceous time with the deposition of arkoses, shales and conglomerates, which are now thin brown coal seam totalling overall more than 3 km in thickness (Knight 1975). In the Late Cretaceous to Early Eocene, renewed rifting activities occurred with the recommencement of subsidence and a sequence of sands, clays and precursors of brown coal seams were deposited over an area about 10 km on-shore and around 100 km off-shore. Subsidence continued through the Oligocene to Late Miocene period, and during this time thick coal seams like Morwell and Yallourn were formed (Durie, 2013). The Morwell formation consists of a complex unit of thick coal seams overlying the Traralgon formation in the Latrobe Valley Depression (Hocking 1972). The Morwell formation is dated to the Late Oligocene and Early Miocene by the occurrence of the middle and upper Proteacidites tuberculatus zone of fossils and radio-metrically by the basal and interbedded volcanic lavas of the Thorpdale volcanic group (Hocking 1972).

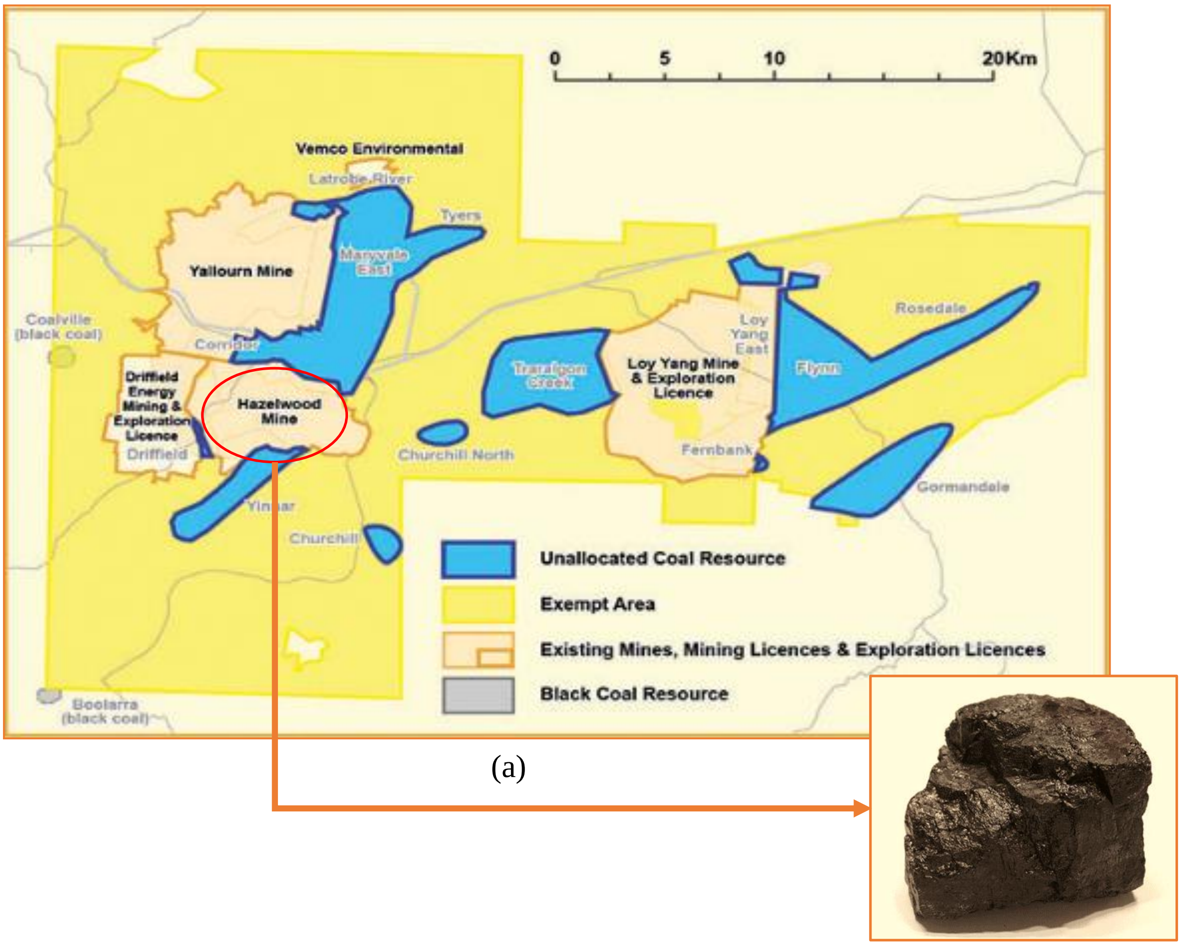

(a)

(b)

Figure 3.2. (a) Hazelwood open-cut coalmine, Gippsland, Victoria (created by the author using data from https://www.foe.org.au/articles/2014-03-18/victorian-government-wants-coal-export-industry) and (b) a brown coal block collected from the site

3.2.2 Structure and properties of Victorian brown coal

Victorian brown coal has unique physical and chemical properties compared to high-rank coals such as bituminous coal and anthracite. The effective and environmentally-friendly utilisation of the Victorian brown coal resource must consider its special structural features and properties and these are listed in the following sections.

3.2.2.1 Petrography of Victorian brown coal

Studies of Victorian brown coal in the Latrobe Valley seams indicate that these coal seams are mainly autochthonous (the coal has been fossilised by in situ grown materials) in origin (Hayashi and Li, 2004). Victorian brown coal has a colour ranging from red brown to dark brown with full natural moisture content (range of 50 - 70 %). In relation to the lithotypes of Victorian brown coal, five main lithotypes are identified, based on a study by George (1982) on coals from the Yallourn and Morwell formations. Further, George and Mackey (1991) summarised the characteristic maceral compositions of these lithotypes. The typical characteristics of the lithotypes and the characteristic maceral compositions are summarised in Table 3.1. According to George and Mackey (1991), Morwell brown coal has a maceral composition of 91.7% of Huminite, 6.9% of Liptinite and 1.2% of Intertinite (all the values are percentages of volume).

3.2.2.2 Physical and chemical properties of Victorian brown coal

Table 3.2 lists the physical properties of the brown coal specimens used for testing. Further, according to Li (2004), Victorian brown coal has various pore structures with a wide range of sizes, including macro-pores (>50 nm in diameter), meso-pores (2-50 nm), micro-pores (0.4-2nm) and sub-micro pores (<0.4 nm). The smaller pores are responsible for the large surface areas of Victorian brown coal (often exceeding 200 m^2/g), while larger pores contribute to the pore volume and porosity (Li, 2004). According to Woskoboenko et al. (1991), Victorian brown coal from the Morwell formation has a surface area of 214 – 313 m^2/g and a micro-pore volume of 0.053 – 0.084 cm^3/g.

Table 3.3 displays the typical mineral and non-mineral contents of Morwell brown coal from the Gippsland basin and Figure 3.3 gives the energy dispersive X-ray spectroscopy (EDS) element composition and the adsorption isotherms (Langmuir) of the brown coal samples used in the study.

Table 3.1. Typical characteristics of lithotypes (George 1982) and maceral composition (George and Mackey 1991) in Victorian brown coal

Lithotype	Dark	Medium- Dark	Medium - Light	Light	Pale
Abbreviation	Dk	M-d	M-l	Lt	Pa
Colour	Dark brown to black brown	Dark brown to medium brown	Medium brown to light brown	Light brown	Pale brown to yellow brown
Texture	High wood content, often small fragments	High to medium wood content, often large pieces	High to low wood content, often well preserved	Medium to low wood content	Wood present but uncommon
Gelification	Gelification particularly of wood material	Some gelification but not extensive	Gelification uncommon, confined mainly to wood	Gelification rare	Gelification very rare
Weathering pattern	Wide and deep cracks, regular pattern	Wide cracks, some regularity of pattern	Shallow cracks, irregular patterns	Generally fine cracks, random orientations	Few extensive cracks
Physical properties	Strong, hard, high density	Variable strength, above average hardness and density	Intermediate physical properties	Generally soft, low density	Soft, crumbles readily, very low density
Maceral composition	- Higher content of destinite - Higher amount of liptinite macerals (suberinite, cutinite and resinite) and inertnite macerals (fusinite and semi-fusinite) - A concomitant decrease in liptinite content (dominated by sporinite and liptodetrinite)		- High concentrations of detrovitrinite and liptinite - Low concentrations of telovitrinite and gelovitrinite		

Table 3.2. Physical properties of Victorian brown coal

Physical property	Typical value
Coal density (g/cm^3)	1.04 – 1.1
Moisture content (% wb)[1]	57 – 66
Fixed carbon (% db)[1]	48[2]
Ash yield (% db)[1]	1.7
Volatile matter content (% db)[1]	50.3[2]
Vitrinite reflectance (%)	0.0 – 0.4[3]
Porosity (%)	67-69[4]

[1]wb – wet basis, db – dry basis; [2]From Li (2004); [3]From De Silva (2013); [4]Jasinge (2010)

Table 3.3. Typical mineral and non-mineral contents of Morwell brown coal (% dry basis) (Brockway and Higgins, 1991)

SiO_2	Al_2O_3	K_2O	TiO_2	FeS_2	Ca	Mg	Na	Cl	Total S	Total Fe
0.14	0.08	0.007	<0.005	0.02	0.54	0.31	0.09	0.07	0.30	0.21

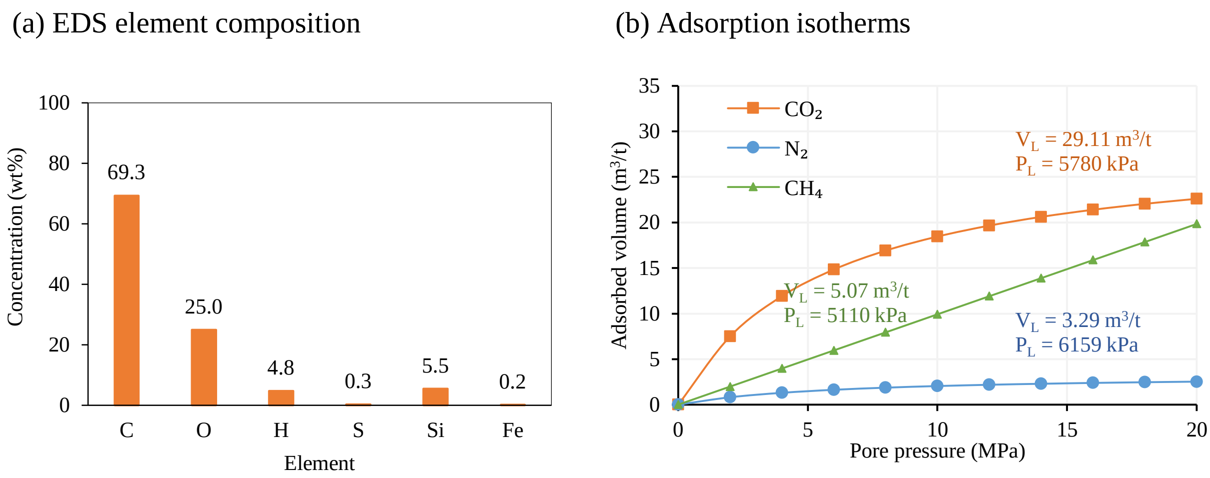

Figure 3.3. Energy dispersive X-ray spectroscopy (EDS) element composition and adsorption isotherms (Langmuir) of the brown coal samples used for the study

3.2.3 Scale of the test samples

For the present research, micro-, meso- and macro-scale brown coal samples were used to conduct the experiments (Figure 3.4), and standard laboratory testing was conducted using meso-scale samples. Further, micro-scale samples were used to gain insight into the underlying physics of the samples during CO_2 injection, while macro-scale samples contributed to making a field-scale environment for the test specimens (Figure 3.4). The instrumentation and experimental methodologies adopted for each type of test are described in the following sections.

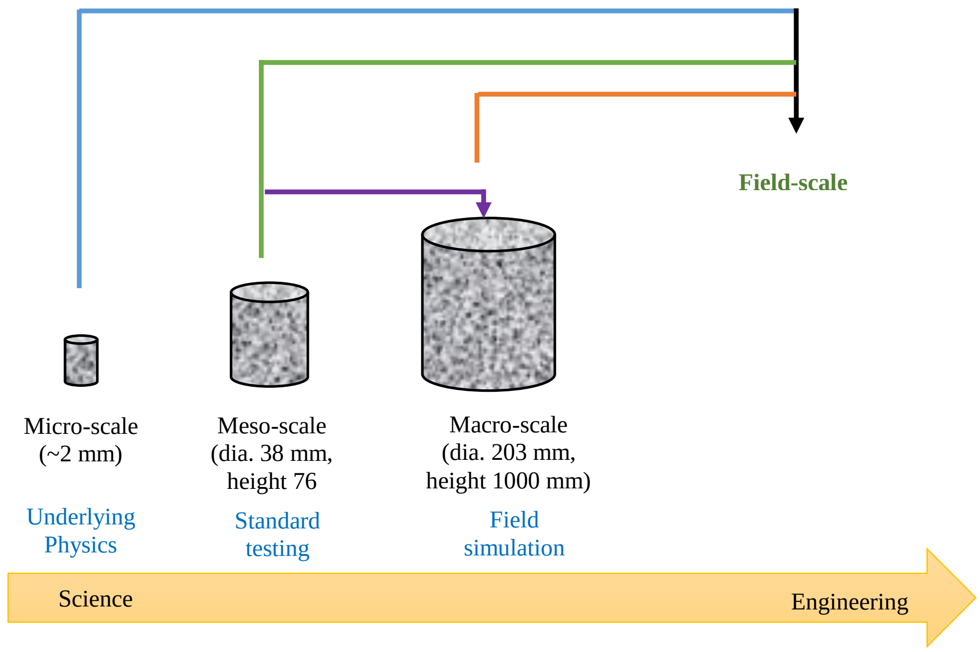

Figure 3.4. Scale of the test samples used for the experimentations

3.3 Micro-scale experiments on brown coal

Micro-scale experiments were conducted using the FEI Quanta 3D Field Emission Scanning Electron Microscope in the Monash Centre for Electron Microscopy (MCEM) and the X-Ray Microscopy Facility for Imaging Geo-materials (XMFIG) at Monash University. The following sections describe the methodology for the micro-scale experiments.

3.3.1 Instrumentation

3.3.1.1 FEI Quanta 3D Field Emission Scanning Electron Microscope

Figure 3.5 shows the FEI Quanta 3D field emission scanning electron microscope which was used for the micro-scale tests. The MCEM FEI Quanta 3D is a dual-beam scanning electron microscope (SEM) that is also equipped with a focused ion beam (FIB). The SEM functions permit microscopic observations of specimens, while the FIB functions allow cutting of samples with sub-micron precision. The Quanta is equipped with a “warm” or Schottky-type field emission gun (FEG), capable of both high-resolution imaging, low vacuum operation (for analysis of uncoated samples) and environmental SEM (ESEM) operation. The microscope is equipped with a range of detectors, including an in-chamber secondary electron detector (E-T type), a detachable four-quadrant back-scattered electron detector (BSED), a retractable annular scanning transmission electron microscopy detector (STEM), an in-chamber low vacuum secondary electron detector (LVSED), a detachable gaseous secondary electron detector (GSED – ESEM), a detachable Deben cool stage (-25 °C to +50 °C at 300Pa), an Edax Apollo XP 10 mm^2 silicon drift detector (SDD) for energy-dispersive X-ray analysis (EDX), an Edax Hikari XP electron back-scattered electron detector (EBSD) and a Gatan X-ray ultra-microscope (XuM) detector and detachable target module and rotation stage (MCEM, 2016).

(a) Front view

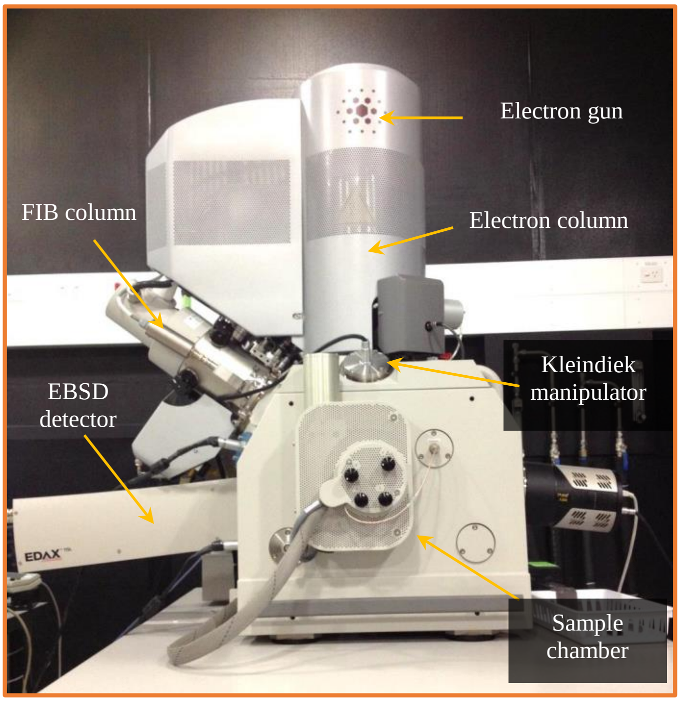

(b) Rare view

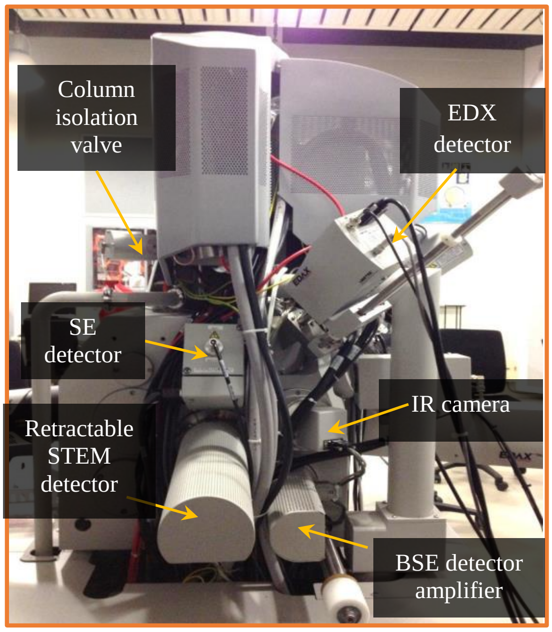

Figure 3.5. FEI Quanta 3D field emission scanning electron microscope

3.3.1.2 X-Ray Microscopy Facility for Imaging Geo-materials (XMFIG)

Figure 3.6 shows the high-resolution X-ray computed tomography (CT) machine in the Civil Engineering Department at Monash University which was used for the non-destructive three-dimensional imaging of coal samples. This X-Ray CT facility has a Zeiss Xradia 520 Versa 3D X-ray microscope, which enables sub-micron viewing of the micro-structural characteristics of samples. It has a unique set of objectives (0.4X, 4X, 20X, 40X), which allows scanning of small sub-regions within a large specimen. Further, this machine can achieve spatial resolution of 0.7 µm and has a minimum achievable voxel of 70 nm. Further, two-stage magnification that provides resolution at a distance (RaaD), delivering large, flexible working distances while maintaining sub-micron resolution is another advantage of this machine. Enhanced absorption contrast detectors maximize the collection of contrast-forming low-energy X-ray photons that are critical to imaging numerous material types. Tuneable propagation phase contrast is used to visualize low Z materials and biological samples that tend to have limited absorption contrast. Non-destructive X-ray microscopes uniquely characterize the microstructure of materials in simulated conditions in situ as well as the evolution of properties over time (4-D) and support a wide variety of in situ rigs for sub-micron imaging of samples up to inches in size in environmental chambers (triaxial, UCS and 1-D compression) and under varying conditions (Zeiss.com, 2016). RaaD enables the Xradia Versa to maintain high resolution as the space between the X-ray source and sample grows, whereas the resolution of conventional micro-CT architecture degrades when samples are placed in spacious in-situ chambers.

Figure 3.6. X-Ray microscopy facility for imaging geo-materials

3.3.2 Sample preparation

3.3.2.1 For SEM analysis

For the SEM analysis, 2 mm size coal particles were carefully obtained from the coal sample by tapping one end of the sample (in order not to damage the pore structure). The particles were then saturated under different CO_2 pressures, similar to the test conditions used for the meso-scale sample saturation. Upon saturation of the samples, they were stored in a small container and sealed until the samples were taken to MCEM for sample preparation. Next, the samples were adhered onto double-sided adhesive carbon tape attached to a circular specimen stub (Figure 3.7). Three to four particles were adhered to each specimen tub and N_2 gas was then spread all over the tub using a compressed air line to confirm the removal of loose particles. The specimens were double-coated with platinum (Pt) to enhance their conductivity and avoid the charging effect during exposure to the electron beam.

Figure 3.7. Specimens prepared for SEM analysis

3.3.2.2 For X-ray CT scanning

The non-destructive X-ray CT scanning process did not require any special sample preparation procedure. The meso-scale (54 mm in diameter and 108 mm high) reconstituted coal samples were scanned under the X-ray CT facility after completing the different fluid (CO_2 and water) saturations. The CT scanning was done in three stages added together to achieve the108 mm sample height.

3.3.3 Experimental procedure

3.3.3.1 SEM analysis

The micro-structural changes in the natural coal samples saturated with CO_2 and N_2 were observed by SEM analysis. Here, the specimens were viewed at 15 kV voltage with 4.5 spot size. The voltage and spot sizes used for the SEM analysis of brown coal samples were comparatively low values to avoid the charging effect produced by the build-up of electrons in the sample. It occurs when the number of electrons leaving the sample is less than those entering. As brown coal is an insulating material, the electrons have no escape path from the sample and this results in charging. Charging can cause many unusual side-effects, including bright flashing on the screen, image distortions, image shift and unusual contrast. Reducing the voltage, spot size or aperture and sample coating can minimise this charging effect. Further, the low-vacuum mode was used while operating the SEM machine, as brown coal is subjected to higher outgassing. Twelve to twenty SEM images were captured at different magnifications for each sample to clearly visualise and compare the changes in the pore structure. Figure 3.8 shows a sample holder of the FEI Quanta 3D, and Figure 3.9 presents a schematic of how SEM images are captured.

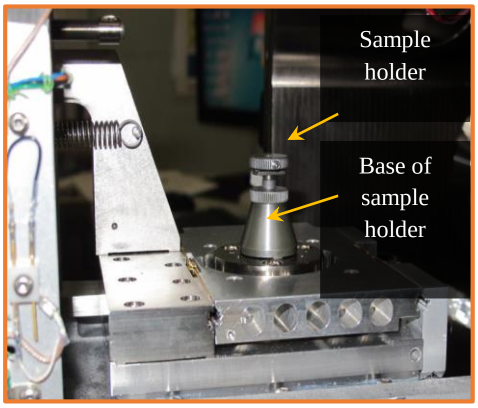

Figure 3.8. Sample holder of FEI Quanta 3D

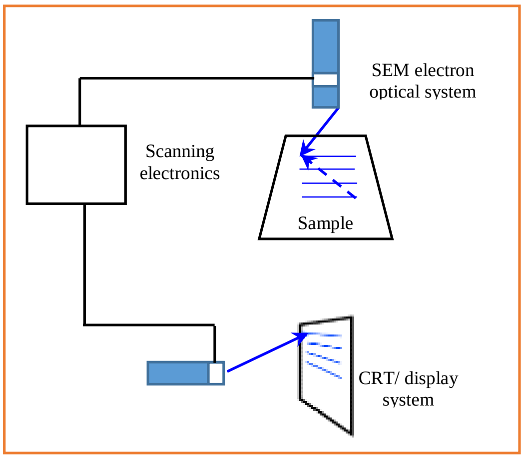

Figure 3.9. Sample scanning and image display in SEM analysis

3.3.3.2 X-ray CT scanning

High-resolution images were also taken of the RC samples with unsaturated, water-saturated and CO_2-saturated conditions. Image projections were acquired by rotating the load stage 360° around its vertical axis and the frame size of the projections was 1024×1024 pixels. The scanning was carried out under full view mode using the scanning in Table 3.4, thus providing a fixed resolution of 60 microns for the qualitative analysis of all images. The images taken at the middle of each sample were used for the analysis to avoid any possible damage at the ends of the samples. Figure 3.10(a) shows a schematic of how the X-ray CT scanning images are captured and Figure 3.10(b) shows the sample set-up to capture images.

Table 3.4. Scanning parameters used to scan the samples

Parameter	Value/Description
Source-to-sample distance	200 mm
Detector-to-sample distance	57 mm from the central axis of the sample
Voltage	140 keV
Power	10 W
Lens	0.4X macro-detector

(a)

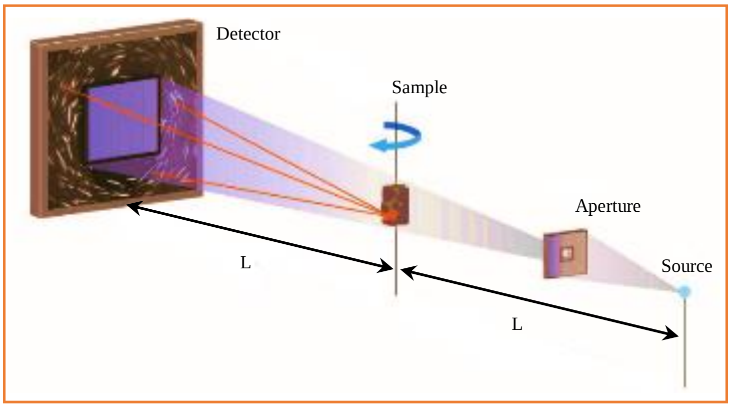

(b)

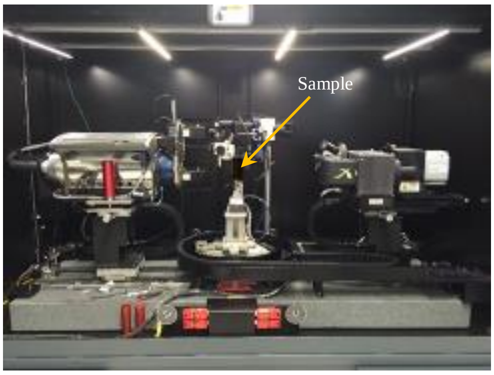

Figure 3.10. (a) X-ray CT image capture and (b) Sample set-up for image capture

3.4 Meso-scale testing

Meso-scale flow and strength experiments were conducted using the high-pressure tri-axial test rig, compressive strength testing apparatus and high-pressure saturation chambers available in the Deep Earth Energy Research Laboratory (DEERL) at Monash University (Ranjith and Perera, 2011). The following sections describe the methodology for the meso-scale experiments.

3.4.1 Instrumentation

3.4.1.1 High-pressure tri-axial test rig

A high-pressure tri-axial test rig (Figure 3.11) was used to conduct both flow and strength meso-scale experiments under representative down-hole pressures and temperature conditions for brown coal specimens. This set-up consists of a pressure cell which has the ability to withstand a 70 MPa confining pressure, 100 kN axial load and a maximum temperature of 80 ^{0}C. The loading unit comprises an S-type load cell and a loading frame capable of withstanding 100 kN. The loading cell placed between the top of the loading frame and the loading shaft applies the load on the sample when the cell base is moved upward. The direction and speed of cell base movement can be controlled using the load control unit (Figure 3.11) and the axial displacement is measured using an LVDT. The plumbing system consists of five major units: confining unit, gas injection unit, gas outlet unit, water injection unit and heating unit.

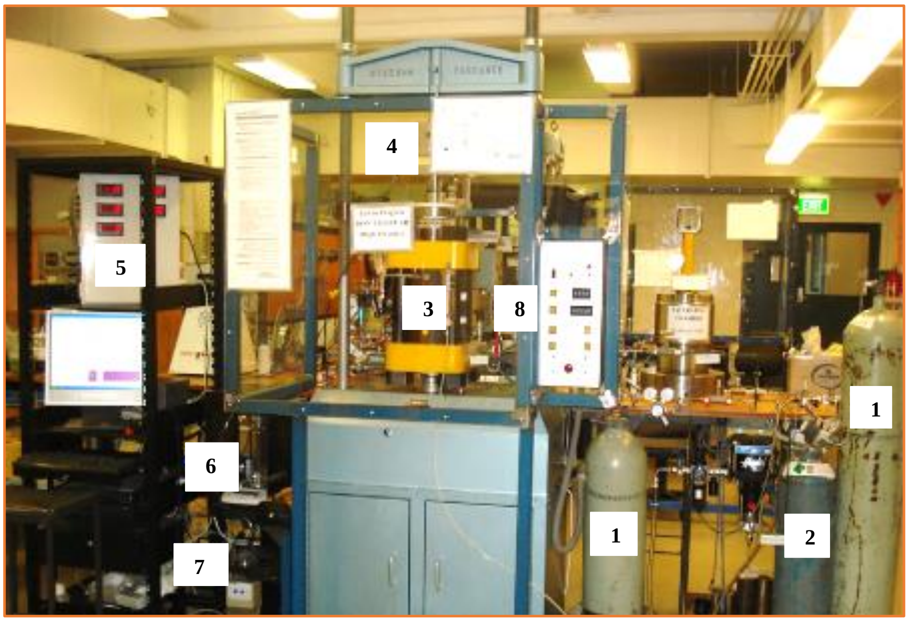

1. CO_2 bottles
2. N_2 bottle
3. Pressure cell
4. Load cell
5. Data acquisition system
6. Deshler bottle
7. Flow meter
8. Load control unit

Figure 3.11. High-pressure tri-axial test rig used for sample testing

The confining unit is used to apply the required down-hole pressures to the samples and is achieved by pressurizing hydraulic oil. The oil is stored in an oil reservoir (Figure 3.12(a)) and a syringe pump (ISCO Teledyne – 260 D) is used to pressurize the oil after sending it to the pressure cell. The oil level variation in the syringe pump is recorded and used to obtain the volumetric strain of the tested coal specimens. The gas injection unit can inject both CO_2 and N_2 into the sample. A compressed gas CO_2 bottle (D size - maximum pressure 5 MPa) is used to inject low-pressure CO_2 and is controlled by a pressure regulator. A CO_2 compressed liquefied gas bottle (G size - maximum pressure 5.7 MPa) is used to inject high-pressure CO_2 and the higher pressures are achieved by an ALG-60 type air-driven gas booster (up to 50 MPa) (Haskel International) (Figure 3.12(b)). To inject N_2, a compressed gas N_2 bottle (E size - maximum pressure 20 MPa) is used and the pressure is varied using a pressure regulator. For higher N_2 pressures, the above-mentioned gas booster is used. Similar to the advanced core-flooding apparatus, the outlet pressure is measured by a pressure transducer and the gas flow rate is measured by a MGC-1V3.0 type Ritter milli gas counter (Ritter Apparatebau) (Figure 3.12(c)). The water flow mass rate is measured by a Deshler bottle, which sits on an electronic balance (Figure 12(d)).

In addition to gas injection, the set-up is able to inject water up to a pressure of 35 MPa using a MP-350 hydraulic pump (Enerpac). To ensure the higher temperatures required in deep coal seams, a heating unit with a working temperature of 50 ^{0}C is used. It has a heating blanket (190 mm diameter and 200 mm in length) around the cell to apply the temperature to the sample and a 2 m long section of the upstream injection unit is wrapped using a heating tape to confirm the injection of super-critical CO_2 (greater than 31.8 ^{0}C) into the sample. The temperature of both cell and tubing is controlled by a temperature control box. All the data acquired from the pressure transducers, LVDT, load cell, temperature unit, and gas outlet unit are translated from analogue to digital data using a DT9834-32-0-16-STP data translation module and recorded using QuickDAQ software. A schematic diagram of the apparatus with the aforementioned units is presented in Figure 3.13. Furthermore, this set-up has the ability to carry out high-pressure tri-axial strength tests, two-phase or three-phase flow tests, and hydro-fracturing using water or gas (N_2/CO_2), together with an acoustic emission facility for sedimentary rocks (see Section 3.4.1.5).

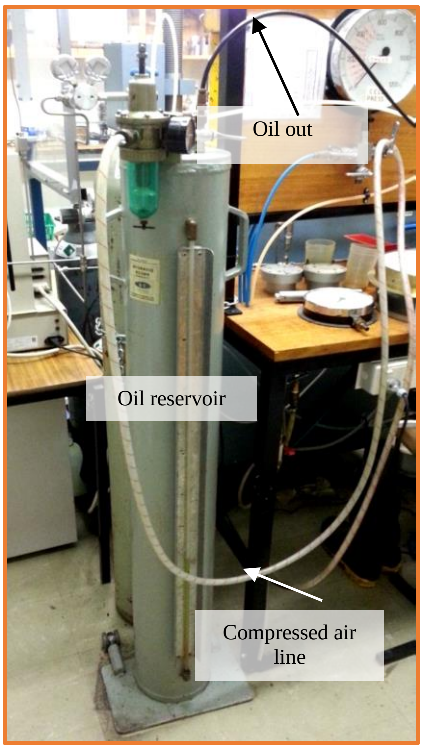

(a) Oil reservoir

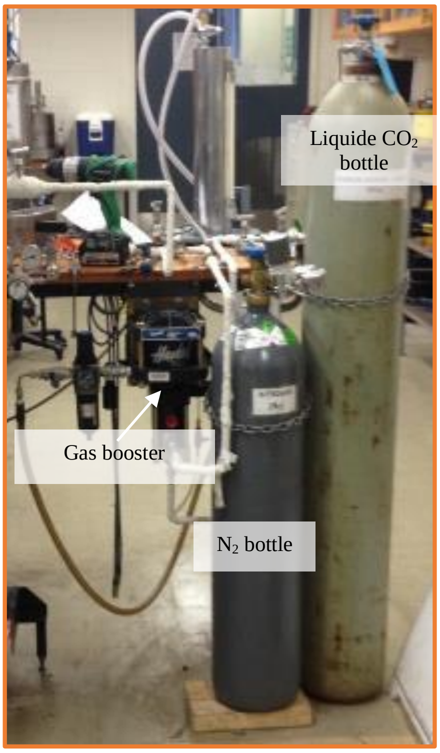

(b) Gas booster

(c) Gas flow meter

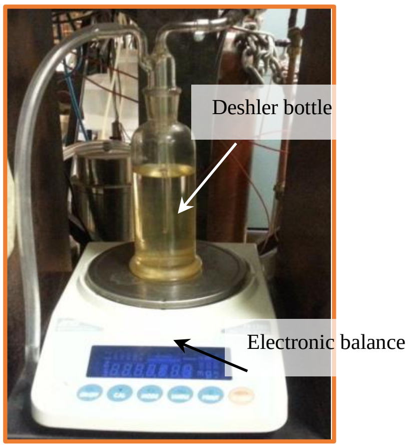

(d) Water mass flow rate measurement unit

Figure 3.12. Components of high-pressure tri-axial test rig

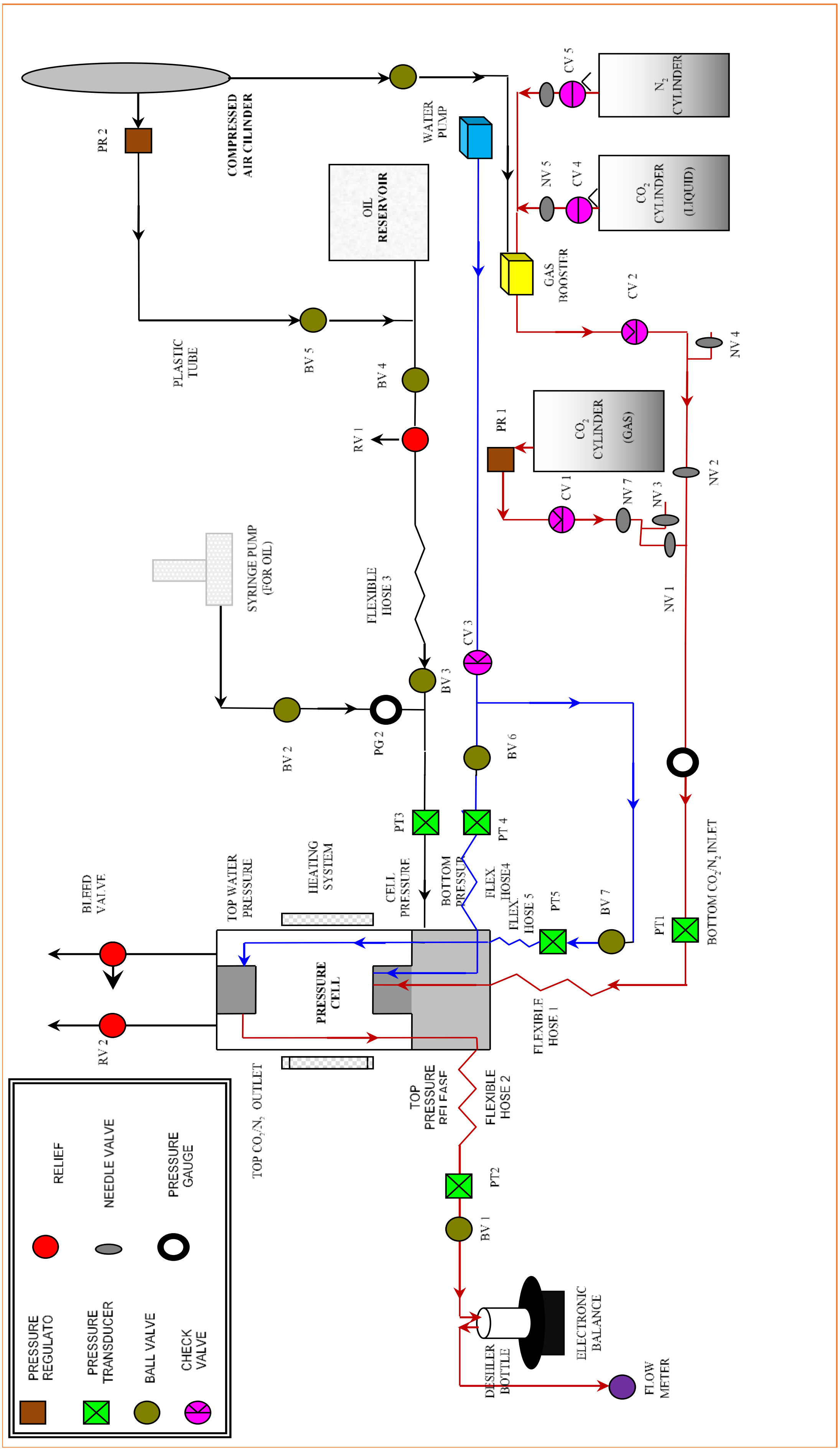

Figure 3.13. Schematic diagram of the high pressure tri-axial test rig

3.4.1.2 Modified high pressure tri-axial test rig for CO_2-ECBM experiments

In order to conduct experiments on CO_2-ECBM, the existing high-pressure tri-axial test rig developed by Ranjith and Perera (2011) was modified by including a CH_4 injection unit upstream and a CO_2/CH_4 concentration measuring unit downstream.

- *CH_4 injection unit at upstream*

A new gas line was added to the existing gas injection unit to inject CH_4 into the coal samples (Figure 3.14). A 750 litre CH_4 bottle (maximum pressure 15 MPa) was used with a purity of 99.95 % of CH_4 and a pressure regulator was used to obtain the required pressures during testing. However, there are strict rules and regulations for using CH_4 in laboratory-level testing, due to the risks associated with the flammability of CH_4. According to Occupational Health and Safety (OHS) guidelines, the safe volume of CH_4 in a room is less than 4.4% of the room volume. Therefore, a simple calculation of the expected maximum CH_4 level in the laboratory was done to ensure that the modified CH_4 system met the safety requirements as follows.

The volume of the room	=	$12 \times 9 \times 4$ m^3
	=	432 m^3
Volume of CH_4 in bottle	=	0.75 m^3

If the whole bottle leaked, the % of CH_4 that would leak into the room

$$= (0.75/432) \times 100$$

$$= 0.173 \text{ \%VOL} <<<< 4.4 \text{ \%VOL}$$

Hence, theoretically an explosion would not occur even if the whole CH_4 volume of the bottle leaked into the room environment. However, CH_4 is lighter than air and can accumulate near the ceiling. Further, the percentage of CH_4 accumulating at the ceiling may be higher, depending on the air circulation in the room. Therefore, a CH_4 detector (Figure 3.15) was installed near the ceiling, reducing the overall risk to a very low level.

- *CO_2/CH_4 concentration measurement unit at downstream*

To identify and measure the concentration of CO_2 and CH_4 in the downstream gas-out line, a CO_2/CH_4 infrared gas sensor (Gascard NG sensor by Edinburgh sensors) (Figure 3.15) was installed downstream after the Deshler bottle. This system includes automatic temperature and pressure corrections and enables real-time environmental condition measurements, thus providing true concentration readings and reliable measurement of target gases. The Gascard NG sensor head and electronics are mounted on a Eurocard printed circuit board (PCB) with a number of bitswitches, which enable the user to control various aspects of the sensor's behaviour including analogue output and filter type selection. It is backward-compatible with outputs from existing Gascard generations and has on-board true RS232 communications along with the option of TCP/iP communications protocol. The Gascard NG has built-in features for multi-gas and multi-sensor operation, together with on-board data logging and has the flexibility to incorporate additional gas detection technologies. This system can ultimately provide the percentage of concentration of CO_2 or CH_4 in the downstream gas at prescribed time intervals (1 s in the present research).

(a) New CH_4 system

(b) CH_4 alarm system

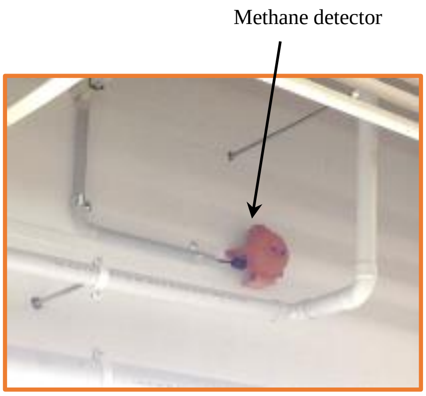

(c) CH_4 detector

Figure 3.14. Components of new CH_4 system

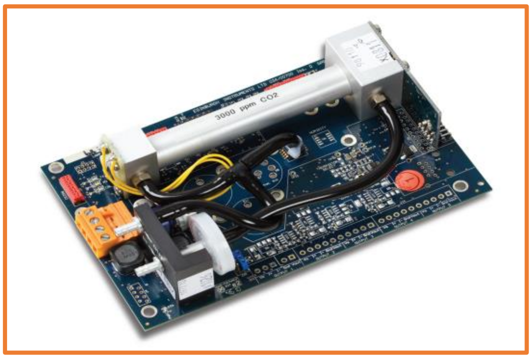

(a) Gascard NG sensor

(b) CO_2/CH_4 infrared gas sensor

Figure 3.15. CO_2/CH_4 measurement unit at downstream

A schematic diagram (main components) of the modified high-pressure tri-axial test rig is shown in Figure 3.16. Figure 3.17 summarises the working capabilities of the high-pressure tri-axial test rig after the modifications. The test conditions used for the experiments on brown coal are explained in Chapters 4, 6 and 7.

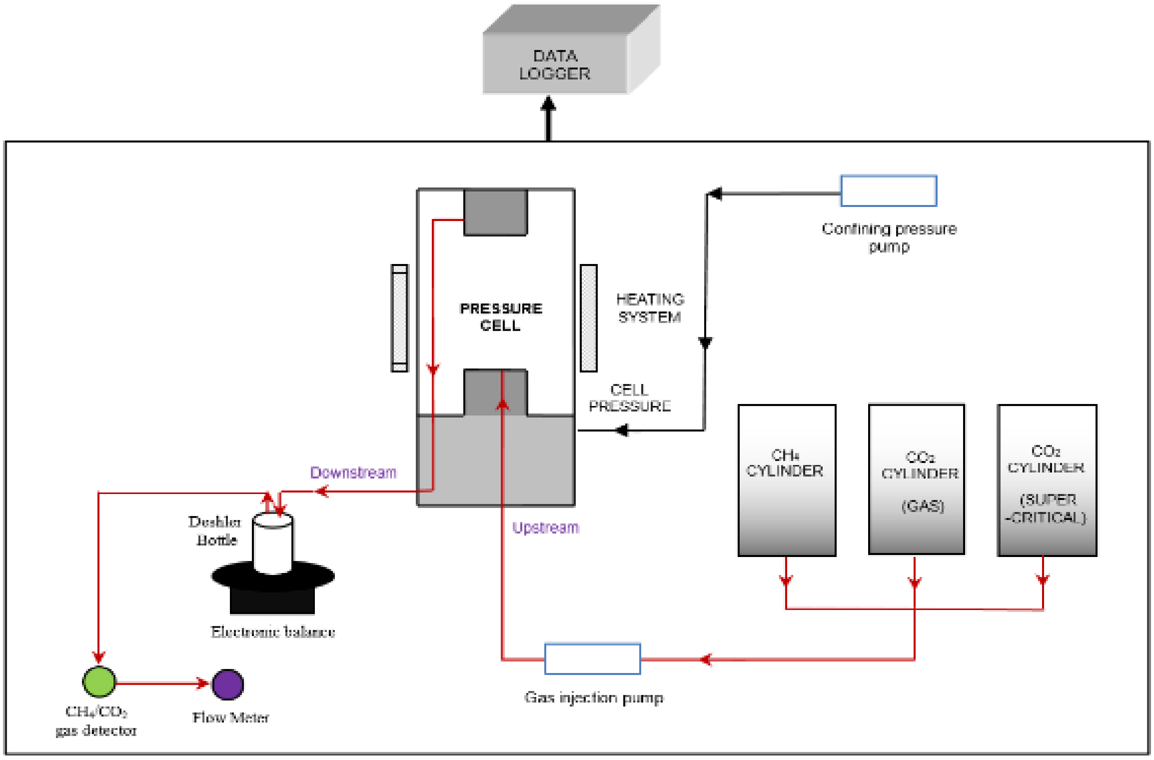

Figure 3.16. Schematic diagram of the modified high-pressure tri-axial test rig

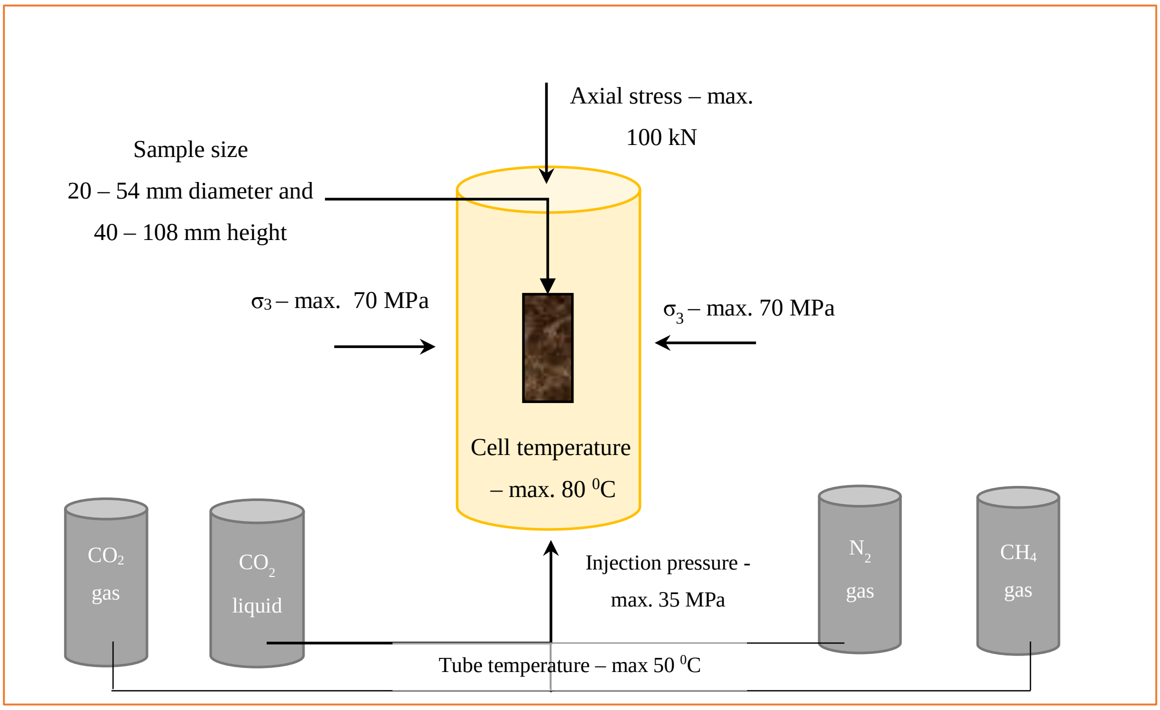

Figure 3.17. Summary of working capabilities of modified high-pressure tri-axial test rig

3.4.1.3 Compressive strength apparatus

A Shimadzu uniaxial compression/tension machine (AGS-X Series dual column electromechanical test frame – floor model) available in the DEERL at Monash University, Australia (Figure 3.18(a)) was used for the compressive strength tests and reconstituted sample preparation. The ±0.5 % accuracy load cells with a wide range from 1/1 to 1/500 of the maximum capacity help improve testing efficiency because multiple tests can be performed without switching load cells and accessories. Furthermore, high-speed data sampling of up to 1 kHz ensures that every possible strength change is captured. The maximum capacity of the set-up is 300 kN and the tests were performed using the displacement control method at specified displacement rates. The axial displacement and the respective loads were recorded using DeFriend software and used to plot stress-strain graphs to obtain the respective strength parameters.

3.4.1.4 ARAMIS optical strain measurement system

An ARAMIS optical strain measurement system (by GOM), with two high-resolution cameras and a software system, was used to capture the strain behaviour during the load application in compression testing. ARAMIS is a non-contact and material-independent measuring system based on digital image correlation. It offers a stable solution for full-field and point-based analyses of test objects of just a few millimetres up to structural components of several meters in size. The system performs high-precision measurements with a 3-D measurement resolution in the sub-micrometre range, regardless of the specimen’s geometry and temperature. For statically- or dynamically-loaded specimens and components, ARAMIS provides accurate 3-D coordinates, 3-D displacements, velocities, accelerations, surface strains and evaluation of 6 degrees of freedom (Gom.com, 2016).

A pair of cameras is used to record the deformation of the structure by tracing discrete correlation areas within stereo images, and the system attempts to counterpart the areas in the stereo images from the cameras at each time step. The ARAMIS 3D camera is a stereo camera system which delivers precise 3-D coordinates based on triangulation and using stochastic patterns or reference-point markers. In order to capture stereo images using the ARAMIS system, the test specimens should have adequate image variation in tone and contrast all over to exclusively identify the correlation areas. This was accomplished by painting the sample surface with matt white paint, followed by spreading a pattern of matt black paint dots on the surface (Figure 3.18(b)). Prior to testing, thorough calibration was carried out using a calibration plate with a known pattern of white dots on a black background. Once the cameras were calibrated, testing of actual specimens was commenced.

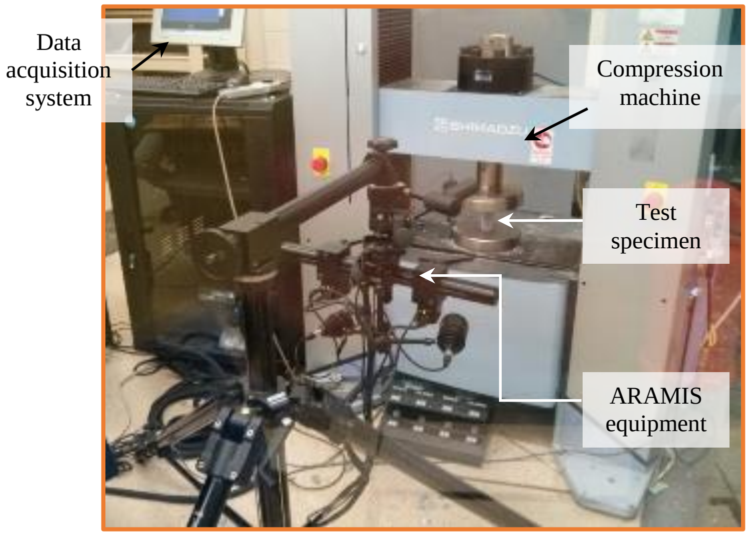

(a) Compression machine and the ARAMIS system

(b) Typical coal sample prepared for ARAMIS image capture

Figure 3.18. Set-up for meso-scale unconfined strength testing

3.4.1.5 Acoustic emission (AE) system

To identify the fracture propagation behaviour and strain energy release of the coal specimens under load application during the UCS testing, an advanced acoustic emission system (AES) manufactured by Physical Acoustic Corporation (PAC: MISTRAS-2001) was used. Generally, AE refers to the elastic waves emitted by materials undergoing microscopic changes of stress state. An AE waveform induced by a propagating crack conveys information regarding the location, crack growth distance, velocity and orientation of the crack (Wadley, 1986). An AE activity is endorsed to the rapid release of energy in a material and that energy release can be related to the energy content of the AE signal (Wasantha et al. 2014). These AE activities can be captured using AE sensors which first convert the mechanical signals from specimens under test to pre-amplified electrical signals and finally to a post-amplified AE count after a suitable filtration process.

Generally, the AE count refers to the number of times an AE signal amplitude exceeds a specified threshold value (refer to Figure 3.19). In the experiments, AE sensors were attached in series to the sample at either side of the specimen (Figure 3.20) to capture the AE activities. To easily attach the sensors and to obtain the same sensitivity for each sensor, an electron wax was used. Considering the brittleness of the brown coal samples, the AE trigger sensitivity was set to 60 dB. When the specimen was ready to be tested, both load application and the AE system were started simultaneously.

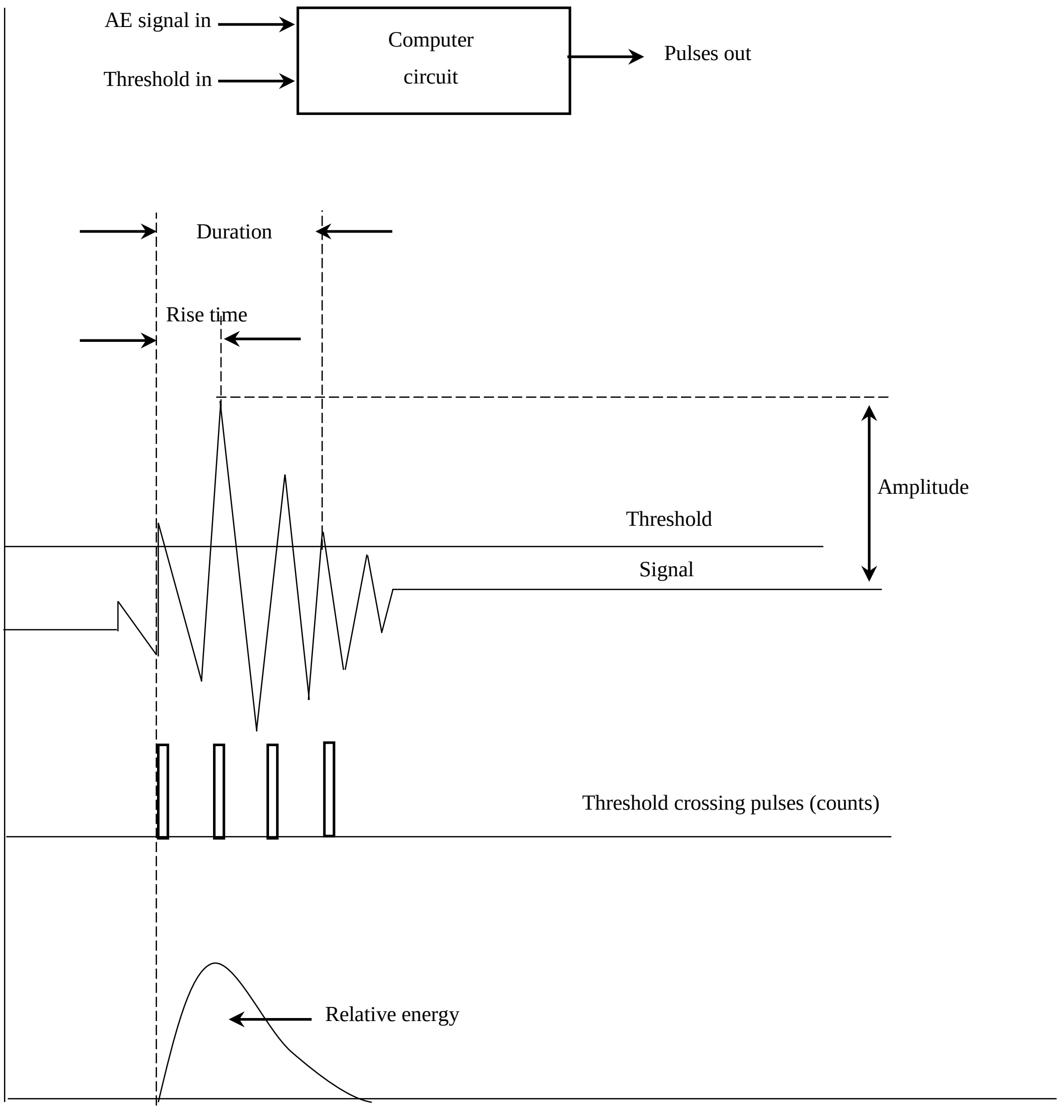

Figure 3.19. Definitions of different parameters of an AE signal (Roberts and Talebzadeh, 2003)

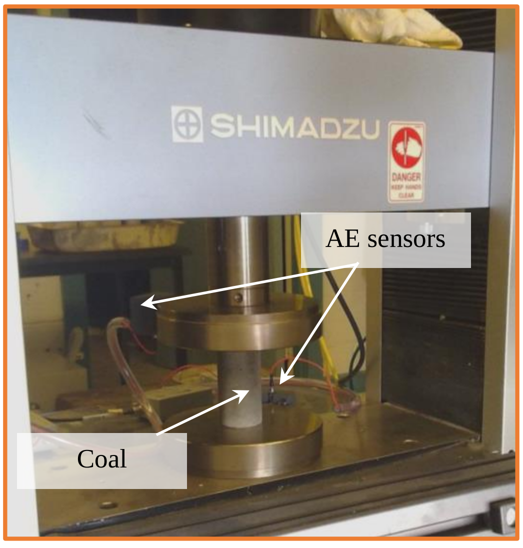

Figure 3.20. Coal sample prepared for capturing acoustic emission signals with AE sensors

3.4.1.6 High-pressure saturation chambers

The high-pressure saturation chamber (Figure 3.21) available in the DEERL (Lakmali and Ranjith, 2015) was used to saturate the coal samples at various CO_2 pressures prior to strength testing. This apparatus can be used to saturate samples up to 10 MPa saturation pressure and includes an advanced temperature control system (a thermal blanket and temperature control box) to maintain the system temperature, which can reach a maximum of 150 ^{0}C. CO_2 is injected using a G-size compressed liquefied gas bottle (maximum pressure 5.7 MPa) through a syringe pump (ISCO Teledyne – 500D). Inlet and outlet gas pressures are measured by pressure transducers and monitored until the end of each test series to check any pressure leakage from the cell. Five such pressure cells are available in the DEERL one of which can accommodate samples with a maximum diameter of 63 mm and a maximum sample height of 126 mm. Further, the cells can hold around 4 ~ 6 samples 38 mm in diameter and 76 mm in height and 10 ~ 12 samples 25 mm in diameter and 50 mm in height. The cells can be customized with a stirrer on the cell instead of the lid to saturate powder samples with a liquid (water or brine) while injecting CO_2 (Lakmali and Ranjith, 2015).

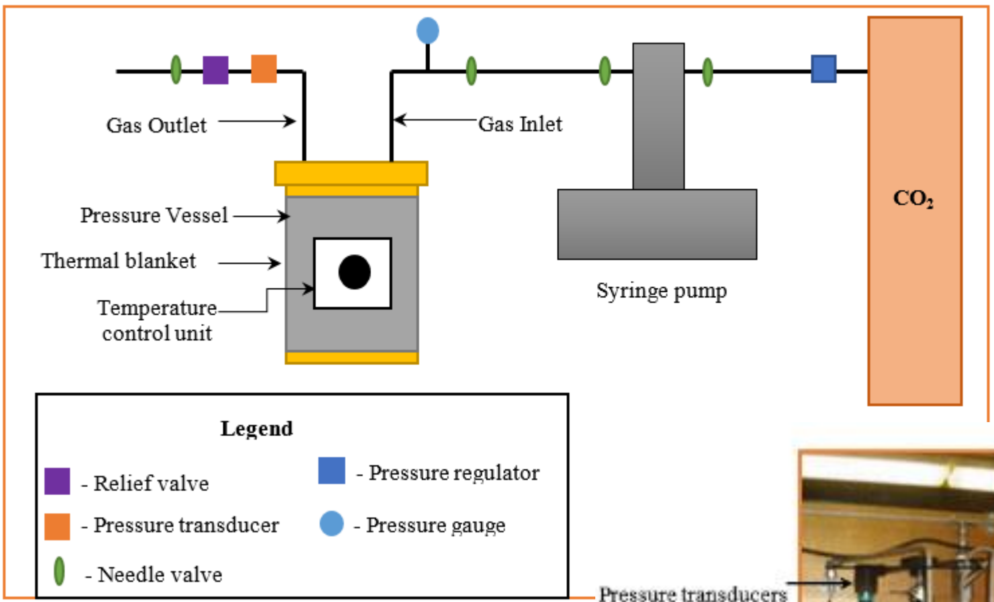

(a) Schematic diagram

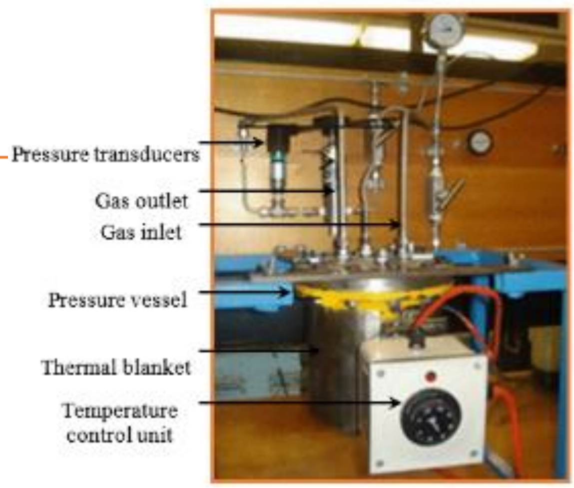

(b) High-pressure saturation chamber

Figure 3.21. High-pressure CO_2 saturation chamber

3.4.2 Sample preparation

3.4.2.1 Natural samples

The large coal blocks acquired from the Hazelwood open-cut coal mine were cored to a 38 mm diameter using the coring machine available in the DEERL (Figure 3.22(b)). The coring barrel consists of an end-diamond cutter and the coring rates can be easily adjusted to the required sample diameter and length. Both wet and dry coring can be performed and wet cutting was used for the present study to obtain smooth axial walls (in some cases dry cutting burns the coal sample). The cored coal samples were then cut to around 80 to 82 mm in height (slightly higher than the required coal sample height of 76 mm) using a diamond cutter available in the DEERL (Figure 3.22(c)). Wet cutting was used to cut the samples at very slow rates to avoid damage to the sample surface. After cutting, the sample surface was smoothened by grinding the two surfaces using a rock grinding machine (Figure 3.22(d)). To achieve two parallel smooth surfaces (for the application of axial compression during loading), after grinding one side of the sample, the whole V-block was rotated 180^0 to grind the other surface (Figure 3.22(d)). After grinding, the coal sample height was approximately 76 mm (Figure 3.22(e)). After the sample preparation process, all the samples were wrapped in polythene bags and kept in the fog room available in the Civil Engineering Department at Monash University to minimise natural moisture loss until they were used for the experiments.

3.4.2.2 Reconstituted (RC) samples

To study the effect of heterogeneity of coal using CO_2 injection, reconstituted (RC) samples were used, as RC samples are more homogeneous than natural samples. Further, previous studies (Jasinge 2010; De Silva 2013; Vishal & Singh 2013) have shown that the development of RC samples has the ability to assist in making useful correlations between the mechanical properties of coal. Furthermore, Jasinge (2010) (for brown coal) and Vishal & Singh (2013) (for black coal) developed a method of preparing reconstituted coal samples, which has focused mainly on no-binder reconstituted coal and was adopted for the present study. The apparatus used for RC sample preparation was a steel mould, 54 mm in diameter and 210 mm in height, with a cylindrical steel compaction ram. All the components of the steel mould, including the inner rim of the mould, base plate, seepage holes and compaction ram, were first cleaned. Once the steel mould was cleaned, the inner rim of the mould and base plate were greased. In addition, a thin layer of plastic wrap was fitted onto the base plate to ensure smooth recovery of the RC sample. The mould was then assembled by tightening the side and bottom bolts.

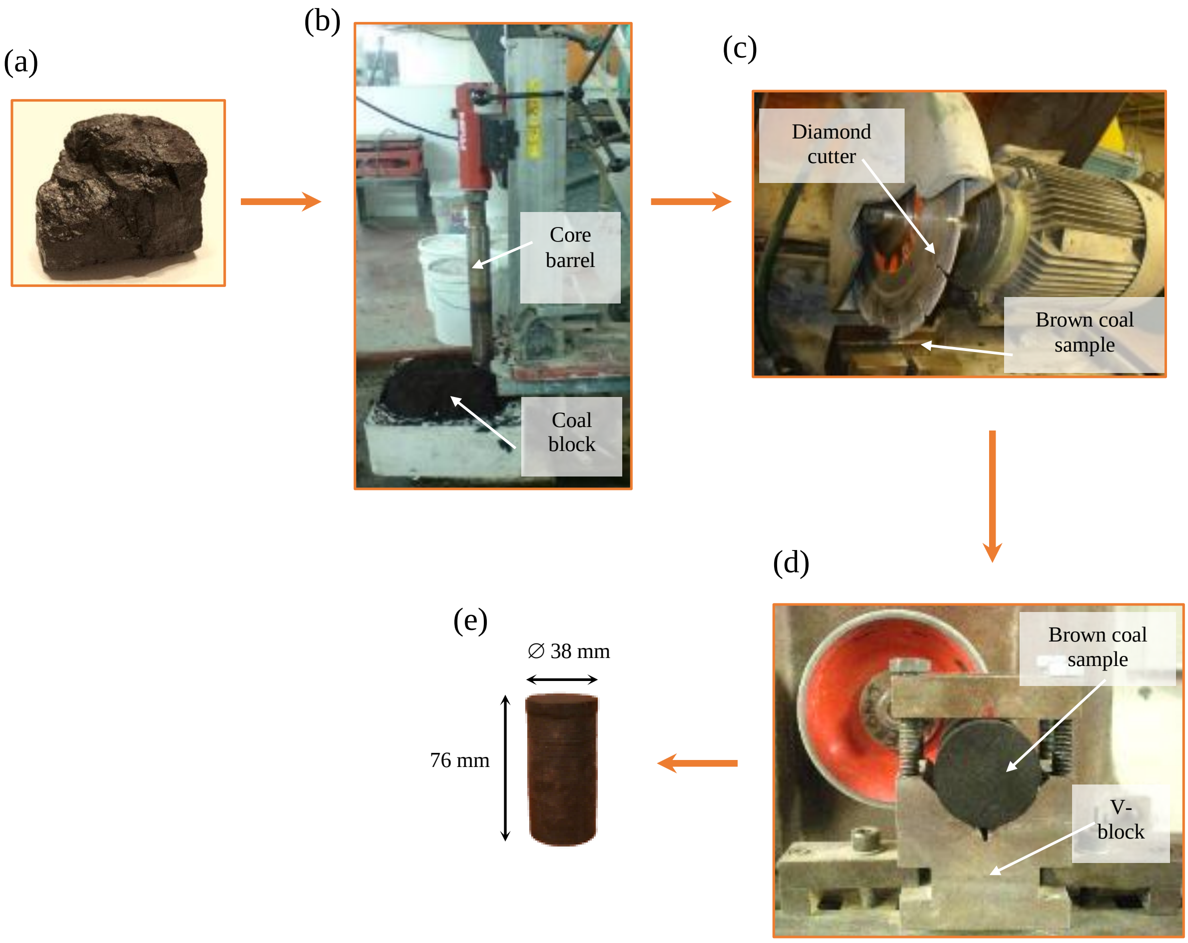

Figure 3.22. Coal sample preparation process for meso-scale tests (a) coal block as received, (b) coring process, (c) cutting process, (d) grinding process and (e) sample after preparation

To prepare the powdered coal, a similar process was used to that described by Jasinge (2010). Initially, the coal blocks were broken into smaller pieces and then crushed using a milling machine. Using a grinder, small pieces of coal were crushed into coal dust. The crushed coal was then sieved using a mechanical sieving machine to separate the coal powder less than 1 mm in size and the sieved coal was then stored in sealed plastic containers.

The moisture content of the powdered coal samples was measured according to ASTM: D3302 before using them for sample preparation, as the brown coal powder was used in its natural wet condition without additional water mixing to prepare the reconstituted meso-scale samples. Based on this standard, a coal powder weight of approximately 50 g was used to check the moisture content. The powder was spread evenly to a depth of 25 mm in a steel container to facilitate a short drying time. As mentioned in the standard, an air-drying oven is required to dry the coal powder. However, since this apparatus was not available, the coal powder was placed in a steel container which was positioned on top of an oven in a room with a temperature of 20 °C. This method was adopted to stimulate the air-drying conditions of an oven at no more than 10 °C above ambient temperature. After each measurement of the coal powder weight, the powder was stirred to ensure adequate drying. This process continued over around a four-day period until there was no change in weight loss. The moisture content of the coal powder used in the sample preparation was found to be approximately 54%.

Next, for sample preparation, the coal powder was filled to the top of the steel mould and compacted in three layers. The surface was roughened after compacting each layer to ensure good bonding between layers. After the placement of each layer, the weight of the coal powder was measured using a weight scale. The first layer and second layer were compacted for approximately 25 and 30 minutes respectively, until displacement became roughly constant. Once the final layer was placed, the sample was then compacted for 24 hours using the Shimadzu uniaxial compression machine. Figure 3.23 depicts a typical displacement versus time graph of a RC sample under compaction. The compaction was assumed to reach the maximum once the displacement versus time curve achieved a constant plateau. Therefore, the coal placed in the mould for compaction remained under a constant compression load.

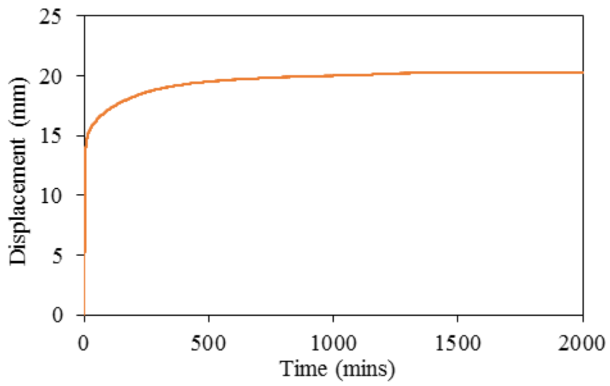

Figure 3.23. Displacement versus time of RC sample developed using 7 MPa compressive stress

Since the degree of consolidation is a time-dependent process, the duration the load is applied affects the sample density and mechanical properties. Therefore, it is crucial to compact the sample for a sufficient time to ensure adequate surface contact between particles and an increase in density, strength and elastic modulus (Jasinge, 2010).

After completing various trial RC samples, it was found that a compaction stress of 7 MPa and a displacement rate of 3 mm/min produced mechanical properties close to those of the natural coal specimens. Following compaction, the sample was extracted from the mould using a hydraulic press. The bottom plate of the steel mould was removed to enable the sample to be pushed out. The hydraulic press applied a small load on the top of the sample which allowed the sample to be extracted from the open bottom end. Once the sample was removed, the weight and dimensions of the sample were measured. The samples were then sealed in plastic bags and placed in the fog room. The sample weight and dimensions were recorded for the next two days to check for swelling and moisture loss.

The samples produced using a mould size of 210 mm were approximately 160 mm in length with a diameter of 54 mm when extruded from the mould. Therefore, to achieve a length of at least twice the diameter, the RC samples were cut to approximately 115 mm. To achieve smooth top and bottom surfaces, the surfaces were ground. This resulted in the RC samples having a length of approximately 113 mm. RC samples 54 mm in diameter by 113 mm high were used for the laboratory tests, and the sample dimensions were recorded before each test. Figure 3.24 shows a flow diagram of how the RC samples were prepared using the methods described.

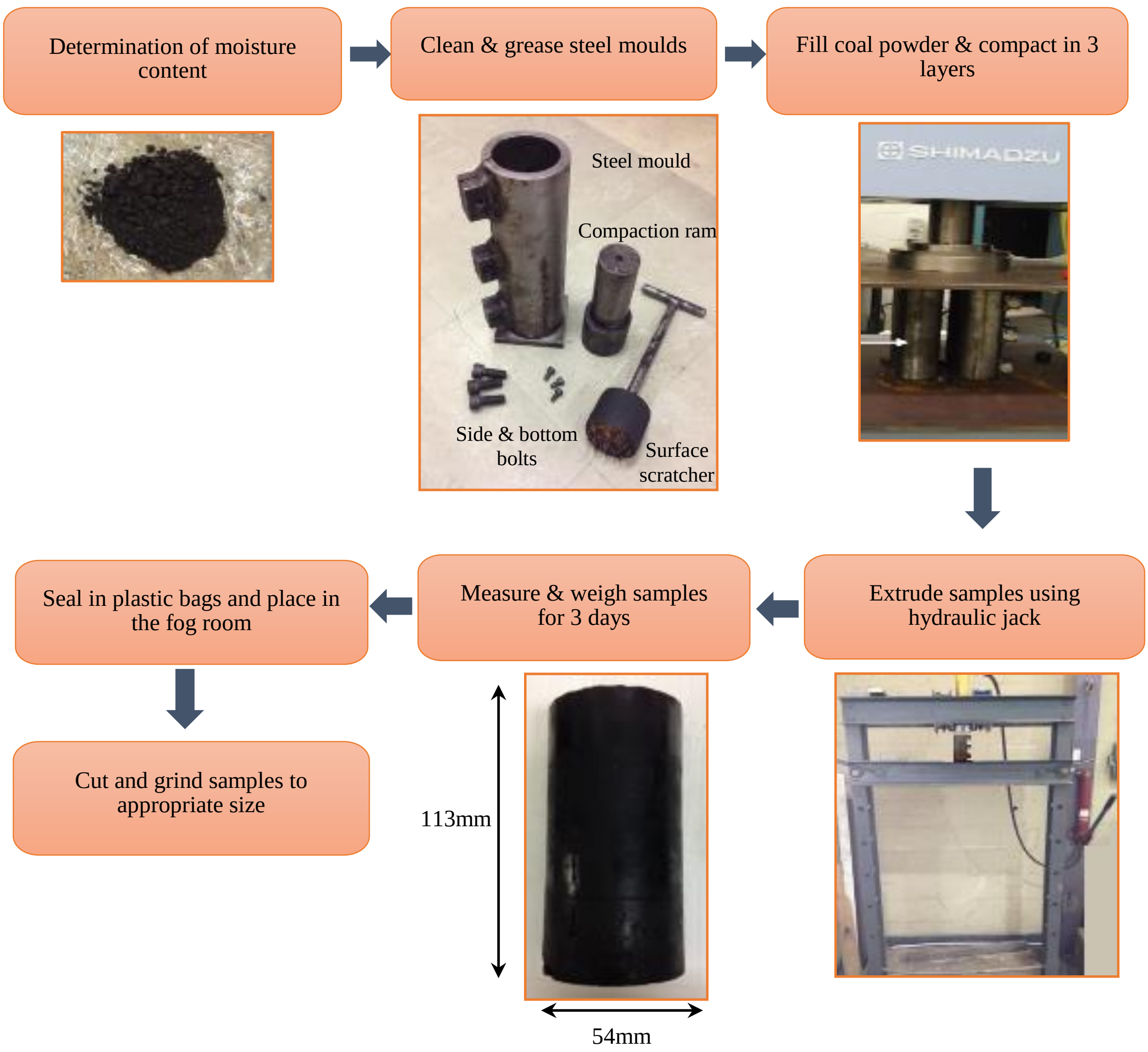

Figure 3.24. Meso-scale reconstituted sample preparation procedure

3.4.3 Experimental procedure

3.4.3.1 Permeability tests

Permeability tests were conducted using CO_2 injections at different injection pressures representing different phase conditions of CO_2. Here, the un-drained condition was maintained to determine the sample permeability using a pressure-transient approach to obtain the super-critical CO_2 injection into the sample and this is further explained in Section 3.6. N_2 was injected to quantify the coal mass changes undergone with CO_2 adsorption, as N_2 is a comparatively less adsorbing gas than CO_2. Hence, comparing the permeabilities for the same injection pressures of CO_2 and N_2 under the same confinement and temperature assisted in finding the CO_2 sorption-induced permeability variations in the coal sample. Gas injection was conducted at the constant pressure required and the corresponding pressure development at downstream was monitored and recorded at one second intervals, using the advanced data acquisition system. The experiments were repeated for several confining pressures to observe the permeability variations of the brown coal specimens at different depths. More details of the experimental procedure are discussed in Chapter 4.

3.4.3.2 Strength tests: unconfined compressive strength (UCS)

Using the pressure chambers (Figure 3.21) available at DEERL, samples were saturated at various CO_2 pressures (from 0 – 10 MPa representing both sub- and super-critical CO_2) prior to testing at a constant temperature (35 ^{0}C in the present study). For the CO_2 saturation, samples were first positioned inside the pressure cell (2 or 3 samples at a time) and gas/liquid was then injected into the pressure cell until the required saturation pressure was reached. All the samples were saturated for several time intervals (21 days, 3 months, 6 months, 9 months and 1 year) to observe the CO_2 adsorption-induced coal matrix strength variation with time. After the saturation period, the pressure cell was gradually de-pressurized at a rate of 0.02 MPa/min to avoid possible damage to the physical structure of the coal specimens due to sudden changes in pressure. After removing the samples from the saturation chamber, they were covered with plastic wrap and tested within around 20 minutes to avoid any possible changes to the saturation state of the samples.

The UCS tests were conducted according to the ASTM standards (Brown, 1981) using the compression machine (Figure 3.18(a)). The strain rate was maintained at 0.1 mm/min for all the tests. The data acquisition system recorded the applied loads on the coal specimens with time, and ARAMIS and AE systems were used to obtain the corresponding strains and fracture patterns during sample failure. When the specimen was ready to be tested, load application, the ARAMIS system and the AE system were started simultaneously to obtain consistent data points from the three machines. More details of the experimental procedure are discussed in Chapters 6 and 7.

3.4.3.3 Strength tests: tri-axial strength

The high-pressure tri-axial test rig in the DEERL (Figure 3.11) was used to conduct the tri-axial tests on the brown coal samples. First the confining pressure (10 MPa) and temperature (35 ^{0}C) were applied to the coal specimen and then the respective CO_2 flow was permeated through the sample (drained conditions). Once the flow upstream and downstream became stable, the specimen was left for another 3 to 4 days to allow the CO_2 to adsorb well into the sample. The load was then applied at a strain rate of 0.1 mm/min until failure. The tests were replicated 2 to 3 times to confirm the experimental observations. The load applied with axial strain was recorded using the advanced data acquisition system. More details of the experimental procedure are discussed in Chapter 6.

3.5 Macro-scale testing

Macro-scale flow experiments were conducted using the advanced core-flooding apparatus available in DEERL at Monash University (De Silva, 2013, De Silva et al., 2013). The following sections describe the methodology for the macro-scale experiments.

3.5.1 Instrumentation

Figure 3.25 shows the advanced core-flooding apparatus used for the macro-scale tests. This set-up consists of a high-pressure plumbing network which can hold pressures up to 35 MPa. The pressure cell can accommodate a sample 1 m in length and 203 mm in diameter and withstand a maximum of 25 MPa working pressure. The axial stress is applied using a hydraulic loading system which can maintain up to 100 T (~30 MPa) (Figure 3.25). The system is provided with CO_2, N_2 and water injection units to conduct single- and multi-phase flow experiments under both drained and undrained conditions. A compressed liquefied CO_2 bottle (G size, maximum pressure 5.7 MPa) is used to inject CO_2 and a compressed gas N_2 bottle (G size, maximum pressure 15 MPa) is used to inject N_2 into the specimen. The CO_2 bottle is placed on a digital platform scale (precision up to 0.01g) to measure the amount of CO_2 by weight injected into the sample, which can be used to investigate the CO_2 storage capacities of the coal specimens under various test conditions. Both the gasses and water are injected into the samples using a syringe pump (ISCO Teledyne – 260 D) (Figure 3.25). There is a gas outlet unit downstream to measure the pressures and the flow rates of the gas coming out of the specimen in the pressure cell. The outlet pressure is measured by a pressure transducer and the gas flow rate is measured by a MGC-1V3.0 type Ritter milli gas counter (Ritter Apparatebau).

Intermediate pressure taps are available at 350, 600 and 850 mm from the upstream injection point to observe the pressure development along the sample (Figure 3.25). A maximum temperature of 100 ^{0}C can be applied to the pressure cell to represent different underground thermal conditions and this is applied by four heat blankets wrapped around the pressure cell (Figure 3.25) and controlled by a temperature control box. A LVDT and a string gauge are used to measure the axial displacement of the specimen during testing. The data collected from the pressure transducers, the LVDT and the string gauges are transferred to the computer using a DT9834-32-0-16-STP data translation module and recorded using QuickDAQ software. This apparatus has the ability to perform hydro-fracturing or other forms of fracturing using foam or non-viscous fluid on sedimentary rocks. A schematic diagram of the apparatus with the aforementioned units is provided in Figure 3.26 and a summary of the working capabilities of the apparatus is shown in Figure 3.27.

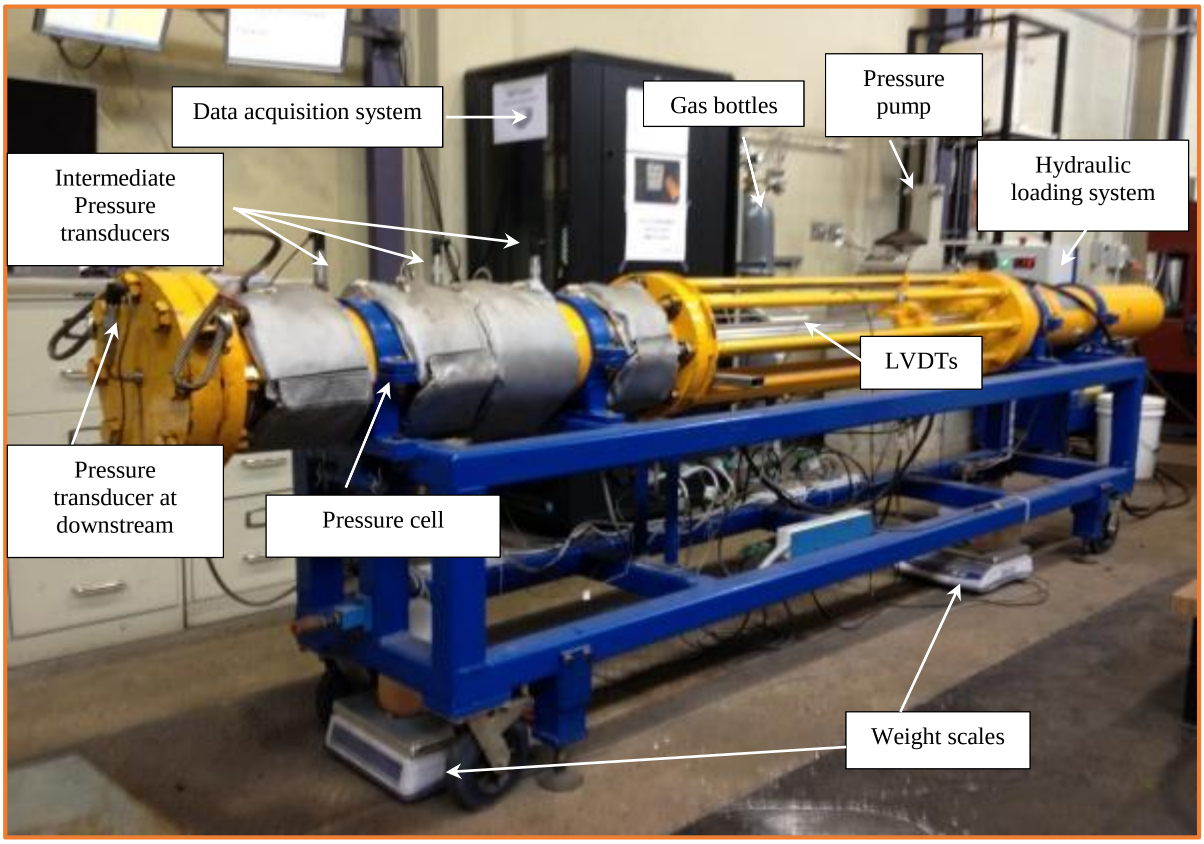

Figure 3.25. Advanced core-flooding apparatus

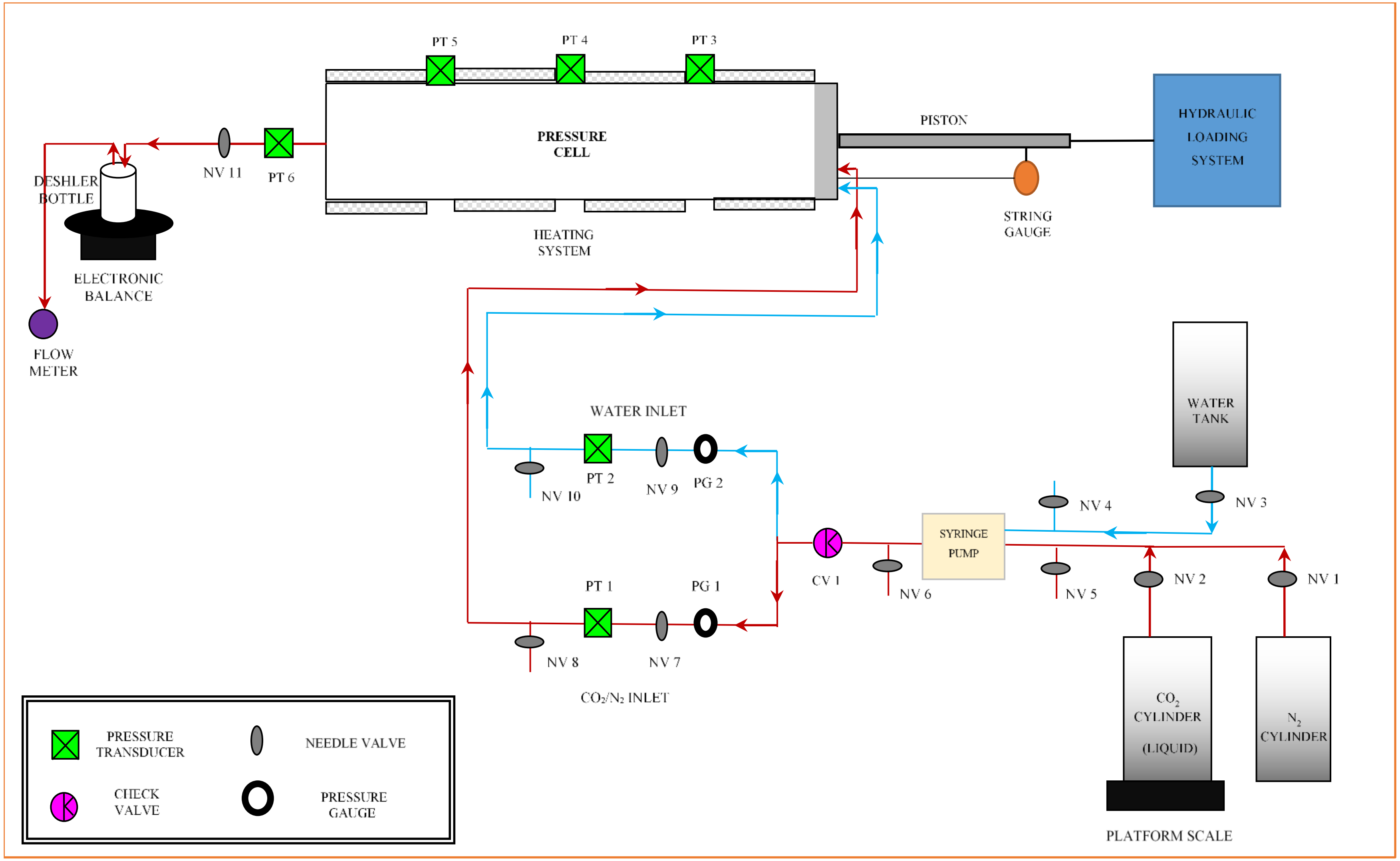

Figure 3.26. Schematic diagram of the advanced core flooding apparatus

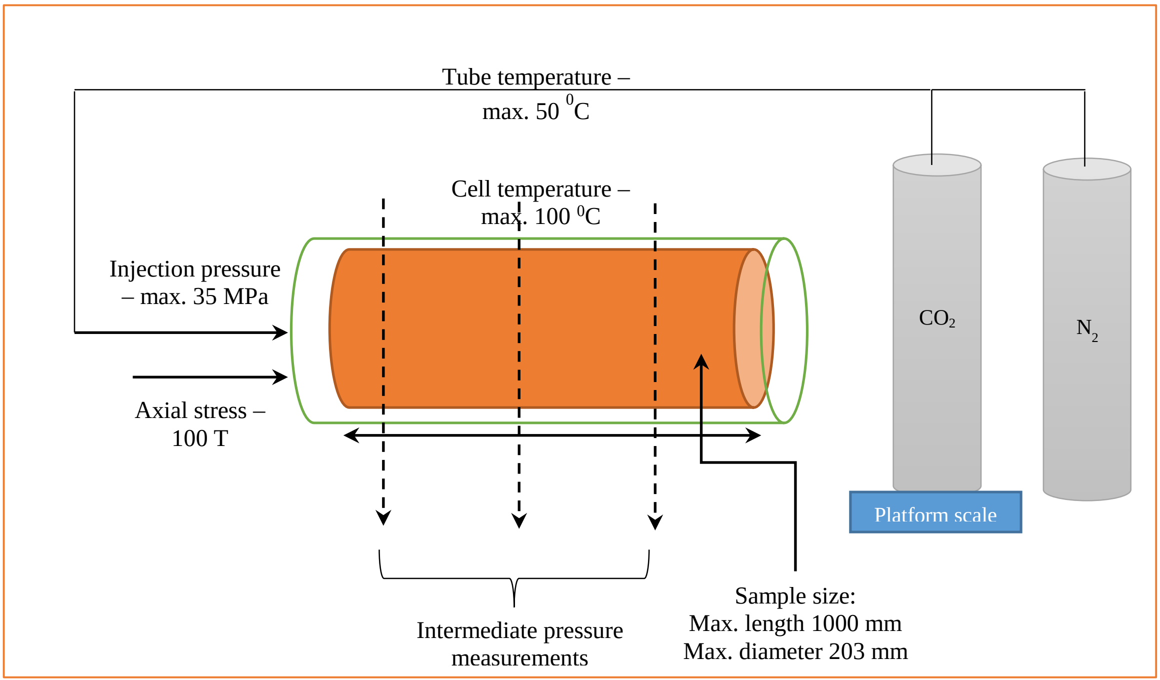

Figure 3.27. Summary of the working capabilities of the advanced core-flooding system

3.5.2 Sample preparation

Due to the difficulty in obtaining a natural coal block 1 m in length, in this experiment reconstituted coal samples were made using powdered brown coal. Further, it is advantageous to use reconstituted specimens to avoid the highly heterogeneous nature of coal (Jasinge, 2010). To prepare the powdered coal, a similar process was used to that described in Section 3.4.2.2. The coal powder used in the sample preparation consisted of particle sizes less than 1 mm with a corresponding well-graded particle size distribution similar to that described for the meso-scale sample preparation, and the moisture content of the powdered samples was measured according to ASTM: D3302, as described in Section 3.4.2.2

The samples for macro-scale testing were prepared in three stages using the powdered coal using similar procedure as for the meso-scale RC samples. First, the required axial stress (11 and 17 MPa were used for the present study) was applied on 1/3 of the coal core sample and compacted for around 30 minutes (here 30 minutes was found to be sufficient for satisfactory compaction of the 1/3 coal layer). The next 1/3 of the coal sample was then added to the cell and compacted for around 30 minutes, followed by the rest of the sample under the same axial stress. Between each compaction, the surface of the coal was disturbed and roughened to ensure sample consistency with good bonding between the layers. The whole coal sample was then consolidated for a sufficient time (around 7 days) and the consolidation level was observed by using a string strain gauge and LVDTs. In order to confirm the fully consolidated condition of the sample, a consolidation profile was used (Figure 3.28(a)) and the water released from the sample was observed (until zero water release from the sample) (Figure 3.28(b)). Permeability testing was conducted only after the consolidation level became stable. After confirming the fully compacted condition of the sample, permeability tests were initiated, maintaining the system temperature at the required constant value (38 ^{0}C for the present study to obtain super-critical CO_2 conditions). Figure 3.28(c) shows a sample after being extruded from the cell at the end of an experiment.

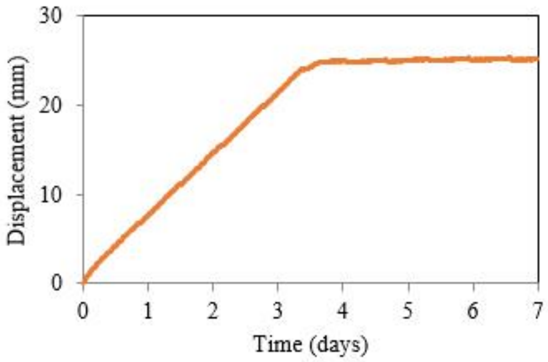

(a) Compaction level of coal sample (at 11 MPa axial stress)

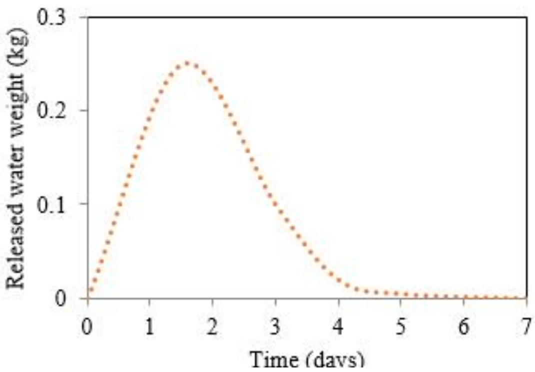

(b) Released water weight from the sample (at 11 MPa axial stress)

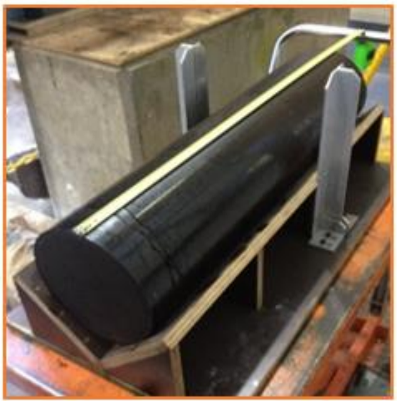

(c) An extruded sample from the apparatus at end of an experiment

Figure 3.28. Sample behaviour at different stages of macro-scale sample preparation

3.5.3 Experimental procedure

Permeability tests were conducted using CO_2 injections at different injection pressures representing different phase conditions of CO_2. Here, the un-drained condition was maintained to determine the sample permeability using a pressure-transient approach to obtain the super-critical CO_2 injection into the sample (under the drained condition downstream pressure is always atmospheric and therefore the super-critical condition cannot be achieved) (Perera et al., 2011). Similar to the meso-scale flow testing, N_2 was injected to quantify the coal mass changes undergone with CO_2 adsorption, as N_2 is a comparatively less adsorbing gas than CO_2. Gas injection was conducted at the constant pressure required and the corresponding pressure development throughout the sample (at 350, 600 and 850 mm from the injection point) and downstream was monitored and recorded, at one second intervals, using the advanced data acquisition system. More details of the experimental procedure are discussed in Chapter 5.

3.6 Experimental permeability calculations

All the meso- and macro-scale flow studies conducted during this research program used the undrained flow conditions at downstream instead of drained conditions. When drained conditions are used, the downstream pressure is at atmospheric conditions and hence it is not possible to obtain the higher CO_2 pressure conditions (super-critical) along the entire sample. In contrast, undrained conditions allow the downstream to develop pressure, resulting in higher pressure conditions even at downstream. Many researchers (Chen et al., 2011; Cui et al., 2009; Feng et al., 2016a; Feng et al., 2016b; Pan et al., 2010; Perera et al., 2011a; Perera et al., 2011b; Siriwardane et al., 2009; Vishal and Singh, 2015; Wang et al., 2011) have used undrained conditions to conduct flow tests on coal specimens. Therefore, undrained conditions were adopted for this research work. Under undrained conditions, pressure development at downstream is monitored and pressure gradient with time is used for the permeability calculations. Two types of equations were used to calculate the undrained coal permeability in this study. The first method was the flow tests which were conducted until the pressure (or flow) reached a steady state and Eqs. [3.1a,b] (Perera et al., 2011b; Siriwardane et al., 2009; Vishal and Singh, 2015) were used for the calculations:

$$Q = \left(\frac{dP}{dt}\right) \times \beta V_d \qquad [3.1a]$$

where, Q is the flow rate through the specimen, V_d is the downstream volume, β is the adiabatic compressibility of the gas, and dP/dt is the rate of change in the downstream pressure with time. Then, Darcy's law (Eq. [3.1b]) was used to calculate the corresponding permeability:

$$k = \frac{2QP_o\mu L}{A(P_i^2 - P_o^2)} \qquad [3.1b]$$

where, Q, μ, P_o, and P_i are the gas flow rate through the coal specimen, the viscosity of the fluid, the downstream pressure and the upstream pressure, respectively. The specimen has a cross-sectional area, A, and mean length, L and permeability, k.

The brown coal samples used for the flow tests took more time to reach the steady-state pressure conditions and in some cases it took around three weeks to 7 weeks under higher effective stresses. Chen et al. (2011), Cui et al. (2009), Feng et al. (2016a), Feng et al. (2016b), Pan et al. (2010) and Wang et al. (2011) used the transient method to calculate the permeability of coal during flows of different fluids, such as CO_2, CH_4, N_2 and He. The transient method requires a shorter duration, which is more feasible for rock masses like coal with lower permeabilities (Pan et al., 2010). In this method, the pressure decay between upstream and downstream vessels through the specimen is used to determine the permeability through the sample upon the variation of either pore pressure or confining pressure reaching an equilibrium state. Brace et al. (1968) first developed the pressure decay approach for tight rocks, however that approach does not account for the sorption effect on coal during the permeation of gases like CO_2. Feng et al. (2016a) suggested that the modified pressure decay approach proposed by Cui et al. (2009) can accurately calculate the permeability of sorptive rocks like coal, and this approach was therefore employed in the present study to calculate the brown coal's permeability using transient method (refer to Eqs. [3.2a] and [3.2b]).

$$\frac{(P_u - P_d)}{\Delta P_0} = e^{-\alpha t} \quad [3.2a]$$

$$k = \frac{\alpha \mu \beta L}{A f_1 \left(\frac{1}{V_u} + \frac{1}{V_d}\right)} \quad [3.2b]$$

where, P_u is upstream vessel pressure, P_d is downstream vessel pressure, ΔP_0 is the step change of pressure in vessels at time = 0, t is time, k is permeability of the specimen, A is the cross-section area of the sample, L is the length of the sample, μ is the viscosity of the injecting fluid, β is the adiabatic compressibility of the injecting fluid, and V_u and V_d are the volume of upstream and downstream pressure vessels, respectively.

Here, $f_1 = \frac{\theta_1^2}{a+b}$ [3.2c]

where, θ_1 is the first solution of the transcendental equation,

$$\tan\theta = \frac{(a+b)\theta}{\theta^2 - ab} \quad [3.2d]$$

In Eq. [3.2d], the a and b parameters are the gas storage capacity ratios of samples with upstream and downstream reservoirs and can be defined as follows (Eqs. [3.2e,f]).

$$a = \frac{\mathrm{V}_p(1+f_a)}{\mathrm{V_u}} \quad [3.2e]$$

$$b = \frac{\mathrm{V}_p(1+f_a)}{\mathrm{V}_d} \quad [3.2f]$$

where, f_a is the ratio of effective porosity contributed by adsorption ($\emptyset_a$) and the porosity ($\emptyset$) of the coal specimen. The $\emptyset_a$ can be calculated by Eq. [3.2g] using the adsorption parameters of the sample for the respective gases at experimental pressures.

$$\emptyset_a = \frac{\rho_s(1-\emptyset)}{V_{std}\beta\rho}\frac{V_L P_L}{(P_L+P)^2} \qquad [3.2g]$$

where, ρ_s is sample density, ρ is the gas density, V_{std} is the mole volume of gas at standard temperature and pressure (22.413E-3 m^3/mol), P is the pore pressure and V_L and P_L are Langmuir constants for volume and pressure, respectively. The permeability of the sample is calculated by plotting the pressure decay curves (in semi-log scale) with time. By substituting the slope of the resulting line "-α" of the pressure decay curves in Eq. [3.2b], the permeability of the sample was obtained.

For both the steady-state approach and the transient approach, substituting the accurate injecting fluid properties is essential. Therefore, the injecting fluid properties, adiabatic compressibility and viscosity of the fluid for different pressure and temperature conditions, were obtained from the REFPROP database (McLinden et al. 1998).

The accuracy of the permeability calculations using the steady-state and transient approach was checked using N_2 gas injection (a comparatively more non-adsorbing gas than CO_2) at 2 MPa injecting pressure under 8 MPa confinement. The permeability tests were conducted under both drained and un-drained conditions and the permeability values obtained under the two conditions were compared. The undrained permeability test was conducted first. Figure 3.29 shows the corresponding permeability values. According to the figure, throughout the injection period permeability remains almost constant. This undrained test was then repeated for 3, 4, and 5 MPa injecting conditions and un-drained permeability values were obtained using Eqs. [3.1a,b] and [3.2a,g]. The permeability values were then compared with the permeability values obtained under the drained condition. Under the drained condition, steady-state flow rates were measured using a milli-gas counter to calculate the permeability using Eq. [3.1b]. Figure 3.30 compares the permeability values obtained under drained and undrained conditions. According to the figure, the undrained permeability calculation can predict the permeability of the coal specimen accurately and can therefore be used for permeability calculations.

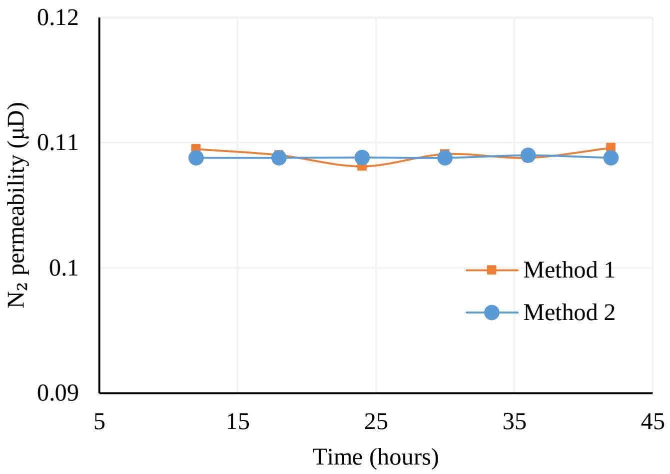

Figure 3.29. Permeability variation with time for 8 MPa confinement and 2 MPa N_2 injection (here Method 1 is the steady-state pressure approach and Method 2 is the transient approach)

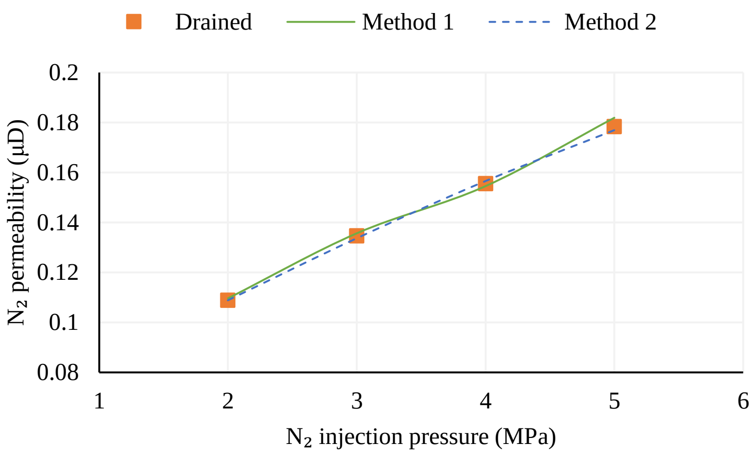

Figure 3.30. Validation of permeability calculated using the drained measurements, steady-state pressure approach (Method 1) and transient approach (Method 2)

3.7 References

ASTM D3302 / D3302M-15, 2015. Standard Test Method for Total Moisture in Coal, *ASTM International*, West Conshohocken, PA.

Brace, W.F., Walsh, J., Frangos, W., 1968. Permeability of granite under high pressure. *Journal of Geophysical Research* 73, 2225-2236.

Brockway, D.J., Higgins, R.S., 1991. Chapter 5 - Brown Coal Sampling, Analysis and Composition Durie, R.A., (ed) *The Science of Victorian Brown Coal*. Butterworth-Heinemann, Oxford, pp. 247-278.

Brown, E.T., 1981. Rock characterization, testing & monitoring: ISRM suggested methods. International Society of Rock Mechanics, Pergamon Press, Oxford, 1981, p 171-183.

Chen, Z., Pan, Z., Liu, J., Connell, L.D., Elsworth, D., 2011. Effect of the effective stress coefficient and sorption-induced strain on the evolution of coal permeability: experimental observations. *International Journal of Greenhouse Gas Control* 5, 1284-1293.

Cui, X., Bustin, A., Bustin, R.M., 2009. Measurements of gas permeability and diffusivity of tight reservoir rocks: different approaches and their applications. *Geofluids* 9, 208-223.

De Silva, P.N.K., 2013. A study of CO_2 storage capacity in sedimentary rocks (*PhD thesis*). Monash University, Melbourne, Australia. [http://arrow.monash.edu.au/vital/access/manager/Repository/monash:120462]

De Silva, P.N.K., Ranjith, P.G., 2013. Advanced core flooding apparatus to estimate permeability and storage dynamics of CO_2 in large coal specimens. *Fuel* 104, 417-425.

Durie, R., 2013. *The science of Victorian brown coal: structure, properties and consequences for utilization.* Butterworth-Heinemann Ltd, Oxford, Chapters 1, 2 and 6.

Feng, R., Harpalani, S., Pandey, R., 2016. Evaluation of Various Pulse-Decay Laboratory Permeability Measurement Techniques for Highly Stressed Coals. *Rock Mechanics and Rock Engineering*, 1-12. [DOI:10.1007/s00603-016-1109-7]

Feng, R., Liu, J., Harpalani, S., 2016. Optimized pressure pulse-decay method for laboratory estimation of gas permeability of sorptive reservoirs: Part 1–Background and numerical analysis. *Fuel*, 191, 555-564.

Garduno, J.L., Morand, H., Saugier, L., Ayers Jr, W., McVay, D.A., 2003. CO_2 sequestration potential of Texas low-rank coals, SPE Annual Technical Conference and Exhibition, Paper ID SPE-84154-MS.

George, A., 1982. Latrobe Valley brown coal—lithotypes: macerals: coal properties. *Australian Coal Geology* 4, 111-130.

George, A., Mackay, G., 1991. Petrology. *The Science of Victorian Brown Coal: Structure, Properties and Consequences for Utilization*. Butterworth Heinemann, Oxford, 46-97.

Gom.com. (2016). ARAMIS: GOM. [online] Available at: http://www.gom.com/metrology-systems/aramis.html [Accessed 13 Oct. 2016].

Hayashi, J.-I., Li, C.-Z., 2004. Structure and properties of Victorian brown coal Li, C.Z., (ed) *Advances in the science of Victorian brown coal*, Elsevier, Oxford, UK. pp 11-84.

Hernandez, G., Bello, R.O., McVay, D.A., Ayers, W.B., Rushing, J.A., Ruhl, S.K., Hoffmann, M.F., Ramazanova, R.I., 2006. Evaluation of the Technical and Economic Feasibility of CO_2 Sequestration and Enhanced Coalbed Methane Recovery in Texas Low-Rank Coals, SPE Gas Technology Symposium, Paper ID SPE-100584-MS.

Hocking, J., 1972. Geologic evolution and hydrocarbon habitat Gippsland Basin. *The APEA Journal* 12, 132-137.

Hooper, B., Murray, L., Gibson-Poole, C. (2005). Latrobe Valley CO_2 Storage Assessment, Cooperative Research Centre for Greenhouse Gas Technologies, Canberra. CO2CRC Publication No. RPT05-0108.

Jasinge, D., 2010. An investigation of the effect of carbon dioxide sequestration on the behaviour of brown coal (*PhD thesis*), Monash University, Melbourne, Australia.

Knight, J., 1975. Wonthaggi and Other Cretaceous Black Coal-Fields, Victoria. *Economic Geology of Australia and Papua New Guinea 2*, 334-338.

Lakmali, U.N., Ranjith, P.G., 2015. Effect of Brine Saturation on Carbonation of Coal Fly Ash for Mineral Sequestration of CO_2 Lollino, G., Manconi, A., Clague, J., Wei, Shan., Charle, M., (ed) *Engineering Geology for Society and Territory-Volume 1*, Springer International Publishing, Switzerland, p. 479-482.

Li, C.Z., 2004. *Advances in the science of Victorian brown coal*. Elsevier, Oxford, UK, p. 11-84.

MCEM, 2016. *FEI Quanta 3D Field Emission Scanning Electron Microscope - User manual*, Monash Centre for Electron Microscopy, Monash University, Australia, p. 5-7.

McLinden, M., Klein, S., Lemmon, E., Peskin, A., 1998. REFPROP, Thermodynamic and transport properties of refrigerants and refrigerant mixtures. NIST Standard Reference Database 23.

Pan, Z., Connell, L.D., Camilleri, M., 2010. Laboratory characterisation of coal reservoir permeability for primary and enhanced coalbed methane recovery. *International Journal of Coal Geology* 82, 252-261.

Perera, M.S.A., Ranjith, P.G., Airey, D.W., Choi, S.K., 2011a. Sub- and super-critical carbon dioxide flow behavior in naturally fractured black coal: An experimental study. *Fuel* 90, 3390-3397.

Perera, M.S.A., Ranjith, P.G., Choi, S.K., Airey, D., 2011b. The effects of sub-critical and super-critical carbon dioxide adsorption-induced coal matrix swelling on the permeability of naturally fractured black coal. *Energy* 36, 6442-6450.

Ranjith, P.G., Perera, M.S.A., 2011. A new tri-axial apparatus to study the mechanical and fluid flow aspects of carbon dioxide sequestration in geological formations. *Fuel* 90, 2751-2759.

Roberts, T., Talebzadeh, M., 2003. Acoustic emission monitoring of fatigue crack propagation. *Journal of Constructional Steel Research* 59, 695-712.

Shimadzu Corporation, (2016). Autograph AGS-X Series Precision Universal / Tensile Tester|Top: SHIMADZU (Shimadzu Corporation). [online] Available at: http://www.shimadzu.com/an/test/universal/ags-x/ags-x.html [Accessed 13 Oct. 2016].

Siriwardane, H., Haljasmaa, I., McLendon, R., Irdi, G., Soong, Y., Bromhal, G., 2009. Influence of carbon dioxide on coal permeability determined by pressure transient methods. *International Journal of Coal Geology* 77, 109-118.

Vishal, V. & Singh, T. 2013. Development of reconstituted Indian coals to investigate coal response to carbon dioxide exposure, in Proceedings ARMA 47th US Rock Mechanics/Geomechanics Symposium 2013, Volume 1, American Rock Mechanics Association, 599-602.

Vishal, V., Singh, T.N., 2015. A Laboratory Investigation of Permeability of Coal to Supercritical CO_2. *Geotech Geol Eng* 33, 1009-1016.

Wadley, H.N., 1986. Acoustic emission: nature’s ultrasound, Review of Progress in Quantitative Non-destructive Evaluation. *in*: Proceedings of the Twelfth Annual Review, 23–28, vol. 5A, Williamsburg, VA, United States, pp. 271-293.

Wang, S., Elsworth, D., Liu, J., 2011. Permeability evolution in fractured coal: The roles of fracture geometry and water-content. *International Journal of Coal Geology* 87, 13-25.

Wasantha, P., Ranjith, P., Shao, S., 2014. Energy monitoring and analysis during deformation of bedded-sandstone: use of acoustic emission. *Ultrasonics* 54, 217-226.

Woskoboenko, F., Stacy, W., Raisbeck, D., 1991. Physical structure and properties of brown coal Durie, R.A., (ed) *The Science of Victorian Brown Coal: Structure, Properties and Consequences for Utilization*. Butterworth-Heinemann Oxford, pp. 151-246.

Zeiss.com. (2016). ZEISS Xradia 520 Versa 3D X-Ray microscope - industry-best resolution and contrast. [online] Available at: http://www.zeiss.com/microscopy/en_de/products/x-ray-microscopy/zeiss-xradia-520-versa.html [Accessed 14 Oct. 2016].

3.8 Chapter summary

To date, little attention has been given to brown coal, in particular Australian brown coal, for CO_2-ECBM studies due to the unlikely existence of brown coal in deep geological formations where geo-sequestration is considered workable. However, recent surveys have confirmed the presence of brown coal seams at un-mineable depths, which can be used for the purpose of geo-sequestration. Hence, brown coal samples from the Hazelwood open-cut coal mine at Morwell, Gippsland, Victoria, Australia were used for the present work to conduct experiments. Experiments were conducted at micro-, meso- and macro-scale to obtain a detailed view of the coal matrix changes during CO_2 storage.

Micro-scale tests were conducted to observe the micro-structural changes in coal samples under different CO_2 saturation conditions. The FEI Quanta 3D microscope at the MCEM facility and the X-Ray microscopy facility for imaging geo-materials (XMFIG) at Monash University eres used to conduct the micro-scale analysis of the brown coal samples. For SEM analysis, the sample sizes were less than 2 mm and they were viewed under a low vacuum to avoid outgassing. Low voltage and spot sizes were used to carry out SEM analysis to minimise the charging effect of the coal particles. For CT scanning, reconstituted coal samples (38 mm in diameter and 76 mm in height) were used and viewed under full-view mode using a macro-detector.

Meso-scale experiments were conducted for both flow and strength tests using natural coal samples (38 mm in diameter and 76 mm in height). Flow tests were carried out using the high-pressure tri-axial test rig and, similar to the macro-scale tests, both CO_2 and N_2 were injected under various confining pressures to represent different depths. The same set-up was used to conduct the tri-axial strength tests for brown coal samples saturated at different CO_2 pressures to investigate seam integrity under CO_2 exposure. UCS tests were carried out on samples saturated at different CO_2 pressures for different time periods to determine the long-term effect of CO_2 adsorption-induced coal matrix swelling on the brown coal samples, using the ARAMIS optical strain system and an AE system.

For the macro-scale experiments, an advanced core-flooding apparatus was used which can accommodate a coal sample 203 mm in diameter and 1000 mm in length. Reconstituted brown coal samples were used for the tests due to the difficulty in finding natural brown coal blocks in such sizes and to avoid the heterogeneity of coal. Both CO_2 and N_2 were used to compare the CO_2 adsorption effect, and these gases were injected under different axial stresses to observe flow behaviour along the coal sample. The amount of CO_2 injected was monitored to quantify the CO_2 storage capacity of the coal.

The experimental permeability tests were conducted under undrained test conditions and the permeability was calculated using two methods. The samples where the downstream pressure development reached the steady state used the steady-state pressure approach to obtain the flow rates, coupled with Darcy's equation. For other permeability tests, the pressure decay approach modified for sorption was used.

Part 2

Investigation of variations of coal flow properties during carbon dioxide sequestration

Part 2: Investigation of variations of coal flow properties during carbon dioxide sequestration

CO_2 sequestration during ECBM process affects both hydro-mechanical properties of coal mass. Hence, the main attention was paid for the CO_2 sequestration induced coal mass flow ability variations and reports the meso-scale and macro-scale experimentations coupled with micro-scale experimentations and their outcomes in this part of the thesis. Mainly, Victorian brown coal (low rank coal) was used for the experiments and the results were compared with the high rank coal results in literature. From the findings of Chapter 2, it was evident that the coal mass flow properties were highly influenced by coal mass properties and injecting fluid properties during CO_2 sequestration. Hence, it would be noteworthy to investigate the effect of those effective factors on flow properties of coal in the course of CO_2 injection. The findings of the studies conducted are presented in this section of the thesis as follows.

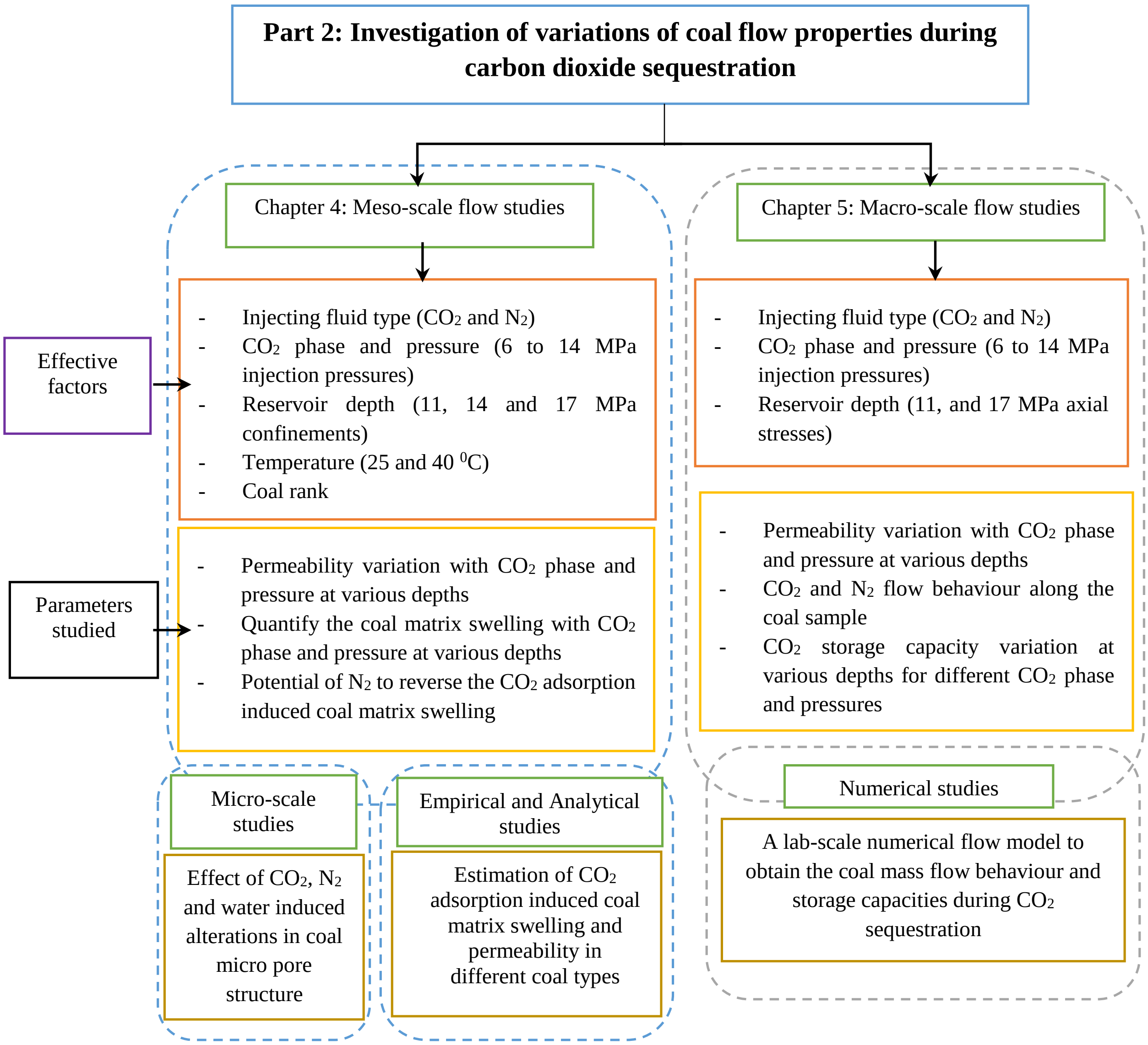

PART 2 - CHAPTER 4

Meso-scale studies of coal flow properties during carbon dioxide sequestration using natural coal specimens

Publications included in Chapter 4

Chapter 4 includes four papers. The details are as follows.

Chapter 4.2

Ranathunga AS, Perera MSA, Ranjith PG, Zhang XG (2017). Super-critical carbon dioxide flow behaviour in low rank coal: A meso-scale experimental study. *J CO_2 Utilization* (under review).

Chapter 4.3

Ranathunga AS, Perera MSA, Ranjith PG (2017). Effect of effective stress and coal matrix swelling on coal flow behaviour during CO_2 sequestration. *Journal of CO_2 Utilization* (under review).

Chapter 4.5

Ranathunga AS, Perera MSA, Ranjith PG, Zhang XG (2017). The influence of CO_2 properties and reservoir depth on coal matrix swelling: A meso-scale experimental study using low rank coal. *Energy Fuel* (under review).

Chapter 4.6

Ranathunga AS, Perera MSA, Ranjith PG (2017). A review and model development for estimation of gas adsorption-induced coal matrix swelling. *Int J of Energy Research* (under review).

4. Meso-scale studies on coal flow properties during carbon dioxide sequestration using natural coal

4.1 Overview

This chapter presents the outcomes of meso-scale studies conducted using natural brown coal to investigate flow property variation due to CO_2 sequestration to fulfil objective 1 of the research work. A series of meso-scale (samples 38 mm in diameter and 76 mm high) core flooding tests were conducted to tests the influence of different effective parameters on the coal mass flow behaviour. The results are presented as follows in this chapter.

- **Section 4.2 -** ***How do injecting CO_2 properties and in situ stresses affect coal mass flow behaviour?***

As discussed in Chapter 2, both coal mass properties and injecting gas properties affect flow behaviour in the coal matrix. Therefore, this section of Chapter 4 is dedicated to the investigation of the influence of in situ stresses (coal mass properties: depth) and CO_2 phase and pressure (injecting gas properties) on low-rank Victorian brown coal.

This section of the chapter is the following paper:
Ranathunga AS, Perera MSA, Ranjith PG, Zhang XG (2017). Super-critical carbon dioxide flow behaviour in low rank coal: A meso-scale experimental study. *J CO_2 Utilization* (under review).

Section 4.3 - ***How can the individual effects of effective stress and sorption-induced strain on the evolution of coal permeability be evaluated?***

In Section 4.2, it was observed that both effective stress and sorption-induced strain (swelling) collective contribute to permeability variations in coal mass. Therefore, an effort was made to distinguish the effective stress-induced and sorption strain-induced permeability variations in coal specimens and the individual effect of these factors in altering coal permeability during CO_2 permeation.

This section of the chapter is the following paper:
Ranathunga AS, Perera MSA, Ranjith PG (2017). Effect of effective stress and coal matrix swelling on coal flow behaviour during CO_2 sequestration. *J of CO_2 Utilization* (under review).

- **Section 4.4 -** ***How does the temperature alter CO_2 permeability in coal?***

According to Chapter 2, higher temperatures have a positive influence on coal permeability during CO_2 injection, due to the reduced adsorption potential to the coal matrix at elevated temperatures in high rank coal. Therefore, it is interesting to identify whether low rank coal behaves similarly at higher temperatures. This is the subject of this section of the chapter.

A conference paper was produced from this section of the chapter as follows:

Ranathunga AS, Perera MSA, Ranjith PG (2014). An Experimental Study to Investigate Temperature Effect on Permeability of Victorian Brown Coal during CO_2 sequestration, ISRM International Symposium and 8th Asian Rock Mechanics Symposium (ARMS8), Sapporo, Japan, 14-16 October, 2014; Paper No. ARMS8_PO-82.

- **Section 4.5 - *How does carbon dioxide adsorption-induced coal matrix swelling vary for various CO_2 properties and reservoir depths?***

Section 4.2 and 4.3 highlighted that coal matrix swelling is one of the main reasons for coal permeability reductions, and it varies with CO_2 pressure and reservoir depth. According to the research literature (refer to Chapter 2), coal matrix swelling varies with CO_2 pressure and reservoir depth and this variation results in different permeability values for high rank coal. However, the behaviour of low rank coal in this respect has not yet been studied comprehensively. This is the subject of this section.

This section of the chapter is the following paper:

Ranathunga AS, Perera MSA, Ranjith PG, Zhang XG (2017). The influence of CO_2 properties and reservoir depth on coal matrix swelling: A meso-scale experimental study using low rank coal. *Energy Fuel* (under review).

- **Section 4.6 - *How can the various gas adsorption-induced coal matrix swellings in coal be estimated?***

There are several models available to predict coal matrix swelling with gas adsorption, however they do not consider all the factors which influence coal matrix swelling. Therefore, an analytical approach was used to estimate coal mass swelling under different effective factors which have been found to be the most influential on sorption-induced strain using the modified D-R model for swelling.

This section of the chapter is the following paper:

Ranathunga AS, Perera MSA, Ranjith PG (2017). A review and model development for estimation of gas adsorption-induced coal matrix swelling. *Int J of Energy Research* (under review).

4.2 How do injecting CO_2 properties and in situ stresses affect coal mass flow behaviour?

The permeability of any material reveals its flow ability and was studied in this section by conducting a series of meso-scale core flooding experiments on low-rank brown coal from the Gippsland basin. The main objective of this study was to investigate the sub- and super-critical CO_2 flow behaviour in low rank brown coal during CO_2 sequestration. Both sub- and super-critical CO_2 was permeated through the coal specimen to study how the different chemical and physical properties in both phases affect the permeability through the material. Further, N_2 (a less adsorbing gas than CO_2) was used to distinguish the coal matrix responses during CO_2 permeation. Three different confinements (11, 14 and 17 MPa) were utilized to represent different reservoir depths (approximately 400, 500 and 600 m). The results were compared with high rank coal data in the research literature to identify the effect of coal rank on the CO_2 sequestration-related variation of coal mass flow ability. Further, SEM analysis was conducted to gain better insights into the micro-structural changes during flow tests.

This section of the chapter is the following paper:

Ranathunga AS, Perera MSA, Ranjith PG, Zhang XG (2017). Super-critical carbon dioxide flow behaviour in low rank coal: A meso-scale experimental study. *J CO_2 Utilization* (under review).

Super-critical carbon dioxide flow behaviour in low rank coal: A meso-scale experimental study

A.S. Ranathunga[1], M.S.A. Perera[1,2], P.G. Ranjith[1], X.G. Zhang[1]

[1]Deep Earth Energy Laboratory, Department of Civil Engineering, Monash University, Building 60, Melbourne, Victoria, 3800, Australia.

[2] Department of Infrastructure Engineering, The University of Melbourne, Building 176, Melbourne, Victoria, 3010, Australia.

Abstract

The carbon dioxide (CO_2) adsorbed in coal seams during CO_2-enhanced coal bed methane recovery (CO_2-ECBM) causes substantial coal matrix alterations, resulting in significantly reduced flow performance. Many studies have been conducted to date on the effect of CO_2 phase on coal mass permeability. However, the effect of coal rank on these permeability changes with CO_2 phase has not yet been studied. Therefore, the main aim of this study is to investigate how the influence of CO_2 phase condition on coal flow performance varies with rank. A series of tri–axial permeability tests was conducted using Australian brown coal samples for both CO_2 and N_2 under various confinements and injections at 35 ^{0}C. The results were then compared with those for high-rank coal reported in the literature. According to the test results, greater coal micro-structure rearrangement occurs with super-critical CO_2 adsorption, resulting in lower permeability in coal, regardless of rank. However, this CO_2 phase influence is much greater for high-rank coal. Although coal permeability reduces with depth for any rank of coal, this depth effect reduces with increasing rank. Furthermore, although N_2 has the ability to recover CO_2 adsorption-induced swelled areas in coal regardless of rank, that capability is much greater for high-rank coal.

Keywords: brown coal, CO_2 sequestration, coal rank, coal matrix swelling, permeability

4.2.1 Introduction and background

Of the various CO_2 mitigation options, CO_2-enhanced coal bed methane (ECBM) recovery is being implemented and tested as a viable option to reduce the amount of CO_2 in the earth's atmosphere, while recovering a valuable energy product: coal bed methane (CH_4) (Baran et al., 2013; Cuéllar-Franca and Azapagic, 2015; Ranathunga et al., 2014a; White et al., 2005; Zhang et al., 2016). The CO_2-ECBM process involves introducing CO_2 through an injecting well into deep coal seams, in which CO_2 acts as a displacing gas that allows the CH_4 already adsorbed in the coal seam to be desorbed, and eventually collected through a recovery well. Ultimately, the extracted methane gas can be stored and used to produce energy in a cost-effective and environmentally-friendly way

(Ranathunga et al., 2014). However, coal matrix swelling upon CO_2 adsorption into the matrix creates many issues in the CO_2-ECBM process, because this coal matrix swelling causes significant alterations in petro-physical properties (permeability, strength, elastic modulus, etc.). These cause reductions in CO_2 injectivity into the coal seam and add risk to the process by increasing the risk of possible CO_2 leakage into the surrounding aquifers (Masoudian, 2016; Pan et al., 2010; Perera and Ranjith, 2012; Vishal et al., 2013).

Coal has a dual porosity system, which is composed of micro-pores (matrix porosity) and macro-pores (the cleat system). Although the micro-pores of the coal structure account for a large percentage of its total porosity, macro-pores contribute significantly to seam permeability (Busch and Gensterblum, 2011). Basically, the gas transportation in any coal seam follows three steps: 1) gas transport through the macro-pores (cleat system), 2) gas diffusion into the micro-pores from the macro-pores and 3) gas adsorption into the micro-pores/desorption from the micro-pores (Harpalani and Schraufnagel, 1990). During CO_2-ECBM, the desorption of coal bed methane with the injection of CO_2 into the coal matrix is due to the higher attraction and stronger Van der Waals bonds between the coal mass and CO_2 compared with the coal mass and CH_4 (Harpalani and Schraufnagel, 1990; Levine, 1993), which is also one of the reasons for the stable storage of CO_2 in coal reservoirs. However, coal's polymer-like structure is greatly influenced by the contacting gases or solvents and is subjected to swelling when CO_2 is adsorbed into the micro-pores (Day et al., 2010). This coal matrix swelling creates large strains between the adsorbing CO_2 gas layer and the macro-pores or cleat walls (Perera et al., 2011a) and as a result, the existing pore space for CO_2 transportation is reduced, and coal mass permeability eventually declines (Gathitu et al., 2009; Perera et al., 2011b).

According to De Silva and Ranjith (2014), coal seam permeability must be more than 1 mD for successful and economical CO_2 sequestration. However, according to recent laboratory-scale experiments (Anggara et al., 2013; Jasinge et al., 2011; Pan et al., 2010; Perera et al., 2011; Ranathunga et al., 2015; Siriwardane et al., 2009; Vishal and Singh, 2015; Wang et al., 2015) and field scale projects (Fujioka et al., 2010; Mavor et al., 2004; Reeves and O'Neill, 1989; Syed et al., 2013), maintaining the favourable conditions required for CO_2 sequestration and ECBM recovery is challenging, due to CO_2 adsorption-induced coal matrix swelling. Therefore, many studies have been conducted to date to investigate the coal mass petro-physical property variations which occur with CO_2 adsorption-induced coal matrix swelling under different in-situ conditions, such as coal seam properties and injecting gas properties. Previous research shows that the swelling process is affected by coal seam properties, including coal seam temperature (Bae and Bhatia, 2006; Perera et al., 2012), coal rank (Reucroft and Sethuraman, 1987; Walker Jr et al., 1988) and depth of CO_2

injection (Pan et al., 2010; Perera et al., 2011b; Vishal and Singh, 2015), and the injecting gas properties, including CO_2 phase and pressure (Anggara et al., 2013; Baran et al., 2013; Day et al., 2010; Harpalani and Chen, 1997; Perera et al., 2011b). Table 4.1 summarises some previous research on the permeability variations caused by coal matrix swelling with different effective factors (coal seam properties and injecting gas properties).

According to Table 4.1, coal CO_2 permeability is greatly altered at higher injection pressures and higher temperatures which exist at greater depths. CO_2 exists in its super-critical state (CO_2 critical point - 7.38 MPa and 31.8^{0}C) in favourable coal seams for CO_2 sequestration (beyond ~ 800 m) (Oldenburg, 2006). This super-critical CO_2 has a higher adsorption capacity than sub-critical CO_2 and creates greater coal matrix swelling (Day et al., 2010; Perera et al., 2011a). Further, significant CO_2 permeability reduction has been identified in existing studies during the CO_2 phase transition from sub- to super-critical (refer to Table 4.1). This indicates the importance of selecting a coal seam with suitable physical properties to achieve operational CO_2 sequestration in coal. However, studies conducted to date on how super-critical CO_2 sequestration performance varies with coal rank at depths applicable for CO_2 sequestration are deficient (refer to Table 1). Although several studies (Pan et al., 2010; Perera et al., 2011b; Vishal and Singh, 2015) have been conducted to identify super-critical CO_2 sequestration performance in high-rank coal, much less attention has been given to low-rank coal in this respect. Australia has a number of low-rank coal resources (White et al. 2005) and the CO_2 sequestration process may be applicable to enhance methane production from them. An effort was therefore made to investigate the effect of CO_2 phase and pressure on the flow properties of low-rank coal using Australian brown coal.

Several previous studies (Perera et al., 2011b; Siriwardane et al., 2009; Kiyama et al., 2011) conducted on high rank coals have reported that N_2 has the potential to enhance CO_2 permeability in the coal mass by reversing the CO_2 adsorption-induced coal matrix swelling. When N_2 is injected into the coal mass, it remains a free gas as it has much lower adsorption potential than CO_2 (Day et al., 2010) in the fracture space. This creates an imbalance between the sorbed and free gas phases and eventually reduces the partial pressure of CO_2, resulting in the release of CO_2 from the coal mass (Reeves, 2003). This release of CO_2 molecules from the coal matrix can therefore partially recover the reversible swelling by the physical adsorption of CO_2 (Kiyama et al., 2011). Therefore, an effort was made to investigate the potential of N_2 to enhance CO_2 permeability in low-rank coal.

Table 4.1. Previous studies of CO_2 adsorption-induced permeability reduction in coal

Coal seam properties

Effective factors	Previous studies and findings: Test conditions	Previous studies and findings: Results	Ref.
Depth (confining pressure)	Low rank coal: Confining pressures – 3 to 12 MPa Injection pressures – 1 to 3.5 MPa Temperature – room temperature	Around 10 to 50% permeability reduction when confining pressure is increased from 3 to 12 MPa.	Jasinge et al. (2011)
	High rank coal: Confining pressures – 15, 20, 25 MPa Injection pressures – 6 to 21 MPa Temperature – 33.5 ^{0}C	Around 37% and 42% average permeability reduction when confining pressure is increased from 15 to 20 MPa and 20 to 25 MPa.	Perera et al. (2011b)
	Key findings	CO_2 permeability is reduced with increasing depth for both high and low rank coals because pore space available for gas movement is reduced with increasing confinement.	Perera et al. (2012a)
Temperature	Low rank coal: Confining pressures – 10 MPa Injection pressures – 5 to 8 MPa Temperature – 25 and 40 ^{0}C	Around 6% permeability increment when temperature is increased from 25 to 40 ^{0}C.	Ranathunga et al. (2014b)
	High rank coal: Confining pressures – 20 and 24 MPa Injection pressures – 8 to 13 MPa Temperature – 25 to 70 ^{0}C	Around 24% and 20% increments in permeability when the temperature is increased from 25 to 70 ^{0}C at 20 and 24 MPa confinements, respectively.	Perera et al. (2012b)
	Key findings	CO_2 permeability increases with increasing temperature for both low and high rank coals because the adsorption capacity of CO_2 reduces with increasing temperature due to increased kinetic energy of gas molecules, which eventually causes them to be released from the adsorbed phase.	Bae and Bhatia (2006)
Coal rank	Low rank coal: Confining pressures – 3 to 12 MPa Injection pressures – 1 to 3.5 MPa Temperature – room temperature	At 7 MPa confining pressure, 1 to 3 MPa injection pressure increment caused around 19% permeability reduction.	Jasinge et al. (2011)
	High rank coal: Confining pressures – 5 to 13 MPa Injection pressures – 1 to 5 MPa Temperature – room temperature	At 7 MPa confining pressure, 1 to 3 MPa injection pressure increment caused around 53% permeability reduction.	Vishal et al. (2013)
	Key findings	CO_2 adsorption-induced permeability reduction is greater for high rank coals than lower rank coals. Well-developed cleat system in high rank coals acts as a locus for CO_2 permeation in the coal matrix, leading to more swelling areas compared to low rank coals.	Ranjith and Perera (2012c)

Injecting gas properties (Phase and Pressure)			
Effective factors	**Previous studies and findings** — **Test conditions**	**Results**	**Ref.**
Sub-critical CO_2	Low rank coal: Axial pressures – 1 to 6 MPa Injection pressures – 0.7 to 5.7 MPa Temperature – 38 ^{0}C	Around 11% average permeability reduction from 5.1 to 5.7 MPa CO_2 injection pressure increment at 6 MPa axial stress.	De Silva (2012)
	High rank coal: Confining pressures – 5 to 13 MPa Injection pressures – 1 to 5 MPa Temperature – room temperature	Around 18% average permeability reduction from 1 to 5 MPa CO_2 injection pressure increment at 5 MPa confining pressure.	Vishal et al. (2013)
	Key findings	CO_2 permeability reduces with increasing CO_2 injection pressures due to the associated greater swelling effect created by higher sorption capacity for both low and high rank coals.	Siriwardane et al. (2009), Durucan and Shi (2009)
Super-critical CO_2	Low rank coal: Axial pressures – 11 MPa Injection pressures – 6 to 14 MPa Temperature – 38 ^{0}C	Around 29% average permeability reduction when CO_2 changes its phase from sub- to super-critical CO_2.	Ranathunga et al. (2015)
	High rank coal: Confining pressures – 16, 20, 24 MPa Injection pressures – 11 to 15 MPa Temperature – 33 ^{0}C	Around 30% average permeability reduction with increase of CO_2 injection pressure from 11 to 15 MPa at 16 MPa confining pressure.	Vishal and Singh (2015)
	Confining pressures – 15, 20, 25 MPa Injection pressures – 6 to 21 MPa Temperature – 33.5 ^{0}C	Around 30%, 42% and 46% average permeability reductions when CO_2 changes its phase from sub- to super-critical CO_2 at 15, 20 and 25 MPa confinements respectively.	Perera et al. (2011b)
	Key findings	CO_2 permeability in coal reduces with increasing CO_2 injection pressures with a greater reduction in the transition point of CO_2 from sub- to super-critical, regardless of rank. This permeability reduction increases with increasing depth for high rank coal and to date no research has yet been conducted for low rank coal in this regard.	Pan et al. (2010), Perera et al. (2011b), Vishal and Singh (2015)

4.2.2 Experimental procedure

4.2.2.1 Sample preparation

Permeability tests were conducted using natural brown coal samples obtained from the Hazelwood coal mine located at Morwell in south Gippsland, Victoria. The coring, cutting and grinding machines available in the Monash University Deep Earth Energy Research Laboratory (DEERL) were used to produce samples 38 mm in diameter and 76 mm high from large coal blocks. These brown coal samples had around 57% natural moisture content, and to avoid moisture loss from the samples, they were wrapped in polythene bags and stored in a plastic container in the fog room in the DEERL until they were used in the experiments.

4.2.2.2 Sample preparation

A series of permeability tests was conducted using the high-pressure tri-axial test rig available in the DEERL and a schematic diagram of the set-up is shown in Figure 4.1. The detailed procedure for using the high-pressure tri-axial test rig for permeability experiments explained in Ranjith and Perera (2011) was used to conduct the experiments for three different confinements (11, 14 and 17 MPa) and different CO_2 inlet pressures (6-14 MPa) (refer to Table 4.2). During the study, an attempt was made to fulfil three main objectives as follows:

(i) Effect of CO_2 phase and pressure on permeability in brown coal:

CO_2 injection pressures ranging from 6-14 MPa, under both sub- and super-critical CO_2 conditions, were injected into samples under three different confinements (11, 14 and 17 MPa), and N_2 was permeated before CO_2 injection to clearly identify the CO_2 adsorption-induced coal matrix alterations (see Table 4.2).

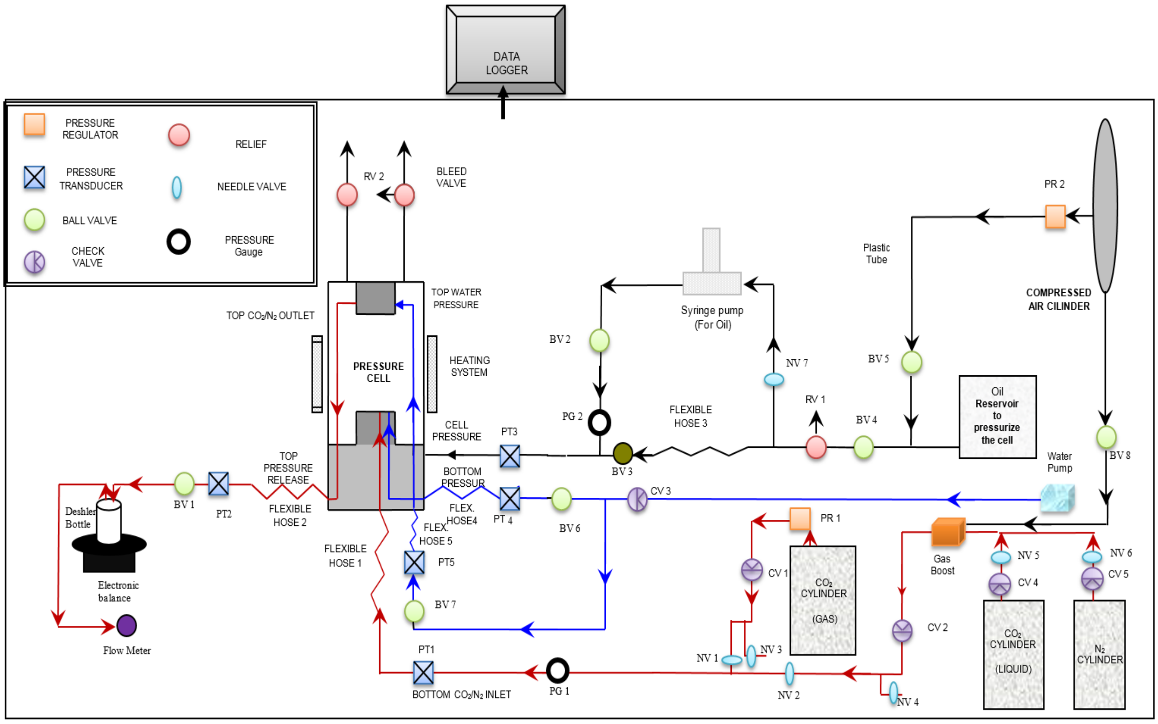

Figure 4.1. Schematic diagram of the high-pressure tri-axial set-up used to conduct flow tests

Table 4.2. Test conditions of the permeability tests

Confinement pressure (MPa)	CO_2 injection pressure (MPa)	N_2 injection pressure (MPa)
11	6	6
	7	7
	8	8
	9	9
14	6	6
	7	7
	8	8
	9	9
	10	10
	12	12
17	6	6
	7	7
	8	8
	9	9
	10	10
	12	12
	14	14

(ii) Potential of N_2 to reverse CO_2 adsorption-induced coal matrix alterations in brown coal:

In order to investigate the potential of N_2 to reverse both sub- and super-critical CO_2 adsorption-induced matrix alterations in brown coal, swelled samples (during CO_2 injection) were permeated with N_2 for 24 hours and CO_2 was then again injected to determine the effect of N_2 on CO_2-induced coal matrix swelling in brown coal.

The temperature of the system was kept constant at 35^0C (> 31.8^0C is the critical temperature of CO_2) throughout the test to confirm that CO_2 injection beyond 7.38 MPa (the critical pressure of CO_2) is at its super-critical state. Therefore, the CO_2 pressures <7 MPa (6 and 7 MPa) were sub-critical conditions while >7 MPa (8 to 14 MPa) were super-critical conditions. All the permeability tests were conducted under undrained conditions to achieve super-critical CO_2 conditions in the downstream, which cannot be achieved using drained tests as the downstream is at atmospheric pressure.

(iii) Effect of CO_2- induced coal matrix alterations on micro-pore structure of brown coal:

An FEI Quanta 3D FEG FIB machine available at the Monash University Centre for Electron Microscopy (MCEM) was used to study the micro-pore structural changes which occur in the coal mass with sub- and super- critical CO_2 adsorption. Two coal slices obtained from the upstream and downstream of the sample were tested prior to permeability testing and three coal slices obtained from upstream, downstream and the middle of the sample were tested after the permeability tests. The coal slices were around 4 to 5 mm in size (length and width) and the thickness was less than 2 mm to avoid high scanning electron contrast formations due to the variations in sample surface morphology. It should be noted that there was potential for the coal samples to release the adsorbed CO_2 into the atmosphere when transporting the specimens for the scanning electron microscopy (SEM) study. Hence, the specimens were transferred as quickly as possible in air-tight containers to minimise this desorption effect. The specimens were adhered to a circular specimen stub using a double-sided adhesive carbon tape followed by a double platinum coating to avoid charging of the specimen (brown coal is an insulating material and the electrons have no escape path from the specimen, causing a charging effect during SEM). During this study, a 15 kV probe current with 4.5 spot size under low vacuum mode was utilized to observe the specimens.

Measuring coal specimen permeability

Both upstream and downstream pressure developments for the different gas injections were recorded using an advanced data acquisition system at one-second intervals. These observations were used to calculate the permeability using the transient method. Unlike steady-state measurements, the transient method requires a short test duration (Pan et al., 2010; Brace et al., 1968), which is more feasible for rock masses like coal with low permeabilities. Further, this method has been used by previous researchers (Pan et al., 2010; Siriwardane et al., 2009; Chen et al., 2011; Wang et al., 2011) to calculate the permeability of coal specimens with the variation of either pore pressure or confining pressure reaching an equilibrium state. In this method, pressure decay between upstream and downstream vessels through the specimen is used to determine the permeability through the sample. However, the pressure decay approach of Brace et al. (1968) does not account for the sorption effect on coal during CO_2 injection. Feng et al. (2016) consider that the modified pressure decay approach by Cui et al. (2009) can accurately calculate the permeability of sorptive rocks like coal, and this approach was therefore employed in the present study to calculate the brown coal's permeability (refer to Eqs. [4.1] and [4.2]).

$$\frac{(P_u - P_d)}{\Delta P_0} = e^{-\alpha t} \qquad [4.1]$$

$$k = \frac{\alpha \mu \beta L}{A f_1\left(\frac{1}{V_u} + \frac{1}{V_d}\right)} \qquad [4.2]$$

where, P_u is upstream vessel pressure, P_d is downstream vessel pressure, ΔP_0 is the step change of pressure in vessels at time = 0, t is time, k is permeability of the specimen, A is the cross-section area of the sample, L is the length of the sample, μ is the viscosity of the injecting fluid, β is the adiabatic compressibility of the injecting fluid, and V_u and V_d are the volume of upstream and downstream pressure vessels, respectively.

Here, $f_1 = \frac{\theta_1^2}{a+b}$ [4.3]

where, θ_1 is the first solution of the transcendental equation,

$$\tan\theta = \frac{(a+b)\theta}{\theta^2 - ab} \quad [4.4]$$

In Eq. [4.4], the a and b parameters are the gas storage capacity ratios of samples with upstream and downstream reservoirs and can be defined as follows (see Eqs. [4.5(a) and (b)]).

$$a = \frac{V_p(1+f_a)}{V_u} \quad [4.5(a)]$$

$$b = \frac{V_p(1+f_a)}{V_d} \quad [4.5(b)]$$

where, f_a is the ratio of effective porosity contributed by adsorption ($\emptyset_a$) and the porosity ($\emptyset$) of the coal specimen. The $\emptyset_a$ can be calculated by Eq. [4.6] using the adsorption parameters of the sample for the respective gases at experimental pressures.

$$\emptyset_a = \frac{\rho_s(1-\emptyset)}{V_{std}\beta\rho}\frac{V_L P_L}{(P_L+P)^2} \quad [4.6]$$

where, ρ_s is sample density, ρ is the gas density, V_{std} is the mole volume of gas at standard temperature and pressure (22.413E-3 m^3/mol), P is the pore pressure and V_L and P_L are Langmuir constants for volume and pressure, respectively. The permeability of the sample is calculated by plotting the pressure decay curves (in semi-log scale) with time. By substituting the slope of the resulting line "-α" of the pressure decay curves in Eq. [4.2], the permeability of the sample was obtained.

In addition, the pressure development of the downstream varies with the CO_2 flowrate along the sample. This CO_2 flowrate is also affected by the coal matrix swelling/shrinkage which occurs during gas permeation at different confining pressures, through which the influence of coal matrix swelling/shrinkage on permeability can also be incorporated (De Silva and Ranjith, 2014).

4.2.3 Experimental results and discussions

The following sections discuss (i) the effect of CO_2 phase and pressure on permeability in brown coal; (ii) the potential of reversing CO_2 adsorption-induced coal matrix alterations using N_2 in brown coal; and (iii) the effect of CO_2-induced coal matrix alterations in the micro-pore structure of brown coal.

4.2.3.1 Effect of CO_2 phase and pressure on coal permeability in brown coal

Figure 4.2 shows the permeability values obtained for first N_2 and first CO_2 injection into the brown coal samples for three different confinements. It should be noted that all the moisture in the sample was drained out before injecting the gasses and hence the permeability values obtained from CO_2 and N_2 injections do not have any influence of moisture in the coal sample.

a. First N_2 injection

According to Figure 4.2, N_2 permeability in brown coal gradually increases with increasing injection pressure at all three confinements. This is because the effective stress acting on the coal matrix reduces with increasing upstream pressure, resulting in an expansion of the coal mass pore spaces for N_2 movement. For example, increasing the injection pressure from 6 to 9 MPa at 11 MPa, 14 MPa and 17 MPa confinements caused the coal mass permeability to be enhanced by around 67%, 54% and 30%, respectively (Figure 4.2). A closer examination of these figures shows that, although increasing permeability with increasing injection pressure is a common fact for any confinement, the amount of increment is reduced with increasing confinement. This is believed to be related to the greater effective stress applying on the coal mass under high confinement, which may act as a barrier to coal mass pore structure expansion, resulting in reduced permeability enhancement. The influence of this greater effective stress at greater confinement can be clearly identified by observing the permeability behaviour for any N_2 injection pressure under various confinements. For example, according to Figure 4.3, increasing the confinement from 11 to 14 MPa and 11 to 17 MPa at 6 MPa injection pressure causes the brown coal permeability for N_2 to be reduced by around 46% and 70%.

Since this confinement effect is largely controlled by the effective stress applied to the coal mass and the coal pore structure’s response to it, it is worthwhile to identify how this influence varies with coal rank. Research has shown a similar permeability reduction with increasing confinement for high-rank coal (Perera et al., 2011b). However, the amount of permeability reduction is much higher for low-rank coal than high-rank coal. For example, increasing the confinement from 14 to 17 MPa (3 MPa increment in confinement) caused the brown coal permeability at 9 MPa N_2 injection pressure to be reduced by around 57% in this study (Figure 4.3), whereas the permeability reduction observed for Australian bituminous coal by Perera et al. (2011b) for the same N_2 injection pressure condition (9 MPa) was around 31% for 15 to 20 MPa confinement increment (5 MPa increment in confinement). This is because high-rank coal has been subjected to a greater degree of biodegradation, resulting in a higher elastic modulus (Australian bituminous coal has an elastic modulus of 3.67 GPa (Perera et al., 2011b)), and Victorian brown coal has an elastic modulus of 41.6 MPa (Jasinge, 2010)) and lower shrinkage compressibility (Australian bituminous coal has a shrinkage compressibility of around 7.69E-7 1/kPa (Pan et al., 2010)) and Victorian brown coal has a shrinkage compressibility around 1.21E-5 1/kPa (Massarotto et al., 2010)) compared to low-rank coal. Therefore, with increasing confinement, it has less ability to shrink compared to low-rank coal.

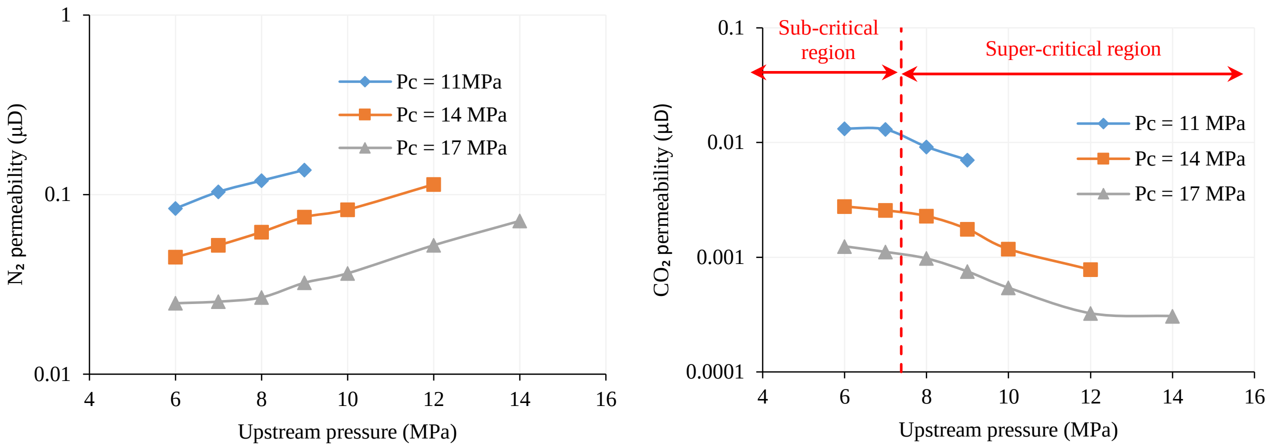

(a) First N_2 injection (b) Frist CO_2 injection

Figure 4.2. Permeability vs. upstream pressure for first N_2 and CO_2 injections during 11, 14 and 17 MPa confinements (Here Pc = confining pressure)

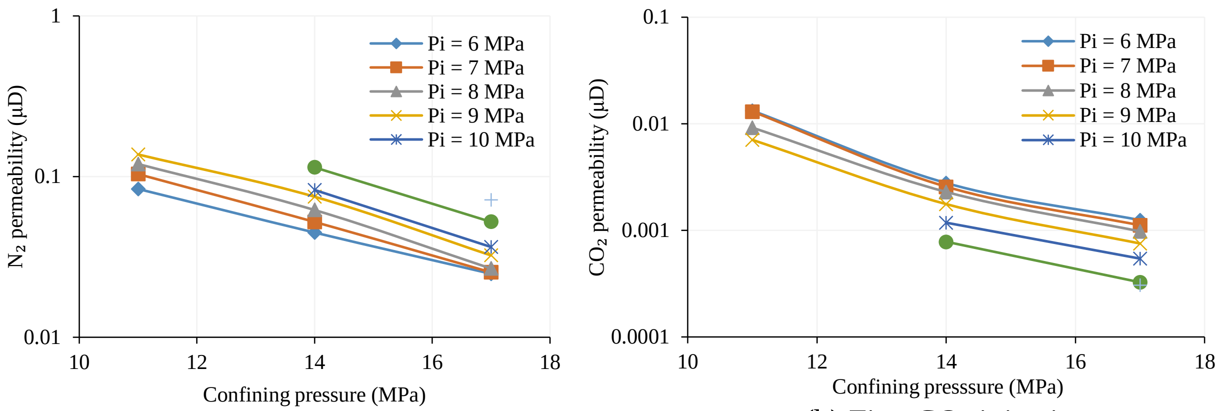

(a) First N_2 injection (b) First CO_2 injection

Figure 4.3. Permeability vs. confining pressure for first N_2 and CO_2 injections during 6 to 14 MPa injection pressures (Here Pi = injection pressure)

b. First CO_2 injection

➢ *Effect of injection pressure*

Unlike for N_2 injection, a reduction of brown coal permeability with increasing injection pressure can be observed for all the confinements for CO_2 injection (Figure 4.2), and the permeability reductions observed with increasing injection pressure (with respect to 6 MPa CO_2 injection) for each confinement are shown in Table 4.3. This permeability reduction with increasing injection pressure for CO_2 flow in coal has also been shown in the research literature (Pan et al., 2010; Perera et al., 2011b; Ranathunga et al., 2015; Vishal and Singh, 2015). Coal matrix swelling, which creates strutural modification in coal, is the cause, because matrix swelling shrinks the coal mass pore volume by increasing the tortuosity for CO_2 movement inside the coal matrix, resulting in reduced CO_2 permeability. Although this CO_2 permeability reduction trend is a new finding for low-rank coal, it has been well proven for high-rank coal (Pan et al., 2010; Perera et al., 2011b; Vishal and Singh, 2015). For instance, Pan et al. (2010) observed around 50% and 70% permeability reductions in bituminous coal when the CO_2 injection pressure was increased from 3 MPa to 13 MPa at 2 MPa and 6 MPa effective stresses, respectively.

Table 4.3. Permeability reduction (%) during first CO_2 injection for all three confinements (with respect to 6 MPa CO_2 injection)

Injection pressure	Confinement	Pc = 11MPa	Pc = 14 MPa	Pc = 17 MPa
Sub-critical region	Pi = 6 MPa	-	-	-
	Pi = 7 MPa	1.83	7.59	10.60
Super-critical region	Pi = 8 MPa	11.71	17.48	21.61
	Pi = 9 MPa	29.83	39.68	46.80
	Pi = 10 MPa	-	56.47	57.52
	Pi = 12 MPa	-	71.85	73.90
	Pi = 14 MPa	-	-	75.34

However, the main focus of this study is to understand the super-critical flow behaviour in low-rank coal. According to Table 4.3, the CO_2 permeability reduction with increasing injection pressure is greater in the super-critical region than in the sub-critical region. For example, at 11 MPa confinement, permeability reductions compared to the 6 MPa first CO_2 injection are around 1.83% and 11.71% for 7 and 8 MPa CO_2 injections, respectively. Therefore, it is important to study how the CO_2 phase condition varies inside the coal sample during each CO_2 injection condition to fully comprehend the phase influence on CO_2 permeability in brown coal. Figure 4.4 demonstrates the approximate CO_2 pressure distribution along the sample (after 24 hours of injection), assuming a linear variation of CO_2 pressures from upstream to downstream along the sample at the three different confinement pressures.

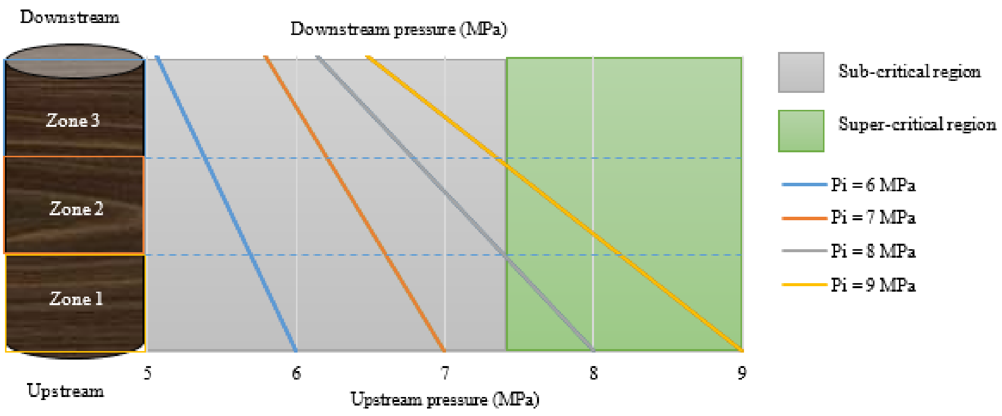

(a) Pc = 11 MPa

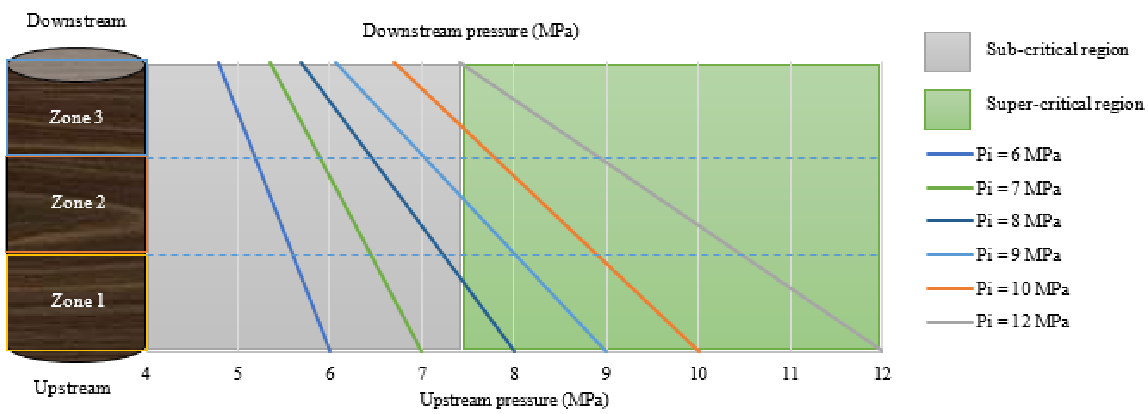

(b) Pc = 14 MPa

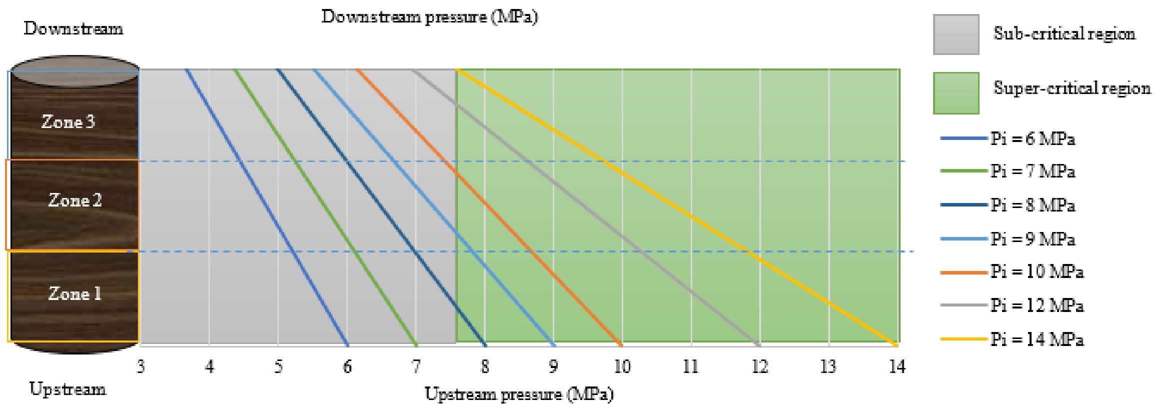

(c) Pc = 17 MPa

Figure 4.4. Downstream pressure variation for different CO_2 injection pressures at various confinements (after 24 hours of gas injection) (Here P_i = injection pressure and P_c = confining pressure)

According to Figure 4.4(a) and (b), during super-critical CO_2 permeation, only some regions are in super-critical condition while the rest of the sample is in sub-critical condition, due to the limited downstream pressure development under each condition (the sample has been divided into three major regions for explanatory purposes: zone 1 (near the upstream region), zone 2 (middle of the sample), and zone 3 (near the downstream region)). According to the figure, at 11 MPa confinement, only zone 1 of the sample is in super-critical condition during 8 MPa CO_2 injection, whereas both zone 1 and 2 are in super-critical condition for 9 MPa CO_2 injection (Figure 4.4(a)). Furthermore, during 14 MPa confinement, zone 1 is fully permeated with super-critical CO_2 at 8 MPa CO_2 injection and only zone 1 and around half of zone 2 have been affected by super-critical CO_2 for 9 MPa CO_2 injection. In the case of 10 MPa CO_2 injection, the effect of super-critical CO_2 extends to a part of zone 3 and the sample is fully flooded with super-critical CO_2 when 12 MPa CO_2 is injected during 14 MPa confinement (Figure 4.4(b)). This shows that a larger area is affected by super-critical CO_2 conditions with the increment of the injection pressure, which further clarifies the reason for the permeability reduction of the sample at higher CO_2 injection pressures. Super-critical CO_2 has greater ability to reduce coal mass flow performance due to its higher adsorption capacity into coal compared to sub-critical CO_2 (Bae and Bhatia, 2006), as super-critical CO_2 molecules create stronger van der Waals bonds with the coal matrix (Massarotto et al., 2010), causing greater swelling in the coal mass and resulting in a decrease in pore volume for CO_2 transport.

This greater CO_2 permeability reduction in its super-critical state has also been observed for high rank-coal by Perera et al. (2011b). A comparison of the permeabilities obtained for both brown coal (the present study) and black coal (Perera et al., 2011b) shows that, although greater CO_2 permeability reduction with increasing injection pressure is common to both coal types, the amount of reduction is rank-dependent. Increasing the injection pressure from 7 to 8 MPa causes the low- and high-rank CO_2 permeability values to be reduced by around 10.71% (at 14 MPa confinement) and 15.79% (for 15 MPa confinement) (Perera et al., 2011b), respectively. Further, brown coal shows only 12.31% reduction of permeability from 7 to 8 MPa CO_2 pressure increase during 17 MPa confinement (Figure 4.2), which is also lower than the reduction percentage observed for black coal under 15 MPa confinement (15.79%) (Perera et al., 2011b). This implies that the influence of CO_2 phase condition on the coal mass structure rearrangement increases with increasing rank, probably due to the well-developed natural cleat system in greatly matured high-rank coal compared with low-rank coal. This cleat system was formed during the coalification process and acts as a flow path for CO_2 movement in the coal matrix. The CO_2 molecules moving through the cleats then gradually adsorb into the coal matrix along the cleat wall. Therefore, the highly developed cleat system in high-rank coal offers a greater locus for CO_2 adsorption, which eventually produces greater swelling-related pore shrinkage, resulting in greater permeability reduction. Perera et al. (2016) have shown a greater strength reduction in high-rank coal compared with low-rank coal for both sub- and super-critical CO_2 injection pressures (up to 10 MPa), due to the greater absorption potential of CO_2 in high-rank coal. According to the findings of the present study, CO_2 adsorption also creates a greater permeability reduction in high-rank coal compared to low-rank coal.

➢ Effect of confining pressure

As expected, the permeability of CO_2 in brown coal greatly reduces with increasing confinement due to the associated effective stress-enhancement. Increasing the confinement from 11 MPa to 14 MPa causes the CO_2 permeability at 6 and 9 MPa injection pressures to reduce by around 80% and 75%, respectively. An important fact is that the influence of confining pressure is much greater for CO_2 than N_2, probably due to the fact that increasing the effective stress has a greater influence on the swelled coal matrix, and the swelled areas are believed to be more significantly subjected to the enhanced effective stress effect with increasing confinement due to their lower strength (Pan and Connell, 2007). This permeability reduction with increasing confinement for both sub- and super-critical CO_2 injections for high-rank coal has been reported previously (Pan et al., 2010; Perera et al., 2011b; Ranathunga et al., 2015; Vishal and Singh, 2015). For example, increasing the confinement from 7 to 11 MPa at 3 MPa CO_2 injection pressure and 16 to 20 MPa at 13 MPa CO_2 injection pressure caused Indian bituminous coal permeability to be reduced by around 80% (Vishal et al., 2013) and 48% (Vishal and Singh, 2015), respectively.

Interestingly, super-critical CO_2 permeability in brown coal is subjected to lower permeability reduction with increasing confinement. For example, around 75% and 57% permeability reductions were exhibited for 9 MPa super-critical CO_2 injection when the confinement increased from 11 to 14 MPa and 14 to 17 MPa (Figure 4.3), respectively. This is possibly because at high confinements, the coal mass pore space has already been significantly reduced by the high effective stress, and therefore further reduction with further increasing effective stress is less likely. According to Vishal and Singh (2015), this phenomenon is common for high-rank coal, and they observed around 48% and 39% permeability reductions for 13 MPa super-critical CO_2 injection when confining pressure was increased from 16 to 20 MPa and 20 to 25 MPa for Indian bituminous coal. This implies that, regardless of rank, the influence of depth on CO_2 permeability in coal reduces with increasing depth.

However, Perera et al. (2011b) observed an increase in CO_2 permeability when larger confinements are applied at higher CO_2 injection pressures (>10 MPa) for Australian bituminous coal. For example, they observed around 20% increase in permeability with increasing confinement from 15 to 20 MPa at 10 MPa super-critical CO_2 injection pressure (Perera et al., 2011b). In relation to the downstream pressure developments, higher CO_2 injections at lower confinements were mostly >7.38 MPa (CO_2 critical pressure) and hence the sample was largely under super-critical conditions (Perera et al., 2011b). However, the reduced permeability at higher confinements caused lower downstream pressure developments (<7.38 MPa), allowing the higher portion of the sample to undergo sub-critical conditions (Perera et al., 2011b). For example, the downstream pressure was around 7.5 MPa (100% of the sample was under super-critical conditions) and 6.2 MPa (around 70% of the sample was under super-critical conditions) for 10 MPa CO_2 injection during 15 and 20 MPa confinements respectively. Therefore, in comparison, larger confinements produced slightly larger permeability values than lower confinements at higher CO_2 injections. This was confirmed by the observed huge swelling effect created by super-critical CO_2 in high-rank coal, which has a greater influence than the depth effect. However, for brown coal, increasing the confinement from 11 to 14 MPa caused the permeability to be reduced by around 80% and 75% at 6 MPa sub-critical CO_2 injection and 9 MPa super-critical CO_2 injection, respectively (see Figure 4.3). These observations show that, although the influence of confinement on permeability is reduced with the phase transition from sub- to super-critical, the confinement effect remains much greater than the swelling effect in low-rank coal compared to high-rank coal, probably due to the much higher coal matrix shrinkage-related pore space reduction, which occurs with increasing depth in partially-matured low-rank coal.

Figure 4.4 clearly shows how confinement changes the influence of super-critical CO_2 injection on the coal matrix. According to the figure, at 11 MPa confinement, zone 1 of the sample is in fully super-critical condition during 8 MPa CO_2 injection, whereas both zone 1 and 2 are in fully super-critical permeated condition for 9 MPa CO_2 injection, and at 17 MPa confinement, only half of zone 1 is covered with super-critical CO_2-permeated coal for 8 MPa CO_2 injection and only around 25% of zone 2 is permeated with super-critical CO_2 at 9 MPa CO_2 injection. Therefore, the portion of super-critical CO_2 permeated in the sample reduces with increasing confinement, resulting in less influence of super-critical CO_2 adsorption at greater confinement.

4.2.3.2 Potential of N_2 to reverse CO_2 adsorption-induced coal matrix alterations in low rank coal

When N_2 is injected into the coal mass, it remains as a free gas (with very little adsorption potential compared to CO_2) in the fracture space, which creates an imbalance between the sorbed and free gas phases and eventually reduces the partial pressure of CO_2, resulting in the release of CO_2 from the coal mass (Reeves, 2003). This release of CO_2 molecules from the coal matrix can therefore partially recover the reversible swelling by physical adsorption of CO_2 (Kiyama et al., 2011). Although research has shown the ability of N_2 to partially reverse CO_2 adsorption-induced swelled areas in high-rank coal (Perera et al., 2011b), the influence of coal rank on it has not yet been discovered. This was therefore considered next. N_2 was again injected into swelled coal samples (with CO_2 injection) at the same injection pressures, and the total N_2 injection took around 24 hours. After this second N_2 injection, CO_2 was again injected into the samples to find how N_2 injection alters the coal mass flow ability or its ability to reverse the swelled areas created during the first CO_2 injection.

Firstly, the CO_2 adsorption-induced swelling effect was checked by observing the permeability values at first and second N_2 injections for all the confinements. According to Figure 4.5, the second N_2 injection also displays a behaviour consistent with that of the first N_2 injection, which depicts an increment in permeability with increasing injection pressure and a reduction of permeability with increasing confining pressure. However, the permeability of the coal mass for the second N_2 injection appears to be much lower than its permeability at first N_2 injection, which confirms the swelling-induced coal matrix rearrangement made during the CO_2 injection, and the effect is higher at higher confinements. The average permeability reductions observed during the second N_2 injection compared to the first N_2 injection were around 12%, 18% and 22% for 11 MPa, 14 MPa and 17 MPa confinements, respectively. As discussed previously, the greater permeability reduction observed at greater confinements is believed to be related to the greater influence of swelling-created pore space shrinkage at high confinements.

The ability of N_2 to recover CO_2 adsorption-induced swelled areas was then investigated by comparing the permeability of coal samples during the first (before the second N_2 injection) and second CO_2 injections (after the second N_2 injection) for all the confinements (Figure 4.6 and Table 4.4). According to Figure 4.6, for any confinement N_2 injection causes the CO_2 permeability to be enhanced at high injection pressures, and the degree of permeability enhancement reduces with increasing confinement. For example, at 9 MPa injection pressure, CO_2 permeability increases by around 21%, 9%, and 0.3% at 11, 14, and 17 MPa confinements (see Figure 4.6), respectively. This shows that N_2 injection also contributes to recovering the swelling areas created by CO_2 in low-rank coal. However, this enhancement disappears with lower injection pressure and increasing confinement, due to the large effective stress acting on low-rank brown coal compared to high-rank coal due to its highly porous, soft matrix. This compression of coal mass by the effective stress appears to be more significant than the permeability of the swelling area recovery. Therefore, although considerable permeability enhancement occurs at even low injection pressures and high confinements, the influence is concealed by the large coal matrix compression which occurs at such high effective stresses.

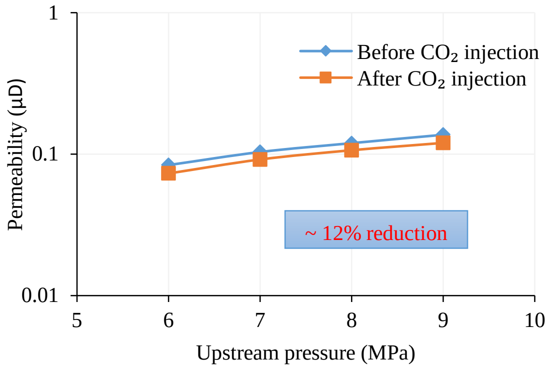

(a) P_c = 11 MPa

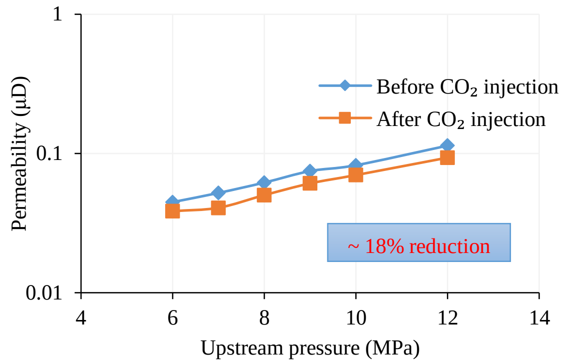

(b) P_c = 14 MPa

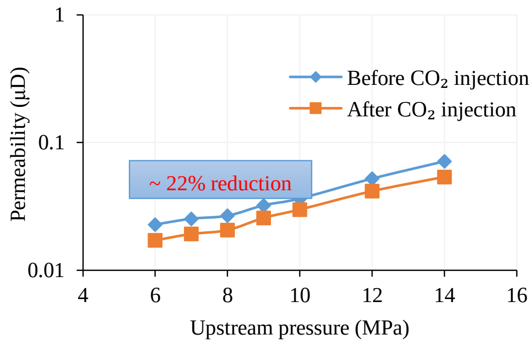

(c) P_c = 17 MPa

Figure 4.5. Permeability vs. upstream pressure for N_2 injection, before and after CO_2 injection during different confinements (Here P_c is confining pressure)

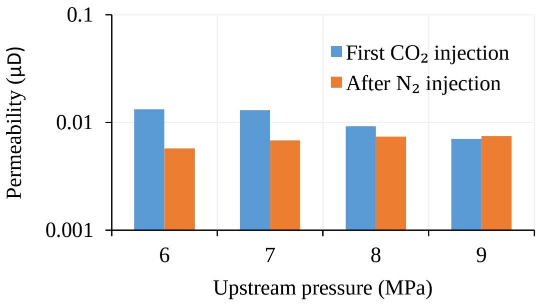

(a) P_c = 11 MPa

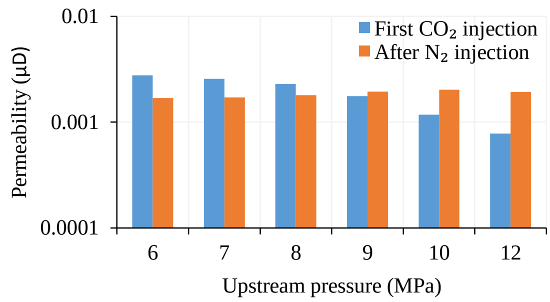

(b) P_c = 14 MPa

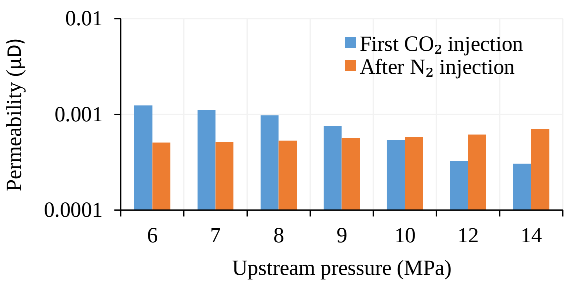

(c) P_c = 17 MPa

Figure 4.6. Permeability vs. upstream pressure for CO_2 injection, before and after N_2 injection during different confinements

Table 4.4. Permeability change (%) after N_2 flooding during CO_2 injection for all three confinements

Injection pressure \ Confinement		P_c = 11MPa	P_c = 14 MPa	P_c = 17 MPa
Sub-critical region	Pi = 6 MPa	-11.33	-10.11	-9.60
	Pi = 7 MPa	-10.49	-9.63	-4.42
Super-critical region	Pi = 8 MPa	7.71	-7.53	-1.23
	Pi = 9 MPa	19.19	9.07	0.27
	Pi = 10 MPa	-	11.28	8.12
	Pi = 12 MPa	-	16.65	12.31
	Pi = 14 MPa	-	-	14.01

In relation to the effect of coal rank on the potential of N_2 to reverse CO_2 adsorption-induced coal matrix alterations, Perera et al. (2011b) observed a comparatively higher permeability enhancement ability of N_2 in high-rank coal compared to low-rank coal. According to their study, N_2 flooding causes the enhancement of permeability for CO_2 of high-rank bituminous coal at 9 MPa injection pressure by around 15% at 15 MPa confinement, which is considerably greater than the N_2 permeability recovery potential observed for low-rank brown coal in this study under similar injection conditions (around 9% at 9 MPa CO_2 injection at 14 MPa confinement). This observed lower potential of N_2 to recover CO_2 adsorption-induced swelled areas is believed to be related to the high effective stress acting on soft and highly porous low-rank brown coal compared to dense high-rank bituminous coal. Furthermore, Perera et al. (2011b) observed an enhancement in swelling area recovery potential of N_2 with increasing confinement, where N_2 injection enhanced CO_2 permeability at 10 MPa injection pressure by around 15% and 17% at 15 and 20 MPa confinements, respectively. According to these researchers, this is due to the slower N_2 flow rate through the coal matrix offering more time to interact with the CO_2 adsorbed areas in the coal matrix, which enhances the swelling area recovery process performed by N_2. However, this greater recovery potential at higher confinement is contradictory to the reduced permeability recovery potential observed at higher confinement in low-rank brown coal. Potentially, although N_2 has greater permeability recovery potential in brown coal, that influence may be obscured by the influence of greater effective stress on soft, highly porous brown coal. However, this permeability behaviour after N_2 flooding for brown coal may vary with the duration of N_2 flooding, because, in the present study, N_2 was permeated for only 24 hours, which may not be enough to obtain higher recovery potential at higher effective stresses due to the low permeability. Therefore, offering more time for N_2 permeation through the coal mass may create enhanced recovery abilities, even for higher effective stresses in brown coal. This requires further attention in future studies.

4.2.3.3 Effect of CO_2-induced coal matrix alterations in micro-pore structure of brown coal

According to Pan and Connell (2007), the gas transport process in coal is greatly influenced by the pore structure of the coal mass. The continuity of the micro-pore structure and the connectivity with the macro-pore structure of the coal mass create efficiency in drainage and gas storage in the coal matrix (Davis et al., 1986). Therefore, a micro-structural analysis using SEM was carried out to determine the coal matrix alterations caused by CO_2 adsorption. The analysis was carried out on five specimens prior to and after the permeability tests and after scanning several random particles of each sample, and representative SEM images are shown in Table 4.5.

As the table shows, the SEM images after the experiment (CO_2 permeated) have a comparatively smoother surface compared to the images prior to the experiment (natural brown coal). Similar observations were made by Kutchko et al. (2013) for bituminous coal after exposing the specimens to CO_2 adsorption at 15.3 MPa at 55 ^{0}C. In addition, the natural brown coal specimens display more clear particle boundaries than the samples after CO_2 permeation, especially at the upstream (refer to Table 4.5). Further, the specimens before the experiment have a more uniform cellular-like micro-pore structure with relatively large pores. This cellular-like structure is still visible in some portions of the images of the specimens after the experiment, which display a reorganized and altered pore structure with CO_2 adsorption (see Table 4.5). These amorphous regions may have developed due to the plasticisation of coal polymer with CO_2 adsorption (Masoudian et al., 2014). According to Figure 4.4, the upstream was under super-critical conditions during all the super-critical CO_2 injections. The higher adsorption capacity of super-critical CO_2 may result in greater plasticisation in coal polymers, which eventually creates more amorphous regions than in the other specimens (middle and downstream). Similarly, Masoudian et al. (2014) observed amorphous spots due to plasticisation in bituminous coal after saturating the coal sample with 2.9 MPa CO_2 pressure under 3 MPa confining pressure for 72 hours, confirming the effect of coal matrix rearrangements for any coal type. In addition, the images taken under 1000 magnification show some striations (see the circled sections of the images) in CO_2 permeated coal samples, mainly in the upstream compared to the natural specimens. According to Davis et al. (1986), this striation is a characteristic of maceral collinite (structure-less maceral vitrinite). Therefore, referring to Table 4.5, the adsorption of super-critical CO_2 tends to generate collinite-type carbon structures in coal. This striation was also observed by Gathitu et al. (2009) for both lignite (from Beulah) and bituminous coal (from Illinois) samples after saturation at 22.75 MPa CO_2 under 130 ^{0}C for 48 hours and 55.85 MPa CO_2 under 80 ^{0}C for 48 hours, respectively. They further explained that the striation effect is greater at deeper depths of coal seams (higher pressures and temperatures) compared to lower depths (lower pressures and temperatures) (Gathitu et al., 2009).

However, it should be noted that the SEM results obtained may vary due to the following conditions. According to Tomasko et al. (2003), once the CO_2 pressure is released using a well-controlled slow depressurisation procedure, the morphological changes due to CO_2-induced plasticisation can be reversed. For the present study, it took around 12 hours to conduct the SEM analysis after the flow experiments, which may have caused desorption of adsorbed CO_2 from the sample with the long waiting time. In addition, further desorption of gasses may occur after applying the vacuum (low vacuum mode) for degassing, which may create changes in the results due to the potential reversibility during SEM analysis. Since the sample was also subjected to N_2 flooding, the expected large coal matrix alterations may not be visualized under this SEM analysis. However, these observations contribute to the demonstration of the altered flow behaviour during CO_2 injection into the coal mass.

Table 4.5. SEM images of sample before and after experiment at upstream, middle and downstream

Zone[1]	**Before experiment**		**After experiment**	
	Magnification – 10k[2]	**Magnification – 1k**[3]	**Magnification – 10k**[2]	**Magnification – 1k**[3]
Zone 1 (Upstream)	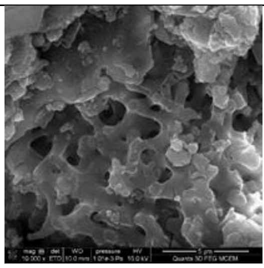	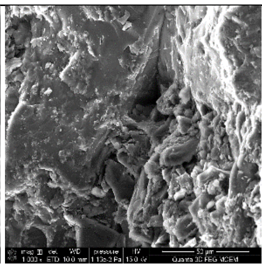	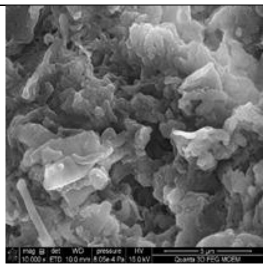	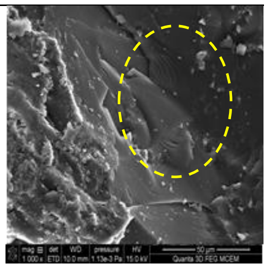
Zone 2 (Middle)	Not conducted	Not conducted	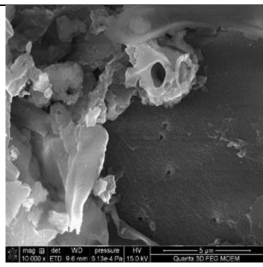	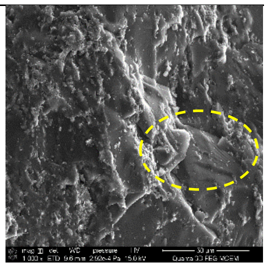
Zone 3 (Downstream)	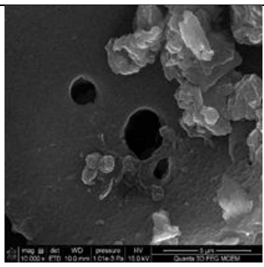	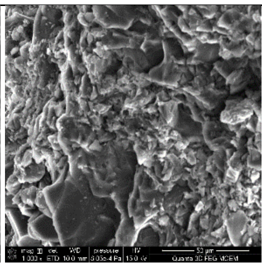	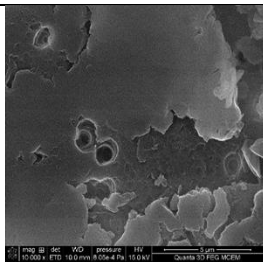	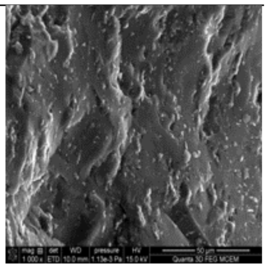

[1] Refer to Figure 4.4 to identify the zones in the brown coal specimen
[2] Conditions used to obtain SEM images: scale – 5 µm, probe current – 15 kV and spot size 4.5 under low vaccum
[3] Conditions used to obtain SEM images: scale – 50 µm, probe current – 15 kV and spot size 4.5 under low vaccum

6.2.3.4 Implications for CO_2 sequestration in coal seams

Generally, super-critical CO_2 is preferred for CO_2-ECBM recovery due to its higher adsorption capacity to the coal matrix (Day et al., 2010) and the ability for stable storage of CO_2 due its higher densities (Hendricks and Blok, 1993). However, reduction of CO_2 flow ability through the coal matrix during super-critical CO_2 sequestration makes the CO_2-ECBM process less productive, since the targeted amount of CO_2 cannot be stored in the coal mass, leading to unpredictable CH_4 recovery. The field-scale CO_2-ECBM projects which exhibited a decrease in CO_2 injection capacity within the first six months to two years after CO_2 injection (Ranathunga et al., 2014a) support the findings of this study. However, the possible permeability reduction with super-critical CO_2 injection reduces with reducing rank, which shows the suitability of low-rank coal seams for the CO_2-ECBM process. However, considering other factors, such as safety-related issues and availability, medium-rank coal seams are more suitable.

Furthermore, according to the findings of this study, regardless of rank, CO_2 permeability in coal reduces with increasing depth. Currently, there is interest in utilising extremely deep underground coal seams for CO_2 sequestration, due to the possibility of mining shallow seams. Generally, the permeability of the coal mass is reduced with depth, which is a main drawback for these types of projects. However, according to the current findings, this depth effect does not have such a great influence on CO_2 permeability as one would expect, especially in high-rank coal, and it would be useful to implement field projects in deep coal seams.

The findings indicate that the injection of an inert gas like N_2 has the potential to recover coal matrix rearrangements due to CO_2 adsorption by desorbing CO_2 molecules from the coal matrix in any rank coal, although the recovery ability may be somewhat less for low-rank than high-rank coal, particularly under higher effective stresses. Several field-scale projects have incorporated pure N_2 in order to enhance CO_2 injection capacity, including those in the Ishikari basin in Japan (CO_2 injection rate from 2.3 tons/day to 6.6 tons/day) (Fujioka et al., 2010) and the Fenn Big Valley basin in Canada (CO_2 absolute permeability from 1 mad to 13.8 mad) (Mavor et al., 2004). Some field-scale projects have used a mixture of CO_2 and N_2 (flue gas) to increase CO_2 permeability through the coal mass, including the Fenn Big Valley basin project in Canada (CO_2 absolute permeability from 1 mad to 5.6 mad) (Mavor et al., 2004). However, these increments are insufficient for economical and efficient CO_2 sequestration.

Considering all these facts, the findings of this study verify the complications when using super-critical CO_2 for CO_2-ECBM recovery in terms of CO_2 storage capacity and CH_4 production enhancement. Nevertheless, this is compensated by the anticipated larger and more stable super-critical CO_2 storage capacity in coal masses. Field-scale reservoir studies are very useful for investigating the possible effects of CO_2 adsorption-induced coal matrix alterations on permeability. Laboratory tests conducted for various reservoir conditions under a controlled environment can be used to obtain better insights into the effects of CO_2 sequestration on the coal mass, which can be used to support reservoir studies by developing laboratory-scale models which can then be extended to a field-scale reservoir study. The SEM analysis of brown coal specimens demonstrates the possible micro-structural behaviours with CO_2 adsorption that can be adapted with the real case scenario of coal matrix rearrangement during CO_2-ECBM recovery. These results are expedient for a thorough evaluation of possible matrix alterations with CO_2 adsorption in coal reservoirs, and to assist reservoir studies.

4.2.4 Conclusions

The following major conclusions can be drawn from the study:

- Although the reduction of permeability with increasing depth due to associated effective stress variations is common for any type of coal, the amount of permeability reduction with increasing depth is much higher for low-rank coals compared to high-rank coal, due to their partially mature, soft and highly compressible nature.
- The uniform cellular-like micro-pore structure with relatively large pores in natural brown coal significantly alters with CO_2 adsorption, which negatively affects the coal mass flow performance. This matrix re-arrangement is much greater for super-critical CO_2 adsorption compared to sub-critical CO_2. Therefore, super-critical CO_2 has much lower permeability than sub-critical CO_2, regardless of coal rank.
- However, the influence of CO_2 phase condition increases with increasing rank, probably due to the well-developed natural cleat system in high-rank coal compared to low-rank coal, which acts as a locus for CO_2 transportation in the coal mass. This causes greater swelling in high-rank compared to low-rank coal.
- The influence of depth on permeability reduces with phase transition from sub- to super-critical in any type of coal due to the greater swelling effect created by super-critical CO_2. However, the effect of greater super-critical CO_2 adsorption-induced swelling in high-rank coal causes this depth effect on coal permeability to reduce with increasing rank.
- Regardless of rank, the influence of depth on CO_2 permeability in coal reduces with increasing depth. However, the depth effect does not have such a great influence on CO_2 permeability as one would expect.
- Although N_2 has the ability to recover CO_2 adsorption-induced swelled areas in coal regardless of rank, the recovery ability is much higher for high-rank coal due to the greater effective stress on soft and highly porous low-rank brown coal compared to dense high-rank coal.

4.2.5 References

Anggara, F., Sasaki, K., Sugai, Y., (2013). Swelling Measurements of a Low Rank Coal in Supercritical CO_2. *International Journal of Geosciences* 4, 863.

Bae, J.-S., Bhatia, S.K., (2006). High-Pressure Adsorption of Methane and Carbon Dioxide on Coal. *Energ Fuel* 20, 2599-2607.

Baran, P., Cygankiewicz, J., Zarębska, K., (2013). Carbon dioxide sorption on polish ortholignite coal in low and elevated pressure. *Journal of CO_2 Utilization* 3–4, 44-48.

Brace, W.F., Walsh, J., Frangos, W., (1968). Permeability of granite under high pressure. *Journal of Geophysical Research* 73, 2225-2236.

Busch, A., Gensterblum, Y., (2011). CBM and CO_2-ECBM related sorption processes in coal: a review. *International Journal of Coal Geology* 87, 49-71.

Chen, Z., Pan, Z., Liu, J., Connell, L.D., Elsworth, D., (2011). Effect of the effective stress coefficient and sorption-induced strain on the evolution of coal permeability: experimental observations. *International Journal of Greenhouse Gas Control* 5, 1284-1293.

Cuéllar-Franca, R.M., Azapagic, A., (2015). Carbon capture, storage and utilisation technologies: A critical analysis and comparison of their life cycle environmental impacts. *Journal of CO_2 Utilization* 9, 82-102.

Cui, X., Bustin, A., Bustin, R.M., (2009). Measurements of gas permeability and diffusivity of tight reservoir rocks: different approaches and their applications. *Geofluids* 9, 208-223.

Davis, M., White, A., Deegan, M., (1986). Scanning electron microscopy of coal macerals. *Fuel* 65, 277-280.

Day, S., Fry, R., Sakurovs, R., Weir, S., (2010). Swelling of Coals by Supercritical Gases and Its Relationship to Sorption. *Energ Fuel* 24, 2777-2783.

De Silva, P.N.K., (2013). A study of CO_2 storage capacity in sedimentary rocks (*PhD Thesis)*. Monash University, Melbourne, Australia.

De Silva, P.N.K., Ranjith, P.G., (2014). Understanding the significance of in situ coal properties for CO_2 sequestration: An experimental and numerical study. *Int J Energ Res* 38, 60-69.

Durucan, S., Shi, J.-Q., (2009). Improving the CO_2 well injectivity and enhanced coalbed methane production performance in coal seams. *International Journal of Coal Geology* 77, 214-221.

Feng, R., Harpalani, S., Pandey, R., (2016). Evaluation of Various Pulse-Decay Laboratory Permeability Measurement Techniques for Highly Stressed Coals. *Rock Mechanics and Rock Engineering*, 1-12.

Fujioka, M., Yamaguchi, S., Nako, M., (2010). CO_2-ECBM field tests in the Ishikari Coal Basin of Japan. *International Journal of Coal Geology* 82, 287-298.

Gathitu, B.B., Chen, W.-Y., McClure, M., (2009). Effects of coal interaction with supercritical CO2: physical structure. *Industrial & Engineering Chemistry Research* 48, 5024-5034.

Harpalani, S., Schraufnagel, R.A., (1990). Shrinkage of coal matrix with release of gas and its impact on permeability of coal. *Fuel* 69, 551-556.

Hendriks, C., Blok, K., (1993). Underground storage of carbon dioxide. *Energy Conversion and Management* 34, 949-957.

Jasinge, D., (2010). An investigation of the effect of carbon dioxide sequestration on the behaviour of brown coal (*PhD thesis*), Monash University, Melbourne, Australia.

Jasinge, D., Ranjith, P.G., Choi, S.K., (2011). Effects of effective stress changes on permeability of Latrobe Valley brown coal. *Fuel* 90, 1292-1300.

Kiyama, T., Nishimoto, S., Fujioka, M., Xue, Z., Ishijima, Y., Pan, Z., Connell, L.D., (2011). Coal swelling strain and permeability change with injecting liquid/supercritical CO_2 and N_2 at stress-constrained conditions. *International Journal of Coal Geology* 85, 56-64.

Kutchko, B.G., Goodman, A.L., Rosenbaum, E., Natesakhawat, S., Wagner, K., (2013). Characterization of coal before and after supercritical CO_2 exposure via feature relocation using field-emission scanning electron microscopy. *Fuel* 107, 777-786.

Levine, J.R., (1993). Coalification: The Evolution of Coal as Source Rock and Reservoir Rock for Oil and Gas: Chapter 3 In: Law, B.E., Rice, D.D. (Eds.), *Hydrocarbons from Coal*. American Association of Petroleum Geologists, AAPG Studies in Geology, 38, pp. 39–77.

Masoudian, M.S., (2016). Multiphysics of carbon dioxide sequestration in coalbeds: A review with a focus on geomechanical characteristics of coal. *Journal of Rock Mechanics and Geotechnical Engineering* 8, 93-112.

Masoudian, M.S., Airey, D.W., El-Zein, A., (2014). Experimental investigations on the effect of CO_2 on mechanics of coal. *International Journal of Coal Geology* 128–129, 12-23.

Massarotto, P., Golding, S., Bae, J.-S., Iyer, R., Rudolph, V., (2010). Changes in reservoir properties from injection of supercritical CO_2 into coal seams - A laboratory study. *International Journal of Coal Geology* 82, 269-279.

Mavor, M., Gunter, W., Robinson, J., (2004). Alberta multiwell micro-pilot testing for CBM properties, enhanced methane recovery and CO_2 storage potential, SPE Annual Technical Conference and Exhibition, Paper No. SPE 90256.

Oldenburg, C.M., (2006). Geologic carbon sequestration: CO_2 transport in depleted gas reservoirs, *Gas Transport in Porous Media,* Ho, C.K., Webb, S.W. (Eds.), Springer, Netherland, Chapter 26, pp 419-425.

Pan, Z., Connell, L.D., (2007). A theoretical model for gas adsorption-induced coal swelling. *International Journal of Coal Geology* 69, 243-252.

Pan, Z., Connell, L.D., Camilleri, M., (2010). Laboratory characterisation of coal reservoir permeability for primary and enhanced coalbed methane recovery. *International Journal of Coal Geology* 82, 252-261.

Perera, M.S.A., Ranjith, P.G., Airey, D.W., Choi, S.K., (2011a). Sub- and super-critical carbon dioxide flow behaviour in naturally fractured black coal: An experimental study. *Fuel* 90, 3390-3397.

Perera, M.S.A., Ranjith, P.G., Choi, S.K., Airey, D., (2011b). The effects of sub-critical and super-critical carbon dioxide adsorption-induced coal matrix swelling on the permeability of naturally fractured black coal. *Energy* 36, 6442-6450.

Perera, M.S.A., Ranjith, P.G., (2012). Carbon dioxide sequestration effects on coal's hydro-mechanical properties: a review. *Int J Energ Res* 36, 1015-1031.

Perera, M.S.A., Ranjith, P.G., Choi, S.K., Airey, D., (2012). Investigation of temperature effect on permeability of naturally fractured black coal for carbon dioxide movement: An experimental and numerical study. *Fuel* 94, 596-605.

Perera, M.S.A., Ranathunga, A.S., Ranjith, P.G., (2016). Effect of Coal Rank on Various Fluid Saturations Creating Mechanical Property Alterations Using Australian Coals. *Energies* 9, 440.

Ranathunga, A.S., Perera, M.S.A., Ranjith, P.G., (2014a). Deep coal seams as a greener energy source: a review. *Journal of Geophysics and Engineering* 11, 063001.

Ranathunga, A.S., Perera, S.A., Gamage, R.P., (2014b). An Experimental Study to Investigate the Temperature Effect on Permeability of Victorian Brown Coal during CO_2 Sequestration, ISRM International Symposium-8th Asian Rock Mechanics Symposium. International Society for Rock Mechanic s, Sapporo, Japan, (2014) paper ID 88.

Ranathunga, A.S., Perera, M.S.A., Ranjith, P.G., Ju, Y., Vishal, V., De Silva, P.N.K., (2015). A macro-scale experimental study of sub-and super-critical CO_2 flow behaviour in Victorian brown coal. *Fuel* 158, 864-873.

Ranjith, P.G., Perera, M.S.A., (2012). Effects of cleat performance on strength reduction of coal in CO_2 sequestration. *Energy*, 45, 1069-1075.

Reeves, S., O'Neill, P., (1989). Preliminary results from the broad meadow pilot, project Bowen basin Australia, Proc. 1989 Coalbed Methane Symposium, University of Alabama School of Mines and Energy Development and Gas Research Inst., Tuscaloosa, AL, pp. 273-291.

Reeves, S.R., (2003). Enhanced CBM recovery, coalbed CO_2 sequestration assessed, *The Oil and Gas Journal*, 101.27, 49-53.

Reucroft, P.J., Sethuraman, A.R., (1987). Effect of pressure on carbon dioxide induced coal swelling. *Energ Fuel* 1, 72-75.

Siriwardane, H., Haljasmaa, I., McLendon, R., Irdi, G., Soong, Y., Bromhal, G., (2009). Influence of carbon dioxide on coal permeability determined by pressure transient methods. *International Journal of Coal Geology* 77, 109-118.

Syed, A., Durucan, S., Shi, J.Q., Korre, A., (2013). Flue Gas Injection for CO_2 Storage and Enhanced Coalbed Methane Recovery: Mixed Gas Sorption and Swelling Characteristics of Coals. *Energy Procedia* 37, 6738-3745.

Tomasko, D.L., Li, H., Liu, D., Han, X., Wingert, M.J., Lee, L.J., Koelling, K.W., 2003. A Review of CO_2 Applications in the Processing of Polymers. *Industrial & Engineering Chemistry Research* 42, 6431-6456.

Vishal, V., Ranjith, P., Pradhan, S., Singh, T., (2013). Permeability of sub-critical carbon dioxide in naturally fractured Indian bituminous coal at a range of down-hole stress conditions. *Engineering Geology* 167, 148-156.

Vishal, V., Singh, T.N., (2015). A Laboratory Investigation of Permeability of Coal to Supercritical CO_2. *Geotech Geol Eng* 33, 1009-1016.

Walker Jr, P.L., Verma, S.K., Rivera-Utrilla, J., Khan, M.R., (1988). A direct measurement of expansion in coals and macerals induced by carbon dioxide and methanol. *Fuel* 67, 719-726.

Wang, L., Wang, Z., Li, K., Chen, H., (2015). Comparison of enhanced coalbed methane recovery by pure N_2 and CO_2 injection: Experimental observations and numerical simulation. *Journal of Natural Gas Science and Engineering* 23, 363-372.

Wang, S., Elsworth, D., Liu, J., (2011). Permeability evolution in fractured coal: The roles of fracture geometry and water-content. *International Journal of Coal Geology* 87, 13-25.

White, C.M., Smith, D.H., Jones, K.L., Goodman, A.L., Jikich, S.A., LaCount, R.B., DuBose, S.B., Ozdemir, E., Morsi, B.I., Schroeder, K.T., (2005). Sequestration of Carbon Dioxide in Coal with Enhanced Coalbed Methane Recovery: A Review. *Energ Fuel* 19, 659-724.

Zhang, X., Ranjith, P.G., Perera, M.S., Ranathunga, A., Haque, A., (2016). Gas Transportation and Enhanced Coalbed Methane Recovery Processes in Deep Coal Seams: A Review. *Energ Fuel* 30, 8832-8849.

4.3 How can the individual effect of effective stress and sorption-induced strain on the evolution of coal permeability be evaluated?

4.3.1 Overview

According to the findings of Section 4.2, both effective stress and the sorption-induced strain in the coal mass cause the observed permeability variations with CO_2 permeation. For an effective application of CO_2-ECBM, identification of the influence of permeability alterations due to each parameter (effective stress and swelling) is needed. The reduction of permeability with the application of higher effective stresses is a common effect for any rock type (Al-Wardy and Zimmerman, 2004; Chen et al., 2011; Ghabezloo et al., 2009; Jasinge et al., 2011; Rathnaweera et al., 2015; Zhao et al., 2003). Hence, the permeability evolution in coal due to CO_2 adsorption requires attention in regard to investigating the CO_2 flow behaviour in coal. Hence, the present study attempted to differentiate the effect of the effective stress and the sorption-induced swelling on coal mass permeability by calibrating the adsorbing-gas permeabilities (CO_2) using the effective stress parameters for comparatively non-adsorbing gas permeabilities (N_2) for both Australian low and high rank coals.

This section of the chapter is the following paper:

Ranathunga AS, Perera MSA, Ranjith PG (2017). Effect of effective stress and coal matrix swelling on coal flow behaviour during CO_2 sequestration. *J of CO_2 Utilization* (under review).

Effect of effective stress and coal matrix swelling on coal flow behaviour during CO_2 sequestration

A.S. Ranathunga[1], M.S.A. Perera[1,2], P.G. Ranjith[1]

[1]Deep Earth Energy Laboratory, Department of Civil Engineering, Monash University, Building 60, Melbourne, Victoria, 3800, Australia.

[2] Department of Infrastructure Engineering, The University of Melbourne, Building 176, Melbourne, Victoria, 3010, Australia.

Abstract

Permeability is one of the most important parameters for CO_2 injection in coal to enhance coalbed methane recovery. Generally, when the adsorbing gasses are injected, the permeability of the coal matrix can be reduced due to both gas adsorption-induced coal mass alterations and in situ stress application-induced coal matrix shrinkage. Laboratory characterization of coal permeability due to these effects provides useful information on the in situ permeability behaviour of coal seams. In this study, a series of experiments were conducted on Victorian brown coal samples using both non-adsorbing (N_2 has much less adsorption compared to CO_2) and adsorbing gases (CO_2) under various confining stresses and pore pressures. In order to determine the causes of permeability reduction for adsorbing gases, non-adsorbing N_2 was used to determine the effective stress coefficient. In these experiments using N_2, the impact of gas sorption was ignored and any permeability reduction was considered as being due to the variation in the effective stress, which is controlled by the effective stress coefficient.

The results show that the effective stress coefficient in the coal studied is significantly pore pressure-dependent and less than unity, and results reported in the research literature indicate that this behaviour is similar for high rank coal. The permeability reduction behaviour obtained from N_2 injecting experiments was then used to calibrate the subsequent flow-through experiments using the adsorbing gas CO_2. Through this calibration, the sole effect of sorption-induced strain on permeability change was obtained for these adsorbing gas flow experiments. The sorption strain-induced permeability clearly showed an over-estimation of permeability reduction, and the error is greater at higher effective stresses, regardless of rank. Importantly, the swelling effect on permeability is dominant in high-rank coal and in contrast, effective stress influence is dominant for low-rank coal. This swelling-induced permeability alteration in coal can be predicted using the D-R model by empirically deriving the D-R model parameters, regardless of rank.

Keywords: brown coal, CO_2 sorption-induced swelling, coal rank, effective stress, permeability

4.3.2 Introduction

To date, numerous studies (Chen et al., 2012; Jasinge et al., 2011; Pan et al., 2010; Perera et al., 2011; Pini et al., 2009; Shi et al., 2014; Siriwardane et al., 2009; Vishal and Singh, 2015) have been conducted on coal mass flow behaviour during CO_2 sequestration in deep coal seams and the CO_2 enhanced methane recovery process in them. Adsorption of CO_2 into coal induces strains between the adsorbing gas layer and the coal pore walls called coal matrix swelling, and these strains cause a reduction in permeability. For example, Chen et al. (2011), Jasinge et al. (2011), Pan et al. (2010), Patching (1965), Perera et al. (2011), Pini et al. (2009), Ranathunga et al. (2015) and Somerton et al. (1975) found that the permeability of coal for CO_2 is comparatively lower than that for non-adsorbing gases (N_2, He, etc.), regardless of coal type. It is therefore important to quantify the permeability alteration in coal with sorption-induced swelling. However, permeability values obtained through laboratory experiments include the effects of both effective stress and swelling (Figure 4.7). It is therefore necessary to eliminate the influence of effective stress in order to precisely understand the effect of swelling on coal permeability.

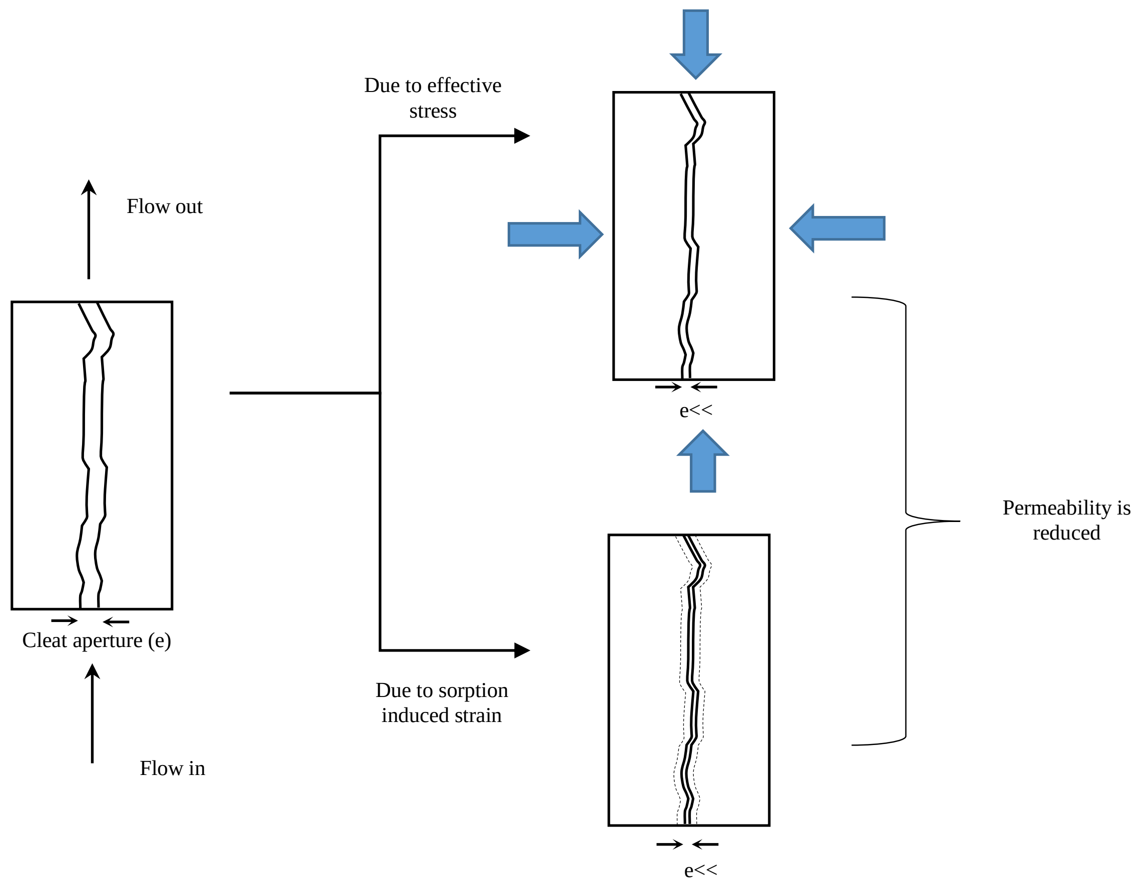

Figure 4.7. Permeability reduction due to effect of effective stress and swelling strain in coal samples

Pan et al. (2010), Lin et al. (2008), Mavor and Gunter (2004), Huy et al. (2010) Siriwardane et al. (2009) and Pini et al. (2009) conducted flow experiments on CO_2 permeability in coal at a given effective stress condition ($P_{eff} = P_c - \alpha P_i$: where P_{eff} is effective stress, P_c is confining pressure, P_i is pore pressure and α is the effective stress parameter) to obtain the permeability variation in coal due to CO_2-induced swelling and observed a reduction of permeability with increasing pore pressure. However, they assumed the effective stress coefficient (α) to be unity, which may not be accurate, particularly for some confining pressures, pore pressure conditions and rock types (Chen et al., 2011). For example, according to Walsh (1981), the effective stress parameter, α is 0.9 for rocks with polished joints and according to Kranzz et al. (1979), it is 0.56 for rocks with tensile joints. A linear increment of effective stress parameter, α, with increasing pressure difference between confining pressure and pore pressure has been reported by Ghabezloo et al. (2009), and according to Rathnaweera et al. (2015), it linearly decreases with increasing degree of salinity in the pore fluid. Nur and Byerlee (1971) calculated the effective stress parameter, α, as 0.64 for sandstone, observing the variation of permeability for sandstone, and Bernabe (1987) showed a decreasing trend of effective stress parameter for permeability with increasing confining pressure for crystalline rocks.

However, to date little attention has been given to the variation of the effective stress coefficient in coal. Zhao et al. (2003) suggested a bilinear function for the effective stress coefficient with pore pressure and volumetric stress, and George and Barakat (2001) proposed α = 0.71 for sub-bituminous coal using non-adsorbing helium after conducting a series of loading and un-loading gas pressure tests. However, for these experiments only the volumetric strain was used as the physical parameter to determine the effective stress coefficient. According to existing studies (Nur and Byerlee, 1971; Bernabe, 1987), not only volumetric strain, but also permeability, confining pressure and pore pressure variations should be incorporated in predicting the effective stress parameter.

Chen et al. (2011) examined helium permeation through high-rank Australian coal at constant pressure differences ($dP = P_c - P_i$: where dP is the pressure difference, P_c is the confining pressure and P_i is the pore pressure) to obtain the effective stress coefficient of coal paying attention to the influences of permeability, confining pressure and pore pressure variations. They applied the widely-used exponential relationship between permeability and effective stress (Eq. [4.7]) proposed by McKee et al. (1988) to obtain the effective stress coefficient.

$$k = k_0 exp\left[-3c_f(\Delta\sigma - \alpha\Delta p)\right] \qquad [4.7]$$

where, k is the permeability, k_0 is the initial permeability, c_f is the cleat compressibility, $\Delta\sigma$ is the confining stress change, Δp is the pore pressure change and α is the effective stress coefficient.

They obtained a less than unity (< 1) effective stress coefficient for coal, importantly as a variable with pore pressure (the effective stress coefficient increases with increasing pore pressure). Assuming the effective stress does not change for similar pressure conditions for CO_2 and CH_4 permeations (dP was constant throughout the tests series), Chen et al. (2011) eliminated the effective stress-induced permeability variation of high rank coal to find the swelling-induced permeability variation in coal, and showed that the swelling-induced permeability reduction is much higher (1.5 to 2.1 times) than the effective stress-induced permeability reduction (high rank bituminous coal). However, to date no similar study has been conducted on low rank coal, which is however essential to understand how such influences vary with coal maturity or rank.

This has therefore been considered in the present study to investigate the swelling- induced permeability variations in low-rank brown coal by eliminating the influence of effective stress. A similar approach was used in the present study to investigate the permeability variations due to sorption-induced strain for low-rank coal brown coal. The results were then compared with those of Chen et al. (2011) to understand the effect of coal rank on swelling-created permeability alterations in coal. Furthermore, an effort was made to predict the swelling- induced permeability changes in coal by applying the widely-used Dubinin–Radushkevich (D-R) model for both low-rank (present study) and high rank coal (Chen et al., 2011)).

4.3.3 Methods and procedures

Following procedures were adopted to investigate the effect of effective stress and the sorption-induced strain on coal permeability variations.

4.3.3.1 Measure permeability using N_2

To calibrate the permeability of adsorbing gas CO_2, N_2 permeability under various pore pressures and confining pressures was used. Figure 4.8 shows the variation of adsorbed gas volume of CO_2 and N_2 for the tested Victorian brown coal samples measured using the gravimetric method. According to Figure 4.8, N_2 has much lower adsorption potential to the tested coal samples compared to CO_2 (more than 9 times lower) and hence, N_2 was considered as a comparatively inert gas for calibration purposes. The permeability data obtained by Ranathunga et al. (2017a) based on meso-scale tri-axial tests under constant pressure differences were used in this study (Figure 4.9).

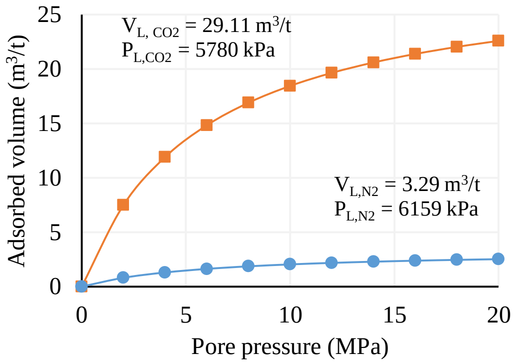

Figure 4.8. Langmuir isotherms for CO_2 and N_2 for the brown coal samples under 40 ^{0}C (here V_L and P_L are Langmuir volume and pressure)

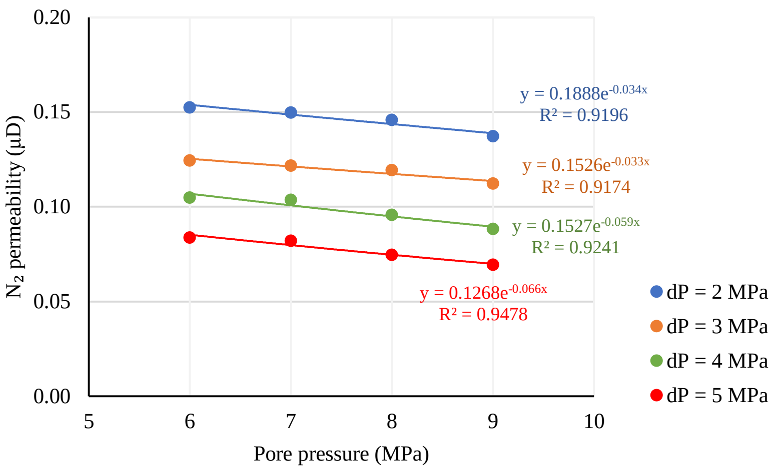

Figure 4.9. N_2 permeability vs. pore pressure with pressure difference (here P_i is pore pressure and the P_c is confining pressure) (Ranathunga et al. 2016a)

4.3.3.2 Understanding the influence of effective stress

According to Figure 4.9, N_2 permeability shows a reduction with pore pressure for the given pressure differences. As mentioned earlier, since N_2 is almost a non-adsorbing gas to brown coal, the effect of matrix swelling on permeability change by N_2 adsorption is negligible, which is further confirmed by the test results obtained by Ranathunga et al. (2017b). The observed reduction in N_2 permeability with pore pressure increase is therefore be due to the Klinkenberg effect and the effective stress effect. In regard to the Klinkenberg effect, Laubach et al. (1998) stated that the mean free path of the gas molecules at higher pressures is much lower than the aperture of the coal cleats (3-40 μm) and hence collisions between the gas molecules are more common than collisions between the coal pore walls and the gas molecules (Han et al., 2010), resulting in minor slip flow or the Klinkenberg effect. Hence, the effect of effective stress is the reason for the observed permeability reduction with the pore pressure.

a. Calculation of coal cleat compressibility

Here, the exponential function proposed by McKee et al. (1988) was used to obtain the effective stress parameter (refer to Eq. [4.8]). If the pore pressure (P_i) is kept constant and only the confining pressure (P_c) is varied, the cleat compressibility of the coal sample can be obtained using the simple permeability relationship with confining stress change (refer to Eq. [4.8]).

$$k = k_0 exp\left(-3c_f \Delta\sigma\right) \quad [4.8]$$

The cleat compressibility values for N_2 and CO_2 obtained from Eq. [4.8] are summarised in Table 4.6. The average compressibility values were used to calculate the effective stress coefficients.

Table 4.6. Compressibility values for different gases and pore pressures

Pore pressure (MPa)	**C_f for N_2 (1/MPa)**	**C_f for CO_2 (1/MPa)**
6	0.0784	0.1189
7	0.0778	0.1197
8	0.0766	0.1214
9	0.0757	0.1233
Average C_f	0.0771	0.1208

b. Calculation of coal effective stress coefficient

For a considered constant pressure difference ($\Delta\sigma = \Delta p$), Eq. [4.7] can be further simplified as follows (refer to Eq. [4.9]).

$$k = k_0 exp\left[-3c_f(1-\alpha)\Delta p\right] \quad [4.9]$$

By substituting the cleat compressibility values obtained from Eq. [4.9], the effective stress coefficient (α) can be obtained for different pore pressures, and the values obtained are shown in Table 4.7. According to the table, it is clear that the effective stress coefficient for brown coal is not equal to unity as proposed by McKee et al. (1988), and the coefficient appears to increase with increasing pore pressure. For example, α increases by 0.96% with increasing pore pressure from 6 to 7 MPa and 1.4% for 8 to 9 MPa pore pressure increment. This is consistent with the results obtained by Chen et al. (2011), who also observed a 1.52% increase in α with a 2 to 3 MPa pore pressure increment in high rank coal. This implies that the α increment observed with pore pressure increase can be expected for any coal type.

Table 4.7. Effective stress coefficient for N_2 under different pore pressures

Pore pressure (MPa)	α for N_2
6	0.835
7	0.843
8	0.855
9	0.867

4.3.3.3 Calculate the additional effective stress value and obtain the real effective stress value

As the $\alpha \neq 1$, an extra effective stress is acting on the coal core and here onwards is referred as "additional effective stress" for this study. According to Chen et al. (2011), this additional effective stress can be calculated using the term $(1-\alpha)\Delta p$ and should be added to the conventional effective stress term by McKee et al. (1988) (refer to Eq. [4.10]).

$$\text{Effective stress acting on the coal core} = (\Delta\sigma - \Delta p) + (1-\alpha)\Delta p \quad [4.10]$$

Here, the first term represents the effective stress calculated considering the effective stress coefficient as 1 (McKee et al., 1988) and the second term represents the additional effective stress acting on the coal sample (Chen et al., 2011). A comparison for N_2 permeation of the original results and corrected magnitudes is shown in Figure 4.10. According to the figure, considering $\alpha = 1$ is not accurate, as it under-estimates the effective stress effect on coal permeability variations. This error was calculated using Eq. [4.11] for each condition and the results are presented in Table 4.8. As the table shows, the error increases with increasing pore pressure. For example, the error at 6 MPa pore pressure is increased by around 10% when the pore pressure is increased to 9 MPa. The permeability data were obtained for constant pore pressure differences and hence, at higher pore pressures, the confining stress acting on the sample is also higher. For example, the confining pressure applied on the sample is 11 MPa for 6 MPa CO_2 pressure and 14 MPa for 9 MPa CO_2 pressure for a constant pressure difference of 5 MPa. The observed enhancement in the effective stress-related error in permeability calculation with increasing pore pressure is therefore affected by the corresponding greater confining stresses at greater pore pressures (because the pressure difference remains the same). Therefore, this is more likely due to the confining stress influence rather than the pore pressure influence. Chen et al. (2011) also witnessed this increase in effective stress calculation error with increasing pore pressure at a given pressure difference for high rank coal under the same stress difference between pore and confining pressure, and around 6.13% error was observed by them with increasing pore pressure from 2.1 to 10.1 MPa. This confirms that the observed effective stress error with varying confining and pore pressures is applicable to any rank of coal. Interestingly, this error is higher for low rank coal than high rank coal, which may be due to the higher strength and lower compressibility of high rank coal and the resulting lower compression with effective stress application.

Underestimation of effective stress (e, %)

$$= \left(\frac{\text{Corrected permeability value - Original permeability value}}{\text{Corrected permeability value}}\right) \times 100\% \qquad [4.11]$$

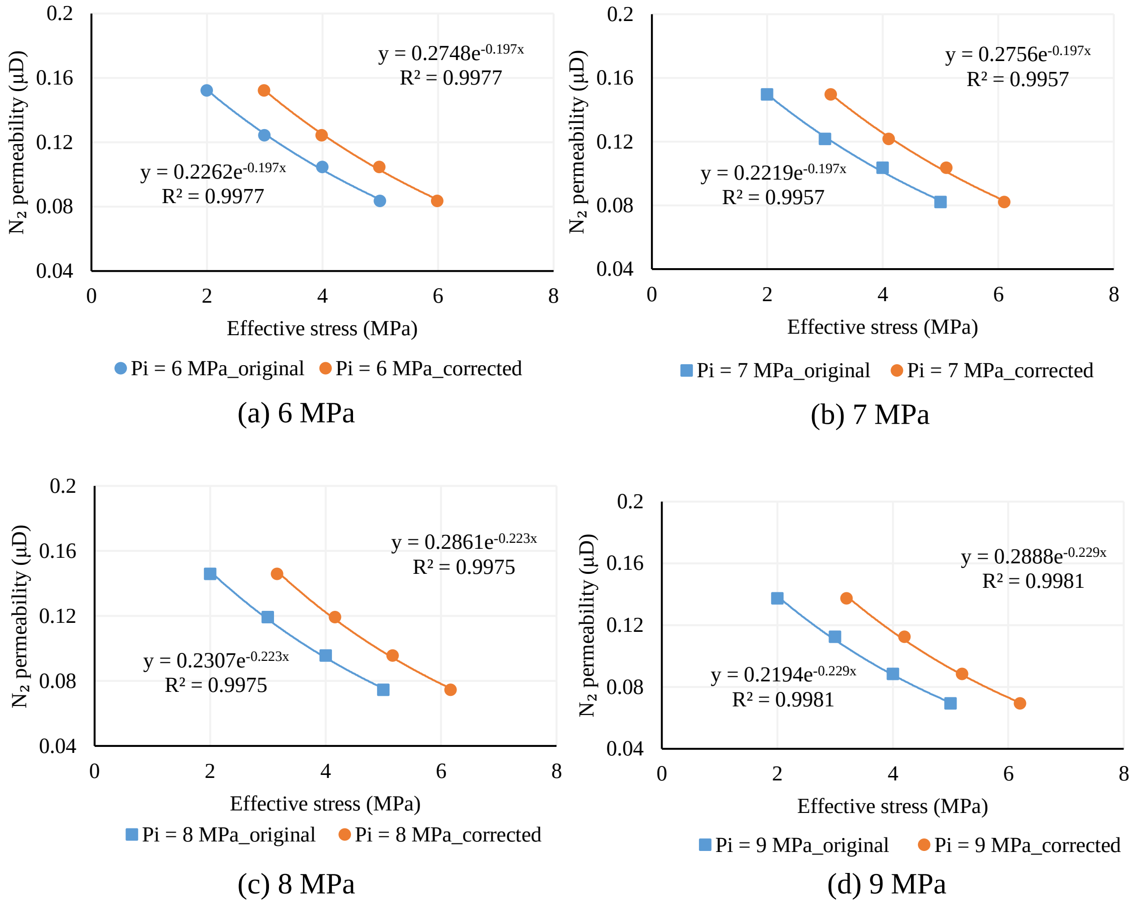

Figure 4.10. Comparison of N_2 permeability behaviour with original and corrected effective stresses under 6, 7, 8 and 9 MPa pore pressures (here Pi is pore pressure)

Table 4.8. Under-estimation of permeability (e%) for N_2 under different pore pressures

Pore pressure (MPa)	**Under-estimation of effective stress (e,%)**
6	21.49
7	24.20
8	29.65
9	31.63

4.3.3.4 Investigate the permeability alteration due to pure swelling effect by eliminating the effective stress effect

As the permeability results used for this study are for constant pressure difference (*dP*) conditions, it is reasonable to assume that the effective stress coefficient is also constant during CO_2 permeation (Chen et al., 2011). The CO_2 permeability data were therefore corrected using the calculated effective stress coefficients from N_2 permeation, by subtracting the additional effective stress-induced permeability reduction (calculated using Eq. [4.9]) from the original data. The initial permeability for each case was calculated from the calibrated expression for N_2 permeability, as shown in Figure 4.10. Figure 4.11 shows the comparison of the original permeability values (including the effect of both sorption-induced strain and effective stress) and the corrected permeability values (only the effect of sorption-induced strain) by eliminating the effective stress effect on CO_2 permeability.

Figure 4.11 shows a clear difference between the original permeability data and the CO_2 sorption-induced permeability data. Table 4.9 demonstrates the permeability increments associated with permeability calculation (using Eq. [4.11]) for CO_2 permeation. As Table 4.9 shows, when the pressure difference (*dP*) is increased from 2 to 5 MPa, the permeability increment is increased by around 22% and 40% for 6 and 9 MPa pore pressures. Further, the permeability increment increased by 43% under 5 MPa pressure difference when the CO_2 pore pressure increased from 6 to 9 MPa. Similar behaviour of higher permeability increments can be observed for higher confining pressures. For example, when the pressure difference increased from 4 to 5 MPa, the permeability increment increased by 49% and 67% for 13 MPa confinement. The pressure difference (*dP*) is higher, meaning that the effect of effective stress on permeability is also higher (refer to Eq. [4.7]). Therefore, for greater pressure differences, the permeability reduction is highly influenced by the applied effective stress and hence the over-estimation of swelling-induced permeability is also greater. Further, the higher permeability over-estimations for higher confining pressures (and therefore for higher pore pressures, as the pressure difference remained constant) can also be observed. This is because generally, permeability is reduced under higher confinements due to the pore volume shrinkage with the application of higher in situ stresses. Next, the effect of coal rank on these permeability over-estimations was studied.

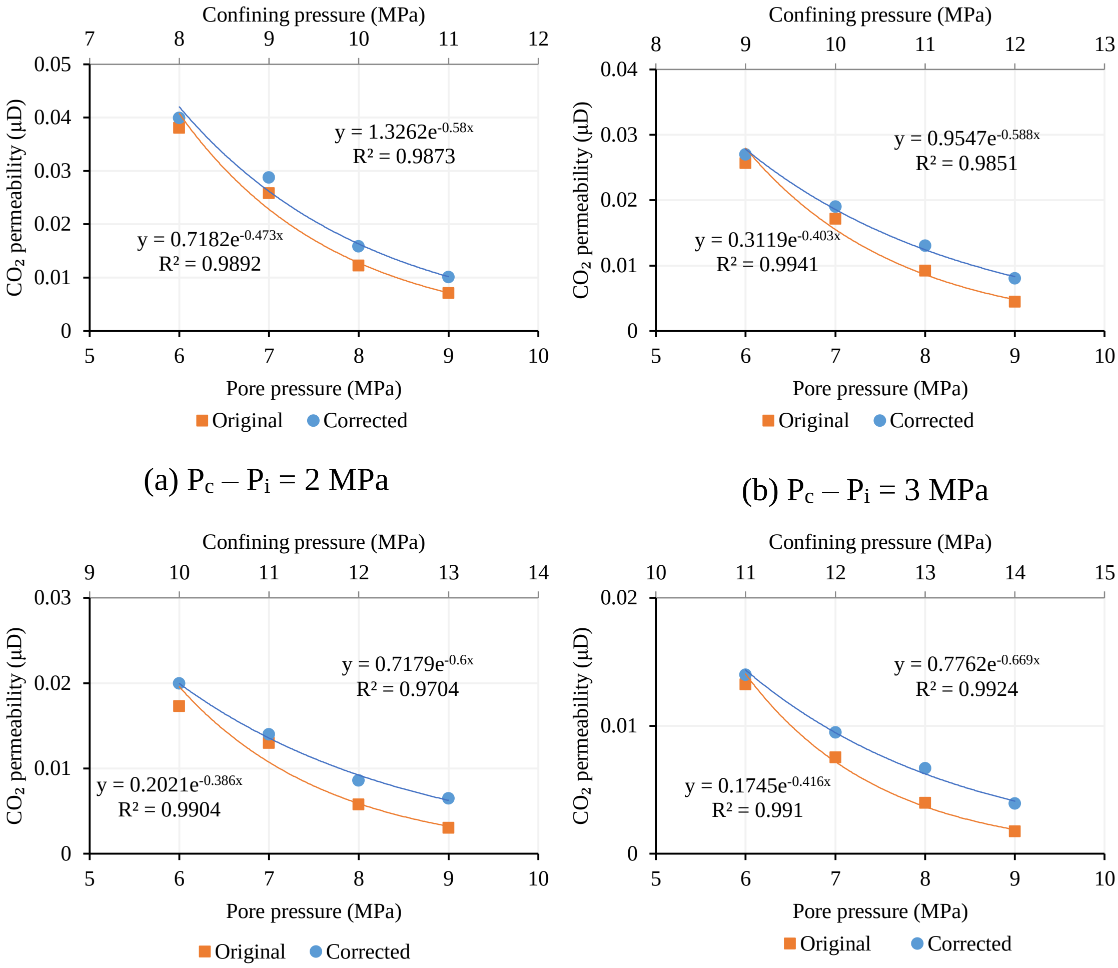

(a) $P_c - P_i = 2$ MPa

(b) $P_c - P_i = 3$ MPa

(c) $P_c - P_i = 4$ MPa

(d) $P_c - P_i = 5$ MPa

Figure 4.11. Comparison of CO_2 permeabilities between the original data (Ranathunga et al. 2017a) and the corrected data for sorption-induced strain only for P_c-P_i = 2, 3, 4 and 5 MPa

Table 4.9. Over-estimation of permeability values for CO_2 permeation

Pore pressure (MPa)	**Permeability error due to the effect of effective stress (%)**			
	Pc-Pi = 2 MPa*	**Pc-Pi = 3 MPa***	**Pc-Pi = 4 MPa***	**Pc-Pi = 5 MPa***
6	4.84	9.26	12.60	13.45
7	15.98	21.56	25.74	44.41
8	22.03	29.41	46.45	67.46
9	30.76	48.78	48.87	70.83

*Here Pc and Pi are the confining pressure and pore pressure, respectively

Figure 4.12 compares the permeability over-estimation caused by the effective stress effect for low rank coal (the present study) with that for high rank coal (Chen et al., 2011) during CO_2 permeation. According to Figure 4.12, similar error increasing behaviour with increasing confining pressure and pore pressure can be seen for high rank coal as well. However, the error (%) for high rank coal is comparatively low compared to that for low rank coal for similar pressure differences. For example, a 2 MPa constant pressure difference shows around 2 times higher positive error gradient for low rank coal (refer to Figure 4.12(a)) and that for dP = 4 MPa is around 5 times higher compared to high rank coal (refer to Figure 4.12(b)). As stated previously, low rank coal undergoes a greater effective stress influence on permeability compared to high rank coal, and therefore, the expected permeability variation due to effective stress change is also higher, eventually producing greater over-estimation of swelling-induced permeability in low rank coal. This was further studied by comparing the swelling-induced permeability and effective stress-induced permeability reductions, to evaluate the contribution of each process for both low and high rank coal. The results are shown in Figure 4.13.

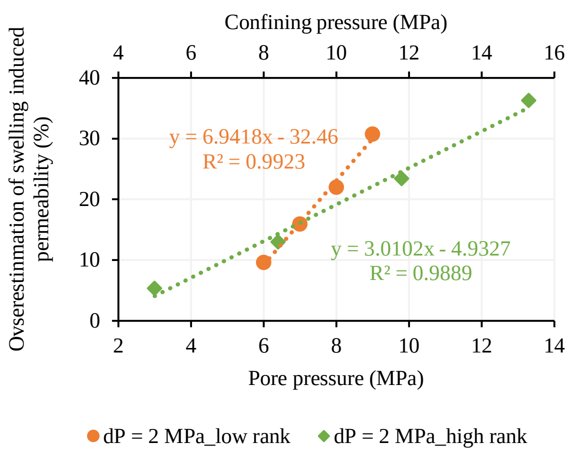

(a) $P_c - P_i$ = 2 MPa

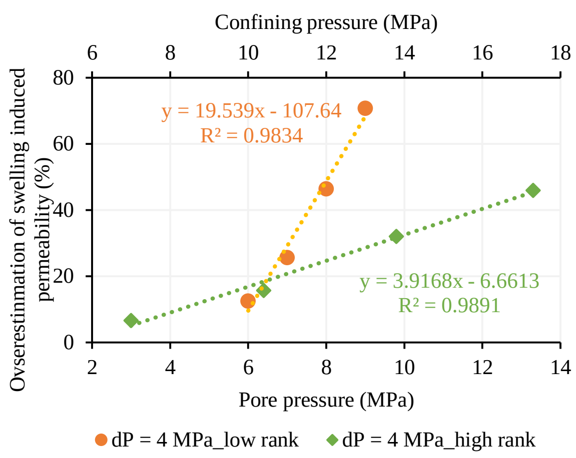

(a) $P_c - P_i$ = 4 MPa

Figure 4.12. Comparison of swelling-induced permeability over-estimation due to the effective stress effect in low rank coal (present study) and high rank coal (Chen et al., 2011) for CO_2 permeation

Here, the permeability reduction percentage was calculated as the difference between initial permeability (regressed from the permeability values for each case) and the permeability value at the final experimental pore pressure for respective permeabilities of effective stress induced and swelling induced strain related permeability. According to Figure 4.13, both effective stress-induced and swelling-induced permeability reductions reduce with increasing pressure difference (*dP*), regardless of coal rank. Further, the CO_2 sorption-induced permeability reduction is around 1.5 times and 2 times greater than the effective stress-induced permeability reductions for low rank and high rank coals, respectively. As explained previously, for greater pressure differences, coal permeability is low and therefore the expected permeability reduction by effective stress is reduced. Further, this lower permeability allows less swelling strain in the coal mass, which eventually also reduces the sorption-induced permeability reduction (Figure 4.13). Furthermore, Figure 4.13 confirms the greater effective stress-induced permeability reduction in low rank coal than high rank coal. Interestingly, the swelling-induced permeability reduction appears to be greater for high rank coal than low rank coal (Figure 4.13). As discussed by Ranathunga et al (2017a), mature high rank coal has a well-developed cleat system that provides more provision for CO_2 transport and adsorption processes, which may eventually enhance the coal swelling strain resulting in permeability reduction. However, these observations indicate that it is necessary to correct the permeability data for sorptive gases by eliminating the influence of the additional effective stress from the swelling strain of coal. This certainly requires precise estimation of the swelling-created permeability changes. Therefore, an effort was made to predict swelling-induced permeability reduction. This is the subject of the next section.

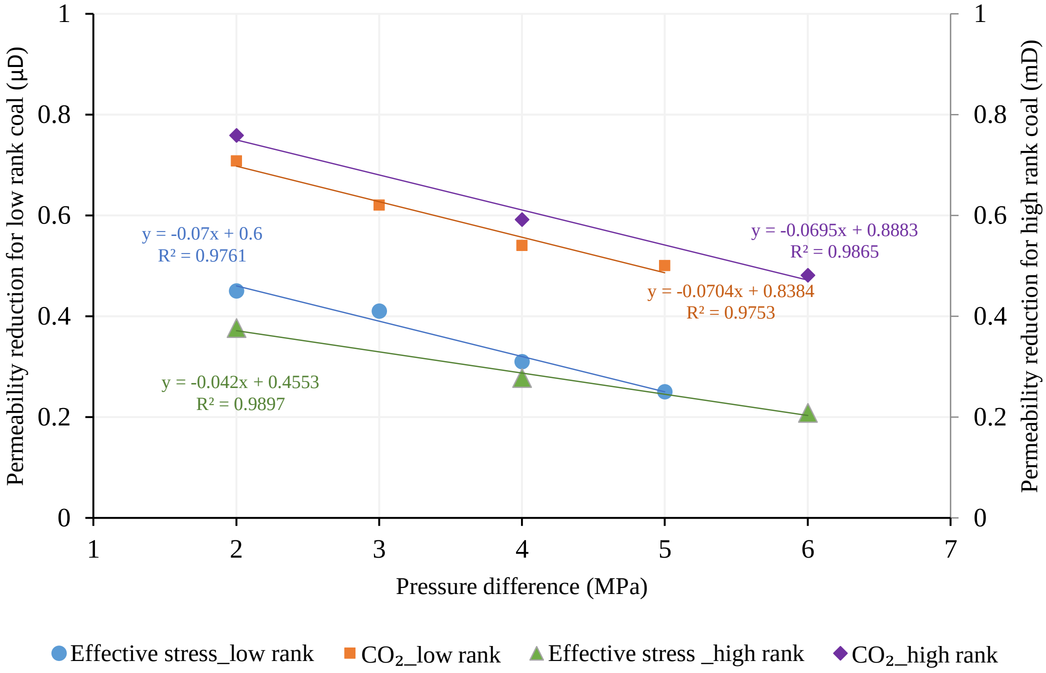

Figure 4.13. Comparison of permeability change caused by effective stress and swelling strain for low rank and high rank coal

4.3.4 Prediction of swelling-induced permeability alterations in coal

The modified Dubinin–Radushkevich (D-R) (refer to Eq. [4.12]) equation has often been used by researchers to predict the adsorption capacity of coal, because of its ability to predict the adsorption capacity of various gases at high pressures (super-critical) on different coal types (Sakurovs et al., 2010; Sakurovs et al., 2007, 2008).

$$W_{ads} = W_o \left(1 - \frac{\rho_g}{\rho_a}\right) exp\left\{-D\left[\ln\left(\frac{\rho_a}{\rho_g}\right)\right]^2\right\} \quad [4.12]$$

where, W_{ads} excess sorption, W_o is the surface adsorption capacity of the substrate, ρ_g is the gas density, ρ_a is the density of the adsorbed phase and D is a constant related to the affinity of the sorbent of the gas. This model has been successfully used to estimate sorption-induced swelling in coal mass (Anggara et al., 2013; Day et al., 2008; Day et al., 2010; Ranathunga et al., 2017b) (refer to Eq. [4.13]).

$$S = S_{max} exp\left\{-D\left[\ln\left(\frac{\rho_L}{\rho_g}\right)\right]^2\right\} \quad [4.13]$$

where, S is volumetric swelling (%), S_{max} is maximum swelling of the coal, ρ_g is the gas density at the temperature and pressure used for the testing, ρ_L is the van der Waals density of the gas (ρ_L = 1028 kg/m^3 for CO_2 (Day et al., 2010)) and D is an empirical curve-fitting parameter. Therefore, an effort was made during the present study to represent sorption-induced CO_2 permeability by the D-R model. The model was modified as follows (refer to Eq. [4.14]) for application to the permeability of coal:

$$k = k' exp\left\{-D'\left[\ln\left(\frac{\rho_L}{\rho_g}\right)\right]^2\right\} \quad [4.14]$$

where, k is the sorption-induced permeability, k' and D' are empirical curve-fitting parameters and ρ_g and ρ_L carry similar meanings as in Eq. [4.13].

4.3.4.1 Prediction of swelling-induced permeability variations for low rank coal

The results obtained by applying Eq. [4.14] to brown coal swelling-induced permeability data are demonstrated in Figure 4.14 and Table 4.10, and both show a better representation of experimentally- derived CO_2 sorption-induced permeability changes with a good fit of less than 0.95. This implies that this modified D-R model (Eq. [4.14]) can be used to predict the sorption-induced permeability alterations in brown coal. As shown in Table 4.10, both k' and D' parameters for permeability are reduced with increasing pressure difference (confining and pore pressures). Figure 4.15 displays the variation of both k' and D' with pressure difference using the experimental data for CO_2 permeation. As shown in the figure, k' follows a decreasing exponential variation while D' follows a decreasing linear variation with pressure difference.

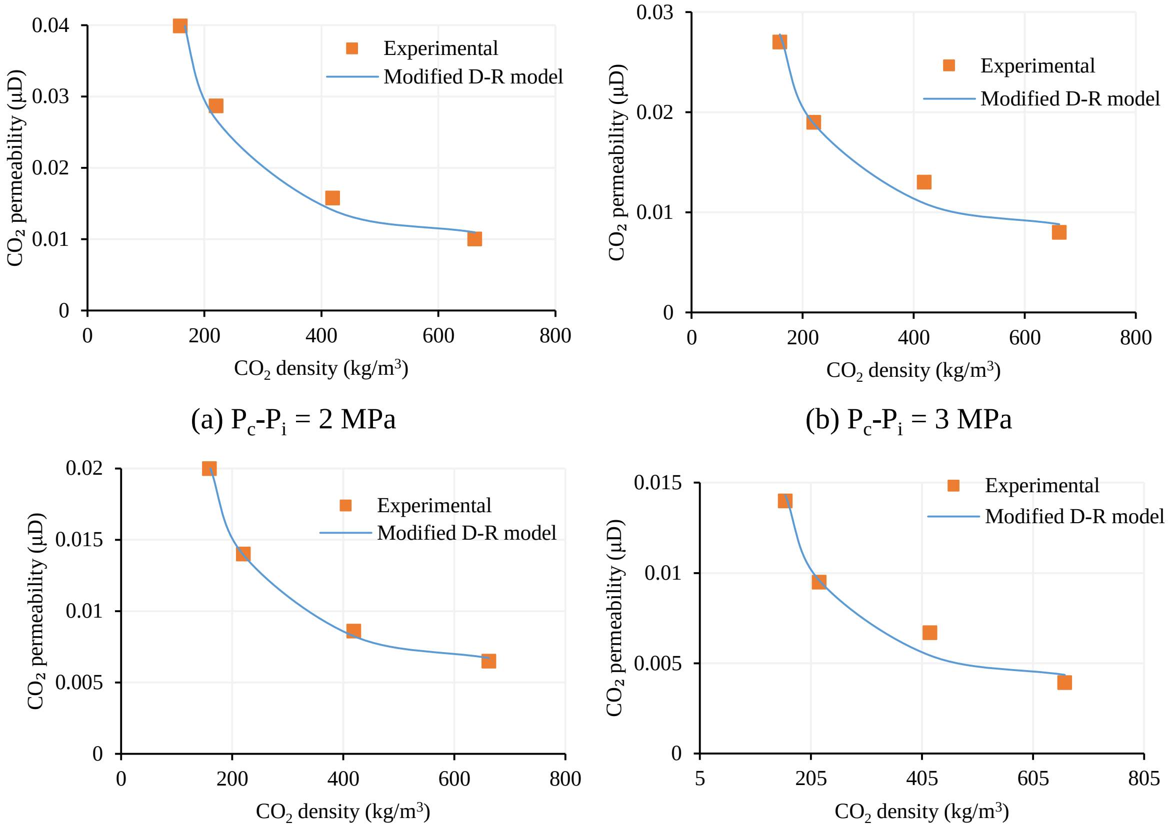

(a) P_c-P_i = 2 MPa (b) P_c-P_i = 3 MPa

(c) P_c-P_i = 4 MPa (d) P_c-P_i = 5 MPa

Figure 4.14. Comparison of experimental and D-R model-predicted CO_2 sorption-induced permeability values for different pressure changes ($P_c – P_i$) of low rank coal

Table 4.10. D-R model parameters for CO_2 sorption-induced permeability in low rank coal

Pressure difference (MPa)	k' (μD)	D'	R²
2	0.0101	-0.334	0.9718
3	0.0082	-0.348	0.9628
4	0.0063	-0.361	0.9970
5	0.0041	-0.408	0.9518

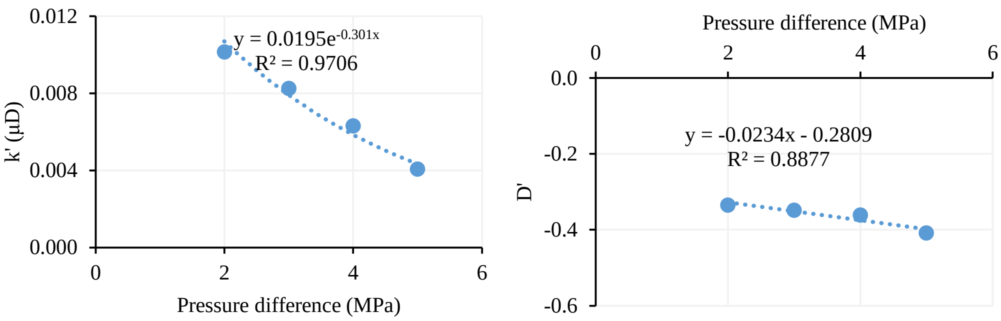

(a) k' (b) D'

Figure 4.15. Variation of Dubinin–Radushkevich parameters k' and D' with pressure diffference ($P_c – P_i$) for low rank coal

4.3.4.2 Prediction of swelling-induced permeability variations for high rank coal

Eq. [4.14] was used to predict the permeability alterations in high rank coal upon CO_2 adsorption-induced swelling using the data obtained by Chen et al. (2011) for Australian bituminous coal (refer to Figure 4.16 and Table 4.11 for the results) and a good fit of data with less than 0.96 R^2 value can be observed for high rank coal, confirming the applicability of this simple permeability model to any type of coal.

A comparison of the D-R model parameters of two coal types (Tables 4.10 and 4.11) shows that similar to low rank coal, high rank coal also exhibits a reduction in both $k'$and D' parameters with increasing pressure difference. Interestingly, high rank coal too follows a similar type variation as for low rank coal which is an exponential reduction of k' and linear reduction of D' parameters with the pressure difference between confining pressure and pore pressure (refer to Figure 4.17).

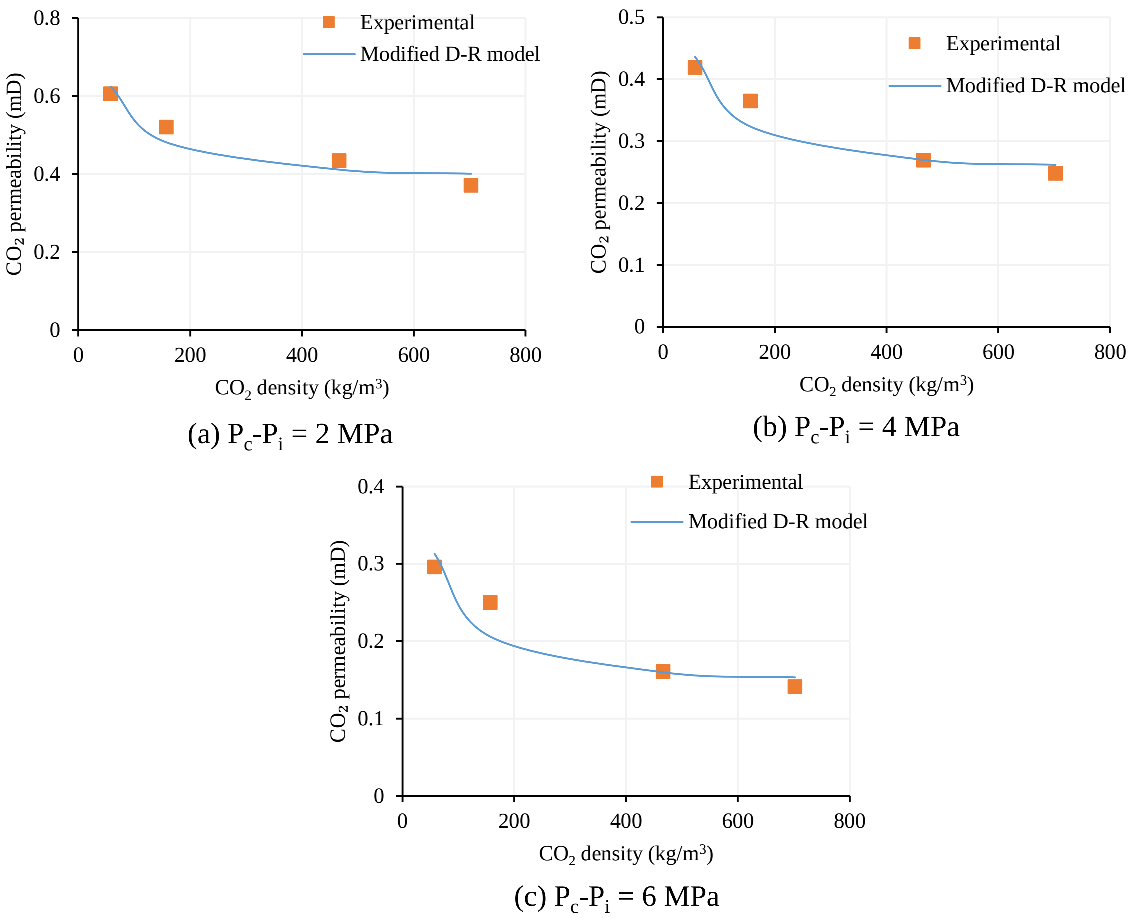

Figure 4.16. Comparison of experimental and D-R model-predicted CO_2 sorption-induced permeability values for different pressure changes (P_c – P_i) of high rank coal

Table 4.11. D-R model parameters for CO_2 sorption-induced permeability in high rank coal

Pressure difference (MPa)	k' (mD)	D'	R^2
2	0.3976	-0.054	0.9846
4	0.2592	-0.062	0.9822
6	0.1513	-0.087	0.9586

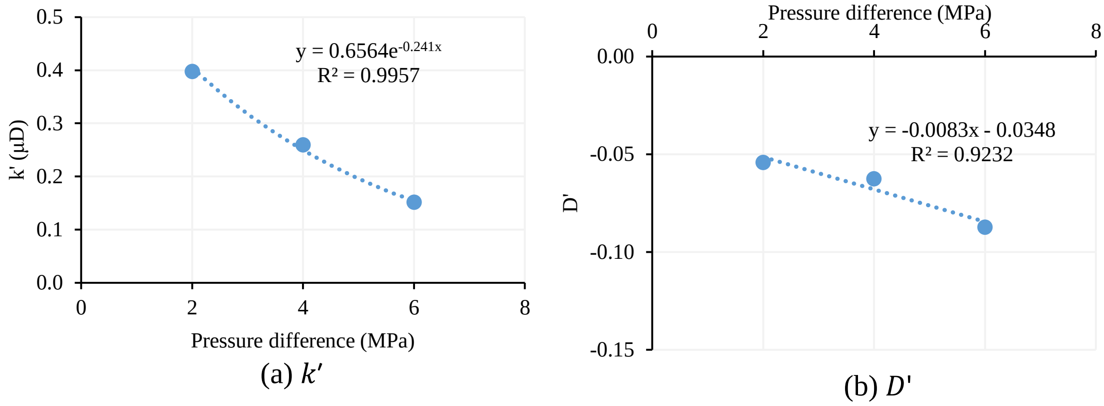

Figure 4.17. Variation of Dubinin–Radushkevich parameters k' and D' with pressure difference ($P_c - P_i$) for high rank coal

The modified D-R model can be presented as in Eqs. [4.15a-c] to calculate the CO_2 sorption- induced permeability variations for any type of coal, including the empirical relationships obtained for k' and D' from the present study (low rank coal) and Chen et al.'s (2011) data (high rank coal).

$$k = k_i' exp\left\{-D_i'\left[\ln\left(\frac{\rho_L}{\rho_g}\right)\right]^2\right\} \quad [4.15a]$$

$$k_i' = a_i exp(b_i dP) \quad [4.15b]$$

$$D_i' = c_i dP + d_i \quad [4.15c]$$

where, dP is the pressure difference between the confining pressure and the pore pressure, and a_i, b_i, c_i and d_i are empirically-derived constants for low and high rank coals where i denotes the coal type. The empirical constants (a, b, c and d) for the two coal types used for the permeability predictions are demonstrated in Table 4.12 and the estimated swelling-induced permeabilities for those two coal types for higher pressure differences (dP) are shown in Figure 4.18. According to Figure 4.18, the estimated sorption strain-induced permeability is reduced with increasing pressure difference for both low and high rank coals. This is possibly due to the lower sorption potential for higher in situ stress applications that reduces the influence of sorption strain on permeability. However, low rank coal shows a much steeper reduction in swelling-induced permeability reduction with pore pressure. The higher effective stress effect on low rank coal plays the main role in permeability variation and the resulting lesser influence of CO_2 sorption-induced permeability reduction may be the reason. Therefore, these findings suggest that low rank coal is subject to less structural modification through sorption strain-induced swelling than high rank coal.

Table 4.12. Empirical constant of Eqs. [4.15b, c] to derive CO_2 sorption- induced permeability variations

Empirical constant	Low rank coal	High rank coal
a_i	0.0195	0.6564
b_i	-0.3010	-0.2410
c_i	-0.0234	-0.0083
d_i	-0.2809	-0.0348

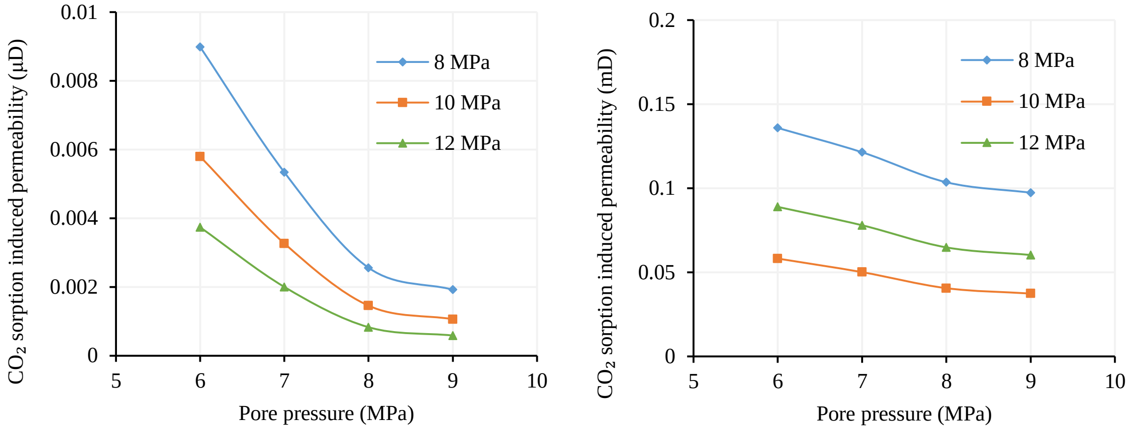

(a) low rank coal (present study)

(b) high rank coal (Chen et al., 2011)

Figure 4.18. Predicted CO_2 sorption-induced permeability variations using modified D-R model for low rank coal (present study) and high rank coal (Chen et al., 2011)

4.3.5 Conclusions

The following major conclusions were drawn from the present study of the influence of effective stress- and sorption-induced strain on coal's mass structure and its flow ability during CO_2 sequestration. According to the findings,

- Often, the effective stress coefficient of any rank coal may not be equal to unity and this non-unity of the effective stress parameter ($\alpha \neq 1$) causes an additional effective stress influence to be induced on the coal sample compared to the condition of $\alpha = 1$. Therefore, the $\alpha = 1$

assumption often causes an under-estimation of the influence of effective stress on coal's structure, and the situation becomes more critical with increasing pore pressure.

- In addition to the effective stress effect, gas adsorption-induced swelling has a considerable influence on coal permeability. However, this is affected by the effective stress effect.
- High rank coal is subjected to a greater reduction in permeability through swelling compared to low rank coal, possibly due to the potential greater swelling ability of high rank coal due to its well-developed cleat system.
- Both low and high rank coals experience permeability reductions with increasing effective stresses, and these reductions are comparatively higher for low rank coal due to its lower strength and higher compressibility.
- Tests results exhibit an over-estimation of the permeability reduction caused by swelling in both high and low rank coals due to the effective stress effect, which is greater at greater effective stresses (higher pressure differences → higher confining pressures and pore pressures).
- Finally, the modified Dubinin–Radushkevich (D-R) model was used to predict the swelling-induced permeability reductions in the coal mass and produced successful results for both low and high rank coals with a reasonable fitting value of less than 0.96. Therefore, the modified D-R model can be applied to any coal type with known empirical relationships for $k'$and D'.

4.3.6 References

Al-Wardy, W., Zimmerman, R.W., (2004). Effective stress law for the permeability of clay-rich sandstones. *Journal of Geophysical Research: Solid Earth* 109, B4.

Anggara, F., Sasaki, K., Sugai, Y., (2013). Swelling Measurements of a Low Rank Coal in Supercritical CO_2. *International Journal of Geosciences* 4, 863.

Bernabe, Y., (1987). The effective pressure law for permeability during pore pressure and confining pressure cycling of several crystalline rocks. *Journal of Geophysical Research: Solid Earth* 92, 649-657.

Chen, Z., Liu, J., Pan, Z., Connell, L.D., Elsworth, D., (2012). Influence of the effective stress coefficient and sorption-induced strain on the evolution of coal permeability: Model development and analysis. *International Journal of Greenhouse Gas Control* 8, 101-110.

Day, S., Fry, R., Sakurovs, R., (2008). Swelling of Australian coals in supercritical CO_2. *International Journal of Coal Geology* 74, 41-52.

Day, S., Fry, R., Sakurovs, R., Weir, S., (2010). Swelling of Coals by Supercritical Gases and Its Relationship to Sorption. *Energ Fuel* 24, 2777-2783.

George, J.S., Barakat, M., (2001). The change in effective stress associated with shrinkage from gas desorption in coal. *International Journal of Coal Geology* 45, 105-113.

Ghabezloo, S., Sulem, J., Guédon, S., Martineau, F., (2009). Effective stress law for the permeability of a limestone. *International Journal of Rock Mechanics and Mining Sciences* 46, 297-306.

Han, F., Busch, A., van Wageningen, N., Yang, J., Liu, Z., Krooss, B.M., (2010). Experimental study of gas and water transport processes in the inter-cleat (matrix) system of coal: anthracite from Qinshui Basin, China. *International Journal of Coal Geology* 81, 128-138.

Huy, P.Q., Sasaki, K., Sugai, Y., Ichikawa, S., (2010). Carbon dioxide gas permeability of coal core samples and estimation of fracture aperture width. *International Journal of Coal Geology* 83, 1-10.

Jasinge, D., Ranjith, P.G., Choi, S.K., (2011). Effects of effective stress changes on permeability of Latrobe Valley brown coal. *Fuel* 90, 1292-1300.

Kranzz, R., Frankel, A., Engelder, T., Scholz, C., (1979). The permeability of whole and jointed Barre granite, *International Journal of Rock Mechanics and Mining Sciences & Geomechanics Abstracts*. Elsevier, pp. 225-234.

Laubach, S., Marrett, R., Olson, J., Scott, A., (1998). Characteristics and origins of coal cleats: A review. *International Journal of Coal Geology* 35, 175-207.

Lin, W., Tang, G.Q., Kovscek, A.R., (2008). Sorption-induced permeability change of coal during gas-injection processes. *SPE Reservoir Evaluation & Engineering* 11, 792-802.

Mavor, M.J., Gunter, W.D., (2004). Secondary porosity and permeability of coal vs. gas composition and pressure, SPE Annual Technical Conference and Exhibition. Society of Petroleum Engineers, Paper No. SPE-90255-MS.

McKee, C., Bumb, A., Koenig, R., (1988). Stress-dependent permeability and porosity of coal and other geologic formations. *SPE Formation Evaluation* 3, 81-91.

Nur, A., Byerlee, J.D., (1971). An exact effective stress law for elastic deformation of rock with fluids. *Journal of Geophysical Research* 76, 6414-6419.

Pan, Z., Connell, L.D., Camilleri, M., (2010). Laboratory characterisation of coal reservoir permeability for primary and enhanced coalbed methane recovery. *International Journal of Coal Geology* 82, 252-261.

Patching, T.H., (1965). Variations in permeability of coal. In: Proc. 3rd Rock Mech. Symp., Univ. of Toronto, UK, pp. 185–199.

Perera, M.S.A., Ranjith, P.G., Airey, D.W., Choi, S.K., (2011). Sub- and super-critical carbon dioxide flow behaviour in naturally fractured black coal: An experimental study. *Fuel* 90, 3390-3397.

Pini, R., Ottiger, S., Burlini, L., Storti, G., Mazzotti, M., (2009). Role of adsorption and swelling on the dynamics of gas injection in coal. *Journal of Geophysical Research: Solid Earth* 114, B04203.

Ranathunga, A.S., Perera, M.S.A., Ranjith, P.G., Ju, Y., Vishal, V., De Silva, P.N.K., (2015). A macro-scale experimental study of sub-and super-critical CO_2 flow behaviour in Victorian brown coal. *Fuel* 158, 864-873.

Ranathunga, A.S., Perera, M.S.A., Ranjith, P.G., Zhang, X.G. (2017a). Super-critical carbon dioxide flow behaviour in low rank coal: A meso-scale experimental study. *Journal of CO_2 Utilization* (under review).

Ranathunga, A.S., Perera, M.S.A., Ranjith, P.G., (2017b). The influence of CO_2 properties and reservoir depth on coal matrix swelling: A meso-scale experimental study using low rank coal. *Enrg Fuel* (under review).

Rathnaweera, T.D., Ranjith, P.G., Perera, M.S.A., Yang, S., (2015). Determination of effective stress parameters for effective CO_2 permeability in deep saline aquifers: An experimental study. *Journal of Natural Gas Science and Engineering* 24, 64-79.

Sakurovs, R., Day, S., Weir, S., (2010). Relationships between the critical properties of gases and their high pressure sorption behaviour on coals. *Energ Fuel* 24, 1781-1787.

Sakurovs, R., Day, S., Weir, S., Duffy, G., (2007). Application of a modified Dubinin-Radushkevich equation to adsorption of gases by coals under supercritical conditions. *Energ Fuel* 21, 992-997.

Sakurovs, R., Day, S., Weir, S., Duffy, G., (2008). Temperature dependence of sorption of gases by coals and charcoals. *International Journal of Coal Geology* 73, 250-258.

Shi, J.Q., Durucan, S., Shimada, S., (2014). How gas adsorption and swelling affects permeability of coal: A new modelling approach for analysing laboratory test data. *International Journal of Coal Geology* 128, 134-142.

Siriwardane, H., Haljasmaa, I., McLendon, R., Irdi, G., Soong, Y., Bromhal, G., (2009). Influence of carbon dioxide on coal permeability determined by pressure transient methods. *International Journal of Coal Geology* 77, 109-118.

Somerton, W.H., Söylemezoḡlu, I., Dudley, R., (1975). Effect of stress on permeability of coal, *International Journal of Rock Mechanics and Mining Sciences & Geomechanics Abstracts.* Elsevier, pp. 129-145.

Vishal, V., Singh, T.N., (2015). A Laboratory Investigation of Permeability of Coal to Supercritical CO_2. *Geotech Geol Eng* 33, 1009-1016.

Walsh, J., (1981). Effect of pore pressure and confining pressure on fracture permeability, *International Journal of Rock Mechanics and Mining Sciences & Geomechanics Abstracts.* Elsevier, pp. 429-435.

Zhao, Y., Yaoqing, H., Jingping, W., Dong, Y., (2003). The experimental approach to effective stress law of coal mass by effect of methane. *Transport in Porous Media* 53, 235-244.

4.4 How does the temperature alter CO_2 permeability in coal?

4.4.1 Overview

In deep coal seams, the temperature becomes higher (>40^{0}C) depending on the depth and geological conditions, which causes the kinetic energy of the gas molecules to increase. Accordingly, this increases the rate of diffusion and results in reduction of adsorption capacity, which affects coal's gas permeability. In several previous studies (Perera et al., 2012; Shao et al., 2016; Yang et al., 2008; Zhao et al., 2010) on temperature effect on coal gas permeability, much less attention has been paid to brown coal, which indicates the necessity of a detailed study. Therefore, the main objective of this study is to investigate the effect of temperature on the permeability of Victorian brown coal. A series of tri-axial experiments was conducted on brown coal specimens collected from the Latrobe Valley basin, Victoria. Permeability tests were carried out under 10 MPa confinement for two different temperatures (25 and 40^{0}C). Both CO_2 and N_2 were injected into the samples under various injecting pressures to obtain a detailed comparison between reactive and non-reactive gas permeability.

A conference paper was produced from this section of the chapter as follows:

Ranathunga AS, Perera MSA, Ranjith PG (2014). An Experimental Study to Investigate Temperature Effect on Permeability of Victorian Brown Coal during CO_2 Sequestration, ISRM International Symposium and 8th Asian Rock Mechanics Symposium (ARMS8), Sapporo, Japan, 14-16 October, 2014; Paper No. ARMS8_PO-82.

4.4.2 Introduction

As explained in previous sections, the injection of CO_2 into the coal mass causes its chemical and physical properties to change greatly, which causes the amount of injectable CO_2 and producible CH_4 to become unpredictable. There has been much research conducted into the effects of CO_2 on coal, which has revealed that a great degree of swelling is caused by CO_2 adsorption that, in turn, can cause the permeability of the coal mass to severely decrease. Beyond 7.38 MPa pressure and 31.8^{0}C temperature, CO_2 exists in its super-critical condition (Oldenburg, 2006) (Figure 4.19), which creates a greater swelling effect in coal due to its greater sorption capacity compared to gas or liquid CO_2 (Perera et al., 2011b). Generally, unmineable coal seams are present beyond 1000 m depths from the ground surface, where the pressures and temperatures are higher than the critical value of CO_2 (7.38 MPa and 31.8^{0}C) and therefore, CO_2 is present in the super-critical state (Figure 4.19). Many researchers have identified various factors that influence CO_2 permeability in coal seams, including both coal mass and adsorbing gas properties, such as coal rank, moisture content, temperature, depth, gas composition and adsorbing gas pressure, gas type and phase and injection and production well operations (Bustin and Clarkson, 1998; Harpalani and Schraufnagel, 1990; Jasinge et al., 2011; Pan et al., 2010; Perera et al., 2011; Ranathunga et al., 2015; Skawiński, 1999). However, very few studies have been conducted on the effect of temperature on gas permeability in coal (Perera et al., 2012; Shao et al., 2016; Yang et al., 2008; Zhao et al., 2010).

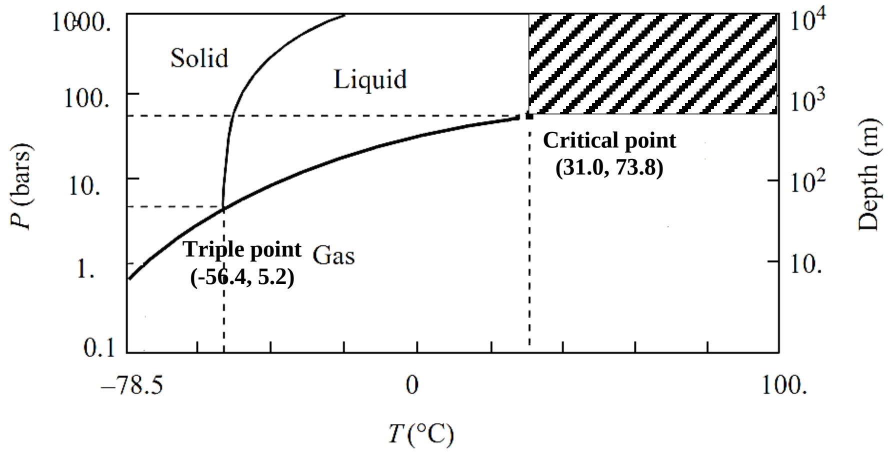

Figure 4.19. Phase diagram for CO_2 (Oldenburg, 2006)

At 1 km depth the San Juan basin, New Mexico has a temperature of around 52 ^{0}C (Reeves and Oudinot, 2005), at 2 km depth the Black Warrior basin, Alabama has a temperature of around 50 ^{0}C (Pashin and McIntyre, 2003) and at 3 km depth the Altmark natural gas field in Germany has a temperature of around 120 ^{0}C (Rebscher et al., 2006). The figures indicate that the temperatures of deep coal seams at different geological locations are different and higher than the ground surface temperature.

According to Azmi et al. (2006), deeper and warmer coal seams adsorb less CO_2 at a given pressure than shallower and cooler ones. Perera et al. (2012), Bae and Bhatia (2006) and Kronimus et al. (2008) found that super-critical CO_2 is subjected to the temperature effect more significantly than gas or liquid sub-critical CO_2 (Figure 4.20). Further, Perera et al. (2012) investigated the temperature effect on coal permeability for CO_2 movement, using naturally- fractured black coal. They observed a significant increase in coal permeability with increasing temperature for higher CO_2 injection pressures (>10MPa), and an insignificant effect on permeability at low CO_2 injection pressures (<9 MPa) (Figure 4.21). This is basically due to the fact that, with increasing temperature, the sorption capacity and the swelling effect in coal are reduced (Bae and Bhatia, 2006), causing an increment in coal permeability at higher temperatures. This shows the importance of selecting a coal seam with appropriate physical properties in order to achieve an effective CO_2-ECBM process. In relation to the temperature effect in low rank coal, Shao et al. (2016) conducted a series of permeability tests on Chinese lignite samples, varying the temperatures from 20 to 650 ^{0}C using 0.5 to 5 MPa N_2 injections under 10 MPa confinement. They observed a fluctuation of N_2 permeability when the temperature increased and both pore pressure and temperature were found to be highly influential on N_2 permeation. A summary of their findings is listed in Table 4.13.

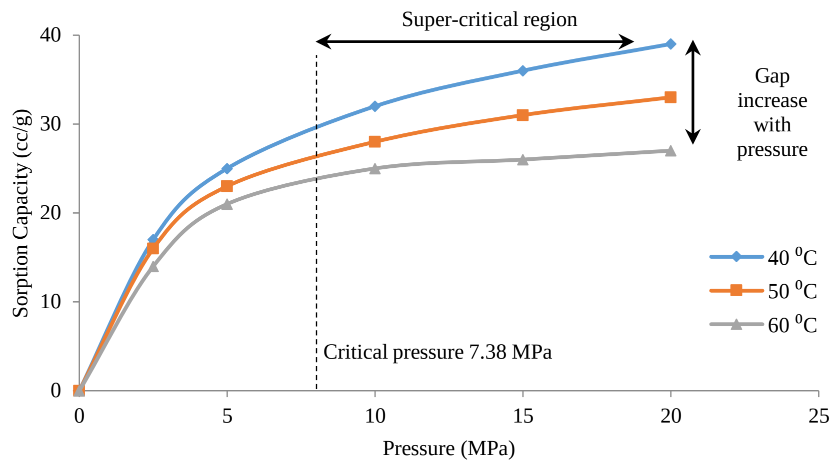

Figure 4.20. Effect of temperature on sorption capacity of coal (Kronimus et al., 2008)

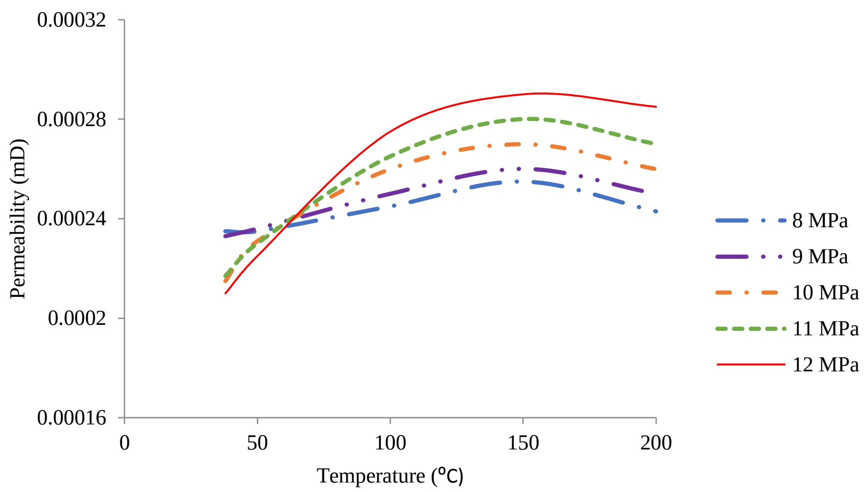

Figure 4.21. Temperature effects on CO_2 permeability at 20 MPa confinement (Perera and Ranjith, 2012)

Table 4.13. Results of N_2 permeability variation with pore pressure and temperature in low rank coal (Shao et al., 2016)

Pore pressure range	**Permeability variation due to temperature change**	
0.5 – 2 MPa	**Observation**	**Reason**
Permeability varies in five stages with temperature		20^0C – 75^0C
	Permeability decreases with increasing temperature	Temperature increases for coal, thereby closing the pores and fractures available for gas movement (Shao et al., 2016)
		75^0C – 150^0C
	Permeability increases with increasing temperature	Moisture and some volatile components are exuded at higher temperatures. Evaporation moisture causes thermal cracks to propagate, inducing more permeable channels (Zou et al., 2015)
		150^0C – 300^0C
	Permeability decreases with increasing temperature	Due to the pyrolysis of lignite, fractures and pores are propagated, creating more flow paths. However, this pyrolysis also causes coal softening, eventually reducing permeable channels with the application of confining pressure and thermal expansion, reducing permeability (Zou et al., 2015).
		300^0C – 350^0C
	Permeability increases with increasing temperature	The effect of pyrolysis continues. However, more pore channels are created than in the previous temperature range due to the greater pyrolysis which happens within this range of temperature in lignite, creating more flow paths for N_2 movement (Shao et al., 2016; Zou et al., 2015).
		350^0C – 650^0C
	Permeability decreases with increasing temperature	Drastic depolymerisation and poly-condensation reactions occur in the coal mass, resulting in obstruction of pores and fractures by the plastic mass formed by the softening and melting of the coal (Zou et al., 2015). Further, greater softening effect causes lower bearing capacities in lignite, resulting in shrinkage of inter-connected pores and therefore, low permeability (Shao et al., 2016).
2.5 – 3.5 MPa	**Observation**	**Reason**
Permeability is varied in five stages with temperature	- Similar to 0.5 MPa to 2 MPa pore pressure range permeability variations -	
4 – 5 MPa	**Observation**	**Reason**
Permeability varies in five stages with temperature		20^0C – 75^0C
	Similar to 0.5 MPa to 2 MPa pore pressure range permeability variations	
		75^0C – 150^0C
	Similar to 0.5 MPa to 2 MPa pore pressure range permeability variations	
		150^0C – 350^0C
	Permeability increases slowly with increasing temperature	Lower effective stress at higher pore pressures increases permeability (Siriwardane et al., 2009)

	$350^0C – 450^0C$
Permeability decreases with increasing temperature	Lignite continues to pyrolyse and new permeable channels are created. Meanwhile, the rising temperature further softens the coal. When the strength of the coal can no longer resist the effective stress, the volume of the coal skeleton becomes smaller, thereby closing the permeable channels (Shao et al., 2016).
	$450^0C – 650^0C$
Permeability increases gradually with increasing temperature	Higher pore pressures combined with the enhanced kinetic energy at higher temperatures mean that gas has the ability to flow through the blocked coal pores, with depolymerisation and polycondensation reactions creating higher permeabilities (Shao et al., 2016).

However, the influence of temperature on CO_2 permeability in low rank coal has not yet been studied, although it is very important for the efficient sequestration of CO_2. Therefore, the main objective of this study is to investigate the effect of temperature on CO_2 permeability in coal using coupled flow-thermal-mechanical experiments on Victorian brown coal.

4.4.3 Experimental methodology

Coal samples with around 53% moisture content were taken from large coal blocks from the Latrobe Valley, Hazelwood open-cut mine in Gippsland, Australia, and stored in black garbage bags in the fog room in the Monash University Civil Engineering Laboratory (MUCEL) to preserve the natural moisture content and other chemical properties. First, 25 mm diameter samples were cored using the coring machine and then cut to around 54 mm lengths using the rock saw available in MUCEL. Samples were then end-ground and polished to 50 mm lengths using the grinder machine at MUCEL to ensure the faces were parallel and smooth (refer to Chapter 3).

Experiments were carried out using the high-pressure tri-axial set up (50 MPa) available in the MUCEL (Ranjith and Perera, 2011). Detailed descriptions of this set-up and the general test procedure are provided in Ranjith and Perera (2011). Permeability tests were conducted for both CO_2 and N_2 injections at four different injecting pressures under 10 MPa confining pressure (to represent a coal seam at around 400 m depth) as shown in Table 4.14. To study the temperature effect, these permeability tests were repeated for two different temperatures: 25 and 40 ^0C (the possible temperature of coal at the depth of 400 m (Suggate, 1974)). The undrained condition was used to determine permeability using a transient flow approach, as suggested by Siriwardane et al., (2009). The downstream boundary condition was maintained at a constant volume of 10.9 cm^3, while the upstream boundary condition was maintained at a constant pressure equal to the injection pressure (Table 4.14).

Table 4.14. Test conditions used for permeability tests.

Confining pressure (MPa)	CO_2 injecting pressure (MPa)	N_2 injecting pressure (MPa)
10	5	5
	6	6
	7	7
	8	8

Using an advanced data acquisition system, downstream pressure development (under undrained conditions) after injecting gas upstream was monitored and recorded at one-second intervals. The downstream pressure vs. time curve was used to calculate the permeability of the coal sample upon reaching steady state using Eq. [4.16] (Siriwardane et al., 2009):

$$Q = \left(\frac{dP}{dt}\right) \times \beta V \qquad [4.16]$$

where, Q is the flow rate through the specimen, V is the downstream volume, β is the adiabatic compressibility of the gas, and dP/dt is the rate of change in the downstream pressure with time. Darcy's law (Eq. [4.17]) was then used to calculate the corresponding permeability:

$$k = \frac{2QP_O\mu L}{A(P_i^2 - P_O^2)} \qquad [4.17]$$

where, Q, μ, P_o, and P_i are the gas flow rate through the coal specimen, the viscosity of the fluid, the downstream pressure and the upstream pressure, respectively. The specimens had cross-sectional area, A, and mean length, L and initial permeability, k. The adiabatic compressibility and the viscosity of the fluid for different pressure and temperature conditions were obtained from the REFPROP data base (McLinden et al. 1998).

In the first stage, a series of experiments was conducted to investigate the effect of temperature on the permeability of brown coal specimens. First, CO_2 was injected into the coal samples at various injection pressures (Table 4.14) under 10 MPa confining pressure at 25 ^{0}C. The downstream pressure developments were observed and recorded to calculate the permeability for each injection pressure. The temperature of the set-up was then increased to 40 ^{0}C and maintained until the sample reached 40 ^{0}C. The same test series was repeated to check the temperature effect on CO_2 permeability. The downstream pressure development curves during 12 hours for the four CO_2 injecting pressures under 10 MPa confining pressure for 25 and 40 ^{0}C conditions are shown in Figure 4.22. After the completion of the permeability tests for CO_2 injection, N_2 gas was injected into the coal sample under the same conditions to study the effect of temperature on the permeability of N_2.

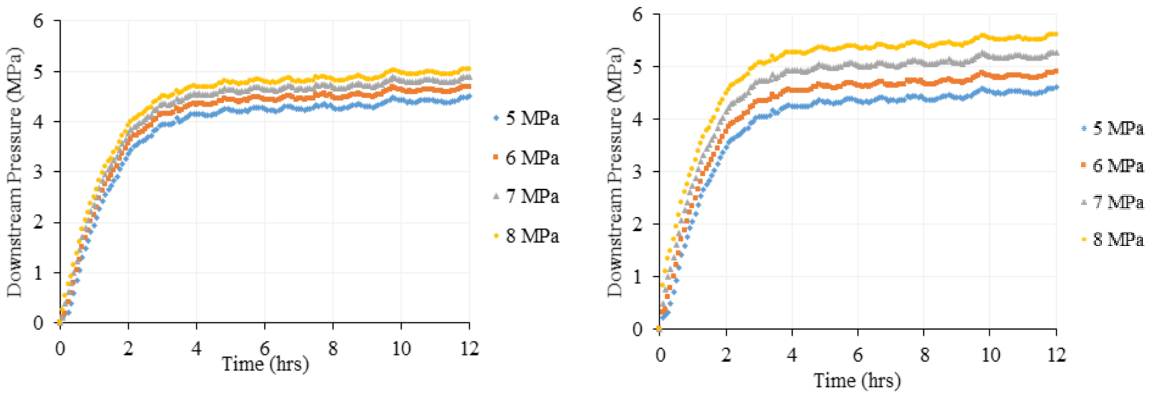

(a) At 25 ^{0}C (b) At 40 ^{0}C

Figure 4.22. Downstream pressure developments at 25 ^{0}C and 40 ^{0}C temperatures for different CO_2 injection pressures

4.4.4 Results and Discussion

As described above, the temperature effect on CO_2 permeability was investigated for four different injecting pressures at 10 MPa confining pressure (Table 4.14). Figure 4.23 shows the permeability values for CO_2 injection calculated for each experimental condition. This shows a noteworthy effect of temperature on CO_2 permeability and hence on the injectivity of CO_2 into deep coal seams. According to the results, CO_2 permeability decreases with increasing injecting pressures at both 25 and 40 ^{0}C, while CO_2 permeability for 8 MPa injecting pressure at 40 ^{0}C shows a higher permeability reduction than at 25 ^{0}C. For instance, when the injecting pressure is increased from 7 MPa to 8 MPa, the permeability is decreased by 4.4% at 25 ^{0}C, whereas there is 8.2% reduction of CO_2 permeability at 40 ^{0}C. The CO_2 permeability reduction observed with increasing injecting pressure at lower temperatures (25 and 40 ^{0}C) is basically due to the process of swelling inside the coal sample during CO_2 injection (Vishal et al., 2013). According to Perera et al. (2011), this volumetric swelling causes the fracture aperture to close down, resulting in a reduction of coal sample permeability (Figure 4.23). Further, at 40 ^{0}C and 8 MPa the CO_2 flood is under super-critical conditions. As observed in Section 4.2, super-critical CO_2 causes greater permeability reductions in brown coal and this is also evident in the present study. Therefore, the percentage decrease in permeability is dominated by the CO_2 phase condition (gas/liquid/super-critical) and the coal permeability varies with the CO_2 phase condition for a given depth (refer to Sections 4.2 and 4.3).

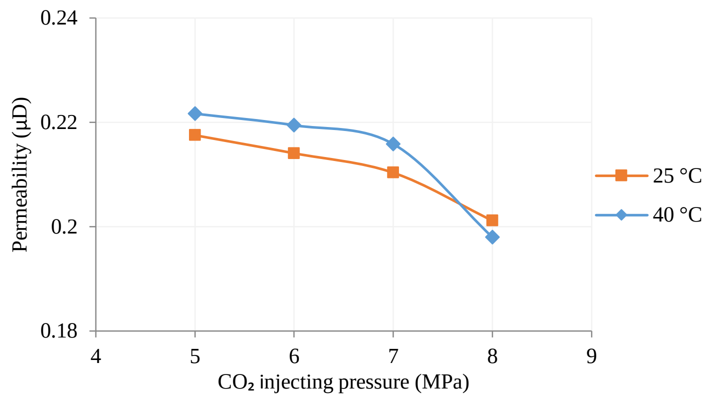

Figure 4.23. Variation of CO_2 permeability with different injecting pressures for 10 MPa confinement at 25 and 40 ^{0}C

However, a small increment of permeability can be seen from 5 to 7 MPa CO_2 injecting pressures when the temperature is increased from 25 to 40 ^{0}C. The CO_2 permeability increases by around 2.5% for 6 MPa injecting pressure after the temperature is elevated from 25 to 40 ^{0}C. Azmi et al. (2006) found that the amount of CO_2 molecules sorbed into the coal matrix reduces with increasing temperature (Figure 4.24) and Bae and Bhatia (2006) found that this reduction increases with increasing injection pressure (Figure 4.24). Therefore, CO_2 permeability should increase with increasing temperature, as observed for 5 to 7 MPa injecting pressures (Figure 4.23).

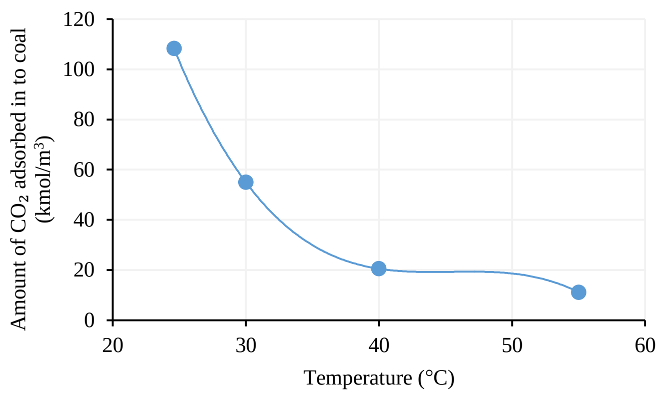

Figure 4.24. Variation of CO_2 adsorption capacity with temperature in low rank coal for a given pressure of 17 kPa (Azmi et al., 2006)

However, higher CO_2 pore pressures (super-critical – 8 MPa) at lower temperatures (40 ^{0}C) still have a greater influence on CO_2 permeability than lower pore pressures (5 – 7MPa) in spite of the reduced adsorption capacity. The results obtained from this test series for brown coal) are consistent with the findings of Perera et al. (2012) for naturally fractured black coal, which showed similar behaviour for lower temperatures (Figure 4.23), and higher pore pressures (8 – 12 MPa) showed around 22% reduction in permeability at 40 ^{0}C. Hence, we can deduce that CO_2 permeability is decreased for higher injection pressures (above 8 MPa) at lower temperatures, regardless of the rank of the coal. Conversely, Perera et al. (2012) observed an increment in CO_2 injectivity for higher temperatures (greater than 40 ^{0}C) in high rank coal, even at higher CO_2 pore pressures. For instance, the permeability increased by around 24% for 12 MPa CO_2 flooding when the temperature was raised from 50 to 70 ^{0}C. As witnessed by Bae and Bhatia (2006), the reduction of adsorption capacity of CO_2 is greater at higher pore pressures at elevated temperatures (refer to Figure 4.20), which may be the reason for this increase in permeability for high rank coal (Perera et al., 2012). A similar type of behaviour can be expected for low rank coal. However, it should be further investigated to draw a definitive conclusion on the effect of higher temperatures on brown coal permeability.

After completing the CO_2 injection, N_2 gas was injected into the coal sample under the same conditions to study the effect of temperature on N_2 permeability (see Figure 4.25). However, the influence of temperature on N_2 permeability was negligible (Figure 4.25) compared to the CO_2 permeability (Figure 4.25), which showed only around 0.75 to 1.3% increment in permeability when the temperature was raised from 25 to 40 ^{0}C. N_2 is a non-reactive gas that causes a negligible adsorption or swelling effect in the coal matrix compared to CO_2 (Kiyama et al., 2011), and therefore does not create any noticeable change in permeability when pore pressure is increased.

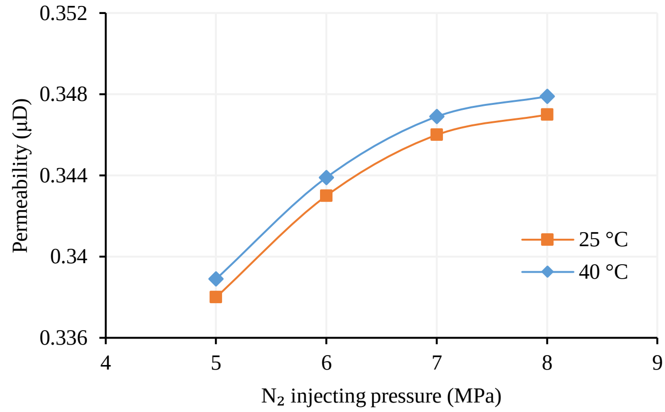

Figure 4.25. Variation of N_2 permeability with different injecting pressures for 10 MPa confinement at 25 and 40 ^{0}C temperatures.

However, Shao et al. (2016) observed a reduction in permeability in the 20 to 75^{0}C temperature range when injecting 4 to 5 MPa N_2 into lignite due to the thermal expansion of coal matrix. The higher pore pressures used in the present study (>5 MPa) and the comparatively low temperature range 25 to 40 ^{0}C may have conceded the permeability reduction in this study (see

Figure 4.25). Further, irrespective of the rank of the coal, the effect of temperature on N_2 permeability for coal is negligible, comparing the results of the current study (for brown coal) and the results obtained by Perera et al. (2012) (for naturally fractured black coal).

4.4.5 Conclusions

The following major conclusions can be drawn from the experimental results:

- CO_2 permeability increases when the temperature is increased from 25 to 40 ^{0}C.
- However, CO_2 permeability decreases for higher injecting pressures at 8 MPa, at temperatures less than 40 ^{0}C. This is due to the process of swelling in the coal sample during CO_2 injection, which decreases CO_2 permeability with increasing injecting pressure, especially under super-critical phase conditions.
- This greater permeability reduction during CO_2 flow at temperatures lower than 40 ^{0}C is common for any coal type. Hence, both the phase condition of CO_2 and its adsorption capacity at different temperatures are highly influential for CO_2 injectivity at different temperatures.
- The influence of temperature on N_2 permeability is negligible compared to CO_2 permeability, basically because N_2 is a comparatively more inert gas than CO_2 and does not cause a noteworthy swelling effect in the coal matrix.

4.4.6 References

Azmi, A., Yusup, S., Muhamad, S., (2006). The influence of temperature on adsorption capacity of Malaysian coal. *Chemical Engineering and Processing: Process Intensification* 45, 392-396.

Bae, J.-S., Bhatia, S.K., (2006). High-Pressure Adsorption of Methane and Carbon Dioxide on Coal. *Energ Fuel* 20, 2599-2607.

Bustin, R.M., Clarkson, C.R., (1998). Geological controls on coalbed methane reservoir capacity and gas content. *International Journal of Coal Geology* 38, 3-26.

Harpalani, S., Schraufnagel, A., (1990). Measurement of parameters impacting methane recovery from coal seams. *International Journal of Mining and Geological Engineering* 8, 369-384.

Jasinge, D., Ranjith, P.G., Choi, S.K., (2011). Effects of effective stress changes on permeability of latrobe valley brown coal. *Fuel* 90, 1292-1300.

Kiyama, T., Nishimoto, S., Fujioka, M., Xue, Z., Ishijima, Y., Pan, Z., Connell, L.D., (2011). Coal swelling strain and permeability change with injecting liquid/supercritical CO_2 and N_2 at stress-constrained conditions. *International Journal of Coal Geology* 85, 56-64.

Kronimus, A., Busch, A., Alles, S., Juch, D., Jurisch, A., Littke, R., (2008). A preliminary evaluation of the CO_2 storage potential in unminable coal seams of the Münster Cretaceous Basin, Germany. *International Journal of Greenhouse Gas Control* 2, 329-341.

McLinden, M., Klein, S., Lemmon, E., Peskin, A., (1998). REFPROP, Thermodynamic and transport properties of refrigerants and refrigerant mixtures. NIST Standard Reference Database 23.

Oldenburg, C.M., (2006). Geologic carbon sequestration: CO_2 transport in depleted gas reservoirs, *Gas Transport in Porous Media.* Springer, pp. 419-426.

Pan, Z., Connell, L.D., Camilleri, M., (2010). Laboratory characterisation of coal reservoir permeability for primary and enhanced coalbed methane recovery. *International Journal of Coal Geology* 82, 252-261.

Pashin, J.C., McIntyre, M.R., (2003). Temperature–pressure conditions in coalbed methane reservoirs of the Black Warrior basin: implications for carbon sequestration and enhanced coalbed methane recovery. *International Journal of Coal Geology* 54, 167-183.

Perera, M.S.A., Ranjith, P.G., Airey, D.W., Choi, S.K., (2011a). Sub- and super-critical carbon dioxide flow behaviour in naturally fractured black coal: An experimental study. *Fuel* 90, 3390-3397.

Perera, M.S.A., Ranjith, P.G., Choi, S.K., Airey, D., (2011b). The effects of sub-critical and super-critical carbon dioxide adsorption-induced coal matrix swelling on the permeability of naturally fractured black coal. *Energy* 36, 6442-6450.

Perera, M.S.A., Ranjith, P.G., Choi, S.K., Airey, D., (2012). Investigation of temperature effect on permeability of naturally fractured black coal for carbon dioxide movement: An experimental and numerical study. *Fuel* 94, 596-605.

Ranathunga, A.S., Perera, M.S.A., Ranjith, P.G., Ju, Y., Vishal, V., De Silva, P., (2015). A macro-scale experimental study of sub-and super-critical CO_2 flow behaviour in Victorian brown coal. *Fuel* 158, 864-873.

Ranjith, P.G., Perera, M.S.A., (2011). A new tri-axial apparatus to study the mechanical and fluid flow aspects of carbon dioxide sequestration in geological formations. *Fuel* 90, 2751-2759.

Rebscher, D., May, F., Oldenburg, C., (2006). Sequestration of CO_2 in the Altmark natural gas field, Germany: Mobility control to extend enhanced gas recovery, Paper LBNL 60157, 2006, Lawrence Berkeley National Laboratory, University of California.

Reeves, S., Oudinot, A., (2005). The Allison Unit CO_2-ECBM Pilot–A Reservoir and Economic Analysis, 2005 International Coalbed Methane Symposium, Paper, pp. 16-20.

Shao, J., Hu, Y., Meng, T., Song, S., Jin, P., Feng, G., (2016). Effect of Temperature on Permeability and Mechanical Characteristics of Lignite. *Advances in Materials Science and Engineering* 2016. DOI: http://dx.doi.org/10.1155/2016/1430641.

Siriwardane, H., Haljasmaa, I., McLendon, R., Irdi, G., Soong, Y., Bromhal, G., (2009). Influence of carbon dioxide on coal permeability determined by pressure transient methods. *International Journal of Coal Geology* 77, 109-118.

Skawiński, R., (1999). Considerations referring to coal swelling accompanying the sorption of gases and water. *Archives of Mining Sciences* 44, 425-434.

Suggate, R., (1974). Coal ranks in relation to depth and temperature in Australian and New Zealand oil and gas wells. *New Zealand Journal of Geology and Geophysics* 17, 149-167.

Vishal, V., Ranjith, P., Singh, T., (2013). CO_2 permeability of Indian bituminous coals: Implications for carbon sequestration. *International Journal of Coal Geology* 105, 36-47.

Yang, X.-l., Zjang, Y.-l., Li, C.Q., (2008). An experimental study of temperature effect on seepage rule of coal seam gas. *Chin J Geotech Eng* 30, 1811-1814.

Zhao, Y., Fang, Q., Zhijun, W., Yuan, Z., Weiguo, L., Qiaorong, M., (2010). Experimental Investigation on Correlation between Permeability Variation and Pore Structure during Coal Pyrolysis. *Transport in Porous Media* 82, 401-412.

Zou, L., Jin, L., Wang, X., Hu, H., (2015). Pyrolysis of Huolinhe lignite extract by in-situ pyrolysis-time of flight mass spectrometry. *Fuel Processing Technology* 135, 52-59.

4.5 How does carbon dioxide adsorption-induced coal matrix swelling vary with various CO_2 properties and reservoir depths?

Coal matrix swelling with CO_2 adsorption is one of the main problems in the process of CO_2-ECBM in deep coal seams, as it causes coal seam flow ability to be considerably reduced (refer to Section 4.2). Hence, it would be interesting to observe the volumetric strain variations of coal specimens to quantify coal matrix swelling during CO_2 flow. Therefore, the main objective of this study was to investigate the effect of coal mass swelling on the permeability of Victorian brown coal. The coal matrix swelling was measured during the meso-scale permeability test series mentioned in Section 4.2. As explained in Section 4.2, a series of tri-axial permeability tests was conducted on brown coal specimens 38 mm in diameter by 76 mm high. These tests were carried out for CO_2 and N_2 injections from 5 - 14 MPa injection pressures under 11 to 17 MPa confining pressures at 35 ^{o}C. The changes in volumetric strain of the samples during different CO_2 properties and reservoir depths and the corresponding effects on CO_2 and N_2 permabilities were examined.

This section of the chapter is the following paper:

Ranathunga AS, Perera MSA, Ranjith PG, Zhang XG (2017). The influence of CO_2 properties and reservoir depth on coal matrix swelling: A meso-scale experimental study using low rank coal. *Energy Fuel* (under review).

The influence of CO_2 properties and reservoir depth on coal matrix swelling: A meso-scale experimental study using low rank coal

A.S. Ranathunga[1], M.S.A. Perera[1,2], P.G. Ranjith[1], X.G. Zhang[1]

[1]Deep Earth Energy Laboratory, Department of Civil Engineering, Monash University, Building 60, Melbourne, Victoria, 3800, Australia.

[2] Department of Infrastructure Engineering, The University of Melbourne, Building 176, Melbourne, Victoria, 3010, Australia.

Abstract

Although the greater adsorption potential of carbon dioxide (CO_2) in coal is an appealing fact in relation to the long-term safe storage of CO_2 in coal seams, the resulting coal structure modification, particularly through coal matrix swelling, adds many uncertainties to the process. To date, many studies have been initiated, particularly on the effects of injecting CO_2 and reservoir properties on this swelling process and the associated reservoir permeability depletion. These influences are largely dependent on the maturity of the coal mass and its structure, including the cleat system. However, little attention has been given to date to the effect of coal rank on CO_2 adsorption-induced coal matrix swelling. Ranathunga et al. (2017) conducted a series of tri-axial permeability tests using Australian brown coal samples for both CO_2 and N_2 under various confinements and injections at 35 ^{0}C to investigate the influence of CO_2 properties and reservoir depth on CO_2 adsorption-induced flow reductions in coal of various ranks. However, this understanding cannot be achieved without detailed analysis of the coal's swelling characteristics. This is the focus of the present study.

Based on the experimental evaluation of coal matrix swelling under various CO_2 and reservoir conditions, super-critical CO_2 adsorption leads to greater coal matrix swelling in coal, and the degree of swelling is dependent on reservoir depth and coal maturity. This coal matrix swelling reduces with increasing reservoir depth, due to the associated reduction in CO_2 sorption capacity into coal. However, this also depends on the pore pressure conditions, and lower effective stresses lead to greater swelling reduction, regardless of coal rank. The potential of N_2 to recover the swelled areas was tested by permeating the coal mass with N_2 at different pressures and for different durations (24, 48 and 72 hours). The results show a greater potential for recovery at lower depths and for longer durations of N_2 flooding. Finally, the applicability of the Dubinin–Radushkevich (D-R) model for the prediction of low rank coal swelling was tested and good agreement between the model data and the measured swelling data was found.

Keywords: brown coal, CO_2 phase and pressure, coal matrix swelling, reservoir depth

4.5.1 Introduction

The storage of CO_2 in deep un-mineable coal seams is currently identified as a potential approach to the minimization of anthropogenic CO_2 in the atmosphere. Numerous research studies have therefore been commenced on this method, particularly related to the alteration of coal seam properties (hydro-mechanical properties) upon CO_2 injection. According to these studies, CO_2 has greater potential to be adsorbed into the coal mass compared to the existing CH_4 in the coal matrix, which confirms the great storage potential for CO_2 in underground coal reservoirs (Skawiński, 1999).

Generally, CO_2-ECBM is carried out in deep coal seams, where CO_2 is in its super-critical state (beyond the critical temperature of 31.8^{0}C and critical pressure of 7.38 MPa) due to the high temperatures and pressure conditions at such depths (Oldenburg, 2006). Interestingly, super-critical CO_2 has greater adsorption potential than sub-critical CO_2 due to its inherent chemical and physical characteristics (liquid-type densities and viscosities and gas-type compressibilities) (Perera et al., 2015). In the CO_2 adsorption process in coal, CO_2 first flows through the macro-pores (butt and face cleats) and adsorbs into the fracture walls. Then it slowly diffuses into the micro-pores (pores in the coal matrix) and adsorbs into the micro-pores (Pan and Connell, 2007). However, during this process of CO_2 adsorption into the coal matrix, a strain is induced between the coal matrix and the adsorbing CO_2 layer, which is commonly known as coal matrix swelling (Gale, 2004; Mazumder and Wolf, 2008; Vandamme et al., 2010).

Coal matrix swelling reduces the pore spaces available for gas movement, resulting in reduced overall permeability (White et al., 2005). This is evident in field-scale projects, such as the San Juan basin, USA and the Ishikari basin, Japan, which showed around 50 to 70% reduction of CO_2 injection capacity within the first six months to one year (Fujioka et al., 2010; Reeves, 2001). Further, according to Botnen et al. (2009), the initial CO_2 permeability of the Williston basin lignite coal seam in North Dakota was reduced by 10 times within the first year as a result of coal matrix swelling. In addition, Gale (2004) stated that this swelling process can create significant stress on the cap rock, which may lead to cap rock failure and hence possible CO_2 back-migration into the atmosphere. Therefore, it is clear that the effect of coal matrix swelling on coal's flow and strength characteristics is of crucial importance.

Day et al. (2008), Hol et al. (2011), Karacan (2007), Pan et al. (2010), Perera et al. (2011a), Siriwardane et al. (2009), and Zutshi and Harpalani (2004) have studied this coal matrix swelling effect using tri-axial experiments on high-rank coal, and Jasinge (2010) and Balan and Gumrah (20209) conducted similar tri-axial tests on low-rank coal. However, these researchers used only low injecting pressures and examined only gas and liquid state CO_2. Although Anggara et al. (2013) conducted swelling experiments on crushed lignite from Indonesia for super-critical CO_2 (up to 10 MPa) using coal blocks of 30 x 10 x 10 mm^3, they did not consider the effect of confining pressure on coal swelling. The incorporation of this confining pressure effect is important for the correct identification of the swelling effect in field stress environments. Therefore, a knowledge gap exists on the effects of coal matrix swelling on permeability under super-critical conditions, especially for low-rank brown coal in confined environments.

The main purpose of this study is therefore to investigate the influence of CO_2 phase condition (sub-critical and super-critical) on coal matrix swelling and the corresponding alterations in brown coal flow characteristics in various in-situ stress environments. This study is an extension of the work by Ranathunga et al. (2017) on the effect of CO_2 phase and pressure on Australian brown coal permeability under in-situ stress conditions. The scientific reasons for the observed degraded CO_2 flow behaviours in that study are discussed in the present study through the concept of coal matrix swelling.

Ranathunga et al. (2017) observed the potential of pressurised N_2 to partially recover CO_2 adsorption-induced coal matrix swelling, particularly under lower effective stresses. This is because the injected N_2 reduces the partial pressure of the coal mass, which eventually leads to the desorption of physically-adsorbed CO_2 from the coal matrix, resulting in reversible swelling recovery. In this study, further attention is paid to this coal matrix swelling behaviour after N_2 permeation to clarify the results of Ranathunga et al. (2017) on permeability enhancement. Ranathunga et al. (2017) found a lower recovery potential at higher effective stresses due to the corresponding reduction in flow rates, and they explained the importance of offering more time for alternative N_2 permeation for greater swelling recovery. This has been taken into consideration in this study by investigating the influence of N_2 flooding duration on the degree of CO_2 permeability enhancement.

4.5.2 Experimental Methodology

A series of swelling experiments was conducted simultaneously with the permeability tests conducted by Ranathunga et al. (2017), and the sample preparation and the experimental methodology for the flow tests are explained in Ranathunga et al. (2017). A summary is given in Figure 4.26 below.

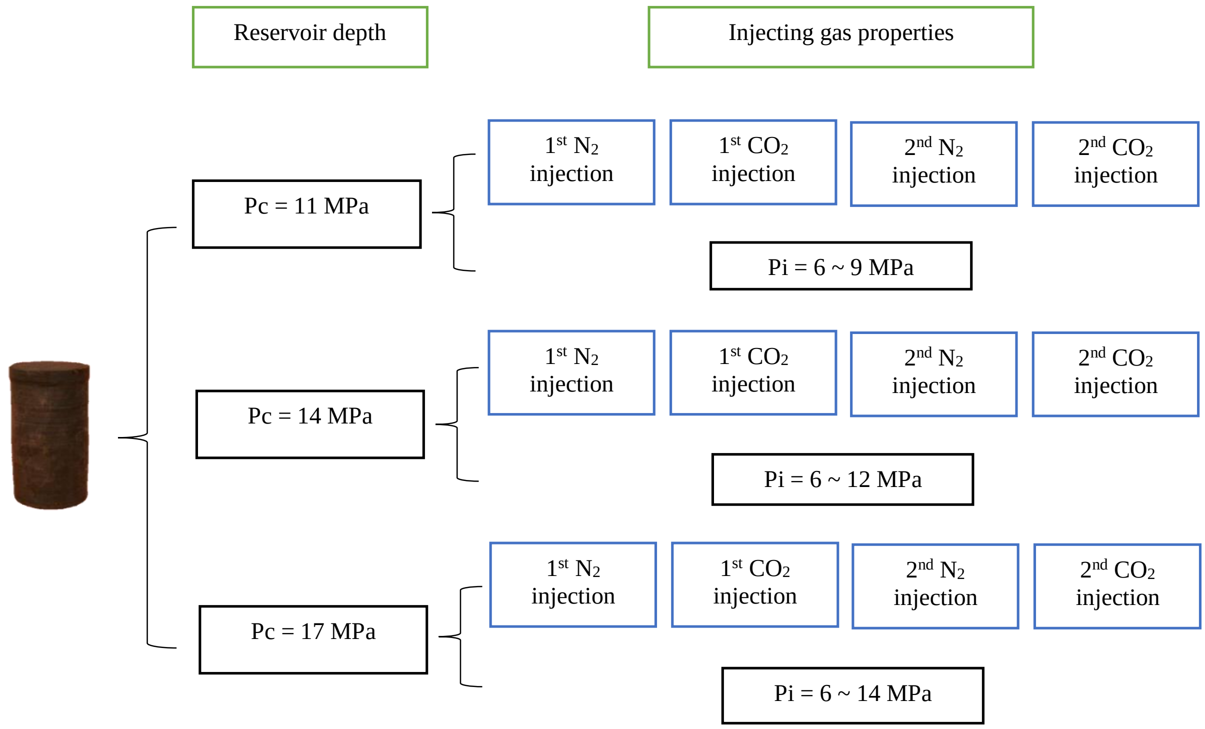

Figure 4.26. Experimental program for tri-axial flow studies (here Pc is confining pressure and Pi is injection pressure)

N_2 was injected into the coal sample before and after CO_2 injection at various pressures to identify the alterations created by CO_2 injection in the coal matrix, this could be done due to the comparatively less adsorptive nature of N_2 than CO_2. As explained by Ranathunga et al. (2017), N_2 has the potential to recover coal matrix swelling-induced matrix alterations. CO_2 was therefore re-injected after 24 hours of N_2 permeation to identify the corresponding enhancement in coal permeability. Further, the influence of N_2 permeation duration on swelling recovery was also studied by flooding N_2 for different time periods of 24, 48 and 72 hours on swelled coal samples under 6 MPa (sub-critical) and 8 MPa (super-critical) CO_2 pressures.

During this complete test series, the volumetric strain in the coal sample was recorded using an advanced data acquisition system at one-second intervals to quantify the CO_2 adsorption-induced coal matrix swelling of the brown coal specimens in various stress environments. The volumetric swelling was calculated using the volume change data given by a syringe pump (see Eq. [4.18]) which was used to apply the confining pressure. When the sample swells, the excess oil volume inside the cell is pumped out towards the syringe pump, and when the sample shrinks oil is sent towards the sample from the pump (Figure 4.27).

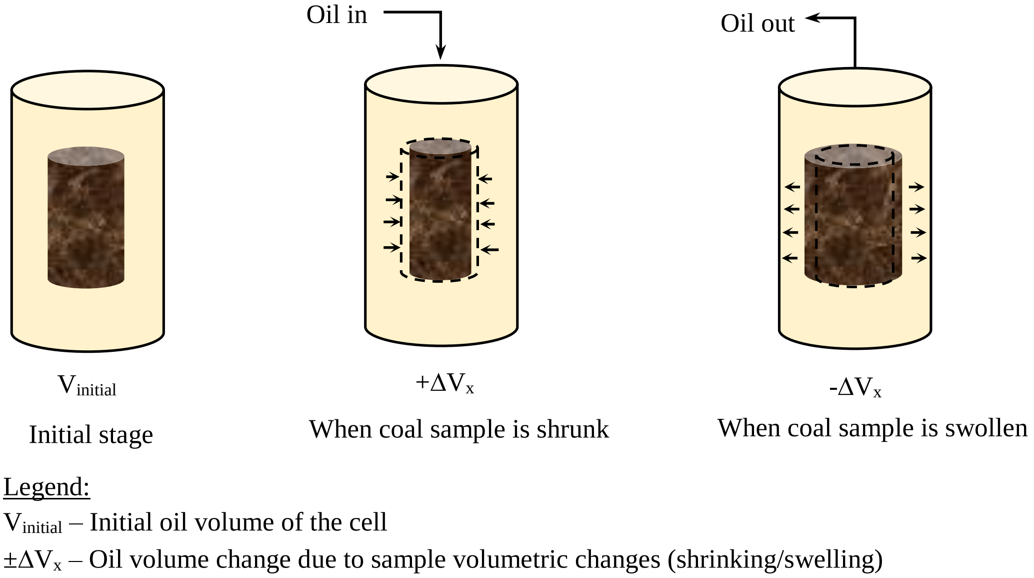

Figure 4.27. Oil volume change of pressure cell due to coal sample volume changes

Eq. [4.18] was used to calculate the volumetric strain in the coal sample under various injection conditions.

$$\text{Volumetric strain of the sample } (\varepsilon_V) = \left(\frac{\pm\ \Delta V_x}{V_{initial}}\right) \times 100\% : \ \Delta V_x = V_{initial} - V_t \qquad [4.18]$$

where, $V_{initial}$ is the initial pump volume for the respective test condition (stable pump volume after applying the confining pressure), V_t is the pump volume at time t and ΔV_x is the oil volume change (pumped in or out from the syringe pump). Therefore, positive volumetric strains represent sample shrinkage ($V_{initial} > V_t$) and negative volumetric strains represent sample swelling ($V_{initial} < V_t$) (Figure 4.27). The whole test series was conducted at 35 ^{0}C (> 31.8 ^{0}C is the critical temperature of CO_2) constant temperature to obtain the super-critical condition of the injected CO_2 when the pressure went beyond 7.38 MPa (the critical pressure of CO_2). The volumetric strain variations of the coal samples for 6 MPa CO_2 and N_2 injections under 11, 14 and 17 MPa confinements are shown in Figure 4.28.

4.5.3 Results and Discussion

4.5.3.1 Effect of sub- and super-critical CO_2 adsorption on coal matrix swelling

According to Figure 4.28, CO_2 flow through low rank brown coal causes clear coal matrix swelling (negative volumetric strain) compared to N_2, and the matrix swelling gradually increases over time, regardless of confinement (Figure 4.28). The influence of CO_2 phase and pressure on coal matrix swelling was therefore studied first.

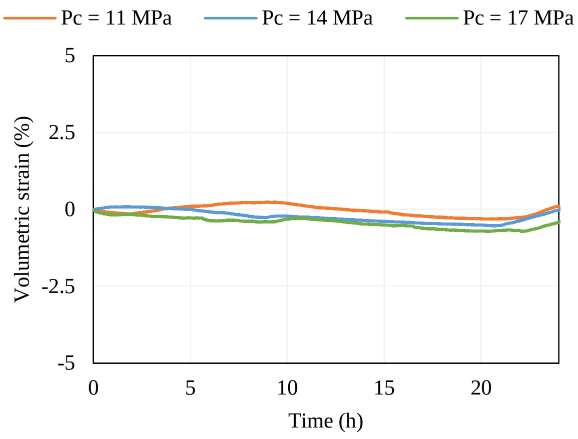

(a) N_2 injection

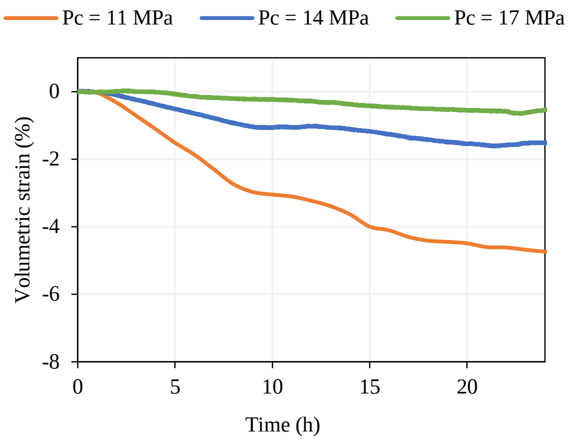

(b) CO_2 injection

Figure 4.28. Volumetric strain variation of brown coal samples for 6 MPa N_2 and CO_2 injections under various confining pressures (here Pc is confining pressure)

For the purposes of comparison, the sample volume increase or *coal matrix swelling* is denoted by positive volumetric strains (note that Eq. [4.18] gives a negative result for swelling; refer to Figure 4.27) and the sample volume decrease or *coal matrix shrinkage* is denoted by negative volumetric strains (note that Eq. [4.18] gives a positive result; refer to Figure 4.27) in Figure 4.29. Figure 4.29 shows the alteration of brown coal's volumetric strain following 24 hours of CO_2 and N_2 flooding at 11 MPa confining pressure. According to the figure, increasing CO_2 injection pressure results in greater volumetric strain in the tested brown coal. For example, 6 to 7 MPa and 8 to 9 MPa CO_2 pressure increments cause around 1.96% and 3.68% volumetric strain increments under 11 MPa confining pressure. Importantly, under the same pressure conditions, N_2 injection exhibits only around 0.08% (6 to 7 MPa) and 0.11% (8 to 9 MPa) volume changes, which are insignificant compared to the CO_2 effect. The other important fact is that the increase of volumetric strain under super-critical CO_2 permeation is much greater compared to that for sub-critical CO_2 permeation. For instance, 8 to 9 MPa super-critical CO_2 permeation causes coal mass swelling around 1.7% greater than the swelling caused by 6 to 7 MPa sub-critical CO_2 permeation (Figure 4.29) under 11 MPa confining pressure. Ranathunga et al. (2017) found around 20% greater reduction in coal mass permeability when the CO_2 phase condition transitioned from sub-critical (6 to 7 MPa) to super-critical (8 to 9 MPa). Hence, around 2% increase in swelling causes the reduction of the flow ability by 10 times, which confirms the influence of adsorbing CO_2 phase condition on coal mass swelling and the associated permeability for low-rank coal.

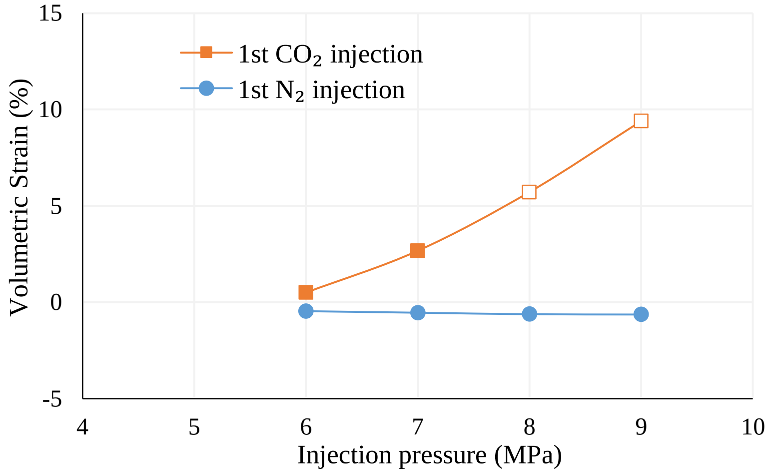

Figure 4.29. Volumetric strain variation with injection pressure under 11 MPa confining pressures for first N_2 and CO_2 injections (here the hollow data points represent the super-critical CO_2 pressures)

In relation to the CO_2 phase effect on swelling, this coal matrix swelling occurs due to the sorbed volume of the adsorbate (Ottiger et al., 2006), and hence this sorbed volume is proportional to the amount of coal matrix swelling (Battistutta et al., 2010). Therefore, increasing pore pressure inside the coal mass causes the CO_2 adsorption-induced swelling to gradually increase. In the present study, when the injection pressure of CO_2 increased from 6 to 9 MPa, the average pore pressure inside the coal sample increased from around 5.53 MPa (< 7.38 - sub-critical range) to 7.73 MPa (> 7.38 – super-critical range) under 11 MPa confinement (here, the *average pore pressure* is taken as the mean value of the upstream and the steady-state downstream pressures). Therefore, with increasing CO_2 injection pressure, coal matrix swelling increases (Figure 4.29). Further, this sorbed volume is greater for super-critical CO_2 due to the higher adsorption capacity (Day et al., 2008), which causes greater coal matrix swelling and consequently greater permeability reduction, as observed by Ranathunga et al. (2017) for brown coal. Similarly, Perera et al. (2011b) observed around 14% radial strain increase for 5 MPa sub-critical CO_2 injection and around 50% strain increment for 8 MPa super-critical CO_2 flow for high-rank coal (Australian bituminous coal). This shows that the greater coal matrix swelling observed under super-critical CO_2 permeation is applicable to any coal seam, regardless of its rank.

According to Figure 4.28, CO_2 absorption-induced swelling occurs at a maximum rate within the first 7 to 8 hours for 6 MPa CO_2 injection under 11 MPa confining pressure. In comparison with the swelling behaviour reported in the research literature for high-rank coal, Perera et al. (2011b) observed a maximum radial strain increment within the first 3 to 4 hours of sub-critical CO_2 injection under 10 MPa confinement. Unlike the intact coal samples used in the present study, the fractured black coal used by Perera et al. (2011b) had more provision for CO_2 permeation through the sample and this may have caused a quicker occurrence of maximum swelling compared to intact brown coal. In relation to the other two confinements considered (14 and 17 MPa), the maximum swelling rate was seen within the first 11 to 12 hours for 14 MPa confinement and within the first 17 to 18 hours for 17 MPa confinement. The maximum swelling rates for these in-situ stresses (11, 14 and 17 MPa) were 0.36, 0.1 and 0.03, respectively. According to these values, the swelling rate reduces with increasing confining pressure. According to Hol et al. (2011), CO_2 adsorption capacity reduces at high effective stresses due to reduced CO_2 molecule permeation into the fine pores in the coal mass, which explains the reason for the reduced volumetric swelling effect observed at greater confining pressures. This reduction of coal matrix swelling with increasing confinement is important in field-scale applications, because this represents the influence of coal seam reservoir depth on its swelling characteristics. This is therefore considered in detail in the following section.

4.5.3.2 Effect of reservoir depth on coal matrix swelling

Figure 4.30 shows the variation of volumetric strain developed in the tested low rank brown coal with CO_2 and N_2 flows in various confining stress environments. Note that here CO_2 density is used instead of CO_2 pressure to characterize the volumetric strain data, because gas density more precisely represents the injecting CO_2 properties due to its dependency on both temperature and pressure (Day et al., 2008). The density of CO_2 was calculated for each injection condition (35 ^{0}C and 6 to 14 MPa injection pressures) using the REFPROP data base (McLinden et al., 1998). As shown in Figure 4.30(a), the volumetric strain of coal for CO_2 flow increases with increasing CO_2 density, regardless of confinement. However, the strain developed clearly reduces with increasing confinement. Figure 4.31 shows the volumetric strain reductions observed for different CO_2 and N_2 injection conditions for 11 to 14 MPa and 14 to 17 MPa confining pressure increments, where the coal matrix swelling is subjected to a reduction with increasing confining stress. However, this confining stress influence on coal matrix swelling is more significant at low confinements (11 to 14 MPa) compared to high confinements (14 to 17 MPa). For example, around 1.08% and 5.45% strain reductions can be seen for 6 MPa (sub-critical) and 9 MPa (super-critical) CO_2 permeation in the coal mass under 11 to 14 MPa confining stress increment and only around 0.6% and 3.02% for 6 MPa (sub-critical) and 9 MPa (super-critical) CO_2 permeation in the coal mass under 14 to 17 MPa confining pressure increment. This greater swelling reduction under greater confinements is related to the much shrunken pore space that the coal mass undergoes at greater confinements, which reduces the surface area available for CO_2 adsorption.

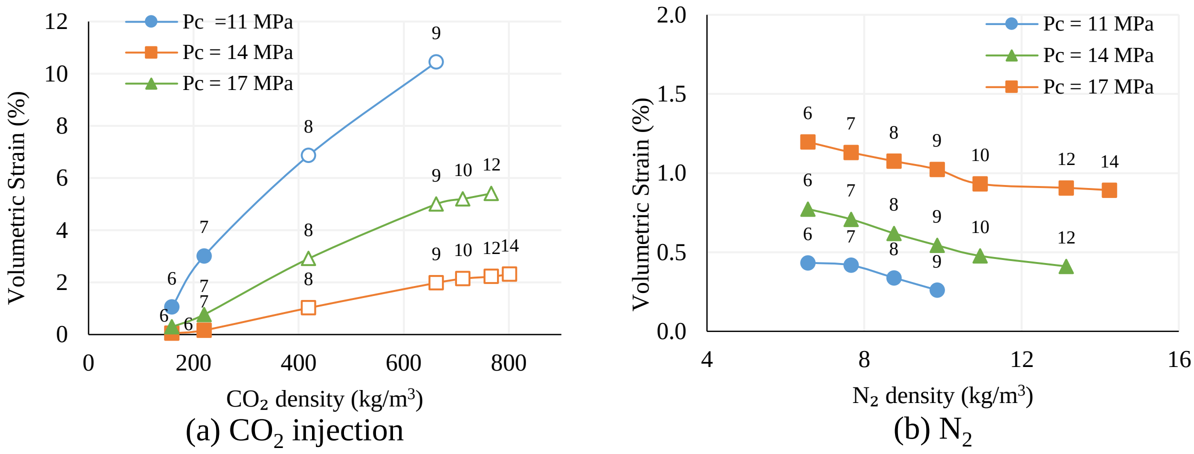

Figure 4.30. Variation of volumetric strain under 11, 14 and 17 MPa confinements during first CO_2 and N_2 injection (here the hollow data points represent the super-critical CO_2 conditions and the data labels denote the respective injection pressures)

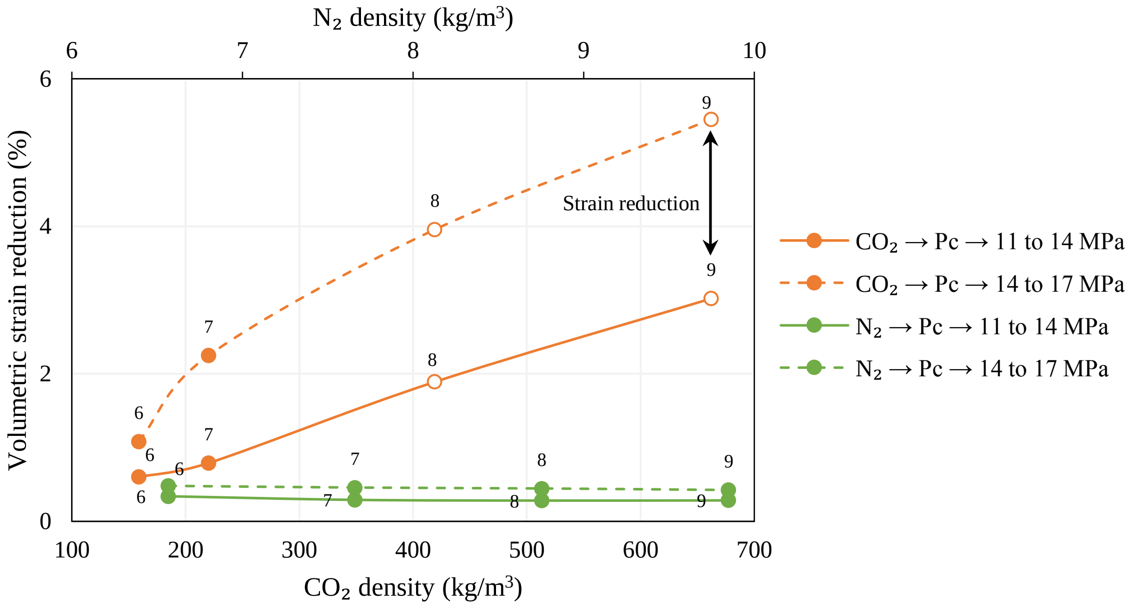

Figure 4.31. Volumetric strain reduction from 11 to 14 MPa and 14 to 17 MPa confinement increase during first CO_2 and N_2 injection (here the hollow data points represent the super-critical CO_2 conditions and the data labels denote the respective injection pressures)

The other important observation is the greater swelling under super-critical CO_2 permeation compared to sub-critical CO_2. Super-critical CO_2 has a greater adsorption capacity due to its highly chemically reactive nature (McLinden et al., 1998) and therefore causes greater coal matrix swelling. The average pore pressure conditions for the different CO_2 injections under the three confining pressures (11, 14 and 17 MPa) are plotted against the upstream CO_2 pressures in Figure 4.32. According to the figure, the average pore pressure has a similar behaviour to strain variation, which shows a reduction of the pore pressure within the sample with increasing confining pressure for all the injection pressures. Hence, as explained previously, the reduced CO_2 sorbed volume of the sample causes the reduction of coal matrix swelling. Further, the higher compressive forces available at higher effective stresses may also restrict the volumetric swelling. Therefore, the increase in volumetric strain reduction is a combined influence of the effective stress increment under higher compressive forces and the lower CO_2 adsorption capacity in the shrunken pore structure. Hol et al.(2011) confirmed this lower swelling effect under greater effective stresses for high-rank coal. Therefore, the results of the present study confirm that, regardless of the rank of the coal seam, it is subjected to a lower swelling effect if the depth of the seam is great.

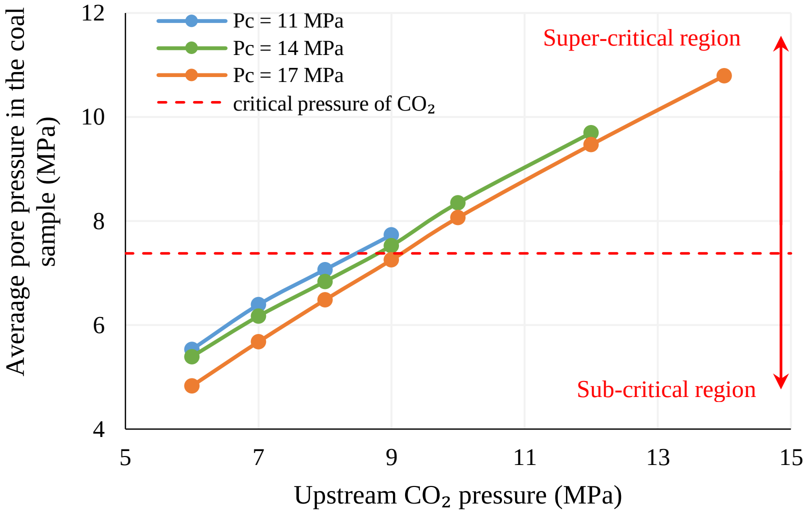

Figure 4.32. Average pore pressure variation in the coal sample during the first CO_2 injection (after 24 hours of injection)

Interestingly, this reduction of strains is greater for higher injection pressures for both 11 to 14 MPa and 14 to 17 MPa stress increments. For instance, a 1.71% increase in strain reduction was observed for 7 to 8 MPa injection pressures for an 11 to 14 MPa stress increase, while a 1.1% increase in strain reduction was observed for the same injection pressures for a 14 to 17 MPa stress increase (Figure 4.31). This can be explained by the portion of the sample which undergoes different CO_2 pressures under the respective conditions, as shown in Figure 4.33. Ranathunga et al. (2017) studied the CO_2 pressure variation along coal samples, assuming a linear variation from upstream to downstream for each injection condition, and the same concept was used here for 7 and 8 MPa CO_2 injections for the three different confinements.

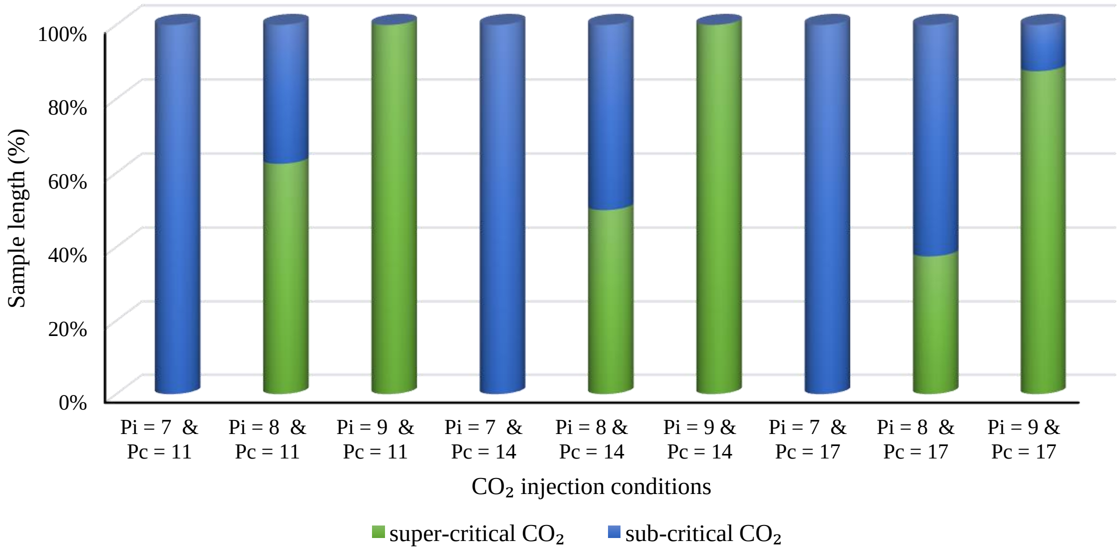

Figure 4.33. CO_2 pressure variation along the sample for 7, 8 and 9 MPa CO_2 injection under 11, 14 and 17 MPa confining pressures (here Pi = injection pressure and Pc = confining pressure)

According to Figure 4.33, under the confinements considered here, 7 MPa CO_2 injection (< 7.38 MPa, the critical pressure of CO_2) causes the sample to undergo 100% CO_2 adsorption under sub-critical conditions, while 8 MPa CO_2 injection (> 7.38 MPa, the critical pressure of CO_2) causes the sample to undergo both sub- and super-critical CO_2 adsorption. However, the portion of the sample subjected to super-critical CO_2 adsorption is reduced with increasing confinement. For example, around 63%, 50% and 32% of the sample (assuming a linear variation from upstream to downstream) is subjected to super-critical CO_2 adsorption under 11, 14 and 17 MPa confinements, respectively. As discussed previously, the coal mass has much reduced pore space under higher confinements and therefore CO_2 has less ability to move through it, which results in a reduced super-critical CO_2 distributed area of the sample under greater confinements. Since super-critical CO_2 creates much greater swelling in the coal mass, the reduction of super-critical CO_2 adsorbed in the coal mass eventually reduces the degree of swelling. Therefore, when the confinement is increased from 11 to 14 MPa (1.71%) and 14 to 17 MPa (1.1%), a reduction in volumetric strain increment (swelling) is shown for 7 to 8 MPa CO_2 pressures in Figure 4.31.

When 9 MPa CO_2 permeates through brown coal, around 100%, 100% and 87.5% of the sample is in super-critical condition (Figure 4.33) under the three confinements considered here. Therefore, as explained above, the greater CO_2 sorbed volume in the sample due to the larger proportion of super-critical CO_2 creates much greater swelling with super-critical CO_2 flooding. In relation to permeability for these conditions, a 7 to 8 MPa CO_2 pressure increase causes 3.2% and 1.8% permeability reduction increments with 11 to 14 MPa and 14 to 17 MPa confining stress increments, respectively, while 5.2% and 2.7% increase of permeability reduction for the similar confinement increase was observed for 8 to 9 MPa super-critical CO_2 permeation (Ranathunga et al. 2017). This confirms the influence of the effective stress changes on strain variations and the effect on CO_2 flow.

Moreover, similar to the CO_2 injection, the strain developed in the coal mass during N_2 injection was also checked under changing confining stress environments and the results are shown in Figure 4.30. According to the figure, 0.34% and 0.28% strain reductions occur for 6 and 9 MPa CO_2 permeations when the confining stress increases from 11 to 14 MPa. In addition, the confinement-created strain reductions are greater for greater confinements, producing strain reductions of 0.48% for 6 MPa and 0.44% for 8 MPa with increasing confinement from 14 to 17 MPa. However, unlike in CO_2 flow, here the influence of N_2 pressure on swelling reduction which occurs with increasing confining pressure is negligible (Figure 4.31). This is because, compared to CO_2, N_2 is a less adsorptive, inert gas (Day et al., 2010). Therefore, the expected volumetric strain increase for N_2 with increasing pore pressure is minimal. Hence, the strain variations observed in Figure 4.31 are mainly due to the effective stress variation with in situ stresses.

4.5.3.3 Potential of N_2 to reverse CO_2 induced coal matrix swelling

As discussed in previous sections, CO_2 flow through the coal matrix causes considerable matrix rearrangements, creating a negative impact on CO_2 sequestration. Although this swelling effect reduces with increasing reservoir depth, the swelling seems to happen at considerably higher rates for super-critical injected CO_2, which is the most common CO_2 phase expected in potential unmineable coal seams (Vishal and Singh, 2015). This matrix swelling causes a reduction of injection capacities in many field-scale CO_2-ECBM projects, making the projects uneconomical (refer to Section 1). Hence, appropriate precautions to reduce this swelling effect are necessary for reservoir productivity enhancement in CO_2-ECBM projects. According to Perera et al. (2011a), the injection of a stream of N_2 into the swelled coal mass creates a considerable improvement in the permeability of high-rank coal by partially reversing the CO_2-induced coal matrix swelling. The applicability of this interesting technique to low rank coal was tested by Ranathunga et al. (2017) using lignite. The researchers found that N_2 injection has the ability to improve the permeability of low-rank brown coal, particularly at lower effective stresses (Ranathunga et al. (2017). However, the precise identification of this ability of N_2 requires a comprehensive overview of the swelling characteristic variations of the coal mass during this remediation process. In order to quantify the ability of N_2 flooding to partially recover CO_2 adsorption-induced coal matrix swelling, the coal sample was subjected to 24 hours of N_2 flooding after each CO_2 injection, and the CO_2 injection was then repeated at the same pressure. For 6 and 8 MPa CO_2 injection pressures the samples were also subjected to an additional 48 hours of the third N_2 flooding after the second CO_2 injection, followed by the third CO_2 injection. Similarly, 72 hours of N_2 flooding (fourth N_2 flooding) for 6 and 8 MPa CO_2 injection pressures was carried out after the third CO_2 injection, followed by the fourth CO_2 injection.

a. After 24 hours of N_2 flooding

Figure 4.34 shows the swelling reduction observed with the second CO_2 injection after 24 hours of N_2 flooding for each CO_2 injection pressure under the three different in-situ stresses considered here. As the figure shows, under all three confinements, swelling recovery is exponentially increased with increasing injection pressure, confirming that high-pressure N_2 flooding is more effective in recovering the reversible swelling areas created by CO_2. For example, the swelling recovery percentages observed for 6 and 8 MPa CO_2 injection pressures are around 1.3% and 8.9% under 11 MPa confinement, and 0.7% and 2.9% under 17 MPa confinement, respectively (see Figure 4.34). According to Kiyama et al. (2011), N_2 has the ability to desorb CO_2 molecules from the pore faces by creating a partial pressure reduction in the sample, which contributes to the reduced swelling percentage in the sample. At higher N_2 pressures, the amount of N_2 entering the coal matrix is greater and eventually the amount of partial recovery of swelling is also greater. Furthermore, at higher CO_2 pressures, the sample is also subjected to greater volumetric strains and therefore N_2 has more ability to recover the swelled areas (Figure 4.34). However, this recovery rate reduces with increasing reservoir depth. For instance, 0.6% and 6% reductions in swelling recovery can be seen for 6 and 8 MPa CO_2 floods with increasing confinement from 11 to 17 MPa. This is because, for higher confinements N_2 flow ability through the coal matrix slows down, which eventually gives less opportunity for swelling recovery for N_2 (Figure 4.34).

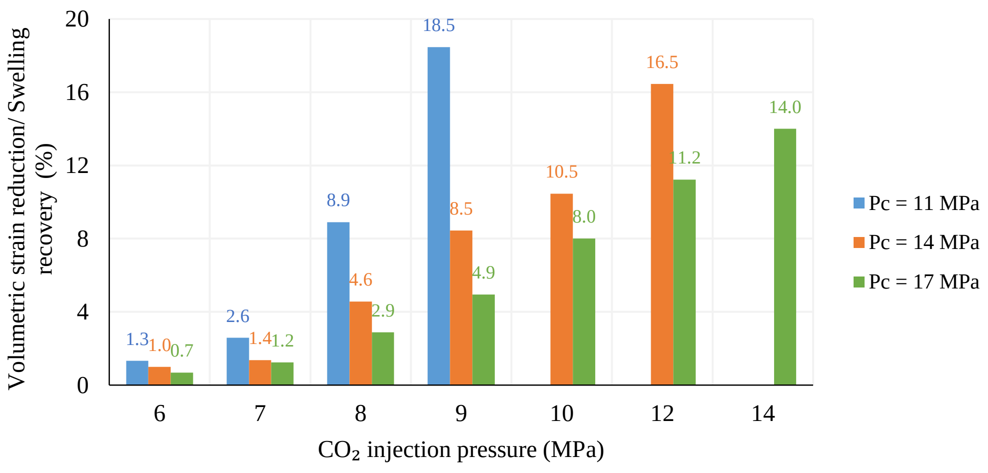

Figure 4.34. Volumetric strain reduction for second CO_2 injection compared to first CO_2 injection after N_2 flooding for 24 hours

It should be noted that before the second CO_2 injection, the sample had already been subjected to swelling during the first CO_2 injection. Hence, less matrix rearrangement can be expected due to the second CO_2 flow than the first (Perera et al., 2011b). Under higher CO_2 pressures, the coal matrix undergoes considerable macro-molecular structural alterations due to the inherent chemical and physical interactions of super-critical CO_2 and coal pore walls (Perera et al., 2011b; Pini et al., 2009). Hence, the expected swelling at higher injection pressures for the re-injection of CO_2 will be less (Figure 4.34). In addition, the swelling is also reduced by reservoir depth, which causes much less swelling at higher confinements for the second CO_2 injection. Therefore, both N_2 flooding and swelling reduction due to the alteration in the coal matrix caused by previous CO_2 flows collectively influence the strain reductions observed during the second CO_2 flow.

Figure 4.35 shows the CO_2 permeability increment against strain reduction with the second CO_2 flow, which confirms that the observed permeability increments after the N_2 flood in Ranathunga et al. (2017) are clearly due to the swelling recovery which occurred before the second CO_2 injection by the N_2 flood. Further, for all three confinements, the CO_2 permeability increment against swelling recovery exhibits a perfect linear variation (y = x) with an overall goodness fit of 0.99 (R^2). This shows the ability of N_2 to be used as a catalyst to improve coal mass permeability by partially recovering CO_2 adsorption-induced matrix swelling.

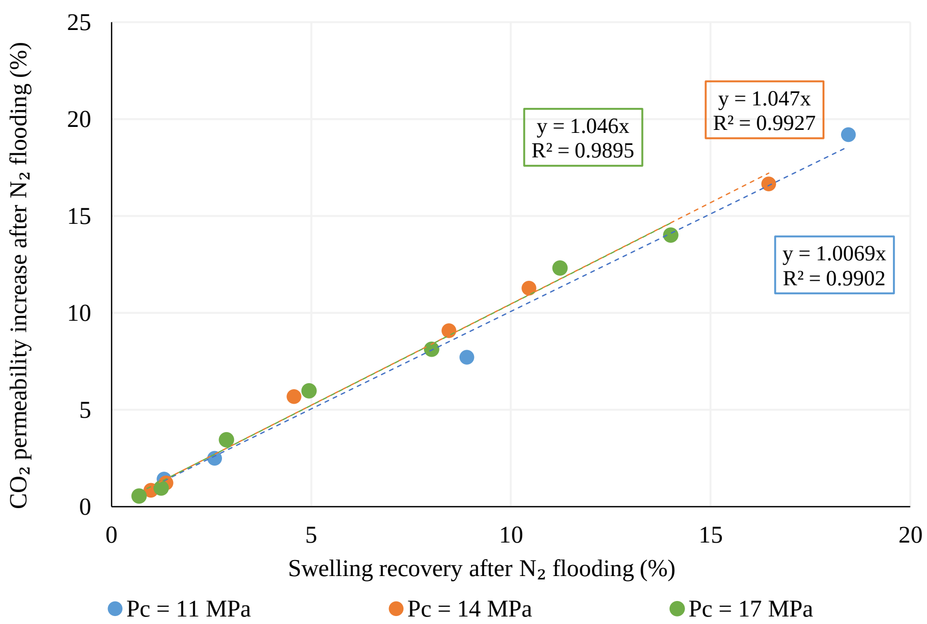

Figure 4.35. CO_2 permeability increase vs. swelling recovery after N_2 flooding

However, this method is only effective for low-rank coal under low confining stresses, because the higher permeability at lower confining stresses allows more N_2 to enter the coal mass, which eventually reverses the swelling. Therefore, it can be expected that if N_2 is injected into the coal matrix for a longer time, the amount of swelling recovery will increase. The following section discusses the swelling recovery by N_2 of brown coal specimens after permeation for a further 48 and 72 hours.

b. Permeation of N_2 for 48 and 72 hours

As described above, the duration of N_2 flooding has a significant influence on swelling recovery, as it offers more opportunity for N_2 to be involved in the recovery process. Figure 4.36 shows the CO_2 permeability after flooding of N_2 for 24, 48 and 72 hours of brown coal specimens at 6 and 8 MPa CO_2 injections. According to the figure, an increase in CO_2 permeability occurs with increasing N_2 flooding duration. For example, 6 MPa sub-critical CO_2 permeability increases by around 9.4% and 13.1% when the N_2 flooding duration is increased up to 48 and 72 hours for 11 MPa confining pressure. Similarly, for 11 MPa confinement, 8 MPa super-critical CO_2 permeability increases by 10.5% and 17.7% for 48 hours and 72 hours N_2 floods compared to 24 hours N_2 flooding. As explained previously, the longer durations allow more N_2 to enter the coal matrix and a greater amount of CO_2 to desorb from the coal mass, allowing an increment in swelling recovery. Interestingly, this increment is reduced for higher confinements (Figure 4.36). For example, around 7.2% and 8.3% decrease compared to 11 MPa confinement can be seen for 14 and 17 MPa confinements when N_2 flooding duration is increased to 48 hours for 6 MPa CO_2 injection. For similar conditions, around 4.9% (14 MPa confinement) and 7.1% (17 MPa confinement) reductions in CO_2 permeability compared to 11 MPa confinement were observed for 8 MPa CO_2 flow after 48 hours of N_2 flooding. In addition, the permeability increment is greater for higher injection pressures (Figure 4.36). For example, when the CO_2 injection pressure is increased from 6 to 8 MPa, around 4.6%, 4.7% and 1.2% increases in CO_2 permeability increments (compared to 24 hours of N_2 permeation) were observed for 11, 14 and 17 MPa confining pressures, respectively after 72 hours of N_2 flooding. This can be explained by the volumetric strain variation observed during these various N_2 floods through the coal specimens, as demonstrated in Figure 4.37.

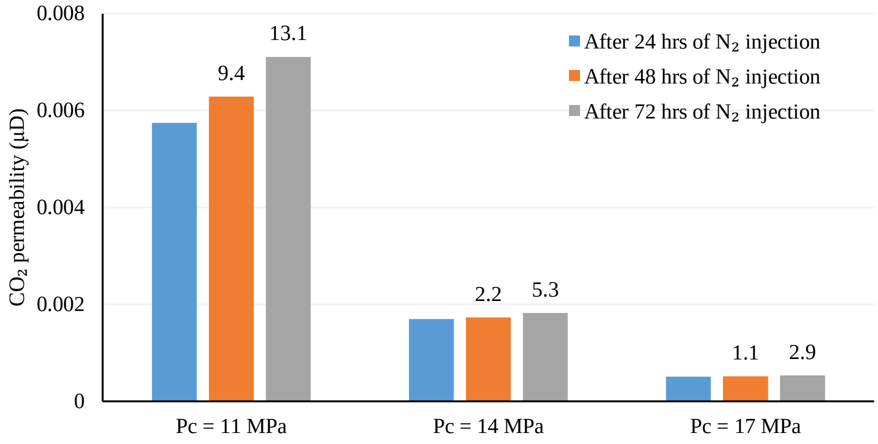

(a) 6 MPa CO_2 injection

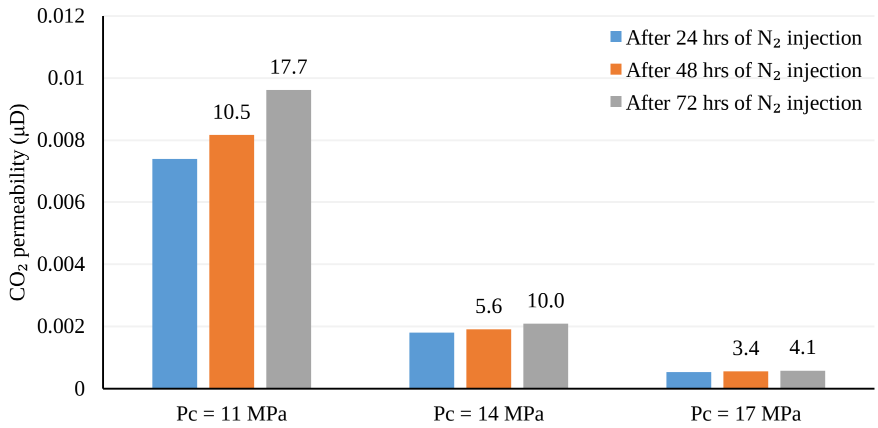

(b) 8 MPa CO_2 injection

Figure 4.36. CO_2 permeability after flooding N_2 for 24, 48 and 72 hours for 6 MPa and 8 MPa CO_2 injections during 11, 14 and 17 MPa confining pressures (here the data labels denote the CO_2 permeability increase compared to 24 hours N_2 flooding)

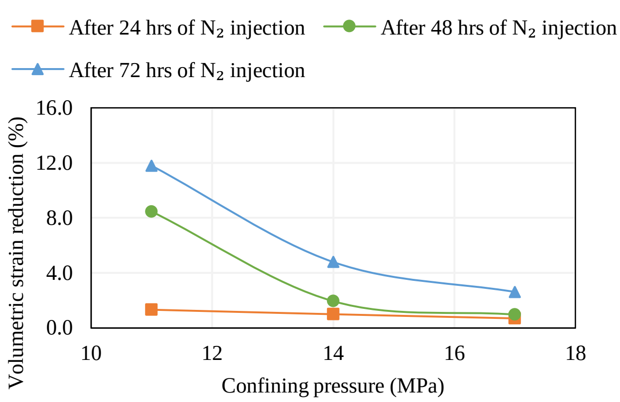

(a) 6 MPa CO_2 injection

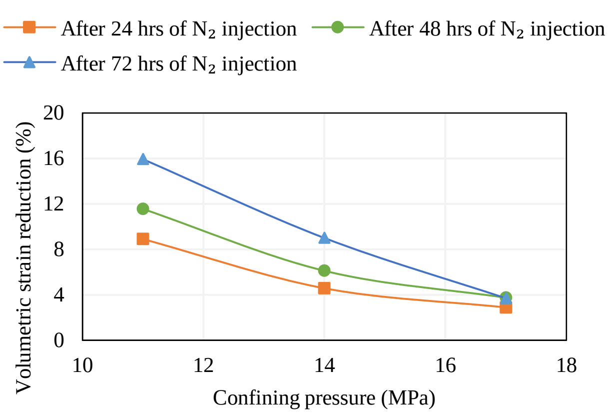

(b) 8 MPa CO_2 injection

Figure 4.37. Volumetric strain reduction of brown coal samples after flooding N_2 for 24, 48 and 72 hours for 6 MPa and 8 MPa CO_2 injections under 11, 14 and 17 MPa confining pressures

According to Figure 4.37, the volumetric strain reduction is increased with N_2 flooding time for both 6 and 8 MPa CO_2 injections. This observation confirms the higher permeability increments (Figure 4.36) when N_2 flooding time is increased, because the increased coal mass swelling recovery for longer N_2 flow durations is subjected to enhanced permeability in the coal matrix. In addition, the volumetric strain reduction is gradually reduced with confining pressure, and this reduction is comparatively higher for 8 MPa CO_2 injection compared to 6 MPa. This indicates the higher permeability increments shown for lower effective stresses compared to higher effective stresses in Figure 4.36. According to Ranathunga et al. (2017), the effective stress effects on low-rank coals are higher than those for high-rank coals due to the lower strength and elastic modulus and higher shrinkage compressibilities of low-rank coal, which result in a more shrunken pore structure under higher stresses. Hence, although the N_2 is flooded for a longer time, the expected swelling recovery is restricted with lower permeabilities at higher effective stresses. This warrants more research using time durations for N_2 flooding longer than 72 hours for low rank coals.

Interestingly, Perera et al. (2011a) observed greater permeability increments in high rank coals under higher confining stress after 24 hours of N_2 flooding. According to Perera et al. (2011a), the reduced flow rates under higher effective stresses allow more time for N_2 to interact with CO_2 adsorbed coal and to recover more swelling areas. As mentioned above, high-strength high-rank coals undergo less pore structure shrinkage due to higher stresses than low rank coals. Therefore, unlike for low rank coals, much higher permeability increments with longer durations of N_2 permeations at higher effective stresses can be expected following the above-mentioned phenomena. This needs to be confirmed by further research for much longer N_2 flooding durations.

However, this method is only efficient at low confining stresses for low-rank coal. Therefore, future research is needed to investigate the most effective applicability of N_2 flooding for the swelling recovery process. Several researchers (Connell et al., 2011; Jessen et al., 2008; Perera et al., 2015; Reznik et al., 1984; Zhou et al., 2013) have tested various approaches. For example, field and laboratory studies have implemented the injection of a CO_2/N_2 binary mixture to recover coal mass swelling-induced permeability reductions (Mavor et al., 2004; Reeves and O'Neill, 1989). However, almost all the studies have been conducted on high-rank coals and have ignored low-rank coals. Hence, future research on the effective use of CO_2 and N_2 mixtures to recover coal matrix swelling and related permeability issues for low-rank coals is necessary.

4.5.3.4 Prediction of CO_2 induced coal matrix swelling under various CO_2 pressures and reservoir depths in low rank coal

The swelling in coal reservoirs upon CO_2 injection is clearly a serious issue for enhanced coal seam gas production and CO_2 sequestration in deep coal seams. The precise prediction of potential swelling in a selected coal seam is therefore of utmost importance. This was considered in the next stage by incorporating the experimental data in widely-used models in the field. Although the Langmuir model has been widely applied to predict CO_2 adsorption behaviour in coal, according to the research literature, this model is not appropriate for high CO_2 pressures (> 6 MPa) (Day et al., 2008). The Dubinin–Astakhov model (D-A) and the Dubinin–Radushkevich model (D-R) have also been used and have been found to better fit experimental adsorption data (Day et al., 2008; Ottiger et al., 2006; Ozdemir et al., 2004). Therefore, the more commonly-used model, the Dubinin–Radushkevich model (D-R), was considered in this study.

Sakurovs et al. (2007) replaced the gas pressure term in the classical D-R isotherm (see Eq. [4.19]) with gas density (see Eq. [4.20]) for a better fit for a wide range of sorption data, including super-critical CO_2 adsorption in coal. Later, this modified D-R model (see Eq. [4.20]) was tested for coal swelling during CO_2 adsorption by Day et al. (2008), who found an extremely good fit for Australian high rank coals.

$$W_{ads} = W_o\left(1-\frac{\rho_g}{\rho_a}\right) exp\left\{-D\left[\ln\left(\frac{P_s}{P}\right)\right]^2\right\} \qquad [4.19]$$

where, W_{ads} excess sorption, W_o is surface adsortion capacity of the substrate, ρ_g is the gas density, ρ_a is the density of the adsorbed phase, D is a constant related to the affinity of the sorbent of the gas, P_s is the saturation pressure (equal to the pressure at which the gas condenses at the temperature of the test) and P is gas pressure.

$$S = S_{max} exp\left\{-D\left[\ln\left(\frac{\rho_a}{\rho_g}\right)\right]^2\right\} + k\rho_g \qquad [4.20]$$

where, S is volumetric swelling (%), S_{max} is maximum swelling of the coal, ρ_g is the gas density at the temeparture and pressure used for the testing, ρ_a is the density of the adsorbed phase (taken to be 1000 kg/m^3) (Day et al., 2008), D is an empirical curve fitting parameter and k is a constant related to the solubility of CO_2 in the coal. However, Day et al. (2010) found the modified D-R Equation (Eq. [4.21]) was more appropriate to precisely incorporate the swelling behaviour in coal upon adsorption of gases such as CO_2, CH_4, N_2, He.

$$S = S_{max} exp\left\{-D\left[\ln\left(\frac{\rho_L}{\rho_g}\right)\right]^2\right\} \qquad [4.21]$$

In this model, Day et al. (2010) adopted van der Waals density (ρ_L) instead of adsorbed phase gas density (ρ_a) which is 1028 kg/m^3 for CO_2 at its critical point (7.38 MPa pressure and 31.8 ^{0}C temperature) (Day et al., 2010) after the study by Sakurovs et al. (2010), who found a better relation to sorption of gases into coal using this van der Waals density. Further, Anggara et al. (2013) found a good fit of this swelling model (Eq. [4.21]) for crushed low-rank coal to predict CO_2 sorption-induced volumetric strains. However, the prediction of swelling based on this equation has become a challenge due to the terms of S_{max} and D. Therefore, an effort was made in this study to derive relationships for these two parameters using the measured brown coal swelling data.

Figures 4.38 and 4.39 demonstrate the experimental and model-predicted volumetric swelling of the brown coal samples under 11, 14 and 17 MPa confinements during first (initial) and second CO_2 injections after 24 hours of N_2 flooding, and Table 4.15 shows the corresponding D-R parameters. According to Table 4.15, the model-predicted maximum swelling (S_{max}) reduces with increasing confining pressure, proving the previously described fact that there is a decrease in volumetric strain with increasing depth or confienment (see Section 3.2). In addition, the empirical curve fitting parameter (D) used in the D-R model increases with increasing confining pressure. Figure 4.40 displays the variation of both S_{max} and D with confining stress for both first and second CO_2 injections. As shown in the figure, S_{max} follows a decreasing exponential variation, while D follows an increasing exponential variation with increasing confining pressure for both CO_2 injections. However, the values obtained for the second CO_2 injection are lower than those for the first CO_2 injection for both S_{max} and D. The reduction of swelling during the second CO_2 injection, as described in Section 3.2, leads to these lower values.

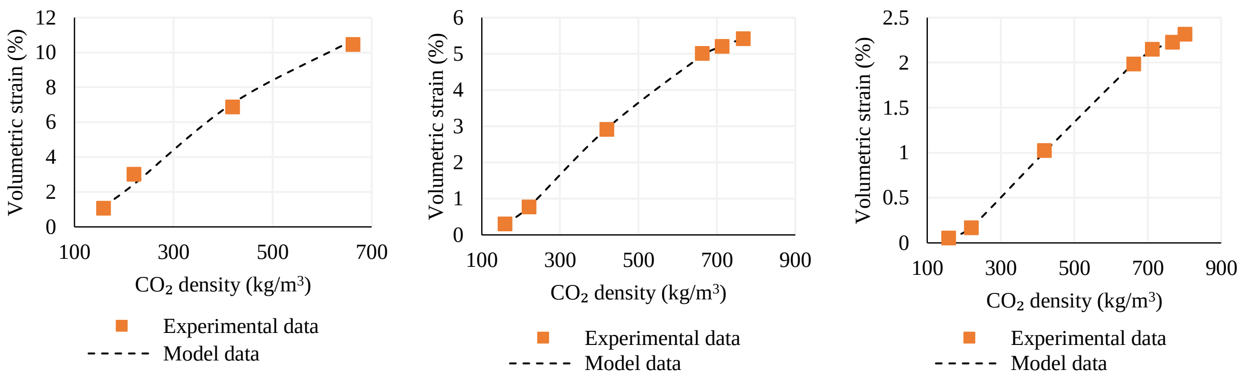

(a) Pc = 11 MPa (b) Pc = 14 MPa (c) Pc = 17 MPa

Figure 4.38. Experimental and model-predicted volumetric swelling of brown coal samples for the different confining pressures during first CO_2 injection

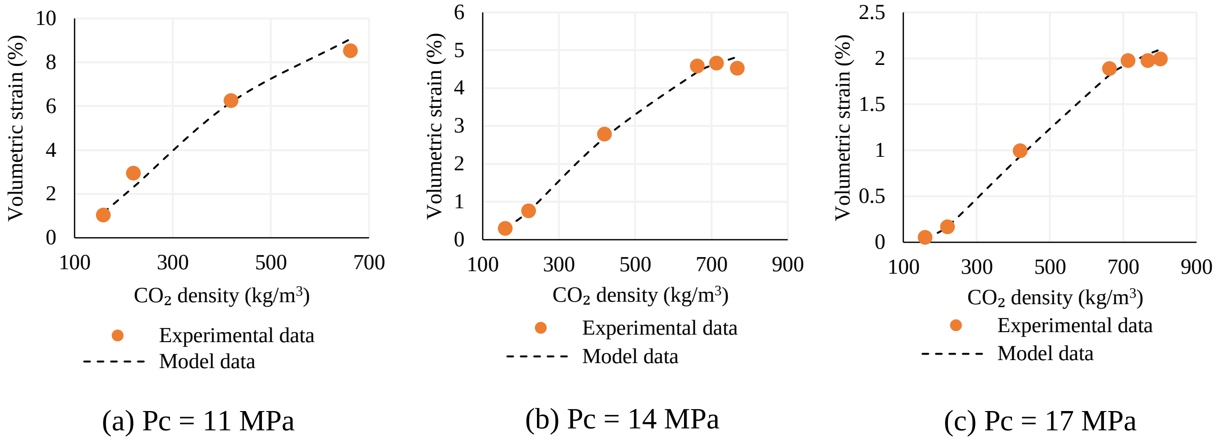

Figure 4.39. Experimental and model-predicted volumetric swelling of brown coal samples for the different confining pressures during second CO_2 injection

Table 4.15. Dubini-Radushkevich parameters for the experimental swelling data

Confining pressure (MPa)	1st CO_2 injection			2nd CO_2 injection		
	S_{max} (%)	D	R^2	S_{max} (%)	D	R^2
11	12.22	0.678	0.974	10.23	0.627	0.990
14	5.84	0.854	0.991	5.17	0.816	0.992
17	2.47	1.117	0.987	2.24	1.085	0.959

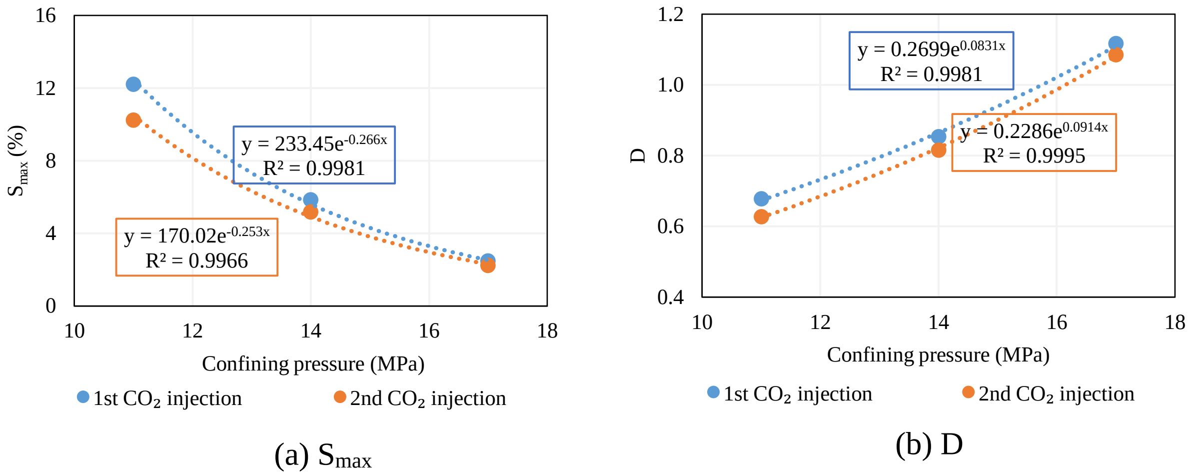

Figure 4.40. Variation of Dubini-Radushkevich parameters (a) S_{max} and (b) D with confining pressure

According to Figure 4.38, the D-R model parameters S_{max} and D have the following relationship with confining pressure (Eqs. [4.22a-c]) for low-rank brown coal for the first and second CO_2 injections:

$$S_i = S_{i,max} exp\left\{-D_i\left[\ln\left(\frac{\rho_L}{\rho_g}\right)\right]^2\right\} \quad [4.22a]$$

$$S_{1,max} = 233.45e^{-0.266P_c}\, ; D_1 = 0.2699e^{0.0831P_c} \quad [4.22b]$$

$$S_{2,max} = 170.02e^{-0.253P_c}\, ; D_2 = 0.2286e^{0.0914P_c} \quad [4.22c]$$

where, P_c is the confining pressure and S_i, $S_{i,max}$ and D_i are the brown coal sample swelling and the D-R parameters for i^{th} CO_2 injection (*i = 1,2*). Figure 4.41 shows the predicted coal matrix swelling due to 1^{st} and 2^{nd} CO_2 injections for greater confinements of 20, 23 and 26 MPa obtained from Eqs. [4.22a-c] According to Figure 4.41, the projected swelling reduces with reservoir depth.

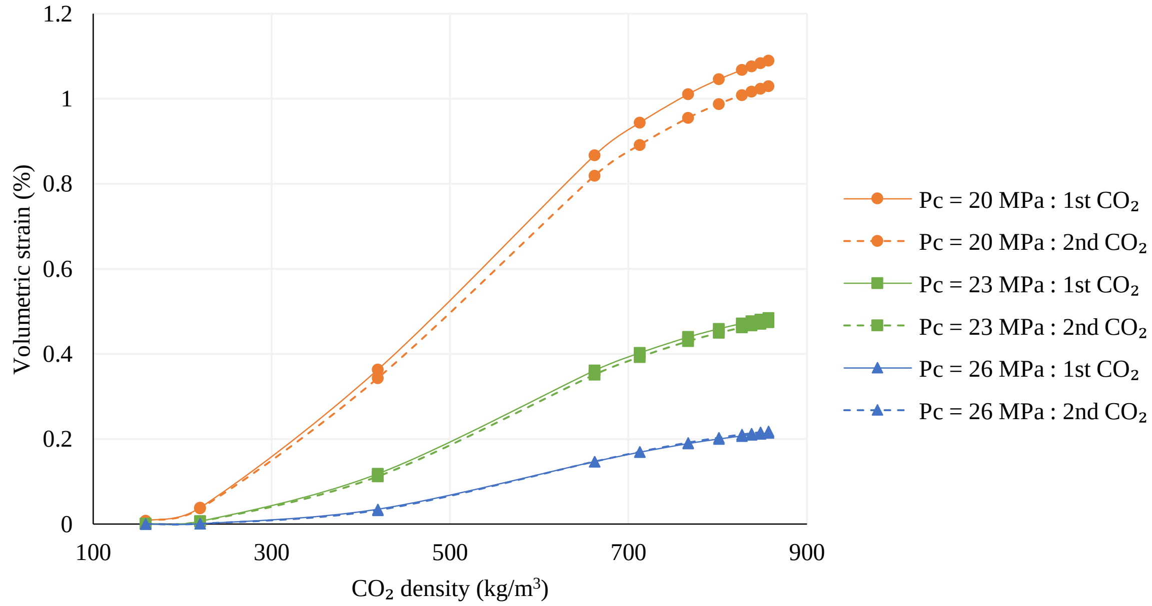

Figure 4.41. Predicted volumetric strain variations using modified D-R model for brown coal during 1^{st} and 2^{nd} CO_2 flow

4.5.4 Conclusions

This study provides a comprehensive understanding of CO_2 adsorption-induced coal matrix swelling, particularly for low-rank brown coal. The behaviour of volumetric swelling for different CO_2 injections at different confining stresses (depths) was studied, and according to the results the following conclusions can be drawn:

- CO_2 adsorption-induced coal matrix swelling is greater at higher CO_2 pressures, particularly for the super-critical phase condition of CO_2, regardless of reservoir depth or the maturity of the coal. This is mainly due to the greater adsorption potential of high-pressure CO_2, which is significantly accelerated with the phase transition from sub- to super-critical.

- Coal matrix swelling decreases with increasing reservoir depth or confining stress, which is beneficial for field applications of CO_2-ECBM, preferably in deep coal formations. However, this also depends on the pore pressure conditions, as lower effective stresses (lower confinements and higher injection pressures) lead to greater swelling reduction, regardless of coal maturity or rank.
- Nitrogen (N_2) exhibits comparatively inert behaviour in coal, producing negligible swelling, regardless of pore pressure and reservoir depth.
- However, the partial pressure depletion created by N_2 in the coal mass has the ability to recover CO_2 adsorption-induced swelled areas in coal to some extent, and that ability is greater if N_2 flooding is carried out for a sufficiently long period under lower effective stress conditions, and it is probable that a greater amount of N_2 can enter the coal mass under such conditions.
- The modified D-R model can effectively be used to predict low-rank coal swelling upon first or repeated injections of CO_2, if appropriate relationships for the Dubinin–Radushkevich parameters, S_{max} and D, are used. The swelling data can be used to derive empirical relationships for the D-R parameters, S_{max} and D, to predict the swelling behaviour of Victorian brown coal.

4.5.5 References

Anggara, F., Sasaki, K., Rodrigues, S., Sugai, Y., (2014). The effect of megascopic texture on swelling of a low rank coal in supercritical carbon dioxide. *International Journal of Coal Geology* 125, 45-56.

Anggara, F., Sasaki, K., Sugai, Y., (2013). Swelling Measurements of a Low Rank Coal in Supercritical CO_2. *International Journal of Geosciences* 4, 863-870.

Balan, H.O., Gumrah, F., (2009). Assessment of shrinkage–swelling influences in coal seams using rank-dependent physical coal properties. *International Journal of Coal Geology* 77, 203-213.

Battistutta, E., van Hemert, P., Lutynski, M., Bruining, H., Wolf, K.-H., (2010). Swelling and sorption experiments on methane, nitrogen and carbon dioxide on dry Selar Cornish coal. *International Journal of Coal Geology* 84, 39-48.

Connell, L., Sander, R., Pan, Z., Camilleri, M., Heryanto, D., (2011). History matching of enhanced coal bed methane laboratory core flood tests. *International Journal of Coal Geology* 87, 128-138.

Day, S., Fry, R., Sakurovs, R., (2008). Swelling of Australian coals in supercritical CO_2. *International Journal of Coal Geology* 74, 41-52.

Day, S., Fry, R., Sakurovs, R., Weir, S., (2010). Swelling of Coals by Supercritical Gases and Its Relationship to Sorption. *Energ Fuel* 24, 2777-2783.

Hol, S., Peach, C.J., Spiers, C.J., (2011). Applied stress reduces the CO_2 sorption capacity of coal. *International Journal of Coal Geology* 85, 128-142.

Jasinge, D., (2010). An investigation of the effect of carbon dioxide sequestration on the behaviour of brown coal (*PhD thesis*). Monash University, Melbourne, Australia.

Jessen, K., Tang, G.Q., Kovscek, A.R., (2008). Laboratory and simulation investigation of enhanced coalbed methane recovery by gas injection. *Transport in Porous Media* 73, 141-159.

Karacan, C.Ö., (2007). Swelling-induced volumetric strains internal to a stressed coal associated with CO_2 sorption. *International Journal of Coal Geology* 72, 209-220.

Kiyama, T., Nishimoto, S., Fujioka, M., Xue, Z., Ishijima, Y., Pan, Z., Connell, L.D., (2011). Coal swelling strain and permeability change with injecting liquid/supercritical CO_2 and N_2 at stress-constrained conditions. *International Journal of Coal Geology* 85, 56-64.

Mavor, M., Gunter, W., Robinson, J., (2004). Alberta multiwell micro-pilot testing for CBM properties, enhanced methane recovery and CO_2 storage potential, SPE Annual Technical Conference and Exhibition, Paper No. SPE 90256.

McLinden, M., Klein, S., Lemmon, E., Peskin, A., (1998). REFPROP, Thermodynamic and transport properties of refrigerants and refrigerant mixtures. NIST Standard Reference Database 23.

Ottiger, S., Pini, R., Storti, G., Mazzotti, M., Bencini, R., Quattrocchi, F., Sardu, G., Deriu, G., (2006). Adsorption of pure carbon dioxide and methane on dry coal from the Sulcis Coal Province (SW Sardinia, Italy). *Environmental Progress* 25, 355-364.

Ozdemir, E., Morsi, B.I., Schroeder, K., (2004). CO_2 adsorption capacity of Argonne premium coals. *Fuel* 83, 1085-1094.

Pan, Z., Connell, L.D., Camilleri, M., (2010). Laboratory characterisation of coal reservoir permeability for primary and enhanced coalbed methane recovery. *International Journal of Coal Geology* 82, 252-261.

Perera, M.S.A., Ranjith, P.G, Ranathunga, A.S, Koay, A., Zhao, J., Choi, S., (2015). Optimization of enhanced coal-bed methane recovery using numerical simulation. *Journal of Geophysics and Engineering* 12, 90.

Perera, M.S.A., Ranjith, P.G., Airey, D.W., Choi, S.K., (2011a). Sub- and super-critical carbon dioxide flow behaviour in naturally fractured black coal: An experimental study. *Fuel* 90, 3390-3397.

Perera, M.S.A., Ranjith, P.G., Choi, S.K., Airey, D., (2011b). The effects of sub-critical and super-critical carbon dioxide adsorption-induced coal matrix swelling on the permeability of naturally fractured black coal. *Energy* 36, 6442-6450.

Pini, R., Ottiger, S., Burlini, L., Storti, G., Mazzotti, M., (2009). Role of adsorption and swelling on the dynamics of gas injection in coal. *Journal of Geophysical Research: Solid Earth* 114, B04203.

Ranathunga, A.S., Perera, M.S.A., Ranjith, P.G., (2017). Super-critical carbon dioxide flow behaviour in low rank coal: A meso-scale experimental study, *Journal of CO_2 Utilization* (under review).

Reeves, S., O'Neill, P., (1989). Preliminary results from the broad meadow pilot, project Bowen basin Australia, Proc. 1989 Coalbed Methane Symposium, University of Alabama School of Mines and Energy Development and Gas Research Inst., Tuscaloosa, AL, pp. 273-291.

Reznik, A.A., Singh, P.K., Foley, W.L., (1984). An analysis of the effect of CO_2 injection on the recovery of in-situ methane from bituminous coal: an experimental simulation. *Society of Petroleum Engineers Journal* 24, 521-528.

Sakurovs, R., Day, S., Weir, S., (2010). Relationships between the critical properties of gases and their high pressure sorption behaviour on coals. *Energ Fuel* 24, 1781-1787.

Sakurovs, R., Day, S., Weir, S., Duffy, G., (2007). Application of a modified Dubinin-Radushkevich equation to adsorption of gases by coals under supercritical conditions. *Energ Fuel* 21, 992-997.

Siriwardane, H., Haljasmaa, I., McLendon, R., Irdi, G., Soong, Y., Bromhal, G., (2009). Influence of carbon dioxide on coal permeability determined by pressure transient methods. *International Journal of Coal Geology* 77, 109-118.

Vishal, V., Singh, T.N., (2015). A Laboratory Investigation of Permeability of Coal to Supercritical CO_2. *Geotech Geol Eng* 33, 1009-1016.

Zhou, F., Hussain, F., Cinar, Y., (2013). Injecting pure N_2 and CO_2 to coal for enhanced coalbed methane: experimental observations and numerical simulation. *International Journal of Coal Geology* 116, 53-62.

Zutshi, A., Harpalani, S., (2004). Matrix swelling with CO_2 injection in a CBM reservoir and its impact on permeability of coal, International Coalbed Methane Symposium, University of Alabama, Tuscaloosa, Alabama, pp. 12-14.

4.6 How can gas adsorption-induced coal matrix swelling in coal be estimated?

According to Section 4.5, coal matrix swelling due to CO_2 adsorption plays an important role in the CO_2 sequestration process in deep coal seams. Therefore, the correct estimation of gas sorption-induced swelling strains is important for field-work in order to estimate CO_2 flow behaviours in a selected coal seam. The Dubinin–Radushkevich (DR) model is a widely-used adsorption model, which can accurately predict the adsorption potential of coal mass for different gasses even under super-critical conditions. This model was developed for coal matrix swelling prediction and has been successfully applied to different coal types. However, the maximum swelling parameter of this model needs to be obtained from experimental evaluations. Therefore, in this section of the thesis, a new descriptive model for the gas sorption-induced swelling of coal as a function of the effective coal mass and adsorbing gas physical properties is proposed. The new model is based on the existing D-R equation, which is modified by inserting a new expression for the term of maximum swelling. The swelling data for coal samples from different locations with various gas adsorptions are considered for the model development.

This section of the chapter is the following paper:

Ranathunga AS, Perera MSA, Ranjith PG (2017). A review and model development for estimation of gas adsorption-induced coal matrix swelling. *Int J of Energy Research* (under review).

A review and model development for estimation of gas adsorption-induced coal matrix swelling

A.S. Ranathunga[1], M.S.A. Perera[1,2], P.G. Ranjith[1]

[1]Deep Earth Energy Laboratory, Department of Civil Engineering, Monash University, Building 60, Melbourne, Victoria, 3800, Australia.

[2] Department of Infrastructure Engineering, The University of Melbourne, Building 176, Melbourne, Victoria, 3010, Australia.

Abstract

The significant influence of coal matrix swelling on CO_2 enhanced coal bed methane recovery is well accepted in the field, and has a strong negative influence on the long-term implementation of the process. According to the research literature, both adsorbate properties (gas type, phase, pressures) and adsorbent properties (rank, depth, moisture content, and temperature) affect the swelling behaviour of coal. To date, several analytical and theoretical models have been developed to estimate this gas adsorption-induced coal matrix swelling effect. Among the analytical models, the modified Dubini-Radushkevich (D-R) model for swelling provides fairly accurate swelling predictions for different coal types and for different fluid adsorptions under various phase conditions, including super-critical conditions. To date, although few theoretical models have been developed to predict coal matrix swelling, following various approaches such as elasticity theory and adsorption thermodynamics, finding model parameters to predict swelling using most of these equations has often been challenging. In addition, none of these analytical or theoretical models is sufficiently descriptive to show the influence of various surrounding factors on coal matrix swelling.

A novel descriptive equation for coal matrix swelling was developed for maximum swelling (in the D-R model) in high rank coal, effectively incorporating the contributions of various effective factors (fixed carbon content, moisture content and critical temperature). Coal matrix swelling data obtained from six different locations (the Kutai basin, the Bowen basin, the Hunter Valley basin and the Illawarra basin) with different moisture contents (0 to 22%) for six different adsorbing gasses (CO_2, CH_4, N_2, Ar, CF_4 and C_2H_6) available in the research literature were used to develop the model in the temperature range of 298.15 to 328.15 K. The model shows fairly good agreement with an accuracy of ±1% with the experimental data.

Keywords: coal matrix swelling, descriptive model, effective factors, gas adsorption, super-critical gasses

4.6.1 Introduction

Coal is a source rock, which contains relatively pure methane, mostly adsorbed into the micro-pore structure (Harpalani and Schraufnagel, 1990a). To recover this methane from coal seams, CO_2 is injected, due to its higher affinity to adsorb into the coal matrix while desorbing the pre-adsorbed methane from it (Pan and Connell, 2007). However, numerous previous researchers (Anggara et al., 2016; Chikatamarla et al., 2004; Cui and Bustin, 2005; Cui et al., 2007; Day et al., 2008a; Day et al., 2010; Durucan and Shi, 2009; Guo et al., 2016; Han et al., 2017; Harpalani and Chen, 1995; Harpalani and Schraufnagel, 1990b; Hol and Spiers, 2012; Hol et al., 2012; Jasinge et al., 2012; Karacan, 2003; Levine, 1996; Pan and Connell, 2012; Peng et al., 2016; Perera et al., 2011; Robertson and Christiansen, 2005; Shi et al., 2008; Zang and Wang, 2017) have highlighted that coal swells during CO_2 adsorption and shrinks during methane desorption. This coal matrix volume change is a unique characteristic of coal seams, that alters the coal matrix porosity, eventually changing coal's permeability during CO_2 enhanced coal bed methane recovery (CO_2-ECBM) (Anggara et al., 2016). These coal volume changes can induce localised strain and stress variations in confined coal seams through effective stresses (overburden pressure), further modifying the gas transport process through its cleat system (Anggara et al., 2016; Cui and Bustin, 2005; Shi and Durucan, 2004). It is therefore important to comprehensively address the effect of coal matrix swelling/shrinkage on its permeability in order to achieve efficient CO_2 sequestration/methane production.

4.6.2 Experimental studies of gas adsorption-induced coal matrix swelling and corresponding coal flow property alterations

4.6.2.1 Factors affecting CO_2 adsorption-induced coal matrix swelling

To date, experimental studies have mainly focused on finding factors affecting CO_2 adsorption-induced coal matrix swelling, adsorbing gas properties and coal seam properties.

a. Studies of the effect of adsorbing gas type and properties on coal swelling

According to previous research (Battistutta et al., 2010; Day et al., 2011; Day et al., 2010; Wang et al., 2013), CO_2 swells coal more than other gasses. As shown in Figure 4.42, CO_2 adsorption-induced swelling is around one-fold higher than the swelling created in coal by CH_4 adsorption. The higher affinity of CO_2 to adsorb into the coal matrix due to the associated greater degree of van der Waals bonds causes physical and chemical structure alterations (Viete and Ranjith, 2006), resulting in greater matrix alterations compared to other gases. Sakurovs et al. (2010) explained that CO_2 has a higher adsorption capacity in coal due to its higher critical temperature (304.95 K) and hence this leads to a greater swelling effect on the coal mass. According to Day et al. (2010), even gases with similar critical temperatures like Xe (Xenon – 289.7 K) and C_2H_6 (Ethane – 305.4 K) have less swelling ability in coal compared to CO_2 due to their larger molecular size compared to CO_2 (CO_2 van der Waals volume is 4.28E-5 m^3/mol, which is smaller than that of Xe (van der Waals volume – 5.16E-5 m^3/mol) and C_2H_6 (van der Waals volume – 6.5E-5 m^3/mol)), which cayses its greater potential to permeate and adsorb into the coal pore structure.

In regard to the effect of injecting CO_2 properties on coal matrix swelling, CO_2 phase condition has a significant influence on coal matrix swelling. CO_2 reaches its super-critical state when its temperature and pressure go beyond 304.95 K and 7.38 MPa. Interestingly, the preferable coal seams for CO_2-ECBM exist at depths where CO_2 is in its super-critical state (Perera et al., 2012b). According to previous research (Anggara et al., 2013; Day et al., 2008b; Hol and Spiers, 2012; Perera et al., 2011), super-critical CO_2 swells coal more than sub-critical CO_2, regardless of coal type (refer to Figure 4.43). For example, Perera et al. (2011) observed around three times greater swelling potential of super-critical CO_2 in high-rank bituminous coal compared to sub-critical CO_2 (see Figure 4.43(a)). Low rank coalalso exhibits around 60% greater swelling under super-critical CO_2 injection (8 MPa) compared to sub-critical CO_2 (7 MPa) (refer to Figure 4.43(b)). This is due to the more chemically-reactive nature of super-critical CO_2 and its high compressibility values compared to liquid CO_2, all of which cause greater adsorption capacity (Perera et al., 2012b). Therefore, the influence of coal matrix swelling is also significant, and this is discussed in the next section.

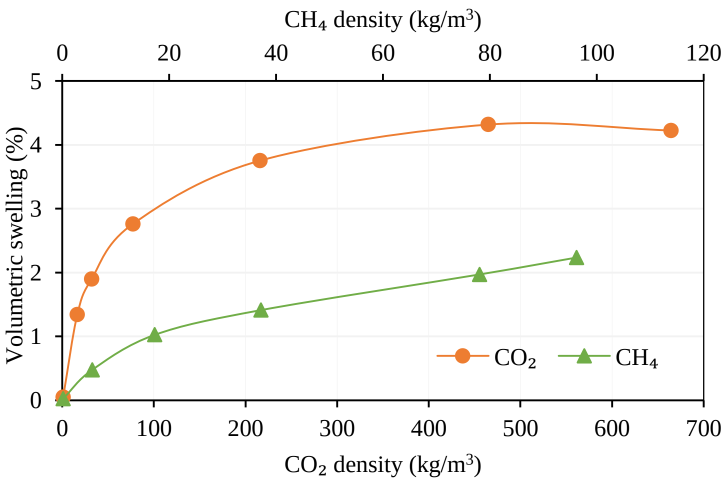

Figure 4.42. Volumetric strain variation with CO_2 and CH_4 in coal (Day et al., 2011)

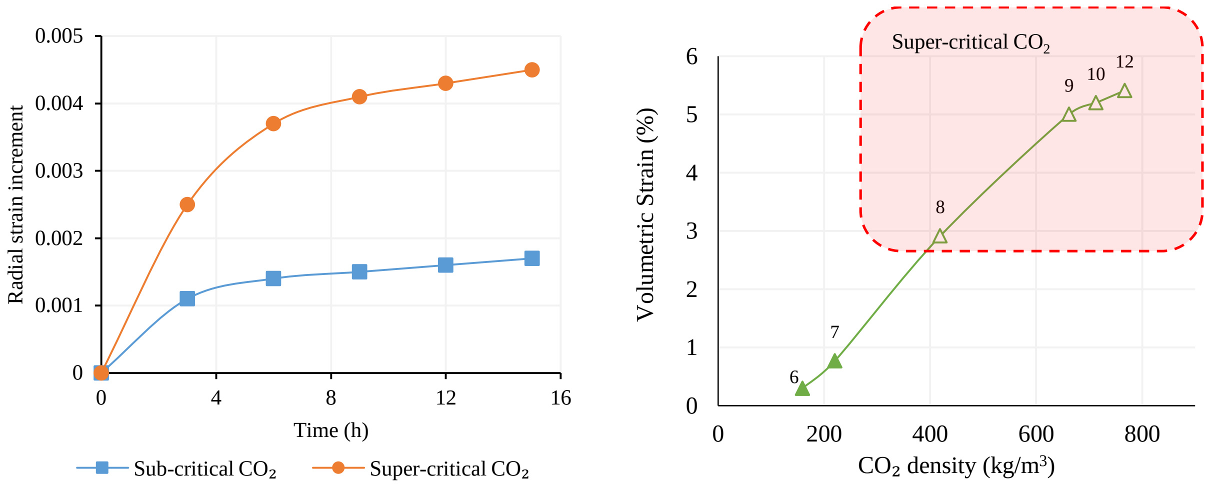

(a) Radial strain increase in bituminous coal

(b) Volumetric strain variations in lignite

Figure 4.43. Radial strain increase in Australian bituminous coal with time during sub- and super-critical CO_2 permeation under 15 MPa confinement (Perera et al., 2011) and volumetric strain variation in Victorian brown coal with CO_2 density during 14 MPa confinement (Ranathunga et al., 2016)

b. Studies on the effect of coal mass properties on coal swelling

To date there have been a number of experimental studies on the influence of coal seam properties on CO_2 adsorption-induced coal matrix swelling. For example, Reucroft and Patel (1986), Ceglarska-Stefańska and Czapliński (1993), Day et al. (2008a) and Day et al. (2011) showed that coal with lower carbon content (low rank coal) undergoes higher coal matrix swelling compared to coal with greater carbon content (high rank coal) (Figure 4.44(a)), mainly due to the lesser degree of mobile polymers present in high rank coal compared to low rank coal. However, Durucan et al. (2009) reported a contradictory behaviour after permeating CO_2 in a range of European coals (carbon content varying from 56.4 to 90.9%), according to which swelling ability in coal was enhanced with the increased carbon content (greater swelling in high rank coal compared to low ranked coal with low carbon content) (refer to Figure 4.44(b)). They observed a polynomial correlation between average CO_2 swelling coefficients with carbon content; an initial swelling coefficient decline from high to low volatile bituminous coal, followed by its increment with increasing coal rank (Durucan et al., 2009). Such contradictory observations warrant future studies to comprehensively understand the effect of carbon content on coal matrix swelling behaviour. Further, Anggara et al. (2014), Cody Jr et al. (1988), Larsen et al. (1997) and Larsen (2004) explained that this CO_2 adsorption-induced strain development is an anisotropic process that depends on the heterogeneity, anisotropy and the lithotypes of the coal. However, according to

Cody Jr et al. (1988), this anisotropy of swelling can be seen only in the first stage of swelling and the repeated swelling of the coal matrix is more isotropic.

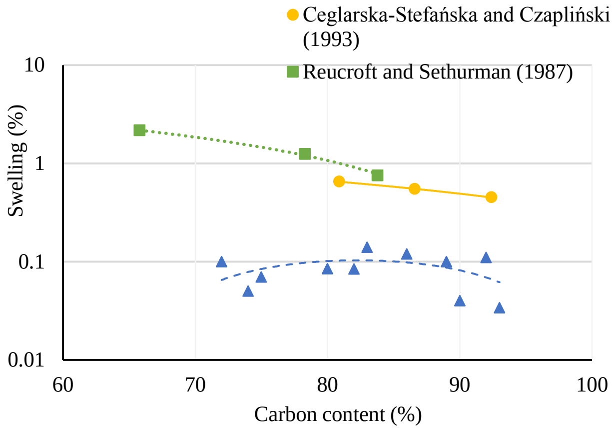

(a) swelling percentage

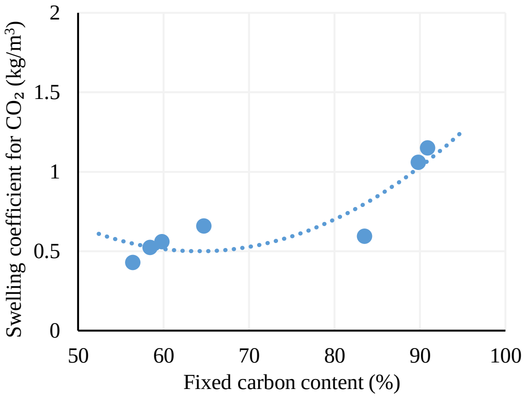

(b) swelling coefficient

Figure 4.44. Coal mass swelling variation (Ceglarska-Stefańska and Czapliński, 1993, Reucroft and Sethuraman, 1987, Walker Jr et al., 1988) and variation of CO_2 swelling coefficient (Durucan et al., 2009) with carbon content

In relation to the effect of temperature on coal swelling, Bae and Bhatia (2006), Ceglarska-Stefańska and Czapliński (1993), Day et al. (2008a); Kronimus et al. (2008) and Perera et al. (2012b) found that coal matrix swelling is reduced with increasing temperature. This is because CO_2 sorption capacity in coal decreases with increasing temperature, because upon temperature increment, gas molecules are released from the adsorbed phase as their kinetic energy is increased accordingly. In addition, the swelling has been found to be less at greater depths compared to shallow depths, due to the associated greater effective stress applying on the coal matrix, that eventually reduces coal mass porosity, offering less adsorption capacity (Hol and Spiers, 2012; Hol et al., 2012; Jasinge et al., 2012; Perera et al., 2011; Wang et al., 2013) (refer to Figure 4.44). The moisture content of coal has also been found to have a positive influence on coal matrix swelling, and comparatively reduced swelling has been reported in wet coal compared to dry coal (Anggara et al., 2013; Day et al., 2011; Wang et al., 2013) (refer to Figure 4.45). This is because the moisture present in the coal mass reduces the area available for CO_2 adsorption (Anggara et al., 2013; Perera et al., 2012a; Wang et al., 2013). This has been clearly demonstrated by Anggara et al., 2013) and is shown in Figure 4.46, according to which the existence of moisture in coal reduces its swelling ability by around half compared to dry coal. All of these findings confirm that CO_2 injection-induced coal matrix volume change is highly dependent on the seam's location.

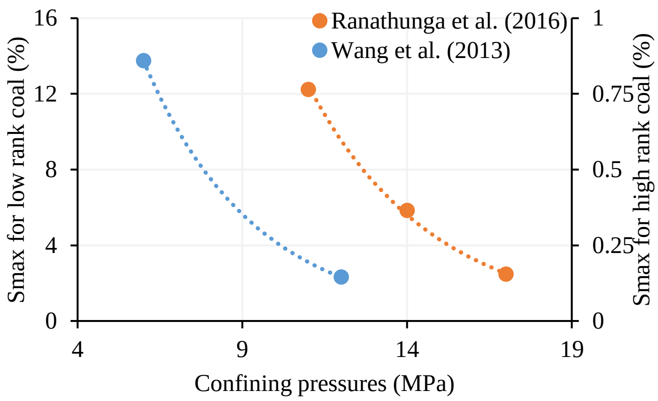

Figure 4.45. Variation of maximum swelling (S_{max}) for low rank coal (Ranathunga et al., 2017) and high rank coal (Wang et al., 2013) with reservoir depth (here S_{max} was calculated using the modified Dubinin–Radushkevich (DR) equation for coal matrix swelling (Day et al., 2010))

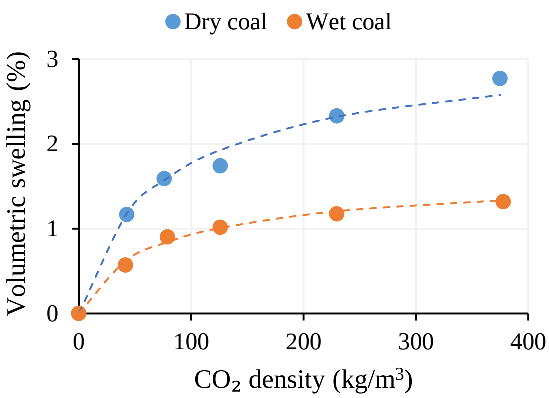

Figure 4.46. Volumetric swelling variation with CO_2 density for dry and wet coal (Anggara et al., 2013)

4.6.2.2 The swelling effect on coal permeability

Although CO_2 adsorption-induced coal swelling has become a well-known fact in the field, to date only a few studies have been conducted on the effect of swelling on flow characteristics and CO_2 storage ability in coal seams. According to Durucan and Shi (2009), Siriwardane et al. (2009), Jasinge et al. (2012); Perera et al. (2011), Wang et al. (2013), Anggara et al. (2016) and Ranathunga et al. (2017), swelling causes reduction in coal flow ability or permeability, and the permeability reduction increases with increasing swelling. Pan et al. (2010) measured CO_2 permeability, strain and adsorption in Australian high rank coal for CO_2 pressures up to 13 MPa and confining pressures up to 20 MPa and found that coal permeability declines with increasing pore pressure at constant effective stress, due to the associated enhancement in the swelling effect, and they observed up to around 70% permeability reduction, depending on CO_2 gas injection pressure and confining pressure (Pan et al., 2010). A similar effect was observed by Jasinge et al. (2012) for Australian low rank coal after permeating CO_2 at pressures up to 3.4 MPa under confining pressures up to 11 MPa, and they observed more than a one-fold permeability reduction due to coal matrix swelling, depending on the CO_2 pressure and confining pressure. Further, Durucan and Shi (2009) (for high rank coal) (Figure 4.47(a)) and Ranathunga et al. (2017) (for low rank coal) (refer to Figure 4.47(b)) observed a reduction in coal permeability due to coal matrix swelling, irrespective of the effective stress condition due to pore pressure increase, which indicates that coal swelling is more significant for coal permeability than the effective stress. In contrast, after conducting a series of permeability tests on low rank coal, Anggara et al. (2016) observed less influence of swelling on permeability compared to effective stress (refer to Figures 4.47(c)), and they observed a significant increment in CO_2 permeability with increasing pore pressure made by enlarged pore space by reducing effective stress. All of these observations confirm that coal mass properties are very important for comprehending the CO_2 adsorption-induced coal matrix swelling-induced permeability changes in coal.

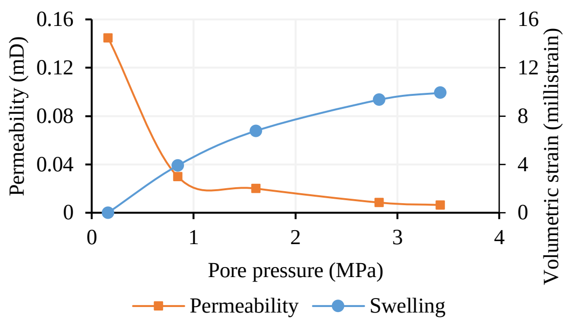

(a) European high rank coal

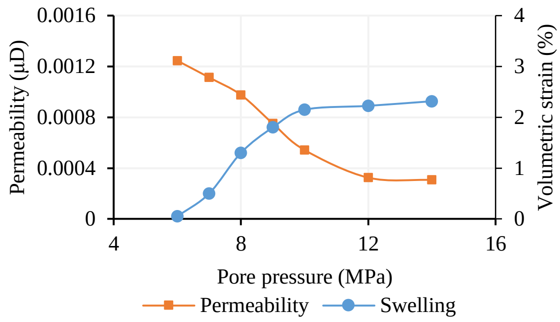

(b) Australian low rank coal

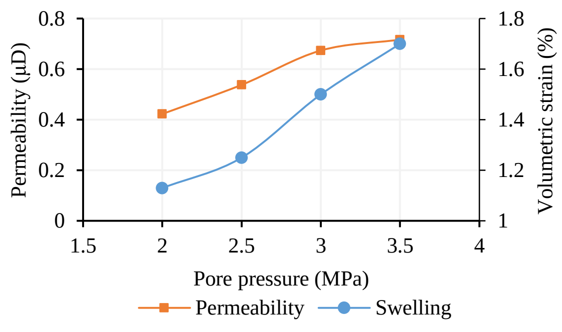

(c) Japanese low rank coal

Figure 4.47. Permeability and coal matrix swelling variation with CO_2 pore pressure for (a) 7 MPa confining pressure for European high rank coal (Durucan et al., 2009), (b) 17 MPa confining pressure (Australian brown coal) (Ranathunga et al., 2017) and (c) 5 MPa confining pressure for Japanese low rank coal (Anggara et al., 2016)

4.6.3 Available models to estimate coal matrix swelling with gas adsorption

There are limitations to conducting experimental investigations on coal mass swelling due to the capabilities of experimental apparatuses, the long-time durations required and the associated high costs. Hence, the development of analytical or theoretical models based on basic experimental observations is essential to precisely estimate coal mass swelling behaviour under field conditions. A number of analytical/theoretical models have been developed to estimate these coal mass volume changes (swelling/shrinkage) and they are summarised in Table 4.16. According to the table, to date various approaches have been adopted to develop models to find coal mass strain variations with gas adsorption. A linear variation between the coal mass strain and pore pressure was proposed by Gray (1987) and a Langmuir-type model for coal mass swelling was proposed by Levine (1996) (refer to Table 4.16), considering the possible over-prediction of errors associated with the linear relationship between strain and pressure. Similar Langmuir-type equations to describe the swelling strain have also been proposed by Palmer and Mansoori (1996) and Shi and Durucan (2004), and an extension of this Langmuir-type model to estimate the mixed gas adsorption induced swelling has been proposed by Mavor and Gunter (2004). According to Shi and Durucan (2004), sorption-induced swelling in coal is equivalent to thermal expansion (refer to Table 4.16) and Connell (2009) extended this extended Langmuir model to incorporate the influence of various stresses, assuming an isotropic swelling strain (refer to Table 4.16). Sawyer et al. (1990) and Seidle and Huitt (1995) proposed a linear relationship between swelling strain and adsorbed amount, which has been widely used in the field (Connell, 2009; Cui and Bustin, 2005; Shi and Durucan, 2005) to develop permeability models. In addition, Day et al. (2008b) proposed the use of gas density instead of gas pressure in the modified Dubinin–Radushkevich (DR) model (Sakurovs et al., 2007) to estimate the swelling percentage of coal (refer to Table 4.16). Day et al. (2010) further modified this model using van der Waals density (refer to Table 4.16) to better relate the swelling of coal for various gas types, even under super-critical conditions.

In addition to these analytical models, some theoretical models have also been developed to obtain the swelling strain of coal with different gas adsorptions. Pan and Connell (2007) developed a theoretical model using elasticity theory and adsorption thermodynamics (refer to Table 4.16), based on the assumption that surface energy change with gas adsorption is equal to the elastic energy change of the coal's solid structure. Vandamme et al. (2010) used molecular-level simulations to determine the surface stress modifications in coal with gas adsorption. In addition, Yang et al. (2010) developed a relationship (refer to Table 4.16) between methane sorption capacity and solvation pressure. To describe methane and carbon dioxide adsorption-induced coal swelling, Guo et al. (2016) used the adsorption and deformation behaviour of slit pores of different sizes using the Grand Canonical Monte Carlo (GCMC) algorithm (refer to Table 4.16). Further, Han et al. (2017) have recently developed a theoretical model (refer to Table 4.16) to estimate coal matrix swelling considering the surface free energy reduction which occurs with sorption, based on the assumption that the swelling ratio is proportional to the Gibbs free energy induced by sorption.

Table 4.16. Analytical and theoretical models developed to estimate coal mass strain changes with gas adsorption

Reference	Model	Remarks
Levine (1996)	$\varepsilon_s = \varepsilon_{max}\left[\frac{P}{P+P_{50}}\right]$ ε_s – linear sorption strain ε_{max} – theoretical maximum strain P_{50} – pressure at which coal has attained 50% of its maximum strain	Assumed that swelling follows a Langmuir type behaviour
Shi and Durucan (2004)	$\sigma-\sigma_o=-\frac{\vartheta}{1-\vartheta}(p-p_o);\ p_c<p\le p_o$ $\sigma-\sigma_o=-\frac{\vartheta}{1-\vartheta}(p-p_o)+\frac{E}{3(1-\vartheta)}\varepsilon_1\left[\frac{p}{p+P_\varepsilon}-\frac{p_c}{p_c+P_\varepsilon}\right]$ $;\ 0<p\le p_c$ $\sigma_c-\sigma_o=-\frac{\vartheta}{1-\vartheta}(p_c-p_o);\ p=p_c$ σ – mean stress ϑ – Poisson’s ratio E – elastic modulus p – pore pressure ε_1 maximum swelling strain at fully saturation condition of coal P_ε – gas pressure at which the matrix strain is half of the maximum value subscript “o” and “c”- initial and critical parameter values	Assumed that sorption-induced swelling is equivalent to thermal expansion.
Pan and Connell (2007)	$\varepsilon = RTL\ ln(1+BP)\frac{\rho_s}{E_s}f(x,\vartheta_s)-\frac{P}{E_s}(1-2\vartheta_s)$ $f(x,\vartheta_s)=\frac{[2(1-\vartheta_s)-(1+\vartheta_s)cx][3-5\vartheta_s-4(1-2\vartheta_s)cx]}{(3-5\vartheta_s)(2-3cx)}$ $\emptyset = 1-3\pi x^2(1-cx)$ ε – swelling strain ρ_s – density of the coal solid E_s – elastic modulus of the coal solid x – coal structure parameter c – a constant (=1.2 x) R – gas constant (8.314 J mol^{-1} K^{-1}) L – Langmuir constant (mol/kg) B – Langmuir constant (1/Pa)	Developed a theoretical model based on the energy balance between changes in the surface potential energy caused by gas adsorption and the elastic energy change caused by solid volume change.
Connell (2009)	$\overline{\sigma}_{xx}=\overline{\sigma}_{yy}=\frac{\vartheta}{1-\vartheta}\overline{\sigma}_{zz}+\frac{E}{1-\vartheta}\overline{\varepsilon}_{xx}+\frac{E}{1-\vartheta}\overline{\varepsilon}^s_{xx}+\frac{1-2\vartheta}{1-\vartheta}\alpha\overline{p}$ α – Biot coefficient $\overline{\varepsilon}$ - normal strain $\overline{\varepsilon}^s$ – sorption strain	Assumed that the geomechanical properties, such as Young's modulus and Poisson’s ratio are still isotropic.
Day et al. (2008b)	$S = S_{max}exp\left\{-D\left[\ln\left(\frac{\rho_a}{\rho_g}\right)\right]^2\right\}+k\rho_g$ S - volumetric swelling S_{max} - maximum swelling of the coal ρ_g - the gas density at the temperature and pressure used for the testing ρ_a - the density of the adsorbed phase (taken to be 1000 kg/m^3) D - an empirical curve fitting parameter k - a constant related to the solubility of gas into the coal.	Used the pore filling model (Dubinin–Radushkevich (DR)) modified with gas density to determine coal matrix swelling with different gas adsorptions
Day et al. (2010)	$S = S_{max}exp\left\{-D\left[\ln\left(\frac{\rho_L}{\rho_g}\right)\right]^2\right\}$ S - volumetric swelling S_{max} - maximum swelling of the coal ρ_g - the gas density at the temperature and pressure used for the testing ρ_L - the van der Waals density	Further modified the modified DR model after finding a better relation to sorption of gases in coal using the van der Waals density by Sakurovs et al., (2010)

Vandamme et al. (2010)	$\Delta\varepsilon = -\frac{\overline{\mu}_F}{K_s} + \alpha_\varepsilon \Gamma_F^{max} \int_{\overline{\mu}_F=-\infty}^{\mu_F(p)} \frac{1}{1+f_F e^{-\overline{\mu}_F/RT}} d\overline{\mu}_F$ K_s – solid bulk modulus α_ε – constant material parameter Γ_F^{max} and f_F - parameters which determine the shape of the adsorption isotherm for each pore fluid $\overline{\mu}_F$ - chemical potential of the pore fluid $\Delta\varepsilon$ - macroscopic strains	Used a thermodynamic approach by extending poromechanics to surface energy and surface stress.
Yang et al. (2010)	$\varepsilon = \frac{\emptyset}{k} \overline{f}_s$ $f_s = \frac{1}{A}\left(\frac{\partial\Omega}{\partial H}\right)_{T,\mu,A} - p_\infty$ $\Omega[\{\rho_i(r)\}] = F_{int}[\{\rho_i(r)\}] + \sum_i \int dr\rho_i(r)[\psi_i(r) - \mu_i]$ k – Elastic modulus where $K = k/\emptyset$, K is bulk modulus f_s – solvation pressure A – surface area Ω – grand free energy H – pore width μ – chemical potential p_∞ - bulk fluid pressure F_{int} - intrinsic Helmholtz free energy ρ_i and μ_i – local number density and chemical potential of component *i* ψ_i – local external potential	Used the quenched solid density functional theory (QSDFT) to study methane adsorption in coal under reservoir conditions.
Guo et al. (2016)	$\varepsilon = \frac{\sigma}{k}$ $\sigma = \frac{\int_{H_{min}}^{H_{max}} f_{SH} S(H) dH}{A_u}$ $f_{SH} = \frac{1}{A}\left[-\sum_{i=1}^{n} \frac{\partial U_{fs}(z_i)}{\partial z}\right] - p_\infty$ $U_{fs}(z_i) = 4\pi\rho_{atoms}\varepsilon_{fs}\sigma_{fs}^2 \left(\frac{\sigma_{fs}^{10}}{5(z_i)^{10}} - \frac{1}{2}\sum_{i=1}^{4} \frac{\sigma_{fs}^4}{(z_i + (i+1)\sigma_{ss})^4}\right)$ ε - linear strain σ – specific surface area stress k – elastic modulus of coal matrix f_{SH} – pressure exerted by the adsorbed gas molecules on a unit surface area of a carbon wall $S(H)$ – surface area as a function of pore size distribution H – pore width A_u – surface area of a unit mass of coal matrix, A – surface area, $U_{fs}(z_i)$ – interaction energy between one gas molecule and one carbon wall p_∞- bulk fluid pressure, ρ_{atoms} - carbon atom density ε_{fs} – fluid -solid interaction energy parameter σ_{fs} – average value of the fluid and solid molecular diameter	The Grand Canonical Monte Carlo (GCMC) algorithm was used to study the distribution of gas molecules under various pressures and Lennard-Jones potential is then used to analyse the effects of gas molecules on the swelling of coal matrix.
Han et al. (2017)	$\varepsilon = DG\frac{c}{c_a} + D\left(1 - \frac{G}{F}\right) ln\left(1 + F\frac{c}{c_a}\right)$ $D = \frac{A\rho RT n_m a}{E(a-1)}; G = 2ec_a; F = a - 1; c < c_a$ $\frac{c}{c_a} = \frac{\sqrt{\left(\frac{(F+1)n_m}{n_a} + 1 - F\right)^2 + 4F} - \frac{(F+1)n_m}{n_a} - 1 + F}{2F}$ ε – swelling ratio c – concentration of sorbate in bulk phase c_a – concentration of sorbed phase ρ – density of coal R – universal gas constant T – temperature E – Young's modulus of coal n_m – sorption amount required to form a monolayer n_a – absolute sorption amount per kilogram of coal G, F, D, a, A – constants	The concept of reduction of surface energy by sorption was considered to develop this theoretical model to obtain swelling using sorption data.

As explained in Section 4.6.2, current studies clearly show that coal mass properties and injecting gas properties are very influential on coal mass swelling. Although different models have been proposed to predict the swelling in coal with gas adsorption-induced swelling, none of these models shows the total effect of all the effective factors (adsorbing gas type, temperature, carbon content, moisture content, etc.) on swelling behaviour in coal. However, understanding of the total effect is necessary for the precise estimation of the swelling behaviour experienced by coal under field conditions. This was therefore considered in this study by developing a model incorporating all of the factors affecting coal matrix swelling. This is described in the following section.

4.6.4 Development of swelling model

According to the research literature (Day et al., 2010; Pan and Connell, 2007; Perera et al., 2012a; Ranathunga et al., 2014; Wang et al., 2013; Zhang et al., 2016), sorption capacity in coal is directly proportional to its matrix swelling. Therefore, several swelling models have been developed by researchers by modifying the existing adsorption models to estimate the coal matrix swelling which occurs with gas adsorption. For example, Durucan et al. (2009), Anggara et al. (2013), Battistutta et al. (2010), Levine (1996) and Anggara et al. (2016) used the Langmuir adsorption models to predict coal matrix swelling with gas adsorption. However, these Langmuir-type models fail to predict the swelling behaviourfort higher adsorption pressures (> 6 MPa) (Day et al., 2008b). Hence, Day et al. (2008b) used a modified version of the Dubinin–Radushkevich (D-R) model to predict coal mass swelling behaviour (refer Eq. [4.23]), and Day et al. (2010) tested this model for different types of coal for various gas adsorptions (CO_2, CH_4, N_2, He, Ne, Ar, Kr, Xe, CF_4, and C_2H_6) at up to 16 MPa pressures and confirmed the applicability of the model for the tested conditions.

$$S = S_{max} exp\left\{-D\left[\ln\left(\frac{\rho_L}{\rho}\right)\right]^2\right\} \quad [4.23]$$

where, S is volumetric swelling (%), S_{max} is maximum swelling of the coal, D is a constant related to the enthalpy of adsorption and ρ is the gas density at the temperature and pressure used for the testing. In this model, Day et al. (2010) adopted van der Waals density (ρ_L) instead of adsorbed phase gas density (ρ_a), which is 1028 kg/m^3 for CO_2 at its critical point (7.38 MPa pressure and 304.95 K temperature) fallowing the study by Sakurovs et al. (2010), which showed a better relation to sorption of gases into coal using the van der Waals density. Here, the constant D is a function of the heat of adsorption and the affinity of the gas to the sorbent (refer Eq. [4.24]).

$$D = \left(\frac{RT}{\beta E}\right)^2 \quad [2]$$

where, R is the universal gas constant, β is the affinity coefficient of the adsorbate and E is the enthalpy of adsorption. However, experimental evaluations are needed to acquire the parameter S_{max} to use this model to predict coal matrix swelling. Therefore, to obtain a more descriptive swelling model for gas adsorption-induced coal matrix swelling, a new equation was inserted into maximum swelling, S_{max}.

4.6.4.1 Samples used for the model development

Different types of high rank coal samples (carbon content > 75%) tested in the research literature under various temperature and pressure conditions for different adsorbing gases were used for the model development, calibration and validation process. Here, only high rank coal was used for the model development due to some contradictory behaviour of low and high rank coals (refer to Section 4.6.2.1). Table 4.17 shows the physical properties and the D-R model parameters (S_{max} and D) (refer to Eq. [4.23]) for the coal types used.

4.6.4.2 Model development, calibration and validation

Since maximum coal swelling, S_{max},, is dependent on several factors, such as adsorbing gas type, temperature, carbon content and moisture content (Day et al., 2008b, 2011; Day et al., 2010; De Silva et al., 2012; Perera et al., 2012a), the variation of S_{max} with each of these individual parameters was first examined using the swelling data (Table 4.17) obtained from the research literature for different coal types under different temperatures and with different moisture contents under various gas adsorptions (refer to Figure 4.48). General trends were observed for the maximum swelling variations with fixed carbon content and moisture content, and it appears that these parameters have reasonably good linear correlations, as the maximum swelling of all the high rank coal types shows a general reduction trend with these coal mass properties (fixed carbon content and moisture content) (refer to Eqs. [4.25, 4.26]). Apart from these two coal mass properties, the temperature of the coal seam may also play an important role in the swelling process and is therefore worth consideration. As explained in Section 4.6.2, temperature is inversely proportional to the sorption capacity in coal and therefore, a reduction in swelling can be expected with increasing temperature. However, Day et al. (2008b) and Kelemen and Kwiatek (2009) showed that temperature has only a little effect on maximum swelling in the range of 298.15 to 348.15 K, the temperature range in preferable coal seams for the ECBM process. Hence, for the present study, the effect of temperature on maximum swelling was ignored.

Table 4.17. Physical properties and D-R model parameters of the coal samples used for model development

Reference	Vitrinite reflectance (%)	Fixed Carbon content (%)	Moisture content (%)	S_{max}[1] (%)	D[1]	Adsorbing gas type	Temperature (K)	Samples taken from*	Remarks
Anggara et al. (2014)[2]	0.37	79.65	21.7	1.70	0.120	CO_2	316.15	Kutai basin (A)	Dry
	0.38	80.74	21.8	1.76	0.076	CO_2	316.15	Kutai basin (B)	Dry
	0.37	79.67	20.8	1.91	0.078	CO_2	316.15	Kutai basin (C)	Dry
	0.47	77.76	12	2.22	0.078	CO_2	316.15	Kutai basin (D)	Dry
	0.47	75.53	13.3	2.07	0.071	CO_2	316.15	Kutai basin (E)	Dry
	0.47	77.16	11	1.90	0.052	CO_2	316.15	Kutai basin (F)	Dry
	0.46	75.47	13.4	2.55	0.072	CO_2	316.15	Kutai basin (G)	Dry
	0.5	77.41	10.1	2.40	0.067	CO_2	316.15	Kutai basin (H)	Dry
Day et al. (2008b)	0.89	83.6	2.4	2.60	0.087	CO_2	328.15	Hunter Valley basin	Dry
	1.29	88.6	1	2.10	0.080	CO_2	328.15	Illawarra basin (A)	Dry
	0.95	84.1	1.5	2.30	0.070	CO_2	298.15	Bowen basin (A)	Dry
				2.20	0.081	CO_2	313.15		Dry
				2.40	0.085	CO_2	328.15		Dry
Day et al. (2010)	1.4	88.9	1.1	1.81	0.062	CO_2	328.15	Illawarra basin (B)	Dry
				1.17	0.090	CH_4	328.15		Dry
				0.54	0.127	N_2	328.15		Dry
				0.78	0.121	Ar	328.15		Dry
				1.33	0.086	Kr	328.15		Dry
	0.69	83	8.5	4.41	0.068	CO_2	328.15	Bowen basin (B)	Dry
				2.46	0.107	CH_4	328.15		Dry
				1.19	0.136	N_2	328.15		Dry
				4.34	0.067	Xe	328.15		Dry
				1.39	0.077	CF_4	328.15		Dry
				4.25	0.080	C_2H_6	328.15		Dry
	0.62	80.7	9.3	5.14	0.090	CO_2	328.15	Bowen basin (C)	Dry
				2.7	0.127	CH_4	328.15		Dry
				1.03	0.116	N_2	328.15		Dry
				1.45	0.127	Ar	328.15		Dry
				2.73	0.109	Kr	328.15		Dry
				4.91	0.070	Xe	328.15		Dry
				1.58	0.091	CF_4	328.15		Dry
				4.49	0.087	C_2H_6	328.15		Dry
Day et al. (2011)	0.69	83.4	5.7	4.4	0.070	CO_2	328.15	Bowen basin (D)	Dry
				2.62	0.081	CO_2	328.15		Wet
				2.60	0.105	CH_4	328.15		Dry
				0.97	0.121	CH_4	328.15		Wet

0.95	82.9	1.7	2.39	0.067	CO_2	328.15	Bowen basin (E)	Dry
			1.96	0.076	CO_2	328.15		Wet
			1.45	0.107	CH_4	328.15		Dry
			0.96	0.125	CH_4	328.15		Wet
0.62	79.3	11.5	5.08	0.073	CO_2	328.15	Bowen basin (F)	Dry
			0.99	0.069	CO_2	328.15		Wet
			2.85	0.103	CH_4	328.15		Dry
			0.68	0.101	CH_4	328.15		Wet
1.4	88.9	1.1	1.24	0.086	CO_2	328.15	Illawarra basin (C)	Dry
			0.99	0.095	CO_2	328.15		Wet
			1.98	0.061	CH_4	328.15		Dry
			1.98	0.070	CH_4	328.15		Wet

[1]Existing D-R model parameters where S_{max} is maximum swelling and D is a constant related to the enthalpy of adsorption

[2]D-R model parameters were obtained using curve-fitting techniques for the experimental swelling data

*Upper case letters identify different samples from the same basin

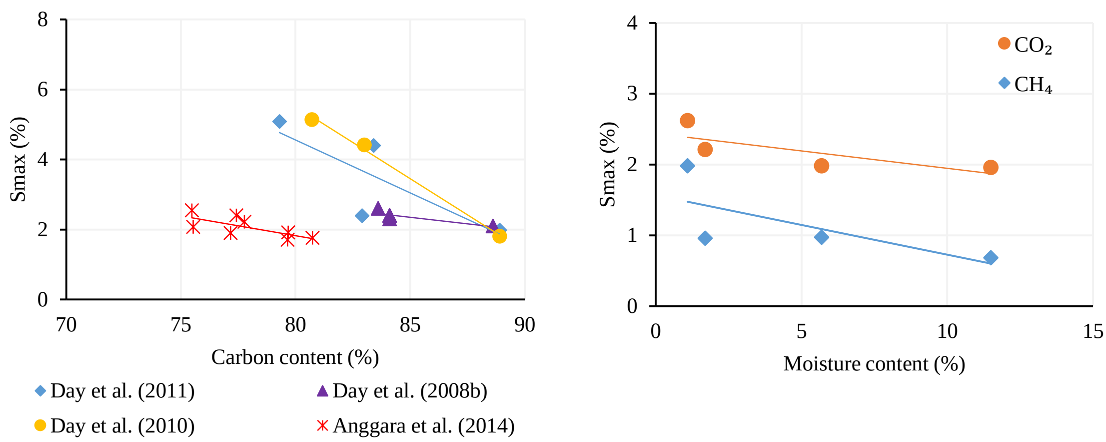

(a) fixed carbon content

(b) moisture content

Figure 4.48. Variation of maximum swelling with vitrinite reflectance, fixed carbon content, and moisture content (Anggara et al., 2013, 2014; Day et al., 2008b, 2011; Day et al., 2010)

$$S_{max} = aC + a_0 \text{ (for fixed carbon content)} \quad [4.25]$$

$$S_{max} = bW_c + b_o \text{ (for moisture content)} \quad [4.26]$$

where, C is the fixed carbon content (%), W_c is the moisture content (%) and $a, b, , a_0$ and b_o are constants.

The influence of adsorbing gas type on swelling should not be ignored, as different gases have different sorption capacities in coal and therefore, the swelling produced by each is different. According to Day et al. (2010), this can be successfully incorporated through the critical temperature (T_c) of the adsorbing gas, as it is proportional to the maximum swelling (Figure 4.49). Hence, the effect of adsorbing gas type on maximum swelling was introduced as a positive linear relationship to its critical temperature (refer to Eq. [4.27]).

$$S_{max} = cT_c + c_o \text{ (for critical temperature)} \qquad [4.27]$$

where, c and c_0 are constants.

Now, S_{max} can be written as a multilinear regression equation as shown in Eq. [4.28].

$$S_{max} = aC + bW_c + cT_c + f_1(CW_c) + f_2(CT_c) + f_3(W_cT_c) + d \qquad [4.28]$$

where f_1, f_2, f_3 and d are constants.

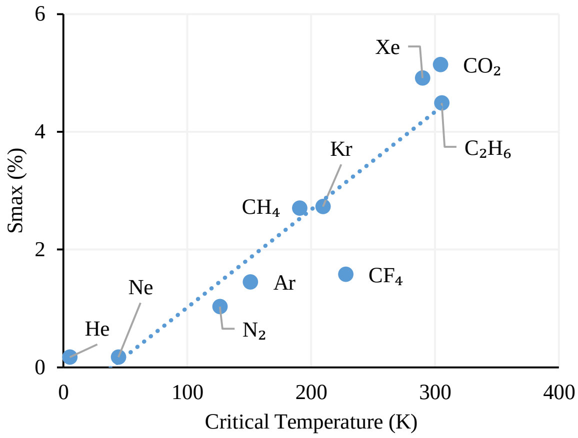

Figure 4.49. Variation of maximum swelling with critical temperature of adsorbing gas type for Australian bituminous coal (Day et al., 2010)

Then, the multicollinearities among the independent parameters (fixed carbon content (C), moisture content (W_c) and critical temperature of the adsorbing gas (T_c)) were checked using the correlation coefficient (calculated by Eq. [4.29]) and the variance inflation factor (VIF) (calculated by Eq. [4.30]) among the parameters. The results are shown in Tables 4.18 and 4.19.

$$R_{xy} = \frac{n\sum x_i y_i - (\sum x_i)(\sum y_i)}{\sqrt{n(\sum x_i^2) - (\sum x_i)^2}\sqrt{n(\sum y_i^2) - (\sum y_i)^2}} \qquad [4.29]$$

$$VIF = \frac{1}{(1 - R_{xy})^2} \qquad [4.30]$$

where, i ranges from 1 to n, n is the number of elements for each parameter and R_{xy} is the correlation coefficient factor.

Table 4.18. Correlation coefficient matrix between parameters used Eq. [4.29]

	R_{vit}	C	W_c	Tc
R_{vit}	1	0.51	-0.38	0.14
C	0.51	1	-0.77	-0.18
W_c	-0.38	-0.77	1	0.29
Tc	0.14	-0.18	0.29	1

Table 4.19. Variance inflation factor matrix between parameters used Eq. [4.30]

	R_{vit}	C	W_c	Tc
R_{vit}	-	1.34	1.17	1.02
C	1.34	-	2.49	1.03
W_c	1.17	2.49	-	1.09
Tc	1.02	1.03	1.09	-

When the R_{xy} is 1, the two parameters are totally dependent and when it is 0, the two parameters are totally independent. If the R_{xy} varies between -0.8 to 0.8, the two parameters can be considered as independent (Field, 2013). As the correlation coefficients of the parameters are between the range in Table 4.18, they can be considered as independent from each other. This conclusion can be further confirmed by the VIF values in Table 4.19 which are less than 2.5. According to Menard (2002), if the VIF is less than 5, the two parameters can be considered as independent from each other. Therefore, Eq. [4.28] can be simplified into the following form (see Eq. [4.31]) by neglecting the multicollinearties among the parameters.

$$S_{max} = aC + bW_c + cT_c + d \quad [4.31]$$

Next, the coefficients a, b, c and d were determined using the swelling data obtained from Anggara et al. (2014) (Kutai basin samples (A)-(E)) and Day et al. (2010) (for CO_2, N_2, and CH_4 adsorption-induced swelling in Bowen (A) and Illawarra (A) basin samples) and Day et al. (2011) (for the effect of moisture during CO_2 adsorption in Bowen basin (E) and (F) samples and Illawarra basin (C) samples) (refer to Table 4.17 for the experimental data). To observe the contribution of each parameter on maximum swelling, a sensitivity analysis was also conducted (Eqs. [4.32a-c], which has a missing independent parameter in each equation). Using the Microsoft Excel Solver tool, best-fitting parameters were investigated for the new equations (Eqs. [4.32a-c]) and compared with the maximum swelling values obtained by the existing D-R equation for swelling (Eq. [4.23]) (refer to Table 4.17 and Figure 4.50).

$$S_{max} = aC + bW_c + d \qquad \text{(without } T_c\text{)} \qquad [4.32a]$$

$$S_{max} = aC + cT_c + d \qquad \text{(without } W_c\text{)} \qquad [4.32b]$$

$$S_{max} = bW_c + cT_c + d \qquad \text{(without } C\text{)} \qquad [4.32c]$$

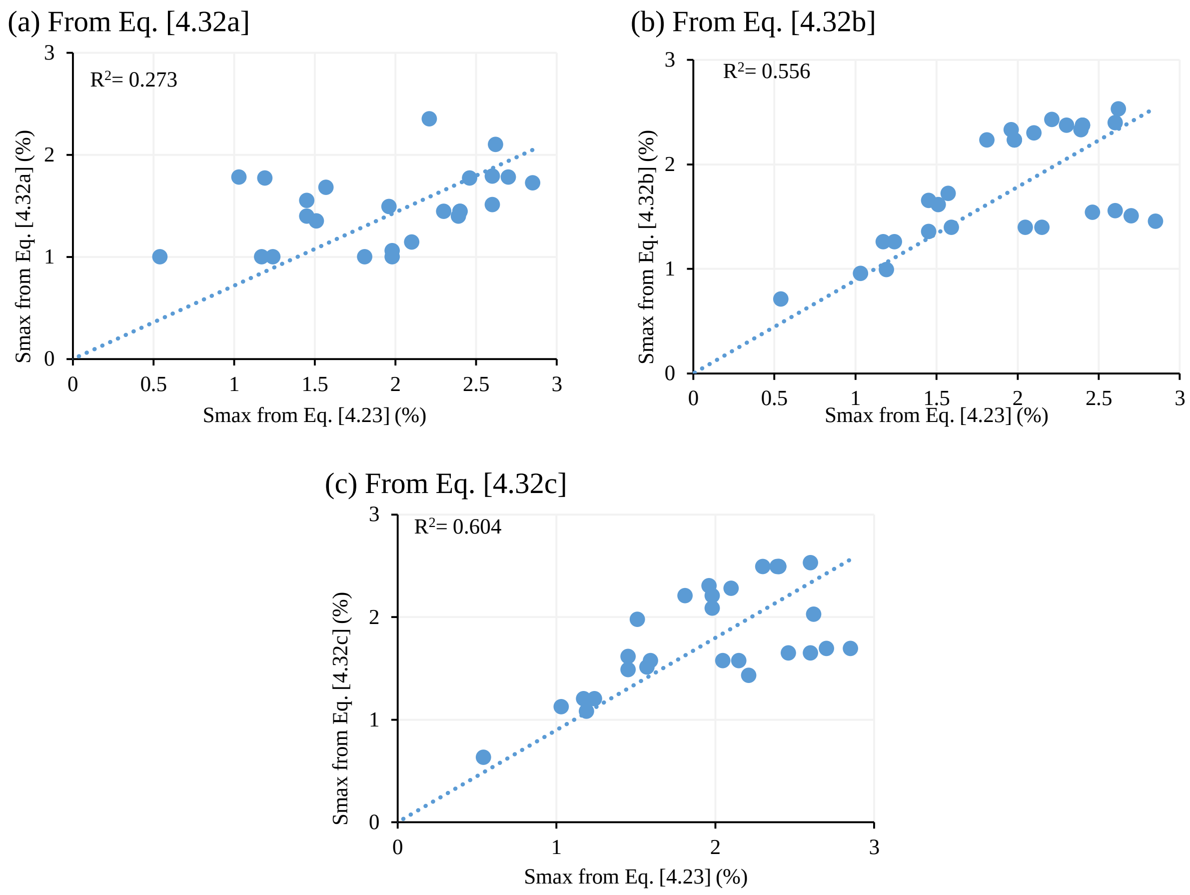

Figure 4.50. Sensitivity analysis for Eq. [4.31] with (a) Critical temperature of the adsorbing gas (Eq. [4.32a]), (b) Moisture content (Eq. [4.32b]) and (c) Fixed carbon content (Eq. [4.32c]) using the swelling data from Anggara et al. (2014) and Day et al. (2011); Day et al. (2010).

Figure 4.50(a) shows the very strong influence of the critical temperature of the adsorbing gas on the maximum swelling, which is confirmed by the very low fitting value (R^2 = 0.217) in that equation. Further, the other two parameters (moisture content (Figure 4.50(b)) and fixed carbon content (Figure 4.50(c))) also have considerable effects on the maximum swelling as shown in Eq. [4.31].

This sensitivity study shows the importance of incorporating the influence of all four parameters in the final swelling equation due to their strong contribution to swelling. Therefore, the best-fitting coefficients for constants were determined to be a = -0.012, b = -0.09, c = 0.008

and $d = 0.796$. As mentioned earlier, the data obtained from Anggara et al. (2014), Day et al. (2011) and Day et al. (2010) (refer to Figure 4.51) were used for the model calibration and the new model is found to be able to predict the maximum swelling accurately with a best fit of 0.88 for the coal samples used for the calibration.

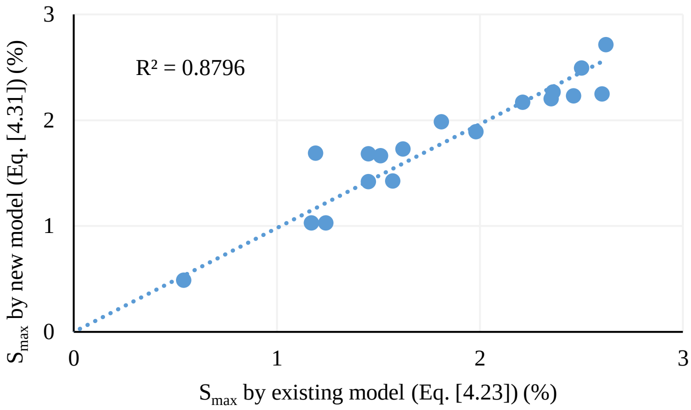

Figure 4.51. Model calibration (Eq. [4.31]) using the data from Anggara et al. (2014), Day et al. (2011) and Day et al. (2010)

The developed swelling model was then validated using the data obtained from Day et al. (2008b) (for Bowen basin (A) coal at 298.15, 313.15 K and 328.15 K temperatures), Day et al. (2010) (Ar, CF_4 and Xe adsorption in Bowen basin coal (C)) and Day et al. (2011) (for CO_2 and CH_4 adsorption in dry and wet coal from Bowen basin (D)) (Figure 4.52) and fairly good agreement with ±1 % (-0.8 to 1%) accuracy could be seen between the predicted maximum swelling values (Eq. [4.31]) and the swelling values obtained using the existing D-R equation (Eq. [4.23]).

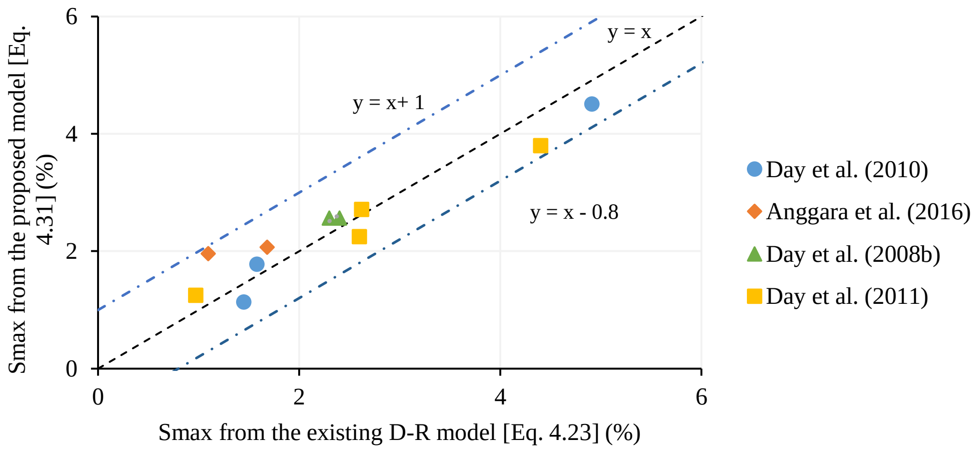

Figure 11. Proposed model validation using data from Day et al. (2008b, 2011) and Day et al. (2010)

Finally, the proposed model (Eq. [4.31]) was incorporated into the Eq. [4.23] (existing D-R equation) to predict the gas adsorption-induced coal matrix swelling in a more descriptive way. In this Eq. [4.33], fixed carbon content (C, %) and moisture content (W_c, %) vary with the coal sample properties and the critical temperature (T_c, %), van der Waals density (ρ_L, kg/m^3) and gas density (ρ, kg/m^3) vary with the adsorbing gas type and its conditions. Further, the constant D is influenced by the affinity of both sorbate and sorbent material properties (refer to Eq. [4.24]). Figure 4.53 displays the predicted coal matrix swelling using the proposed model for different coal properties and adsorbing gas properties. The data used for the model validation were also used in this case. The critical temperature (T_c) and van der Waals density (ρ_L) were taken from Day et al. (2010) and the respective gas densities at their tested pressures and temperatures were obtained by the REFPROP database (McLinden et al., 1998). Coal mass properties (C, W_c) and the D (constant related to enthalpy of adsorption) were acquired from the respective data sources (Day et al., 2008b, 2011; Day et al., 2010) (see Table 4.17).

$$S = (aR_{vit} + bC + cW_c + dT_c + e)exp\left\{-D\left[\ln\left(\frac{\rho_L}{\rho}\right)\right]^2\right\} \quad [4.33]$$

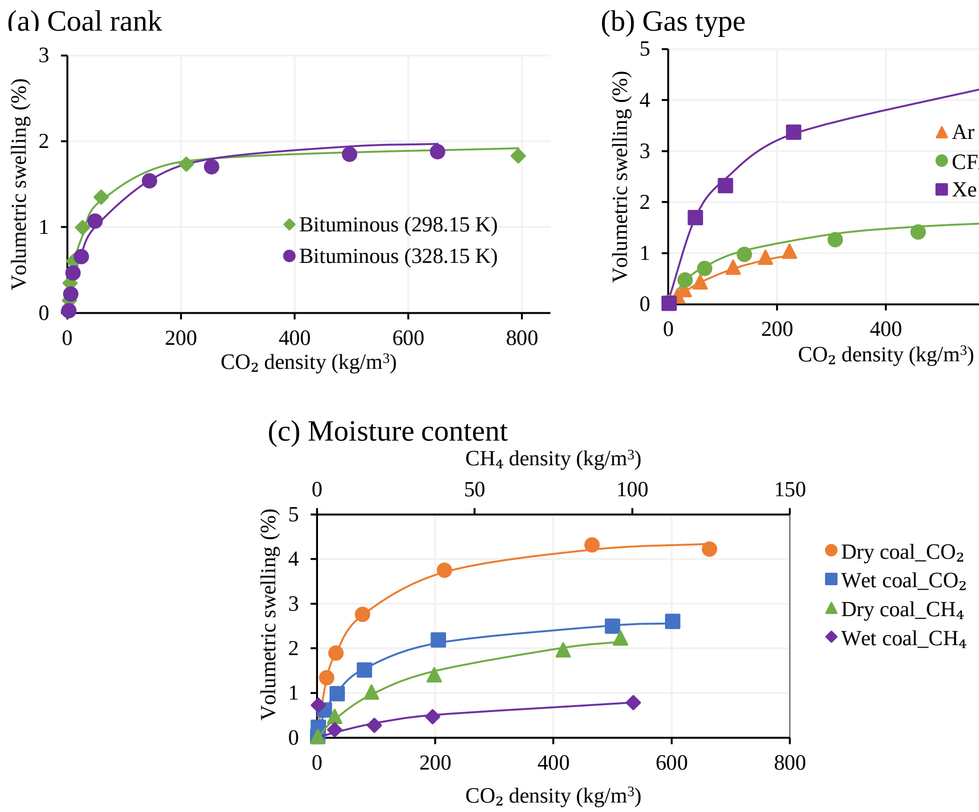

Figure 4.53. Coal mass volumetric swelling (%) in different coal samples under different conditions obtained using proposed model (Eq. [4.31]) for data obtained from Day et al. (2008b, 2011); Day et al. (2010) (line plots are the model-predicted swelling values)

According to Figure 4.53, the predicted coal matrix swelling data show good agreement with the experimental observations. To further check the accuracy of the model-predicted data, bias and the root mean square errors (RMSEs) were calculated and are shown in Table 4.20. According to Table 4.20, the bias varies between -0.8 – 0.4 and the RMSE (<0.3) values are quite small for the model-predicted values with the experimental values, which further confirms that the use of the proposed model is acceptable.

Table 4.20. Statistical analysis of experimental data and data predicted by the proposed model

Swelling data taken from (reference)	Tested sample conditions	Bias	RMSE
Day et al. (2008b)	Bituminous (298.15 K)	0.251	0.090
	Bituminous (328.15 K)	0.346	0.079
Day et al. (2010)	Ar (328.15 K)	-0.240	0.048
	CF_4 (328.15 K)	0.332	0.071
	Xe (328.15 K)	0.302	0.091
Day et al. (2011)	Dry coal_CO_2	0.017	0.075
	Wet coal_CO_2	-0.211	0.066
	Dry coal_CH_4	-0.112	0.065
	Wet coal_CH_4	-0.702	0.301

4.6.5 Limitations and recommendations

As the predicted swelling data from the proposed model (Eq. [4.33]) indicate, this model can accurately estimate the expected coal matrix swelling in coal for different gas adsorptions. The importance of this model is the ability to directly relate the effect of different factors of sorbate and sorbent on the swelling process. However, it should be noted that all the data used for the development of the model had a fixed carbon content >75% (high rank coal). Therefore, the values obtained for the constants in Eq. [4.31] may not accurately fit coal properties which are out of the range.

For this model, several effective factors were considered, which are believed to have a strong influence on maximum swelling. However, the effect of temperature was not considered, because the effect of temperature was negligible within the range of 293.15 to 333.15 K for the data used (Day et al., 2008b). As explained in Section 4.6.2.1, at higher temperatures, the adsorption capacity is reduced (Bae and Bhatia, 2006) and hence the expected maximum swelling is less. However, studies of the effect of high temperatures on coal mass swelling in different types of coal are scarce and hence, could not be effectively incorporated into the present study. Therefore, it is proposed to conduct experimental studies to observe the effect of temperature on the swelling of different coal types to include that influence in the present model.

Further, the mineral contents and the micro-pore diameter of the coal specimens affect the gas adsorption capacity of coal (Perera et al., 2012a), and may also contribute to the swelling of coal. This needs to be studied in the future.

The swelling data used for the present study were obtained from gas adsorption experiments conducted on crushed coal samples/small coal blocks without applying any confinement. As explained in Section 4.6.2.2, the application of stresses reduces the maximum swelling in both low and high rank coals (refer to Figure 4.45). However, among the large number of studies of gas adsorption-induced coal matrix swelling, very few have been conducted with the application of stresses on coal mass for swelling. Therefore, more studies need to be conducted on different coal types under different effective stresses, in order to include the effect of confinement on coal mass swelling in the proposed model.

In addition, as explained in Section 4.6.2, there are some contradictory findings on the effect of coal rank on coal mass swelling (refer to Figure 4.43). The data used for the present study showed a reduction of swelling with increasing carbon content and hence used a negative linear relationship for model development, but the situation is different for low rank coals. Therefore, in-depth studies are required to precisely incorporate the influence of rank on coal matrix swelling.

However, within these limitations, the proposed model could predict the swelling behaviour quite accurately and can be fine-tuned when the answers to the above knowledge gaps are found.

4.6.6 Conclusion

The estimation of coal matrix swelling with different gas adsorptions (e.g. CO_2, CH_4 and N_2) is required for the efficient and effective implementation of enhanced coal bed methane recovery projects. To-date, studies have shown that both adsorbing gas properties and coal mass properties are affect coal mass strain variations due to gas adsorption. Therefore, a comprehensive review was undertaken.

In experimental work on the effect of adsorbing gas type on coal swelling, CO_2 has been found to be the most dominant adsorbent compared to other gasses, such as CH_4, N_2, CF_4, C_2H_6, Xe, etc. This is because CO_2 has a higher affinity to be adsorbed into the coal mass, with its unique physical and chemical properties creating stronger van der Waals bonds with the coal pore walls. In addition, the phase of the adsorbing gas is also important, and super-critical CO_2 exhibits greater adsorption potential in coal compared to gaseous/liquid CO_2, which results in greater coal matrix swelling compared to sub-critical CO_2. In relation to the influence of coal mass properties on CO_2 adsorption-induced swelling, the positive effects of carbon content, moisture content, temperature and depth on swelling have been confirmed in the field. However, there have been some contradictory observations on the effect of coal rank on CO_2 induced swelling, because both positive and negative influences of rank on swelling have been reported.

The coal swelling models currently available were then reviewed in order to understand the contribution of modelling to the prediction of coal swelling, and some analytical and theoretical models developed to predict the coal matrix swelling caused by different gases were found. Of the analytical models, to date Langmuir-type behaviour for swelling has been widely used to estimate coal mass swelling upon gas adsorption, although it exhibits significant inaccuracy in predicting swelling under high pressures. Therefore, the modified Dubinin–Radushkevich (DR) model could be used, as it exhibits a better fit for various coal types, even under super-critical conditions. Furthermore, to date some theoretical models have been developed to predict coal matrix swelling, following various approaches, including elasticity theory, adsorption thermodynamics, quenched solid density functional theory, and the Grand Canonical Monte Carlo (GCMC) algorithm. Although these models are more reliable, finding model parameters to predict swelling using these equations has often been challenging. In addition, neither these analytical and theoretical models are not sufficiently descriptive to show the influence of various surrounding factors on coal matrix swelling.

A novel approach was therefore taken to develop a descriptive analytical model for coal matrix swelling in high rank coal with gas adsorption, which effectively shows the influences of various effective factors. The existing D-R model was used to develop the model, inserting a new expression for maximum swelling (Eq. [4.32]) as a function of fixed carbon content (%) and moisture content (%) to represent coal mass properties, and critical temperature (K) to represent the effect of adsorbing gas properties. These effective factors were chosen after checking the contribution of each factor on maximum swelling. The model was calibrated for a range of high rank coal samples with various moisture contents and temperatures and for various adsorbing gas types (CO_2, CH_4 and N_2). The model was then validated using the swelling data obtained for a range other coal samples with different coal mass properties. The model was then incorporated into the existing D-R model (Eq. [4.33]). The proposed equation can estimate the coal mass swelling with gas adsorption with an accuracy of around ±1.0%, and hence can be used as a descriptive analytical model to estimate swelling. However, the model was developed for a range of coals with a fixed carbon content of >75% and hence, provides a better fit of data for this range.

4.6.7 References

Anggara, F., Sasaki, K., Rodrigues, S., Sugai, Y., (2014). The effect of megascopic texture on swelling of a low rank coal in supercritical carbon dioxide. *International Journal of Coal Geology* 125, 45-56.

Anggara, F., Sasaki, K., Sugai, Y., (2013). Swelling Measurements of a Low Rank Coal in Supercritical CO_2. *International Journal of Geoscience*s 4, 863-870.

Anggara, F., Sasaki, K., Sugai, Y., (2016). The correlation between coal swelling and permeability during CO_2 sequestration: A case study using Kushiro low rank coals. *International Journal of Coal Geology* 166, 62-70.

Bae, J.S., Bhatia, S.K., (2006). High-Pressure Adsorption of Methane and Carbon Dioxide on Coal. Energ Fuel 20, 2599-2607.

Battistutta, E., van Hemert, P., Lutynski, M., Bruining, H., Wolf, K.H., (2010). Swelling and sorption experiments on methane, nitrogen and carbon dioxide on dry Selar Cornish coal. *International Journal of Coal Geology* 84, 39-48.

Ceglarska-Stefańska, G., Czapliński, A., (1993). Correlation between sorption and dilatometric processes in hard coals. *Fuel* 72, 413-417.

Chikatamarla, L., Cui, X., Bustin, R.M., (2004). Implications of volumetric swelling/shrinkage of coal in sequestration of acid gases, Coalbed Methane Symposium, Tuscaloosa, AL, paper 0435.

Cody Jr, G.D., Larsen, J.W., Siskin, M., (1988). Anisotropic solvent swelling of coals. Energ *Fuel* 2, 340-344.

Connell, L., (2009). Coupled flow and geomechanical processes during gas production from coal seams. *International Journal of Coal Geology* 79, 18-28.

Cui, X., Bustin, R.M., (2005). Volumetric strain associated with methane desorption and its impact on coalbed gas production from deep coal seams. *AAPG Bulletin* 89, 1181-1202.

Cui, X., Bustin, R.M., Chikatamarla, L., (2007). Adsorption-induced coal swelling and stress: Implications for methane production and acid gas sequestration into coal seams. *Journal of Geophysical Research: Solid Earth* 112 (B-10).

Day, S., Duffy, G., Sakurovs, R., Weir, S., (2008a). Effect of coal properties on CO_2 sorption capacity under supercritical conditions. *International Journal of Greenhouse Gas Control* 2, 342-352.

Day, S., Fry, R., Sakurovs, R., (2008b). Swelling of Australian coals in supercritical CO_2. *International Journal of Coal Geology* 74, 41-52.

Day, S., Fry, R., Sakurovs, R., (2011). Swelling of moist coal in carbon dioxide and methane. *International Journal of Coal Geology* 86, 197-203.

Day, S., Fry, R., Sakurovs, R., Weir, S., (2010). Swelling of Coals by Supercritical Gases and Its Relationship to Sorption. *Energ Fuel* 24, 2777-2783.

De Silva, P.N.K., Ranjith, P.G., Choi, S.K., (2012). A study of methodologies for CO_2 storage capacity estimation of coal. *Fuel* 91, 1-15.

Durucan, S., Ahsanb, M., Shia, J.Q., (2009). Matrix shrinkage and swelling characteristics of European coals. *Energy Procedia* 1, 3055-3062.

Durucan, S., Shi, J.Q., (2009). Improving the CO_2 well injectivity and enhanced coalbed methane production performance in coal seams. *International Journal of Coal Geology* 77, 214-221.

Field, A., (2013). Discovering statistics using IBM SPSS statistics. 4th edition, Sage, London, pp 163-391.

Gray, I., (1987). Reservoir engineering in coal seams: Part 1-The physical process of gas storage and movement in coal seams. *SPE Reservoir Engineering* 2, 28-34.

Guo, X., Wang, Z., Zhao, Y., 2016. A comprehensive model for the prediction of coal swelling induced by methane and carbon dioxide adsorption. *Journal of Natural Gas Science and Engineering* 36, 563-572.

Han, F., Chen, G., Liu, Z., Yang, J., (2017). Correlation of swelling and sorption properties of block coal sample. *Fuel* 188, 452-461.

Harpalani, S., Chen, G., (1995). Estimation of changes in fracture porosity of coal with gas emission. *Fuel* 74, 1491-1498.

Harpalani, S., Schraufnagel, A., (1990a). Measurement of parameters impacting methane recovery from coal seams. *International Journal of Mining and Geological Engineering* 8, 369-384.

Harpalani, S., Schraufnagel, R.A., (1990b). Shrinkage of coal matrix with release of gas and its impact on permeability of coal. *Fuel* 69, 551-556.

Hol, S., Spiers, C.J., (2012). Competition between adsorption-induced swelling and elastic compression of coal at CO_2 pressures up to 100 MPa. *Journal of the Mechanics and Physics of Solids* 60, 1862-1882.

Hol, S., Spiers, C.J., Peach, C.J., (2012). Microfracturing of coal due to interaction with CO_2 under unconfined conditions. *Fuel* 97, 569-584.

Jasinge, D., Ranjith, P.G., Choi, X., Fernando, J., (2012). Investigation of the influence of coal swelling on permeability characteristics using natural brown coal and reconstituted brown coal specimens. *Energy* 39, 303-309.

Karacan, C.Ö., (2003). Heterogeneous sorption and swelling in a confined and stressed coal during CO_2 injection. *Energ Fuel* 17, 1595-1608.

Kelemen, S., Kwiatek, L., (2009). Physical properties of selected block Argonne Premium bituminous coal related to CO_2, CH_4, and N_2 adsorption. *International Journal of Coal Geology* 77, 2-9.

Kronimus, A., Busch, A., Alles, S., Juch, D., Jurisch, A., Littke, R., (2008). A preliminary evaluation of the CO_2 storage potential in unminable coal seams of the Münster Cretaceous Basin, Germany. *International Journal of Greenhouse Gas Control* 2, 329-341.

Larsen, J.W., (2004). The effects of dissolved CO_2 on coal structure and properties. *International Journal of Coal Geology* 57, 63-70.

Larsen, J.W., Flowers, R.A., Hall, P.J., Carlson, G., (1997). Structural rearrangement of strained coals. *Energ Fuel* 11, 998-1002.

Levine, J.R., (1996). Model study of the influence of matrix shrinkage on absolute permeability of coal bed reservoirs. *Geological Society, London, Special Publications* 109, 197-212.

Mavor, M.J., Gunter, W.D., 2004. Secondary porosity and permeability of coal vs. gas composition and pressure, SPE Annual Technical Conference and Exhibition, Houston, Texas, Paper 80255.

McLinden, M., Klein, S., Lemmon, E., Peskin, A., (1998). REFPROP, Thermodynamic and transport properties of refrigerants and refrigerant mixtures. NIST Standard Reference Database 23 (http://webbook.nist.gov/chemistry/fluid/)

Menard, S., (2002). Applied logistic regression analysis. Sage University Paper Series on Quantitative Applications in Social Sciences, vol. 106, Thousand Oaks, California, pp 41-90.

Palmer, I., and J. Mansoori, (1998), How permeability depends on stress and pore pressure in coalbeds: A new model: Society of Petroleum Engineers Reservoir Evaluation and Engineering, SPE Paper 52607, pp. 539–544.

Pan, Z., Connell, L.D., (2007). A theoretical model for gas adsorption-induced coal swelling. *International Journal of Coal Geology* 69, 243-252.

Pan, Z., Connell, L.D., (2012). Modelling permeability for coal reservoirs: a review of analytical models and testing data. *International Journal of Coal Geology* 92, 1-44.

Pan, Z., Connell, L.D., Camilleri, M., (2010). Laboratory characterisation of coal reservoir permeability for primary and enhanced coalbed methane recovery. *International Journal of Coal Geology* 82, 252-261.

Peng, Y., Liu, J., Pan, Z., Connell, L.D., Chen, Z., Qu, H., (2017). Impact of coal matrix strains on the evolution of permeability. *Fuel* 189, 270-283.

Perera, M.S.A., Ranjith, P.G., Choi, S.K., Airey, D., Weniger, P., (2012a). Estimation of gas adsorption capacity in coal: a review and an analytical study. *International Journal of Coal Preparation and Utilization* 32, 25-55.

Perera, M.S.A., Ranjith, P.G., Choi, S.K., Airey, D., (2011). The effects of sub-critical and super-critical carbon dioxide adsorption-induced coal matrix swelling on the permeability of naturally fractured black coal. *Energy* 36, 6442-6450.

Perera, M.S.A., Ranjith, P.G., Choi, S.K., Airey, D., (2012b). Investigation of temperature effect on permeability of naturally fractured black coal for carbon dioxide movement: An experimental and numerical study. *Fuel* 94, 596-605.

Ranathunga, A.S., Perera, M.S.A., Ranjith, P.G., (2014). Deep coal seams as a greener energy source: a review. *Journal of Geophysics and Engineering* 11, 063001.

Ranathunga, A.S., Perera, M.S.A., Ranjith, P.G., (2017). The influence of CO_2 properties and reservoir depth on coal matrix swelling: A meso-scale experimental study using low rank coal. *Energ Fuel* (under review).

Reucroft, P., Patel, H., (1986). Gas-induced swelling in coal. *Fuel* 65, 816-820.

Reucroft, P.J., Sethuraman, A.R., (1987). Effect of pressure on carbon dioxide induced coal swelling. *Energ Fuel* 1, 72-75.

Robertson, E.P., Christiansen, R.L., (2005). Measuring and Modelling Sorption-Induced Coal Strain, 4th Annual DOE/NETL Conference on Carbon Capture and Sequestration, Alexandria, Virginia, pp. 2-5.

Sakurovs, R., Day, S., Weir, S., (2010). Relationships between the critical properties of gases and their high pressure sorption behaviour on coals. *Energ Fuel* 24, 1781-1787.

Sakurovs, R., Day, S., Weir, S., Duffy, G., (2007). Application of a modified Dubinin-Radushkevich equation to adsorption of gases by coals under supercritical conditions. *Energ Fuel* 21, 992-997.

Sawyer, W., Paul, G., Schraufnagel, R., (1990). Development and application of a 3D coalbed simulator. CIM/SPE, 90-119.

Seidle, J.R., Huitt, L., (1995). Experimental measurement of coal matrix shrinkage due to gas desorption and implications for cleat permeability increases, International Meeting on Petroleum Engineering, Beijing, China, Paper 30010.

Shi, J., Durucan, S., (2004). Drawdown induced changes in permeability of coalbeds: a new interpretation of the reservoir response to primary recovery. *Transport in Porous Media* 56, 1-16.

Shi, J.Q., Durucan, S., (2005). CO_2 Storage in Deep Unmineable Coal Seams. *Oil Gas Sci Technol* 60, 547-558

Shi, J.Q., Mazumder, S., Wolf, K.H., Durucan, S., (2008). Competitive Methane Desorption by Supercritical CO_2 Injection in Coal. *Transport in Porous Media* 75, 35-54.

Siriwardane, H., Haljasmaa, I., McLendon, R., Irdi, G., Soong, Y., Bromhal, G., (2009). Influence of carbon dioxide on coal permeability determined by pressure transient methods. *International Journal of Coal Geology* 77, 109-118.

Vandamme, M., Brochard, L., Lecampion, B., Coussy, O., (2010). Adsorption and strain: The CO_2-induced swelling of coal. *Journal of the Mechanics and Physics of Solids* 58, 1489-1505.

Viete, D.R., Ranjith, P.G., (2006). The effect of CO_2 on the geomechanical and permeability behaviour of brown coal: Implications for coal seam CO_2 sequestration. *International Journal of Coal Geology* 66, 204-216.

Walker Jr, P.L., Verma, S.K., Rivera-Utrilla, J., Khan, M.R., (1988). A direct measurement of expansion in coals and macerais induced by carbon dioxide and methanol. *Fuel* 67, 719-726.

Wang, S., Elsworth, D., Liu, J., (2013). Permeability evolution during progressive deformation of intact coal and implications for instability in underground coal seams. *International Journal of Rock Mechanics and Mining Sciences* 58, 34-45.

Yang, K., Lu, X., Lin, Y., Neimark, A.V., (2010). Deformation of coal induced by methane adsorption at geological conditions. *Energ Fuel* 24, 5955-5964.

Zang, J., Wang, K., (2017). Gas sorption-induced coal swelling kinetics and its effects on coal permeability evolution: Model development and analysis. *Fuel* 189, 164-177.

Zhang, X.G., Ranjith, P.G., Perera, M.S.A., Ranathunga, A.S., Haque, A., (2016). Gas Transportation and Enhanced Coalbed Methane Recovery Processes in Deep Coal Seams: A Review. *Energ Fuel* 30, 8832-8849.

4.7 Chapter summary

The main objective of this chapter was to investigate the influence of CO_2 adsorption on brown coal flow behaviour. Various meso-scale experimental programs were conducted to observe the effect of different effective factors on coal mass permeability with CO_2-ECBM and the major finding are summarised below.

- **Section 4.2 - *How do injecting CO_2 properties and in situ stresses affect coal mass flow behaviour?***

The reduction of permeability with increasing depth due to the associated effective stress variation is much higher for low-rank coal compared to high-rank coal. Further, super-critical CO_2 has much lower permeability than sub-critical CO_2, regardless of coal rank. However, this influence of CO_2 phase condition increases with increasing rank. Interestingly, the influence of depth on permeability reduces with phase transition from sub- to super-critical in any type of coal due to the greater swelling effect created by super-critical CO_2. Although N_2 has the ability to recover CO_2 adsorption-induced swelled areas in coal regardless of rank, the recovery ability is much higher for high-rank coal.

- **Section 4.3 – *How can the individual effect of effective stress and sorption-induced strain on the evolution of coal permeability be evaluated?***

The effective stress coefficient for coal is not equal to unity and is effective stress-dependent, this behaviour being common for any coal type. This non-unity of the effective stress parameter ($\alpha \neq 1$) causes an under-estimation of permeability due to the additional effective stress application and it increases with increasing pore pressure. The swelling-induced permeability clearly shows an over-estimation of permeability reduction which is higher at higher effective stresses and is also common for high rank coal. However, high rank coal exhibits a higher reduction in permeability than low rank coal due to sorption-induced strains. Finally, the modified Dubinin–Radushkevich (D-R) model was used to predict the swelling-induced permeability reductions in coal mass and provided successful results for both low and high rank coals with a goodness fit >0.96.

- **Section 4.4 – *How does the temperature alter CO_2 permeability in coal?***

CO_2 permeability decreases for higher injecting pressures at low temperatures, whereas permeability increases when the temperature is increased. However, the influence of temperature on N_2 permeability is negligible compared to CO_2 permeability. Interestingly, these observations are common for both low and high rank coals.

- **Section 4.5 – *How does carbon dioxide adsorption-induced coal matrix swelling vary for various CO_2 properties and reservoir depths?***

CO_2 adsorption-induced coal matrix swelling is greater at higher CO_2 pressures, particularly for the super-critical phase condition of CO_2, regardless of reservoir depth or the maturity of the coal. N_2 exhibits comparatively inert behaviour in coal, producing negligible swelling, regardless of pore pressure and reservoir depth. However, the partial pressure depletion created by N_2 in the coal mass has the ability to recover CO_2 adsorption-induced swelled areas in coal to some extent, and that ability is greater if N_2 flooding is done for a sufficiently long period under lower effective stress conditions, and it is probable that a greater amount of N_2 can enter the coal mass under such conditions. The modified D-R model can effectively be used to predict low-rank coal swelling upon first or repeated injections of CO_2, if appropriate relationships for the Dubinin–Radushkevich parameters, S_{max} and D, are used.

- **Section 4.6 – *How can the various gas adsorption- induced coal matrix swellings in coal be estimated?***

A new descriptive model is proposed for coal matrix swelling with gas adsorption using the effective factors. The existing D-R model was used to develop the model by inserting a new expression for the maximum swelling, including fixed carbon content (%) and moisture content (%) to represent coal mass properties and critical temperature (K) to represent the effect of adsorbing gas properties. The proposed equation can estimate coal mass swelling due to gas adsorption with an accuracy of around ±1% and hence can be used as a descriptive analytical model to estimate swelling. However, the equation was developed for a range of coals with a fixed carbon content of >75%, and hence provides a better fit of data for this range.

PART 2 - CHAPTER 5

Macro-scale studies of coal flow properties during carbon dioxide sequestration using reconstituted coal

Publications included in Chapter 5

Chapter 5 includes two publications. Details of the publications are as follows:

Chapter 5.2

Ranathunga AS, Perera MSA, Ranjith PG, Ju Y, Vishal V, De Silva PNK (2015). A macro-scale experimental study of sub- and supercritical CO_2 flow behaviour in Victorian brown coal. *Fuel* 158: 864-873.

Chapter 5.4

Ranathunga AS, Perera MSA, Ranjith PG (2017). A laboratory-scale numerical study of CO_2 flow through coal under down-hole stress conditions: Application for CO_2 storage. *Energy Fuel* (under review).

Declaration for Thesis Chapter 5.2

In the case of Chapter 5.2, the nature and extent of my contribution to the work was the following:

Nature of contribution	Extent of contribution (%)
Initiation, key ideas, experimental work, data analysis and writing up	85

The following co-authors contributed to the work. If co-authors are students at Monash University, the extent of their contribution in percentage terms must be stated:

Name	Nature of contribution	Extent of contribution (%) for student co-authors only
Perera MSA	Key ideas, reviewing and editing the manuscript	N/A
Ranjith PG	Key ideas, reviewing and editing the manuscript	N/A
Ju Y	Reviewing and editing the manuscript	N/A
Vishal V	Reviewing and editing the manuscript	N/A
De Silva PNK	Reviewing and editing the manuscript	N/A

The undersigned hereby certify that the above declaration correctly reflects the nature and extent of the candidate's and co-authors' contributions to this work*.

Candidate's signature	[redacted]	**Date** 25/01/2017

Main Supervisor's signature	[redacted]	**Date** 25/01/2017

*Note: Where the responsible author is not the candidate's main supervisor, the main supervisor should consult with the responsible author to agree on the respective contributions of the authors.

5. Macro-scale studies of coal flow properties during carbon dioxide sequestration using reconstituted coal

5.1 Overview

For field-scale simulations in the laboratory, macro-scale experiments are crucial. Therefore, an effort was made to quantify the coal mass flow variations during CO_2 injection using a macro-scale (samples 203 mm in diameter and 1000 mm long) experimental program. The experiments were conducted using the advanced core-flooding apparatus available in the Deep Earth Energy Research Laboratory (refer to Chapter 3). Reconstituted samples were used for this study to eliminate the great heterogeneity of coal, as discussed in Chapter 2.

- **Section 5.2 – *How does coal mass flow behaviour vary along the coal sample due to different CO_2 properties?***

A series of injection pressures was used to inject the fluid into the coal mass to obtain both sub- and super-critical CO_2 phase conditions. N_2 flooding was also done to quantify the coal matrix alterations due to CO_2 flow. Unlike in the meso-scale tests, it was possible to observe the fluid flow behaviour along the coal sample in this experiment, which provides an overview of the expected CO_2 flow along the coal mass.

This section of the chapter details the following paper:

Ranathunga AS, Perera MSA, Ranjith PG, Ju Y, Vishal V, De Silva PNK (2015). A macro-scale experimental study of sub- and super-critical CO_2 flow behaviour in Victorian brown coal. *Fuel* 158: 864-873.

- **Section 5.3 – *How do CO_2 properties and in situ stresses affect CO_2 storage capacity?***

In this section, the effect of in situ stresses on the coal flow behaviour along the sample was tested. In this set of experiments, the in situ stress was applied by varying the axial load, which may represent a thin coal seam, as the deformation is most likely in one direction for thin coal seams. Further, how the amount of CO_2 injected into the coal specimen varies with different CO_2 phase and pressure and in situ stresses was tested to quantify the CO_2 storage capacity of brown coal.

The following journal paper was produced from this chapter:

Ranathunga AS, Perera MSA, Ranjith PG, De Silva GPD (2016). A macro-scale view of the influence of effective stress on carbon dioxide flow behaviour in coal: An experimental study. *Geo-mechanics and Geo-physics for Geo-Energy and Geo-Resources*, 1-16.

- **Section 5.4 – *Prediction of expected fluid flow along the coal seam and storage capacity variations in coal with various CO_2 properties under different down-hole stresses***

Finally, a macro-scale numerical model was developed using the COMSOL Multiphysics simulator to extend the experimental findings to deeper reservoir conditions (higher in situ stresses), and to predict the expected fluid flow along the coal seam and storage capacity variations in brown coal for various CO_2 phase and pressures under different down-hole stresses.

This section of the chapter details the following paper:

Ranathunga AS, Perera MSA, Ranjith PG (2017). A laboratory-scale numerical study of CO_2 flow through coal under down-hole stress conditions: Application to CO_2 storage. *Energy Fuel* (under review).

5.2 How does coal mass flow behaviour vary along the coal sample due to different CO_2 properties?

As stated in Chapter 2, a number of studies have been conducted on coal mass flow behaviour during CO_2 injection. However, most have been conducted on small coal samples (up to 100 mm in length), which are incapable of representing the coal mass rearrangements during CO_2 flow and CO_2 storage capacities at a substantial scale. Hence, the main objective of this study is to determine the permeability behaviour of coal for different CO_2 injections using macro-scale coal specimens (203 mm in diameter and 1000 mm in length). A series of core flooding experiments was conducted on Victorian brown coal specimens using an advanced core flooding apparatus, for a range of injection pressures (6 – 10 MPa) at 11 MPa axial stress and 38 ^{0}C constant system temperature using both CO_2 and N_2. The CO_2 flow behaviour along the sample was also studied to observe the expected CO_2 flow patterns through the coal seams and these were compared with the N_2 flow to enable the identification of the CO_2-induced flow variations. An effort was also made to quantify the swelling of the sample during CO_2 flow.

This section of the chapter details the following publication:

Ranathunga AS, Perera MSA, Ranjith PG, Ju Y, Vishal V, De Silva PNK (2015). A macro-scale experimental study of sub- and super-critical CO_2 flow behaviour in Victorian brown coal. *Fuel* 158: 864-873.

Fuel 158 (2015) 864–873

Contents lists available at ScienceDirect

Fuel

journal homepage: www.elsevier.com/locate/fuel

A macro-scale experimental study of sub- and super-critical CO_2 flow behaviour in Victorian brown coal

A.S. Ranathunga [a], M.S.A. Perera [a,*], P.G. Ranjith [a], Y. Ju [b], V. Vishal [c], P.N.K. De Silva [d]

[a] *Deep Earth Energy Laboratory, Department of Civil Engineering, Monash University, Building 60, Melbourne, Victoria 3800, Australia*
[b] *China University of Mining & Technology, Xueyuan RD, 100083 Beijing, PR China*
[c] *Department of Energy Resources Engineering, Stanford University, CA 94305, USA*
[d] *UCL Australia, University College London, Torrens Building, Adelaide, SA 5000, Australia*

H I G H L I G H T S

- Sub- and super-critical CO_2 flow behaviours in Victorian brown coal.
- Testing of macro scale samples using an advanced core-flooding apparatus.
- CO_2 adsorption induced swelling causes significant coal structure modification.
- Super-critical CO_2 injection causes a greater reduction in CO_2 permeability.
- CO_2 phase and pressure influences on coal matrix swelling and flow properties.

A R T I C L E I N F O

Article history:
Received 13 April 2015
Received in revised form 10 June 2015
Accepted 14 June 2015
Available online 19 June 2015

Keywords:
CO_2 sequestration
Permeability
Macro-scale samples
Core-flooding apparatus

A B S T R A C T

In deep coal seams carbon dioxide (CO_2) exists in its super-critical state, which emphasizes the importance of studying super-critical CO_2 flow behaviour in coal, especially for field applications, such as CO_2 sequestration and enhanced coal bed methane recovery. Although there has been some research on the subject, the studies have been conducted on only certain types of coal (e.g., naturally fractured black coal) using small coal samples, which makes it difficult to verify the applicability of adsorption theories at a higher scale to estimate field CO_2 storage capacity. The main objective of this study is therefore to determine the permeability behaviour of coal for sub-critical and super-critical CO_2 flows using large coal specimens (203 mm in diameter and 1000 mm in length). A series of core flooding experiments was conducted on brown coal specimens collected from the Latrobe Valley basin, Victoria, using an advanced core flooding apparatus, for a range of injection pressures (6–10 MPa) at 11 MPa axial stress and 38 °C temperature.

According to the test results, CO_2 permeability in coal may reduce with increasing injection pressure due to the phase transition of CO_2 from sub-critical to super-critical during pressure increment. N_2 injection into a coal mass permeated with CO_2 shows lower permeability values compared to N_2 injection into a fresh coal mass, because in the former case, the coal mass structure has already been critically reformed during the CO_2 flood. Although the pressure development trends for first N_2, CO_2 and second N_2 injections along the sample are similar, there may be a noticeable pressure reduction, especially closer to the injection point during the second N_2 injection. This is due to the coal structure re-arrangement during the CO_2 flood, where the pressure development is less in the regions, when CO_2 is in the super-critical state. Such CO_2 and N_2 migration patterns through coal seams after injection are highly important for field applications.

5.2.1 Introduction

Today, global warming is happening at an alarming rate, and is considered a serious risk to human beings around the world. The amount of greenhouse gases in the atmosphere is the main cause and therefore, it is necessary to investigate appropriate greenhouse gas mitigation options. CO_2 sequestration in deep coal seams has been identified as an effective CO_2 mitigation option, due to the added advantage of the production of coal bed methane (CBM), which offsets the cost of CO_2 sequestration (enhanced coal bed methane (ECBM)) [1–7]. Further, the CO_2 injected into the coal

* Corresponding author. [redacted]
[redacted] *address:* samintha.perera@monash.edu (M.S.A. Perera).

http://dx.doi.org/10.1016/j.fuel.2015.06.047
0016-2361/

seams is in an adsorbed state and can therefore be stably stored for a geologically significant period [4], which is important for the long term safety of the process. CBM is a natural gas formed during the coalification process which is extracted from coal beds. CBM can be used to produce energy in a more economical and greener way and the process has been tested in many countries in the world including Canada, the USA, Japan, Poland and Australia [1,4,8,9]. According to Perera and Ranjith [1], White et al. [4], and Reeves [10], injection of a CO_2 stream into the coal bed during CBM recovery can significantly enhance CBM production due to its higher affinity to adsorb CO_2 compared to CH_4. This is because, the greater chemical potential of CO_2 causes the creation of stronger Van der Waals bonds with the coal surface than CH_4, resulting in greater attraction to the coal matrix surface [11,12]. The processes of ECBM production and CO_2 sequestration have therefore become attractive means of producing energy, while mitigating the atmospheric CO_2 level.

In coal beds, most gas exists in an adsorbed phase in the coal matrix and some as free gas in the fracture pore space [13]. Unless a large joint exists, the natural cleat system of the coal mass, formed during the coalification process, governs gas movement through it. In the gas transport process in coal, first it moves through its natural cleat system and then adsorbs into the coal matrix along the cleat walls [14]. When the gas molecules reach the micro pores in the coal matrix, they follow the diffusion process, as the mean flow path of the gas molecules is greater than the micro pore diameter. In contrast, when the gas molecules reach the cleats, flow is controlled by coal mass permeability, as the mean flow path of the gas molecules is smaller than the cleat width. According to Harpalani and Chen [15], diffusional flux into the coal matrix can be simulated using the diffusion equation (Eq. (1)) and the fluid movement through fractures or the cleat system can be simulated using Darcy's law (Eq. (2)). However, the diffusion process is a quite slow process and therefore, takes much greater time than the pressure-driven advection process in cleats.

$$m = -D\nabla C \tag{1}$$

$$m = -\frac{\rho \mathrm{k}}{\mu}\nabla P \tag{2}$$

where m is mass flow rate, D is the diffusion coefficient and ∇C is the concentration gradient, ∇P is the pressure gradient, μ is the viscosity of gas and ρ is the density of gas. According to existing findings, both CO_2 sequestration and CBM recovery processes are dependent on coal mass and adsorbing gas properties, such as coal rank, moisture content, temperature, depth, existing gas composition and adsorbing gas pressure, gas type and phase and injection and production well operations [4,13,16,17].

However, according to Jasinge et al. [18] and Vishal et al. [19], injection of CO_2 into coal causes its chemical and physical properties to be greatly changed, resulting in unpredictable amounts of injectable CO_2 and producible CH_4 in coal seams. There has been much research conducted on this process, which has revealed that there is a great degree of swelling caused by CO_2 adsorption into the coal matrix that, in turn, can cause the permeability of the coal mass to be severely decreased [8,19–21]. This is because swelling induces a strain between the injecting CO_2 molecules and the coal matrix, which reduces the pore spaces available for gas movement, resulting in reduced permeability in the coal seam [19,20]. For successful CO_2 – enhanced methane recovery, the seam permeability should be more than 1 mD [17]. Hence, in this context the CO_2 adsorption-induced call matrix swelling is of great concern.

Under the high pressure and temperature conditions in deep un-mineable coal seams, CO_2 exists in its super-critical condition (beyond 7.38 MPa pressure and 31.8 °C temperature CO_2 exists as super-critical fluid), which is believed to create a greater swelling effect in coal compared to gas or liquid CO_2 due to its higher chemical potential and sorption capacity [2]. All of these facts imply that un-mineable coal seams are more vulnerable to the swelling effect.

Coal matrix swelling depends on the injecting CO_2 pressure and phase condition. The effect of CO_2 pressure on coal swelling has been studied by Harpalani and Chen [15] and Day et al. [22], who have confirmed the increased swelling effect with increasing CO_2 pressure. According to these researchers, increment of CO_2 injection pressure expands the pore space, thereby offering a greater number of effective areas for the adsorption and later swelling processes. This enhanced swelling effect and the associated permeability reduction with increasing CO_2 injection pressure have also been shown by Perera et al. [23]. According to Perera et al. [23], the CO_2 phase transition from sub- to super-critical also significantly affects the swelling-related permeability reduction in coal.

However, maintaining consistency during laboratory experiments on coal has become a difficult task due to coal's highly heterogeneous nature, which has been a major obstacle to the verification of the effects of in-situ coal properties on coal's behaviour. The production of homogenous reconstituted coal samples with reproducible properties is the only solution identified to date to overcome this issue, and the effectiveness of this method has been shown by Jasinge et al. [18]. On the other hand, to date most coal CO_2 injection studies have been conducted using small-scale samples (up to around 100 mm in length), which makes it difficult to verify the applicability of adsorption theories at a higher scale to estimate CO_2 storage capacity. As a result, De Silva and Ranjith [17,24], conducted advance core-flooding tests using 1 m long and 203 mm diameter coal samples to effectively estimate the CO_2 flow behaviour in coal. However, only sub-critical CO_2 injection has been considered by these researchers, which cannot represent actual CO_2 flow behaviour in deep coal seams.

This study therefore focuses on identifying the influences of both sub- and super-critical CO_2 injection on coal matrix swelling and the associated permeability alterations using macro-scale (1 m long and 203 mm diameter) reconstituted Victorian brown coal samples.

5.2.2 Methodology

This study was conducted using the advanced core-flooding apparatus located in the Deep Earth Energy Research Laboratory (DEERL) at Monash University (Fig. 1). A detailed description of the apparatus can be found in De Silva and Ranjith [24] and the experimental methodology is described below.

5.2.2.1 Sample preparation

The coal samples used were taken from the Hazelwood open-cut coal mine at Morwell in Gippsland, Victoria as coal blocks, which had a natural moisture content of around 52–55%. Due to the difficulty in obtaining a natural coal block 1 m in length (brown coal being very weak with many cleats compared to black coal), in this experiment reconstituted coal samples were made using powdered coal. To prepare the powdered coal, a similar process was used to that described by Jasinge et al. [18]. Initially, the coal blocks were broken into smaller pieces and then crushed using a milling machine. Using the grinder, small pieces of coal were crushed into coal dust. The crushed coal was then sieved using a mechanical sieving machine to separate the coal powder less than 1 mm in size and the sieved coal was then stored in sealed plastic containers.

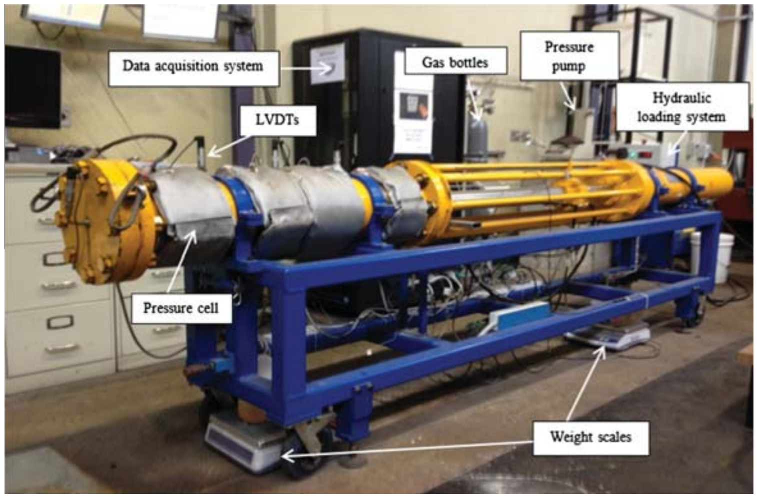

Fig. 1. Advanced core flooding apparatus.

The samples required for the macro-scale testing were then prepared in three stages using this powdered coal. First, an axial stress of 11 MPa was applied on 1/3 of the coal core sample and compacted for 30 min. Then, the next 1/3 of the coal sample was added to the cell and compacted for 30 min, followed by the rest of the sample under 11 MPa axial stress. Between each compaction, the surface of the coal was disturbed and roughened to ensure sample consistency. The whole coal sample was then consolidated for a further 7 days and the consolidation level was observed by using a string strain gauge and linear variable differential transformers (LVDTs). In order to confirm the fully consolidated condition of the sample, a consolidation profile was used (see Fig. 2) and the water released from the sample was observed (until zero water release from the sample). The permeability testing was conducted only after the consolidation level became stable. The permeability testing was conducted only after the consolidation level became stable (see Fig. 2). After confirming the fully compacted condition of the sample, permeability tests were initiated, maintaining the system temperature at 38 °C constant value.

5.2.2.2 Permeability tests

Permeability tests were conducted for both CO_2 and N_2 injections at five different injecting pressures (6, 7, 8, 9, and 10 MPa) under 11 MPa axial stress (Fig. 3). Here, the un-drained condition was maintained to determine the sample permeability using a pressure-transient approach to obtain the super-critical CO_2 injection into the sample (under the drained condition downstream pressure is always atmospheric and therefore the super-critical condition cannot be achieved) [1]. CO_2 injection was conducted at the constant pressure required and the corresponding pressure development throughout the sample (at two intermediate points, 600 mm and 850 mm from the injection point) and downstream was monitored and recorded, at one second intervals, using an advanced data acquisition system (Fig. 3).

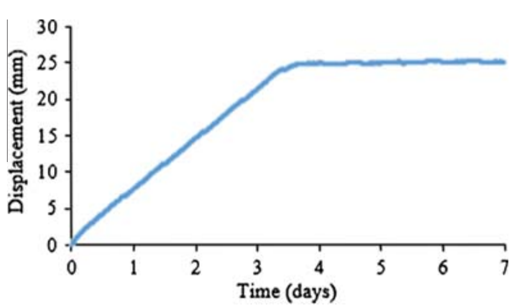

Fig. 2. Compaction of coal sample under 11 MPa axial stress.

The downstream pressure vs. time curve was used to calculate the permeability of the coal sample using Eq. (3) [25]:

$$Q = \left(\frac{dP}{dt}\right) \times \beta V \tag{3}$$

where Q is the flow rate through the specimen, V is the downstream volume, β is the adiabatic compressibility of the gas, and dP/dt is the rate of change in the downstream pressure with time. Then, Darcy's law (Eq. (4)) was used to calculate the corresponding permeability [17]:

$$K = \frac{2QP_o\mu L}{A(P_i^2 - P_o^2)} \tag{4}$$

where Q, μ, P_o, and P_i are the gas flow rate through the coal specimen, the viscosity of the fluid, the downstream pressure and the upstream pressure, respectively. The specimen had a cross-sectional area, A, and mean length, L and initial permeability, K.

N_2 was first injected into the coal sample at five different injection pressures (Fig. 3) under 11 MPa axial stress and CO_2 injection was then initiated. N_2 was then again injected into the sample to check the CO_2 flow-induced physical structure modification of the coal sample (Fig. 3). The downstream pressure development curves for first N_2 injection, CO_2 injection and second N_2 injection under 11 MPa axial stress are shown in Fig. 4(a)–(c). In addition, during each injection, fluid flow behaviour throughout the sample was recorded by measuring the pressure development at two intermediate points (600 mm and 850 mm from the injection point) along the length of the sample (Fig. 5) and the swelling effect was investigated by measuring the sample volume change (Fig. 6).

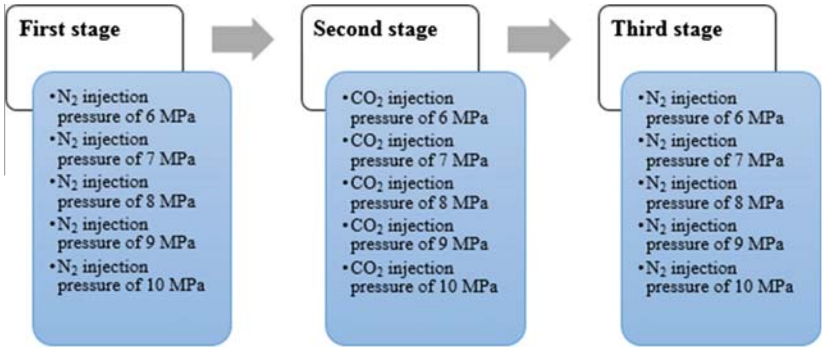

Fig. 3. Test sequence used for permeability tests.

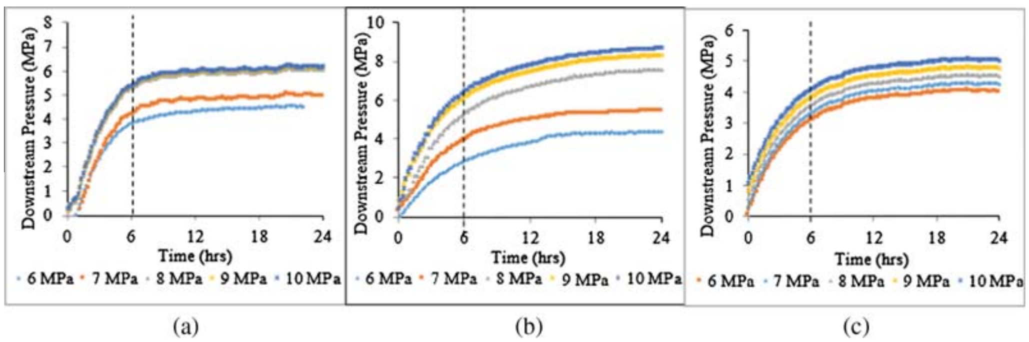

Fig. 4. Downstream pressure developments for different injection pressures in (a) first N_2 injection, (b) CO_2 injection and (c) second N_2 injection under 11 MPa axial stress.

5.2.3 Results and discussion

5.2.3.1 CO_2 and N_2 flow behaviour in coal

According to Fig. 4, after around 6 h of CO_2 injection, reasonable steady-state behaviour in downstream pressure was be achieved. The downstream pressures developed at 6, 12, 18 and 24 h after the injection during first N_2, CO_2 and second N_2 injections were then analysed to check the pressure development in the sample with time. For example, Fig. 7 shows the sample pressure developments for 6 and 9 MPa injection pressures. According to the figure, although the pressure development increases with increasing injection pressure for both first and second N_2 injections, the first N_2 injection shows a higher downstream pressure development at all the selected time periods for any injection pressure, and the second N_2 injection displays the lowest pressure developments. It appears that an obstruction to pressure development formed during the CO_2 flux. If the pressure development during this CO_2 injection is then considered, according to Fig. 7, there is greater pressure development at lower injection pressure (6 MPa), which exhibits a higher amount of CO_2 molecule movement or a higher CO_2 mass flow rate into the downstream at lower injection pressure (Eq. (2)). The CO_2 flow ability through the coal mass therefore seems to reduce with increasing injection pressure.

It should be noted that, in this program the system temperature was maintained at a constant value of 38 °C (>31.8 °C, critical temperature) throughout the experiment, which cause CO_2 to be transferred to its super-critical state when it reached the critical pressure (7.38 MPa). During 9 MPa injection, CO_2 was therefore at its super-critical state at the injection point, and according to Fig. 7, downstream CO_2 also became super-critical after around 18 h of injection (it goes beyond the critical pressure of CO_2), at which the pure super-critical CO_2 condition throughout the sample can be confirmed. According to Fujioka et al. [8], movement of super-critical CO_2 in coal results in greater coal matrix swelling and eventually reduced CO_2 injectability into the coal mass, which is likely to be the reason for the observed decline in CO_2 flux at increased injection pressure.

In order to clarify this, permeability under each injection pressure was then determined and the results are shown in Fig. 8. According to the figure, although the coal mass permeability for both first and second N_2 injections increases with increasing injection pressure, CO_2 permeability clearly reduces with increasing injection pressure. This may be related to the previously-mentioned phase transition influence of CO_2 during the pressure increment (sub-critical to super-critical). In general, increase of injection pressure causes the coal mass pore pressure to be raised, which reduces the effective stress applied on the coal matrix and eventually expands the coal mass pore space for gas movement, resulting in enhanced permeability. The comparatively inert nature of N_2 in coal is well accepted [15,26–28], and therefore, the observed permeability increment of N_2 with increasing injection pressure is clearly the effective stress effect mentioned previously.

This is not the only interesting result shown in Fig. 8; the lower permeability values for the second N_2 injection (after the CO_2 injection) compared to the first N_2 injection (Fig. 8) are also critical. This is believed to be related to coal matrix swelling. During the CO_2 movement through the coal sample, the CO_2 adsorbs into the coal matrix, causing the coal matrix to swell by reducing the pore space available for gas movement. According to the past studies, this swelling-induced strain in coal is not auto-recoverable and

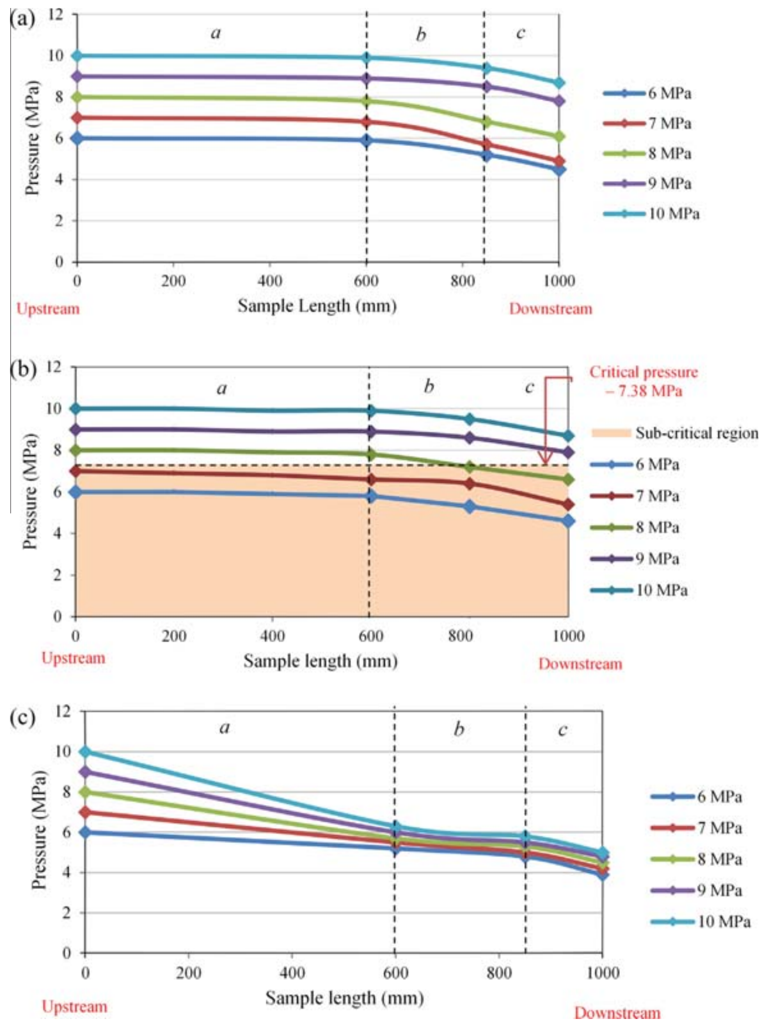

Fig. 5. Pressure profiles along the length of the sample for different injection pressures in (a) first N_2 injection, (b) CO_2 injection and (c) second N_2 injection under 11 MPa axial stress.

remains as permanent damage to the coal mass [4]. The second N_2 injection was preceded to this swelled and re-structured coal mass and therefore the lower permeability values should be expected.

A closer examination of this feature is required for full understanding and this can be done using Table 1, which shows how the coal sample permeability reduces due to the CO_2 flow at each injection pressure. According to Table 1, although the increased permeability reduction between the first and second N_2 flux with increasing injection pressure is a common trend, there is clearly a greater N_2 permeability reduction after 8 MPa injection pressure. For example, increasing the CO_2 injection pressure from 6 to 7 MPa causes the N_2 permeability reduction to be increased by only around 2%, and the further increase of injection pressure from 7 to 8 MPa, causes the permeability reduction to be increased by around 11%. This is clearly related to the unique properties of super-critical CO_2, which has greater chemical strength and therefore, greater swelling potential. As mentioned earlier, the entire core-flooding set-up was maintained at 38 °C constant temperature in this study (>31.8 °C, critical temperature of CO_2) and therefore, increasing the pressure beyond 7.38 MPa causes the injecting CO_2 phase to be transferred from the sub- to the super-critical state, and at least a portion of CO_2 in the coal mass to be super-critical (regions *a* and *b* in Fig. 5(b)), resulting in higher permeability reduction in the coal mass. According to Bae and Bhatia [29], phase transition from sub- to super-critical causes a higher degree of sorbed CO_2 volume in coal, and according to Massarotto et al. [30], super-critical CO_2 molecules create much stronger bonds with the coal's surface than sub-critical CO_2 molecules. Furthermore, Okamoto et al. [31] found that, the organic materials in the coal mass can be dissolved by the super-critical CO_2, resulting in reduced pore space due to the deposition of organic matter. All of these reasons are believed to conjointly contribute to the greater permeability reduction caused by super-critical CO_2 flux.

5.2.3.2 Fluid flow behaviour along the coal sample

As described above, CO_2 flow through the coal matrix creates significant differences when CO_2 reaches its super-critical state, which also affects other gas transport behaviours in coal. It is therefore, important to study the CO_2 and N_2 flow patterns along the coal sample for different injection pressures to understand

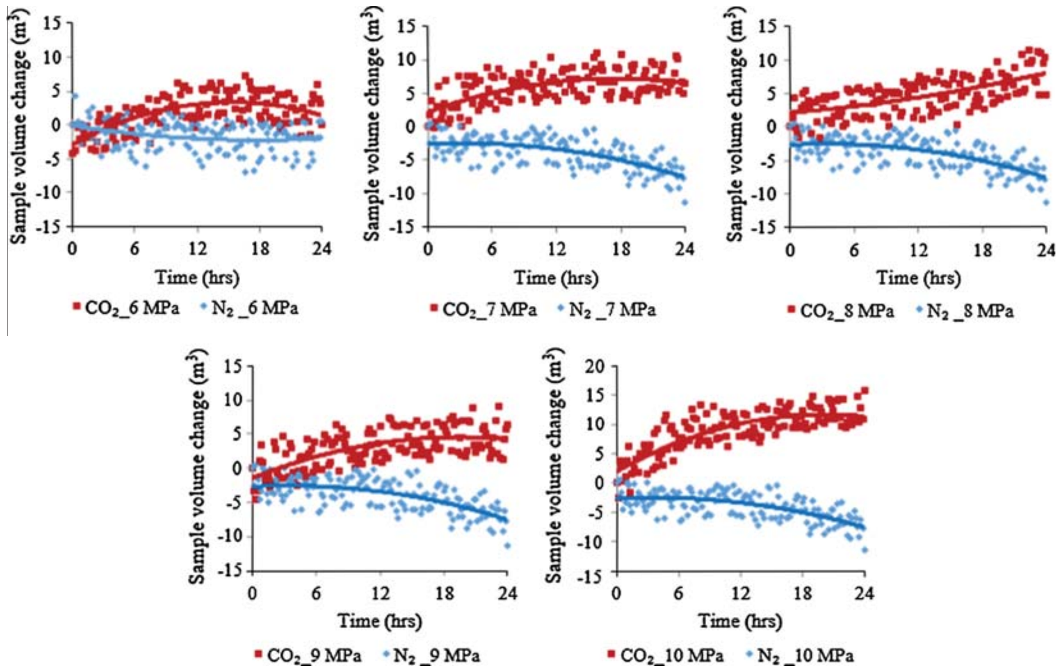

Fig. 6. Coal sample volume change with different injection pressures for first N_2 injection and CO_2 injection.

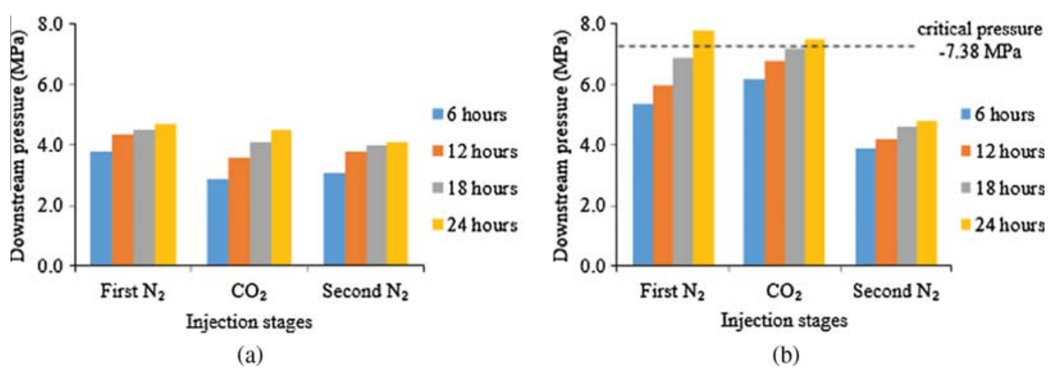

Fig. 7. Downstream pressure development at 6 h, 12 h, 18 h and 24 h during (a) 6 MPa (sub-critical) and (b) 9 MPa (super-critical) injection pressures.

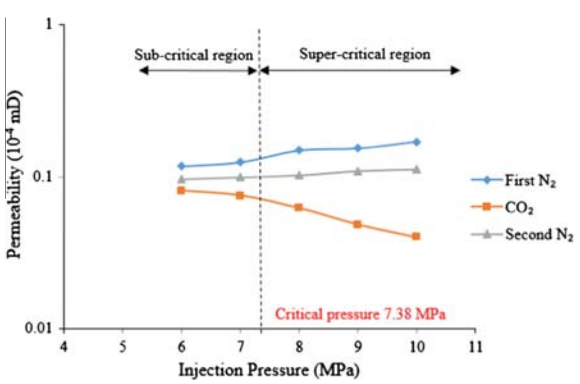

Fig. 8. Permeability changes with different injection pressures for first N_2 injection, CO_2 injection and second N_2 injection.

the actual CO_2 phase transition behaviour inside the coal sample. The results are shown in Fig. 5. According to this figure, all the injections (first N_2, CO_2 and second N_2) show similar fluid flow behaviour through the coal sample, with the exception of the steeper pressure reduction in region "*a*" during the second N_2 injection (Fig. 5(c)). Here, the three regions; "*a*", "*b*" and "*c*" are the distance between the injection point to the first intermediate pressure transducer, the first to second intermediate pressure transducer, and the second pressure transducer to the end of the sample, respectively. Table 2 gives the steady state pressure gaps in the three regions ("*a*", "*b*" and "*c*") for all the injections (first N_2, CO_2 and second N_2) after 24 h of injection. According to Fig. 4, the pressure development downstream clearly becomes steady after 24 h of injection and therefore, the pressure development throughout the sample after 24 h of injection can be considered as the ultimate or steady-state pressure distribution along the sample. The following sections reveal the fluid flow behaviour along the coal sample

Table 1
Permeability reduction for CO_2 and second N_2 injection for different injection pressures.

	Injection pressure (MPa)	Permeability reduction (%)		
		Compared to first N_2 injection		Compared to second N_2 injection
		Second N_2	CO_2	CO_2
Sub-critical region	6	17.89	31.04	16.02
	7	20.49	39.62	24.06
Super-critical region	8	31.24	58.19	39.20
	9	32.79	68.29	55.48
	10	34.25	76.36	64.05

for each injection condition to enable full understanding of the process.

a. Flow behaviour along the coal sample during the first N_2 injection

The pressure development along the coal sample for the first N_2 injection is shown in Fig. 5(a). According to the figure, during the first N_2 injection, the steady-state injection pressure up to 600 mm away from the injection point, at region "*a*", is almost same as the pressures for all the injections. The pressure gap is negligible in region "*a*", and there are slight pressure gaps in region "*b*" between two intermediate points, and "*c*" (the second interme-diate point to the sample end). The pressure gap in region "*c*" is much steeper and the pressure gaps of both regions "*b*" and "*c*" decrease with increasing injection pressures (Table 2). As stated previously, throughout the N_2 injection, the system temperature was maintained at 38 °C constant value and injecting pressure was increased from 6 MPa to 10 MPa. Within this pressure–temperature region N_2 is not subjected to any phase transition (for N_2 the critical temperature is −146.8 °C and the critical pressure is 3.39 MPa). Therefore, there is no phase changing influence on N_2 flow, such as changing of chemical potential and the corresponding adsorption reaction with coal matrix or kinetic energy change (fluid release/energy absorption during their phase transition) throughout the samples in the entire test series. However, according to Fig. 5, there is a clear pressure gap throughout the sample under steady-state conditions (24 h after the injection). For example, only around 4.5 MPa downstream pressure could be achieved at 6 MPa injection pressure and only around 8.7 MPa downstream pressure could be achieved at 10 MPa injection pressure. As mentioned above, the pressure development downstream becomes steady by 24 h of injection (Fig. 4) and therefore, the pressure development throughout the sample after 24 h of injection can be considered as the ultimate pressure distribution along the sample. The pressure gap or gradient shown in Fig. 5(a) exhibits a pore pressure gradient throughout the coal sample, probably caused by the destruction of the advection flux after a certain pressure development due to the reduction of the pressure gap available for the flowing fluid. In actual field conditions, when a fluid is injected into a coal seam, it maintains its injection pressure in the critical zone of influence and a pressure gap exists thereafter. Therefore, for this experiment a 600 mm length from upstream can be considered as the critical zone of influence, as it maintains the injection pressure throughout the region. In addition, pressure development at 800 mm is around 87% of the injection pressure and at 1000 mm length is around 75% of the injection pressure.

Table 2
Pressure gradient along the sample for first N_2, CO_2 and second N_2 injection.

Region	Stage	Pressure gradient (%)				
		6 MPa	7 MPa	8 MPa	9 MPa	10 MPa
a (0–600)	1st N_2	1.67	1.56	1.50	1.11	1.00
	CO_2	3.33	5.71	2.50[a]	1.01[a]	0.95[a]
	2nd N_2	13.33	17.43	28.75	33.33	37.00
b (600–850)	1st N_2	11.86	11.18	10.89	4.49	5.05
	CO_2	7.69	8.62	4.04[a]	3.37[a]	3.03[a]
	2nd N_2	7.02	7.69	9.94	11.33	13.94
c (850–1000)	1st N_2	14.04	13.86	12.84	8.33	8.42
	CO_2	13.21	15.63	8.14	4.24[a]	3.45[a]
	2nd N_2	12.73	13.79	14.09	16.00	18.75

[a] Areas where CO_2 was in its super-critical state.

b. Flow behaviour along the coal sample during CO_2 injection

According to Fig. 5, the CO_2 migration pattern along the coal sample generally exhibits a trend similar to the N_2 migration pattern observed at the first N_2 injection, discussed above, and injection pressure is maintained throughout region "*a*" and considerable pressure gaps exist in regions "*b*" and "*c*" at steady state. Interestingly, increasing the injection pressure from 7 to 8 MPa significantly reduces the pressure gap for CO_2 compared to the first N_2 injection in both regions "*b*" (8.62–4.04% at CO_2 flow compared to 11.18–10.89% at first N_2 flow) and "*c*" (15.63–8.14% at CO_2 flow compared to 13.86–12.84% at first N_2 flow) (Table 2). It should be noted that CO_2 changes its phase condition from sub-critical to super-critical when the CO_2 pressure goes beyond 7.38 MPa, because the system temperature was maintained at 38 °C during the test, which is above the critical temperature of CO_2. This contrasts with the permeability behaviour of super-critical CO_2 discussed in the previous section, as super-critical CO_2 has much lower permeability values than sub-critical CO_2. Therefore a lower pressure development rate and eventually a higher pressure gap can be expected during super-critical CO_2 injection due its slow flow rate under the increased swelling effect. However, according to Fig. 5, super-critical CO_2 creates greater pressure development (fewer gaps) throughout the sample and therefore, there must exist another factor causing this pressure development. According to Perera et al. [23], super-critical CO_2 has liquid-like density, which is probably the key cause. Due to the higher density values of super-critical CO_2 (304.14 kg/m^3 for 8 MPa pressure and 38 °C temperature) compared to gas CO_2 (114.97 kg/m^3 for 5 MPa pressure and 38 °C temperature) [32], the amount of pressure development created by super-critical CO_2 within a fixed volume is clearly higher than the pressure created by the same amount of gas CO_2 in that volume. For this reason, although the number of CO_2 molecules passing through the coal sample is less under super-critical conditions, those molecules may create a higher pressure development throughout the sample.

The other important observation is the comparatively lower pressure gap in the sample under 9 MPa injection pressure at region "*c*" compared to that at 8 MPa injection pressure. Although the reduction of the pressure gap with increasing injection pressure seems to be common to all the injection pressures, the increment of injection pressure from 8 to 9 MPa causes the pressure gap to be significantly reduced at region "*c*" (8.14–4.24%). According to Fig. 5 (a), during 8 MPa CO_2 injection, although the CO_2 molecules in regions "*a*" and "*b*" are in super-critical condition, in region "*c*" they are at the sub-critical state. Therefore, CO_2 molecules in region "*c*" are in the gas condition at 8 MPa injection pressure and super-critical condition at 9 MPa injection pressure (the system temperature is 38 °C). As explained earlier, in the super-critical state gas molecules have higher density values and create greater pressure development within the same volume. This is confirmed by the fact that increasing the injection pressure from 9 to 10 MPa creates only a minor reduction in the pressure gap in regions "*b*" (3.37–3.03%) and "*c*" (4.24–3.45%). This is because, under both 9 MPa and 10 MPa injection pressures, all the CO_2 molecules inside the sample are in super-critical state after 24 h of injection, steady state (see Fig. 5(b)) and therefore, there is no influence of phase transition.

The CO_2 migration pattern through the coal seam after injection, is an important feature to study for both CO_2 sequestration and enhanced coal bed methane recovery projects. The reason is that the longer the CO_2 moves, the greater the amount of CO_2 stored and eventually, the greater the amount of methane produced.

c. Flow behaviour along the coal sample during the second N_2 injection

During the CO_2 flood the coal mass was subjected to internal structure modification due to CO_2 adsorption-induced swelling and the second N_2 injection was carried out into this reformed sample. A careful examination of pressure development patterns during the second N_2 injection was therefore made to identify the effect of this modification on the fluid flow behaviour inside the coal sample. According to Fig. 5(c) and Table 2, the pressure profiles along samples during the second N_2 injection are quite dif-ferent from the initial N_2 injection and CO_2 injection-caused pres-sure profiles, and there is a large pressure gap for each injection pressure in region "*a*" (Fig. 5(c)). In addition, in regions "*b*" and "*c*", the gap between the pressure developments corresponding to each injection pressure is greatly reduced and the corresponding pressure values are lower than the injection pressures (Fig. 5(c)). For example, the downstream pressures for 6 MPa and 10 MPa injection pressures are 3.9 MPa, and 5 MPa, respectively.

In order to understand this phenomenon, pressure development profiles along the sample for first and second N_2 injections were compared and the results are shown in Fig. 9. Fig. 9 clearly exhibits a steeper drop in the pressure profiles for the second N_2 injection compared to the first N_2 injection. Interestingly, the gap between the pressure profiles increases with increasing injection pressure, especially after 8 MPa injection pressure. As discussed previously, N_2 does not change its phase throughout the flow during the experiment as its critical point (critical temperature is −146.8 °C and critical pressure is 3.39 MPa) is well below the test conditions. The reason for these greater pressure drops after the 8 MPa injection pressure is therefore possibly related to the coal matrix swelling-created structure re-arrangement caused by the prior CO_2 flow. Now, N_2 is moving in this reformed coal sample and the steeper pressure gap after 8 MPa injection indicates that the super-critical CO_2 (>8 MPa) has created a greater structural re-arrangement in the coal mass compared to sub-critical or gas CO_2 (<8 MPa) (Table 2). This was expected, due to the greater chemical potential and swelling ability of super-critical CO_2. This implies that the pressure profiles made by the repeated N_2 flux after the CO_2 injection more clearly exhibit the swelling-caused structural re-arrangement effect than the CO_2 injection-caused pressure profile. It will be highly important in future CO_2 sequestration and ECBM research to closely examine the internal structural modification created by CO_2 adsorption in coal.

However, as it moves along the sample towards downstream, the steepness of the pressure reducing trend generally reduces. For example, at 8 MPa injection pressure, the pressure gap between the injection pressure and the end of region "*a*", region "*b*", and region "*c*" are around 28.75%, 9.94% and 14.09%, respectively. This also relates to the phase changing effect of CO_2. According to Fig. 5(b), throughout region "*a*" CO_2 exists in its super-critical state when the injecting CO_2 is super-critical (>7.38 MPa) and therefore, region "*a*" should have been subjected to greater internal structural modification caused by swelling. According to Fujioka et al. [8], the swelling due to super-critical CO_2 increases with the pressure. This is the reason for the increasing pressure gap with increased injection pressure in region "*a*". The reduced pressure gap in region "*b*" is due to the fact that under this injection pressure the CO_2 molecules in region "*b*" are only partially super-critical, whereas the CO_2 molecules in the latter portion of the region are in the sub-critical state (Fig. 5(b)). Therefore, the coal mass has been partially subjected to super-critical CO_2 adsorption, resulting in the effect of less structural modification on the second N_2 flux at region "*b*". Similarly, since the CO_2 molecules are in the sub-critical or gaseous state

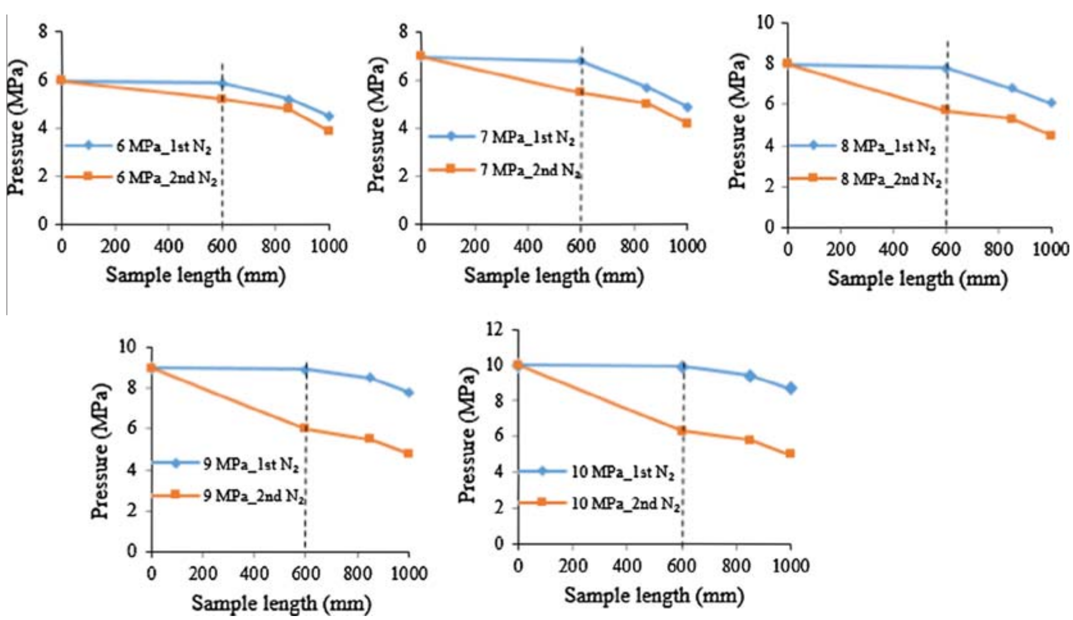

Fig. 9. Pressure profiles along the length of the sample for different injection pressures in first and second N_2 injection.

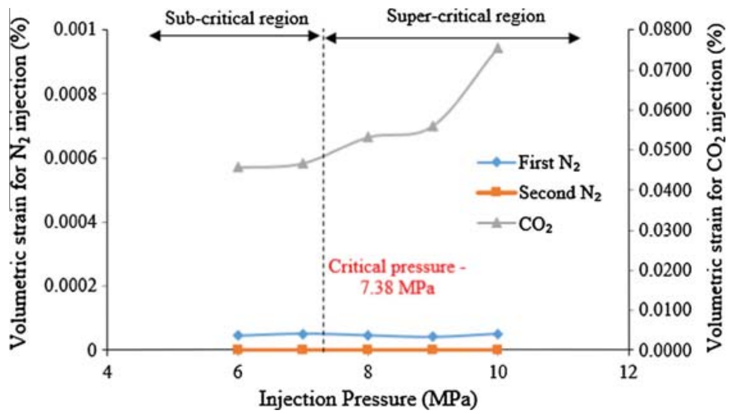

Fig. 10. Volumetric strain with different injection pressures for first N_2 injection, CO_2 injection and second N_2 injection.

throughout region "*c*" for 8 MPa injection, one would expect less swelling and structure modification compared to regions "*a*" and "*b*", resulting in a lower pressure gap. Although the pressure gap in region "*c*" is comparatively much less than the pressure gap observed in region "*a*", the gap is slightly higher than that in region "*b*". This is due to the greater distance from the injection point, since the longer the distance, the fewer the migrated N_2 molecules, resulting in less pressure development and accordingly a higher gap. As mentioned earlier, after the build-up of a certain pressure downstream (and the corresponding pressure development throughout the sample), there is insufficient pressure gap to create an advection flux (the pressure-driven flow of coal in cleats).

5.2.3.3 A quantitative approach to CO_2 adsorption-induced coal matrix swelling

According to the above findings, CO_2 adsorption-induced coal matrix swelling creates significant changes to the fluid flow behaviour in coal. A quantitative approach was therefore adopted to identify this real swelling effect created by CO_2 adsorption under different injection conditions, by measuring the sample volume change under each injection condition (Fig. 6). According to Fig. 6, the coal sample volume increases with time during all the CO_2 injections, probably due to the coal matrix swelling caused by CO_2 adsorption. Since this may also have been influenced by the injection pressure created pore pressure increment, the sample volume change under N_2 injection for the same injection pressures (6–10 MPa) was also examined. According to Fig. 6, the sample seems to be subjected to shrinkage during all the N_2 injection conditions. Such shrinkage might occur in the coal mass with time due to the external stress application creating compaction, and this shows that the previously reported sample expansion during CO_2 injection is related to the coal matrix swelling created by CO_2 adsorption.

These sample volume changes were then used to calculate the volumetric strain (sample volume change after 24 h/initial sample volume) under each injection condition and the results are shown in Fig. 10. According to this figure, although there is a clear volumetric swelling in the coal sample during CO_2 injection, both first and second N_2 injections do not create such noticeable volumetric changes to the coal sample. Katyal et al. [33] suggested that swelling is caused by the vastly cross-linked macromolecular network of coal, which is subjected to swelling in the presence of CO_2. According to Harpalani and Chen [15], this swelling alters the surface area and the pore structure of the coal mass, resulting in reduced seam permeability. As discussed earlier, N_2 is a relatively inert gas which does not cause any noticeable swelling in the macromolecular network of coal, and therefore, creates a negligible swelling effect. However, the first N_2 injection seems to create a very small volumetric strain (average volumetric strain of 4.74E−05%) in the coal sample compared to the later N_2 injection (average volumetric strain of 2.82E−07%) (see Fig. 10). This is suspected to be related to the pore space expansion created by the increased pore water pressure during N_2 injection in the fresh coal sample. Katyal et al. [33] stated that water and CO_2 share a similar kind of relationship with coal and consequently, coal mass is likely to create small changes in volume (Fig. 10) which may be the reason for the comparatively higher volumetric strain during the first N_2 injection. For the second N_2 injection, the sample has already been subjected to expansion with pore water pressure increment, and therefore, there is no further volumetric strain for the same injection pressures.

Moreover, according to Fig. 10, the volumetric swelling produced by CO_2 adsorption appears to significantly increase with increasing CO_2 injection pressure. For example, swelling causes the induction of 12% and 38% volumetric strain in the coal sample for 8 MPa and 10 MPa, injection pressures, respectively. A similar swelling behaviour has been observed by Ozdemir et al., [5] after conducting a series of experiments for different coal types including lignite, which showed an increasing trend of swelling with increasing CO_2 pressure. As discussed earlier, super-critical CO_2 creates greater swelling in coal mass than sub-critical CO_2 (Fig. 10) and increasing injection pressure causes more of the CO_2 inside the coal sample to be super-critical (Fig. 5). Therefore, increasing injection pressure clearly causes a greater degree of swelling in the coal matrix.

5.2.4 Conclusions

This study was conducted to identify the influences of sub- and super-critical CO_2 injections on coal matrix swelling and the associated permeability alterations using macro-scale reconstituted Victorian brown coal samples. The following major conclusions can be drawn from the experimental results:

CO_2 permeability in coal may reduce with increasing injection pressure due to the phase transition of CO_2 from sub-critical to super-critical during the pressure increment. This is because the movement of super-critical CO_2 in coal results in greater coal matrix swelling and eventually reduced CO_2 injectability into the coal mass. This has been confirmed by the fact that N_2 injection into a coal mass permeated with CO_2 produces much lower permeability values than N_2 injection into a fresh coal sample, because the coal mass structure has already been critically reformed during the CO_2 flood.

Pressure profiles along the sample length were then examined for each injection by considering the pressure gaps at three main regions along the sample; region "*a*" (600 mm from the injection point), region "*b*" (between 600 to 850 mm) and region "c" (850 mm to sample end, 1 m). According to the results, although the pressure development trends for all three injections along the samples are similar, there is a noticeable pressure reduction in the initial region of the samples (region "*a*") during the second N_2 injection. This is due to the coal structure re-arrangement which occurred during the CO_2 flood, and the pressure development seems to be much less in the regions where CO_2 was in the super-critical state. This is because super-critical CO_2 adsorption-induced swelling is higher than that of sub-critical CO_2.

Increasing the injection pressure beyond the critical pressure of CO_2 (7.38 MPa) may cause a greater pressure development (fewer gaps) along the coal mass, even under the greater permeability reduction created by the super-critical CO_2 adsorption-induced swelling. This is due to the higher density values of super-critical CO_2 compared to gas CO_2 that create a higher pressure development within a fixed volume compared to the same amount of gas CO_2 in that volume. This is confirmed by the fact that with further increase of injection pressure after the whole sample has super-critical CO_2, may create only minor changes in pressure gaps along the sample. These CO_2 and N_2 migration patterns through coal seams after injection are highly important for field applications such as CO_2 sequestration and enhanced coal bed methane recovery. The reason is that, the longer the distance that CO_2 and N_2 travel, the greater the amount of CO_2 stored, and eventually, the greater the amount of methane produced. CO_2 adsorption-induced coal matrix swelling was then quantitatively determined by measuring the volumetric strain of samples under each injection condition. According to the results, super-critical CO_2 causes greater swelling of the coal mass than sub-critical CO_2 and the swelling of coal mass increases with injection pressure. This is consistent with the prescribed pressure development and permeability made conductions.

5.2.5 Acknowledgement

The authors want to express their appreciation for the funding provided by Australian Research Council (DE130100124).

5.2.6 References

[1] Perera MSA, Ranjith PG. Carbon dioxide sequestration effects on coal's hydro-mechanical properties: a review. Int J Energy Res 2012;36:1015–31.
[2] Perera MSA, Ranjith PG, Choi SK, Bouazza A, Kodikara J, Airey D. A review of coal properties pertinent to carbon dioxide sequestration in coal seams: with special reference to Victorian brown coals. Environ Earth Sci 2011;64:223–35.
[3] Stevens SH, Kuuskraa VA, Gale J, Beecy D. CO_2 injection and sequestration in depleted oil and gas fields and deep coal seams: worldwide potential and costs. Environ Geosci 2001;8:200–9.
[4] White CM, Smith DH, Jones KL, Goodman AL, Jikich SA, LaCount RB, et al. Sequestration of carbon dioxide in coal with enhanced coalbed methane recovery: a review. Energy Fuels 2005;19:659–724.
[5] Ozdemir E, Morsi BI, Schroeder K. CO_2 adsorption capacity of Argonne premium coals. Fuel 2004;83:1085–94.
[6] Perera MSA, Ranjith PG, Peter M. Effects of saturation medium and pressure on strength parameters of Latrobe Valley brown coal: carbon dioxide, water and nitrogen saturations. Energy 2011;36:6941–7.
[7] Vishal V, Ranjith PG, Singh TN. CO_2 permeability of Indian bituminous coals: implications for carbon sequestration. Int J Coal Geol 2013;105:36–47.
[8] Fujioka M, Yamaguchi S, Nako M. CO_2-ECBM field tests in the Ishikari Coal Basin of Japan. Int J Coal Geol 2010;82:287–98.
[9] Reeves S, Taillefert A. Reservoir modeling for the design of the RECOPOL CO_2 sequestration project, Poland. In: Topical Report 2002. <http://citeseerx.ist.psu.edu/viewdoc/download?doi=10.1.1.463.4379&rep=rep1&type=pdf> [accessed 03.04.14].
[10] Reeves SR. Enhanced CBM recovery, coalbed CO_2 sequestration assessed. Oil Gas J 2003;101:49–53.
[11] Levine JR. Hydrocarbons from coal, chapter 3 – coalification: the evolution of coal as source rock and reservoir rock for oil and gas; 1993, p. 40.
[12] Flores RM. Coal and coalbed gas: fueling the future. Waltham, MA: Newnes Elsevier; 2013. p. 44.
[13] Jing X, Mingzhong G, Bin Y, Ru Z, Wencheng J. Coal permeability model on the effect of gas extraction within effective influence zone. Geomech Geophys Geo-Energy Geo-Resour 2015. http://dx.doi.org/10.1007/s40948-015-0002-2.
[14] Sawyer W, Paul G, Schraufnagel R. Development and application of a 3D coalbed simulator. CIM/SPE 1990:90–119.
[15] Harpalani S, Chen G. Estimation of changes in fracture porosity of coal with gas emission. Fuel 1995;74:1491–8.
[16] Ranathunga AS, Perera MSA, Ranjith PG. Deep coal seams as a greener energy source. a review. J Geophys Eng 2014;11:063001.
[17] De Silva PNK, Ranjith PG. Understanding the significance of in situ coal properties for CO_2 sequestration: an experimental and numerical study. Int J Energy Res 2014;38:60–9.
[18] Jasinge D, Ranjith PG, Choi SK. Effects of effective stress changes on permeability of Latrobe Valley brown coal. Fuel 2011;90:1292–300.
[19] Vishal V, Ranjith PG, Pradhan S, Singh TN. Permeability of sub-critical carbon dioxide in naturally fractured Indian bituminous coal at a range of down-hole stress conditions. Eng Geol 2013;167:148–56.
[20] Viete DR, Ranjith PG. The effect of CO_2 on the geomechanical and permeability behaviour of brown coal: implications for coal seam CO_2 sequestration. Int J Coal Geol 2006;66:204–16.
[21] Stacy WO, Jones JC. The swelling and adsorption characteristics of Victorian brown coals. Fuel 1986;65:1171–3.
[22] Day S, Fry R, Sakurovs R, Weir S. Swelling of coals by supercritical gases and its relationship to sorption. Energy Fuels 2010;24:2777–83.
[23] Perera MSA, Ranjith PG, Airey DW, Choi SK. Sub- and super-critical carbon dioxide flow behavior in naturally fractured black coal: an experimental study. Fuel 2011;90:3390–7.
[24] De Silva PNK, Ranjith PG. Advanced core flooding apparatus to estimate permeability and storage dynamics of CO_2 in large coal specimens. Fuel 2013;104:417–25.
[25] Siriwardane H, Haljasmaa I, McLendon R, Irdi G, Soong Y, Bromhal G. Influence of carbon dioxide on coal permeability determined by pressure transient methods. Int J Coal Geol 2009;77:109–18.
[26] Huy PQ, Sasaki K, Sugai Y, Ichikawa S. Carbon dioxide gas permeability of coal core samples and estimation of fracture aperture width. Int J Coal Geol 2010;83:1–10.
[27] Somerton WH, Söylemezoğlu I, Dudley R. Effect of stress on permeability of coal. Int J Rock Mech Min Sci Geomech Abstr 1975:129–45.
[28] Kiyama T, Nishimoto S, Fujioka M, Xue Z, Ishijima Y, Pan Z, et al. Coal swelling strain and permeability change with injecting liquid/supercritical CO_2 and N_2 at stress-constrained conditions. Int J Coal Geol 2011;85:56–64.
[29] Bae J-S, Bhatia SK. High-pressure adsorption of methane and carbon dioxide on coal. Energy Fuels 2006;20:2599–607. http://dx.doi.org/10.1021/ef060318y.
[30] Massarotto P, Golding S, Bae J-S, Iyer R, Rudolph V. Changes in reservoir properties from injection of supercritical CO_2 into coal seams—A laboratory study. Int J Coal Geol 2010;82:269–79.
[31] Okamoto I, Li X, Ohsumi T. Effect of supercritical CO_2 as the organic solvent on cap rock sealing performance for underground storage. Energy 2005;30:2344–51.
[32] McLinden M, Klein S, Lemmon E, Peskin A. REFPROP, thermodynamic and transport properties of refrigerants and refrigerant mixtures. NIST Stand Ref Database 1998:23.
[33] Katyal S, Valix M, Thambimuthu K. Study of parameters affecting enhanced coal bed methane recovery. Energy Sources Part A 2007;29:193–205.

5.3 How do CO_2 properties and in situ stresses affect CO_2 storage capacity?

As stated in Section 5.2, CO_2 adsorption-induced coal matrix rearrangements lead to reduced flow abilities in coal. These flow abilities can further vary due to the greater effective stress on the coal mass, as discussed in Sections 4.2 and 4.3 for natural meso-scale brown coal samples. Therefore, it is interesting to investigate the effect of effective stress on macro-scale reconstituted coal specimens and this is the subject of this section. A series of core flooding experiments was conducted on Australian brown coal using the advanced core flooding apparatus. A range of CO_2 injection pressures (6 to 14 MPa) under 17 MPa axial stress were utilised for the study and the results were compared with the results of 11 MPa axial stress (see Section 5.2) to obtain the effect of greater in situ stresses. The volume changes of the sample and the CO_2 flow along the coal sample were also measured, to comprehend CO_2-induced coal matrix swelling and its effect on coal permeability. Finally, the CO_2 storage capacity was measured under different test conditions to quantify the ability of brown coal to store CO_2 which is important for CO_2 sequestration.

The following journal paper was produced from this chapter:

Ranathunga AS, Perera MSA, Ranjith PG, De Silva GPD (2016). A macro-scale view of the influence of effective stress on carbon dioxide flow behaviour in coal: An experimental study. *Geomechanics and Geophysics for Geo-Energy and Geo-Resources*, 1-16.

5.3.1 Introduction

Due to its ability to reduce the amount of anthropogenic carbon dioxide (CO_2) in the environment, CO_2 sequestration in deep un-mineable coal seams has been identified as an effective method to address global warming (Jing et al. 2015; Verma and Sirvaiya 2016; White et al. 2005). Based on the fact that the coal mass has greater affinity to CO_2 than other gases like methane (CH_4) and nitrogen (N_2) due to its greater chemical and physical interaction, in return the sequestration process releases coal bed methane (CBM), which is an environmentally-friendly energy source with higher efficiency (White et al. 2005). However, according to the research literature (Day et al. 2008; Hol and Spiers 2012; Jing et al. 2015; Larsen et al. 1997; Pan and Connell 2007; Wang et al. 2013), the sequestration of CO_2 disrupts the stability of the original coal structure with apparent changes in coal matrix swelling, which decreases the CO_2 injectivity into the coal seam and affects its long-term stability. It is therefore important to study the principles of coal mass swelling and to have a better understanding of the factors affecting this process.

A number of studies have been conducted on coal seam permeability upon CO_2 sequestration and the effects of various factors on this have been highlighted, including injecting

CO_2 properties (Jasinge 2010; Day et al. 2008; Pan and Connell 2007; Perera et al. 2011; Siriwardane et al. 2009; Vishal and Singh 2015) and coal mass properties (Merkel et al. 2015; Wang et al. 2013). According to the research, potential coal seams for CO_2 sequestration with higher temperatures and pressures have limited CO_2 flow ability, because CO_2 is in its super-critical state (beyond 7.38 MPa pressure and 31.8^{0}C temperature CO_2 exists as super-critical fluid) and has greater sorption capacity in such seams.

On the other hand, it is well known that coal is a highly heterogeneous material and it is therefore quite difficult to validate the results obtained from natural coal samples for in situ coal seams (De Silva 2013). Jasinge (2010) and Liu et al. (2016) found that reconstituted coal (RC) samples with reproducible properties can be used to successfully represent natural coal specimens to overcome such difficulties. The following section focuses on some previous studies conducted on RC and natural samples.

5.3.2 Comparison of fluid flow behaviour in reconstituted and natural coal

To date, many studies have been conducted to identify the flow behaviour in natural coal seams using reconstituted coal samples and satisfactory results have been obtained. Figure 5.1 illustrates a study that compares N_2 and CO_2 permeability and the related swelling in natural and reconstituted Australian low rank coal (Jasinge, 2010).

According to Figure 5.1(a), N_2 flow linearly reduces with increasing effective stress in both natural and RC samples, and CO_2 flow (Figure 5.1(b)) follows a negative exponential variation, exhibiting the unfavourable effect of CO_2 exposure on coal permeability. Further, the RC specimens show higher permeability than natural specimens for both N_2 and CO_2 flow (see Figs. 5.1(a) and (b)). Similar results were obtained by Liu et al. (2016), who injected CH_4 (~0.69 MPa) into coking coal from the Hexi coal mine, China under different confining pressures (from around 2-7 MPa), and showed higher permeability for RC specimens than natural coal samples. This indicates the differences in fracture system characteristics, such as fracture porosity and connectivity, of the reconstituted coal sample and the natural coal sample. Further attention to coal mass swelling with N_2 and CO_2 permeation reveals that N_2 injection does not show any significant variation in swelling with effective stress (Figure 5.1(c)) for both natural and RC samples. Conversely, CO_2 flow causes the coal mass swelling to undergo an increasing trend with the increase of injection pressure (Figure 5.1(d)) for both natural and RC specimens. However, RC specimens display a comparatively higher coal matrix swelling compared to natural specimens during CO_2 flow. This is probably caused by the greater amount of CO_2 molecules entering the coal mass due to the higher permeability in RC samples than natural samples, which interact with the coal mass and cause greater swelling. This may also contribute to the observed permeability variations (Figure 5.1(b)), with lower permeability reductions for natural samples than RC samples during CO_2 permeation. However, the correlation between swelling and permeability of coal generally shows a similarity in both natural and RC specimens, allowing the use of RC specimens for experimental purposes (Jasinge 2010; Liu et al. 2016).

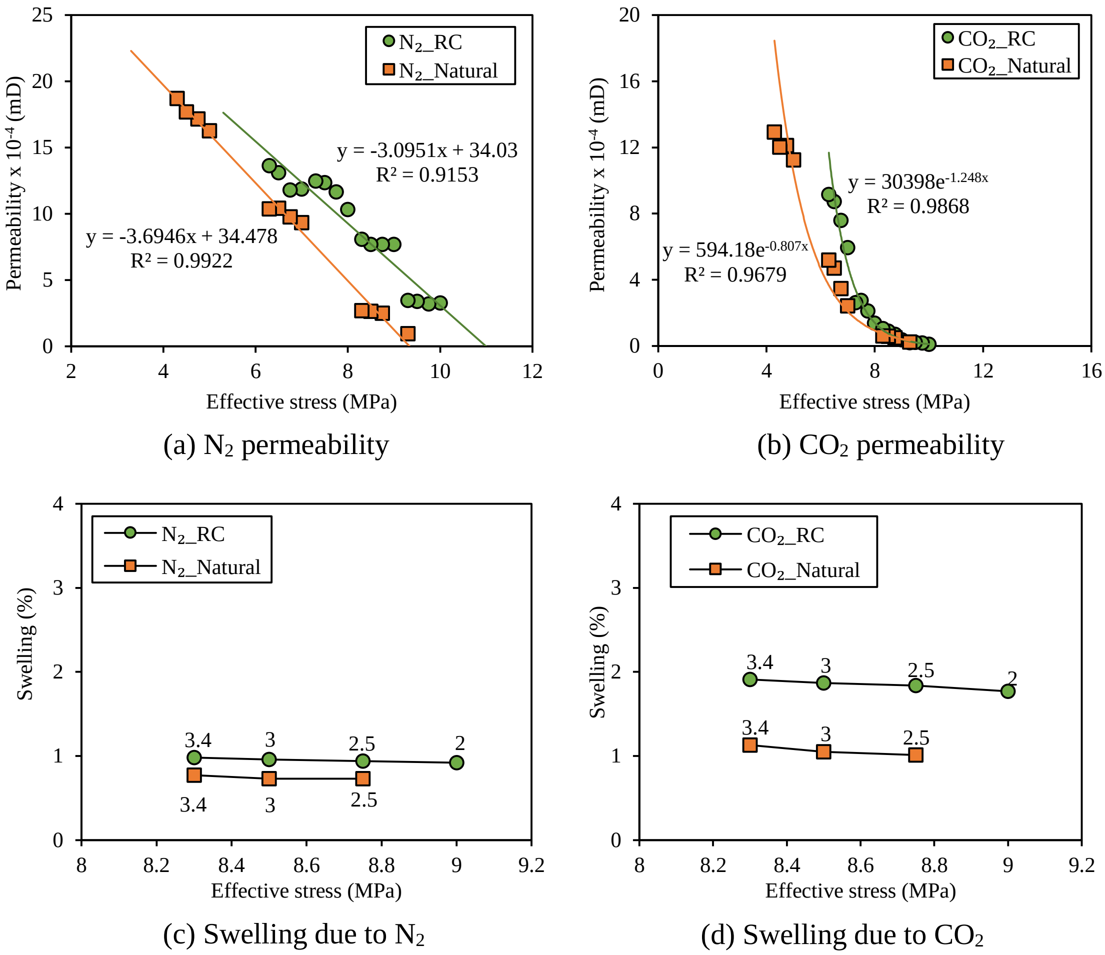

Figure 5.1. N_2 and CO_2 permeability and coal mass swelling variation with effective stress for reconstituted coal (RC) and natural coal specimens (Jasinge 2010) (The data labels in (c) and (d) denote the respective injection pressures)

5.3.3 Studies of CO_2 flow behaviour using macro-scale coal specimens

As reported in the literature (Day et al. 2008; Jasinge 2010; Pan et al. 2010; Perera et al. 2011; Siriwardane et al. 2009; Sun et al. 2016; Vishal and Singh 2015), most coal CO_2 injection studies have been conducted using meso-scale samples (up to around 100 mm in length). This has caused difficulties in confirming the applicability of adsorption theories at a higher scale to the estimation of CO_2 storage capacity (De Silva 2013). Hence, De Silva (2013) conducted advanced core-flooding tests using 1 m long and 203 mm diameter (macro-scale) RC low rank coal samples to estimate CO_2 flow behaviour in coal, in order to overcome the scale effect. De Silva (2013) basically focused on the sub-critical CO_2 flow in large coal samples and Ranathunga et al. (2015) extended this study to super-critical CO_2 to represent actual CO_2 flow behaviour in deep coal seams, considering the CO_2 flow behaviour along the sample. The following sections summarise some major findings of the macro-scale core flooding experiments conducted on CO_2 injection.

5.3.3.1 Sub-critical CO_2 injection

De Silva (2013) conducted a series of tests of sub-critical CO_2 injection (from 0.4 MPa to 7.4 MPa) under 1, 2, 4, 6 and 8 MPa axial stresses and observed a reduction in CO_2 permeability with increasing CO_2 injection pressure and axial stress (Figure 5.2). CO_2 adsorption-induced coal matrix swelling is the main cause of this permeability reduction and this was proved by the related swelling data (Figure 5.2). According to Figure 5.2, the coal volumetric strain is increased with increasing injection pressure. Further, according to the figure, the increase of axial stress causes a reduction in permeability for CO_2 movement, probably due to the greater effective stresses on the coal mass.

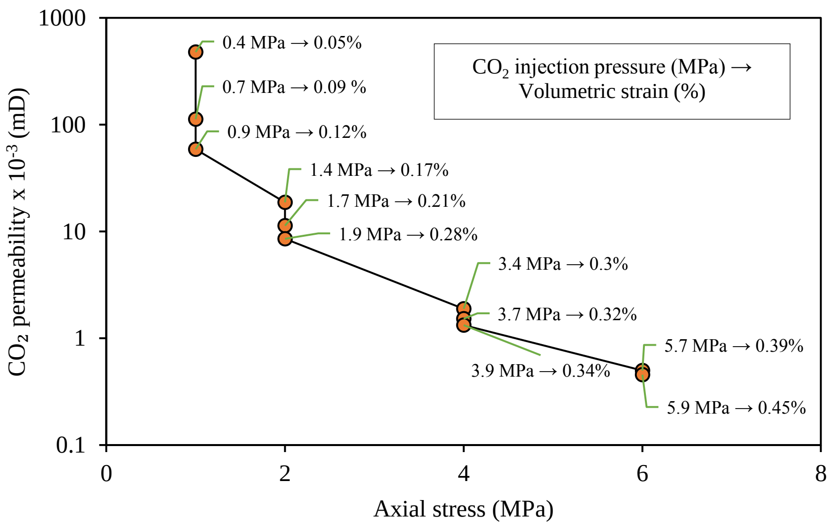

Figure 5.2. CO_2 permeability variation with axial stress and volumetric strain for different CO_2 injection pressures (The first value of the label denotes the CO_2 injection pressure (MPa) and the second value denotes the respective volumetric strain (%)) (De Silva 2013)

5.3.3.2 Super-critical CO_2 injection

As potential coal seams for CO_2 sequestration undergo super-critical CO_2 injection, Ranathunga et al. (2015) conducted a series of tests using super-critical CO_2 to understand the variations of CO_2 phase in large-scale coal specimens. They injected 6 to 10 MPa CO_2 into low rank RC specimens under a constant temperature of 38 ℃ (> 31.8 ℃, the critical temperature of CO_2) and under 11 MPa axial stress. They injected N_2 before (first N_2 injection) and after the CO_2 injection (second N_2 injection) to quantify the CO_2 flow-induced coal mass changes, and the N_2 and CO_2 permeability variations obtained are illustrated in Figure 5.3.

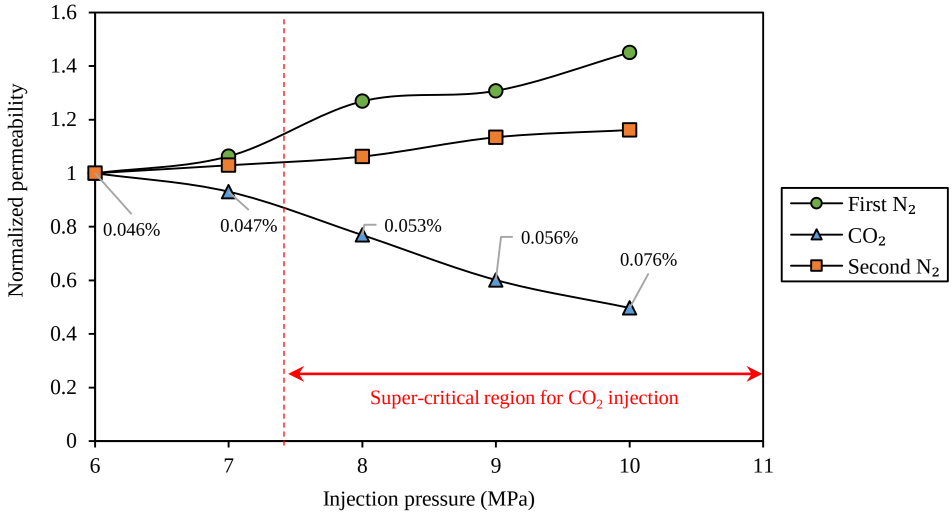

Figure 5.3. Permeability variation with different injection pressures for first N_2 injection, CO_2 injection and second N_2 injection (Ranathunga et al. 2015) (The data labels indicate the coal specimen's volumetric strain (%) under CO_2 injection. The permeability values have been normalized by dividing each value by the permeability obtained for 6 MPa in each injection condition)

According to Figure 5.3, the results are consistent with the results obtained by De Silva (2013) for sub-critical CO_2, showing a reduction of permeability with increasing CO_2 injection pressure. However, it can be noted that the reduction is comparatively higher in the super-critical region compared to sub-critical CO_2. For example, there is around a 7% decrease in permeability from 6 to 7 MPa for sub-critical CO_2 injection and around 21% permeability decrease from 8 to 9 MPa for super-critical CO_2 injection. This reduction is three times higher than in sub-critical CO_2 flow. The main reason for this observation is the greater adsorption capacity of super-critical CO_2, as a result of its more chemically active nature, liquid-like density and viscosity, which cause greater coal mass swelling compared to sub-critical CO_2 (Day et al. 2008). This is further evident from the volumetric swelling data for both regions (Figure 5.3). Furthermore, the comparative reduction of the second N_2 flow compared to the first N_2 flow clearly illustrates the coal mass changes which occur upon exposure to CO_2. For example, at 6 MPa, the first N_2 to the second N_2 injection shows around 17% permeability reduction, and that for 8 MPa is around 31%. As N_2 is a comparatively less adsorptive gas than CO_2 (Perera et al. 2011), this observed flow variation clearly occurs due to coal mass swelling during CO_2 flux.

In addition, De Silva (2013) observed a decrease in CO_2 permeability in coal with increasing effective stress (axial stress) for sub-critical CO_2. Hence, it is important to investigate how super-critical CO_2 flow changes with increasing effective stress. Ranathunga et al. (2017) conducted a series of meso-scale experiments to investigate this super-critical CO_2 effect for similar low rank natural coal samples and observed the similar behaviour of CO_2 flow and permeability reduction with increasing effective stress. Table 5.1 lists some of the results obtained by Ranathunga et al. (2017) for 6 to 7 MPa (sub-critical CO_2), 7 to 8 MPa (the CO_2 phase-changing region), and 8 to 9 MPa (super-critical CO_2) flow increments under 11, 14 and 17 MPa axial stresses.

According to Table 5.1, reduction of permeability with increasing effective stress is evident, and greater permeability reduction in deep coal seams is shown during CO_2 sequestration. Furthermore, this reduction is gradually increased (around 18%) when the CO_2 phase is changed, being comparatively greater in super-critical CO_2 compared to sub-critical CO_2. The opportunity for more adsorptive super-critical CO_2 molecules to interact with the coal matrix, creating increased matrix rearrangements, is the main reason for this observation (Perera et al. 2011). However, this may create complications for CO_2-ECBM in deeper coal seams for CO_2 injectivity and productivity. Hence, further research is needed to gain a better understanding of this phenomenon for application in the field.

Table 5.1. Variation of CO_2 permeability with effective stress (Ranathunga et al. 2017)

	Permeability variation (%)		
Confining pressure (MPa)	**6 to 7 MPa sub-critical CO_2 flow increment**	**7 to 8 MPa CO_2 phase changing region**	**8 to 9 MPa super-critical CO_2 flow increment**
11 (around 400m depth)	-1.8*	-9.7*	-19.2*
14 (around 500m depth)	-7.6*	-12.4*	-25.1*
17 (around 600m depth)	-10.6*	-23.2*	-30.3*

*A negative sign indicates permeability reduction

The main objective of this study is therefore to develop knowledge of coal mass behaviour with CO_2 exposure using macro-scale reconstituted low rank coal samples, and in particular to identify the influence of axial stress on large-scale samples. The present study can therefore be considered as an extension of the work of De Silva (2013) and Ranathunga et al. (2015), which pays more attention to super-critical CO_2 flow behaviour in coal located at various depths using macro-scale coal samples. An effort is also made to quantify the corresponding CO_2 storage capacity variation with various effective factors (CO_2 phase, pressure and seam depth).

5.3.4 Experimental methodology

The advanced core-flooding apparatus available in the Deep Earth Energy Research Laboratory (DEERL) at Monash University was used to conduct this study. A detailed description of the apparatus can be found in Chapter 3 and the experimental procedure is briefly described below.

5.3.4.1 Sample preparation

In this experiment, RC samples were prepared using powdered low rank brown coal. The coal powder was obtained from coal blocks taken from the Hazelwood open-cut coal mine at Morwell in Gippsland, Victoria. The samples had a natural moisture content of around 55%. The RC specimen construction procedure is shown in Figure 5.4, and the detailed methodology adopted to construct the RC samples can be found in Chapter 3.

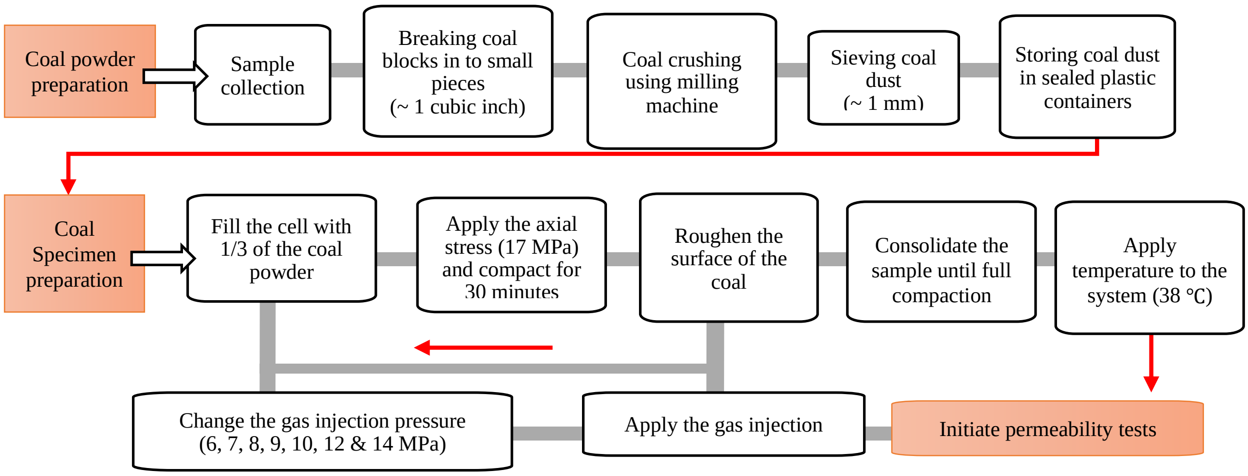

Figure 5.4. Experimental program for core flooding tests

5.3.4.2 Permeability tests

Permeability tests were conducted for CO_2 injections for seven different injecting pressures (6, 7, 8, 9, 10, 12 and 14 MPa) under 17 MPa axial stress, maintaining the system temperature at 38 ℃. Since the system temperature was maintained at 38 ^{0}C, 6 and 7 MPa CO_2 injections were under sub-critical conditions and the rest of the CO_2 injections were under super-critical conditions (beyond 7.38 MPa pressure and 31.8^{0}C temperature CO_2 exists as a super-critical fluid). The undrained condition was maintained to determine the sample permeability, and the pressure-transient approach was used calculate the permeability (Pan et al. 2010; Perera et al. 2011). CO_2 injection was performed, maintaining the injection pressure at a steady state for each injection pressure (6, 7, 8, 9, 10, 12 and 14 MPa). The corresponding pressure developments at intermediate points along the sample and downstream were monitored and recorded using an advanced data acquisition system.

The permeability of the coal sample was then calculated using Eqs. [5.1] and [5.2] (Perera et al. 2011) upon downstream pressure development reaching steady state:

$$Q = \left(\frac{dP}{dt}\right) \times \beta V_d \qquad [5.1]$$

$$k = \frac{2QP_O\mu L}{A(P_i^2 - P_O^2)} \qquad [5.2]$$

where, Q is the flow rate through the specimen, V_d is the downstream volume, β is the adiabatic compressibility of the gas, and *dP/dt* is the rate of change in the downstream pressure with time, μ is the viscosity of the injecting fluid, A is the cross-section area of the sample (0.0324 m^2), L is the length of the sample (937 mm for this study after full consolidation), and P_i and P_o are the upstream and downstream pressures, respectively. The viscosity and the adiabatic compressibility were calculated using the REFPROP database (McLinden et al. 1998) for the respective CO_2 pressures and a constant temperature (38 ℃). The corresponding permeability values of the sample for 17 MPa axial stress are shown in Figure 5.5.

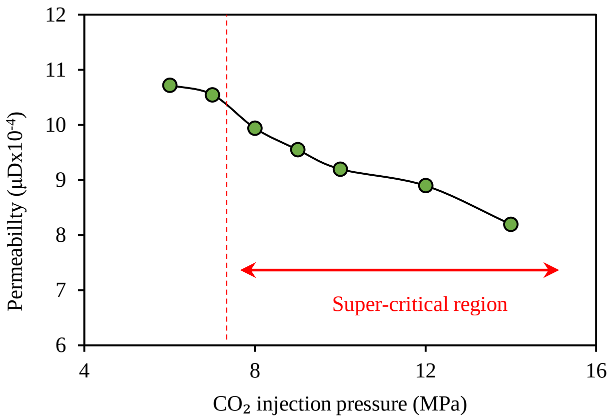

Figure 5.5. CO_2 permeability variation with CO_2 injection pressures for 17 MPa axial stress

5.3.4.3 Coal matrix swelling measurement

During each test, the sample length variation was recorded using a linear variable differential transformer (LVDT) at 1s intervals to quantify the CO_2 adsorption-induced coal matrix swelling in the RC specimen. The volumetric swelling was then calculated using the measured length change of the sample using Eq. [5.3], because movement in the radial direction was restrained in the tests by the steel casing. When the sample was subjected to swelling, the sample length was accordingly increased and for shrinkage, the sample length was consequently decreased.

$$\text{Volumetric strain of the coal sample} = \frac{L_t - L_o}{L_o} \times 100\% \qquad [5.3]$$

It should be noted that this volumetric strain value includes the effect of both CO_2 adsorption-induced coal mass alterations and consolidation due to the application of axial stress.

5.3.5 Results and discussion

A series of permeability tests was conducted for seven different CO_2 injection pressures under 17 MPa axial stress using a macro-scale RC low rank coal sample, and the results obtained are discussed in the following sections.

5.3.5.1 Carbon dioxide flow along the coal sample

a. Effect of injected carbon dioxide properties on coal mass permeability

According to Figure 5.5, CO_2 permeability reduces with increasing CO_2 injection pressure at 17 MPa axial stress, and the reduction is relatively higher for super-critical CO_2. For example, increasing the injection pressure from 6 to 7 MPa sub-critical CO_2 flow caused around 11% permeability reduction and increasing the injection pressure from 8 to 9 MPa super-critical CO_2 flow caused a much larger permeability reduction of around 38%. As explained previously, CO_2 adsorption-induced coal matrix swelling is the main cause of this observed permeability reduction with increasing injection pressure. Similar results were reported by Ranathunga et al. (2015) for 11 MPa axial stress following similar macro-scale tests using the same type of RC coal samples, and a comparison of CO_2 permeability variations under 11 and 17 MPa axial stresses with respective to volumetric strain is presented in Figure 5.6.

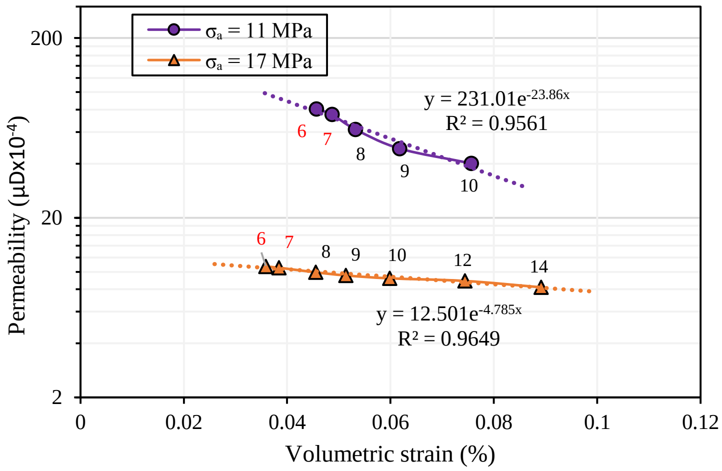

Figure 5.6. CO_2 permeability vs. coal mass volumetric strain variation under 11 MPa (Ranathunga et al. 2015) and 17 MPa axial stresses (Red data labels denote sub-critical and black data labels denote super-critical CO_2 injections)

According to Figure 5.6, CO_2 permeability and the volumetric swelling of the specimen follow a negative exponential variation for both axial stresses, confirming the reason for the observed reduced CO_2 flow ability with injection pressure. According to Day et al. (2010), the greater adsorption capacity of CO_2 at higher pressures results in greater matrix alterations, causing reduced permeabilities. Figure 5.7 shows the variation of CO_2 properties of viscosity and compressibility with increasing CO_2 pressure at 38 ^{0}C (the temperature used for the current experiment). According to Figure 5.7, CO_2 properties are significantly changed in the super-critical region, where significant increments in viscosity and reductions in compressibility with increasing pressure can be seen. This inordinate increment of viscosity (Figure 5.7(a) and (c)) provides greater fluidity for super-critical CO_2, which increases the adsorption capacity of the coal mass, and the reduction of compressibility of super-critical CO_2 (Figure 5.7(b)) constrains the amount of CO_2 molecules entering the coal matrix. These are the reasons for greater coal mass swelling and the lower permeabilities obtained with increasing CO_2 injection pressures.

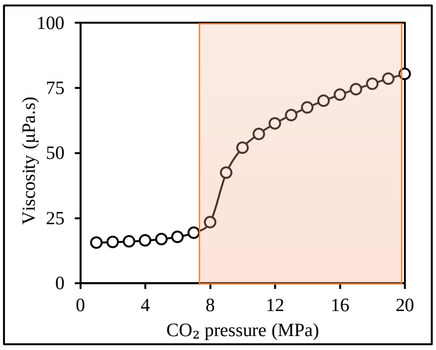

(a) Viscosity

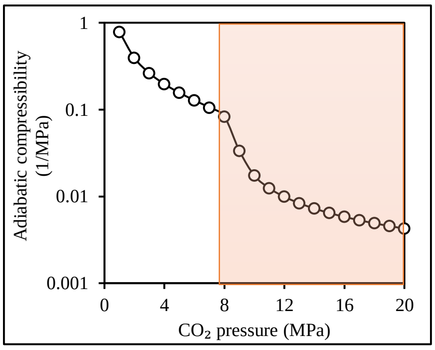

(b) Compressibility

Figure 5.7. Variation of CO_2 properties with pressure (McLinden et al. 1998) (The shaded area is under super-critical conditions)

However, this coal matrix swelling also varies with time and this was considered next. Figure 5.7 exhibits the volumetric strain variations with time (the injection period is the time taken to reach the steady state at downstream and the additional 10 days (approximately) allowed for swelling-induced matrix changes.). According to the figure, the volumetric strain exponentially increases with time. Due to the lower permeabilities under higher CO_2 pore pressures, it took longer durations to obtain the steady-state conditions than for lower CO_2 permeabilities. Therefore, this additional time allowed CO_2 and coal to have greater interactions, creating larger volumetric strain variations for higher CO_2 floods (Figure 5.7). If this concept is applied to the field conditions, long-term sequestration of CO_2 can reduce CO_2 injectivity by causing greater coal matrix swelling, confirming the observed reductions of CO_2 injections within 6 months to 2 years in field projects (refer to Chapter 2).

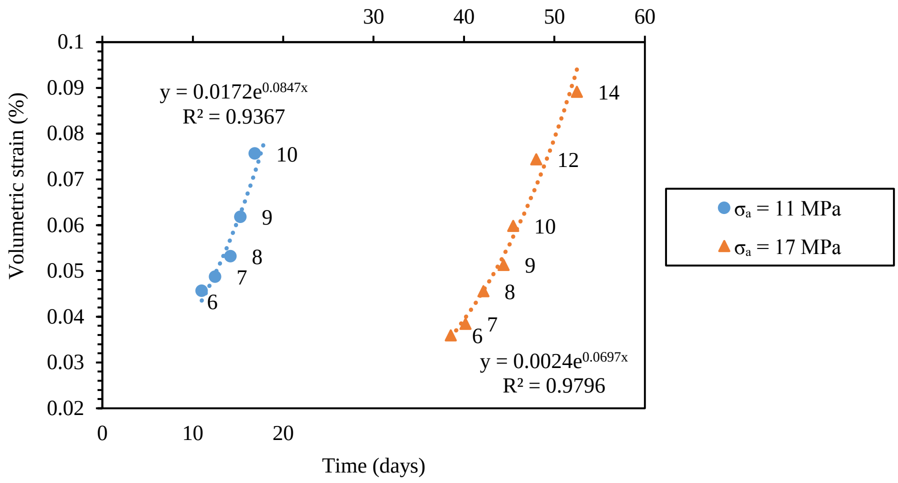

Figure 5.7. Coal mass volumetric strain vs. time variation under 11 MPa (Ranathunga et al. 2015) and 17 MPa axial stresses after the injection period (Red data labels denote sub-critical and black data labels denote super-critical CO_2 injections)

b. Effect of coal seam depth on permeability

According to Figure 5.6, a reduction of permeability from 11 to 17 MPa axial stress increment can be observed, similar to previous studies using small coal samples (Ranathunga et al. 2017; Vishal and Singh 2015). The disruptions to the flow with increased effective stresses cause these permeability decreases. However, the CO_2 flow reduction is comparatively less for super-critical CO_2 injection than for sub-critical CO_2. For example, a reduction of around 86% for 6 MPa sub-critical CO_2 injection and around 80% for 8 MPa super-critical CO_2 injection can be seen when the axial stress is increased from 11 to 17 MPa. Similar results were obtained by Ranathunga et al. (2017) for small coal samples of similar low rank coal and these researchers observed 82% and 77% decreases of permeability for 6 MPa (sub-critical) and 9 MPa (super-critical) CO_2 injections for an 11 to 17 MPa confining pressure increase. This may be due to the already reduced flow with greater coal mass swelling and greater effective stress application in deeper coal seams that lead only to a lower reduction of super-critical CO_2 flow. This suggests that, regardless of sample size, the effect of seam depth on its permeability is significant.

As discussed previously, increases of CO_2 injection pressure from 6 to 7 MPa (sub-critical flow) and 8 to 9 MPa (super-critical flow) cause a permeability reduction of 11 % and 38% respectively for 17 MPa axial stress. For similar CO_2 injection pressure increments during 11 MPa axial stress, Ranathunga et al. (2015) observed around 5% (6 to 7 MPa) and 23% (8 to 9 MPa) permeability reductions for similar macro-scale RC samples made with the same brown coal. This implies that the permeability reduction with increasing injection pressure observed at 17 MPa axial stress is greater than the reduction observed at 11 MPa axial stress (Ranathunga et al., 2015). Similar results have been obtained in a meso-scale study by Ranathunga et al. (2017) on similar rank coal samples, which showed around 2% and 11% permeability reductions for 11 and 17 MPa confining pressures when CO_2 injection pressure was increased from 6 to 7 MPa, and 19% and 30% permeability reductions when CO_2 injection pressure was increased from 8 to 9 MPa under the same confining pressures (see Table 5.1). The reason is the lower flow ability under higher applied effective stresses, which offers a longer residential time for the CO_2 molecules within the coal mass. This may lead to greater matrix alterations causing lower permeability, especially for super-critical CO_2 flow (Vishal and Singh 2015).

The other important fact is that the coal matrix swelling is comparatively less at 17 MPa than for 11 MPa axial stress (Figure 5.6). For example, around 0.045% and 0.036% volumetric strains can be seen for 6 MPa (sub-critical) CO_2 flow and 0.053% and 0.046% for 8 MPa (super-critical) CO_2 flow under 11 MPa and 17 MPa axial stresses, respectively (Figure 5.6). This may be due to the obstruction of sample length variation by the higher stresses applying at higher axial stresses. In addition, this volumetric strain increment with injection pressures is higher for 11 MPa axial stress compared to 17 MPa axial stress. For instance, a 6 to 7 MPa sub-critical CO_2 flow increment shows around 7.2% and 4% volumetric strain increases for 11 and 17 MPa axial stresses, while that for 8 to 9 MPa super-critical flow is around 16.1% and 12.6%, respectively (Figure 5.6). Similar results have been reported by Jasinge (2010) for RC low rank coal of a similar type. Jasinge (2010) observed around 8.9% and 3.8% swelling increments for 9 to 10 MPa confining pressure increments when CO_2 pressure was increased from 2.5 to 3.4 MPa. As explained previously, the higher effective stresses acting on the coal mass under greater axial stresses slow the CO_2 flow along the coal matrix, offering less opportunity for CO_2 to interact with the coal mass by increasing the matrix rearrangements. Hol et al. (2011) also confirmed this observation after finding a lower CO_2 sorption capacity for bituminous coal due to the higher in situ stresses applied on the coal mass which result in less matrix swelling. This shows the lower coal matrix swelling effect expected for CO_2 injection at greater seam depths. This is favourable for CO_2 sequestration, as most potential seams for CO_2 sequestration are at quite deep depths (> 1 km).

c. How does carbon dioxide flow behaviour vary along the seam?

As discussed in Sections 5.3.5.1(a) and (b), lower CO_2 injection pressures at shallow depths produce higher permeability through the coal mass, while higher CO_2 pressures at deeper depths cause flow reduction with enhanced coal matrix swelling and higher effective stresses applied on the coal mass. The meso-scale study conducted by Perera et al. (2011) on black coal (high rank), showed a considerable reduction in pressure along the coal mass during CO_2 injection. For example, around 6 MPa downstream pressure was observed for 10 MPa CO_2 injection under 15 MPa confinement, and around 3 MPa for 20 MPa confinement for the same injection pressure. Similar lower pressure gradients were observed by Ranathunga et al. (2015) for a low rank macro-scale coal sample, and non-linear pressure variation along the specimen could be seen. Therefore, it was interesting to study how this CO_2 flow varies through the coal sample length (937 mm for the current study) during each injection condition under this greater axial stress condition. Figure 5.9 illustrates how the CO_2 pressure varied along the length of the sample during 6 MPa (sub-critical) and 8 MPa (super-critical) CO_2 injections at both 11 and 17 MPa axial stresses at the end of 10 days, measured using intermediate pressure transducers.

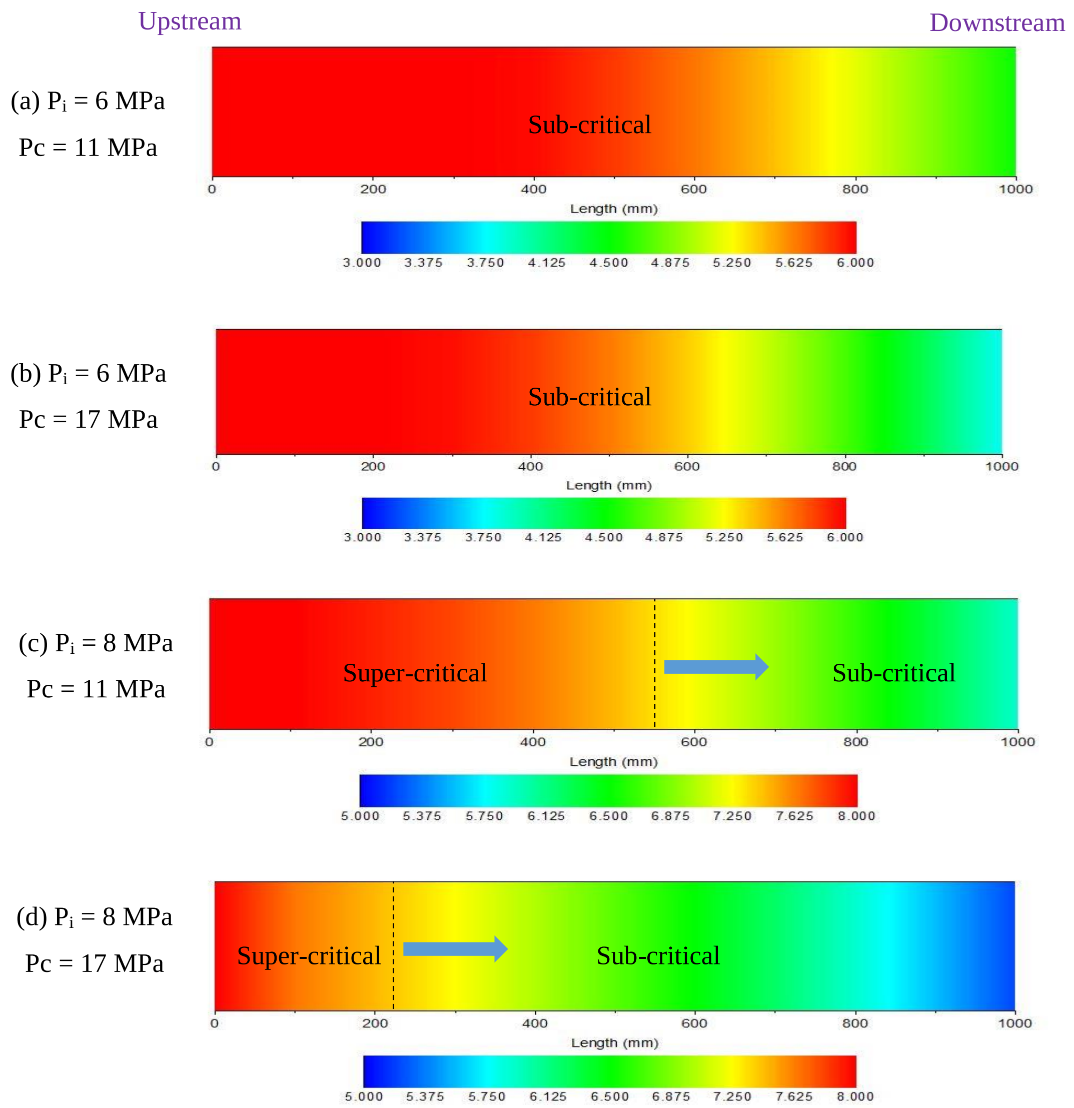

Figure 5.9. Pressure variation along the length of the sample after 10 days under 11 MPa (Ranathunga et al. 2015) and 17 MPa axial stresses (Here, P_i is injection pressure and σ_a is axial stress. The colour scale of each figure depicts the CO_2 pressure variation (in MPa) along the coal sample)

As shown in Figure 5.9, the respective injection pressures dropped gradually from upstream to downstream, regardless of injection pressure or depth (axial stress). The important thing is that this decrease is greater at higher injection pressures (super-critical) and greater depths compared to lower pressures and shallow depths. For example, 6 MPa sub-critical CO_2 flow under 11 MPa axial stress caused a decrease of 21.4% from upstream to downstream, while the same injection under 17 MPa axial stress caused a greater reduction of 32.9%. In addition, 8 MPa super-critical CO_2 flow under 11 MPa axial stress produced a 29.8% drop in pressure, and 17 MPa axial stress caused a greater reduction of 43.6%. These lower pressure gradients caused lower permabilities through the sample (Figure 5.6). Interestingly, the injected pressure remained constant up to around 500 m, 200 m, 400 m and 50 m during 6 MPa and 8 MPa CO_2 injection under 11 MPa and 17 MPa axial stress, respectively. Nevertheless, this length reduced with increasing injection pressure and axial stress. Hence, it can be deduced that the critical zone of influence (the area of CO_2 injection pressure kept constant) during CO_2 injection into a coal seam is larger at lower injection pressures at shallow depths, while it is reduced when higher CO_2 pressures are injected into deeper coal seams. This is important for the CO_2 storage process in deep coal seams.

Furthermore, only around 50% of the sample is under super-critical conditions under 11 MPa axial stress for 8 MPa CO_2 injection, and this proportion becomes less (around 25% of the sample) under 17 MPa axial stress (see Figures 5.8(c) and (d)). This observation clearly indicates the lower volumetric strain increments at higher effective stresses (refer to Section 5.3.5.1). The reason is that the coal matrix alterations due to more adsorptive super-critical CO_2 occur over a smaller area of the sample due to the lower permeabilities under higher effective stresses. Hence, the volumetric strain increment is less at greater depths than shallow depths.

d. An empirical relationship for carbon dioxide flow variation along a low rank coal seam

As CO_2 permeability along the coal sample varies with both axial stress and CO_2 injection pressure, a multi-variable regression equation was developed for permeability variations using the experimental data from Section 4.2 and the present study. Refer to Eq. [5.4]:

$$k = e^{(-0.2944\sigma_a - 0.1105P_i - 7.9127)} \qquad R^2 = 0.936 \qquad [5.4]$$

where, σ_a is axial stress (MPa), P_i is CO_2 injection pressure (MPa) and k is CO_2 permeability (mD).

The predicted permeability variations with the axial stresses and CO_2 injection pressures are shown in Figure 5.10. The figure clearly indicates that CO_2 permeability is higher at lower axial stresses and lower CO_2 injection pressures. In addition, it is reduced gradually with the increment of both axial stress and CO_2 injection pressure, confirming the experimental observations.

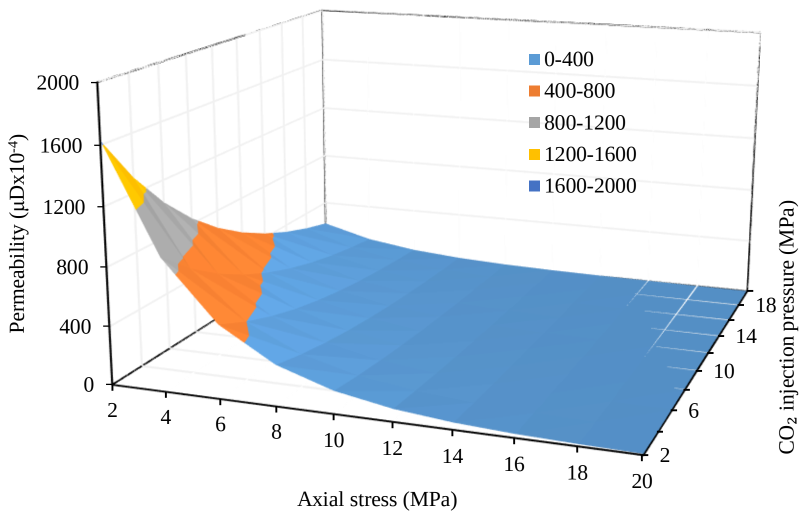

Figure 5.10. Predicted permeability variation with axial stress and CO_2 injection pressure

5.3.5.2 CO_2 storage capacity variation

One of the main purposes of the CO_2-ECBM process is to store anthropogenic CO_2 in deep un-mineable coal seams. It is therefore vital to investigate the amount of CO_2 that can be stored in the coal mass under various conditions, including various seam depths (axial stress) and injecting fluid properties (CO_2 phase and pressure). The next stage of analysis was therefore to quantify the CO_2 storage capacity in the coal mass under the various test conditions. This was accurately monitored using a digital platform scale at the CO_2 injection point. The amount of gas injected was monitored over time after changing the injection pressure and maintaining it for more than 10 days, to allow sufficient time for swelling. Figure 5.11 shows the variation in the amount of CO_2 injected into the coal mass (after around 10 hours) with effective stress under 11 MPa and 17 MPa axial stress conditions for each injection pressure. The effective stress was calculated as the difference between the applied axial stress and the mean gas pressure (the average of the pressures applied at upstream and downstream).

According to Figure 5.11, the amount of CO_2 injected is increased with increasing effective stress for both 11 and 17 MPa axial stresses. This increment is greater when the CO_2 injection pressure is greater than 7 MPa (super-critical flow) and lower for 6 to 7 MPa (sub-critical flow) CO_2 injections. For example, around 4.9% increment in injected CO_2 weight was observed with a 6 to 7 MPa pressure increment, and that for 8 to 9 MPa was 14.9% at 11 MPa axial stress. Similarly, for 17 MPa axial stress, the injected CO_2 weight was around 1.9% for an increase from 6 to 7 MPa pressure and 9.8% for 8 to 9 MPa pressure increment. The main reason for this observation is the reduction of CO_2 flow with increasing injection pressure (refer to Figure 5.6) due to the coal matrix rearrangements which adsorb less CO_2 injected into the coal sample.

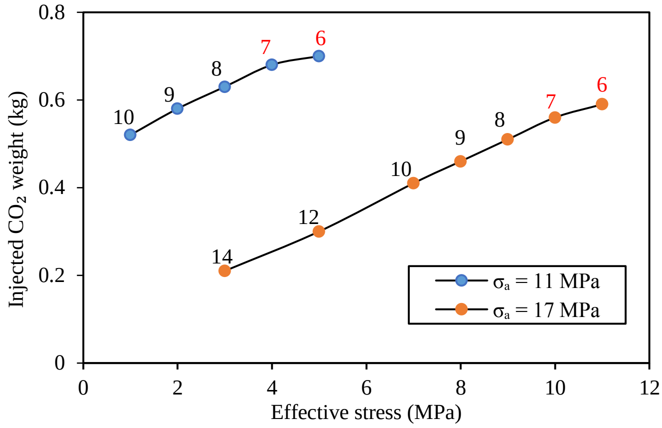

Figure 5.11. Variation of injected CO_2 weight (after 10 days) and CO_2 permeability with effective stress for 11 and 17 MPa axial stresses (The red data labels denote the sub-critical and the black data labels denote the super-critical CO_2 injections).

In addition, the observed injected CO_2 weight is different for a given effective stress. For example, during 5 MPa effective stress, 6 MPa sub-critical CO_2 injection injected 0.7 kg of CO_2 while 12 MPa super-critical CO_2 injected only 0.3 kg of CO_2 for the same effective stress. Here, the effective stress was calculated as the difference between the axial stress and the average pore pressure of the sample from upstream to downstream. In the case of 6 MPa CO_2, the whole sample (100%) is filled with sub-critical CO_2 (Figure 5.8), while a larger portion of the sample (around 60%) is filled with super-critical CO_2. Hence, greater coal matrix alterations can be expected for 12 MPa CO_2 adsorption than for 6 MPa CO_2, which may be the reason for this difference in CO_2 injection capacity. Hence, it can be concluded that CO_2 pore pressure has a much greater influence on CO_2 adsorption capacity in a coal seam than the applied in situ stresses. This was confirmed in Chapter 4.3, where the CO_2 sorption strain-induced permeability reduction was greater than the effective stress-induced permeability reduction.

However, this CO_2 storage process is time-dependent, and a longer time offers more opportunity for CO_2 adsorption and storage. Figure 5.12 shows the injected CO_2 weight variation with time at 6 MPa (sub-critical) and 8 MPa (super-critical) injection pressures under both 11 and 17 MPa axial stresses. According to Figure 5.12, the cumulative weight of injected CO_2 increases over time, and the rate of increase is lower at higher CO_2 injection pressures and greater axial stresses. For example, the average increases are around 0.0031 and 0.0025 at 6 and 8 MPa CO_2 injection pressures under 11 MPa axial stress, while they are around 0.0008 and 0.0005 for the same injection pressures (6 and 8 MPa) under 17 MPa axial stress. This observation clearly explains the CO_2 storage behaviour observed in Figure 5.11, which shows greater CO_2 storage capacity at lower depths and lower CO_2 injection pressures.

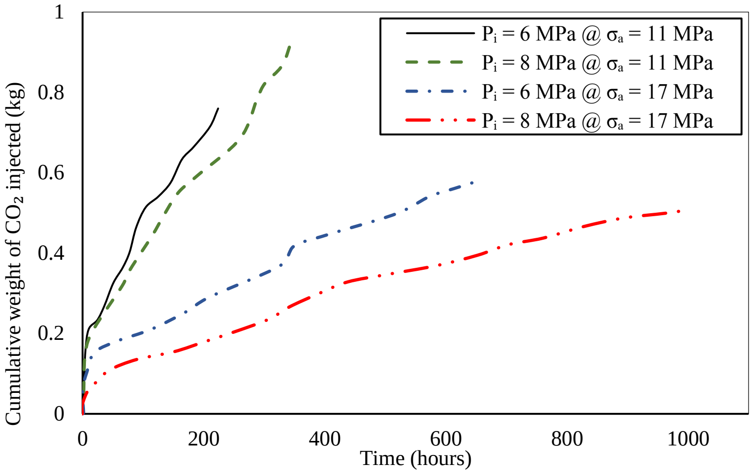

Figure 5.12. Cumulative weight of injected CO_2 variation with time for 6 MPa and 8 MPa injection pressures at 11 MPa and 17 MPa axial stresses

Interestingly, in relation to the weight of CO_2 injected at the end of the injection period, a contrasting behaviour compared to that shown in Figure 5.12 was obtained. Figure 5.13 illustrates a comparison of the weight of CO_2 injected after 10 days of injection and at the end of the injection period under both 11 and 17 MPa axial stresses. According to Figure 5.13, it can be noted that, although flow ability reduces at higher CO_2 injection pressures, a comparatively larger amount of CO_2 can be stored if a long time is offered for CO_2 sequestration at greater depths. The reason is, as stated in Figure 5.8, the inherent liquid-like properties of super-critical CO_2 permit greater adsorption potential within the coal matrix, which requires some time to complete.

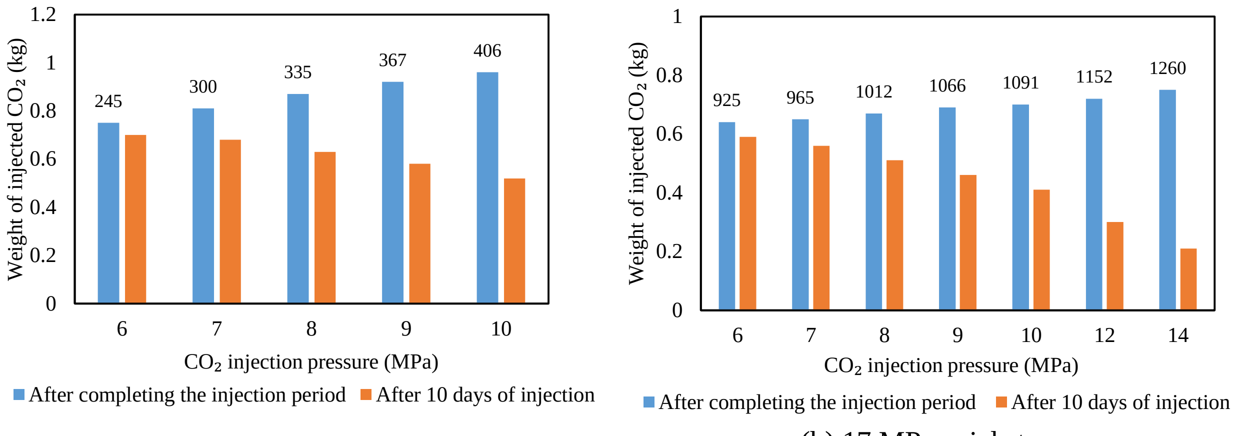

Figure 5.13. Comparison of weight of CO_2 injected after completing the injection period and after 10 days during 11 MPa and 17 MPa axial stress (The data labels denote the injection period (in hours) for each injection pressure)

However, in the case of the variation of CO_2 storage capacity with axial stress, the injected CO_2 weight reduction with axial stress is not much lower than the permeability reduction observed with axial stress (Figure 5.6). A comparison of the observed permeability reductions and the CO_2 storage capacity reductions under 11 to 17 MPa axial stress increment is shown in Table 5.2 after completing the injection period (time to reach steady state plus around 10 days).

Table 5.2. Comparison of permeability and CO_2 injectivity reductions with 11 MPa to 17 MPa axial stresses

	CO_2 injection pressure (MPa)	**Permeability reduction (%)**	**Injected CO_2 weight reduction (%)**
Sub-critical region	6	86.72	27.08
	7	85.96	25.01
Super-critical region	8	83.98	22.99
	9	80.31	19.75
	10	77.06	14.67

According to Table 5.2, similar to permeability reduction, the injected CO_2 or stored CO_2 weight is greatly reduced in the super-critical region, and the permeability reduction is around 60~70% higher than the injected CO_2 weight reductions (see Table 5.2). The longer residential time for CO_2 molecules with higher effective stresses may offer greater adsorption possibility for CO_2 molecules within the coal matrix (De Silva 2013) with time and the increased amount of CO_2 molecules entering the coal mass under higher CO_2 pressures, warranting lower reductions than in flow ability.

Another interesting point can be seen in Table 5.2, which is that the super-critical CO_2 undergoes lower reductions in both permeability and CO_2 injected weight than for sub-critical CO_2. As explained before, with greater CO_2 floods, the CO_2 flow is greatly influenced by the CO_2 pore pressure compared to the effective stresses applied on the sample. Hence, the expected reduction of permeability or CO_2 injectivity with effective stress is less for higher CO_2 injections than for lower CO_2 injections.

5.3.5.3 Suggestions for CO_2-ECBM field applications

Potential coal seams for CO_2-ECBM are located deep underground, where the injected CO_2 is in its super-critical state (beyond 7.38 MPa and 31.8 ^{0}C). The liquid-like viscosities (Figure 5.6) of super-critical CO_2 provide more potential for stable CO_2 storage within the coal matrix. Nevertheless, the observed decrease in CO_2 flow ability along the coal matrix, especially during super-critical CO_2 injection, raises concerns in relation to the productivity of the ECBM process. On the other hand, according to the findings, regardless of the permeability reductions, CO_2 storage capacity in coal increases with increasing injection pressure, offering sufficient time for sequestration. Furthermore, a comparatively lower reduction of CO_2 storage capacity was witnessed with increasing axial stress from 11 MPa (representing an approximately 400 m deep coal seam) to 17 MPa (representing an approximately 600 m deep coal seam). This information is very useful for CO_2 sequestration field projects, because there is current interest in utilising extremely deep underground coal seams for CO_2 sequestration. According to current findings, this depth effect does not have much influence on CO_2 storage potential.

However, attention should be paid to the flow reductions which occur with coal matrix swelling, because they might affect long-term CO_2 sequestration processes by allowing more CO_2 adsorption, which has been witnessed in several field-scale projects (White et al. 2005). Therefore, the implementation of flow-enhancement techniques (e.g. hydro fracturing, alternative injection of N_2) (White et al. 2005) will provide more opportunities to store greater amounts of CO_2 in deeper coal seams. Hence, resolving complications when using super-critical CO_2 for CO_2-ECBM recovery in terms of CO_2 storage capacity and CH_4 production enhancement using flow-enhancement techniques is essential prior to field-scale projects.

5.3.6 Conclusions

Following a series of CO_2 permeability tests using macro-scale low rank coal specimens, the following conclusions can be drawn:

- CO_2 permeability in coal is greater at lower depths and lower CO_2 injection pressures, while it gradually reduces with increasing depth and injection pressure, and the associated effective stress variation and the coal matrix swelling caused by CO_2 adsorption are the main causative factors, respectively.
- Super-critical CO_2 causes greater swelling in the coal mass compared to sub-critical CO_2, and the swelling increases with increasing injection pressure, regardless of depth. However, this swelling increment is reduced with increasing seam depth, probably due to the associated greater effective stresses that obstruct CO_2 flow along the coal matrix, offering less opportunity for CO_2 to interact with the coal mass.
- The permeability variation along the coal sample under the tested coal seam and injecting CO_2 conditions can be effectively represented using a simple multivariable regression model, and such models play an important role in field projects to predict CO_2 flow migration along the seam.
- The observed CO_2 permeability along the tested coal specimen indicated that the critical zone of influence for CO_2 injection into a selected coal seam is greater at lower injection pressures and at shallow depths, and it reduces with increasing CO_2 pressure and seam depth.

- Finally, the observed CO_2 storage capacity of the tested coal under various conditions revealed that CO_2 storage capacity in a coal seam is greatly influenced by the CO_2 pore pressure. However, the reduction of CO_2 storage capacity with depth was not significant, which is important for field CO_2 sequestration projects, which normally use deep seams to store CO_2.

5.3.7 References

Day, S., Fry, R., Sakurovs, R. (2008) Swelling of Australian coals in supercritical CO_2. *International Journal of Coal Geology* 74, 41-52.

De Silva, P.N.K. (2013) A study of CO_2 storage capacity in sedimentary rocks (*PhD thesis*), Monash University, Melbourne, Australia.

Hol, S., Spiers, C.J. (2012) Competition between adsorption-induced swelling and elastic compression of coal at CO_2 pressures up to 100MPa. *Journal of the Mechanics and Physics of Solids* 60, 1862-1882.

Jasinge, D. (2010) An investigation of the effect of carbon dioxide sequestration on the behaviour of brown coal. (*PhD thesis*), Monash University, Melbourne, Australia.

Xie, J., Gao, M., Yu, B., Zhang, R., Jin, W. (2015) Coal permeability model on the effect of gas extraction within effective influence zone. *Geomechanics and Geophysics for Geo-Energy and Geo-Resources* 1:15-27

Larsen, J.W., Flowers, R.A., Hall, P.J., Carlson, G. (1997) Structural rearrangement of strained coals. *Energ Fuel* 11, 998-1002.

Liu, Q., Cheng, Y., Ren, T., Jing, H., Tu, Q., Dong, J. (2016) Experimental observations of matrix swelling area propagation on permeability evolution using natural and reconstituted samples. *Journal of Natural Gas Science and Engineering* 34, 680-688.

Masoudian, M.S., Airey, D.W., El-Zein, A., (2014) Experimental investigations on the effect of CO_2 on mechanics of coal. *International Journal of Coal Geology* 128, 12-23.

McLinden, M., Klein, S., Lemmon, E., Peskin, A. (1998) REFPROP, Thermodynamic and transport properties of refrigerants and refrigerant mixtures. NIST Standard Reference Database 23, Gaithersburg, MD.

Merkel, A., Gensterblum, Y., Krooss, B.M., Amann, A. (2015) Competitive sorption of CH_4, CO_2 and H_2O on natural coals of different rank. *International Journal of Coal Geology* 150, 181-192.

Pan, Z., Connell, L.D. (2007) A theoretical model for gas adsorption-induced coal swelling. *International Journal of Coal Geology* 69, 243-252.

Pan, Z., Connell, L.D., Camilleri, M. (2010) Laboratory characterisation of coal reservoir permeability for primary and enhanced coalbed methane recovery. *International Journal of Coal Geology* 82, 252-261.

Perera, M.S.A., Ranjith, P.G., Airey, D.W., Choi, S.K. (2011) Sub- and super-critical carbon dioxide flow behaviour in naturally fractured black coal: An experimental study. *Fuel* 90, 3390-3397.

Ranathunga, A.S., Perera, M.S.A., Ranjith, P.G., Ju, Y., Vishal, V., De Silva, P.N.K. (2015) A macro-scale experimental study of sub-and super-critical CO_2 flow behaviour in Victorian brown coal. *Fuel* 158, 864-873.

Ranathunga, A.S., Perera, M.S.A., Ranjith, P.G. (2017) Super-critical carbon dioxide flow behaviour in low rank coal: A meso-scale experimental study. *Journal of CO_2 Utilization* (under review)

Sun, Y., Li, Q., Yang, D., Liu, X. (2016) Laboratory core flooding experimental systems for CO_2 geosequestration: An updated review over the past decade. *Journal of Rock Mechanics and Geotechnical Engineering* 8, 113-126.

Siriwardane, H., Haljasmaa, I., McLendon, R., Irdi, G., Soong, Y., Bromhal, G. (2009) Influence of carbon dioxide on coal permeability determined by pressure transient methods. *International Journal of Coal Geology* 77, 109-118.

Verma, A.K., Sirvaiya, A. (2016) Comparative analysis of intelligent models for prediction of Langmuir constants for CO_2 adsorption of Gondwana coals in India. *Geomechanics and Geophysics for Geo-Energy and Geo-Resources* 2, 97-109.

Vishal, V., Singh, T.N. (2015) A Laboratory Investigation of Permeability of Coal to Supercritical CO_2. *Geotechnical and Geological Engineering* 33, 1009-1016.

Wang, S., Elsworth, D., Liu, J. (2013) Permeability evolution during progressive deformation of intact coal and implications for instability in underground coal seams. *International Journal of Rock Mechanics and Mining Sciences* 58, 34-45.

Wang, Y., Liu, S., Elsworth, D. (2015) Laboratory investigations of gas flow behaviors in tight anthracite and evaluation of different pulse-decay methods on permeability estimation. *International Journal of Coal Geology* 149, 118-128.

White, C.M., Smith, D.H., Jones, K.L., Goodman, A.L., Jikich, S.A., LaCount, R.B., DuBose, S.B., Ozdemir, E., Morsi, B.I., Schroeder, K.T. (2005) Sequestration of Carbon Dioxide in Coal with Enhanced Coalbed Methane Recovery: A Review. *Energy and Fuels* 19, 659-724.

5.4 Prediction of expected fluid flow along the coal seam and storage capacity variations in coal with various CO_2 properties under different down-hole stresses

The previous sections (5.2 and 5.3) detailed the coal mass flow behaviour for various CO_2 properties and in situ stresses expected during the CO_2-ECBM process. However, the experimental studies were conducted only for 11 and 17 MPa axial stresses, which approximately represent a thin coal seam at a depth of 400 and 600 m respectively. Therefore, this work aims to study the coal mass flow behaviour under the deep underground conditions expected during CO_2 sequestration by developing numerical models extending the experimental results obtained during the present study. The COMSOL Multiphysics numerical simulator was first used to simulate the core-flooding experimental results for brown coal, and then to model the behaviour of black coal expected under different CO_2 conditions using the experimental results reported in the research literature.

This section of the chapter details the following publication:

Ranathunga AS, Perera MSA, Ranjith PG (2017). A laboratory-scale numerical study of CO_2 flow through coal under down-hole stress conditions: Application to CO_2 storage. *Energy Fuel* (under review).

A laboratory-scale numerical study of CO_2 flow through coal under down-hole stress conditions: Application to CO_2 storage

A.S. Ranathunga[1], M.S.A. Perera[1,2], P.G. Ranjith[1]

[1]Deep Earth Energy Laboratory, Department of Civil Engineering, Monash University, Building 60, Melbourne, Victoria, 3800, Australia.

[2] Department of Infrastructure Engineering, The University of Melbourne, Building 176, Melbourne, Victoria, 3010, Australia.

Abstract

Existing studies highlight the uncertainty in the process of CO_2 sequestration in deep coal seams, mainly due to the associated CO_2 adsorption-induced coal matrix rearrangements. Therefore, it is important to investigate how the CO_2 flow varies through the coal seam and the related effect on CO_2 storage capacity. Several experimental studies have been conducted on this, however, the inability to represent deep coal seam conditions in laboratory experiments is one of the main drawbacks in relating experimental results to field conditions. The main objective of this study is therefore to determine the permeability behaviour in coal for CO_2 flow and the corresponding CO_2 storage capacity using a laboratory-scale numerical model of deep coal seams. A macro-scale (203 mm diameter and 1000 mm long) model was developed using COMSOL Multiphysics software to represent a thin coal seam, and the model was successfully calibrated and validated using the data obtained using the experimental results of reconstituted brown coal specimens by Ranathunga et al. (2015) and Ranathunga et al. (2016b). The model was then extended to predict the flow characteristics such as permeability, CO_2 pressure and CO_2 concentration distributions, and CO_2 storage capacity in coal under higher injection pressures and deeper reservoir depths.

According to the model results, CO_2 permeability through the coal mass is negatively affected by both CO_2 pressure and the depth of the coal seam, whereas this effect is decreased at higher depths and CO_2 pressures. Further, the flow parameters, such as CO_2 pressure and CO_2 concentration, reduce along the sample length with increasing depth. The model can accurately predict the experimental observations of CO_2 storage capacities, which showed an increment in CO_2 storage over time. However, for a given depth, CO_2 concentration increases with increasing injection pressure. In spite of the lower pressure developments and permeabilities existing under higher effective stresses, greater amounts of CO_2 can be sequestrated into coal seams if sufficient time is allowed for CO_2 permeation.

Keywords: CO_2 storage; Core flooding test; Effective stress; Laboratory-scale model

5.4.1 Introduction

The injection of CO_2 into deep coal seams causes their chemical and physical properties to change greatly, which causes the amount of injectable CO_2 into and producible CH_4 from these seams to become unpredictable. Much research has been conducted on the effects of CO_2 injection on coal and has revealed that there is a great degree of swelling caused by CO_2 adsorption that, in turn, can cause the permeability of the coal mass to be severely reduced (Anggara et al., 2013; Day et al., 2008; Perera et al., 2011; Ranathunga et al., 2015). In these research studies, De Silva and Ranjith (2013), Ranathunga et al. (2015) and Ranathunga et al. (2016b) conducted several macro-scale studies using reconstituted low rank brown coal samples to study the effect of CO_2 and reservoir properties on the CO_2 flow behaviour in coal using reconstituted coal samples to minimise the effect of heterogeneity. The macro-scale tests provide a better location-dependent representation of the CO_2 adsorption-induced coal structure modification and have the ability to capture the changes in CO_2 storage capacity along the coal mass, offering a good correlation of measured data with field conditions.

However, these studies were conducted under limited test conditions, due to the extensive time required to conduct such macro-scale tests. Therefore, an effort was made in this study to model the experimental observations using the COMSOL Multiphysics simulator. The results were then extended to simulations using COMSOL Multiphysics, particularly on the impact of CO_2 properties on CO_2 sequestration and its influence on CO_2 storage for macro- scale experimental conditions. These have not been studied to date using numerical modelling. For the proposed numerical model, the experimental results obtained by Ranathunga et al. (2015) based on core-flooding tests conducted under different CO_2 phase and pressure conditions were used and the results were validated using the experimental results obtained by Ranathunga et al. (2016b). The validated model was then extended to higher axial stresses and CO_2 pressures to represent the situation of potential deep coal seams which are preferable for CO_2 sequestration. The model effectively represents the field conditions, confirming the reliability of the modelling approach used.

5.4.2 Model Development

This section presents the methodology adopted to develop the numerical model using COMSOL. A two-dimensional finite element model to simulate the core-flooding tests performed under different CO_2 saturation conditions was developed using COMSOL Multiphysics using the *Poroelasticity* interface in the Structural Mechanics module and the *Transport of diluted species in porous media* interface in the Chemical Species Transport module.

5.4.2.1 Theory used for model development

a. Structural mechanics: Poroelasticity

Generally, the poroelastic model describes the linked interactions between fluid and deformation in porous media. This module assumes the domain of the material consists of both the porous matrix and the fluid filling the pore (solutes), and both carry loads. The formulation used for structural analysis in COMSOL for both small and finite deformations is totally Lagrangian. As explained in Section 4.5, displacement is considered as a function of the material coordinates (X, Y, Z) in the total Lagrangian configuration, and hence the total strain tensor is written in terms of the displacement gradient (∇u) (see Eq. [5.5]).

$$\nabla u = \begin{bmatrix} \frac{\partial u}{\partial X} & \frac{\partial u}{\partial Y} & \frac{\partial u}{\partial Z} \\ \frac{\partial v}{\partial X} & \frac{\partial v}{\partial Y} & \frac{\partial v}{\partial Z} \\ \frac{\partial w}{\partial X} & \frac{\partial w}{\partial Y} & \frac{\partial w}{\partial Z} \end{bmatrix} \qquad [5.5]$$

The physical components of the radial and axial displacement, u and w, are used as independent variables for the axially symmetric geometry.

Therefore, the Green-Lagrange strain tensor (ε) can be defined as in Eq. [5.6].

$$\varepsilon = \frac{1}{2}[\nabla u + (\nabla u)^T + (\nabla u)^T \nabla u] \qquad [5.6]$$

An elastoplastic model was assumed for the numerical study. Here, the structural mechanics equation from the solid mechanics module is modified to incorporate the fluid pressure gradient, and hence an additional term $\alpha_B p_f I$, is inserted as the fluid to the structure coupling term. This coupling term links the structural deformation to fluid flow, and consequently the stress, strain and the pore pressure of linear poroelastic material are related with the following equation (Eq. [5.7]):

$$S - S_0 = C:(\varepsilon - \varepsilon_0 - \varepsilon_{inel}) - \alpha_B p_f I \qquad [5.7]$$

where, S and ε are stress and strain tensor, S_0 and ε_0 are the initial stress and strain, ε_{inel} is the sum of all inelastic strains, C is the 4th order elasticity tensor, α_B is the Biot-Willis coefficient and p_f is the fluid pore pressure.

b. Structural mechanics: Darcy's law

Darcy law can be used to model the fluid flow in a porous medium, where the major driving force is the pressure difference. Darcy's equation in the subsurface flow module is modified to include the additional term, the time rate change of volumetric strain ($\frac{\partial e_{vol}}{\partial t}$) to link fluid flow with structural deflection, as shown in Eq. [5.8]

$$p_f S \frac{\partial p_f}{\partial t} + \nabla . \rho \left[-\frac{k}{\mu} \nabla p_f \right] = Q_m - p_f \alpha_B \frac{\partial e_{vol}}{\partial t} \qquad [5.8]$$

where, $\frac{\partial e_{vol}}{\partial t}$ is the rate of change in volumetric strain derived from solid displacement, Q_m is the mass source term, ρ is fluid density, S is the storage coefficient, k is the permeability of the porous medium and μ is the dynamic viscosity of the fluid. Here, the storage coefficient S is calculated by Eq. [5.9].

$$S = \frac{\varepsilon_p}{K_f} + (\alpha_B - \theta)\left(\frac{1-\alpha_B}{K_d}\right) \qquad [5.9]$$

where, ε_p is the porosity of the material, K_f is the bulk modulus of fluid (inverse of fluid compressibility), K_d is the drained bulk modulus ($K_d = \left(1 - \varepsilon_p\right)K_s$, and $K_s$is the bulk modulus of the material).

c. Transport of diluted species in porous media

The transport of diluted species in porous media interface was used to model the CO_2 concentration in the brown coal sample, and this interface was coupled with the Darcy law interface using Darcy velocity (u) in Eq. [5.10].

$$\frac{\partial}{\partial t}(\theta c_i) + \frac{\partial}{\partial t}\left(\rho_b c_{P,i}\right) + \frac{\partial}{\partial t}\left(\alpha_v c_{G,i}\right) + u . \nabla c_i = \nabla . \left[\left(D_{D,j} + D_{e,j}\right). \nabla c_i\right] + R_i + S_i \qquad [5.10]$$

where, θ is liquid volume fraction, c_i is the concentration of species, ρ_b is the bulk density, $c_{P,i}$ is the amount adsorbed to the solid particles, α_v is the resulting gas volume fraction ($\varepsilon_p - \theta$), $c_{G,i}$ is concentration of species in the gas phase, $D_{D,j}$ is the dispersion tensor, $D_{e,j}$ is the diffusion tensor, u is the directional velocity, R_i is the reaction rate expression, and S_i is an arbitrary term. In this model, CO_2 adsorption into the coal mass was modelled by the Langmuir equation and this is shown in Eq. [5.11].

$$c_{P,i} = \frac{V_L p}{(p+P_L)} \qquad [5.11]$$

where, V_L and P_L are Langmuir volume and pressure coefficients respectively.

5.4.2.2 Model validation using experimental data

The numerical study is based on the results of a previous experimental study conducted on CO_2 flow variation in reconstituted Victorian brown coal under different CO_2 phase and pressures by

Ranathunga et al. (2015) and Ranathunga et al. (2016b). Here, reconstituted brown coal samples results were used to avoid the complexities related to the heterogeneity of coal. In the previous studies, sub-critical (6 and 7 MPa) and super-critical (8, 9 and10 MPa) CO_2 were permeated in reconstituted brown coal samples 203 mm in diameter and 1000 mm in length at 38 ^{0}C (>31.8 ^{0}C is the critical temperature of CO_2). The material properties for the modelling were obtained from the experimental results and are further discussed in the following sections.

5.4.2.3 Basic assumptions

1. Brown coal is a linear poro-elastic isotropic material, and poro-elasticity theory can be used to model the linked interaction between the flow and solid deformation.
2. The major fluid driving force across the coal specimen is the pressure gradient, and hence Darcy's law is valid.
3. The adsorption of CO_2 into the coal matrix can be modelled using Langmuir isotherms.
4. CO_2 flow through the coal specimen is due to advection, diffusion and dispersion, and sorption.
5. No moisture or other gasses were present in the coal sample before CO_2 permeation.

5.4.2.4 Model definition and boundary conditions

To simulate the experimental conditions, a 2-D model was first developed for a width of 1000 mm (the length of the tested coal specimen) and a height of 203 mm (the diameter of the tested coal specimen), which was then converted into a 3-D model using the Model builder interface in the COMSOL Multiphysics simulator. The boundary conditions adopted for the structural mechanics module (mechanical boundary conditions) are as follows:

Under laboratory condition, the circumference and the left-side base of the sample consist of a fixed pressure cell casing and hence are assumed to be a fixed boundary. The right side of the sample moves inward and outward from the cell to compress the sample and hence the axial load (F_a) was applied to the right-side base of the sample. CO_2 was injected from the right-side base of the sample and was introduced as an *Inflow flux*. The circumference of the sample (top and bottom boundaries) has no flow boundaries. When considering the downstream of the sample, the experiments were conducted under undrained conditions, and the pressure development of a fixed volume at the downstream was observed to calculate the pressure gradients along the coal specimen. Further, there was no outflow from the downstream during the gas injection. A 8 mm long area was introduced to the left side of the model to represent the fixed downstream volume (32.36 cm^3) with a 100% initial porosity (empty volume). The initial permeability of the downstream volume was selected as 1000 mD (>>> brown coal initial permeability, to better represent the initial void volume there) and the end boundary of the downstream volume was set as fixed with a no-flow boundary (Perera et al., 2012). Parametric sweeps were used in the model for CO_2 injection and axial loads, and injection pressures of 5-20 MPa and axial loads of 0-15 MPa were applied to the sample. The overall details of the geometry and boundary conditions adopted for the model are shown in Figure 5.14.

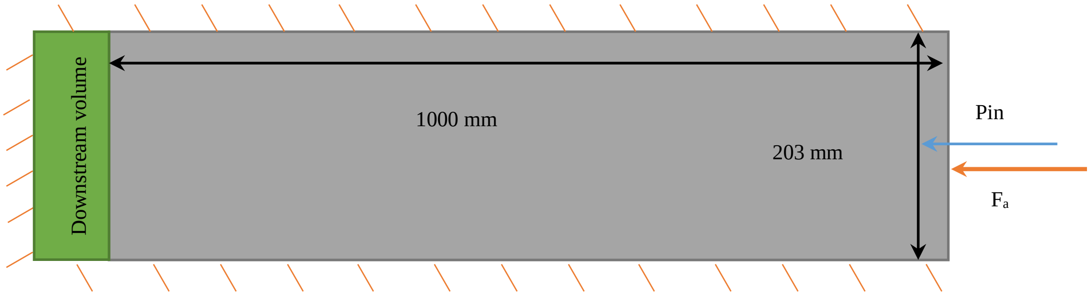

Figure 5.14. Dimensions, boundary conditions, and boundary load for the macro-scale COMSOL model

5.4.2.5 Model input parameters

The thermodynamic properties, such as density, viscosity and adiabatic compressibility of CO_2, vary with the fluid pressure for a given temperature. The relationships between the thermodynamic properties and mean CO_2 pressure within the sample (*Pm*) (the temperature was kept constant throughout the experiments) were derived using the REFPROP database (McLinden et al., 1998), and these formulations were entered into COMSOL (see Eqs. [5.12-5.14]). Further, the CO_2 concentration of the sample was obtained from Eq. [5.16] using the COMSOL model parameter for Darcy's velocity field *X* component. The material properties for the model were obtained from the experimental results. The input parameters for the model are shown in Table 5.3.

<u>Density of CO_2 (ρ_{CO2}):</u>

$$\rho_{CO2,sub} = 15.216\exp(4E-07P_m) \qquad R^2 = 0.9789 \qquad \text{for } P_m \leq 7.38\text{ MPa} \qquad [5.12a]$$

$$\rho_{CO2,super} = -1E-12P_m^2 + 6E-05P_m + 266.85 \qquad R^2 = 0.9886 \qquad \text{for } P_m > 7.38\text{ MPa} \qquad [5.12b]$$

<u>Dynamic viscosity of CO_2 (μ_{CO2}):</u>

$$\mu_{CO2,sub} = 5E-19P_m^2 - 3E-12P_{in} + 2E-05 \qquad R^2 = 0.9987 \qquad \text{for } P_m \leq 7.38\text{ MPa} \qquad [5.13a]$$

$$\mu_{CO2,super} = 6E-09P_m^{0.5689} \qquad R^2 = 0.9757 \qquad \text{for } P_m > 7.38\text{ MPa} \qquad [5.13b]$$

Adiabatic compressibility of CO_2 (β_{CO2}):

$$\beta_{CO2,sub} = 2.5416\, P_m^{-1.081} \qquad R^2 = 0.9867 \qquad \text{for } P_m \leq 7.38 \text{ MPa} \qquad [5.14a]$$

$$\beta_{CO2,super} = 149609 P_m^{-1.866} \qquad R^2 = 0.9810 \qquad \text{for } P_m > 7.38 \text{ MPa} \qquad [5.14b]$$

where, $P_m = \frac{P_{in} + P_{out}}{2}$, where P_m is mean CO_2 pressure through the sample, P_{in} is the CO_2 injection pressure (or upstream pressure) and P_{out} is the downstream pressure (when the pressure developments of the downstream achieve the steady state). P_{out} varies with the injection pressure and the axial load applied on the sample and Eq. [5.16] was developed to obtain downstream pressure at steady state using the experimental data from Ranathunga et al. (2015) and Ranathunga et al. (2016b).

$$P_{out} = -0.0527 F_a + 0.7839 P_{in} - 2.2347 \qquad [5.15]$$

Concentration of CO_2:

$$c = \frac{[poro.uf \times \rho_{CO2}]}{0.04401}\ [mol/(m^2 s)] \qquad [5.16]$$

where, $poro.uf$ is the Darcy's velocity field *X* component obtained from the model.

The major flow driving mechanism is assumed to be the pressure gradient through the sample, and hence Darcy's law is valid. The CO_2 flow rate (Q, steady state) and the permeability (k) of coal specimen are given by Eqs. [5.17] and [5.18].

$$Q = -1.4602 \times 10^{-11} F_a - 8.651794 \times 10^{-13} P_{in} + 0.00028\ [l/h] \qquad [5.17]$$

$$k = \frac{2QP_{out}(\mu_{CO2,i})L}{A(P_{in}^2 - P_{out}^2)}\ [m^2] \qquad [5.18]$$

where, $\mu_{CO2,i}$ is the dynamic viscosity of the CO_2 present in the sample and *i* = sub- and super-critical CO_2 phases (refer to Eqs. [5.13a,b]). It should be noted that only the steady-state flow rate values for 6, 8 and 10 MPa CO_2 injection pressures under 11 and 17 MPa axial stresses were used to develop the empirical relationship shown in Eq. [5.17], and the rest of the data were used to validate the model. Finally, the model was extended to higher axial loads and CO_2 injection pressures to obtain the effect of CO_2 properties and in situ stresses on the brown coal sample.

Table 5.3. The input parameters for the model

Model Parameter	Value
Coal sample properties	
Sample diameter (D)	203 mm
Sample length (L)	1000 mm
Density (ρ)	1097.8 kg/m^3
Young's modulus (E)	72.01 MPa (Jasinge, 2010)
Poisson's ratio (ϑ)	0.27 (Jasinge, 2010)
Porosity (ε_p)	0.41 (Jasinge, 2010)
Biots-Willis coefficient (α_B)	0.9 (Perera et al., 2013)
Pore volume compressibility (c_p)	2.96E-05 1/Pa (De Silva and Ranjith, 2014)
Matrix shrinkage/swelling compressibility(c_m)	1.21E-05 1/Pa (De Silva and Ranjith, 2014)
Langmuir volume for CO_2 adsorption for brown coal (V_L)	29.11 m^3/kg (Jasinge, 2010)
Langmuir pressure for CO_2 adsorption for brown coal (P_L)	0.578 MPa (Jasinge, 2010)
Downstream properties (explained in Section 5.4.2.4)	
Downstream length (L_{ds})	8 mm
Porosity (ε_{ds})	1
Initial permeability ($k_{o,ds}$)	1000 mD (Perera et al., 2012)
CO_2 properties (explained in Section 5.2.2.4)	
Density (ρ_{CO2})	Refer Eqs. [5.12a,b]
Dynamic viscosity (μ_{CO2})	Refer Eqs. [5.13a,b]
Adiabatic compressibility (β_{co2})	Refer Eqs. [5.14a,b]
Initial CO_2 concentration (c_o)	0 kg/m^3
CO_2 concentration (c)	Refer Eq. [5.16]
Boundary conditions (parametric sweep)	
Axial load (F_a)	5 - 20 MPa
CO_2 injection pressures (P_{in})	0 - 15 MPa

7.4.3.6 Meshing and element sizes

A 2-D mapped meshing was assumed for the model since it consists of a simple rectangular geometry bounded by four boundary segments with no holes. By defining the number of elements at each side, a mapped mesh was introduced to the model. The meshing parameters are shown in Table 5.4 and the assumed mapped mesh and mesh quality plot are shown in Figure 5.15. The colour range 0 means poor quality and 1 means good quality in Figure 5.15, which indicates the assumed mesh pattern fits the geometry well.

Table 5.4. CO_2 saturation-dependent material parameters

Property	Value
Number of degrees of freedom	23526
Number of elements (rectangle)	158118
Number of boundary elements	1763

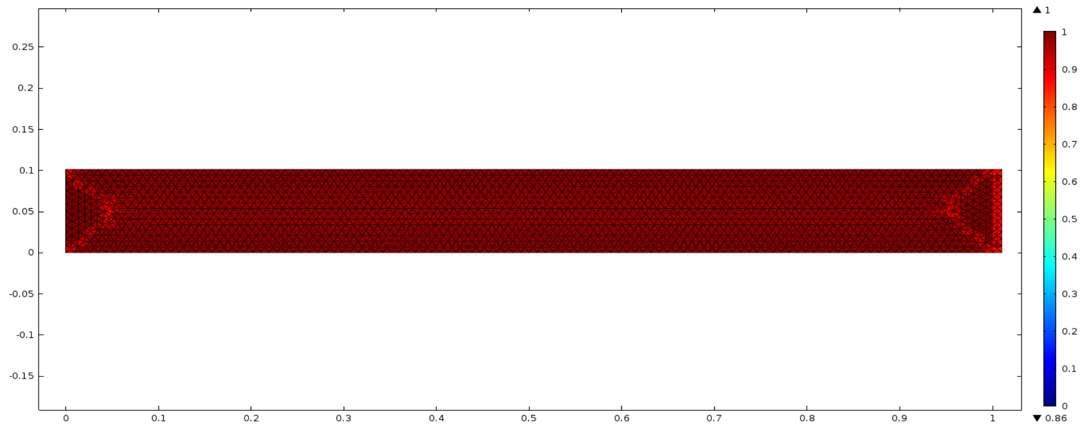

Figure 5.15. Mesh quality plot for the mesh pattern used in the model

5.4.3 Model results and discussion

5.4.3.1 Effect of CO_2 injection pressure on coal mass permeability

A comparison of the coal mass permeability values obtained from the experiments and the COMSOL model for 11 and 17 MPa axial loads is shown in Figure 5.16. According to the figure, the model-predicted permeability values are in good agreement with the experimental results. Particularly for higher CO_2 pressures (12 and 14 MPa were not used for the empirical relationship developments), the model-predicted permeability values show only around 7 to 9 % errors compared with the experimental results (see Table 5.5). Next, the model was extended to calculate the CO_2 permeability of brown coal under higher injection pressures, which could not be found under laboratory conditions. The results are shown in Figure 5.17.

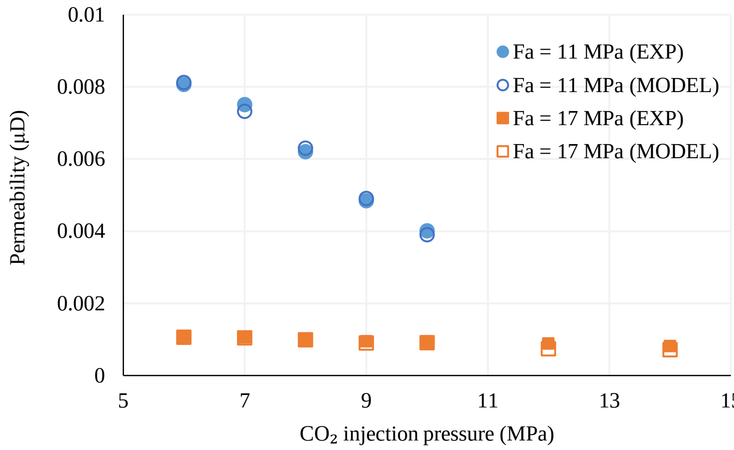

Figure 5.16. Comparison of permeability values obtained from experiments (solid points) (Ranathunga et al., 2015; Ranathunga et al., 2016b) and COMSOL model (hollow points) for 11 and 17 MPa axial loads

Table 5.5. Error between experimental and model-predicted permeability values

Axial load (MPa)	CO_2 injection pressure (MPa)	Error (%)
11	7	6.12
	9	4.07
17	7	1.54
	9	4.97
	12	7.47
	14	8.94

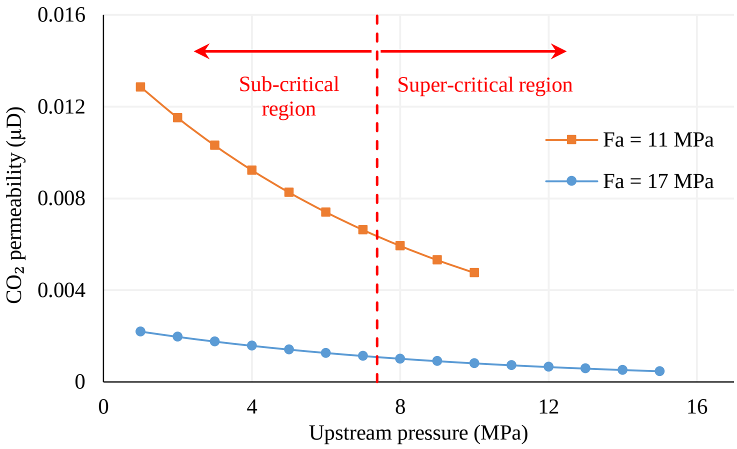

Figure 5.17. CO_2 permeability for further sub- and super-critical CO_2 flows under 11 and 17 MPa axial loads

According to Figure 5.17, the expected permeability reduction with CO_2 adsorption is continued at both lower (< 6 MPa) and higher (> 14 MPa) injection pressures. As observed by Ranathunga et al. (2015) and Ranathunga et al., (2016b), the flow reduction is increased under higher pore pressures than lower pressures. For example, a 5 to 6 MPa sub-critical CO_2 pressure increase causes a flow reduction of 9.15%, while the reduction for 15 to 16 MPa CO_2 pressure increment is around 54.7% Therefore, flow reduction is increased by around 6- fold when the upstream pressure is raised by 10 MPa. As explained previously, the greater adsorption potential under higher CO_2 pore pressures reduces the flow through the coal sample, resulting in greater permeability reductions under higher CO_2 pressures compared to lower pressures. It would be interesting to investigate whether this flow behaviour continues in deeper coal seams. This was studied next by extending the model to higher axial loads representing different depths.

5.4.3.2 Effect of reservoir depth on coal mass permeability

Figure 5.18 shows the CO_2 flow variation at different reservoir depths obtained from the extended laboratory-scale COMSOL model. As observed by Ranathunga et al. (2016b), the CO_2 flow ability along the coal mass is reduced at greater depths due to the higher effective stress. For example, during 6 MPa sub-critical CO_2 flow, around 65.9% and 54.7% reduction of CO_2 flow was observed when the depth was increased from 0.4 to 0.5 km and 0.5 to 0.6 km, respectively (see Figure 5.18). This flow reduction is less at greater depths than lower depths. Similar results were observed by Ranathunga et al. (2016a) (refer to Section 5.1.2), who observed around 69% and 56% reduction of CO_2 permeability when the depth was increased by similar values (from 0.4 to 0.5 km and 0.5 to 0.6 km respectively) for low rank coal, based on tri-axial experiments. Hence, these findings from the COMSOL model confirm the lesser influence of seam depth on CO_2 flow reduction.

In addition, when the coal seam depth is increased from 0.8 to 0.9 km, the CO_2 permeability is reduced by 78.4% for 4 MPa sub-critical CO_2 injection, while there is around a 53.5% reduction for 14 MPa super-critical CO_2 injection (refer to Figure 5.18). Similar behaviour was observed in Section 5.1.2 in meso-scale flow studies on brown coal, which obtained around 80% and 75% flow reduction for 6 MPa (sub-critical) and 9 MPa (super-critical) CO_2 injections when the confining pressure increased from 11 to 14 MPa (approximately 0.4 to 0.5 km). Under higher effective stresses, the CO_2 permeability through the coal mass is reduced and hence the expected flow reductions under higher CO_2 pressures (super-critical CO_2) are also lower. Therefore, the experimental findings of greater CO_2 flow reduction under higher effective stresses which gradually decrease with increasing depth and injection pressure are further confirmed by the model results. This implies that the influence of CO_2 phase is more dominant in shallow coals seams than deep seams, which is preferable for CO_2 storage, as it is often carried out at deep depths.

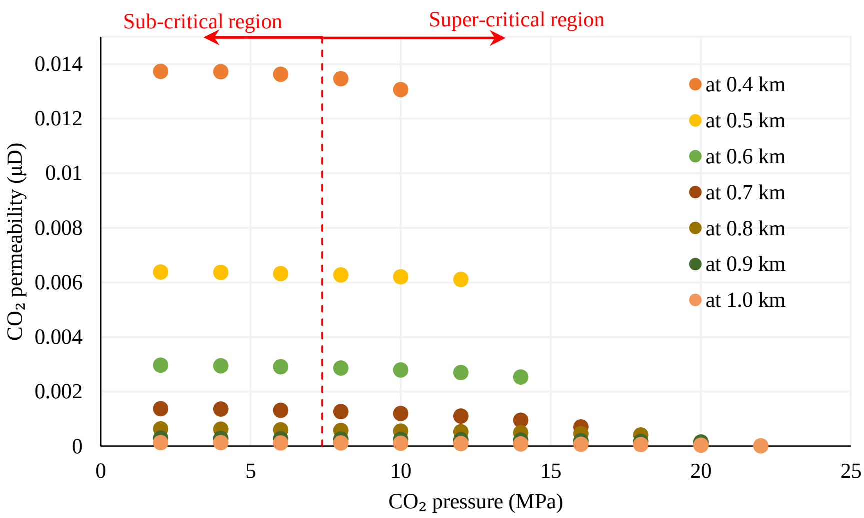

Figure 5.18. CO_2 permeability variation at greater depths

5.4.3.3 CO_2 pressure and concentration distribution along the coal sample

a. CO_2 pressure distribution along the coal specimen

The steady-state flow under experimental conditions at 6 MPa injection and 17 MPa axial load was obtained after around 18 hours of CO_2 injection (Ranathunga et al., 2016b). The CO_2 pressure distribution in brown coal up to 18 hours of CO_2 injection (steady-state time under experimental conditions) at 6 MPa injection pressure and 17 MPa axial load is shown in Figure 5.19. According to the figure, CO_2 moves gradually with time due to the pressure difference (advection) and reaches the steady-state condition. As there is a greater pressure difference between the upstream (P_{in}) and downstream boundaries, CO_2 movement through brown coal is mainly governed by the pressure-driven advection process (Darcy's flow). Under the steady-state condition, the CO_2 pressure at the right boundary is equal to the injection pressure (P_{in}) and the left boundary is at steady-state downstream pressure (P_{out}).

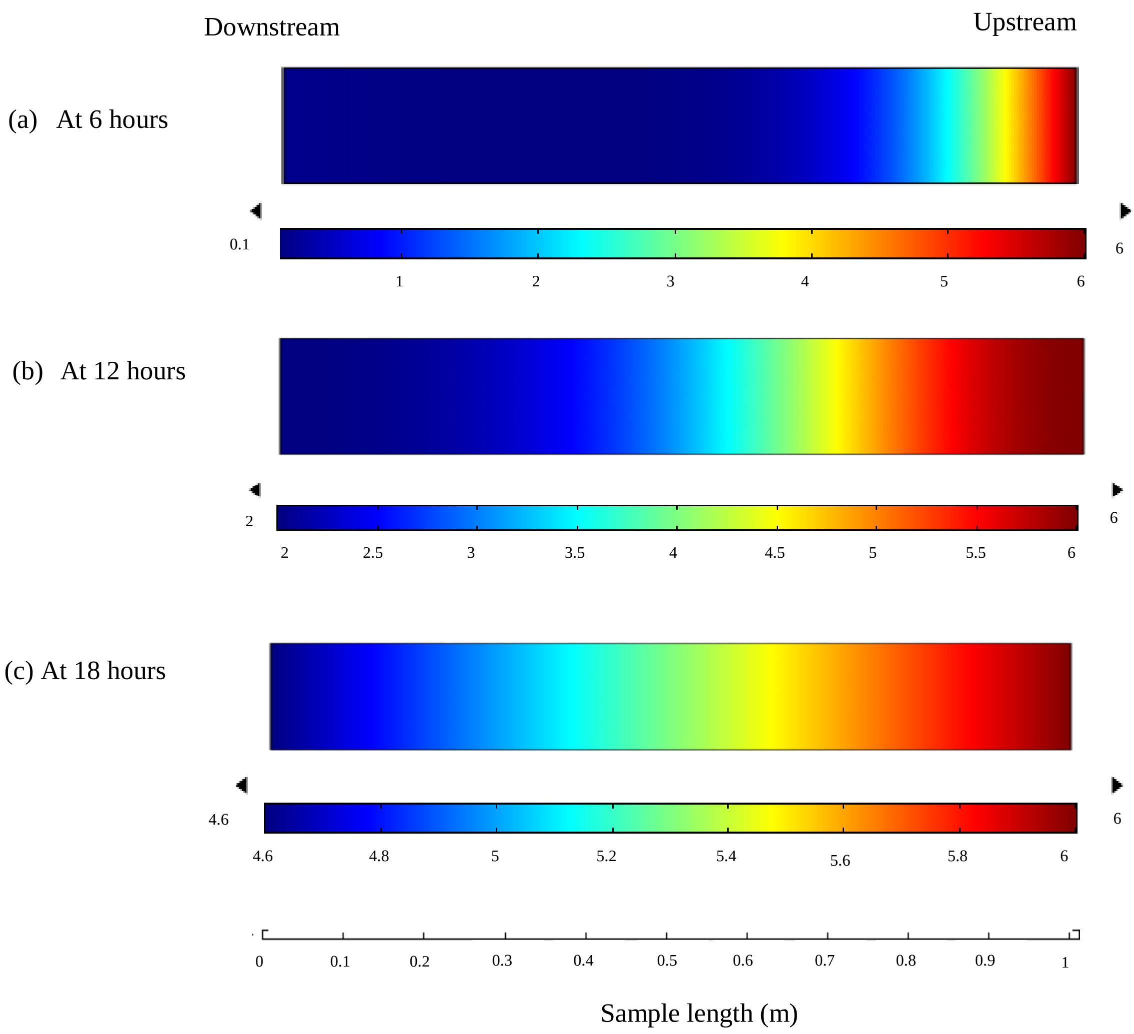

Figure 5.19. CO_2 pressure distribution (in MPa) in brown coal after 6, 12, and 18 hours of 6 MPa CO_2 injection under 17 MPa axial load

Then the CO_2 pressures through the brown coal specimen after 24 hours (assuming 24 hours is sufficient time to achieve the steady-state condition for all the injection pressures) were plotted for 6 and 8 MPa CO_2 injections for 11 MPa axial stress and compared with the experimental results observed for the respective conditions (refer to Figure 5.20). According to the figure, there is good agreement between the experimental predictions of pressure development along the coal specimen and the model-predicted data. The pressure distribution along the sample is almost constant up to around 1/3 of the sample length from the injection point and is gradually reduced up to downstream.

Figure 5.21 displays the model-predicted pressure development of the coal sample at 6 and 8 MPa CO_2 under different axial stresses. As observed in Figure 5.20, the CO_2 pressure reduces gradually along the length of the sample for any injection and axial load conditions. For a given injection pressure, the CO_2 pressure decreases with the increase in axial load (depth) after around 1/3 of the sample length at any distance from the injection surface (Figure 5.21). This may be due to the reduction in pore volume with increases in stress. The effective stress (the difference between axial load and mean injection pressure) increases as the depth increases, and an increase in effective stress causes pore volume shrinkage, leading to reduced flow pathways (Ranjith and Perera, 2011). However, as the injection pressure increases, the effect of depth on CO_2 pressure distribution gradually decreases (Figure 5.21(b)). This is possibly due to the reduced CO_2 flow during higher injection pressures (super-critical conditions), which creates lower pressure developments across the coal specimen that eventually has less variation with depth (Nasvi et al., 2014). These results are consistent with the CO_2 pressure variations observed by Ranathunga et al. (2016a) for similar low rank coal along the sample.

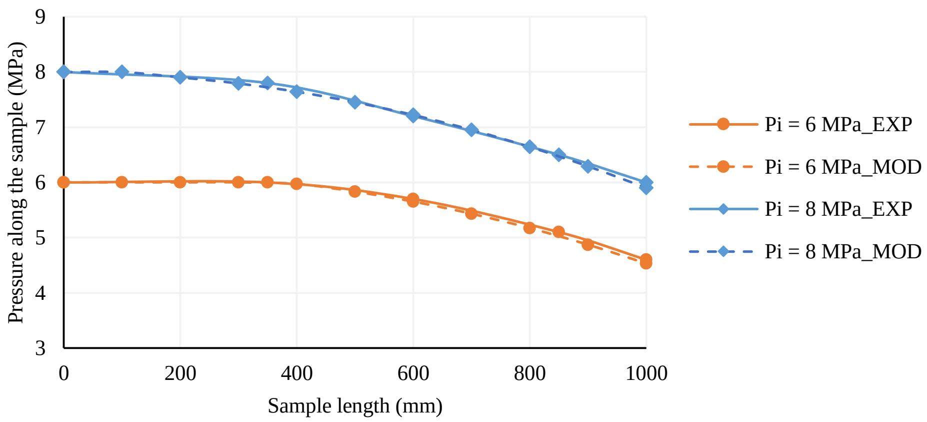

Figure 5.20. Pressure distribution along the coal sample under 11 MPa axial stress for 6 and 8 MPa CO_2 injections from flow experiments (Ranathunga et al., 2015) and model prediction after 24 hours

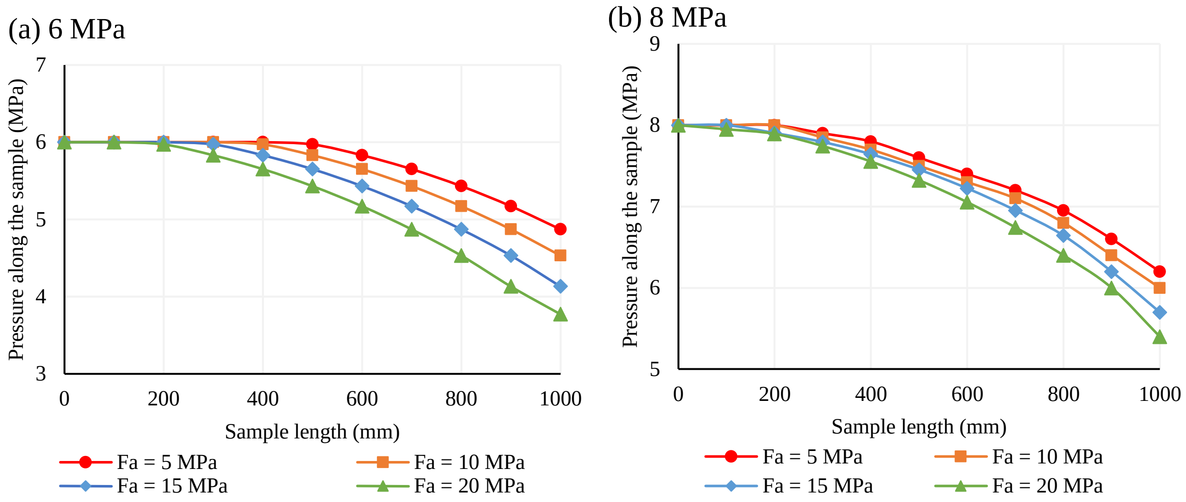

Figure 5.21. CO_2 pressure development along the brown coal specimen during 6 and 8 MPa CO_2 injection for different axial stresses applied on the sample

b. Distribution of CO_2 concentration along the coal specimen during CO_2 permeation

The CO_2 concentration distribution for different injection and axial stresses was studied. The concentration of CO_2 up to 18 hours of CO_2 injection for 6 MPa injection and 17 MPa axial load is shown in Figure 5.22. The CO_2 mass spreads with time due to advection and reaches a stable condition after 18 hours of CO_2 permeation. The concentration at the upstream boundary (right-side boundary) of the coal increases from 2.77 to 7.02 kg/m^3 after 6 to 18 hours of CO_2 injection, while the concentration at the downstream boundary (left-side boundary) increases from 1.96 to 5.62 kg/m^3 during the same time period.

Figure 5.23 shows the CO_2 concentration distribution in coal after 24 hours of CO_2 injection for different injection and axial loads. In the figure, the CO_2 concentration reduces along the coal sample following a slight exponential behaviour for both 6 and 8 MPa CO_2 permeations. As expected, for a given injection pressure, CO_2 concentration reduces with increases in axial stresses and the results are consistent with the pressure distribution trends obtained for various axial loads. In addition, for a given axial load, CO_2 concentration increases with the increase in injection pressures (Figures 5.23(a) and (b)). For example, under 20 MPa axial load, CO_2 concentration at the upstream (left-side boundary) increases from 6.61 to 13.59 kg/m^3 as the injection pressure is increased from 6 to 8 MPa. This is due to the increase in net CO_2 flux with the increase in CO_2 injection pressure through the coal sample.

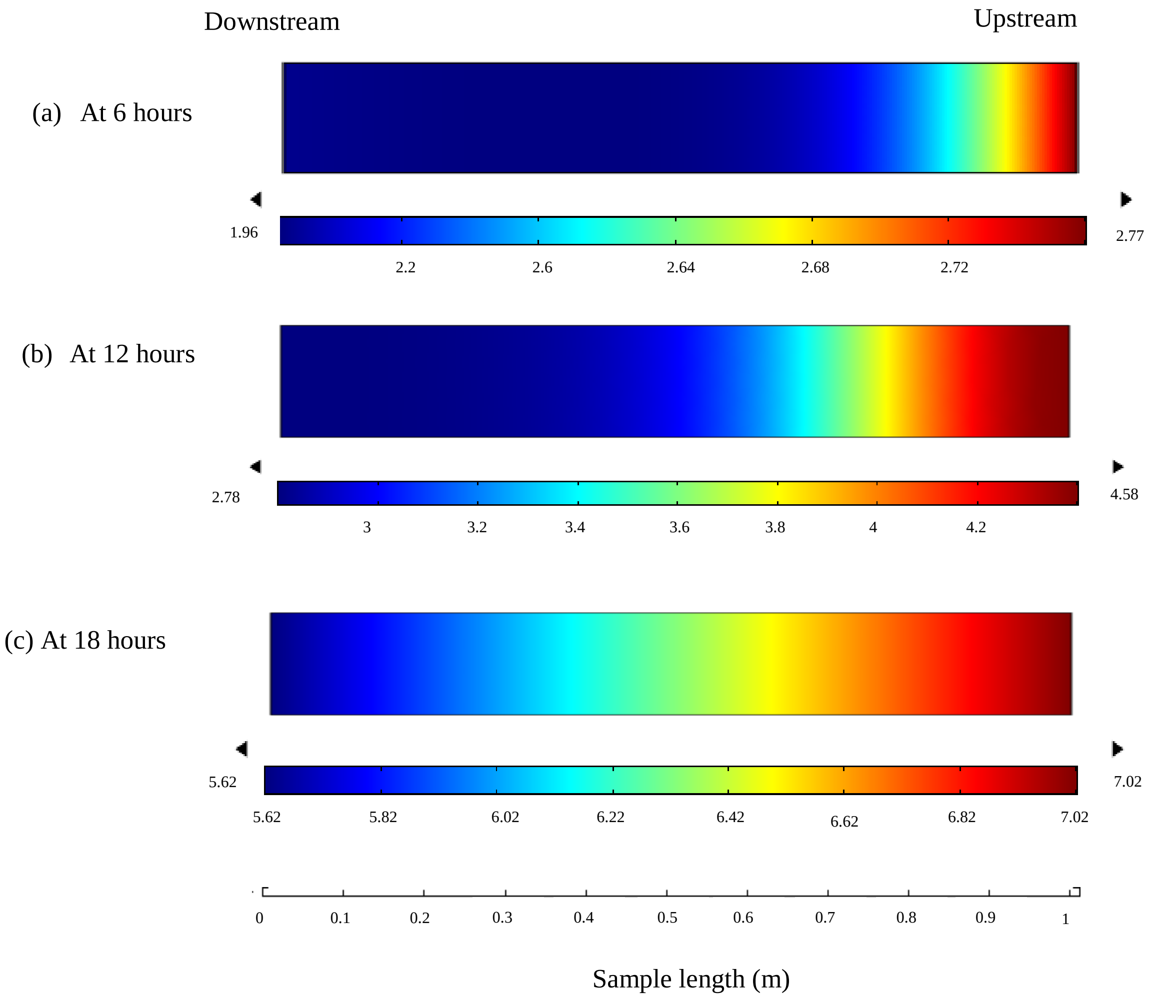

Figure 5.22. CO_2 concentration (in kg/m^3) distribution in brown coal after 6, 12, and 18 hours of 6 MPa CO_2 injection under 17 MPa axial load

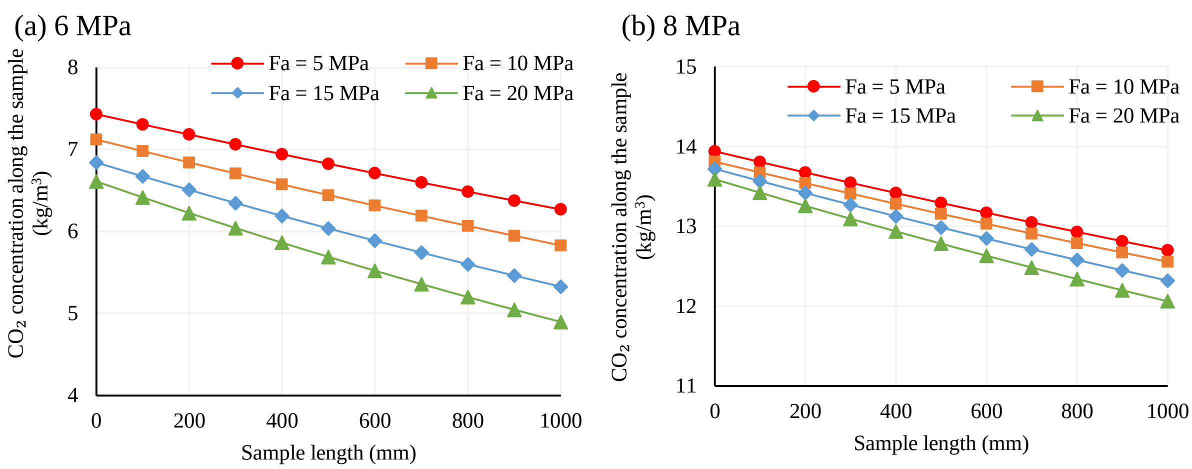

Figure 5.23. CO_2 concentration along the brown coal specimen during 6 and 8 MPa CO_2 injections for different axial stresses applied on the sample

5.4.3.4 CO_2 storage capacity of the coal sample

The main purpose of CO_2 sequestration in coal is to store CO_2 stably due to its high adsorption potential to the coal matrix. Therefore, identification of the adsorption potential of a given coal seam is important for the evaluation of the amount of CO_2 that can be stored in the coal mass. According to Ranathunga et al. (2016b), a brown coal specimen showed an increment of cumulative weight of CO_2 injected into the coal sample with time under both 11 and 17 MPa axial stress applications. Assuming that the total amount of CO_2 injected into the coal mass equals the total amount of CO_2 adsorbed into the coal mass (note that the flow tests were conducted under undrained conditions, therefore the CO_2 injected into the coal sample had no escape paths from the sample during permeation), this observation was compared with the model-predicted cumulative weight of CO_2 adsorbed into the coal mass with time. The results are shown in Figure 5.24. The amounts of CO_2 adsorbed into the coal specimen under different injection pressures and axial loads were obtained using Eq. [5.19].

$$W_{ads} = \left(\frac{\rho_{CO2,i}}{tds.cP\_c}\right) AL \qquad [5.19]$$

where, $\rho_{CO2,i}$ is the density of CO_2 at a given injection pressure (here $\rho_{CO2,i}$ was substituted in mol/m^3), i = sub- and super-critical phase conditions (refer to Eqs. [5.12a,b]), and $tds.cP\_c$ is a model parameter for the concentration of species adsorbed into the solid in mol/kg.

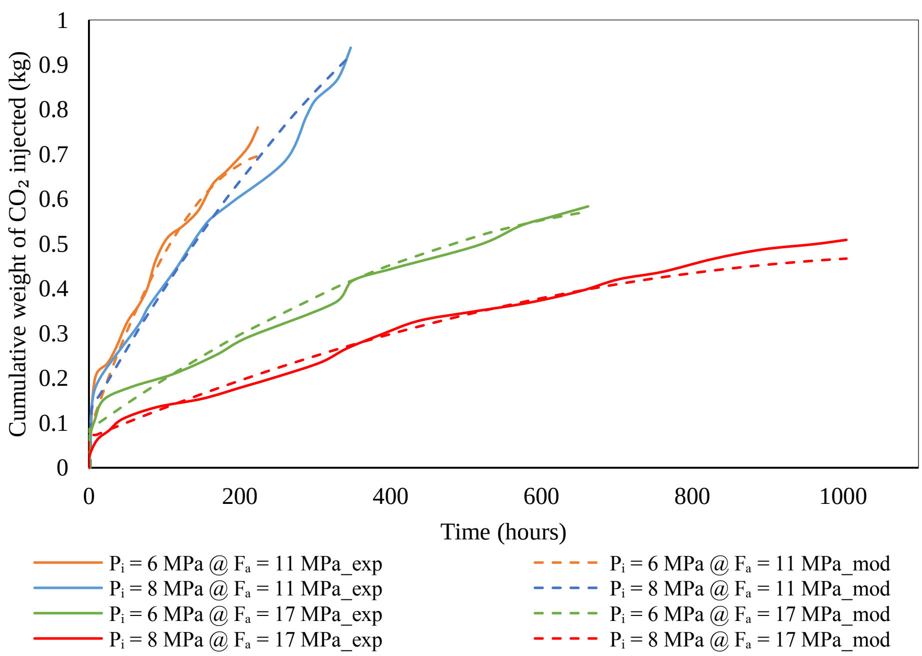

Figure 5.24. Comparison of model predicted and experimental observations for cumulative CO_2 weight injected into the coal specimen at 6 and 8 MPa CO_2 permeations under 11 and 17 MPa axial stresses

As shown in the figure, the experimental observations for the cumulative amount of CO_2 adsorbed into the sample are predicted well by the numerical model for different injection pressures and axial stresses. Further, there is only <8% difference in the experimental and model-predicted total amount of CO_2 adsorbed into the coal mass at the end of 10 days of CO_2 injection (see Table 5.6). Here, a duration of 10 days means the time after the specimen accomplishes the steady-state. Therefore, the total weight of CO_2 that can be adsorbed for various CO_2 pressures under different axial loads after injecting CO_2 for 10 days (after approaching steady-state conditions) was evaluated and the results are shown in Figure 5.25. According to the figure, the adsorbed CO_2 weight is exponentially reduced with increasing axial loads for a given CO_2 injection pressure. For an example, around 24% and 32% reduction of total CO_2 adsorption was observed for 4 and 12 MPa CO_2 injections when the axial loads are increased from 4 to 20 MPa (refer to Figure 5.25). This is due to the reduced adsorption capacity with CO_2 reduced permeability under higher stress applications (Hol et al., 2011). In addition, for a given axial load, the adsorbed CO_2 weight is also increased. For instance, around 45% increase in adsorbed weight is observed for 4 MPa axial load when CO_2 injection pressure is increased from 4 to 12 MPa. As explained by Ranathunga et al. (2016b), the greater adsorption capacity that increases with the injection pressure due to CO_2's inherent physical and chemical properties may increase the adsorbed CO_2 weight. It should be noted that, due to the sufficient time allowed for CO_2 permeation (time to reach steady-state condition plus 10 days), the lower permeabilities at higher CO_2 pressures are increased. Interestingly, the depth effect is reduced at higher CO_2 pressures, possibly due to the larger number of CO_2 molecules entering the sample at higher pressures leading to greater adsorption into the coal mass.

Table 5.6. Error between the experimental and model-predicted total adsorbed CO_2 weight

Axial load (MPa)	**CO_2 injection pressure (MPa)**	**Experimental value (kg)**	**Model predicted value (kg)**	**Error (%)**
11	6	0.75	0.71	5.33
	8	0.87	0.92	-5.82*
17	6	0.64	0.60	6.25
	8	0.67	0.61	7.46

*Negative sign means that the model-predicted value is higher than the experimental value

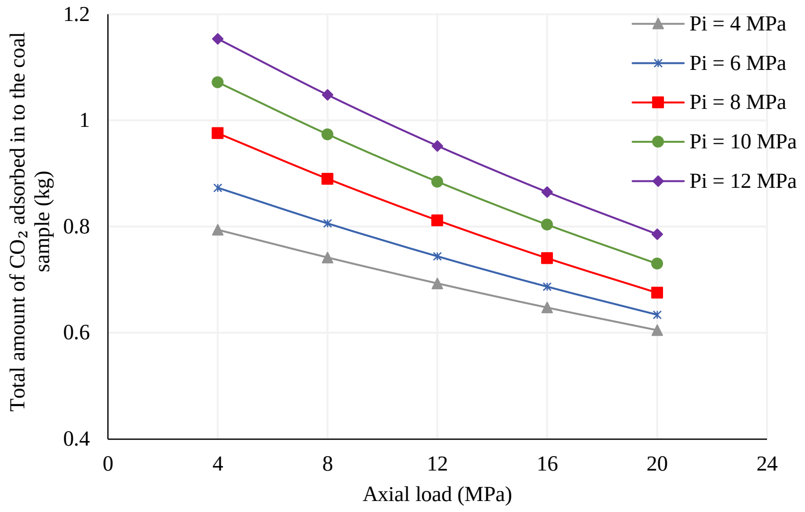

Figure 5.25. Total amount of CO_2 adsorbed into the coal sample during various CO_2 permeations under different axial loads (10 days after reaching steady-state condition)

5.4.4 Conclusions

This work focused on the numerical modelling of CO_2 flow through low rank brown coal using the COMSOL Multiphysics numerical simulator for different CO_2 injections and axial loads. The *Poro-elasticity* interface in the Structural Mechanics module and the *Transport of diluted species in porous media* interface in the Chemical species transport module were used to build the model in COMSOL. The model was first calibrated using part of the experimental data for CO_2 permeability (6, 8 and 10 MPa injections under 11 and 17 MPa axial loads) and validated using the rest of the data. It was noted that the CO_2 permeability values of coal predicted by the model were consistent with the experimental results. Next, the model was extended to different injection pressures and axial loads to observe the behaviour of a thin coal seam during CO_2 sequestration. The following major conclusions were drawn from the model results.

- ➢ CO_2 permeability through the coal mass is negatively affected by both CO_2 pressure and the depth of the coal seam, and this effect is decreased for greater depths and CO_2 pressures.
- ➢ CO_2 pressure distribution along the coal sample can be predicted reasonably well by the COMSOL model. Further, the flow parameters, such as CO_2 pressure and CO_2 concentration, reduce along the sample length with greater depths, and this is related to pore volume shrinkage caused by increased effective stress application.
- ➢ However, for a given axial load, CO_2 concentration increases with the increase in injection pressure, and this is due to the increase in net advective CO_2 flux with the increase in injection pressure.
- ➢ The CO_2 storage capacity in coal mass from the experiments and the model estimations followed a similar behaviour, showing an increase in cumulative adsorbed CO_2 weight with

time. In addition, the experimentally-derived total CO_2 adsorption 10 days after approaching steady-state condition deviated by <8% from the model predictions.

- According to the model results for different CO_2 pressures and depths, greater amounts of CO_2 can be sequestrated into coal seams even at higher depths and higher CO_2 pressures despite the flow reduction observed if a sufficient time is allowed for CO_2 permeation.

5.4.5 References

Anggara, F., Sasaki, K., Sugai, Y., 2013. Swelling Measurements of a Low Rank Coal in Supercritical CO_2. *International Journal of Geosciences* 4, 863-870.

Day, S., Fry, R., Sakurovs, R., 2008. Swelling of Australian coals in supercritical CO_2. *International Journal of Coal Geology* 74, 41-52.

De Silva, P.N.K., Ranjith, P.G., 2013. Advanced core flooding apparatus to estimate permeability and storage dynamics of CO_2 in large coal specimens. *Fuel* 104, 417-425.

De Silva, P.N.K., Ranjith, P.G., 2014. Understanding the significance of in situ coal properties for CO_2 sequestration: An experimental and numerical study. *Int J Energ Res* 38, 60-69.

Hol, S., Peach, C.J., Spiers, C.J., 2011. Applied stress reduces the CO_2 sorption capacity of coal. *International Journal of Coal Geology* 85, 128-142.

Jasinge, D., 2010. An investigation of the effect of carbon dioxide sequestration on the behaviour of brown coal (*PhD thesis*). Monash University, Melbourne, Australia.

Liu, G., Smirnov, A.V., 2009. Carbon sequestration in coal-beds with structural deformation effects. *Energy Conversion and Management* 50, 1586-1594.

McLinden, M., Klein, S., Lemmon, E., Peskin, A., 1998. REFPROP, Thermodynamic and transport properties of refrigerants and refrigerant mixtures. NIST Standard Reference Database 23.

Nasvi, M.C.M., Ranjith, P.G., Sanjayan, J., 2014. A numerical study of CO_2 flow through geopolymer under down-hole stress conditions: Application for CO_2 sequestration wells. *Journal of Unconventional Oil and Gas Resources* 7, 62-70.

Perera, M.S.A., Ranjith, P.G., Choi, S.K., Bouazza, A., 2013. A parametric study of coal mass and cap rock behaviour and carbon dioxide flow during and after carbon dioxide injection. *Fuel* 106, 129-138.

Perera, M.S.A., Ranjith, P.G., Choi, S.K., Airey, D., 2011. The effects of sub-critical and super-critical carbon dioxide adsorption-induced coal matrix swelling on the permeability of naturally fractured black coal. *Energy* 36, 6442-6450.

Perera, M.S.A., Ranjith, P.G., Choi, S.K., Airey, D., 2012. Investigation of temperature effect on permeability of naturally fractured black coal for carbon dioxide movement: An experimental and numerical study. *Fuel* 94, 596-605.

Ranathunga, A., Perera, M., Ranjith, P., Ju, Y., Vishal, V., De Silva, P., 2015. A macro-scale experimental study of sub-and super-critical CO_2 flow behaviour in Victorian brown coal. *Fuel* 158, 864-873.

Ranathunga, A.S., Perera, M.S.A., Ranjith, P.G., 2016a. Super-critical carbon dioxide flow behaviour in low rank coal: A meso-scale experimental study, *Journal of CO_2 Utilization* (under review).

Ranathunga, A.S., Perera, M.S.A., Ranjith, P.G., De Silva, G.P.D., 2016b. A macro-scale view of the influence of effective stress on carbon dioxide flow behaviour in coal: an experimental study. *Geomechanics and Geophysics for Geo-Energy and Geo-Resources*, 1-16.

Ranjith, P.G., Perera, M.S.A., 2011. A new tri-axial apparatus to study the mechanical and fluid flow aspects of carbon dioxide sequestration in geological formations. *Fuel* 90, 2751-2759.

Zhou, L., Feng, Q., Chen, Z., Liu, J., 2012. Modelling and upscaling of binary gas coal interactions in CO_2 enhanced coalbed methane recovery. *Procedia Environmental Sciences* 12, 926-939.

5.5 Chapter summary

The main objective of this chapter was to investigate how the flow behaviour of coal is influenced by reservoir depth and CO_2 properties and the corresponding variation of CO_2 storage capacity. Macro-scale reconstituted coal samples were used for the experiments to represent a homogeneous thin coal seam, and the major findings are summarised below.

- Similar results were obtained for macro-scale homogeneous samples as for meso-scale experimental studies on natural intact brown coal specimens, as follows:
  - CO_2 permeability in coal reduces with increasing injection pressure due to the phase transition of CO_2 from sub-critical to super-critical during the pressure increment.
  - Further, CO_2 permeability in coal is greater at lower depths and lower CO_2 injection pressures, while it gradually reduces with increasing depth and injection pressure.
  - Super-critical CO_2 causes greater swelling in the coal mass than sub-critical CO_2, and the swelling increases with increasing injection pressure, regardless of depth. This swelling increment is however reduced with increasing seam depth.

- The pressure profiles along the sample length were then examined for each injection pressure by considering the pressure gaps at three main regions along the sample. The following observations were made:
  - There were similar pressure development trends for CO_2 and alternative N_2 injections along the sample, which were non-linear.
  - However, there was a noticeable pressure reduction in the initial region of the samples during the second N_2 injection due to the coal structure re-arrangement which occurred during the CO_2 flood.
  - The observed CO_2 permeability along the tested coal specimen indicated that the critical zone of influence for CO_2 injection into a selected coal seam is greater at lower injection pressures and at shallow depths, and it reduces with increasing CO_2 pressure and seam depth.

- The observed CO_2 storage capacity of the tested coal under various conditions revealed that CO_2 storage capacity in a coal seam is greater at greater depths and higher CO_2 injection pressures. However, the reduction of CO_2 storage capacity with depth was not significant, which is important for field CO_2 sequestration projects, which normally use deep seams to store CO_2.

- The laboratory-scale model developed, calibrated and validated based on the experimental results could predict the coal mass flow behaviours, pressure development along the coal samples and CO_2 storage capacities fairly accurately. According to the model results, if sufficient time is allowed for CO_2 permeation, greater amounts of CO_2 can be sequestrated into coal seams even at higher depths and higher CO_2 pressures despite the flow reduction observed.

Part 3: Chapters 6 and 7

Investigation of variation of coal's mechanical properties during carbon dioxide sequestration

Part 3: Investigation of variation of coal's mechanical properties during carbon dioxide sequestration

CO_2 sequestration during the ECBM process affects the hydro-mechanical properties of the coal mass. Hence, in this chapter, the main focus is the CO_2 sequestration-induced coal mass mechanical property variations. This chapter reports on the meso-scale experiments coupled with micro-scale experiments and their outcomes. For the experiments, mainly Victorian brown coal (low-rank coal) was used and the results are compared with those for high-rank coal reported in the research literature. As summarised in Chapter 2, several factors affect CO_2 adsorption-induced coal matrix rearrangements, such as the fluid properties in the coal mass (CO_2 phase and pressure, different fluids etc.) and coal mass properties (coal rank, depth etc.). The findings are presented in this section of the thesis as follows.

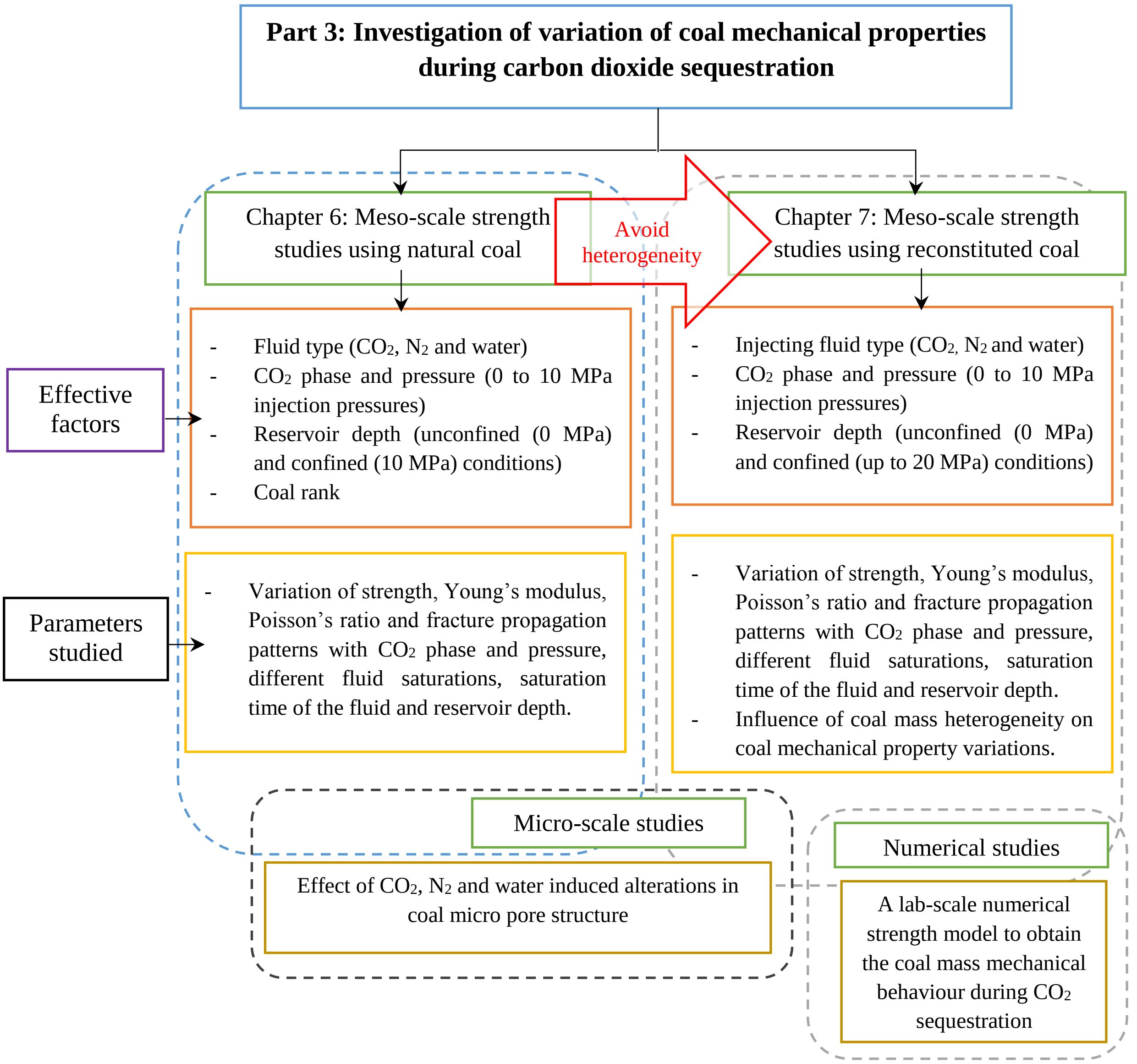

PART 3 - CHAPTER 6

Investigation of coal mechanical property variations during carbon dioxide sequestration using natural coal

Publication included in Chapter 6

Chapter 6 includes three publications. Details of the publications are as follows.

Chapter 6.2

Ranathunga AS, Perera MSA, Ranjith PG, Bui H (2015). Supercritical CO_2 saturation-induced mechanical property alterations in low rank coal: An experimental study. *The Journal of Supercritical Fluids* 109, 134-140.

Chapter 6.3

Perera MSA, **Ranathunga AS**, Ranjith PG (2016). Effect of coal rank on various fluid saturations creating mechanical property alterations using Australian coals. *Energies* 9(6), 440. DOI: doi:10.3390/en9060440.

Chapter 6.4

Ranathunga AS, Perera MSA, Ranjith PG (2016). Influence of CO_2 adsorption on the strength and elastic modulus of low rank Australian coal under confining pressure. *International Journal of Coal Geology* 167, 148-156.

Declaration for Thesis Chapter 6.2

In the case of Chapter 6.2, the nature and extent of my contribution to the work was the following:

Nature of contribution	**Extent of contribution (%)**
Initiation, key ideas, experimental work, data analysis and writing up	85

The following co-authors contributed to the work. If co-authors are students at Monash University, the extent of their contribution in percentage terms must be stated:

Name	**Nature of contribution**	**Extent of contribution (%) for student co-authors only**
Perera MSA	Key ideas, reviewing and editing the manuscript	N/A
Ranjith PG	Key ideas, reviewing and editing the manuscript	N/A
Bui H	Reviewing and editing the manuscript	N/A

The undersigned hereby certify that the above declaration correctly reflects the nature and extent of the candidate's and co-authors' contributions to this work*.

Candidate's signature	[redacted]	**Date** 25/01/2017

Main Supervisor's signature	[redacted]	**Date** 25/01/2017

*Note: Where the responsible author is not the candidate's main supervisor, the main supervisor should consult with the responsible author to agree on the respective contributions of the authors.

Declaration for Thesis Chapter 6.3

In the case of Chapter 6.3, the nature and extent of my contribution to the work was the following:

Nature of contribution	Extent of contribution (%)
Initiation, key ideas, experimental work, data analysis and writing up	85

The following co-authors contributed to the work. If co-authors are students at Monash University, the extent of their contribution in percentage terms must be stated:

Name	Nature of contribution	Extent of contribution (%) for student co-authors only
Perera MSA	Key ideas, reviewing and editing the manuscript	N/A
Ranjith PG	Key ideas, reviewing and editing the manuscript	N/A

The undersigned hereby certify that the above declaration correctly reflects the nature and extent of the candidate's and co-authors' contributions to this work*.

Candidate's signature	[redacted]	**Date** 25/01/2017

Main Supervisor's signature	[redacted]	**Date** 25/01/2017

*Note: Where the responsible author is not the candidate's main supervisor, the main supervisor should consult with the responsible author to agree on the respective contributions of the authors.

Declaration for Thesis Chapter 6.4

In the case of Chapter 6.4, the nature and extent of my contribution to the work was the following:

Nature of contribution	**Extent of contribution (%)**
Initiation, key ideas, experimental work, data analysis and writing up	85

The following co-authors contributed to the work. If co-authors are students at Monash University, the extent of their contribution in percentage terms must be stated:

Name	**Nature of contribution**	**Extent of contribution (%) for student co-authors only**
Perera MSA	Key ideas, reviewing and editing the manuscript	N/A
Ranjith PG	Key ideas, reviewing and editing the manuscript	N/A

The undersigned hereby certify that the above declaration correctly reflects the nature and extent of the candidate's and co-authors' contributions to this work*.

Candidate's signature	[redacted]	**Date** 25/01/2017

Main Supervisor's signature	[redacted]	**Date** 25/01/2017

*Note: Where the responsible author is not the candidate's main supervisor, the main supervisor should consult with the responsible author to agree on the respective contributions of the authors.

6. Investigation of coal mechanical property variations during carbon dioxide sequestration using natural coal

6.1 Overview

This chapter reports the results of experimental studies conducted using natural coal samples (Victorian brown coal) to investigate the variations of coal mass mechanical properties, strength, Young's modulus, Poisson's ratio and fracture propagation patterns during CO_2 sequestration, to fulfil objective 2 of this research work. The experiments were carried out to test the influence of different effective parameters on the coal mass strength properties and are presented as follows in this chapter.

- **Section 6.2**: ***How do CO_2 phase and pressure affect coal mass integrity?***

The injecting gas properties (CO_2 pressure and phase effect) of the coal mass strength were studied using a series of uniaxial compressive strength (UCS) tests on brown coal. Another objective of this study was to reveal some insights regarding CO_2-induced micro-structural changes.

This section of the chapter is the following publication:

Ranathunga AS, Perera MSA, Ranjith PG, Bui H (2015). Supercritical CO_2 saturation-induced mechanical property alterations in low rank coal: An experimental study. *The Journal of Supercritical Fluids* 109, 134-140.

- **Section 6.3**: ***How do various fluid saturations alter coal mass strength properties with coal rank?***

An effort was made to quantify the coal mass strength variations during different fluid saturations with water and N_2. Further, how this variation changes with coal maturity (coal rank) was also investigated using both brown coal (lignite from the Gippsland basin) and black coal (bituminous coal from the Sydney basin). The results acquired from the UCS tests were compared with CO_2 saturation-induced mechanical property variations to obtain a comparison of the effect of different fluids on coal mass during the ECBM process.

This section of the chapter is the following publication:

Perera MSA, **Ranathunga AS**, Ranjith PG (2016). Effect of coal rank on various fluid saturations creating mechanical property alterations using Australian coals. *Energies* 9(6), 440.

- **Section 6.4**: ***How does the influence of CO_2 adsorption on coal mechanical properties vary under different confining pressure and with various fluid saturation times?***

Several test sequences were executed under confinement to study the influence of confining pressure on coal mass strength deviations which represent field conditions during ECBM. Both sub- and super-critical CO_2 injections were used to saturate the brown coal samples during the experiments. The results are presented as Langmuir-type equations which can be utilised for numerical studies regarding CO_2-ECBM for different CO_2 pressures under various confining pressures. At the same time, the long-term effect of CO_2 adsorption-induced coal mass strength property changes was studied, as CO_2 sequestration is a long-term process. Brown coal was used in the experiments and it was saturated for 3, 6, 9 and 12 months to study the time effect.

This section of the chapter is the following publication:

Ranathunga AS, Perera MSA, Ranjith PG (2016). Influence of CO_2 adsorption on the strength and elastic modulus of low rank Australian coal under confining pressure. *International Journal of Coal Geology* 167, 148-156.

6.2 How do CO_2 phase and pressure affect coal mass integrity?

According to Chapter 2, CO_2 phase and pressure play the main role in CO_2 adsorption- induced coal mass flow behaviour and super-critical CO_2 injection has greater effects on the coal matrix. Therefore, it is also important to find how these CO_2 properties change the coal mass strength. There have been several studies on the effect of CO_2 properties on high- rank coal strength. However, with the exception of a few studies on low-rank coal using sub-critical CO_2 saturation, to date no study has been conducted on the effect of super-critical CO_2 saturation on low-rank coal strength. Therefore, a series of UCS tests was carried out on low-rank brown coal from the Gippsland basin under both sub- and super-critical CO_2 saturations to investigate the effect of CO_2 properties on coal strength and Young's modulus. The ARAMIS optical strain system was used to obtain the strain development in coal together with the AE system to capture the strain energy released under different CO_2 saturation conditions. The results were compared with the data on high-rank coal data in the literature to identify the effect of coal rank on CO_2 sequestration-related coal mass strength variations. Furthermore, SEM analysis was conducted to gain insight into the micro-structural changes under different CO_2 saturation conditions.

This section of the chapter is the following publication:

Ranathunga AS, Perera MSA, Ranjith PG, Bui H (2015). Supercritical CO_2 saturation-induced mechanical property alterations in low rank coal: An experimental study. *The Journal of Supercritical Fluids* 109, 134-140.

J. of Supercritical Fluids 109 (2016) 134–140

Contents lists available at ScienceDirect

The Journal of Supercritical Fluids

journal homepage: www.elsevier.com/locate/supflu

Super-critical CO_2 saturation-induced mechanical property alterations in low rank coal: An experimental study

A.S. Ranathunga, M.S.A. Perera*, P.G. Ranjith, H. Bui

Deep Earth Energy Laboratory, Department of Civil Engineering, Monash University, Building 60, Melbourne, Victoria 3800, Australia

ARTICLE INFO

Article history:
Received 11 June 2015
Received in revised form
11 November 2015
Accepted 11 November 2015
Available online 1 December 2015

Keywords:
Brown coal
Mechanical properties
Sub- and super-critical CO_2

ABSTRACT

The adsorption of carbon dioxide (CO_2) into the coal matrix during CO_2-enhanced methane recovery causes significant alterations to the coal mass chemical and physical structures, causing modifications to coal's mechanical properties. Hence, the main objective of this study is to investigate the effects of sequestrated CO_2 phase condition on coal strength. A series of unconfined compressive strength tests was conducted on Australian brown coal samples, saturated under various CO_2 pressures (2–10 MPa) at 35 °C using an advanced acoustic emission (AE) system and optical 3D deformation analysis. According to the results, super-critical CO_2 has the ability to cause a greater reduction of strength (by 46%) and enhancement of elasticity properties (by 20%) in brown coal compared to sub-critical CO_2, because super-critical CO_2 has greater adsorptive potential, which eventually creates greater coal matrix swelling. According to the AE and deformation analysis, the coal mass natural cleat system contributes significantly to the observed CO_2 adsorption-induced changes in mechanical properties.

6.2.1 Introduction and background

With increasing industrialization, carbon dioxide (CO_2) emissions are becoming a major concern, directly affecting global warming. Of the various feasible methods, CO_2 sequestration in deep unmineable coal seams is recognized as one of the most promising CO_2 mitigation methods [1–4]. However, there are certain risks that need to be considered with respect to the long-term safe storage of the sequestered CO_2.

According to Gibbs [5] and Griffith [6], a material can become weaker when a more chemically potential adsorbate substitutes the existing adsorbate of the material. In the CO_2-enhanced methane recovery process (CO_2-ECBM), CO_2 is a more chemically potential gas than pre-adsorbed methane in coal seams [5,6], which implies that the replacement of the CH_4 with CO_2 causes the coal seam strength to be reduced. Further, a natural coal matrix is a vastly brittle structure which confines the free movement of coal molecules [7]. When CO_2 is adsorbed into the coal matrix, it increases the ductile properties of the coal mass, because of the enhancement of free volume due to alterations in the coal matrix [8]. These coal struture modifications may create the potential for injected CO_2 to be released back to the atmosphere by the generation of faults [9]. This may lead to potential damage to infrastructure [10], and may cause hazardous occurrences such as gas outburst due to the increased pore pressure inside the weakened storage medium [11]. Several previous studies [8,10,12–15] have investigated this strength reduction in coal with CO_2 adsorption.

Initially, researchers [12,13] used coal powder or tiny cubes to check the influence of CO_2 on coal strength, and the study conducted by Czaplinski and Holda [13] showed a clear strength reduction in low rank coal with CO_2 adsorption, confirming the findings of Aziz and Ming-Li [12] obtained from drilling experiments on coal cubes saturated with CO_2, CH_4 and air. As these studies were conducted on small coal samples, they cannot represent the real adsorption process in the coal mass natural cleat system. Viete and Ranjith [15] were the first researchers to conduct standard unconfined compressive strength (UCS) tests on coal specimens to investigate the effect of CO_2 adsorption in the coal matrix. The 54 mm diameter and 108 mm high lignite samples used for this study displayed a reduction in both UCS (by 13%) and the elastic modulus (by 26%) for a 1.5 MPa CO_2 saturation at room temperature. However, CO_2 exists in its super-critical state (beyond the critical point of CO_2 – 7.38 MPa and 31.8 °C) in the coal seams suitable for CO_2 injection, due to the higher temperatures and pressures at these deep locations [16]. Super-critical CO_2 has higher adsorption potential [17] and unique physical properties compared to sub-critical CO_2, such as higher viscosities [18] and enhanced propensities [19]. This higher adsorptive nature of CO_2 leads to greater coal matrix swelling [20], which reduces the coal mass pore spaces. Therefore, with the aim of investigating the coal

* Corresponding author.
E-mail address: samintha.perera@monash.edu (M.S.A. Perera).

http://dx.doi.org/10.1016/j.supflu.2015.11.010
0896-8446/

mass strength reduction during super-critical CO_2 injection, Perera et al. [8] conducted several UCS tests using bituminous coal at 33 °C constant temperature. According to their findings, a greater reduction in coal mass strength can be observed due to super-critical CO_2 adsorption compared to sub-critical CO_2 adsorption (51% and 54% reduction of UCS and elastic modulus from 6 MPa to 8 MPa CO_2 saturation respectively) in bituminous coal. Ranjith and Perera [21] used lignite (low rank) and bituminous coal (high rank) to study the effect of carbon content (coal rank) on strength reduction for CO_2 adsorption up to 3 MPa CO_2 saturation pressure at 35 °C. They found a greater strength reduction (around 20%) in high rank coal than low rank coal during sub-critical CO_2 saturation.

However, to date researchers have considered only the response of high rank coal to super-critical CO_2 adsorption, and little is known about how super-critical CO_2 adsorption-induced strength reduction varies with coal rank. This study therefore, intends to fill this gap by determining the effect of super-critical CO_2 adsorption on the strength of low rank coal (lignite), and compares it with the effect on high rank coal [8]. Therefore, the main objective of the present study is to distinguish the effects of sub- and super-critical CO_2 saturation on the mechanical properties of low-ranked brown coal. This study involved an experimental programme of UCS testing on brown coal samples saturated with CO_2 under various sub- and super-critical pressures and unsaturated samples.

6.2.2 Methodology

6.2.2.1 Sample preparation for testing

Brown coal samples obtained from the Hazelwood mine in the Latrobe Valley, south-east Victoria, Australia were used for all testing purposes. The samples were stored in a fog room in the Monash University Deep Earth Energy Research Laboratory (DEERL) after being enclosed in polythene bags to preserve the natural moisture content and the overall chemical properties of the samples. Victorian brown coal is a low-rank coal (lignite) with a specific gravity of 1.035, with 48% fixed carbon, 1.7% ash yield, 50.3% volatile matter content and 0.28% sulphur content (all the percentage values are based on a dry basis) [15]. The samples used for this study (38 mm in diameter and 76 mm in height) were obtained from large coal blocks using the diamond coring and cutting machine available at DEERL, and a rock grinder was used to achieve smooth parallel surfaces for testing. The specimens were enclosed in polythene bags and stored in a plastic container in the fog room again to minimize moisture loss until the samples were used for the experiments.

6.2.2.2 Experimental methods

Using the pressure chamber available at DEERL [22], samples were saturated at various CO_2 pressures (2, 4, 6, 8 and 10 MPa) prior to testing. This apparatus can be used to saturate samples up to 10 MPa saturation pressure and includes a temperature control unit to maintain the system temperature, which was set to 35 °C (greater than the critical temperature of CO_2 31.8 °C). For the CO_2 saturation, samples were first positioned inside the pressure chamber (2 or 3 samples at a time) and gas was then injected into the pressure cell until the required saturation pressure was reached. Altogether, 15 samples were tested, including sub-critical CO_2 saturated samples, super-critical CO_2 saturated samples and unsaturated coal samples for comparison. Since the system temperature was greater than the critical temperature of CO_2 (31.8 °C), 2, 4 and 6 MPa (<7.38 MPa) the CO_2 saturated samples were under sub-critical conditions while the 8 and 10 MPa (>7.38 MPa) CO_2 saturated samples were under super-critical conditions. All the samples were saturated for a period of 21 days [14]. After the saturation period, the pressure chamber was gradually de-pressurized at a rate of 0.02 MPa/min to avoid possible damage to the physical structure of the coal specimens due to sudden changes in pressure. After the samples were removed from the saturation chamber, they were covered with plastic wraps and tested within around 20 min to avoid any possible changes to the saturation state of the samples.

a. UCS testing

The UCS tests were conducted according to the ASTM standards [23]. The testing was conducted using the Shimadzu compression machine located in DEERL and the loading rate was maintained at 0.1 mm/min for all the tests. An automatic data acquisition system was used to record the applied loads on the coal specimens with time, and optical 3D deformation analysis (ARAMIS photogrammetry) and acoustic emission (AE) systems were used to obtain the corresponding strains and fracture patterns during sample failure.

b. Optical 3D deformation analysis

An optical 3D deformation analysis system (ARAMIS photogrammetry), with two high-resolution cameras and a software system, was used to capture the strain behaviour during the load application in UCS testing. A pair of cameras is used to record the deformation of the structure by tracing discrete correlation areas within stereo images, and the system attempts to counterpart the areas in the stereo images from the cameras at each time step. In order to capture stereo images using the ARAMIS system, the test specimens require adequate image variation in tone and contrast all over to exclusively identify the correlation areas. This was accomplished by painting the sample surface with matt white paint followed by spreading a pattern of matt black paint dots on the surface. Prior to testing, a thorough calibration was carried out using a calibration plate with a known pattern of white dots on a black background. When the cameras were calibrated, testing of actual specimens was commenced.

c. Acoustic emission (AE) system

To identify the fracture propagation behaviour of the tested coal specimens under load application during the UCS testing, an advanced acoustic emission (AE) system was used. Two AE sensors in series were attached to the sample at either side of the specimen. To easily attach the sensors and to obtain the same sensitivity for each sensor, an electron wax was used. When the specimen was ready to be tested, both load application and the AE system were started simultaneously. After each test, the AE characteristic parameters were analyzed using the recorded AE data and the relationships between each characteristic parameter during the load application were investigated.

d. Scanning electron microscopy (SEM) analysis

A comprehensive SEM analysis was conducted using the FEI Quanta 3D FEG FIB machine located in the Monash Centre for Electron Microscopy (MCEM) using coal slices obtained before and after the CO_2 saturation. During sample preparation, several slices 2–5 mm in height were cut from each sample and saturated with CO_2 in the saturation chamber together with the samples used for the strength test. At the end of the saturation period, the samples were removed from the chamber by slowly releasing the pressure and prepared for the SEM analysis by adhering them to double-sided adhesive carbon tape attached to a circular specimen stub. Three types of samples were used for SEM analysis: 4 MPa CO_2 saturated (sub-critical); 8 MPa CO_2 saturated (super-critical); and unsaturated for comparison. The samples were viewed under 15 kV voltage with 4.5 spot size and low vacuum mode was used while operating the SEM machine, as brown coal is subjected to higher outgassing.

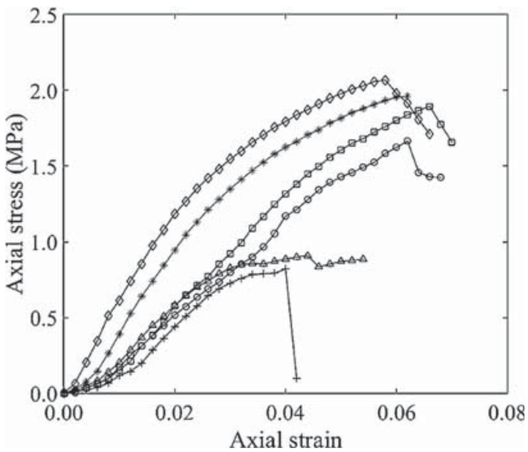

Fig. 1. Axial stress versus strain curves for unsaturated ("◊") and CO_2 saturated ("*" – 2 MPa, "□" – 4 MPa, "o" – 6 MPa, "△" – 8 MPa and "+" – 10 MPa) brown coal samples.

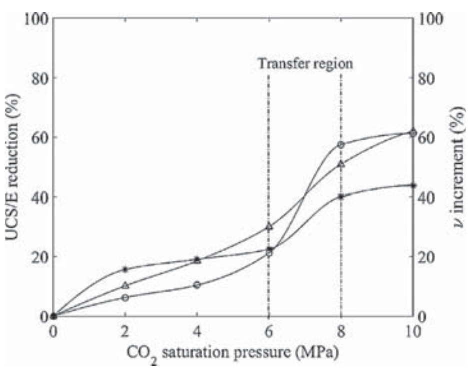

Fig. 2. CO_2 saturation-induced mechanical property alterations in brown coal (samples were saturated in CO_2 at 35 °C constant temperature. Here "o" – unconfined compressive strength (UCS) reduction, "*" – Young's modulus (E) reduction and "△" – Poisson's ratio (ν) increment).

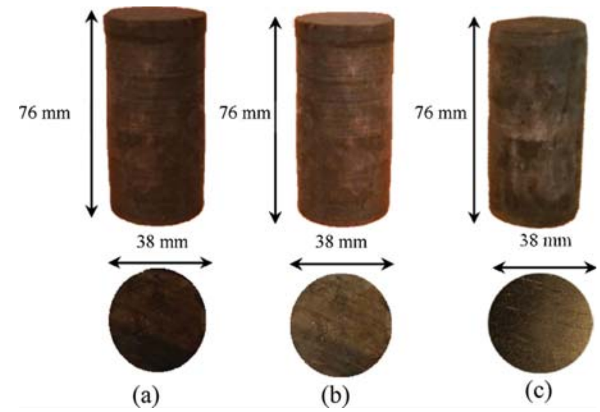

Fig. 3. Appearance of the brown coal samples before failure (a) unsaturated sample, (b) after saturation of 4 MPa CO_2 (sub-critical) and (c) after saturation of 8 MPa CO_2 (super-critical).

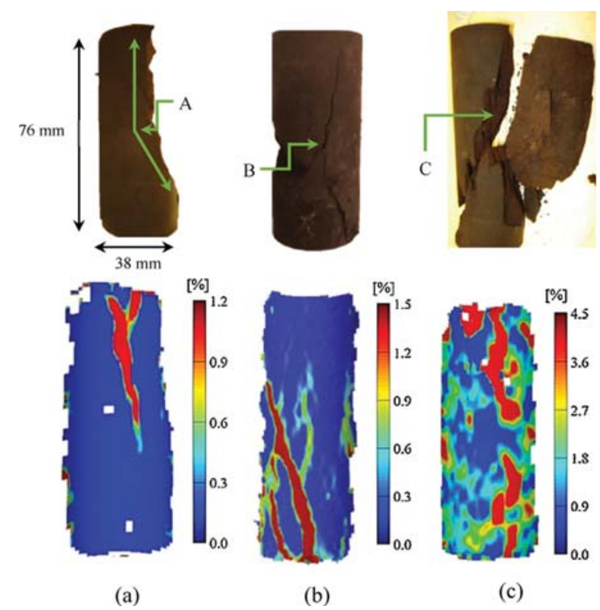

Fig. 4. Appearance of the samples after failure using optical 3D deformation analysis (at failure) (a) unsaturated sample, (b) after saturation of 4 MPa CO_2 (sub-critical) and (c) after saturation of 8 MPa CO_2 (super-critical) (here A: sample fails along a shear plane, B: sample fails along the major cleat system and C: sample fail along major and minor cleat system).

6.2.3 Experimental results and discussion

Axial stress–strains, ARAMIS responses and AE responses were tested for a total of 15 samples. Table 1 shows the UCS, Young's modulus and Poisson's ratio values obtained for all the tested samples and for discussion purposes, the specimens with the highest UCS values were considered to represent each test condition. Finally, the samples were subjected to SEM analysis for microstructural analysis.

6.2.3.1 CO_2 sequestration-induced alterations to geomechanical properties in brown coal

The following sections discuss the variations in brown coal geomechanical properties: UCS, Young's modulus and Poisson's ratio for both sub- and super-critical CO_2 saturation.

a. Unconfined compressive stress (UCS)

The stress–strain behaviours for sub- and super-critical CO_2 saturations are shown in Fig. 1. As Fig. 1 indicates, the UCS of brown coal is considerably reduced for all test conditions after CO_2 saturation, while it is more substantial in super-critical CO_2-saturated samples compared to the sub-critical CO_2-saturated samples.

As shown in Fig. 2, the UCS reduction due to sub-critical CO_2 adsorption gradually increases with increasing CO_2 saturation pressure from 2 to 6 MPa. Coal matrix swelling caused by CO_2 adsorption is the main causative factor for these variations [8]. According to Botnen et al. [24], the natural cleat system in coal acts as a locus for CO_2 adsorption and causes an expansion of the coal matrix along the cleat walls. This behaviour causes the coal structure to be changed by reducing its overall strength, as demonstrated by the physical appearance of the unsaturated and CO_2-saturated coal samples in Figs. 3 and 4. According to Fig. 4(a), the unsaturated brown coal sample failed along a shear plane and the CO_2-saturated sample failed along its major cleats (see Fig. 4(b)).

Interestingly, CO_2 adsorption-induced strength reduction in brown coal is subjected to a sudden increment (from 21.25% to 57.5%) when CO_2 saturation pressure is increased from 6 to 8 MPa (see Fig. 2), at which point CO_2 transfers from its sub- to super-critical state (here onwards the region between 6 to 8 MPa CO_2

Table 1
Mean values of uniaxial compressive strength (UCS), Young's modulus (E) and Poisson's ratio (ν) obtained from testing and changes in these values relative to values obtained from testing of unsaturated samples.

CO_2 saturation pressure (MPa)*	UCS (MPa)	Average UCS (MPa)	ΔUCS (%)	E (MPa)	Average E (MPa)	ΔE (%)	Average ν	Δν (%)
0 (unsaturated sample)	2.46 2.34 2.39	2.40	–	43.16 39.32 42.32	41.60	–	0.226	–
2 (sub-critical)	2.29 2.22 2.24	2.25	−6.25	36.17 33.68 35.39	35.08	−15.67	0.249	10.18
4 (sub-critical)	2.14 2.10 2.22	2.15	−10.42	33.48 32.94 34.53	33.65	−19.11	0.268	18.58
6 (sub-critical)	1.84 1.93	1.89	−21.25	31.26 33.20	32.23	−22.52	0.294	30.09
8 (super-critical)	0.97 1.06	1.02	−57.50	22.47 27.35	24.91	−40.12	0.341	50.88
10 (super-critical)	0.87 0.99	0.93	−61.25	20.18 26.66	23.42	−43.70	0.366	61.95

* Samples were saturated in CO_2 at 35 °C constant temperature.

is referred as the "transfer region"). This is believed to be related to the greater adsorptive capacity of super-critical CO_2 compared to sub-critical CO_2 [25] and the corresponding greater coal matrix swelling under super-critical CO_2 adsorption [26]. CO_2 adsorption in coal occurs along its natural cleat system [27] and therefore an expansion of cleat space occurs with the swelling of the coal matrix with CO_2 adsorption. Alternatively, swelling also causes the density of the coal mass to be reduced, which contributes to coal mass strength reduction. Hence, the greater adsorptive potential of super-critical CO_2 causes a greater strength reduction. This can be physically identified by checking the physical appearance of the failed sub- (see Fig. 3b) and super-critical CO_2 saturated coal samples (see Fig. 3c), where the coal mass breakage has clearly occurred through both minor and major cleats in the super-critical CO_2 saturated brown coal (Fig. 4c). This proves the greater chemical potential of super-critical CO_2 to attract both minor and major cleats.

However, further increase of the CO_2 saturation pressure beyond the transfer region does not cause any perceptible change in the brown coal UCS (see Fig. 2). According to Shi et al. [28], super-critical CO_2 permeability in brown coal significantly reduces with increasing super-critical CO_2 pressure. This may cause CO_2 flow ability through the sample to be reduced with increasing pressure, resulting in less matrix rearrangement at higher super-critical CO_2 pressures (8 MPa>).

Conversely, this observed strength reduction in brown (low rank) coal is comparatively less than the strength reductions reported for CO_2 saturated bituminous coal (high rank) in the research literature [8]. For example, Perera et al. [8] found a 53% and 78% UCS reduction in sub-critical CO_2 saturated (6 MPa) and super-critical CO_2 saturated (8 MPa) high-ranked bituminous coal respectively, compared to unsaturated bituminous coal samples. The lower strength reduction of low-ranked coal compared to high-ranked coal is due to the well-developed natural cleat system in bituminous coal during the coalification process, which acts as a pathway for CO_2 flow through the coal matrix, creating greater matrix alterations.

b. Young's modulus and Poisson's ratio

In addition to the UCS variations during CO_2 saturation, the results show that the Young's modulus and the Poisson's ratio of brown coal are also affected by CO_2 saturation (see Table 1). Due to sub-critical CO_2 saturation (6 MPa), the Young's modulus has a reduction of 22.52% and the Poisson's ratio has an increment of 30% compared to unsaturated specimens. As explained by Larsen et al. [7], coal is a highly brittle material with less freedom of movement, due to its glassy-strained higher energy structure. When CO_2 is adsorbed into this coal matrix, it results in an expansion of free volume by amending its polymer structure. This improves the coal mass ductile properties, resulting in decreased Young's modulus and increased Poisson's ratio.

In the transfer region, the reduction of Young's modulus at 8 MPa (40.12%) is twice that at 6 MPa (22.52%) and the increment in Poisson's ratio is by a factor of 1.5 (50.88% for 8 MPa and 30.09% for 6 MPa) compared to unsaturated samples. Chikatamarla et al. [29] indicated that, unlike sub-critical CO_2, super-critical CO_2 has better solubility for solid constituents due to its higher density. This causes the organic compounds in coal to be polymerized, leading to plasticization of coal during CO_2 saturation, enhancing the ductile properties of the coal [1]. This higher plasticization effect of super-critical CO_2 compared to sub-critical CO_2 causes the sudden changes in Young's modulus in the transfer region (see Fig. 2). Further, the previously mentioned greater coal mass expansion with coal matrix swelling during super-critical CO_2 adsorption results in the sudden enhancement of Poisson's ratio (see Fig. 2).

Further increase of the CO_2 saturation pressure beyond 8 MPa causes a marginal increase in Young's modulus reduction and Poisson's ratio increment (see Table 1). This observation is believed to be related to the previously mentioned permeability reduction in the super-critical region [28], which reduces brown coal's plasticization capacity. Overall, it can be concluded that the influence of CO_2 saturation on brown coal strength is clearly dependent on the adsorbed CO_2 phase condition, and the influence is more significant for super-critical CO_2 adsorption than for sub-critical CO_2 adsorption. However, further increase of CO_2 saturation pressure beyond the transfer region does not have any noticeable influence on brown coal's mechanical properties.

Comparing these results with those of previous studies [8], the Young's modulus reduction in high-ranked bituminous coal at 6 MPa CO_2 saturation is around 35.2% [8], which is higher than the Young's modulus reduction in low-ranked brown coal observed in the present study (22.52%). Further, at 8 MPa CO_2 saturation, 71.3% of Young's modulus reduction was observed by Perera et al. [8] for bituminous coal, while a reduction of 40.12% was observed for brown coal, according to the results of the present study. However, these Young's modulus values are not very different when compared with the UCS reduction values in high- and low-ranked coal (only around 10% different). This implies that, although there is a

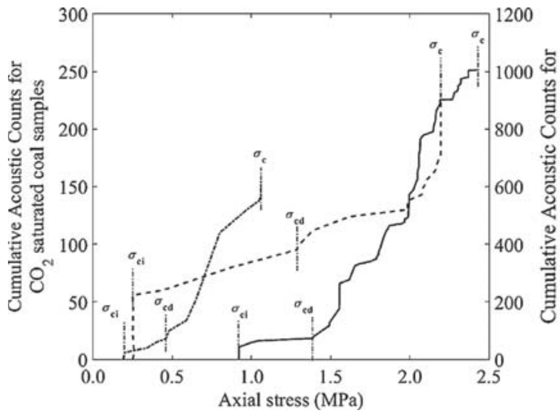

Fig. 5. Cumulative acoustic counts vs. axial stress of tested brown coal samples for unsaturated (continuous line), sub-critical (4 MPa) CO_2 saturated (dash line) and super-critical (8 MPa) CO_2 saturated (dotted line) samples (here σ_{ci} = crack initiation stress, σ_{cd} = crack damage stress and σ_c = unconfined compressive strength (UCS)) (refer to Table 2 for σ_{ci}, σ_{cd} and σ_c values).

higher CO_2 adsorption capacity and swelling in high-ranked coal, the structural rearrangements are comparatively similar in any coal rank.

6.2.3.2 CO_2 saturation effect on strain development in brown coal during load application

Fig. 4 shows ARAMIS images of natural, sub- and super-critical CO_2-saturated brown coal specimens during load application, and the range of colours in each specimen (blue to red) exhibits the variation in the strain values. The points inside the blue zone experienced the minimum stress before failure and the points inside the red zone faced the maximum stress before failure.

According to the ARAMIS images (Fig. 4), the coal samples saturated in CO_2 exhibit a ductile nature, with the super-critical CO_2 (8 MPa) saturated sample displaying greater ductile properties with 4.37% of highest strain at failure compared to the sub-critical CO_2 (4 MPa) saturated sample (1.5% of highest strain at failure). The uneven spread of red spots in the CO_2 saturated specimens just before failure (see Fig. 4(b) and (c)) reflects the heterogeneous nature of brown coal's strain distribution after CO_2 adsorption, and the strain distribution of unsaturated brown coal specimens appears moderately homogeneous in contrast (Fig. 4(a)). In addition, these ARAMIS images confirm that the shear-dominant failure mechanism in unsaturated coal samples changes to failure along the cleat system after CO_2 saturation (refer to Section a).

6.2.3.3 CO_2 saturation effect on fracture propagation patterns in brown coal

The AE system available in the DEERL was used to observe the fracture propagation patterns in brown coal under various saturation conditions. Fig. 5 shows the variation in the cumulative number of AE counts with axial stress for the tested samples (unsaturated, 4 MPa and 8 MPa) and Table 2 presents the stress threshold values obtained from Fig. 5. The AE technology has the ability to detect the energy release in the rock mass during the various stages of material failure [30]: crack closure, stable crack propagation, and unstable crack propagation. Of these, crack closure describes the initial period of the load application, at which the rock mass cracks are in closed position (the period from the start of load application to crack initiation stress (σ_{ci})). During the stable fracture propagation stage, the axial stress causes insignificant damage to the failure plane (the period from crack initiation stress (σ_{ci}) to crack damage stress (σ_{cd})), while the unstable fracture propagation stage occurs when the failure plane is damaged with the load application (the period from crack damage stress (σ_{cd}) to failure load (UCS)).

According to Fig. 5, the unsaturated sample exhibits a greater number of AE counts with load application compared to the CO_2-saturated samples (see Fig. 5). This is probably due to the coal matrix swelling-induced pre-existing cracks in the CO_2 saturated samples, which obviate the need for crack initiation during the loading. In addition, in the CO_2 saturated samples, both crack initiation and damage occur much more quickly than in the unsaturated sample, and the super-critical CO_2-saturated sample exhibits the quickest cracking occurrence. This is because, in addition to the pre-existing cracks, the coal matrix is much weaker after CO_2 saturation due to the surface energy reduction which occurs with coal matrix swelling [30], which is greater with super-critical CO_2 adsorption. This is also confirmed by the broader stable crack propagation period shown in the 4 MPa CO_2 saturated sample ($\cong$1.03 MPa) compared to the 8 MPa CO_2 saturated sample ($\cong$0.27 MPa) (Fig. 5). Interestingly, the fracture propagation periods for CO_2-saturated brown coal samples (Fig. 5 and Table 2) are broader than those for CO_2-saturated high-ranked black coal observed by Perera et al. [8] under the same test conditions. This indicates the greater influence of CO_2 adsorption on high-ranked coal strength compared to low-ranked coal strength. This is believed to be related to the finely honed cleat system in high-ranked coal, which offers a greater extent of locus for CO_2 adsorption, which eventually creates greater coal matrix swelling.

6.2.3.4 CO_2 saturation-induced brown coal's micro pore structure alterations

The coal mass pore structure has an important influence on the gas transport process in coal [31], and according to Katyal et al. [32], the effectiveness of gas storage and drainage in coal greatly depends on its microscopic behaviour, micro pore structure and orientation, density, and the continuity of micro pores and their connectivity to the macro pores. A SEM analysis was therefore carried out to understand the mechanical property alterations caused by CO_2 saturation. The results of unsaturated, 4 MPa and 8 MPa CO_2 saturated coal samples are shown in Fig. 6. According to Fig. 6, natural brown coal exhibits a more uniform cellular-like micro pore structure with comparatively large pores. However, the pores are significantly shrunk and the cellular structure is noticeably rearranged with CO_2 saturation (see Fig. 6). In particular, a greater modification to the coal pore structure is made by super-critical CO_2 saturation. These observations confirm the effect of the CO_2 adsorption-induced strength alterations in coal described in the previous sections.

6.2.3.5 Implications for field application

Due to the potential of CO_2 to exist in its super-critical state, preferable coal seams for CO_2 sequestration exist at depths greater than 800 m [33]. Furthermore, super-critical CO_2 has greater storage capacity in deep underground reservoirs due to its gas-like compressibilities and liquid-like viscosities [20]. According to Oldenburg [34], the pore pressure condition of coal seams at such depths is higher than 8 MPa (hydrostatic pressure). This was considered in this study by testing coal samples saturated up to 10 MPa CO_2 saturation pressures at 35 °C, which covers the pore pressure condition up to around 1 km depth. However, it should be noted that the coal mass is subjected to considerable lithostatic pressures in real case scenarios, which has not been incorporated in the present study, because of the extensive time required for CO_2 saturation to conduct tests with confinement. The real strength

Table 2
Stress threshold values of unsaturated and CO_2 saturated (4 and 8 MPa) samples under axial loading.

Conditions	Crack initiation stress (σ_{ci}, MPa)	Crack damage stress (σ_{cd}, MPa)	Uniaxial compressive strength (σ_c, MPa)
Unsaturated	1.01	1.42	2.46
*Sub-critical CO_2 (4 MPa)	0.25	1.28	2.22
*Super-critical CO_2 (8 MPa)	0.19	0.46	1.06

* Samples were saturated in CO_2 at 35 °C constant temperature.

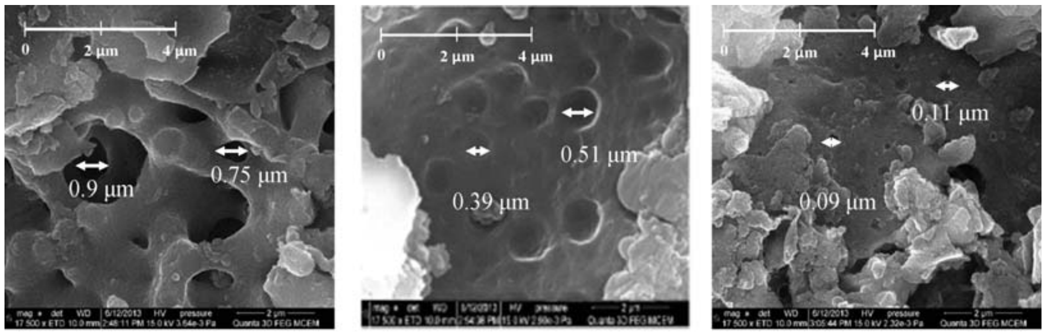

(a) (b) (c)

Fig. 6. Comparison of SEM results for (a) unsaturated sample, (b) sub-critical CO_2-saturated (4 MPa) sample and (c) super-critical CO_2-saturated (8 MPa) sample (SEM images were viewed under a magnification of 17,500×, a working distance of 10 mm and a voltage of 15 kV).

reductions in coal under CO_2 saturation are therefore expected to be lower than the obtained values, because there are higher effective stress conditions in coal seams under such confinement, which reduce the CO_2 flow performance [26]. This indicates the requirement for future studies to incorporate confinement stress conditions to suggest the adsorptive weakening of a coal seam due to CO_2 in field conditions.

According to the findings, although the injection of super-critical CO_2 is preferential due to its stable storage possibility, it may not be a safe CO_2 injection option in coal seams, due to the potential larger strength reduction. Alternatively, the enhancement of ductile properties with super-critical CO_2 injection is not a favourable circumstance for some CO_2 injectability and methane production stimulation techniques such as hydro-fracturing. The effectiveness of the hydro-fracturing process largely depends on the brittleness of the rock mass, because brittle rocks are easily fractured during the hydro-fracturing process and these induced fractures have greater potential to be in an open position [35]. Conversely, the plastically deforming nature of CO_2 saturated coal causes the fractures induced during the hydro-fracturing process to heal with the pressure release, creating unfavourable formation properties.

In summary, the findings of this study exhibit the risks associated with the use of super-critical CO_2 for the CO_2-ECBM process in terms of safety and production enhancement. However, this should be counter-balanced by the expected greater stable super-critical CO_2 storage capacity in coal compared to sub-critical CO_2. Laboratory tests can be used to obtain a better vision of the effects of CO_2 sequestration in coal mass in a controlled environment which can be used to support reservoir studies and then be extended to other advanced studies (risk assessment studies, economic optimization studies, project-screening models, etc.). In addition, these results can be incorporated to further investigate the coal mass behaviour for CO_2 sequestration by developing a laboratory-scale model which can be extended to a field-scale reservoir study [36]. The AE data in this study illustrate the progressive fracture behaviour with load application that can be assimilated with the real case scenario of fault initiation during the CO_2-ECBM process. These results are useful for a detailed understanding of possible migration paths for CO_2 from reservoirs, and to facilitate risk assessment studies.

6.2.4 Conclusions

The influence of CO_2 adsorption on the mechanical properties of brown coal was examined in a UCS testing programme. According to the test results:

- Sub-critical CO_2 adsorption causes brown coal's mechanical properties to be significantly changed due to the associated coal matrix swelling, with the tested coal's UCS strength being reduced by up to around 21.25% with gas CO_2 adsorption and the Young's modulus and Poisson's ratio being reduced and increased by around 22.52% and 30.09%, respectively.
- Super-critical CO_2 adsorption causes significantly greater mechanical property alterations in brown coal. 46% and 22.71% reduction of UCS and Young's modulus and a 16% increment of Poisson's ratio were observed when CO_2 saturation pressure increased from 6 to 8 MPa (the transfer region) respectively. The greater adsorption potential-related ductile property enhancement in brown coal compared to sub-critical CO_2 is the main causative factor for these alterations during super-critical CO_2 adsorption. Furthermore, the geomechanical property alterations observed during the ARAMIS and SEM studies confirm the brittle to ductile property modifications of coal mass with super-critical CO_2 adsorption at the micro-structural level.
- In addition, CO_2 saturation in brown coal causes early stages of fracture development, due to its swelled and reduced surface energy after CO_2 adsorption, and the effect is greater under super-critical CO_2 adsorption.
- Higher strength reductions have been observed in the research literature for black coal compared to brown coal, due to its well-defined cleat system which acts as a locus for CO_2 movement, creating greater structural alterations.

Finally, from the results of this study, it can be concluded that CO_2 phase and pressure have a great influence on the mechanical properties of coal, irrespective of its rank.

6.2.5 Acknowledgements

The authors wish to express their appreciation for the funding provided by the Australian Research Council (DE130100124) and the use of facilities in the Monash Centre of Electron Microscopy (MCEM).

6.2.6 Appendix A. Supplementary data

Supplementary data associated with this article can be found, in the online version, at http://dx.doi.org/10.1016/j.supflu.2015.11.010.

6.2.7 References

[1] S. Bachu, Carbon dioxide storage capacity in uneconomic coal beds in Alberta, Canada: methodology, potential and site identification, Int. J. Greenh. Gas Control 1 (2007) 374–385.
[2] M. Mazzotti, R. Pini, G. Storti, Enhanced coalbed methane recovery, J. Supercrit. Fluids 47 (2009), pp. 619–627.3.
[3] Y. Zhang, K.K. Gangwani, R.M. Lemert, Sorption and swelling of block copolymers in the presence of supercritical fluid carbon dioxide, J. Supercrit. Fluids 11 (1997) 115–134.
[4] A.S. Ranathunga, M.S.A. Perera, P.G. Ranjith, Deep coal seams as a greener energy source: a review, J. Geophys. Eng. 11 (2014) 1–17.
[5] J.W. Gibbs, On the equilibrium of heterogeneous substances, Am. J. Sci. (1878) 441–458.
[6] A.A. Griffith, The phenomena of rupture and flow in solids, Philos. Trans. R. Soc. Lond. Ser A, Contain. Pap. Math. Phys. Character 221 (1921) 163–198.
[7] J.W. Larsen, R.A. Flowers, P.J. Hall, G. Carlson, Structural rearrangement of strained coals, Energy Fuels 11 (1997) 998–1002.
[8] M.S.A. Perera, P.G. Ranjith, D.R. Viete, Effects of gaseous and super-critical carbon dioxide saturation on the mechanical properties of bituminous coal from the Southern Sydney Basin, Appl. Energy 110 (2013) 73–81.
[9] J. Gale, Geological storage of CO_2: what do we know, where are the gaps and what more needs to be done? Energy 29 (2004) 1329–1338.
[10] P.G. Ranjith, D. Jasinge, S.K. Choi, M. Mehic, B. Shannon, The effect of CO_2 saturation on mechanical properties of Australian black coal using acoustic emission, Fuel 89 (2010) 2110–2117.
[11] Y. Ates, K. Barron, The effect of gas sorption on the strength of coal, Min. Sci. Technol. 6 (1988) 291–300.
[12] N.I. Aziz, W. Ming-Li, The effect of sorbed gas on the strength of coal – an experimental study, Geotech. Geol. Eng. 17 (1999) 387–402.
[13] A. Czapliński, S. Hołda, Changes in mechanical properties of coal due to sorption of carbon dioxide vapour, Fuel 61 (1982) 1281–1282.
[14] M.S.A. Perera, P.G. Ranjith, M. Peter, Effects of saturation medium and pressure on strength parameters of Latrobe Valley brown coal: carbon dioxide, water and nitrogen saturations, Energy 36 (2011) 6941–6947.
[15] D.R. Viete, P.G. Ranjith, The effect of CO_2 on the geomechanical and permeability behaviour of brown coal: implications for coal seam CO_2 sequestration, Int. J. Coal Geol. 66 (2006) 204–216.
[16] A. Kronimus, A. Busch, S. Alles, D. Juch, A. Jurisch, R. Littke, A preliminary evaluation of the CO_2 storage potential in unminable coal seams of the Münster Cretaceous Basin, Germany, Int. J. Greenh. Gas Control 2 (2008) 329–341.
[17] S. Day, R. Fry, R. Sakurovs, S. Weir, Swelling of coals by supercritical gases and its relationship to sorption, Energy Fuels 24 (2010) 2777–2783.
[18] J. Huang, T. Moriyoshi, H. Manabe, Patterning of fine particles by means of supercritical CO_2, J. Mater. Sci. 41 (2006) 1605–1610.
[19] P. Randolph, D. Soeder, P. Chowdiah, Porosity and permeability of tight sands, in: SPE Unconventional Gas Recovery Symposium, Society of Petroleum Engineers, Pittsburgh, 1984 (Paper No. 12836).
[20] A.S. Ranathunga, M.S.A. Perera, P.G. Ranjith, Y. Ju, V. Vishal, P.N.K. De Silva, A macro-scale experimental study of sub-and super-critical CO_2 flow behaviour in Victorian brown coal, Fuel 158 (2015) 864–873.
[21] P.G. Ranjith, M.S.A. Perera, Effects of cleat performance on strength reduction of coal in CO_2 sequestration, Energy 45 (2012) 1069–1075.
[22] U.N. Lakmali, P.G. Ranjith, Effect of Brine Saturation on Carbonation of Coal Fly Ash for Mineral Sequestration of CO_2, Engineering Geology for Society and Territory, vol. 1, Springer International Publishing, Switzerland, 2015, pp. 479–482.
[23] ASTM D7012-04, Standard Test Methods for Compressive Strength and Elastic Moduli of Intact Rock Core Specimens under Varying States of Stress and Temperatures PN ASTM International PL West Conshohocken, PA, 2014, http://dx.doi.org/10.1520/D7012-14.
[24] L.S. Botnen, D.W. Fisher, A.A. Dobroskok, T.R. Bratton, K.H. Greaves, T. Robert McLendon, G. Steiner, J.A. Sorensen, E.N. Steadman, J.A. Harju, Field test of CO_2 injection and storage in lignite coal seam in North Dakota, Energy Proc. 1 (2009) 2013–2019.
[25] J.S. Bae, S.K. Bhatia, High-pressure adsorption of methane and carbon dioxide on coal, Energy Fuels 20 (2006) 2599–2607.
[26] M.S.A. Perera, P.G. Ranjith, D.W. Airey, S.K. Choi, Sub- and super-critical carbon dioxide flow behaviour in naturally fractured black coal: an experimental study, Fuel 90 (2011) 3390–3397.
[27] M.S.A. Perera, P.G. Ranjith, S.K. Choi, D.W. Airey, P. Weniger, Estimation of gas adsorption capacity in coal: a review and an analytical study, Int. J. Coal Prep. Util. 32 (2012) 25–55.
[28] J.Q. Shi, S. Durucan, S. Shimada, How gas adsorption and swelling affects permeability of coal: a new modelling approach for analysing laboratory test data, Int. J. Coal Geol. 128 (2014) 134–142.
[29] L. Chikatamarla, X. Cui, R.M. Bustin, Implications of volumetric swelling/shrinkage of coal in sequestration of acid gases, in: Proceedings of International Coalbed Methane Symposium, Tuscaloosa, AL, 2004 (Paper No. 0435).
[30] M. Mehic, P.G. Ranjith, S.K. Choi, A. Haque, The geomechanical behaviour of Australian black coal under the effects of CO_2 injection: uniaxial testing, in: Advances in Unsaturated Soil, Seepage and Environmental Geomechanics – Geotechnical Special Publication, American Society of Civil Engineers (ASCE), Reston, VA, 2006, pp. 290–297.
[31] Z. Pan, L.D. Connell, A theoretical model for gas adsorption-induced coal swelling, Int. J. Coal Geol. 69 (2007) 243–252.
[32] S. Katyal, M. Valix, K. Thambimuthu, Study of parameters affecting enhanced coal bed methane recovery, Energy Sources A 29 (2007) 193–205.
[33] X. Jing, G. Mingzhong, Y. Bin, Z. Ru, J. Wencheng, Coal permeability model on the effect of gas extraction within effective influence zone, Geomech. Geophys. Geo-Energy Geo-Resour. 1 (2015) 15–27.
[34] C.M. Oldenburg, Geologic carbon sequestration: CO_2 transport in depleted gas reservoirs, in: Gas Transport in Porous Media, Springer, 2006, pp. 419–426.
[35] L. Gandossi, An overview of hydraulic fracturing and other formation stimulation technologies for shale gas production, in: Report EUR 26347 EN for Joint Research Centre (Institute for Energy and Transport) of European Commission, Publications Office of the European Union, Luxembourg, 2013, pp. 7–10.
[36] X. Cui, R.M. Bustin, Volumetric strain associated with methane desorption and its impact on coalbed gas production from deep coal seams, AAPG Bull. 89 (2005) 1181–1202.

6.3 How do various fluid saturations alter the coal mass strength properties with coal rank?

During CO_2 sequestration in deep coal seams, the coal mass may be subjected to various fluid (CO_2, N_2, water *etc.*) saturations. Many studies to date have focused on the effect of CO_2 saturation on coal mass. However, to maintain a long-term progression of the CO_2-ECBM process, it is required to identify the mechanical responses of preferable coal seams for various fluid saturations available in the coal mass. Hence, the main objective of this study was to investigate coal's mechanical responses to water and N_2 saturations compared to CO_2 saturation, and to determine the effect of coal rank. A series of UCS tests was conducted on Australian brown coal samples from the Gippsland basin and black coal from the Sydney basin saturated with water and N_2 under various saturation pressures. The AE system was utilized together with UCS tests to identify the crack propagation patterns under each saturation condition. Further, SEM analysis was conducted to gain better insight into the micro-structural changes under water and N_2 saturation conditions.

This section of the chapter is the following publication:

Perera MSA, **Ranathunga AS**, Ranjith PG (2016). Effect of coal rank on various fluid saturations creating mechanical property alterations using Australian coals. *Energies* 9(6), 440.

energies

MDPI

Article

Effect of Coal Rank on Various Fluid Saturations Creating Mechanical Property Alterations Using Australian Coals

Mandadige Samintha Anne Perera *, Ashani Savinda Ranathunga and Pathegama Gamage Ranjith

Deep Earth Energy Laboratory, Department of Civil Engineering, Monash University, Building 60, Melbourne, Victoria 3800, Australia; ashani.ranathunga@monash.edu (A.S.R.); ranjith.pg@monash.edu (P.G.R.)
* Correspondence: samintha.perera@monash.edu; Tel.: +61-399-058-902; Fax: +61-399-054-982

Academic Editor: Thomas E. Amidon
Received: 13 April 2016; Accepted: 1 June 2016; Published: 8 June 2016

Abstract: During CO_2 sequestration in deep coal seams, the coal mass may be subjected to various fluid (CO_2, N_2, *etc.*) saturations. Therefore, in order to maintain the long-term integrity of the process, it is necessary to identify the mechanical responses of preferable coal seams for various fluid saturations. To date, many studies have focused on the CO_2 saturation effect on coal mass strength and less consideration has been given to the influence of other saturation mediums. Hence, this study aims to investigate coal's mechanical responses to water and N_2 saturations compared to CO_2 saturation and to determine the effect of coal-rank. A series of unconfined compressive strength (UCS) tests was conducted on Australian brown and black coal samples saturated with water and N_2 at various saturation pressures. An advanced acoustic emission (AE) system was utilized to identify the changes in crack propagation behaviors under each condition. According to the results, both CO_2 and water act similarly with coal by enhancing the ductile properties of the coal mass and this mechanical weakening is greater for high-rank coal. Conversely, N_2 saturation slightly enhances coal strength and delays crack propagation in coal and this strength enhancement can be improved by increasing the N_2 saturation pressure.

Keywords: coal rank; mechanical properties; N_2 saturation; CO_2 saturation; water saturation

---

6.3.1. Introduction

The process of enhanced coal bed methane (ECBM) recovery is being implemented and tested as a viable option to store and reduce the amount of anthropogenic carbon dioxide (CO_2) in the Earth's atmosphere, as well as for the recovery of useful coal bed methane (CH_4) gas [1–7]. Overall, the ECBM process involves introducing CO_2 through injecting wells into deep coal seams and this CO_2 then acts as a displacing gas, which allows the already adsorbed CH_4 to be desorbed from the coal matrix. Finally, CH_4 is obtained through a recovery well and used to produce energy in a cost-effective and environmentally friendly way.

However, according to previous studies [1–3,6,8–12], this CO_2-ECBM process leads to CO_2 adsorption-induced coal matrix alterations, which in turn affect its hydro-mechanical properties. Particularly in the geomechanical respect, the coal mass becomes weaker with the substitution of existing adsorbate CH_4 with the highly chemically potential CO_2 [13,14]. According to Perera *et al.* [15], Ranathunga *et al.* [16] and Vishal *et al.* [17], the inherent brittleness of the coal mass becomes ductile with the plasticization effect of coal with the adsorption of CO_2, and this phenomena is higher for super-critical CO_2 (beyond the critical temperature of CO_2-31.8 °C and the critical pressure of CO_2-7.38 MPa). Generally, potential CO_2-ECBM reservoirs are located deep underground, where CO_2 is in its super-critical state [2]. Hence, the strength reduction may be hazardous for the overall stability of coal reservoirs, mainly in regard to the cap rock's stability [18]. Table 1 provides a summary of previous studies on the identification of the geomechanical responses of different coal types under various CO_2 adsorption conditions. Those studies show that the coal mass is weakened by CO_2 adsorption and the effect is relatively higher for super-critical CO_2 for any type of coal. For instance, Australian brown coal shows 20.92% and 23.84% of unconfined compressive strength (UCS) and Young's modulus reduction for sub-critical CO_2 saturation at 6 MPa and 57.32% and 41.14% UCS and Young's modulus reduction for super-critical CO_2 saturation at 8 MPa respectively [16]. For Australian black coal, when the CO_2 saturation pressure increased from 6 MPa (sub-critical) to 8 MPa (super-critical), the UCS reduction was increased from 56.67% to 77.58% and the Young's modulus reduction was increased from 42.23% to 70.27% [15]. This is because the higher adsorption potential of super-critical CO_2 results in greater coal matrix alterations, causing greater strength reductions in the coal structure.

Table 1. Geomechanical responses of different coal types under various CO_2 saturation conditions.

Temperature (°C)	Pressure (MPa)	CO_2 Phase Condition	Coal Type	Coal Rank	UCS (MPa)	ΔUCS (%)	E (MPa)	ΔE (%)	Reference
35	0	-	Lignite [1]	Low	2.40	-	41.60	-	[16]
33	0	-	Bituminous [2]	High	33.00	-	3700	-	[15]
Room temperature	0	-	Bituminous [3]	High	15.29	-	5340	-	[17]
Room temperature	1	Gas	Lignite [1]	Low	2.34	2.09	40.32	4.73	[16]
35	2	Gas	Lignite [1]	Low	2.25	5.86	35.08	17.11	[16]
35	3	Gas	Lignite [1]	Low	2.17	9.21	33.78	20.18	[16]
Room temperature	4	Gas	Bituminous [3]	High	12.62	17.60	3940	26.20	[17]
35	4	Gas	Lignite [1]	Low	2.15	10.04	33.65	20.49	[16]
33	4.5	Gas	Bituminous [2]	High	15.80	52.12	2300	37.84	[15]
35	6	Gas	Lignite [1]	Low	1.89	20.92	32.23	23.84	[16]
33	6	Gas	Bituminous [2]	High	14.30	56.67	2130	42.43	[15]
35	8	Super critical	Lignite [1]	Low	1.02	57.32	24.91	41.14	[16]
33	8	Super critical	Bituminous [2]	High	7.40	77.58	1100	70.27	[15]
35	10	Super critical	Lignite [1]	Low	0.93	61.09	23.42	44.69	[16]
33	12	Super critical	Bituminous [2]	High	7.30	77.88	1160	68.65	[15]
33	16	Super critical	Bituminous [2]	High	13.95	57.64	1570	57.58	[15]

[1] Australian brown coal; [2] Australian black coal; [3] Indian black coal.

Interestingly, although both low and high rank coal samples behave similarly under CO_2 saturation, low rank coal exhibits a comparatively lower strength reduction compared to high rank coal (see Table 1). According to Table 1, the average reduction of UCS is around 29% for the tested Australian brown coal and that of the tested Australian black coal is around 61%. Further, the Young's modulus of the tested Australian brown coal exhibits around 26% average reduction, while the tested Australian black coal shows an average reduction of around 47%. In addition, for 3 MPa CO_2 saturation, the tested Australian brown coal shows a UCS reduction of 9.21% and Young's modulus reduction of 20.18%, while the tested Indian black coal shows 17.6% and 26.2% reductions in UCS and Young's modulus, respectively (see Table 1). The reason is the naturally existing well-developed cleat system in high rank coal that acts as a locus for CO_2 movement, permitting a greater matrix alteration compared to low rank coal with a less-developed cleat system.

It is also important to study the geomechanical behavior of the coal mass under other saturation mediums such as water and nitrogen (N_2). Moisture in a rock mass is known to affect the strength of rock by reducing its surface energy [19] and consequently softening the bond structure. Hence, it is vital to identify how different types of coals behave under the effect of moisture. In the case of N_2 saturation, researchers [3,20–23] have found that N_2 has the ability to recover CO_2 adsorption-induced coal matrix alteration, which eventually enhances the hydraulic properties of the coal matrix. Perera, Ranjith and Peter [24] have investigated the behavior of N_2 and CO_2 saturation on low-rank brown coal and observed around 2% increase in strength and Young's modulus for 3 MPa N_2 saturation. This is quite a low pore pressure condition and it is important to see this effect under much greater pore pressure conditions for possible field application. Regarding the rank effect, although there have been some studies to date [16,25] on the effect of CO_2 saturation on different ranks of coal, none of them has considered the rank-dependent mechanical behavior of coal mass under N_2 saturation, particularly under high saturation pressure conditions. Therefore, it is interesting to investigate how coal mechanical property alterations vary under high N_2 saturation conditions and the rank effect on them, which will in turn enable more reliable applications for field projects. This study therefore intends to fill this gap by determining the effect of water and N_2 saturation on the strength of low rank coal (lignite) and high rank coal (bituminous). The main objective of the present study is to distinguish the effects of water and N_2 saturation on the mechanical properties of different coal ranks.

6.3.2. Methodology

6.3.2.1. Samples Used for Testing

Brown coal (lignite) samples acquired from the Hazelwood mine in the Latrobe Valley, Victoria, Australia from approximately 50–75 m depth (from the ground level) were employed to represent low rank coal, while black coal (bituminous) samples collected from the Appin coal mine in the Southern Sydney basin, Australia from approximately 400 m depth (from the ground level) were utilized to represent high rank coal for this study. Both types of coal were obtained immediately after mining and therefore had been subjected to minimal environmental effects such as dusting, water evaporation or sunlight. The samples used for the present study were the same specimens obtained from the same coal blocks used by Perera, Ranjith and Viete [15] (black coal) and Ranathunga *et al.* [16] (brown coal) and the water content of the blocks was checked before coring new samples to ensure that the coal blocks were not subjected to any moisture loss. The physical properties of the samples used are shown in Table 2. Samples of 38 mm in diameter and 76 mm in height were used for testing purposes and the samples were maintained in a fog room wrapped in plastic wraps (after coring from the coal blocks) before being used for the saturations to preserve natural conditions. The detailed methodology adopted to prepare the samples is discussed in Ranathunga, Perera, Ranjith and Bui [16].

Table 2. Physical properties of Victorian brown coal and Southern Sydney basin bituminous coal used for the study.

Physical Property	Brown Coal [16]	Black Coal [15]
Coal density (g/cm^3)	1.04–1.1	1.4–1.9
Moisture content (% wb) [1]	57–66	1–5
Fixed carbon (% db) [1]	48	60–71
Ash yield (% db) [1]	1.7	6–12
Volatile matter content (% db) [1]	50.3	10–25
Vitrinite reflectance (%)	0.0–0.4 [2]	1.1–1.5 [2]

[1] wb-wet basis, db-dry basis; [2] From Silva [24].

6.3.2.2. Samples Preparation for Testing

The procedures implemented for water and N_2 saturations are explained in the following sections.

a. Water Saturation

Three coal samples from each rank were saturated in water for approximately three weeks to allow full water saturation. The samples were placed in vacuum chambers (Figure 1a) and the weight of the coal samples was recorded before placing them into the saturation chamber. The weight was then checked over time for around three weeks until the weight reached a steady state. The samples were then wrapped well with plastic wraps and stored in the fog room for another two weeks to allow an equal distribution of moisture throughout the sample before testing.

(**a**) (**b**)

Figure 1. Coal samples in (**a**) water saturation chamber and (**b**) N_2 saturation chamber.

b. N_2 Saturation

During the study by Perera, Ranjith and Viete [15], the black coal samples were saturated under two different N_2 pressures (8 and 16 MPa) using a high pressure tri-axial test rig (see Figure 1b) to compare the observations of CO_2 saturated samples. Unlike CO_2, N_2 is a comparatively inert gas, which does not cause any significant coal matrix re-arrangement through chemical interactions with the coal mass [23,26]. For this study, brown coal samples were saturated under three different saturation pressures (2, 6 and 8 MPa) using a similar procedure to that reported in Perera, Ranjith and Viete [15]. Further, black coal samples were saturated under two other different saturation pressures (2 and 6 MPa) additional to those used in the study of Perera, Ranjith and Viete [15] for comparison purposes. Here the samples were saturated under 35 °C temperature to provide similar conditions to those used for CO_2 saturation in Ranathunga, Perera, Ranjith and Bui [16] and Perera, Ranjith and Viete [15]. It should be noted that upon the completion of each saturation, the pressure cell was depressurized gradually at a quite slow rate of around 0.02 MPa/min to avoid any possible damage to the coal mass caused by the sudden pressure release.

6.3.2.3. Experimental Procedure

The following sections summarize the experimental methodology adopted for the testing.

a. Unconfined Compressive Strength (UCS) Tests

A series of UCS tests was performed on the coal samples using the Shimadzu compression machine available in the Deep Earth Energy Research Laboratory (DEERL) at Monash University. A displacement rate of 0.1 mm/min [27] was applied for the uniaxial compressive tests of the coal samples and the corresponding load and displacement were recorded.

b. Acoustic Emission (AE) Tests

An advanced acoustic emission (AE) system was used to observe the fracture propagation patterns of the tested brown and black coal samples during the UCS testing. Two AE sensors attached at either side of the specimen were used to capture the acoustic counts during the load application. These AE data were used to characterize the crack propagation stages and to obtain the stress threshold values for each condition.

c. Scanning Electron Microscopy (SEM) Analysis

High-resolution SEM images were also taken of the coal samples under unsaturated, water-saturated, N_2-saturated and CO_2-saturated conditions. The scanning was carried out with 4.5 spot size under 15 kV voltage while maintaining a low vacuum mode using the FEI Quanta 3D FEG FIB machine located at the Monash Centre for Electron Microscopy (MCEM), thus providing a fixed resolution of 2 microns for the qualitative analysis of all images. The complete procedure adopted for SEM analysis is detailed in Ranathunga, Perera, Ranjith and Bui [16].

6.3.3. Experimental Results and Discussion

Axial stress-strains and AE responses were tested for brown and black coal samples under different fluid saturation conditions. The highest UCS values were used to represent the different test conditions for discussion purposes, as the variation of experimental values was minimal. In addition, SEM images were also incorporated to show the micro-structural changes in the coal matrix under different fluid saturations. The following sections discuss and compare how the different coal types behave under the saturation of various fluids.

6.3.3.1. Effect of Coal Rank on Water Saturation Effect on Geomechanical Properties in Coal

Figure 2 shows the variation of axial stress with axial strain for water-saturated brown and black coal samples. According to Figure 2 and Table 3, brown coal exhibits a UCS value of 2.04 MPa and a Young's modulus value of 35.46 MPa after water saturation, which represent around a 14.64% reduction of UCS and a 16.21% reduction of Young's modulus compared to the unsaturated brown coal samples. Black coal exhibits a UCS of 21.01 MPa and Young's modulus of 2.24 GPa after water saturation (refer Table 3), which represents around 36.33% reduction in UCS and a 39.46% reduction in Young's modulus compared to the unsaturated black coal samples. Both black and brown coal show a similar behavior for water saturation; there is a considerable reduction in their mechanical properties with water saturation. The major reason for this water saturation-induced strength reduction is the softening of the rock mass bond structure [19] and the ability of moisture inside the rock mass to decrease the surface energy [28]. Furthermore, moisture in a rock mass can cause its toughness to be increased [29], by enhancing the ductile behavior, resulting in a lower Young's modulus.

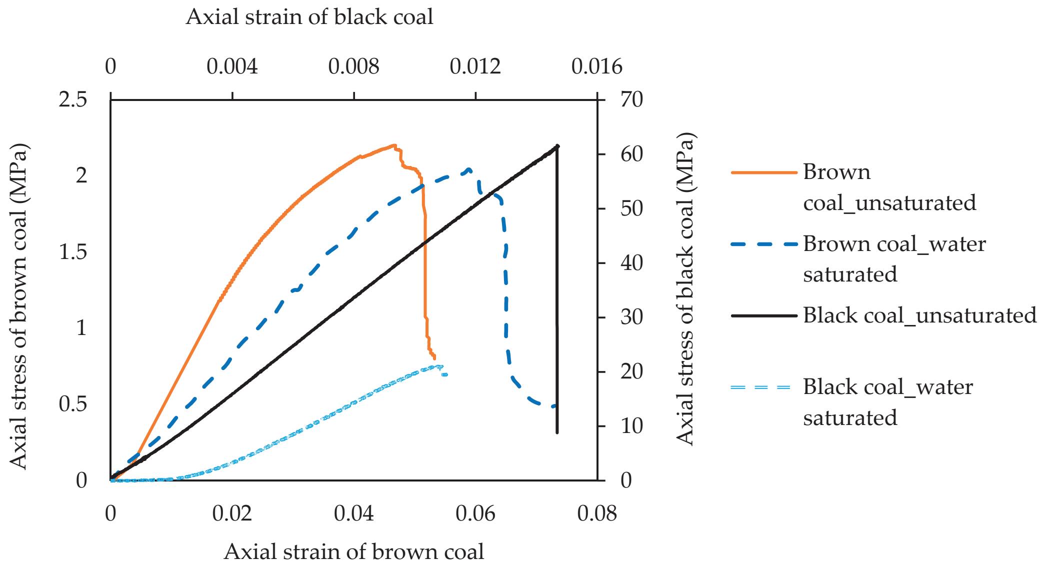

Figure 2. Axial stress *vs.* axial strain curves for brown coal and black coal during water saturation.

Table 3. Unconfined compressive strength (UCS) and Young's modulus (E) values obtained under various saturation conditions for brown coal and black coal.

Saturation Fluid	Pressure (MPa)	Brown Coal				Black Coal			
		UCS (MPa)	ΔUCS (%) [3]	E (MPa)	ΔE (%) [3]	UCS (MPa)	ΔUCS (%) [3]	E (GPa)	ΔE (%) [3]
Unsaturated	-	2.39 [1]	-	42.32 [1]	-	31.01 [2]	-	3.52 [2]	-
	-	2.34 [1]	-	39.32 [1]	-	33.00 [2]	-	3.70 [2]	-
	-	2.36 [1]	-	42.16 [1]	-	-	-	-	-
Water	-	2.07	−14.64	35.46	−16.21	21.01	−36.33	2.24	−39.46
	-	2.01		35.17		20.89		2.14	
	-	2.05		35.28		20.94		2.20	
N_2	2	2.43	1.58	42.52	0.47	33.39	1.18	3.71	0.27
	2	2.39		41.97		32.17		3.54	
	6	2.51	5.05	43.08	1.80	33.76	2.30	3.76	1.62
	6	2.48		43.01		32.89		3.64	
	8	2.57	7.56	44.28	4.63	34.01 [2]	3.06	3.80 [2]	2.70
	8	2.54		44.16		33.20 [2]		3.71 [2]	
	16	-	-	-	-	35.11 [2]	6.39	3.91 [2]	5.68
	16					33.30 [2]		3.71 [2]	

[1] From Ranathunga, Perera, Ranjith and Bui [16]; [2] From Perera, Ranjith and Viete [15]; [3] The sample with the highest UCS value was taken to calculate the UCS and E variations.

Interestingly, compared to brown coal, black coal has around 2.5 times higher reduction in both UCS and Young's modulus. This significant mechanical property weakening in black coal has also been observed by Vishal, Ranjith and Singh [17] for Indian black coal (around 25.5% UCS reduction and 37.8% Young's modulus reduction upon water saturation). This is possibly due to the fact that black coal has more fractures and a well-developed cleat system that allow more intake of moisture into the coal mass. The water molecules can dissolve in the material and can be drawn to the tips of the fractures, causing more stress towards the fracture tips, resulting in their expansion [28]. Hence, black coal exhibits a higher strength reduction than brown coal, which has fewer fractures and under-developed cleats. These observations can be further confirmed by comparing the SEM images of unsaturated and water-saturated coal samples (see Table 4). Here, compared to unsaturated samples, both brown and black coals show altered micro structures after water saturation and these alterations are clearly greater in black coal.

Figure 3 compares the AE counts with axial stress for brown and black coals with and without water saturation. As shown in Figure 3, the unsaturated samples exhibit clear fracture propagation behavior with all the three main stages under load application compared to the water-saturated samples. A crack closure (CC) region can first be observed without any strain energy release. A stable crack propagation (SC) region can then be witnessed, at which crack propagation is initiated (crack initiation stress-σ_{ci}), releasing strain energy linearly without damaging the sample. Unstable crack propagation (UC) can finally be seen, which starts at the crack damage point (σ_{cd}) and progresses until the sample fails (UCS) with an exponential increment in strain energy released.

However, in water-saturated coal samples, these three stages are not clearly visible. Brown coal (see Figure 3a) portrays only crack closure and then sample failure without any stable or unstable crack propagation. As discussed previously, moisture intake into the rock mass causes the fracture tips of the specimen to be weakened, which may result in failure without any crack propagation. However, stable and unstable crack propagation can be observed for water-saturated black coal before it undergoes failure. The reason may be the softer and weaker properties of brown coal compared to black coal that cause it to fail rapidly, with water saturation creating a softening effect.

Table 4. Appearance of the brown and black coal samples under different fluid saturations before and after failure.

Coal Type	Sample Appearance Under Different Test Conditions		SEM Images [3]	Average Pore Size
	Natural samples			
Brown coal	 Before failure [1]	 After failure [1]	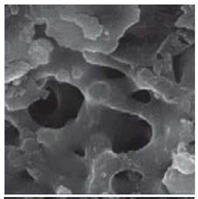	~0.9 μm
Black coal	 Before failure [2]	 After failure [2]	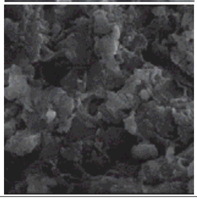	~0.43 μm
	Water-saturated samples			
Brown coal	 Before failure	 After failure	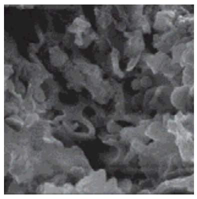	~0.34 μm
Black coal	 Before failure	 After failure	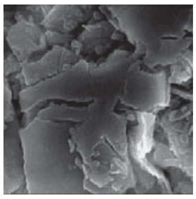	~0.12 μm
	N_2 saturated samples			
Brown coal	 After saturation in 8 MPa N_2	 After saturation in 8 MPa N_2[2]	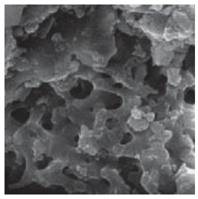	~0.62 μm
Black coal	 After failure	 After failure [2]	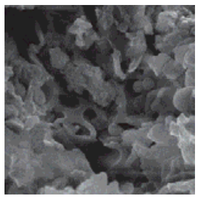	~0.23 μm

[1] From Ranathunga, Perera, Ranjith and Bui [16]; [2] From Perera, Ranjith and Viete [15]; [3] viewed under a magnification of 17,500×, a working distance of 10 mm and a voltage of 15 kV.

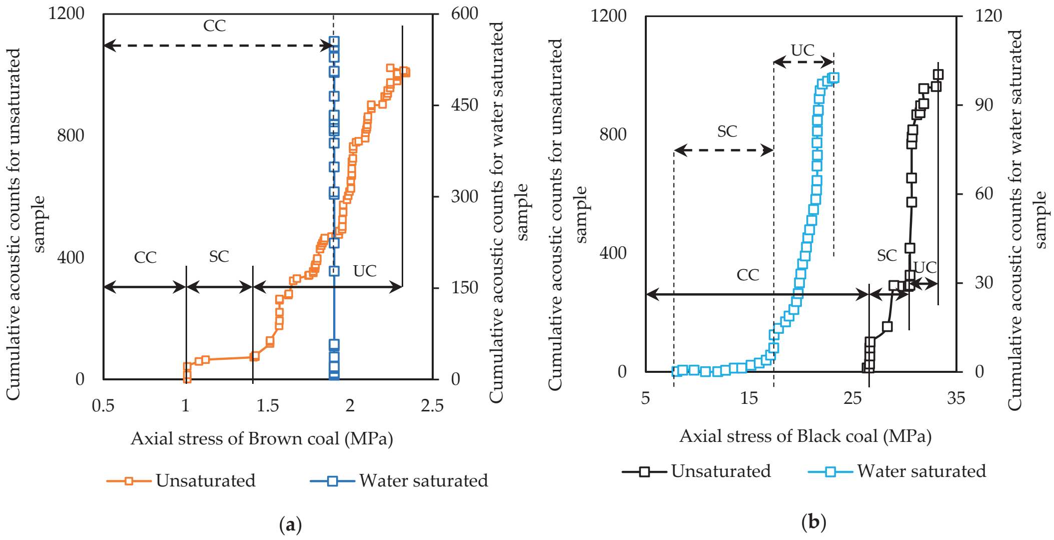

Figure 3. Cumulative acoustic counts *versus* axial stress for unsaturated and water saturated (**a**) brown coal and (**b**) black coal samples (Here CC-Crack closure, SC-Stable crack propagation and UC-Unstable crack propagation).

After water saturation, the brown coal samples were observed to have a very soft and bulgy appearance compared to the water-saturated black coal samples. Further, the water-saturated brown coal had a bulging failure and black coal exhibited a failure along the major and minor cleats (see Table 4). This is possibly because, due to the well-developed cleat system in high rank black coal compared to brown coal, water molecules have more possibility to move through these cleat systems and weaken the coal mass along them in black coal. In the case of brown coal, which has only a poorly developed cleat system, water molecules slowly diffuse into the whole rock matrix, weakening the coal matrix. Black coal shows more rapid crack propagation after water saturation, probably because the weaker cleat system allows fractures to easily propagate through the system. For example, the crack initiation stress for the unsaturated sample is 26.7 MPa while it is 6.74 MPa for the water-saturated sample. Furthermore, the crack damage occurred at 30.5 MPa for the unsaturated sample and at 17.15 MPa for the water-saturated sample (see Figure 3b). In summary, water saturation causes a strength reduction in any coal regardless of rank. However, high rank coal exhibits a greater strength reduction than low rank coal with water saturation, mainly due to the mature fracture network, which easily attracts water molecules. In addition, water saturation causes a direct failure in low rank brown coal (without fracture propagation) compared to high rank coal, which exhibits more rapid fracture propagation after water saturation compared to its dry condition.

6.3.3.2. Rank Effect on N_2 Saturation-Created Geomechanical Alterations in Coal

The effects of N_2 saturation on brown and black coal's mechanical properties were then investigated and the results are shown in Figure 4 and Table 3. According to Figure 4, unlike in water saturation, N_2 saturation causes a slight increment in coal strength for both brown and black coal, and the strength gain is increased by increasing N_2 saturation pressure. The reason may be the ability of N_2 to push the existing moisture from the coal mass. This was evident by the calculated weight variation in the N_2-saturated samples, which was reduced by around 5% to 19% during the saturation period. As mentioned in the previous section, moisture in a coal mass causes its structure to be weakened, and the removal of moisture from the rock mass should therefore cause a strength gain.

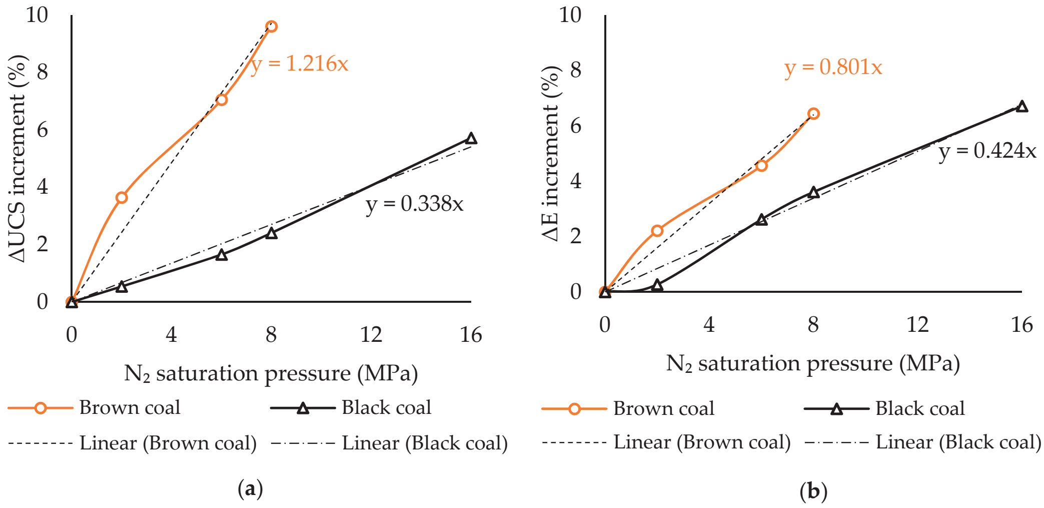

Figure 4. (**a**) Compressive strength (UCS) and (**b**) Young's modulus (E) increment during N_2 saturation for brown and black coal.

Further, according to Table 3, the Young's modulus of both brown coal and black coal slightly increase after N_2 saturation, and this is also related to the moisture removing potential of the N_2 molecules. As described earlier, the existence of water causes the ductile properties of the coal mass to improve. Therefore, the removal of water should improve the brittle behavior, which is proven by the observed Young's modulus increment in both brown and black coal after N_2 saturation. Further, at higher N_2 saturation pressures, the amount of N_2 molecules that enter the coal mass is higher. Therefore, the removal of moisture from the sample is also higher, which causes greater strength gains. Apart from this moisture release, N_2 injection may also cause the release of some adsorbed phase gases such as methane and CO_2 from the coal matrix [22]. The adsorption of any of these coal seam gases (CH_4, CO_2) causes the coal matrix to swell and injecting N_2 causes these swelled areas to recover to some extent. Coal swelling causes its strength to be reduced, and therefore even the partial recovery of swelling by injecting N_2 should contribute to the enhancement of the strength of the coal mass.

The aim of this study is to identify the effect of coal rank on these coal mass mechanical property alterations under various fluid injections. According to Figure 4, the N_2 saturation-created strength gain in brown coal samples is greater than the strength gain in black coal after N_2 saturation (see Figure 4). For example, the UCS shows a 1.216 positive gradient for brown coal and a 0.338 positive gradient for black coal with N_2 saturation pressure, while Young's modulus shows a 0.801 and 0.424 positive gradient with N_2 saturation pressure for brown and black coals, respectively. This is mainly related to the available moisture in black and brown coals. According to Table 2, the moisture content in brown coal (average 62%) is much higher than in black coal (average 3%). The amount of moisture removed from the coal mass by introducing N_2 is therefore higher in brown coal, and this should cause a greater strength gain in brown coal than in black coal. According to the SEM images of 8 MPa N_2 saturated brown and black coal samples (see Table 4), brown coal exhibits a clearer micro pore structure compared to black coal after water saturation, probably due to the water removed from the pore space. The SEM image of N_2 saturated black coal shows some open pore spaces compared to the unsaturated black coal, possibly due to the moisture removed from the coal matrix. This proves the strength gains observed for N_2 saturated black and brown coal.

The AE analysis data for N_2 saturation, unlike water saturation, shows considerable delays in crack initiation to crack damage (stable crack propagation) for both high and low rank coals (see Table 4). For instance, 8 MPa N_2 saturation caused the stable crack propagation in brown coal to increase from around 0.41 MPa to 0.6 MPa and in black coal from around 2.68 MPa to 3.8 MPa. This may be due to the lower water content in the N_2 saturated sample. An increase of surface energy may take place with the water removal from the N_2 saturated coal samples, eventually causing a delay in crack propagation. Interestingly, a comparison of the stress threshold values of N_2 saturated brown and black coal shows that both display very similar behavior, as shown by the UCS and Young's modulus results, which show an increment with increasing N_2 saturation pressure, and a greater increment for brown coal compared to black coal. The previously mentioned moisture removal rate is the reason for this observation, further confirming the ability of N_2 to cause strength gain in the coal mass. Hence, it can be concluded that N_2 has the ability to slightly enhance the strength properties of coal and this ability is higher for low rank coal.

6.3.3.3. How Significant is Water and N_2 Saturation on Coal Strength Compared to That of CO_2

Coal generally has a mixture of pore fluid, composed of water, N_2, CO_2 and CH_4 and their composition can be changed with various applications such as CO_2 sequestration and N_2 injection for ECBM recovery. It is therefore necessary to have comprehensive knowledge of the relative effect created by each component. Particularly in the case of CO_2 sequestration, knowledge of the effects of other fluid saturations compared to CO_2 saturation is necessary to have an overall idea of coal mass strength in this process. In addition, such a comparative study is essential for various ranked coals to determine the effects of these processes on coal seam. In this respect, Perera *et al.* [24] conducted a series of strength tests to compare the influence of water and N_2 saturation with that of CO_2 saturation. However, they conducted this series of strength tests on coal samples saturated under only very low pressure conditions (up to 3 MPa). These are far from the real situation in the field, in which quite high injection pressures of CO_2 and N_2 are used and the natural water is under very high pore fluid pressures. Therefore, the conduct of a comparative study with greater and more realistic saturation pressures is necessary to understand field conditions, while also incorporating other possible influences such as the CO_2 phase effect. Further, a study of different ranked coal is necessary to identify how these influences vary from seam to seam or with coal maturity. This section therefore compares the findings of the present study with those of previous studies on the effect of CO_2 saturation on low ranked brown coal [16] and high-ranked black coal [15].

a. Comparison of Variation of Coal's Mechanical Properties

Figure 5 compares the UCS and Young's modulus of CO_2 and N_2 saturated brown and black coals. According to this figure, there is a clear strength reduction with CO_2 adsorption and in contrast a strength gain with N_2 adsorption regardless of rank, and both types of strength property alterations are enhanced with increasing saturation pressure. However, when comparing brown and black coals, greater reductions in UCS and Young's modulus with CO_2 saturation in black coal can be seen, due to its well-defined cleat system. In contrast, a lower strength gain under N_2 saturation in black coal can be seen due to the previously described lower moisture content of high rank coal. The influence of N_2 and CO_2 saturation on coal mechanical properties varies greatly under high saturation pressure conditions. For example, the CO_2 adsorption-induced strength reduction in both black and brown coals is significantly enhanced after around 8 MPa, with the phase variation of CO_2 from sub- to more chemically reactive super-critical conditions (see Figure 5). This change cannot be seen in N_2 saturation with increasing pressure (a more linear variation with saturation pressure can be seen), because the N_2 phase does not change under such conditions (for N_2 the critical temperature is -146.8 °C and the critical pressure is 3.39 MPa) [23]. This is particularly important for field projects, in which coal seams are under very high saturation pressures and temperatures, and completely different responses to CO_2 and N_2 injections into the seam should be expected.

Now if the water saturation and CO_2 saturation effect on coal strength are compared, quite similar behavior can be observed, as both cause the coal mechanical properties to be weaken, with black coal being subjected to more weakening than brown coal due to its cleat system. However, how the water saturation effect varies with saturation pressure could not be tested in the present study. This would give important information on the pressure effect on water softening and warrants future research.

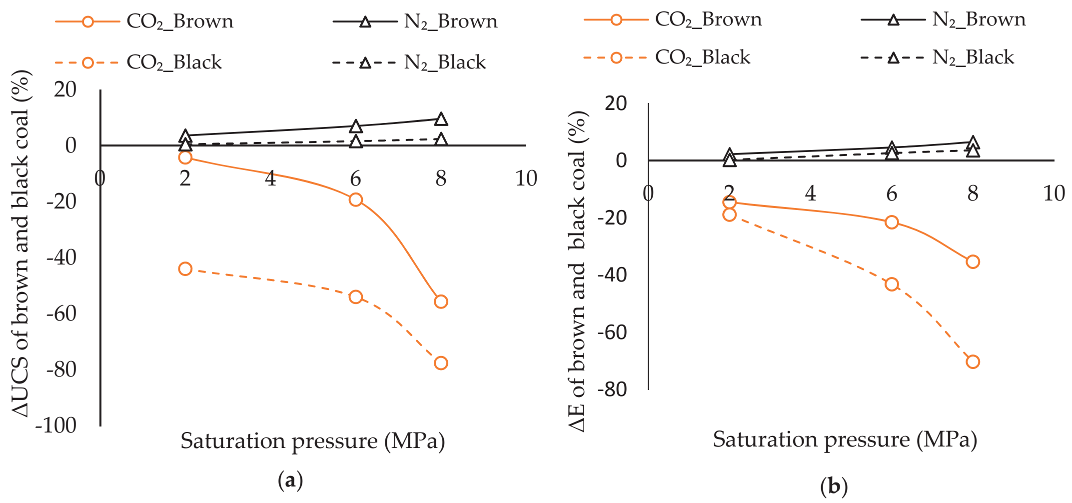

Figure 5. Comparison of (**a**) UCS and (**b**) Young's modulus variation with CO_2 [15,16] and N_2 saturation of brown coal and black coal.

b. Comparison of Fracture Propagation

Figure 6 shows the variation of normalized stress threshold values and Table 5 displays the respective stress threshold values for brown and black coal saturated with CO_2 [15] and N_2 [16]. Here, the values have been normalized by dividing each stress value by the respective stress threshold value under unsaturated condition. According to the AE data, (see Figure 6 and Table 5), unlike in N_2 saturation, CO_2 saturation causes quicker crack initiation and crack damage in both high and low rank coals, probably due to the reduced surface energy with CO_2 adsorption [24]. For instance, at around 4 MPa CO_2 saturation, there is around 0.74 MPa normalized crack initiation stress for brown coal and around 0.51 MPa crack initiation stress for black coal (around 4.5 MPa saturation pressure in black coal). Further, when comparing the stress threshold values in CO_2 saturated brown and black coal, both display very similar behavior in terms of UCS and Young's modulus (see Table 5), and a reducing stress threshold trend with increasing CO_2 saturation pressure, the reduction being greater for black coal than brown coal (see Figure 6). The well-developed cleat system in black coal compared to brown coal might be the reason for this observation. Further, for super-critical CO_2 saturations, black coal exhibits crack propagation without any crack initiation (see Figure 6a), probably due to the enhanced ductile behavior of samples under super-critical CO_2 adsorption, which causes higher plasticization in the coal mass. In addition, crack propagation in N_2 saturation also displays a similar behavior with the variation of strength parameters, which shows an increment in stress threshold with increasing N_2 saturation pressure, the increment being greater for brown coal due to greater moisture removal. Based on these crack propagation changes which occur with CO_2 and N_2 saturations, the use of N_2 to recover the CO_2 adsorption-induced coal matrix alteration appears to be an effective option.

In relation to crack propagation in water- and CO_2-saturated samples, both show more rapid crack propagation (see Table 5) compared to N_2 saturation, and particularly in water-saturated sampled, crack initiation is not even visible (see Figure 6 and Table 5). In the case of CO_2 saturation, CO_2 adsorption-induced coal matrix swelling causes a strain layer to be generated between the adsorbed CO_2 and the fracture/cleat face [9,11]. Hence, with lower axial load applications, this weak layer possibly starts to break, causing rapid crack propagation [30]. During water saturation, the water (H_2O) molecules react with mineral/macerals and also create hydrogen bonds with the existing moisture in the coal mass [17], which results in structural rearrangements. Further, an expansion of fracture tips may occur due to the water molecule-induced internal stress increment [24], therefore initiating an early failure without any visible crack propagation.

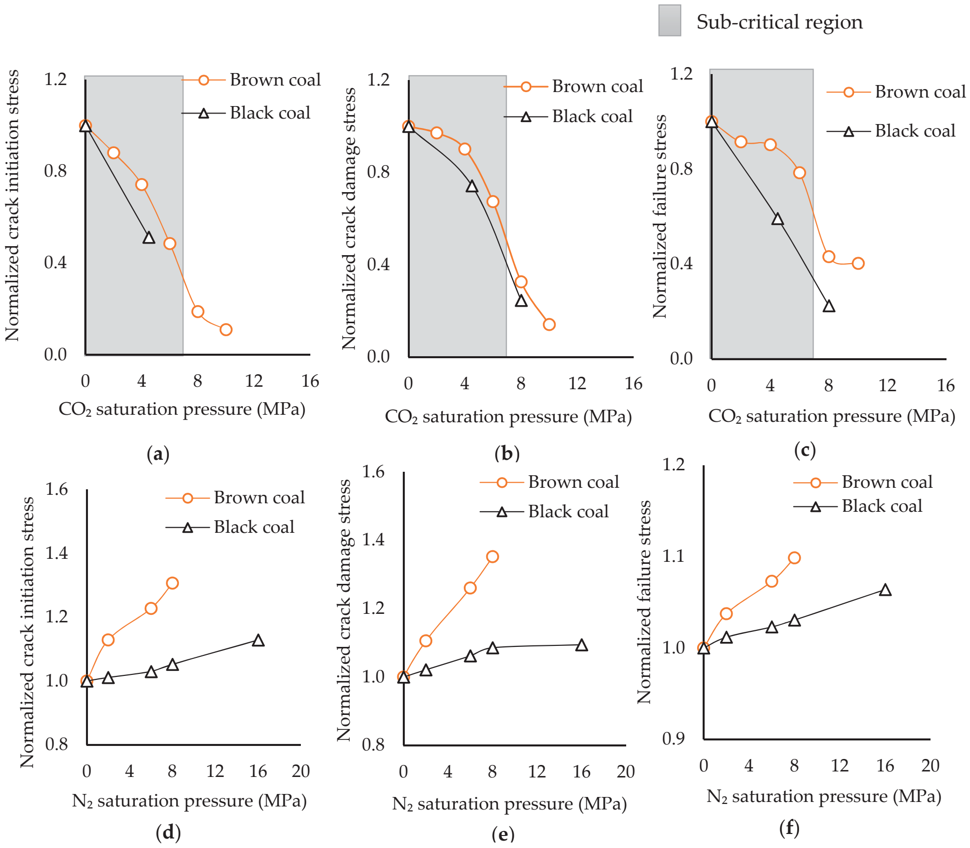

Figure 6. Variation of normalized stress threshold values: (**a**) crack initiation stress, (**b**) crack damage stress, and (**c**) failure stress during different CO_2 saturations for brown coal and black coal; and (**d**) crack initiation stress, (**e**) crack damage stress, and (**f**) failure stress during different N_2 saturations for brown coal and black coal (here the stress threshold values were normalized by dividing by the respective stress threshold value for unsaturated sample).

Table 5. Stress threshold values obtained under various saturation conditions for brown coal and black coal.

Saturation Fluid	Saturation Pressure (MPa)	Brown Coal			Black Coal		
		Crack Initiation Stress (σ_{ci}, MPa)	Crack Damage Stress (σ_{cd}, MPa)	UCS (MPa)	Crack Initiation Stress (σ_{ci}, MPa)	Crack Damage Stress (σ_{cd}, MPa)	UCS (MPa)
Unsaturated	-	1.01 [1]	1.42 [1]	2.39 [1]	26.70 [2]	30.50 [2]	33.00 [2]
Water	-	-	-	2.06	-	17.15	20.94
N_2	2	1.14	1.57	2.43	27.10	29.38	33.39
	6	1.24	1.79	2.51	27.53	30.43	33.76
	8	1.32	1.92	2.57	28.10 [2]	31.90 [2]	34.01 [2]
	16	-	-	-	30.14 [2]	32.16 [2]	35.11 [2]

[1] From Ranathunga, Perera, Ranjith and Bui [16]; [2] From Perera, Ranjith and Viete [15].

6.3.4. Conclusions and Suggestions for Future Research

6.3.4.1. Conclusions Drawn from the Present Study

The influence of coal rank on various fluid saturation-induced coal mechanical properties changes was studied using low rank (Australian brown coal) and high rank (Australian black coal) coal samples. The following conclusions can be drawn:

- Water saturation causes a significant strength reduction in coal regardless of rank, because the moisture penetrating into the coal mass causes its fractures to expand, decreasing the surface energy of the coal mass, and eventually causing the strength to be reduced.
- This strength reduction is enhanced with increasing coal rank due to the well-developed cleats in mature coal which offer more loci for moisture to stay in the coal mass.
- The enhanced ductile nature of coal upon water adsorption delays crack initiation, regardless of rank. It is therefore necessary to have a lot of low injection pressure for coal seams with a greater degree of water saturation in terms of safety.
- In contrast to water saturation, N_2 saturation slightly enhances coal strength, regardless of rank, and this increment increases with increasing N_2 saturation pressures. This is possibly due to the ability of N_2 to partially recover the coal seam gas (methane, CO_2) adsorbed swelled areas and push out the adsorbed water from the coal mass.
- N_2 saturation significantly slows crack initiation and propagation in coal regardless of rank. This is a favorable feature in terms of long-term stability in coal seams and can be used to strengthen weak seams after CO_2 injection.
- The strength gain created by N_2 saturation reduces with increasing rank, probably due to the lower level of moisture stored in high rank coal.
- The variation of mechanical properties of coal upon CO_2 and N_2 saturations shows quite different responses to increasing saturation pressure, as the CO_2 phase condition may change from sub- to super-critical under greater pressures. In contrast, N_2 does not undergo such phase change with increasing pressure, due to its much lower critical conditions.
- The present study was conducted under 35 °C temperature (N_2 saturation) up to 8 MPa saturation pressure, which represents a pore pressure condition of an approximately 800 m deep coal seam [31]. As the study was conducted in an unconfined environment, the observed strength variations are expected to be lower in a confined environment under field conditions, because the confinement causes greater effective stress in the field, leading to a shrunken pore structure in coal seams with reduced gas flow performance through them.

6.3.4.2. Suggestions for Future Research

- Methane is one of the major components in coal seam gas that plays an important role in the overall mechanical response of the coal mass. Hence, to understand the overall influence of coal seam gas on coal's mechanical properties, future research is needed on methane saturation under various pressures for different rank coals.
- It is recommended to conduct further research on coal mass mechanical behavior under confinements for different saturation conditions to represent the real case scenarios existing in the field, where the coal mass has been exposed to lithostatic pressure conditions.
- The water saturation effect of the present study was conducted under atmospheric pressure conditions due to the unavailability of the necessary laboratory facilities. However, it is essential to investigate the water saturation effect under different pressure conditions, so that it can be clearly compared with the different pressure effects of N_2 and CO_2. This is a future research option.
- As found in the present study, coal mass mechanical behavior under various saturations varies with different coal types. However, the results of this study need to be generalized by testing various ranked coal samples taken from various coal basins around the world. Future experimentation is therefore recommended using a wider range of coal specimens taken from different basins in the world with diverse cleat structures and mineral compositions, in order to obtain better insight into the observed strength variations.

Acknowledgments: The authors wish to express their appreciation for the funding provided by the Australian Research Council (DE130100124) and the use of facilities in the Monash Centre of Electron Microscopy (MCEM).

Author Contributions: Ashani Savinda Ranathunga performed the experiments, analyzed the data, and prepared the draft manuscript. Mandadige Samintha Anne Perera mentored the experimental program and reviewed the draft. Ranjith Pathegama Gamage reviewed the final paper and made important suggestions and recommendations for paper revision.

Conflicts of Interest: The authors declare no conflict of interest.

Abbreviations

The following abbreviations are used in this manuscript:

AE	Acoustic emission
CC	Crack closure
CH_4	Methane
CO_2	Carbon dioxide
db	Dry basis
E	Young's modulus
ECBM	Enhanced coal bed methane recovery
MCEM	Monash Center of Electron Microscopy
N_2	Nitrogen
SC	Stable crack propagation
SEM	Scanning electron microscopy
UC	Unstable crack propagation
UCS	Unconfined compressive strength
wb	Wet basis
σ_{cd}	Crack damage stress
σ_{ci}	Crack initiation stress

6.3.5 References

1. Perera, M.S.A.; Ranjith, P.G. Carbon dioxide sequestration effects on coal's hydro-mechanical properties: A review. *Int. J. Energ. Res.* **2012**, *36*, 1015–1031. [CrossRef]
2. Ranathunga, A.S.; Perera, M.S.A.; Ranjith, P.G. Deep coal seams as a greener energy source: A review. *J. Geophys. Eng.* **2014**, *11*, 063001. [CrossRef]
3. Vishal, V.; Singh, T.N. A laboratory investigation of permeability of coal to supercritical CO_2. *Geotech. Geol. Eng.* **2015**, *33*, 1009–1016. [CrossRef]
4. Xie, J.; Gao, M.; Yu, B.; Zhang, R.; Jin, W. Coal permeability model on the effect of gas extraction within effective influence zone. *Geomech. Geophys. Geo-Energy Geo-Resources* **2015**, *1*, 15–27. [CrossRef]
5. Gale, J. Geological storage of CO_2: What do we know, where are the gaps and what more needs to be done? *Energy* **2004**, *29*, 1329–1338. [CrossRef]
6. Zhang, Y.; Gong, B.; Li, J.; Li, H. Discrete fracture modeling of 3D heterogeneous enhanced coalbed methane recovery with prismatic meshing. *Energies* **2015**, *8*, 6153–6176. [CrossRef]
7. Hu, G.; Xu, J.; Zhang, F.; Zhao, C.; Qin, W.; Zhu, Y. Coal and coalbed methane co-extraction technology based on the ground movement in the yangquan coalfield, China. *Energies* **2015**, *8*, 6881–6897. [CrossRef]
8. Aziz, N.I.; Ming-Li, W. The effect of sorbed gas on the strength of coal – an experimental study. *Geotech. Geol. Eng.* **1999**, *17*, 387–402. [CrossRef]
9. Jasinge, D. An investigation of the effect of carbon dioxide sequestration on the behaviour of brown coal. Ph.D. Thesis, Monash University, Melbourne, Australia, 2010.
10. Viete, D.R.; Ranjith, P.G. The effect of CO_2 on the geomechanical and permeability behaviour of brown coal: Implications for coal seam CO_2 sequestration. *Int. J. Coal Geol.* **2006**, *66*, 204–216. [CrossRef]
11. White, C.M.; Smith, D.H.; Jones, K.L.; Goodman, A.L.; Jikich, S.A.; LaCount, R.B.; DuBose, S.B.; Ozdemir, E.; Morsi, B.I.; Schroeder, K.T. Sequestration of carbon dioxide in coal with enhanced coalbed methane recovery: A review. *Energ. Fuel* **2005**, *19*, 659–724. [CrossRef]
12. Pan, Z.; Connell, L.D.; Camilleri, M. Laboratory characterisation of coal reservoir permeability for primary and enhanced coalbed methane recovery. *Int. J. Coal Geol.* **2010**, *82*, 252–261. [CrossRef]
13. Gibbs, J.W. On the equilibrium of heterogeneous substances. *Am. J. Sci.* **1878**, *16*, 441–458. [CrossRef]
14. Griffith, A.A. The phenomena of rupture and flow in solids. *Phil. Trans. R. Soc. Lond. Ser. A* **1921**, *221*, 163–198. [CrossRef]

15. Perera, M.S.A.; Ranjith, P.G.; Viete, D.R. Effects of gaseous and super-critical carbon dioxide saturation on the mechanical properties of bituminous coal from the southern sydney basin. *Appl. Energy* **2013**, *110*, 73–81. [CrossRef]
16. Ranathunga, A.S.; Perera, M.S.A.; Ranjith, P.G.; Bui, H. Super-critical CO_2 saturation-induced mechanical property alterations in low rank coal: An experimental study. *J. Supercrit. Fluids* **2016**, *109*, 134–140. [CrossRef]
17. Vishal, V.; Ranjith, P.; Singh, T. An experimental investigation on behaviour of coal under fluid saturation, using acoustic emission. *J. Nat. Gas Sci. Eng.* **2015**, *22*, 428–436. [CrossRef]
18. Ates, Y.; Barron, K. The effect of gas sorption on the strength of coal. *Min. Sci. Technol.* **1988**, *6*, 291–300. [CrossRef]
19. Brady, B.; Brown, E. *Rock Mechanics: For Underground Mining*, 3rd ed.; Springer: Dordrecht, The Netherlands, 2004.
20. Jasinge, D.; Ranjith, P.; Choi, X.; Fernando, J. Investigation of the influence of coal swelling on permeability characteristics using natural brown coal and reconstituted brown coal specimens. *Energy* **2012**, *39*, 303–309. [CrossRef]
21. Kiyama, T.; Nishimoto, S.; Fujioka, M.; Xue, Z.; Ishijima, Y.; Pan, Z.; Connell, L.D. Coal swelling strain and permeability change with injecting liquid/supercritical CO_2 and N_2 at stress-constrained conditions. *Int. J. Coal Geol.* **2011**, *85*, 56–64. [CrossRef]
22. Perera, M.S.A.; Ranjith, P.G.; Choi, S.K.; Airey, D. The effects of sub-critical and super-critical carbon dioxide adsorption-induced coal matrix swelling on the permeability of naturally fractured black coal. *Energy* **2011**, *36*, 6442–6450. [CrossRef]
23. Ranathunga, A.S.; Perera, M.S.A.; Ranjith, P.G.; Ju, Y.; Vishal, V.; De Silva, P. A macro-scale experimental study of sub-and super-critical CO_2 flow behaviour in victorian brown coal. *Fuel* **2015**, *158*, 864–873. [CrossRef]
24. Perera, M.S.A.; Ranjith, P.G.; Peter, M. Effects of saturation medium and pressure on strength parameters of Latrobe Valley brown coal: Carbon dioxide, water and nitrogen saturations. *Energy* **2012**, *36*, 6941–6947. [CrossRef]
25. Ranjith, P.G.; Perera, M.S.A. Effects of cleat performance on strength reduction of coal in CO_2 sequestration. *Energy* **2012**, *45*, 1069–1075. [CrossRef]
26. Perera, M.S.A.; Ranjith, P.G.; Airey, D.W.; Choi, S.K. Sub- and super-critical carbon dioxide flow behavior in naturally fractured black coal: An experimental study. *Fuel* **2011**, *90*, 3390–3397. [CrossRef]
27. ASTM D7012. *Standard Test Method for Compressive Strength and Elastic Moduli of Intact Rock Core Specimens un-der Varying States of Stress and Temperatures*; ASTM International: West Conshohocken, PA, USA, 2004.
28. Vutukuri, V.S.; Lama, R.D.; Saluja, S.S. *Handbook on Mechanical Properties of Rocks: Testing Techniques and Results*; Trans Tech Publications: Bay Village, OH, USA, 1978; pp. 105–115.
29. Kuvaev, N.; Panchenko, D. Effect of moisture on the dynamic strength of brown coals. *J. Min. Sci.* **1975**, *11*, 220–222. [CrossRef]
30. Ranjith, P.G.; Jasinge, D.; Choi, S.K.; Mehic, M. The effect of CO_2 saturation on mechanical properties of Australian black coal using acoustic emission. *Fuel* **2010**, *89*, 2110–2117. [CrossRef]
31. Oldenburg, C.M. Geologic carbon sequestration: CO_2 transport in depleted gas reservoirs. In *Gas Transport in Porous Media*; Springer: Dordrecht, The Netherlands, 2006; pp. 419–426.

6.4 How does the influence of CO_2 adsorption on coal mechanical properties vary under confining pressure and various fluid saturation times?

In the various strength studies conducted regarding the CO_2-ECBM process, very little attention has been paid to the geo-mechanical property alterations in coal seams during CO_2 adsorption under in-situ stress conditions which represent actual field conditions. As discussed in Chapter 2, coal seam depth or the confining pressure is an important factor affecting CO_2 adsorption-induced coal matrix changes which may induce less matrix rearrangement, due to the higher confinement, resulting in higher tortuosity and consequently lower flow rate through the coal mass. This behaviour may lead to less strength variation at greater depths or in in-situ conditions compared to the unconfined conditions reported in Section 6.2. Therefore, this study aimed to determine how coal seam integrity varies with the introduction of CO_2 under in-situ stress conditions, by conducting a series of tri-axial strength tests on Australian brown coal samples from the Gippsland basin.

The effect of CO_2 exposure time on coal's mechanical properties was also investigated under super-critical CO_2 saturation conditions, in order to determine the effect of long-term CO_2 injection on coal seam mechanical properties, as CO_2-ECBM is a long-term process. Brown coal was used to conduct the experiments and it was saturated for 3, 6, 9 and 12 months to study the time effect. Further, micro-structural changes in the specimens were observed at different durations of CO_2 saturation to better relate the observed strength properties.

This section of the chapter is the following publication:

Ranathunga AS, Perera MSA, Ranjith PG (2016). Influence of CO_2 adsorption on the strength and elastic modulus of low rank Australian coal under confining pressure. *International Journal of Coal Geology* 167, 148-156.

International Journal of Coal Geology 167 (2016) 148–156

Contents lists available at ScienceDirect

International Journal of Coal Geology

journal homepage: www.elsevier.com/locate/ijcoalgeo

Influence of CO_2 adsorption on the strength and elastic modulus of low rank Australian coal under confining pressure

A.S. Ranathunga [a], M.S.A. Perera [b,c,*], P.G. Ranjith [a]

[a] Deep Earth Energy Laboratory, Department of Civil Engineering, Monash University, Building 60, Melbourne, Victoria 3800, Australia
[b] Department of Infrastructure Engineering, The University of Melbourne, Building 176, Melbourne, Victoria, 3010, Australia
[c] Adjuct Research Fellow, Deep Earth Energy Laboratory, Department of Civil Engineering, Monash University, Building 60, Melbourne, Victoria, 3800, Australia

A R T I C L E I N F O

Article history:
Received 16 May 2016
Received in revised form 15 August 2016
Accepted 17 August 2016
Available online 29 September 2016

Keywords:
CO_2 adsorption
Strength and elastic modulus
CO_2 phase and pressure
Coal rank
Stress environment

A B S T R A C T

Precise knowledge of changes in the CO_2 adsorption-induced mechanical properties of deep coal seams is necessary for the safe and successful implementation of carbon dioxide-enhanced coal bed methane (CO_2-ECBM) recovery. To date, little attention has been paid to the geo-mechanical property alterations in coal seams during CO_2 adsorption under in-situ stress conditions. The aim of this study is therefore to discover how coal seam integrity varies with the introduction of CO_2 under in-situ stress conditions, by conducting a series of tri-axial strength tests of Australian brown coal samples. The effect of CO_2 exposure time on coal's mechanical properties was also investigated under super-critical CO_2 saturation (10 MPa) conditions, in order to determine the effect of long-term CO_2 injection on coal seams' mechanical properties, as CO_2-ECBM is a long-term process.
According to the test results, irrespective of coal rank, the strength reduction in coal with CO_2 injection under field conditions is significantly less than would be expected based on simple laboratory testing such as uniaxial tests. However, in any stress environment, high rank coals are subjected to greater strength and stiffness reductions with CO_2 adsorption than low rank coals, due to their well-developed cleat system, and the injection of super-critical CO_2 induces greater mechanical property alterations in coal than sub-critical CO_2 injection. These strength and elastic modulus changes in coal with CO_2 adsorption can be presented using a simple Langmuir-type equation, regardless of rank. Furthermore, the observation of the effect of long-term CO_2 saturation on coal's mechanical properties revealed that, although CO_2 adsorption-induced mechanical property alterations in coal are mostly completed with the first interaction with CO_2, further structural re-arrangement may occur at a slower rate over time.

6.4.1. Introduction

Enhanced coal bed methane (ECBM) recovery is a coal bed methane (CBM) production stimulation technique that provides benefits for atmospheric carbon dioxide (CO_2) mitigation. The ECBM process involves the capture of CO_2 and its injection into un-mineable coal seams, which displaces the CH_4 formed during the coalification process in the seam, which can then be captured and utilised as an energy source. However, swelling of the coal matrix in the presence of CO_2 is a primary issue in the CO_2 sequestration and ECBM recovery process in deep coal seams (Hol and Spiers, 2012; Masoudian, 2016; Nikoosokhan et al., 2014; Vandamme et al., 2010; White et al., 2005), because it reduces the overall strength of the seam (Ates and Barron, 1988; Aziz and Ming-Li, 1999; Wang et al., 2013a; White et al., 2005). This mechanical degradation of the coal seam may greatly affect the seam's integrity, particularly in the presence of geological structures like deformed zones of strike-slip, faults, reverse and thrust (Wang et al., 2013a), by expanding the damaged zones. Further, Viete and Ranjith (2006) (for low rank coal) and Wang et al. (2013a) (for high rank coal) found an accelerated flow behaviour of CO_2 through weakened coal specimens upon CO_2 adsorption due to micro fracture formation under regional and localised in situ stresses. Hence, the combined effect created by coal strength reduction and flow acceleration pose a great threat of CO_2 back-migration into the atmosphere, rendering storage efforts ineffective. For example, the storage of substantial amounts of high pressure CO_2 in a coal seam weakened by CO_2 adsorption may result in adverse incidents, such as gas outburst, a sudden and violent failure of the seam with the release of huge quantities of gas and earth materials, even threatening the lives of people living in the area (Ates and Barron, 1988; Wang et al., 2013a).

In relation to the mechanism of the change in coal matrix strength with fluid adsorption, it should be noted that the coal matrix is not a rigid structure, but is a polymer-like network that readily undergoes volumetric changes with fluid injection (shrinkage and swelling), depending on various factors including adsorbing fluid type and phase (Nikoosokhan et al., 2014; Vandamme et al., 2010; White et al., 2005).

* Corresponding author at: Dr. Mandadige Samintha Anne Perera, Department of Infrastructure Engineering, The University of Melbourne, Building 176, Melbourne, Victoria 3010, Australia.
E-mail address: samintha.perera@unimelb.edu.au (M.S.A. Perera).

http://dx.doi.org/10.1016/j.coal.2016.08.027
0166-5162/© 2016 Elsevier B.V. All rights reserved.

Furthermore, the influence on the coal matrix of the adsorbing fluid is also dependent on the maturity of the seam or the coal's rank (Perera et al., 2016). Table 1 shows a summary of previous studies of the various factors affecting coal mass strength with the adsorption of different fluids. According to Table 1, water saturation creates a reduction in coal mass strength, while N_2 saturation slightly enhances coal strength with the removal of moisture and other adsorbed gases from the coal mass. Furthermore, CO_2 causes a greater strength reduction in coal when it is in its super-critical state compared to the sub-critical state, and this reduction is higher for high rank coal than low rank coal (see Table 1). However, most of these studies have been conducted in uniaxial stress environments that do not represent coal mass behaviour under in-situ stress conditions in the field. This is because the mechanical property alterations in coal mass with CO_2 saturation are higher under uniaxial conditions, due to the absence of higher effective stress under field conditions. In order to account for this in-situ stress condition, it is therefore necessary to perform more reliable tests such as tri-axial tests for the strength performance evaluation of the coal matrix upon fluid injection. In one of the few studies on this subject, Viete and Ranjith (2006) found that the strength loss which occurs due to CO_2 saturation is minimal under tri-axial conditions compared to uniaxial conditions. At 2 MPa CO_2 saturated low rank coal samples showed around 6.25% strength reduction and 15.67% elastic modulus reduction (Perera et al., 2016) in uniaxial testing and insignificant mechanical property variation when the test was performed under tri-axial conditions by applying a 10 MPa confinement to similar 2 MPa CO_2 saturated low rank coal samples (Viete and Ranjith, 2006). However, Masoudian et al. (2014) observed up to 19% strength reductions and up to 20% elastic modulus reductions with sub-critical CO_2 saturation (<5.5 MPa) in high rank coal samples under various confining pressures. To date, the effect of super-critical CO_2 adsorption under tri-axial stress conditions has not been investigated, despite these being the actual in-situ conditions in the field. Further, many studies have been conducted on the mechanical property variation in high rank coal under various possible CO_2 saturations and in-situ stresses (see Table 1) considering the wide application of high rank coal in CO_2 sequestration and ECBM processes.

The infrequent existence of brown coal at sufficient depths for feasible CO_2 sequestration has caused less attention being given to similar investigations for low rank coals such as brown coal. However, according to the Cooperative Research Centre for greenhouse gas technologies (CO2CRC) studies, there possibly exist brown coal storage sites in the offshore Gippsland basin at un-minable depths (400–800 m) (Hooper et al., 2005; Jasinge, 2010). Based on these possibilities, the present study was undertaken to find the storage and ECBM effectiveness of CO_2 in brown coal under various stress environments.

Furthermore, current studies of coal mass strength changes with CO_2 adsorption have been conducted within two to three weeks after the samples were saturated (Aziz and Ming-Li, 1999; Bagga et al., 2015; Masoudian et al., 2014; Ranathunga et al., 2016; Vishal et al., 2015; Wang et al., 2013b). However, with CO_2-ECBM projects, it is intended to sequestrate CO_2 for a geologically significant period. The current observations on coal mass strength reductions for CO_2 adsorption may therefore differ from the actual conditions in the field, and it is vital to investigate how coal mass strength reduction varies over time with CO_2 injection. This was also considered in this study, which attempts to explore the effect of the saturation time of CO_2 on low-ranked brown coal strength changes.

6.4.2. Experimental methodology

6.4.2.1. Sample preparation

Low rank brown coal samples taken from the Hazelwood coal mine in the Latrobe Valley, Victoria, Australia were used for the present study. These samples had an average moisture content of 62% (on a wet basis), around 48% (on a dry basis) fixed carbon content, volatile matters of 50.3% (on a dry basis) (Ranathunga et al., 2016) and an average bulk density of 1.11 g/cm^3. The samples used for the testing program were 38 mm in diameter and 76 mm in height, and Ranathunga et al. (2016) explain the detailed sample preparation procedure. Great care was taken to reduce the heterogeneity of the brown coal specimens, and the samples were taken from the same coal block.

Table 1
Summary of research into factors affecting coal strength.

Effective factors		Key findings	Type of tests	Reference
Saturated medium	Carbon dioxide (CO_2)	– CO_2 decreases coal strength as coal mass becomes weaker with the substitution of existing adsorbate CH_4 with the highly chemically potential CO_2	Uniaxial	Aziz and Ming-Li (1999); Karacan (2007); Larsen (1997); Hol and Spiers (2012); Bagga et al. (2015)
		– Under tri-axial conditions strength loss due to CO_2 saturation is minimal compared to uniaxial conditions.	Tri-axial	Viete and Ranjith (2006); Hol et al. (2012); Pan et al. (2010); Masoudian et al. (2014)
	Nitrogen (N_2)	– N_2 displaces the natural moisture from the pore spaces in the coal, this dries the coal out and slightly increases its strength (up to 10%)	Uniaxial	Perera et al. (2016)
		– No noticeable change in the strength compared to natural samples	Tri-axial	Jasinge (2010)
	Methane (CH_4)	– CH_4 desorption weakens coal mass due to reduction of the effective stress and crushing of coal due to the internal gas energy release controlled by gas pressure and content	Tri-axial	Wang et al. (2013a)
	Water	– Water reduces the strength of coal (up to 30%) with the softening of the rock mass bond structure and the ability of moisture inside the rock mass to decrease the surface energy	Uniaxial	Vishal et al. (2015)
		– Water saturation effect is negligible at any confining stress on both strength and elastic modulus	Tri-axial	Masoudian et al. (2014)
Gas phase	Sub-critical CO_2	– High rank coal (around 26%) showed a comparatively higher reduction of strength and elastic modulus compared to low rank coal (around 20%).	Uniaxial	Bagga et al. (2015); Vishal et al. (2015)
		– Up to 20% reduction of strength and up to 19% reduction of elastic modulus was observed for high rank coal – Increase in elastic modulus with increasing effective confining pressure	Tri-axial	Masoudian (2016); Wang et al. (2013b)
	Super-critical CO_2	– Average reduction of uniaxial strength is around 59% for low rank coal while that for high rank coal is 71% – Higher adsorption potential of super-critical CO_2 results in greater coal matrix alterations causing higher strength reductions in coal structure	Uniaxial	Hol and Spiers (2012); Perera et al. (2016)
		– Around 10–20% reduction of bulk modulus was observed for high rank coal.	Tri-axial	Pan et al. (2010)
Coal rank		– Compared low rank coal, high rank coal exhibits a higher reduction of strength and elastic modulus (from 0.5 to 1.75 times reduction).	Uniaxial	Bagga et al. (2015); Vishal et al. (2015)
		– High rank coal (20%) showed a comparatively slightly higher reduction of strength and elastic modulus compared to low rank coal (17%)	Tri-axial	Jasinge (2010); Masoudian et al. (2014)

6.4.2.2. Sample testing

Tri-axial tests were conducted on brown coal samples after saturating the specimens at 4.5, 5.5, 6.5, 7.5 and 8.5 MPa CO_2 pressures. Furthermore, unsaturated coal samples were also tested to compare the observations of the CO_2 saturated specimens. All the tests were conducted under 10 MPa confining pressure and 35 °C constant temperature. The 10 MPa confining pressure represents a coal specimen located at a depth of approximately 400 m, and the CO_2 pressures of 4.5, 5.5 and 6.5 MPa represent sub-critical conditions (less than the critical point of CO_2–7.38 MPa pressure and 31.8 °C temperature), while 7.5 and 8.5 MPa CO_2 pressure represent super-critical conditions (greater than the critical point of CO_2).

a. Tri-axial strength tests

The high-pressure tri-axial test rig in the Monash University Deep Earth Energy Laboratory (see Fig. 1) was used to conduct the tri-axial tests on the brown coal samples. First the confining pressure (10 MPa) and temperature (35 °C) were applied to the coal specimen and then the respective CO_2 flow (4.5, 5.5, 6.5, 7.5 and 8.5 MPa) was permeated through the sample (drained conditions). Once the flow of upstream and downstream became stable, the specimen was left for another 3 to 4 days to allow the CO_2 to adsorb well into the sample. The load was then applied at a strain rate of 0.1 mm/min until failure. The tests were replicated 2 to 3 times to confirm the experimental observations. The load applied with axial strain was recorded using an advanced data acquisition system and the results were then analysed. The results for axial strain and tri-axial strength are displayed in Fig. 2.

b. CO_2 saturation to investigate long-term saturation effect

Brown coal samples which had been saturated with CO_2 at 10 MPa pressure and 35 °C (super-critical conditions) for 3, 6, 9 and 12 months were then tested to investigate how the mechanical properties of brown coal vary over the duration of CO_2 exposure. Here, 10 MPa CO_2 pressure was chosen, based on the results obtained by Ranathunga et al. (2016) for brown coal, which showed that the highest strength reduction occurs in brown coal when it has been saturated by 10 MPa CO_2 (see Table 1). Two to three samples for each duration (3, 6, 9 and 12 months) were saturated using high-pressure saturation chambers. After the saturation period, the pressure cells were gradually de-pressurized at a slow rate of 0.02 MPa/min to prevent possible damage to the physical structure of the coal specimen caused by sudden pressure changes. Scanning electron microscopy (SEM) was also employed to observe the micro-structural changes in coal specimens over time to further clarify the coal matrix alterations. The detailed procedure used for CO_2 saturation and the SEM study are explained in Ranathunga et al. (2016).

6.4.3. Experimental results and discussion

During the present study, tri-axial tests were conducted for different CO_2 saturated low rank coal samples and unsaturated coal samples for comparison, and the results are shown in Table 2. The stress-strain curves obtained for these coal specimens are shown in Fig. 2. In addition, coal samples were tested for different CO_2 saturation periods (3, 6, 9 and 12 months), and the results are shown in Table 3. The following sections discuss how the coal mass mechanical properties (strength and elastic modulus) changed under the test conditions.

6.4.3.1. Coal mechanical property alterations with CO_2 adsorption under in-situ stress conditions

a. Strength of coal mass

According to Table 2, an average strength of 2.33 ± 0.003 MPa (at a 95% level of confidence) could be seen in unsaturated coal specimens under 10 MPa confining pressure. As expected, CO_2 saturation causes a clear strength reduction in the tested low rank coal (see Table 2). For example, around 12.16% strength reduction can be seen for coal samples saturated with 8.5 MPa CO_2 (see Table 2). As stated by Gibbs (1878), CO_2 adsorption should theoretically reduce the surface energy of the coal mass (see Eq. (1)), as CO_2 has a higher chemical potential than the existing CH_4 in the coal mass.

$$\Delta\gamma = -\frac{RT}{MS}\int_0^P x\, d(\ln P) \qquad (1)$$

where, $\Delta\gamma$ is change in surface energy (J), R is universal gas constant (8.314 J/mol·K), T is temperature (K), M is molecular weight of CO_2 (g), S is surface area of coal (m^2), x is the amount of adsorption (g [adsorbent]/g [coal]) and P is the CO_2 pressure (Pa).

Further, Griffith (1921) indicated that the tensile strength of a material required to form a new crack surface (σ) is (see Eq. (2)):

$$\sigma = \sqrt{\frac{2\gamma E}{\pi b}} \qquad (2)$$

where, E is the elastic modulus of the material, γ is surface energy and b is the half length of the crack.

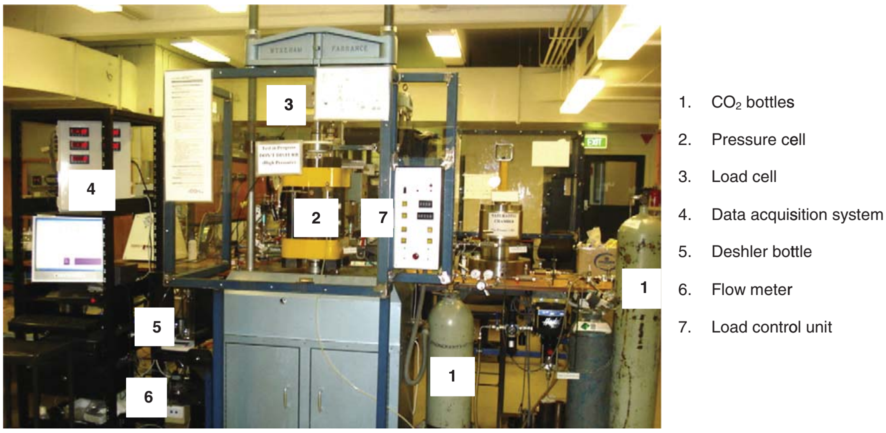

Fig. 1. High-pressure tri-axial test rig used for sample testing.

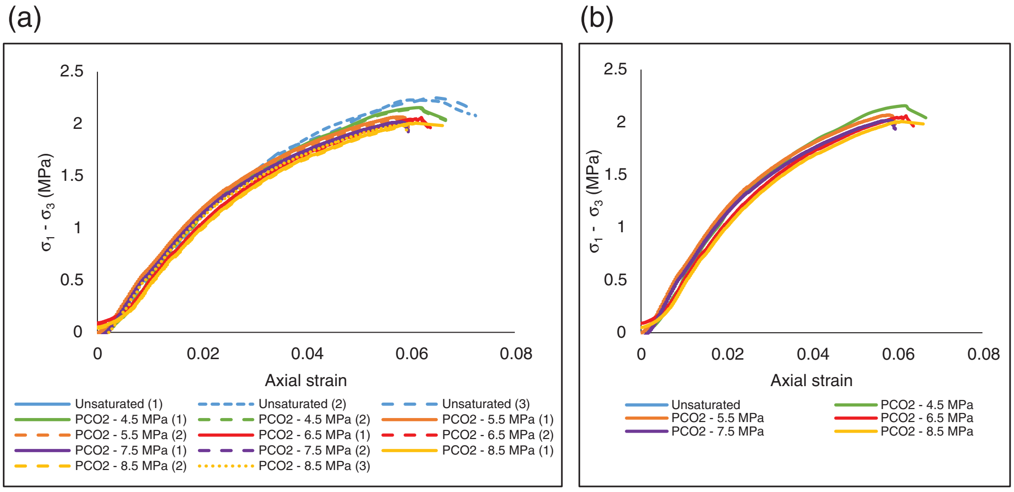

Fig. 2. Stress vs. strain curves for (a) all the tested coal samples and (b) the samples with highest failure strength (here "PCO2" is the CO_2 saturation pressure).

By combining Eqs. (1) and (2), the decrease in the tensile strength required to form a new crack surface during CO_2 adsorption can be obtained, as shown in Eq. (3):

$$\Delta\sigma = \sqrt{\frac{\frac{2ERT}{MS}\left[\int_0^P x\, d(\ln P)\right]}{\pi a}} \tag{3}$$

According to Eq. (3), the higher the CO_2 pressure, the greater the reduction of the surface energy, leading to a lower tensile strength for crack formation and hence an overall strength reduction of the coal mass. Therefore, the observed strength reductions in the present study confirm the expected matrix rearrangement induced in coal with CO_2 adsorption. This strength reduction under tri-axial conditions has also been shown for high rank coal by Masoudian et al. (2014), according to whom the strength of Australian high rank coal (high volatile bituminous) can be reduced by up to around 20% by sub-critical CO_2 adsorption (5.5 MPa). It is therefore clear that CO_2 adsorption causes the strength of coal to be considerably reduced, even under the in-situ stress environment in the field, regardless of the coal's rank.

However, the strength reduction observed under tri-axial conditions is much lower than the strength reductions observed by previous researchers under uniaxial conditions for CO_2 saturated coal. For example, Ranathunga et al. (2016) observed up to 21.25% and 57.50% uniaxial compressive strength (UCS) reductions in low rank Australian brown coal samples similar to those in the present study saturated by sub-critical CO_2 (6 MPa) and super-critical CO_2 (8 MPa). These reductions are much greater than the strength reductions observed in the present study for similar coal saturated under saturation conditions of 6.5 and 8.5 MPa and tested under tri-axial conditions (10.17% and 12.16%).

This observation may be due to both mechanical strengthening of coal mass with the application of higher in-situ stresses and the changes in CO_2 adsorption potential during the higher effective stresses, as explained in the following sections.

➢ Mechanical strengthening of coal

According to Gentzis et al. (2007), the Hoek-Brown failure criterion (see Eq. (4)) is a better representation of the coal strength than Mohr-Coulomb failure criterion:

$$\sigma_1' = \sigma_3' + \sigma_c\left(m\frac{\sigma_3'}{\sigma_c} + s\right)^a \tag{4}$$

where, σ_1' and σ_3' are major and minor effective principal stresses, σ_c is the uniaxial compressive strength of the intact rock and *m, s, a* are Hoek-Brown parameters.

Table 2
Experimental results obtained for different test conditions.

Saturation condition	Differential stress/(σ_1-σ_3) (S, MPa)	Average S (MPa)[a]	ΔS (%)	Elastic modulus (E, MPa)	Average E (MPa)[a]	ΔE (%)	Moisture content (%)
Natural	2.331	2.330 ± 0.003	–	67.141	67.125 ± 0.379	–	61.93
	2.327			66.783			62.41
	2.332			67.452			61.85
4.5 MPa CO_2	2.150	2.174 ± 0.046	6.71	60.597	60.811 ± 0.418	9.41	62.77
	2.197			61.024			62.41
5.5 MPa CO_2	2.104	2.103 ± 0.003	9.76	59.495	59.301 ± 0.38	11.66	62.10
	2.101			59.107			62.64
6.5 MPa CO_2	2.087	2.093 ± 0.012	10.17	57.975	58.32 ± 0.675	13.12	62.53
	2.099			58.664			62.18
7.5 MPa CO_2	2.068	2.065 ± 0.007	11.39	57.713	57.600 ± 0.221	14.19	62.22
	2.061			57.487			62.39
8.5 MPa CO_2	2.047	2.047 ± 0.006	12.16	57.451	57.364 ± 0.324	14.54	62.53
	2.052			57.957			62.34
	2.041			57.044			62.79

[a] At 95% level of confidence.

Table 3
Unconfined compressive strength (UCS) and elastic modulus (E) values obtained under 10 MPa CO_2 saturation for brown coal for different saturation periods.

Time (days)	UCS (MPa)	ΔUCS (%)	ΔUCS compared to 21 days (%)	E (MPa)	ΔE (%)	ΔE compared to 21 days (%)
0	2.40	0.00	–	41.60	0.00	–
21	0.99	58.75	0.00	23.42	43.70	0.00
90	0.91	62.08	8.08	22.89	44.98	2.26
180	0.87	63.75	12.12	22.07	46.95	5.76
270	0.82	65.83	17.17	21.59	48.10	7.81
365	0.74	69.17	25.25	20.93	49.69	10.63

As shown in Eq. (4), with the application of in situ stresses, the material is strengthened. Therefore, compared to uniaxial conditions, tri-axial strength is higher. According to Masoudian et al. (2014), around 44% reduction of the Hoek-Brown parameter "m" for intact coal (14.263) compared to CO_2 treated coal (8.053) was observed. Therefore, CO_2 adsorption can affect the mechanical strengthening of the coal mass.

➢ CO_2 adsorption potential at higher effective stresses

After conducting a series of experiments to investigate the effect of applied stresses on the CO_2 sorption capacity of high volatile bituminous coal, Hol et al. (2011) found that the in situ stresses reduce the CO_2 adsorption capacity of coal primarily and CO_2 adsorption induced coal matrix swelling will reduce the adsorption capacity secondarily. They developed a thermodynamic model to describe the CO_2 adsorption capacity with effective stress (see Eq. (5)) as follows:

$$C_\sigma = \frac{C_s a_f K exp\left(-\frac{\sigma_e \Omega_a}{kT}\right)}{1 + a_f K exp\left(-\frac{\sigma_e \Omega_a}{kT}\right)} \tag{5}$$

where, C_σ is equilibrium concentration of adsorbed CO_2 (mol/kg), C_s is the number of potential adsorption sites per kg of coal (constant), a_f is the chemical activity of the free CO_2 at pressure P, K is the equilibrium constant for the adsorption reaction, Ω_a is partial or effective molecular volume of CO_2 in the adsorbed state, k is the Boltzmann constant, T is temperature and σ_e is the hydrostatic effective stress.

According to Eq. (5), the effect of in-situ stresses on CO_2 adsorption capacity is reduced with higher effective stress applications. The amount of adsorption (x, in Eq. (3)) is reduced at higher stress applications and ultimately increases the tensile strength required to form a crack in the coal mass (refer to Eq. (3)). Therefore, compared to uniaxial conditions, the expected strength reduction due to the CO_2 adsorption is less under tri-axial conditions. Similarly, for high rank Australian black coal, Perera et al. (2013) observed around 53.9% strength reduction for 6 MPa (sub-critical) CO_2 saturation, and the reduction was <20% under tri-axial conditions (Masoudian et al., 2014). Hence, it can be deduced that, irrespective of the coal rank, the actual strength reductions in deep coal seams with CO_2 injection are much lower than the values obtained in uniaxial tests.

b. Stiffness of coal mass

The effect of CO_2 adsorption under in-situ stress conditions on coal's elastic behaviour was then investigated by examining the corresponding elastic modulus changes. As shown in Table 2, the average elastic modulus (E) of unsaturated coal samples is 67.125 ± 0.379 MPa (at a 95% level of confidence) under 10 MPa confining pressure. This elastic modulus value is reduced with increasing CO_2 saturation pressure, similar to the observations of coal strength (see Table 2). For example, there is around a 9.41% E reduction for 4.5 MPa CO_2 saturated samples while around a 14.54% E reduction in specimens saturated by 8.5 MPa CO_2 (see Table 2). The CO_2 adsorption-induced plasticisation effect (Karacan, 2007) is the main reason for these observed variations of elastic modulus. This plasticisation occurs due to the increment of segmental mobility induced in the polymer structure with CO_2 dissolution, which has a softening effect on the coal mass. In addition, this process causes the coal polymer structure to be weakened. Hence, the expansion of the coal mass free volume with polymer structural rearrangement upon CO_2 adsorption (Larsen et al., 1997) results in the enhancement of the ductile nature of coal's structure and this causes the observed E reduction. Similarly, Masoudian et al. (2014) discovered an overall reduction of 19% in E for high rank coal upon sub-critical CO_2 saturation. A comparison of the findings of the present study with those of Masoudian et al. (2014) confirms the enhancement of coal ductile properties with CO_2 adsorption, regardless of coal rank.

Similar to the strength results, the E reduction under tri-axial conditions is lower than those observed under uniaxial conditions with the adsorption of CO_2 into the coal mass. For instance, Ranathunga et al. (2016), observed a 40.12% E reduction for super-critical (8 MPa) CO_2 saturated low rank coal specimens, which is much greater than the E reduction observed under tri-axial conditions in the present study (14.54%) for similar low ranked coal. As explained in Section 3.1.a, due to higher in situ stresses, CO_2 adsorption potential is reduced (refer to Eq. (5)), and hence the expected plasticisation effect is less compared to uniaxial conditions. In addition, the closure of fractures and pores under higher stress applications may result in an increase in the material stiffness (Corkum and Martin, 2007). Further, Gentzis et al. (2007) observed an increment in elastic modulus with confining pressure up to 5 MPa and then a constant value for the rest of confinements for bituminous coal (unsaturated). However, the micro-cracks created at higher loadings with different orientations and frequencies lead to an anisotropy in elastic modulus values (Szwilski, 1984). For CO_2 saturated coal (under 0.5 MPa), Wang et al. (2013b) found increasing elastic modulus with effective confining pressure. Therefore, the effect of in-situ stresses on elastic modulus variations observed with CO_2 adsorption in terms of confinement shrinking warrants further research.

In addition, for high rank coal, Perera et al. (2013) observed around 42.43% elastic modulus reduction under 6 MPa (sub-critical) CO_2 saturation for Australian high rank coal under uniaxial stress conditions, and this is lower than the 19% under tri-axial conditions reported by Masoudian et al. (2014). Hence, according to the experimental results, a comparatively lower ductile enhancement can be expected under field conditions with CO_2 injection for any coal rank.

c. Quantification of CO_2 adsorption-induced mechanical property variations

An attempt was then made to mathematically relate the changes in CO_2 adsorption-induced coal mechanical properties (strength and elastic modulus). Day et al. (2010), found that the amount of swelling in coal mass is directly related to the adsorption of gas into the coal matrix, and Masoudian et al. (2014) assumed that the strength reduction in coal has a Langmuir-type curve that can be successfully related to laboratory results using a mathematical relationship (Eq. (6)):

$$\Delta\sigma_{CO_2} = \frac{\Delta\sigma_{max} P_{CO_2}}{P_{CO_2} + P_\sigma} \tag{6}$$

where, $\Delta\sigma_{co_2}$ is the strength reduction due to CO_2 adsorption (MPa), P_{co_2} is the CO_2 saturation pressure (MPa), and $\Delta\sigma_{max}$ and P_σ are curve fitting parameters.

Therefore, the strength of the CO_2 saturated coal (σ_{co_2}) can be calculated as follows:

$$\sigma_{CO_2} = \sigma_{intact} - \Delta\sigma_{CO_2} \tag{7}$$

where, σ_{intact} is the strength of the intact coal sample.

Fig. 3 shows the CO_2 adsorption-induced strength reductions against the CO_2 saturation pressure curves and the curve fitting parameters. The

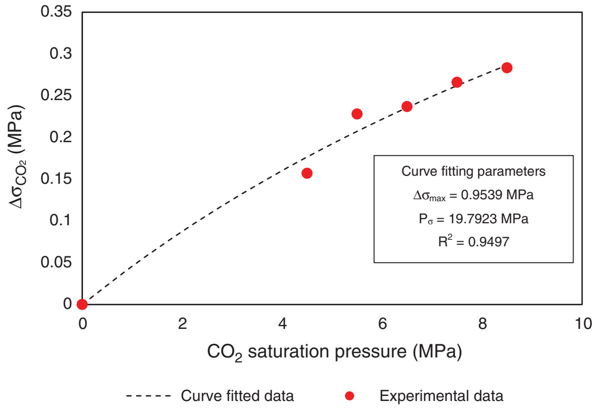

Fig. 3. Strength reduction ($\Delta\sigma_{co_2}$) versus injection pressure and estimated parameters.

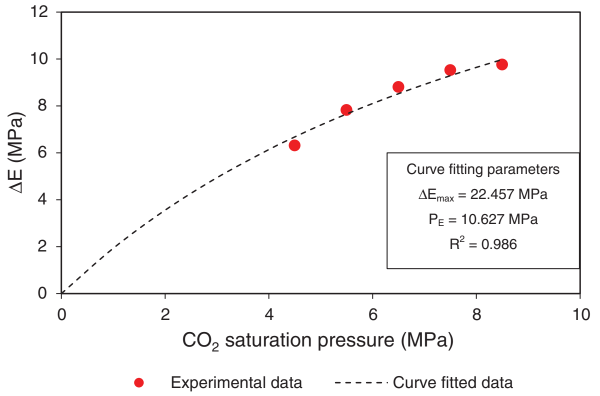

Fig. 4. Elastic modulus reduction (ΔE) versus injection pressure and estimated parameters.

data obtained from the present study show that the relation proposed by Masoudian et al. (2014) is also valid for low-ranked coal. After a least square regression analysis ($R^2 = 0.9497$), $\Delta\sigma_{max}$ was estimated as 0.9539 MPa and P_σ was estimated as 19.7923 MPa for Australian low-rank brown coal and $\Delta\sigma_{max} = 14.59$ MPa and $P_\sigma = 1.307$ MPa for Australian high-rank coal (Masoudian et al., 2014). This shows that the curve fitting parameters in Eq. (6) vary with the coal rank, similar to the Langmuir curve fitting parameters. Furthermore, the curve fitting parameters may also be dependent on the test conditions. Therefore, the testing of a much broader range of coal ranks under different stress environments is required to find a general relation for Eq. (6).

Similarly, the CO_2 adsorption-induced elastic modulus reduction in coal can be given as Eqs. (8) and (9), following Masoudian et al. (2014):

$$\Delta E_{CO_2} = \frac{\Delta E_{max} P_{CO_2}}{P_{CO_2} + P_E} \tag{8}$$

where, ΔE_{co_2} – is the elastic modulus reduction due to CO_2 adsorption (MPa), P_{co_2} is CO_2 saturation pressure (MPa), and ΔE_{max} and P_E are curve fitting parameters.

Therefore, the elastic modulus of CO_2 saturated coal specimens (E_{co_2}) can be calculated as:

$$E_{CO_2} = E_{intact} - \Delta E_{CO_2} \tag{9}$$

where, E_{intact} is the strength of the intact coal sample.

Fig. 4 shows the E reduction due to CO_2 adsorption against CO_2 saturation pressure curves and the estimated values for the curve fitting parameters. After a least square regression analysis ($R^2 = 0.986$), ΔE_{max} was estimated as 22.457 MPa and P_E was estimated as 10.627 MPa. Masoudian et al. (2014) found the curve fitting parameters for E reduction to be $\Delta E_{max} = 0.65$ GPa and $P_E = 1.519$ MPa for high rank coal. Hence, as explained previously, these curve fitting parameters vary with coal rank and the molecular composition of coal. Finally, the predicted strength (σ_{co_2}) variation and elastic modulus variation with the CO_2 adsorption in low rank coal were calculated using Eqs. (6), (7), (8) and (9), and the results are shown in Fig. 5.

6.4.3.2. Factors affecting CO_2 adsorption-induced mechanical property changes under in-situ stress conditions

As discussed previously, injecting CO_2 properties and coal mass properties are the main factors affecting CO_2 adsorption-induced mechanical property alterations in coal. These are discussed in the following section.

a. Effect of CO_2 phase and pressure

The effect of injecting CO_2 properties (phase and pressure) on changes in coal seams' mechanical properties under in-situ conditions was examined, and the results are shown in Fig. 6(a). According to the figure, super-critical CO_2 saturated (7.5 and 8.5 MPa) coal samples exhibit higher mechanical property alterations than sub-critical CO_2 saturated (4.5, 5.5 and 6.5 MPa) samples. The inherent properties of super-critical CO_2, including its ability to greatly enhance the solubility of coal's solid constituents by its higher density and greater chemical potential (Chikatamarla et al., 2004), cause it to act as a plasticizer within the coal mass, resulting in greater reductions in strength and stiffness (Masoudian, 2016). A similar CO_2 phase influence effect on coal strength has been reported in uniaxial stress environments (Perera et al., 2013). Therefore, it is clear that the coal mass is subjected to greater mechanical property reductions with super-critical CO_2 adsorption than sub-critical CO_2 adsorption in any stress environment, and therefore under any field conditions (for example, at any depth) (see Fig. 6(b)).

In relation to the CO_2 pressure effect, according to Table 2, the CO_2 induced strength and elastic modulus reductions in coal clearly increase with increasing CO_2 saturation pressure. For example, around 6.71% and 12.16% strength reductions and 9.41% and 14.54% elastic modulus reductions can be seen for coal samples saturated with 4.5 MPa CO_2 and 8.5 MPa CO_2, respectively (see Table 2). This is because of the greater capacity of high-pressure CO_2 to attack the coal matrix than low pressure CO_2 (refer to Eq. (3)).

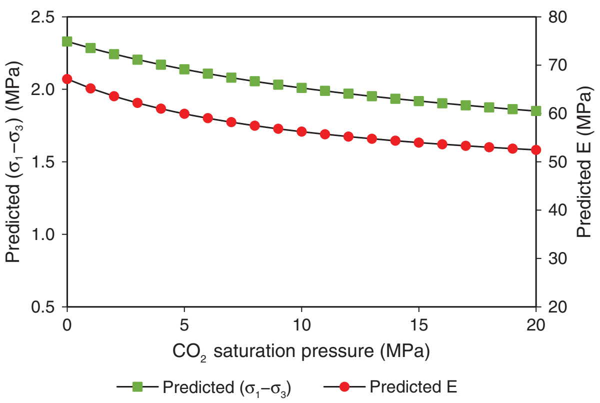

Fig. 5. Predicted strength ($\sigma_1 - \sigma_3$) and elastic modulus (E) of brown coal based on the proposed models with CO_2 saturation.

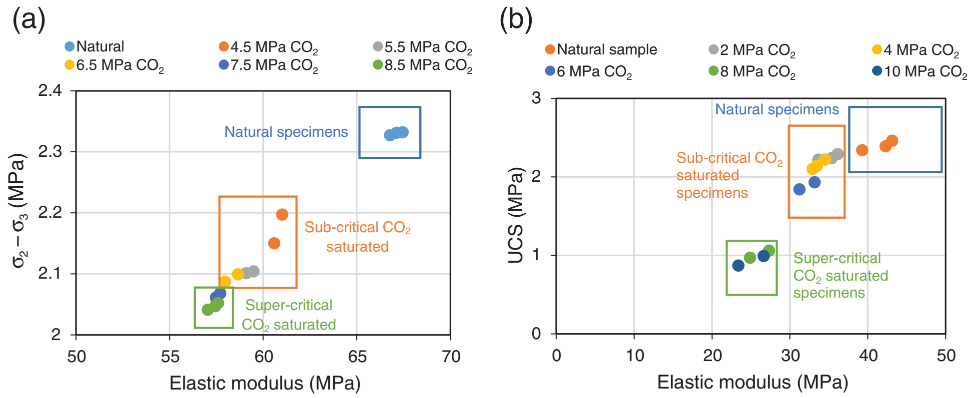

Fig. 6. Strength vs. elastic modulus plots for natural and CO_2 saturated samples tested under (a) tri-axial conditions and (b) uniaxial conditions (Ranathunga et al., 2016).

b. Effect of coal seam properties

The effect of coal seam properties (rank) on its mechanical property changes occur with CO_2 injection under in-situ stress conditions was then examined by comparing the tri-axial test results of low rank coal in the present study with those of high rank coal in Masoudian et al. (2014). These values were obtained by the euqations developed to predict the strength and elastic modulus variation with CO_2 adsorption in the present study (low rank coal) and by Masoudian et al. (2014) (high rank coal) and the results are shown in Fig. 7.

As shown in Fig. 7(a), a greater strength reduction occurs in high rank coal upon CO_2 adsorption compared with low rank coal in a tri-axial stress environment. For example, 4 MPa sub-critical CO_2 saturations cause around 0.16 MPa (around 7%) and 11 MPa (around 17%) strength reductions in low and high rank coals, respectively. Further, with 8 MPa super-critical CO_2 saturation, the coal mass is subjected to around 0.27 MPa (12%) and 12.54 MPa (around 28%) strength reduction in low and high rank coals, respectively. However, it should be noted that a 10 MPa confinement was used in the present study and a much lower (up to 5.5 MPa) confinement was used in Masoudian et al. (2014), which might also affect the greater strength reduction in high ranked coal observed in the tri-axial environment. However, Jasinge (2010) found around 6.84% strength reduction under 5 MPa confinement for 3 MPa CO_2 saturation in low rank coal similar to that in the present study, which is much lower than the 20% strength reduction in high rank coal under 5.5 MPa confinement and the 5.5 MPa CO_2 saturation pressure observed by Masoudian et al. (2014). Although the latter had a slightly higher confining pressure and CO_2 saturation pressure, the result indicates that high rank coal shows a greater strength reduction than low rank coal.

The effect of coal rank on coal elastic properties alterations upon CO_2 adsorption was then considered and the results are shown in Fig. 7(b). According to this figure, 4 MPa sub-critical CO_2 saturation causes around 6.14 MPa (around 9%) and 0.47 GPa (around 16%) elastic modulus reductions in low and high rank coals, respectively, and 8 MPa super-critical CO_2 saturation causes 9.64 MPa (14%) and 0.55 GPa (around 25%) for low rank and high rank coal, respectively. However, it should be noted that a 10 MPa confinement was used in the present study and a much lower (up to 5.5 MPa) confinement was used in Masoudian et al. (2014), which might also affect the observed greater strength reduction in high rank coal in the tri-axial environment. However, Jasinge (2010) observed around 5.44% elastic modulus reduction under 5 MPa confinement for 3 MPa CO_2 saturation compared to the 17% elastic modulus reduction observed in Masoudian et al. (2014) under 5.5 MPa confinement and 5.5 MPa CO_2 saturation pressure. This implies that, similar to strength reductions, E reductions due to CO_2 adsorption under tri-axial conditions also increase with increasing coal rank.

The reason is that the coal mass natural cleat system forms during the coalification process, and higher rank coal has a much more developed cleat system than lower ranked coal. The cleats act as loci for the CO_2 adsorption process. Further, Hol and Spiers (2012), stated that coal seams with higher stiffness (high rank coal) reveal greater CO_2 adsorption-induced swelling, which creates more structural alterations in

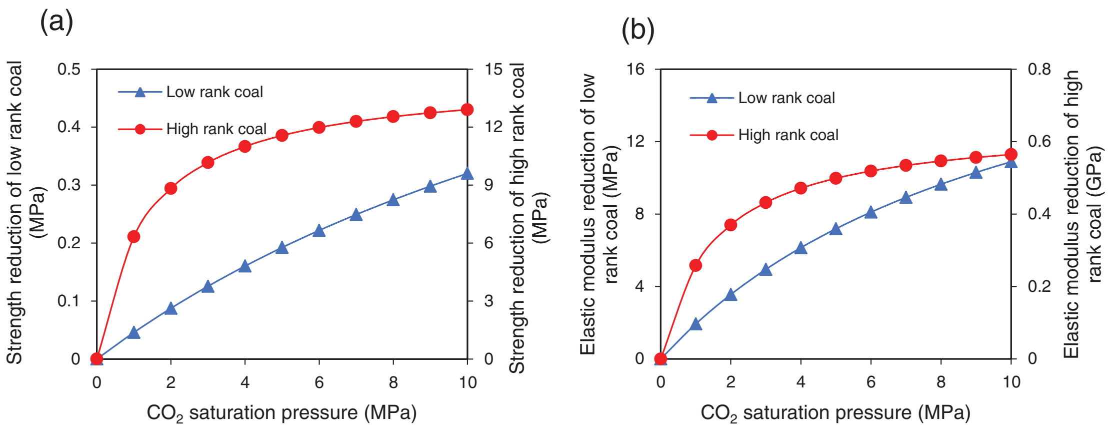

Fig. 7. Comparison of (a) strength reduction and (b) elastic modulus reduction due to CO_2 saturation of low rank coal and high rank coal (Masoudian et al., 2014) under tri-axial conditions.

the coal matrix compared to coal with low stiffness (low rank). This greater reduction in mechanical properties in high rank coal compared to low rank coal in the uniaxial stress environment has been shown by Ranathunga et al. (2016), and the present study shows the applicability of this to real field situations in the presence of in-situ stresses.

6.4.3.3. Effect of time-dependent CO_2 saturation on geo-mechanical properties of coal

Based on the above observations, the adsorption of CO_2 into any rank coal causes its mechanical properties, including strength and elastic modulus, to weaken in any stress environment (tri-axial or uniaxial). This is because CO_2 adsorption causes a reduction in surface energy in coal by causing coal structure re-arrangement and swelling. However, one can expect the above phenomena to result in an increase of the magnitude of adsorption weakening of coal with longer CO_2 exposure.

Jasinge (2010) conducted a series of uniaxial tests on Australian brown coal samples by saturating them at 1, 2 and 3 MPa CO_2 pressures for 1, 2, 3 and 4 days to investigate the effect of saturation time on coal strength. According to this study, 1 MPa CO_2 injected brown coal exhibited 7.36%, 13.97% and 23.53% strength reduction for 2, 3 and 4 days saturation durations compared with 1 day saturation. In addition, an elastic modulus reduction of 13.97%, 30.63% and 31.9% was observed for the same 1 MPa CO_2 saturated brown coal samples for 2, 3 and 4 days saturation durations compared with 1 day saturation. These observations clearly show the effect of saturation time on the strength of the coal mass. Further, Bagga et al. (2015) conducted a series of uniaxial tests for Indian coal (83% carbon content) under 5 MPa constant CO_2 pressure for 25 and 45 days. They observed around 41% and 65% strength reduction and around 23% and 30% reduction in elastic modulus for 25 and 45 days, respectively compared to unsaturated samples. However, these studies were conducted only for lower CO_2 saturation pressures and small time durations, and therefore fail to represent the real case scenario of super-critical CO_2 saturations over geologically significant time periods.

This was therefore considered next by investigating the effect of super-critical CO_2 saturation (10 MPa) on the strength of the low-rank brown coal over time (see Table 3 and Fig. 8). CO_2 saturation was continued up to 365 days to determine how the post-saturation period affects the mechanical properties of brown coal.

6.4.4. Conclusions

Changes in coal seam integrity with the introduction of CO_2 were studied under both tri-axial and uniaxial environments using low ranked Australian brown coal. The following conclusions can be drawn:

- ➢ Coal strength is reduced with CO_2 adsorption, depending on the CO_2 saturation pressure and phase. For example, around 9% and 12% average strength reductions were observed in the tested brown coal for sub-critical (5.5 MPa) and super-critical CO_2 (8.5 MPa) saturations, respectively.
- ➢ Coal mass stiffness is also altered with CO_2 adsorption, leading to a similar reduction to that shown for coal mass strength. For example, an average elastic modulus reduction of 11% for sub-critical CO_2 saturation (5.5 MPa) and 14.3% for super-critical CO_2 saturation (8.5 MPa) were seen in the tested brown coal.
- ➢ A greater strength reduction in coal with CO_2 adsorption occurs under uniaxial stress conditions than tri-axial stress conditions, due to both mechanical confinement and the reduction of CO_2 adsorption with enhanced effective stress conditions in the tri-axial stress environment.
- ➢ High rank coal exhibits greater strength and elastic modulus reductions than low rank coal in any stress environment, mainly due to the existing well-developed cleat system in high rank coal that offers more provisions for CO_2 adsorption.
- ➢ Although CO_2 adsorption-induced coal matrix alterations are largely completed with the initial interaction with CO_2, considerable further coal matrix re-arrangement may occur at a slower rate.

6.4.5. Acknowledgements

The authors wish to express their appreciation for the funding provided by the Australian Research Council (DE130100124) and the use of facilities in the Monash Centre of Electron Microscopy (MCEM).

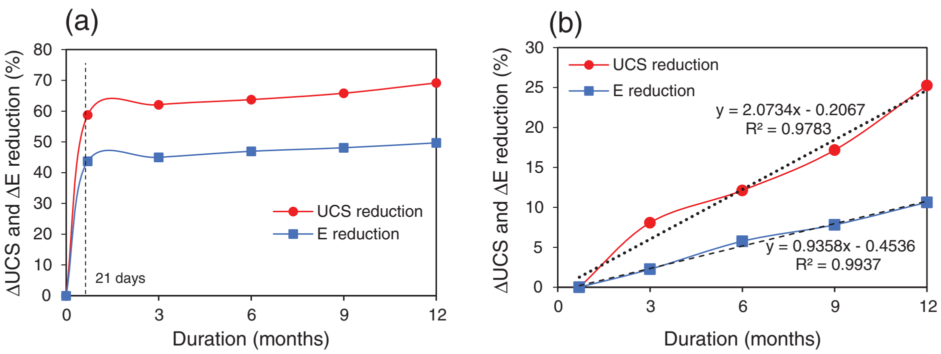

Fig. 8. Unconfined compressive strength (UCS) and elastic modulus (E) variation of brown coal samples for different durations with respect to (a) unsaturated sample and (b) 21 days of saturation. According to Table 3 and Fig. 8, the reduction of strength and elastic modulus with CO_2 saturation are not completed by 21 days and further exposure to CO_2 appears to cause further reduction, but at a slower rate. For example, after 21 days of saturation with CO_2 at 10 MPa, the strength and elastic modulus were reduced by around 59% and 44% respectively (refer Table 3). These values were further reduced up to 70% (UCS) and 50% (E) after 365 days of saturation compared to the unsaturated sample (refer Table 3). This implies that CO_2 adsorption-induced coal matrix alterations largely occur with the first exposure to CO_2. Although it continues to rearrange the coal matrix by reducing the strength parameters over the contact period with CO_2, this latter stage strength reduction is much lower than the initial strength reduction. This is possibly due to the fact that coal matrix swelling starts quickly with CO_2 injection and is largely completed within the first few days. Further, as discussed in Section 6.4.3.1.a above, CO_2 adsorption-induced coal matrix swelling reduces the adsorption capacity, which is the reason for the lower alterations to the mechanical properties of coal mass with time. Therefore, changes in CO_2 adsorption-induced strength properties also mainly occur in the initial CO_2 injection period. This observation was confirmed by SEM analysis, the results of which are shown in Fig. 9. The SEM images show a relative reduction in average pore size of the tested coal specimens after CO_2 saturation, and the average pore sizes were taken by averaging the pore sizes of ten to twelve different SEM images of three different specimens for one condition. The greatest reduction of pore spaces was observed when the specimen was saturated for 21 days with CO_2 and there is a gradual reduction after 21 days of saturation (see Fig. 9(b)). These observations imply that the enhancement of coal mass ductile behaviour with the plasticization of coal mass with CO_2 adsorption and the surface energy reductions are critical at the beginning of CO_2 sequestration and the effect is reduced over time.

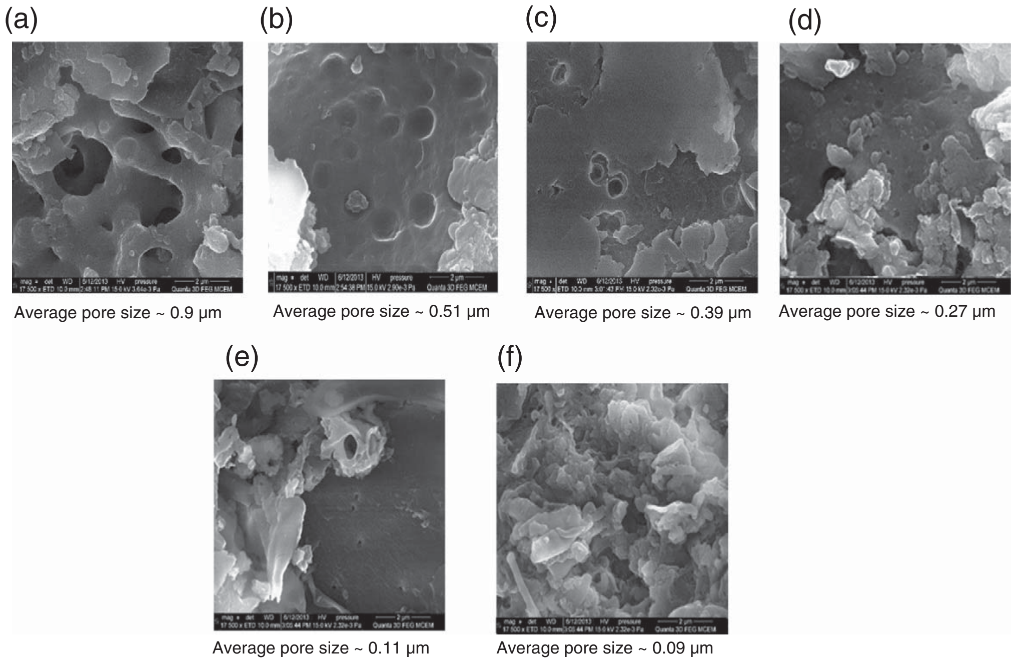

Fig. 9. SEM images of brown coal samples with (a) unsaturated, (b) 21 days, (c) 90 days, (d) 180 days, (e) 270 days and (f) 365 days duration of CO_2 saturation (conditions used to obtain SEM images: scale – 2 μm, magnification – 17 k, probe current – 15 kV and spot size 4.5 under low vacuum).

6.4.6 References

Ates, Y., Barron, K., 1988. The effect of gas sorption on the strength of coal. Min. Sci. Technol. 6, 291–300.

Aziz, N.I., Ming-Li, W., 1999. The effect of sorbed gas on the strength of coal – an experimental study. Geotech. Geol. Eng. 17, 387–402.

Bagga, P., Roy, D.G., Singh, T.N., 2015. Effect of carbon dioxide sequestration on the mechanical properties of Indian coal. ISRM Regional Symposium-EUROCK 2015. International Society for Rock Mechanics (Paper no. 190).

Chikatamarla, L., Cui, X., Bustin, R.M., 2004. Implications of Volumetric Swelling/Shrinkage of Coal in Sequestration of Acid Gases, Coalbed Methane Symposium, Tuscaloosa, AL (Paper no. 0435).

Corkum, A.G., Martin, C.D., 2007. The mechanical behaviour of weak mudstone (Opalinus Clay) at low stresses. Int. J. Rock Mech. Min. Sci. 44, 196–209.

Day, S., Fry, R., Sakurovs, R., Weir, S., 2010. Swelling of coals by supercritical gases and its relationship to sorption. Energy Fuel 24, 2777–2783.

Gentzis, T., Deisman, N., Chalaturnyk, R.J., 2007. Geomechanical properties and permeability of coals from the Foothills and Mountain regions of western Canada. Int. J. Coal Geol. 69, 153–164.

Gibbs, J.W., 1878. On the equilibrium of heterogeneous substances. Am. J. Sci. 441–458.

Griffith, A.A., 1921. The Phenomena of Rupture and Flow in Solids. Philosophical Transactions of the Royal Society of London. Series A, Containing Papers of a Mathematical or Physical Character 221, 163–198.

Hol, S., Spiers, C.J., 2012. Competition between adsorption-induced swelling and elastic compression of coal at CO_2 pressures up to 100 MPa. J. Mech. Phys. Solids 60, 1862–1882.

Hol, S., Peach, C.J., Spiers, C.J., 2011. Applied stress reduces the CO_2 sorption capacity of coal. Int. J. Coal Geol. 85, 128–142.

Hol, S., Spiers, C.J., Peach, C.J., 2012. Micro fracturing of coal due to interaction with CO_2 under unconfined conditions. Fuel 97, 569–584.

Hooper, B., Murray, L., Gibson-Poole, C., 2005. Latrobe Valley CO_2 Storage Assessment. Co-operative Research Centre for Greenhouse Gas Technologies, CO2CRC Publication, Canberra No. RPT05-0108.

Jasinge, D., 2010. An Investigation of the Effect of Carbon Dioxide Sequestration on the Behaviour of Brown Coal (PhD thesis) Monash University, Melbourne, Australia.

Karacan, C.Ö., 2007. Swelling-induced volumetric strains internal to a stressed coal associated with CO_2 sorption. Int. J. Coal Geol. 72, 209–220.

Larsen, J.W., Flowers, R.A., Hall, P.J., Carlson, G., 1997. Structural rearrangement of strained coals. Energy Fuel 11, 998–1002.

Masoudian, M.S., 2016. Multiphysics of carbon dioxide sequestration in coalbeds: a review with a focus on geomechanical characteristics of coal. J. Rock Mech. Geotech. Eng. 8, 93–112.

Masoudian, M.S., Airey, D.W., El-Zein, A., 2014. Experimental investigations on the effect of CO_2 on mechanics of coal. Int. J. Coal Geol. 128–129, 12–23.

Nikoosokhan, S., Vandamme, M., Dangla, P., 2014. A poromechanical model for coal seams saturated with binary mixtures of CH_4 and CO_2. J. Mech. Phys. Solids 71, 97–111.

Pan, Z., Connell, L.D., Camilleri, M., 2010. Laboratory characterisation of coal reservoir permeability for primary and enhanced coalbed methane recovery. Int. J. Coal Geol. 82, 252–261.

Perera, M.S.A., Ranjith, P.G., Viete, D.R., 2013. Effects of gaseous and super-critical carbon dioxide saturation on the mechanical properties of bituminous coal from the southern Sydney Basin. Appl. Energy 110, 73–81.

Perera, M.S.A., Ranathunga, A.S., Ranjith, P.G., 2016. Effect of coal rank on various fluid saturations creating mechanical property alterations using Australian coals. Energy 9, 440.

Ranathunga, A.S., Perera, M.S.A., Ranjith, P.G., Bui, H., 2016. Super-critical CO_2 saturation-induced mechanical property alterations in low rank coal: an experimental study. J. Supercrit. Fluids 109, 134–140.

Szwilski, A.B., 1984. Determination of the anisotropic elastic moduli of coal. Int. J. Rock Mech. Min. Sci. Geomech. Abstr. 21, 3–12.

Vandamme, M., Brochard, L., Lecampion, B., Coussy, O., 2010. Adsorption and strain: The CO_2-induced swelling of coal. J. Mech. Phys. Solids 58, 1489–1505.

Viete, D.R., Ranjith, P.G., 2006. The effect of CO_2 on the geomechanical and permeability behaviour of brown coal: implications for coal seam CO_2 sequestration. Int. J. Coal Geol. 66, 204–216.

Vishal, V., Ranjith, P., Singh, T., 2015. An experimental investigation on behaviour of coal under fluid saturation, using acoustic emission. J. Nat. Gas Sci. Eng. 22, 428–436.

Wang, S., Elsworth, D., Liu, J., 2013a. Permeability evolution during progressive deformation of intact coal and implications for instability in underground coal seams. Int. J. Rock Mech. Min. Sci. 58, 34–45.

Wang, S., Elsworth, D., Liu, J., 2013b. Mechanical behavior of methane infiltrated coal: the roles of gas desorption, stress level and loading rate. Rock Mech. Rock. Eng. 46, 945–958.

White, C.M., Smith, D.H., Jones, K.L., Goodman, A.L., Jikich, S.A., LaCount, R.B., DuBose, S.B., Ozdemir, E., Morsi, B.I., Schroeder, K.T., 2005. Sequestration of carbon dioxide in coal with enhanced coalbed methane recovery: a review. Energy Fuel 19, 659–724.

6.5 Chapter summary

The main objective of this chapter was to investigate the influence of CO_2 adsorption on the mechanical properties of brown coal. Various meso-scale experimental programs were conducted to observe the effect of different effective factors on coal mass strength with CO_2-ECBM and the major findings of the experiments are summarised below.

- ***How do CO_2 phase and pressure affect coal mass integrity?***

After conducting a UCS testing program on brown coal for different CO_2 pressures, it was found that sub-critical CO_2 adsorption causes brown coal's mechanical properties to be significantly changed due to the associated coal matrix swelling. In comparison, super-critical CO_2 adsorption causes significantly greater mechanical property alterations in brown coal with its greater adsorption potential-related ductile property enhancement compared to sub-critical CO_2. In addition, CO_2 saturation in brown coal causes early stages of fracture development, due to its swelled and reduced surface energy after CO_2 adsorption, and the effect is greater for super-critical CO_2 adsorption.

- ***How do various fluid saturations alter the coal mass strength properties with coal rank?***

Using Australian brown coal and Australian black coal samples, the influence of coal rank on various fluid saturation-induced coal mechanical properties changes was studied. According to the results, both water and CO_2 saturation cause a significant strength reduction in coal, regardless of rank. This strength reduction is heightened with increasing coal rank due to the well-developed cleats in mature coal which offer more loci for moisture to stay in the coal mass. In contrast to water and CO_2 saturation, N_2 saturation slightly enhances coal strength, regardless of rank, and this increment increases with increasing N_2 saturation pressures.

- ***How does the influence of CO_2 adsorption on coal mechanical properties vary under confining pressure and various fluid saturation times?***

The following conclusions were drawn after conducting a series of tri-axial tests on brown coal to observe the changes in coal seam integrity with the introduction of CO_2. Both coal strength and stiffness are reduced with CO_2 adsorption, which is higher for super-critical CO_2 saturation than gaseous CO_2 saturation. In addition, these strength and stiffness reductions due to CO_2 adsorption can be represented by a Langmuir-type equation. A greater strength reduction in coal with CO_2 adsorption occurs under uniaxial stress conditions than tri-axial stress conditions, due to both mechanical confinement and the reduction of CO_2 adsorption with enhanced effective stress conditions in the tri-axial stress environment. High rank coal exhibits greater reductions in strength and stiffness than low rank coal in any stress environment. According to the CO_2-saturated strength tests conducted for various saturation time periods, although CO_2 adsorption-induced coal matrix alterations are largely completed with the initial interaction with CO_2, considerable further coal matrix re-arrangement may occur at a slower rate.

PART 3 - CHAPTER 7

Investigation of coal mechanical property variations during carbon dioxide sequestration using reconstituted coal

Publications included in Chapter 7

Chapter 7 includes one paper. Details of the paper are as follows.

Chapter 7.3

Ranathunga AS, Perera MSA, Ranjith PG (2017). Key factors controlling coal's strength property alterations during CO_2 enhanced coal bed methane production: A numerical study. *Journal of Natural Gas Science and Engineering* (under review).

7. Investigation of coal mechanical property variations during carbon dioxide sequestration using reconstituted coal

7.1 Overview

As outlined in Chapter 2, the complexity associated with the heterogeneity of coal samples is the main hindrance to CO_2-ECBM studies. Several researchers have used reconstituted coal samples with reproducible material properties to overcome this problem. Therefore, several experiments and a numerical study were carried out using reconstituted brown coal samples to observe the expected coal matrix behaviours under loading as follows:

- **Section 7.2** – ***How to overcome the effect of coal heterogeneity on the mechanical property variations in coal induced by different fluid saturations?***

The main objective of this section is to investigate the effect of different fluid saturations on the mechanical properties of coal using reconstituted low rank brown coal samples. Powdered brown coal acquired from the Latrobe Valley basin was used to prepare the reconstituted samples. The prepared samples were then saturated in water, N_2 and both sub- and super-critical CO_2 and tested under unconfined conditions to check the influences of various saturations on coal's mechanical properties. Further, the micro-structural variations of the saturated samples were viewed using the X-ray CT facility.

The following conference paper was produced based on this section of the thesis:

Ranathunga AS, Perera MSA, Ranjith PG, Haque RT (2016). An experimental study of the behaviour of reconstituted low rank coal under different fluid saturations, ISRM International Symposium and EUROCK 2016, Cappadocia, Turkey, 29-31 August, 2016; Paper no 166.

Under laboratory conditions, there are limitations in providing the required environmental conditions for the test specimens due to the limited capacities of the instruments or the extensive time-frames required to complete the experiments. Therefore, the observed influences of effective factors on coal mass mechanical properties were numerically modelled to extend the experimental results to the expected reservoir conditions. This is discussed in the following section.

Section 7.3 – ***How do effective factors influence coal mass strength properties? A meso-scale numerical study using reconstituted coal***

The COMSOL Multiphysics simulator was used to develop a meso-scale (laboratory-scale) numerical model to determine the mechanical property changes in brown coal samples during CO_2 sequestration. First, a uniaxial model was developed using the results from Section 5.2, which was then extended to a tri-axial model. Finally, the model was used to predict the expected strength and elastic modulus variations in brown coal for various CO_2 phases and pressures under different down-hole stresses.

This section of the chapter details the following paper:

Ranathunga AS, Perera MSA, Ranjith PG (2017). Key factors controlling coal's strength property alterations during CO_2-enhanced coal bed methane production: A numerical study. *Journal of Natural Gas Science and Engineering* (under review).

7.2 How to overcome the effect of coal heterogeneity for different fluid saturation- induced mechanical property variations in coal?

7.2.1 Overview

Carbon dioxide (CO_2) storage in deep coal seams significantly alters the petro-physical properties of the coal masses and precise evaluation of such alterations is difficult due to the highly heterogeneous nature of coal. This indicates the importance of testing reconstituted homogeneous coal samples. The main objective of this section is therefore to investigate the effect of different fluid saturations on the mechanical properties of coal using reconstituted low-rank coal samples. The reconstituted coal samples were made using powdered Australian brown coal, which were first moulded and then subjected to axial load until the specimens achieved the mechanical properties of natural specimens. The prepared samples were then saturated in water, N_2 and CO_2 to determine the influences of various saturations on the coal's mechanical properties. Several samples from each saturation condition underwent X-Ray computed tomography (X-ray CT) tests to determine the structural alterations which occurred with different fluid saturations.

The following conference paper was produced based on this section of the thesis:

Ranathunga AS, Perera MSA, Ranjith PG, Haque RT (2016). An experimental study of the behaviour of reconstituted low rank coal under different fluid saturations, ISRM International Symposium and EUROCK 2016, Cappadocia, Turkey, 29-31 August, 2016; Paper no 166.

7.2.2 Introduction

Enhanced coal bed methane (ECBM) recovery is being implemented and tested as a viable option to store carbon dioxide (CO_2) and reduce the amount in the Earth's atmosphere, as well as for the recovery of useful methane (CH_4) gas (Perera et al., 2013; Ranathunga et al., 2014). Overall, the ECBM process involves introducing CO_2 through injecting wells into deep coal seams. This CO_2 then acts as a displacing gas, which allows the already-adsorbed CH_4 to be desorbed from the coal matrix. The methane is finally obtained through a recovery well and used to produce energy in a cost-effective and environmentally-friendly way.

However, the ECBM recovery technique has both advantages and disadvantages. One of the major issues involved in the injection of CO_2 is the significant alterations of coal seams' petro-physical properties. Perera et al., (2013) and Ranathunga et al., (2016) have found that the strength and Young's modulus of coal vary with the adsorption of CO_2 into the coal matrix. Moreover, since coal is a highly heterogeneous material, it is difficult to determine the properties of the entire coal seam in the field. Therefore, it is essential to establish an acceptable method of manufacturing reconstituted coal samples to stimulate field properties. Several approaches have been trialled to produce a more homogeneous representation of natural coal that would be more amenable to the experimental investigation of mechanical and flow behaviour.

According to the research literature, the development of reconstituted coal (RC) samples has the ability to assist in making useful correlations between the mechanical properties of coal (Jasinge, 2010; Vishal & Singh, 2013). Furthermore, Jasinge (2010) (for brown coal) and Vishal & Singh (2013) (for black coal) developed a method of preparing RC samples, which has focused mainly on no-binder RC. They produced samples with mechanical properties close to those of natural coal. For example, Jasinge (2010) produced RC low rank coal samples with 1.46 ± 0.14 MPa average uniaxial strength (1.2-1.8 MPa for natural samples), 77.43 ± 2.61 MPa Young's modulus (65-89 MPa for natural samples) with a 95% confidence interval and densities between 1.11 to 1.14 g/cm^3 (1.11 to 1.15 g/cm^3 for natural coal samples). However, studies of the effect of various saturation mediums using RC samples are lacking.

Therefore, in this study, reconstituted Victorian brown coals were developed employing the method proposed by Jasinge (2010). The prepared samples were then treated with water, CO_2 and N_2 in order to observe the mechanical property alterations in homogeneous coal samples.

7.2.3 Preparation of reconstituted coal samples

This section presents the methodology adopted to develop reconstituted brown coal samples. The natural brown coal used for the development of reconstituted brown coal samples originated from the Hazelwood mine in the Latrobe Valley, south-east Victoria, Australia.

7.2.3.1 Sample preparation

Brown coal powder was prepared according to the methodology adopted by Jasinge (2010). The brown coal powder was used under its natural moisture condition of around 54%. The apparatus used in the RC sample preparation is a steel mould 54 mm in diameter and 210 mm in height, using a cylindrical steel compaction ram (see Figure 7.1(a)). The procedure for the sample preparation is summarised in the following section and the more detailed procedure is presented in Chapter 3.

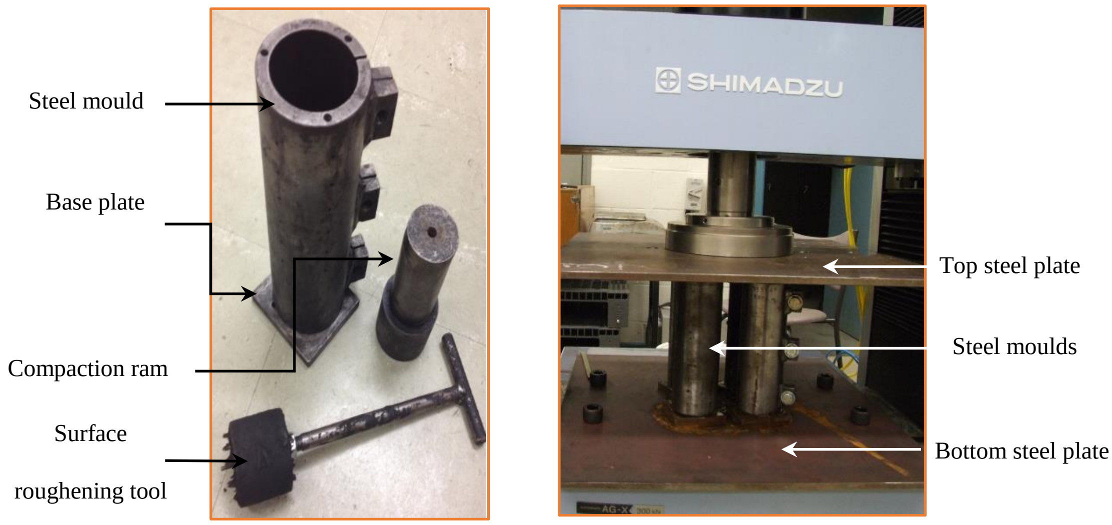

(a) Steel (b) Compaction of sample

Figure 7.1. Reconstituted sample preparation

The coal powder was filled to the top of the steel mould and compacted in three layers. The surface was roughened after compacting each layer to ensure full bonding between layers. After the placement of each layer, the weight of the coal powder was measured. The sample were then subjected to axial load until it reached the natural coal strength using a Shimadzu uniaxial compression machine (see Figure 7.1(b)). The first and second layers were compacted for around 30 minutes. Once the final layer was placed, the sample was then compacted for 24 hours. The compaction was assumed to reach the maximum once the displacement versus time curve achieved a constant plateau. Therefore, the coal placed in the mould for compaction remained under a constant compression load. Since the degree of consolidation is time-dependent, the duration of load application affects the sample's density and mechanical properties. It is therefore required to compact the sample for a sufficiently long time to ensure adequate surface contact between particles and to increase the density, strength and Young's modulus (Jasinge, 2010). After preparing various trial RC samples, it was found that a compaction stress of 7 MPa and a displacement rate of 3 mm/min were sufficient to produce the mechanical properties of natural coal in the RC specimens.

Following compaction, the samples were removed from the mould using a hydraulic press and the weights and dimensions of the samples were measured. The samples were then sealed in plastic bags and placed in the fog room and their weight and dimensions were recorded for the next three days to check for swelling and moisture loss. The RC samples were cut to approximately 113 mm and the top and bottom surfaces were ground, to achieve smooth and parallel surfaces.

The resulting RC samples had a length of approximately 108 mm (see Figure 7.2(a)). Figure 7.2(b) shows the top surface of a typical RC sample after grinding.

(a) After cutting to appropriate size (b) Top surface after grinding (54 mm)

Figure 7.2. A typical reconstituted coal sample after preparation

7.2.3.2 Preparation for testing and experimental procedure

A total of three RC samples were tested under unsaturated conditions. The procedures adopted for water, N_2 and CO_2 saturations are detailed in the following sections.

a. Water saturation

Two RC samples were saturated in water for approximately two weeks to allow full saturation. The samples were placed in vacuum chambers (see Figure 7.3(a)). The weight of the RC samples was recorded before placing them in the saturation chamber. The weight was then checked regularly for two weeks until the weight reached a steady state. The samples were then wrapped carefully with plastic wraps and stored in a fog room for another two weeks to allow an equal distribution of moisture throughout the samples before testing.

b. CO_2 saturation

Various CO_2 saturation pressures were employed to investigate the effects of CO_2 on the mechanical properties of coal. CO_2 saturation pressures of 4, 6, 8 and 10 MPa were applied to the RC samples at a temperature of 40 ^{0}C (>31.8 ^{0}C is the critical temperature of CO_2). Hence, the samples saturated under 4 and 6 MPa CO_2 (<7.38 MPa is the critical pressure of CO_2) were under sub-critical conditions and those saturated under 8 and 10 MPa (>7.38 MPa) were under super-critical conditions. In order to conduct CO_2 saturation, the samples were placed in high-pressure saturation chambers (see Figure 7.3(b)) for a period of two weeks for each saturation pressure condition. After the saturation period, the pressure chambers were gradually de-pressurized at a rate of 0.02 MPa/min to avoid possible damage to the physical structure of the coal specimen caused by sudden pressure changes. After the samples were removed from the saturation chamber, they were covered with plastic wrap and tested within around 20 minutes to avoid any possible changes to the saturation of the samples.

c. N_2 saturation

The RC samples were saturated under two different N_2 pressures (4 and 8 MPa) using a high-pressure tri-axial test rig (see Figure 7.3(c)) to compare the results with the observations of CO_2 saturated samples, because unlike CO_2, N_2 is a comparatively inert gas, which does not cause any significant coal matrix re-arrangement through chemical interactions with the coal mass (Perera et al., 2015). A similar procedure to that used for CO_2 saturation was applied for N_2 saturation.

(a) Water saturation chamber

(b) CO_2 saturation chamber

(c) N_2 saturation chamber

Figure 7.3. Saturation of reconstituted samples in water and different CO_2 and N_2 saturations

7.2.3.3 Experimental procedure

The following sections summarize the experimental methodology adopted for the tests (refer to Chapter 3 for detailed experimental procedures).

- *UCS Testing* - A series of UCS tests was performed on the RC samples using a Shimadzu machine. A displacement rate of 0.1 mm/min (ASTM D7012 2004) was applied for the uniaxial compressive tests of the RC samples and the load and displacement were recorded.
- *X-Ray Computed Tomography (X-ray CT)* – High-resolution images were also taken of the RC samples under unsaturated, water-saturated and CO_2-saturated conditions. The scanning

was carried out under full view mode, maintaining the X-Ray source (140keV/10W) at 200 mm and using the 0.4X macro-detector 57 mm from the central axis of the samples, thus providing a fixed resolution of 60 microns for the qualitative analysis of all images. Images were taken at the middle of each sample.

7.2.4 Test results and discussion

7.2.4.1 Selection of reconstituted coal samples

Various trial RC samples were first developed with similar bulk density, strength, and Young's modulus to natural brown coal. For this study, the application of an axial load of 7 MPa was found to be sufficient to produce RC samples with similar mechanical properties, such as bulk density, strength and Young's modulus, to those of natural coal. For example, the average uniaxial compressive strength of the prepared unsaturated RC samples using a compaction load of 7 MPa was 1.47 MPa, which is in the range of natural brown coal specimens (varying between 1.2 MPa and 1.8 MPa) (Jasinge, 2010), as shown in Figure 7.4. In addition, using a compaction load of 7 MPa, an average Young's modulus of 69.7 MPa (ranging between 65 – 89 MPa for natural brown coal) (Jasinge, 2010) and an average bulk density of 1097.8 kg/m^3 (ranging between 1100 kg/m^3 and 1150 kg/m^3 for natural brown coal) (Jasinge, 2010) were produced. Therefore, the mechanical properties produced by the RC samples using a compaction load of 7 MPa proved to be adequate in terms of strength to represent natural coal specimens in the laboratory experiments.

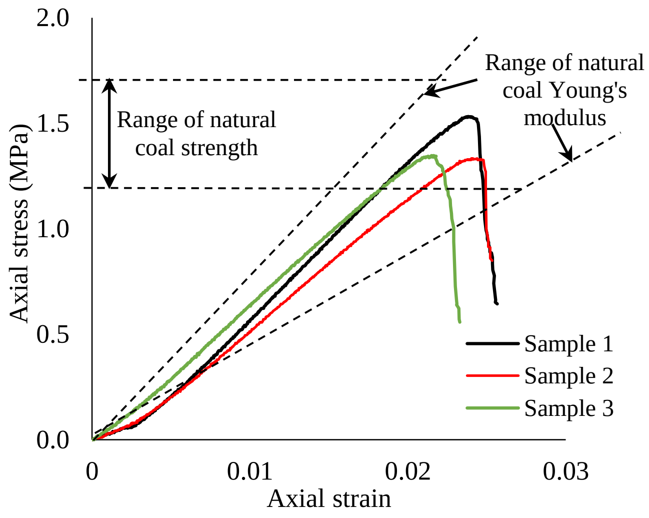

Figure 7.4. Axial stress versus axial strain curves for unsaturated RC samples

A series of uniaxial compression strength tests was then performed to determine the peak strength and Young's modulus of the RC samples. The UCS tests were conducted for unsaturated, water, CO_2- and N_2-saturated RC samples. The results obtained are presented in Table 7.1. Samples with maximum UCS values in each case are used for the discussion here and the stress-strain curves obtained from the CO_2 treated samples for the maximum UCS value are shown in Figure 7.5.

Table 7.1. Saturation effects on UCS and Young's modulus (E) values of RC samples

Saturation condition	UCS (MPa)	ΔUCS (%)*	E (MPa)	ΔE (%)*
Unsaturated	1.66	-	72.01	-
Water	0.26	-84.34	12.14	-83.14
4 MPa N_2	1.68	1.19	72.69	0.94
8 MPa N_2	1.72	3.49	73.42	1.96
4 MPa CO_2	1.16	-30.24	50.46	-29.93
6 MPa CO_2	1.10	-34.03	47.45	-34.11
8 MPa CO_2	0.92	-44.77	39.81	-44.72
10 MPa CO_2	0.79	-52.18	34.47	-52.13

* negative indicates a reduction in UCS and Young's modulus (E)

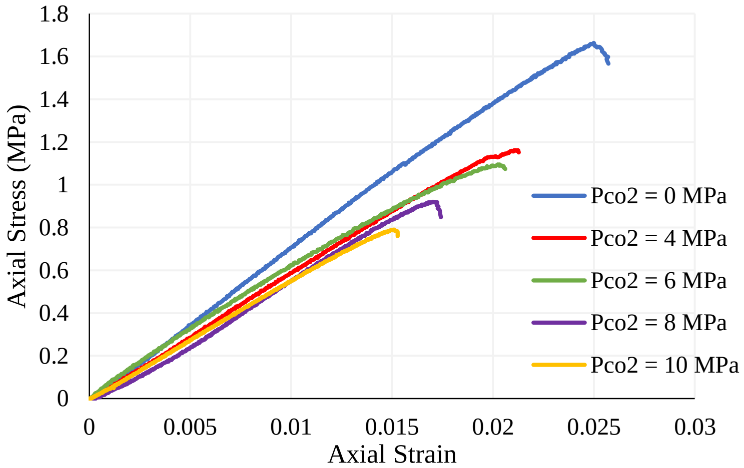

Figure 7.5. Experimental stress-strain curves for CO_2 saturated reconstituted brown coal

7.2.4.2 Water saturation effects on RC strength

According to Table 7.1, there is around 84% reduction in both strength and Young's modulus of water-saturated RC samples compared to the unsaturated RC sample. This reduction was expected, as water significantly influences the strength of any rock mass through the water softening effect (Vásárhelyi and Ván, 2006). Figure 7.6 shows a sectional view of a water-saturated RC sample and a section along the height obtained through X-ray CT scanning that clearly shows the distribution of cracks (the black lines). As mentioned before, the adsorption of water into any coal mass can easily attack its fractures' tips, softening the coal mass and eventually expanding the fractures. According to Figures 7.6(a) and (b), compared to unsaturated RC, there are large number of cracks in water-saturated RC samples.

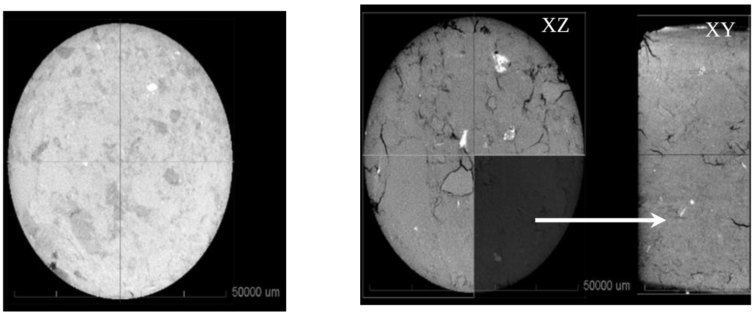

(a) Mid height (b) Quarter section along the height

Figure 7.6. Sectional view of a water-saturated RC sample showing distribution of cracks (black lines are cracks)

Similar reductions in strength and Young's modulus in natural brown coal of around 16.8% and 7.6% have been reported by Perera et al. (2011). However, the effect of water saturation on RC samples is comparatively greater. This greater reduction may be due to the saturation period and surface area of the samples. According to Vásárhelyi and Ván (2006), the longer the saturation time, the greater the water absorption rate into the rock mass. Therefore, the longer saturation period used in this study (two weeks compared to one week in Perera et al., 2011) caused more moisture to be attracted into the coal matrix. In addition, the particle size used for the RC sample preparation was ~1 mm which provides more surface area for moisture adsorption. Overall, the moisture inside the coal samples causes the reduction in surface energy and strength.

7.2.4.3 CO_2 saturation effect on RC samples

The adsorption potential of any gas into the coal matrix greatly depends on the type of gas. According to Ranathunga et al. (2014), CO_2 has a great adsorption capacity than other gases such as N_2 and CH_4 due to the stronger intermolecular forces between hydrocarbons such as CO_2 and the coal mass. This strong relationship plays a significant role in the process of coal- bed methane recovery. However, the adsorption of CO_2 into the coal matrix significantly influences the swelling and strength properties of coal. In this section, the effects of different CO_2 saturation pressures on the strength of the RC samples are reported. Based on the findings of various researchers (Perera et al., 2011; Ranathunga et al., 2016; Viete & Ranjith, 2006), the adsorption of CO_2 causes a clear strength reduction in coal. Similar behaviour was observed for RC samples after CO_2 saturation in the present study, as shown in Table 7.1 and Figure 7.7.

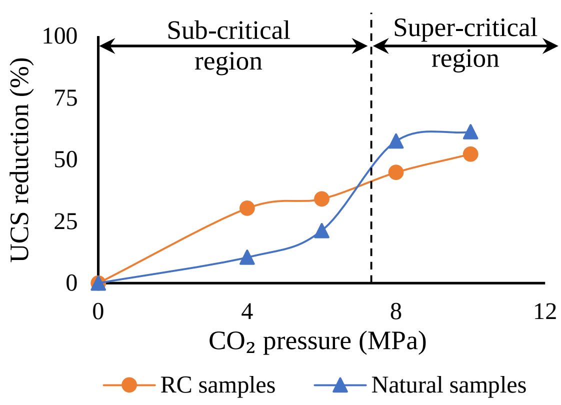

(a) UCS

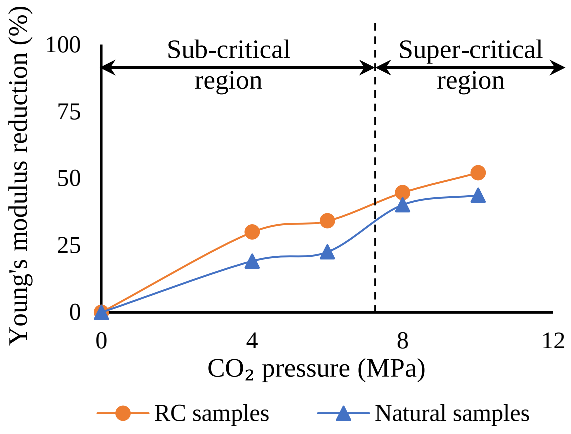

(b) Young's modulus

Figure 7.7. Effect of CO_2 saturation on UCS and Young's modulus for RC and natural brown coal samples

Table 7.1 shows that as the CO_2 saturation pressure increases, the reductions in strength and Young's modulus also increase. Further, this reduction is greater in the super-critical region than in the sub-critical region (see Figure 7.7). In particular, a sudden increment in strength property reduction (by around 16%) between 6 and 8MPa (the transfer region) can be observed where the CO_2 saturation pressure changes from its sub- to super-critical condition. This is consistent with existing studies of natural coal samples (Huang et al., 2006), which show a sudden increment in CO_2 viscosity after the critical point, as super-critical CO_2 possesses gas-like compressibilities and liquid-like densities. Further, Chikatamarla et al. (2004) indicated that, unlike sub-critical CO_2, super-critical CO_2 has better solubility in solid constituents due to its greater density. This causes the organic compounds in coal to be polymerized, leading to greater plasticization of the coal mass during CO_2 saturation, enhancing the ductile properties of the coal (Ranathunga et al., 2016). This greater plasticization effect of super-critical CO_2 compared to sub-critical CO_2 causes sudden changes in its Young's modulus (see Figure 7.7).

These UCS and Young's modulus reductions observed in RC samples were then compared with those in natural brown coal specimens reported in the literature (Ranathunga et al., 2016) under the same CO_2 saturation pressures and the results are shown in Figure 7.7. According to the figure, there are around 46% and 23% reductions in UCS and Young's modulus in natural coal when the CO_2 saturation pressure changes from 6 to 8 MPa.

As shown in Table 7.1, there was a greater reduction in strength and Young's modulus of RC samples saturated at 8 and 10 MPa CO_2 pressures in the super-critical region, similar to natural brown coal (see Figure 7.7). This greater reduction is due to the super-critical CO_2 adsorption, which has greater adsorption potential and dissolution ability in coal compared to sub-critical CO_2, resulting in greater matrix alteration and much reduced strength (Ranathunga et al., 2015). This can be further confirmed by the X-ray CT analysis shown in Figure 7.8, which presents the sectional views of an unsaturated RC sample and RC samples saturated at 4 and 10 MPa CO_2 pressure. The light areas indicate higher density areas and the darker areas show lower densities (see Figure 7.8 (b) (highlighted in dashed lines) and Figure 7.8 (c)). The adsorption of CO_2 causes the polymerisation of the coal matrix, creating a softer and less dense structure and this effect is increased at higher CO_2 pressures (Ranathunga et al. 2016). This observation is confirmed by the CT analysis, which shows a less dense structure (darker areas) under super-critical CO_2 saturation (refer to Figure 7.8(c)). This less dense structure developed with CO_2 saturation is the reason for the strength variations observed in the RC samples.

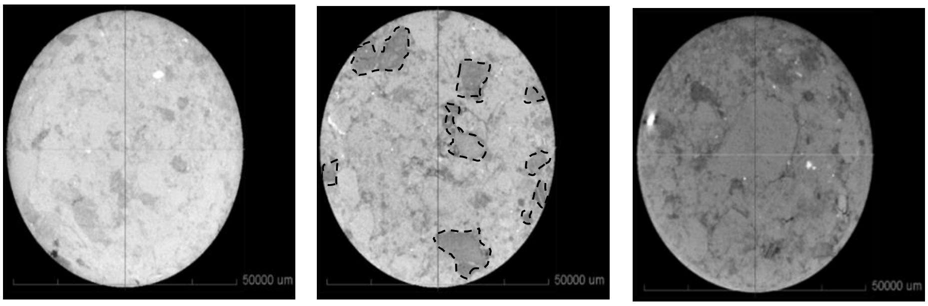

(a) Unsaturated (b) 4 MPa CO_2 (c) 8 MPa CO_2

Figure 7.8. Sectional view through mid-height of RC samples for unsaturated, 4 MPa and 8 MPa CO_2 saturated samples

Interestingly, although both RC and natural brown coal samples behave similarly under CO_2 saturation, RC samples exhibit comparatively less strength reduction than the natural samples (see Figure 7.8). The reason is the naturally-existing cleat system in natural coal that acts as a locus for CO_2 movement, permitting greater matrix alteration compared to RC samples without any cleats.

7.2.4.4 N_2 saturation effects on RC samples

The effect of N_2 saturation on RC coal was then tested for two different saturation pressures and the results are shown in Figure 7.9. According to the figure, N_2 saturation does not reduce the strength of brown coal; rather, it causes a slight increment in coal strength. The observed increment of UCS value due to N_2 saturation is around 1% and 3.5% for samples saturated under 4 and 8 MPa N_2 saturation pressures, respectively (Table 7.1). The reason may be the ability of N_2 to push the moisture out of the coal sample, resulting in a strength increment. This is evident from the calculated weight variation in the N_2-saturated samples, which reduced by around 8 to 13% during the saturation period. Further, according to Table 7.1, the Young's modulus of brown coal slightly increases after N_2 saturation (up to 2%) and this is also related to the moisture-removing potential of the N_2 molecules. As described earlier, the presence of water causes the ductile properties of the coal mass to improve, and therefore its removal should improve the brittle behaviour, which is proven by the Young's modulus increment in RC coal observed after N_2 saturation.

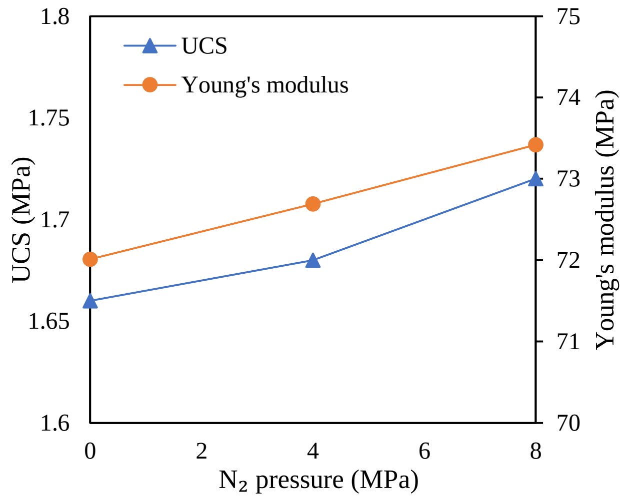

Figure 7.9. Effect of N_2 saturation on UCS and Young's modulus for RC samples

Interestingly, this N_2 saturation-created strength gain in RC coal samples is consistent with the natural brown coal's strength observed by Perera et al. (2016) upon N_2 saturation. Perera et al. (2016) obtained around 7.6% and 4.6% increments in both strength and Young's modulus in natural brown coal. Compared to natural brown coal, RC has a lower increment in strength parameters with N_2 saturation. This might be due to a similar reason to that explained under CO_2 saturation, as the cleat system in natural coal samples may improve the N_2 flow through the coal matrix, causing more removal of moisture from the coal mass, leading to greater strength gain.

7.2.5 Conclusions

Reconstituted low rank coal samples were prepared using Victorian brown coal powder, and a compaction load of 7 MPa was sufficient to manufacture RC samples with similar mechanical properties to natural coal. The effects of different saturation conditions (water and CO_2) on the mechanical properties of the prepared RC samples were then examined. Greater strength reduction was found for water and CO_2 saturation compared to unsaturated samples, particularly under high pressures.

This strength reduction of RC samples under water saturation is significant, and around 84% UCS and Young's modulus reductions compared with unsaturated RC samples were observed. This is because water is known to be one of the most effective strength reducing liquids for coal. The moisture penetrates the coal mass, causing the sample's fractures to expand. This causes the surface energy of the coal mass and eventually its strength to be reduced.

The strength reductions in RC samples were also examined under CO_2 saturation pressures of 4, 6, 8 and 10 MPa. According to the results, CO_2 adsorption causes brown coal's mechanical properties to change significantly due to the associated coal matrix alterations, and super-critical CO_2 adsorption causes much greater mechanical property changes in RC brown coal than sub-critical CO_2. This was proven by the observed around 16% UCS and Young's modulus reductions when CO_2 saturation pressure increased from 6 to 8 MPa (the transfer region). The greater adsorption potential-related ductile property enhancement in brown coal during super-critical CO_2 adsorption compared to sub-critical CO_2 is the main causative factor. The geo-mechanical property alterations observed using X-ray CT studies confirmed this brittle to ductile property modification in coal mass upon CO_2 adsorption and the enhancement of that effect with super-critical adsorption.

However, the strength reduction observed in the RC coal samples in this study upon CO_2 saturation is considerably smaller than the strength reductions observed in natural brown coal in the research literature. This is related with the natural cleat system in natural coal that acts as a locus for CO_2 movement, resulting in greater structural alterations. Interestingly, the saturation of similar coal samples with N_2 under similar pressures increased the strength of RC coal instead of the observed strength reduction in CO_2 saturated RC coal samples, which confirms that pure CO_2 saturation creates interactions with the coal matrix. Although RC and natural samples provided slight variations in strength parameters, they produced similar behaviours for different fluid saturations. Therefore, RC samples can be utilised to study the different effect of different factors on coal during CO_2-ECBM by avoiding the complexities due to the heterogeneity of coal.

7.2.6 References

ASTM D7012. (2004). Standard test method for compressive strength and elastic moduli of intact rock core specimens under varying states of stress and temperatures: *Annual Book of ASTM Standards 19.03*.

Chikatamarla, L. Cui, X. and Bustin, R.M. (2004). Implications of volumetric swelling/shrinkage of coal in sequestration of acid gases, in Proceedings Coalbed Methane Symposium, Tuscaloosa, AL, Paper no. 0435.

Huang, J. Moriyoshi, T. and Manabe, H. (2006). Patterning of fine particles by means of supercritical CO_2. *Journal of Materials Science* 41(5): 1605-1610.

Jasinge, D. (2010). An investigation of the effect of carbon dioxide sequestration on the behaviour of brown coal (*PhD thesis),* Monash University, Melbourne, Australia. [http://arrow.monash.edu.au/vital/access/manager/Repository/monash:63624]

Perera, M.S.A. Ranjith, P.G. and Peter, M. (2011), Effects of saturation medium and pressure on strength parameters of Latrobe Valley brown coal: carbon dioxide, water and nitrogen saturations. *Energy* 36(12): 6941-6947.

Perera, M.S.A. Ranjith, P.G. and Viete, D.R. (2013). Effects of gaseous and super-critical carbon dioxide saturation on the mechanical properties of bituminous coal from the Southern Sydney Basin. *Applied Energy* 110: 73-81.

Perera, M.S.A., Ranathunga, A.S., Ranjith, P.G., (2016). Effect of Coal Rank on Various Fluid Saturations Creating Mechanical Property Alterations Using Australian Coals. *Energies* 9, 440. DOI: 10.3390/en9060440.

Ranathunga, A.S. Perera, M.S.A. and Ranjith, P.G. (2014). Deep coal seams as a greener energy source: a review. *Journal of Geophysics and Engineering* 11(6): 063001.

Ranathunga, A.S. Perera, M.S.A. Ranjith, P.G. & Bui, H. (2016), Super-critical CO_2 saturation-induced mechanical property alterations in low rank coal: An experimental study. *Journal of Supercritical Fluids* 109: 134-140.

Ranathunga, A.S. Perera, M.S.A. Ranjith, P.G. Ju, Y. Vishal, V. and De Silva, P.N.K. (2015), A macro-scale experimental study of sub-and super-critical CO_2 flow behaviour in Victorian brown coal. *Fuel* 158: 864-873.

Vásárhelyi, B. and Ván, P. (2006). Influence of water content on the strength of rock. *Engineering Geology* 84(1): 70-74.

Viete, D. R. & Ranjith, P. G. (2006). The effect of CO_2 on the geomechanical and permeability behaviour of brown coal: Implications for coal seam CO_2 sequestration. *International Journal of Coal Geology* 66(3): 204-216.

Vishal, V. & Singh, T. (2013). Development of reconstituted Indian coals to investigate coal response to carbon dioxide exposure, *in* Proceedings ARMA 47th US Rock Mechanics/Geomechanics Symposium 2013, Volume 1, American Rock Mechanics Association, 599-602.

7.3 How do effective factors influence coal mass strength properties? A meso-scale numerical study using reconstituted coal

The previous sections detailed the coal mass strength behaviour, particularly of Victorian brown coal under various fluid saturation conditions expected during the CO_2-ECBM process. However, the scope of experimental studies conducted at laboratory scale is sometimes restricted, due to limitations in the capability to provide the required experimental conditions apparatuses and time frame. Therefore, this work aims to study the coal mass strength behaviour under the deep underground conditions expected during CO_2 sequestration by developing numerical models which extend the experimental results obtained during the present study. The COMSOL Multiphysics numerical simulator was first used to simulate the uniaxial experimental results, and then to model the tri-axial behaviour of brown coal saturated under different CO_2 conditions.

This section of the chapter details the following publication:

Ranathunga AS, Perera MSA, Ranjith PG (2017). Key controlling factors of coal's strength property alterations during CO_2 enhanced coal bed methane production: A numerical study. *Journal of Natural Gas Science and Engineering* (under review).

Key controlling factors of coal's strength properties alterations during CO_2 enhanced coal bed methane production: A numerical study

A.S. Ranathunga[1], M.S.A. Perera[1,2], P.G. Ranjith[1]

[1]Deep Earth Energy Laboratory, Department of Civil Engineering, Monash University, Building 60, Melbourne, Victoria, 3800, Australia.

[2] Department of Infrastructure Engineering, The University of Melbourne, Building 176, Melbourne, Victoria, 3010, Australia.

Abstract

CO_2-ECBM is considered to be a potential atmospheric CO_2 mitigation strategy while producing methane as a by-product for industrial use. However, many researchers have reported that the CO_2 sequestrated in coal seams rearranges the natural coal mass structure by generating coal matrix swelling. These alterations cause coal mechanical properties to change, creating uncertainties in the CO_2-ECBM process in terms of long-term safety. Although a number of laboratory studies have been conducted to date on this, they have been limited to selected reservoir conditions such as less confinement (depth of the injection), CO_2 pressures and temperatures due to limitations in existing laboratory facilities to conduct tests under field and possibly extreme conditions. Therefore, a laboratory-scale numerical model was developed using the experimental results obtained from the research literature to simulate the mechanical behaviour of CO_2-saturated coal under in-situ stress conditions.

The COMSOL Multiphysics numerical simulator was first used to simulate the uniaxial experimental results, and then extended to model the tri-axial behaviour of coal samples saturated under different CO_2 phase and pressure conditions (0 to 10 MPa). The proposed model has the ability to reasonably predict the coal strength reduction upon CO_2 adsorption and its change with reservoir and injecting CO_2 properties. Based on the model results, confining pressure adds an additional strength (3 to 7%) to the CO_2 treated coal mass through associated pore shrinkage and the corresponding reduced CO_2 adsorption capacities. Importantly, the model clearly shows a reduction in the effect of CO_2 adsorption on reservoir strength with increasing reservoir depth, which is favourable for the CO_2-ECBM process. However, the volume of brown coal experiencing plastic deformation in coal after CO_2 injection is found to increase (up to 40%) with increasing confinement and CO_2 saturation pressure offering more ductile nature to the coal mass.

Keywords: brown coal, CO_2-saturation, Laboratory-scale model, tri-axial, uniaxial

7.3.1 Introduction

Enhanced coalbed methane (ECBM) recovery has now been implemented and tested as a viable option to store and reduce the amount of anthropogenic carbon dioxide (CO_2) in the earth's atmosphere while recovering coalbed methane (CH_4) gas. However, according to previous studies, the CO_2-ECBM process leads to CO_2 adsorption-induced coal matrix alterations, which in turn affect coal's hydro-mechanical properties (Perera et al., 2013a). In regard to the geo-mechanical aspect, the coal mass becomes weaker with the substitution of existing adsorbate CH_4 with the highly chemically-potential CO_2 and its inherent brittleness charecteristics become ductile with the asscociated plasticization effect caused by CO_2 adsorption into it (Karacan, 2007).

Generally, potential CO_2-ECBM reservoirs are located deep underground, where CO_2 is in its super-critical state (beyond the critical temperature of CO_2 of 31.8^0C and the critical pressure of CO_2 of 7.38 MPa) (White et al., 2005). According to previous studies, the effect of CO_2 adsorption on coal's strength properties is comparatively greater in its super-critical state compared to the sub-critical (gas/liquid) state (Perera et al. 2013b; Ranathunga et al. 2016a) . This strength reduction may be hazardous for the overall stability of the coal reservoir, mainly by creating cap rock instability (Wang et al., 2013). However, to date studies of the CO_2 adsorption-induced strength reduction in coal have mainly been limited to low-pressure, low-temperature environments and the effect of CO_2 under lithostatic stress conditions has hardly been considered.

According to studies on the effect of in-situ stress on CO_2 treated coal masses (Hol and Spiers, 2012; Jasinge, 2010; Masoudian et al., 2014; Pan et al., 2010; Ranathunga et al., 2016a; Wang et al., 2013), the coal strength reduction which occurs upon CO_2 adsorption is minimal in a tri-axial stress environment compared to a uniaxial environment. Masoudian et al. (2014) and Wang et al. (2013) observed an increase in elastic modulus with increasing effective confining stress for sub-critical CO_2 adsorption in coal. For super-critical CO_2, Pan et al. (2010) observed around 10 to 20 % bulk modulus reduction in high rank coal. A comparison of the tri-axial strength values obtained by Masoudian et al. (2014) for high rank coal and Ranathunga et al. (2016b) for low rank coal, indicates that high rank coal has a slightly greater strength reduction upon CO_2 adsorption compared to low rank coal. According to these observations, it is evident that the coal mass undergoes structural changes upon CO_2 adsorption, even under high in-situ stresses, and these changes are greater for higher CO_2 injection pressures. However, many of these studies were conducted under very low confinements and for low CO_2 pressures, due to the sophisticated laboratory facilities required, the extensive time necessary and the high cost. However, ordinary tests do not represent the actual situation in the field. Therefore, numerical models can be used to predict the probable behaviours of the coal under the higher CO_2 pressures and temperatures expected in the field.

Although several numerical field simulations have been conducted to date on CO_2 sequestration in coal using different software packages, such as COMET3 (Pekot and Reeves, 2002; Perera et al., 2015), TOUGH 2 (Botnen et al., 2009), FEMLAB (Holzbecher, 2005) and COMSOL (Liu and Smirnov, 2009; Perera et al., 2013a), very few models have been developed for laboratory conditions. Meso-scale numerical models, with experimental input on the hydro-mechanical behaviour of coal, are important to obtain better insight into field- scale coal mass behaviour with CO_2 sequestration. Such meso-scale models will be particularly helpful to fill the existing knowledge gaps on the safe and long-term storage of CO_2 in deep coal seams, based on aprecise studies of their associated mechanical property alterations. The present study therefore focused on the development of a comprehensive meso-scale numerical model to study the strength reduction in coal caused by CO_2 adsorption by combining laboratory strength data with the COMSOL Multiphysics numerical simulator.

In this study the COMSOL simulator (www.comsol.com) was utilised to develop numerical models to obtain the required test conditions, as it provides excellent user interfaces and model-coupling capabilities. Although this simulator has been widely used for the field-scale investigation of the CO_2-ECBM process by various researchers (Liu and Smirnov, 2009; Perera et al. 2013a, Zhou et al. 2012), to date no attention has been given to meso-scale model development based on COMSOL. It is particularly important to study the changes in coal's mechanical behaviour caused by CO_2 adsorption under laboratory test environments such as uniaxial and tri-axial loading, which offer proven accuracy to the model and therefore to the prediction of behaviour. COMSOL is a finite element method (FEM) with a partial differential equation (PDE) solution engine and is therefore capable of simulating a wide range of engineering application areas, such as chemical engineering, earth sciences and structural mechanics. Importantly, COMSOL also has the ability to couple different physical interfaces together to facilitate more accurate simulations under various test conditions.

In this study, a COMSOL-based meso-scale model was developed using the experimental results obtained by Ranathunga et al. (2016c) on a series of uniaxial loading tests conducted for different CO_2 phases and pressures on low rank brown coal obtained from the Gippsland basin, Australia. The validated model was then extended to the tri-axial stress environment and finally to possible real field conditions of higher confining pressures and CO_2 pressures.

7.3.2 Model development

A two-dimensional axisymmetric finite element model was first developed using the COMSOL Multiphysics solid mechanics module to simulate laboratory tests (uniaxial compression tests and tri-axial compression tests) under different CO_2 saturation conditions.

7.3.2.1 Governing equations

The formulation used in the solid mechanics module of COMSOL Multiphysics is totally Lagrangian. Here, in the total Lagrangian configuration, the displacement is considered as a function of the material coordinates (X, Y, Z) and hence the total strain tensor is written in terms of the displacement gradient (∇u) (see Eq. [7.1]).

$$\nabla u = \begin{bmatrix} \frac{\partial u}{\partial X} & \frac{\partial u}{\partial Y} & \frac{\partial u}{\partial Z} \\ \frac{\partial v}{\partial X} & \frac{\partial v}{\partial Y} & \frac{\partial v}{\partial Z} \\ \frac{\partial w}{\partial X} & \frac{\partial w}{\partial Y} & \frac{\partial w}{\partial Z} \end{bmatrix} \qquad [7.1]$$

The axial symmetry uses a cylindrical coordinate system and the implementation assumes independence of the angle, and the torsional component of the displacement is identically zero. The physical components of the radial and axial displacement, u and w, are used as independent variables for the axially symmetric geometry.

Therefore, the Green-Lagrange strain tensor (ε) can be defined as in Eq. [7.2].

$$\varepsilon = \frac{1}{2}[\nabla u + (\nabla u)^T + (\nabla u)^T \nabla u] \qquad [7.2]$$

An elastoplastic model was assumed for the numerical study. For isotropic linear elastic materials, the total stress tensor can be defined as in Eq. [7.3].

$$S - S_0 = C : (\varepsilon - \varepsilon_0 - \varepsilon_{inel}) \qquad [7.3]$$

where, S and ε are the stress and strain tensor, S_0 and ε_0 are the initial stress and strain, ε_{inel} is the sum of all inelastic strains and *C* is the 4th order elasticity tensor.

According to Gentzis et al. (2007), the Hoek-Brown failure criterion (see Eq. [7.4]) is a better representation of the coal strength than the Mohr-Coulomb failure criterion and was therefore adopted for this study. This is a non-linear an empirical model widely used in geomechanics applications because material parameters can be estimated with field observations, together with the uniaxial compressive strength of the intact rock mass.

$$\sigma_1 = \sigma_3 + \sigma_c \left(m \frac{\sigma_3}{\sigma_c} + s \right)^a \qquad [7.4]$$

where, $\sigma_1 \geq \sigma_3 \geq 0$ are major and minor principle stresses respectively, σ_c is the uniaxial compressive strength of the intact rock and *m*, *s* and *a* are the material parameters (Hoek and Brown, 1980). Since intact coal samples were used in the experiments, the original Hoek Brown criterion was adopted for the model and *s* = 1 and a = 0.5 were assigned.

In terms of the invariants I_1 and J_2 the Hoek-Brown criterion can be re-written as in Eq. [7.5].

$$F_y = 2\sqrt{J_2}sin\left(\theta + \frac{\pi}{3}\right) - \sigma_c\sqrt{s - m\frac{\sigma_1}{\sigma_c}} = 0 \qquad [7.5]$$

where, θ is the lodge angle $0 \leq \theta \leq \pi/3$ (Jaeger et al., 2009). I_1 is the first invariant stress tensor (see Eq. [7.6]) and J_2 is the second invariant of stress deviator tensor (Eq. [7.7]).

$$I_1 = \sigma_1 + \sigma_2 + \sigma_3 \qquad [7.6]$$

$$J_2 = \frac{1}{6}[(\sigma_1 - \sigma_2)^2 + (\sigma_2 - \sigma_3)^2 + (\sigma_3 - \sigma_1)^2] \qquad [7.7]$$

7.3.2.2 Model validation using experimental data

The numerical study was based on the experimental data reported in the research literature on mechanical property alterations in reconstituted Victorian brown coal for various CO_2 phases and pressures by Ranathunga et al., (2016c). Here, the data obtained using reconstituted brown coal samples were used as a primary step in model development, in order to avoid the complexities associated with the large heterogeneities in natural coal. In this study, reconstituted brown coal samples 54 mm in diameter and 108 mm in length were saturated in 4 and 6 MPa (sub-critical) and 8 and 10 MPa (super-critical) CO_2 at a temperature of 40 ^oC (>31.8 ^oC is the critical temperature of CO_2) and uniaxial compression tests were conducted with a strain-controlled loading rate of 0.1 mm/min. The material properties for the model were obtained from the experimental results (see Figure 7.10).

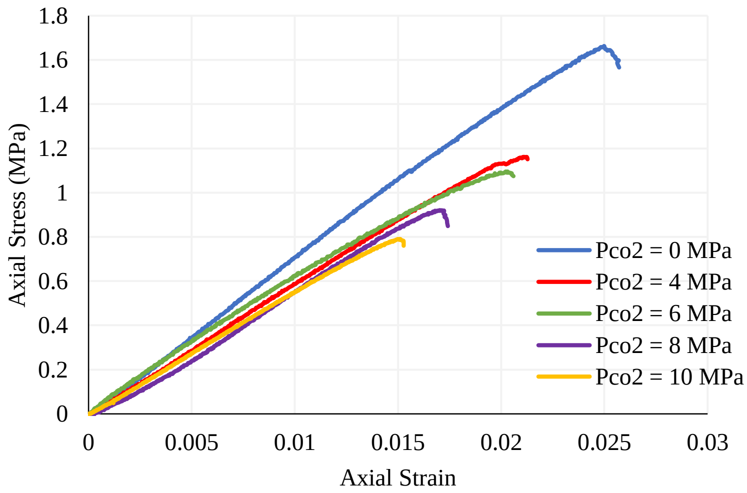

Figure 7.10. Experimental stress-strain curves for CO_2 saturated reconstituted brown coal

7.3.2.3 Basic assumptions

1 Coal is a homogeneous material (this is reasonable as the samples used were reconstituted).

2 The coal sample is at a constant temperature throughout the experiment.

3 All the stress points exist in the defined yield surface.

4 The Hoek-Brown parameters derived for each CO_2 saturation condition do not change with the confining pressure.

5 The axial strain of a brown coal sample (ε) which undergoes confined conditions can be given as:

$$\varepsilon = \left(\alpha_{P_{co2}} P_c + \beta_{P_{co2}}\right)\varepsilon_{uc} \qquad [7.8]$$

where, ε_{uc} is axial strain at failure for unconfined conditions (data from Ranathunga et al., 2016c) and $\alpha_{P_{co2}}$ and $\beta_{P_{co2}}$ (refer to Table 7.3 for the parameters used) are constants empirically derived from experimental data for similar low rank coals by Ranathunga et al. (2016a), Ranathunga et al. (2016b) and Jasinge (2010) under various confinements and P_c and P_{co2} are confining pressure and CO_2 saturation pressure, respectively.

7.3.2.4 Model definition and boundary conditions

To simulate the experimental conditions, an axisymmetric 2-D model was developed with a width of 27 mm (the diameter of the sample is 54 mm) and a height of 108 mm and the developed model was then converted into a 3-D model using the results nodes available in the model builder interface in the COMSOL Multiphysics simulator. The boundary conditions adopted for the solid mechanics module (mechanical boundary conditions) are as follows:

The bottom of the sample was fixed and a prescribed displacement was introduced as an auxiliary sweep to the top of the sample to simulate the axial compression. A boundary load (P_c) was introduced as a radial force simulating the corresponding confining pressure condition. This was introduced as a parametric sweep for different confining pressure conditions from 0 MPa to 25 MPa in 5 MPa steps, where 0 MPa represents unconfined or uniaxial compression. The details of the geometry and boundary conditions adopted for the model are shown in Figure 7.11.

7.3.2.5 Model input parameters

The material properties required for the model were obtained from the experimental results, and the input parameters for the model are shown in Table 7.2. The Young's modulus (E) and Poisson's ratio (n) values of the tested coal under different CO_2 saturation conditions were taken from the literature (Ranathunga et al., 2016b) and the Hoek-Brown parameters were taken from the best fit curves with experimental data from the numerical model (see Table 7.3) (the “m” parameter was changed until the best fit curve for each CO_2 saturated condition was obtained from the numerical model).

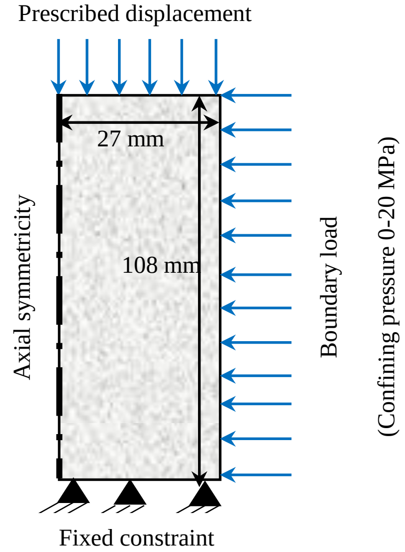

Figure 7.11. Details of the geometry and boundary conditions

Table 7.2. The input parameters for the model

Model Parameter	Value
Coal sample properties	
Sample diameter (D)	54mm
Sample height (H)	108 mm
Density (ρ)	1097.8 kg/m^3
Boundary conditions (parametric sweep)	
Confining pressure (P_c)	0, 10, 15, 20, 25 MPa
CO_2 saturation pressures (P_{co2})	0, 4, 6, 8, 10 MPa

Table 7.3. CO_2 saturation-dependent material parameters

CO_2 saturation pressure (MPa)	**Young's Modulus E (MPa)**	**Uniaxial compressive strength σ_c (MPa)**	**Hoek-Brown Parameter m**	**$\alpha_{P_{co2}}$ For Eq. [7.8]**	**$\beta_{P_{co2}}$ For Eq. [7.8]**
0	72.01	1.66	3.8	0.000141	0.0249
4	50.46	1.16	2.7	0.000136	0.0214
6	47.45	1.10	1.8	0.000132	0.0202
8	39.81	0.92	0.6	0.000126	0.0172
10	34.47	0.79	0.08	0.000119	0.0150

7.3.2.6 Meshing and element sizes

A 2-D mapped meshing was used for the model since it consists of a simple rectangular geometry bounded by four boundary segments with no holes. By defining the number of elements at each side, a mapped mesh was introduced to the model. The assumed mapped mesh and mesh quality plot are shown in Figure 7.12 and the meshing parameters are shown in Table 7.4. It should be noted that the colour range 0 means poor quality and 1 means good quality. The assumed mesh pattern fits the geometry well and therefore indicates a good quality mesh.

Table 7.4. CO_2 saturation-dependent material parameters

Property	Value
Number of degrees of freedom	29250
Number of elements (rectangle)	2500
Number of boundary elements	250

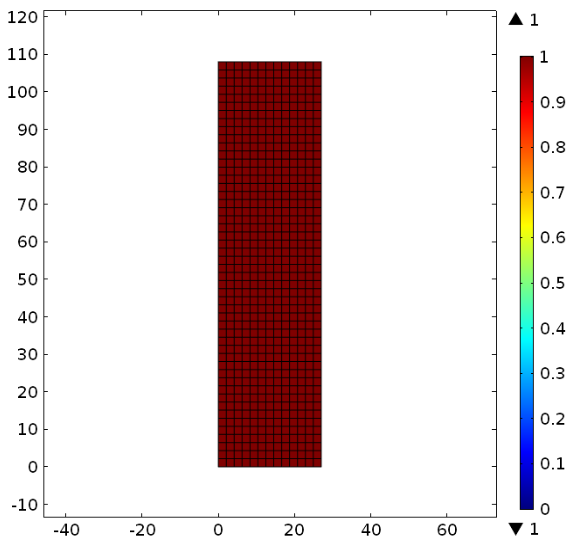

Figure 7.12. Mesh quality plot for the mesh pattern used in the model

7.3.3 Model results and discussion

7.3.3.1 Behaviour of brown coal under uniaxial compression

In order to validate the model, firstly, stress-strain curves were generated and the results were compared with the experimental uniaxial compression results. The resultant vertical force due to mechanical loading can be calculated using Eq. [7.9]:

$$F = \int_0^r \sigma_z \, 2\pi r \, dr \qquad [7.9]$$

where, *F* is the resultant vertical force, *r* is the radius of the coal sample and σ_z is the *z* component of the stress tensor. This was computed using the integration operator of COMSOL Multiphysics by the summation over nodes of the top surface of the coal samples.

The resultant vertical stress due to mechanical loading was calculated using Eq. [7.10].

$$\sigma_z = \frac{F}{\pi R^2} \qquad [7.10]$$

where, *R* is the radius of the sample (27 mm).

Since the axial displacement was applied as a prescribed displacement (*Disp*) at the top surface using an auxiliary sweep from 0 to 1 mm in 0.05mm steps, the mechanical axial strain was defined as in Eq. [7.11].

$$\varepsilon = \frac{Disp}{H} \qquad [7.11]$$

where, ε is the axial strain and *H* is the sample height (108 mm).

The overall experimentally-predicted stress-strain curves from 0 to 10 MPa CO_2 saturation pressures are presented in Figure 7.13. A comparison of the model-predicted and measured stress-strain behaviours of brown coal under 4 MPa (sub-critical) and 8 MPa (super-critical) CO_2 pressures and for the unsaturated sample under uniaxial compression conditions is presented in Figure 7.14. As the figure shows, the model predicts the behaviour of brown coal accurately up to the yield point. The post-failure behavior of brown coal could not be obtained during the experiments due to the sudden failure of the sample under the strain- controlled loading rate used for the tests (0.1 mm/min). Hence, the post-failure behaviour was not considered in the current study. However, after the yield point, the model assumes it is perfectly plastic as no strain hardening could be observed.

As mentioned before, the Hoek-brown parameter “m” was obtained by varying the “m” value until the model acquired the best-fit curve with the experimental results. According to Table 7.3, around 29% reduction of the Hoek-Brown parameter “m” for 4 MPa sub-critical CO_2 treated coal compared to unsaturated coal was observed. Further, this reduction for 8 MPa CO_2 treated coal was around 80% compared to unsaturated coal. Similarly, Masoudian et al. (2014) observed around a 44% reduction of the “m” for CO_2 (up to 5.5 MPa) treated black coal (8.053) compared to intact coal (14.263). Therefore, CO_2 adsorption can affect the mechanical strengthening of the coal mass and the effect is greater for super-critical CO_2. The rearrangement of the natural glassy-strained structure of the coal matrix (Larsen et al., 1997) due to the CO_2 adsorption is the reason for this outcome.

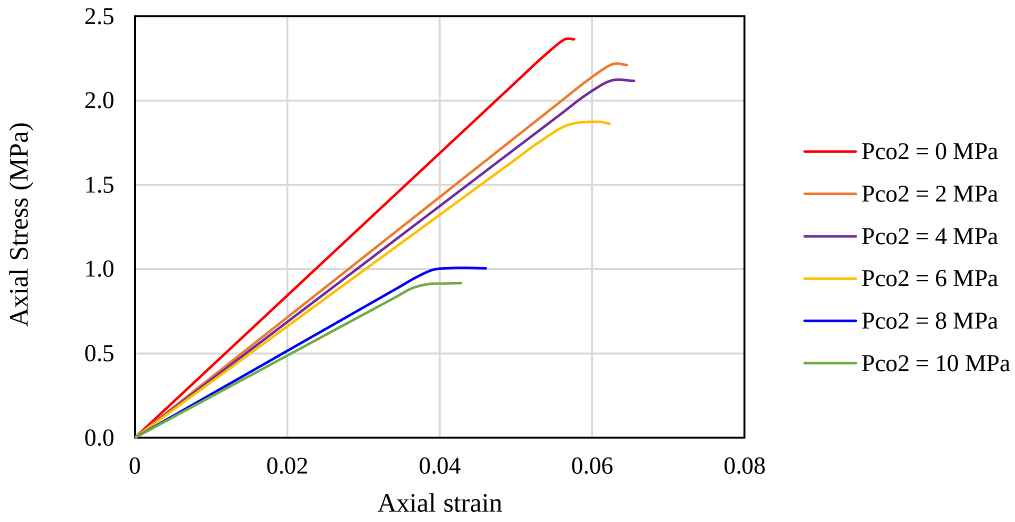

Figure 7.13. Model-predicted stress-strain curves of brown coal under different CO_2 saturation pressures

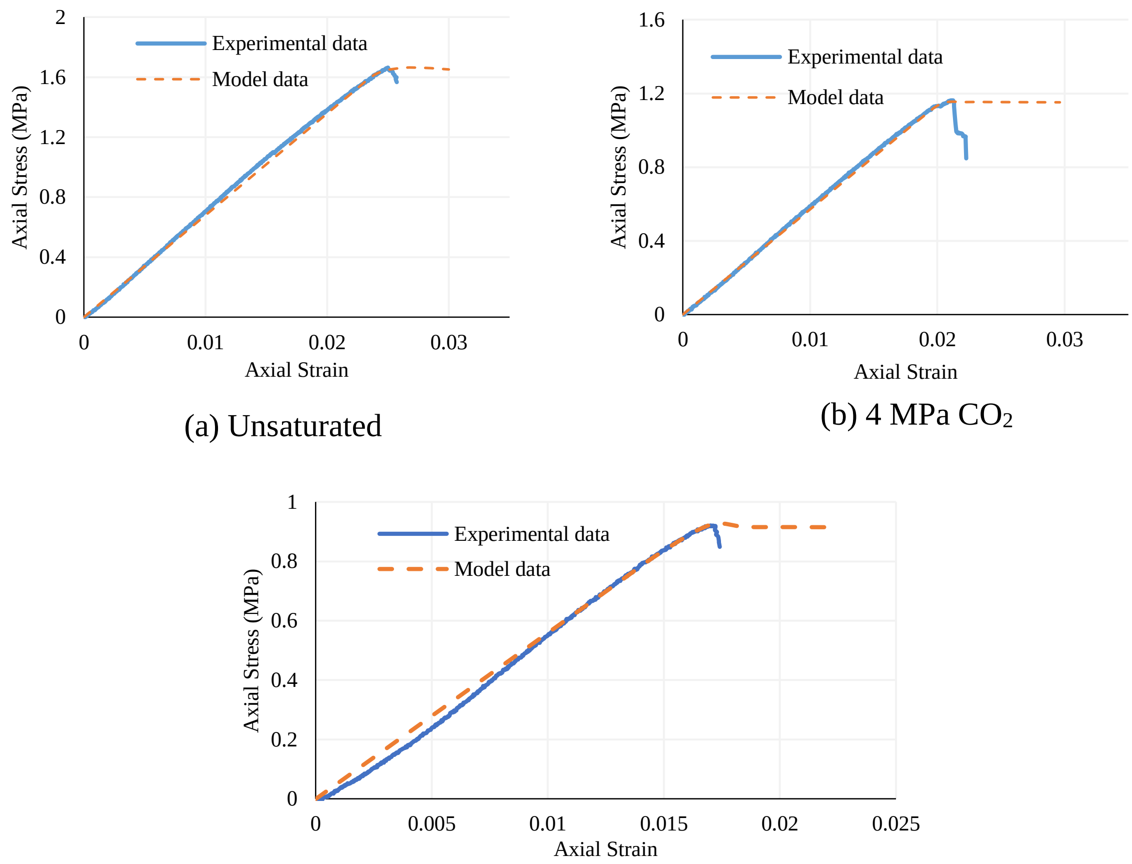

(a) Unsaturated

(b) 4 MPa CO_2

(c) 8 MPa CO_2

Figure 7.14. Comparison of model-predicted and experimental stress-strain curves of brown coal under unsaturated, 4 MPa and 8 MPa CO_2 saturation conditions

7.3.3.2 Alteration of brown coal strength characteristics upon CO_2 adsorption under tri-axial stress environment

When the proposed model for uniaxial conditions was validated using the measured data, the model was extended to study the mechanical behaviour of brown coal under tri-axial stress conditions. To obtain the tri-axial stress conditions, the brown coal sample was subjected to confining pressures of 10 to 25 MPa in 5 MPa increments. For this model, the deviatoric strength was calculated by subtracting the confining stress at failure from the coal mass strength obtained at that particular confining stress (Eq. [7.12]):

$$\sigma_{dev} = \frac{F}{\pi R^2} - P_c \qquad [7.12]$$

where, R is the radius of the sample (27 mm) and P_c is the confining pressure. A parametric sweep was introduced into the model from 0 to 20 MPa in 5 MPa steps to achieve different confinements. Here, deviatoric stress was considered instead of failure strength, as it is the stress change that causes the coal mass failure at that particular confining stress. This is strongly related to field conditions, as natural coal seams located at deep depths are at equilibrium under the naturally-applying confining stresses and only subject to failure upon further increase of load or due to deviatoric stress.

The variation of deviatoric stress with confining stress for unsaturated brown coal is shown in Figure 7.15. As the figure shows, the deviatoric stress of brown coal at failure increases with increasing confining stress. According to Eq. [7.4], when σ_3 is increased, the σ_1 is also subjected to increase, due to the mechanical strengthening which occurs with the associated reduction of the pore voids in the coal matrix, which is confirmed by Figure 7.15.

Although failure strength increases with increasing confining stress, the rate of increase reduces with increasing confining stress. For example, increasing the confining stress from 10 to 15 MPa (lower confinements) and 20 to 25 MPa (higher confinements) caused around 3.4 % and 3.0 % increments in the deviatoric stress in the tested brown coal. This is because there is a greater potential for dilation at low confining pressures, which is supressed at higher confinements (Barton, 2013). Therefore, the ability to open rock micro-cracks and the resulting friction angle are lower at higher confinements. These changes cause the failure mechanism of coal to shift from brittle to ductile with increasing confinement, also changing the shape (Hoek, 1983). Since the rate of increase in the resulting strength reduces with increasing confinement, deviatoric strength remains almost constant at greater depths or confinements (the difference between the resulting strength and confining pressure gives the deviatoric strength). This indicates that confining pressure dominates the behaviour of brown coal at greater depths (with high levels of confinement). The deviatoric strength variations obtained from the model for brown coal saturated under 4 (sub-critical) and 8 MPa (super-critical) CO_2 are shown in Figure 7.16 and Figure 7.17, respectively.

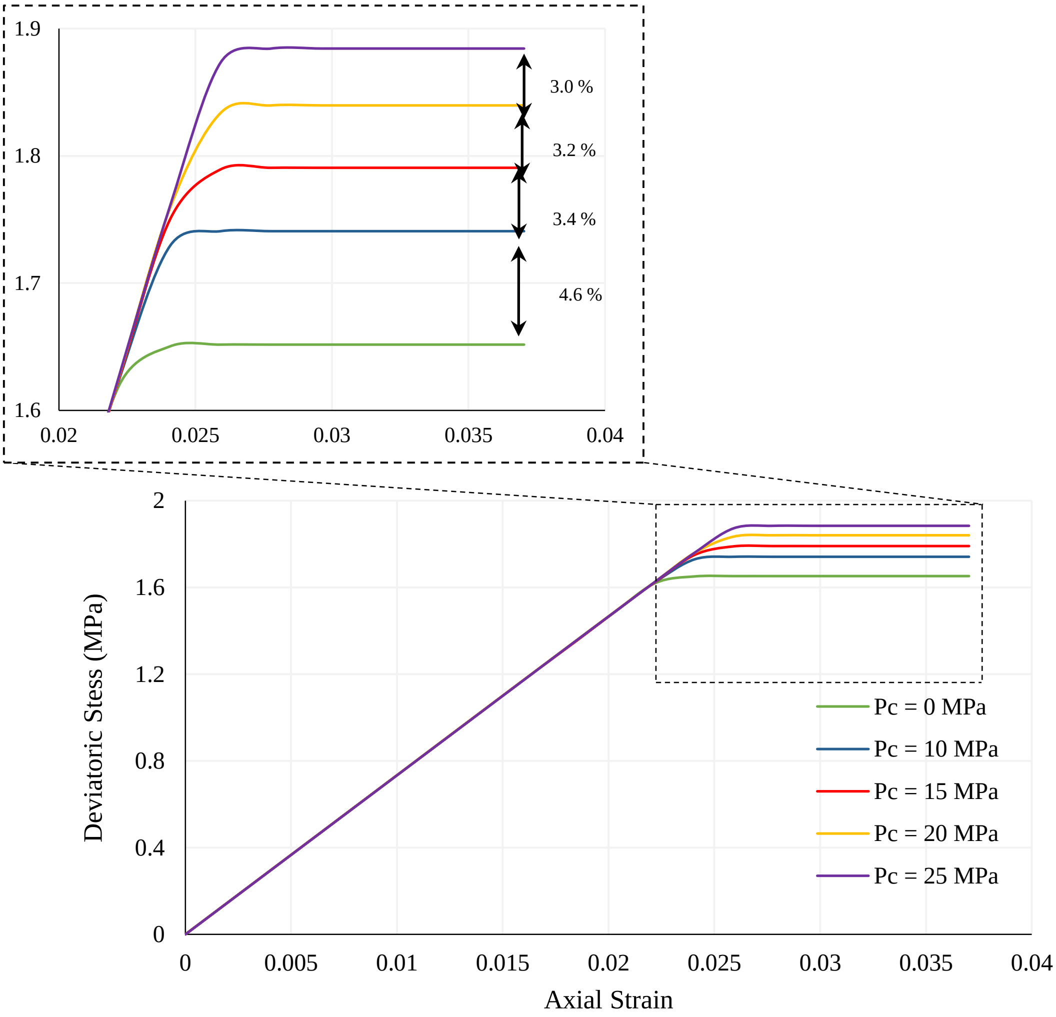

Figure 7.15. Deviatoric stress variation of brown coal without CO_2 saturation

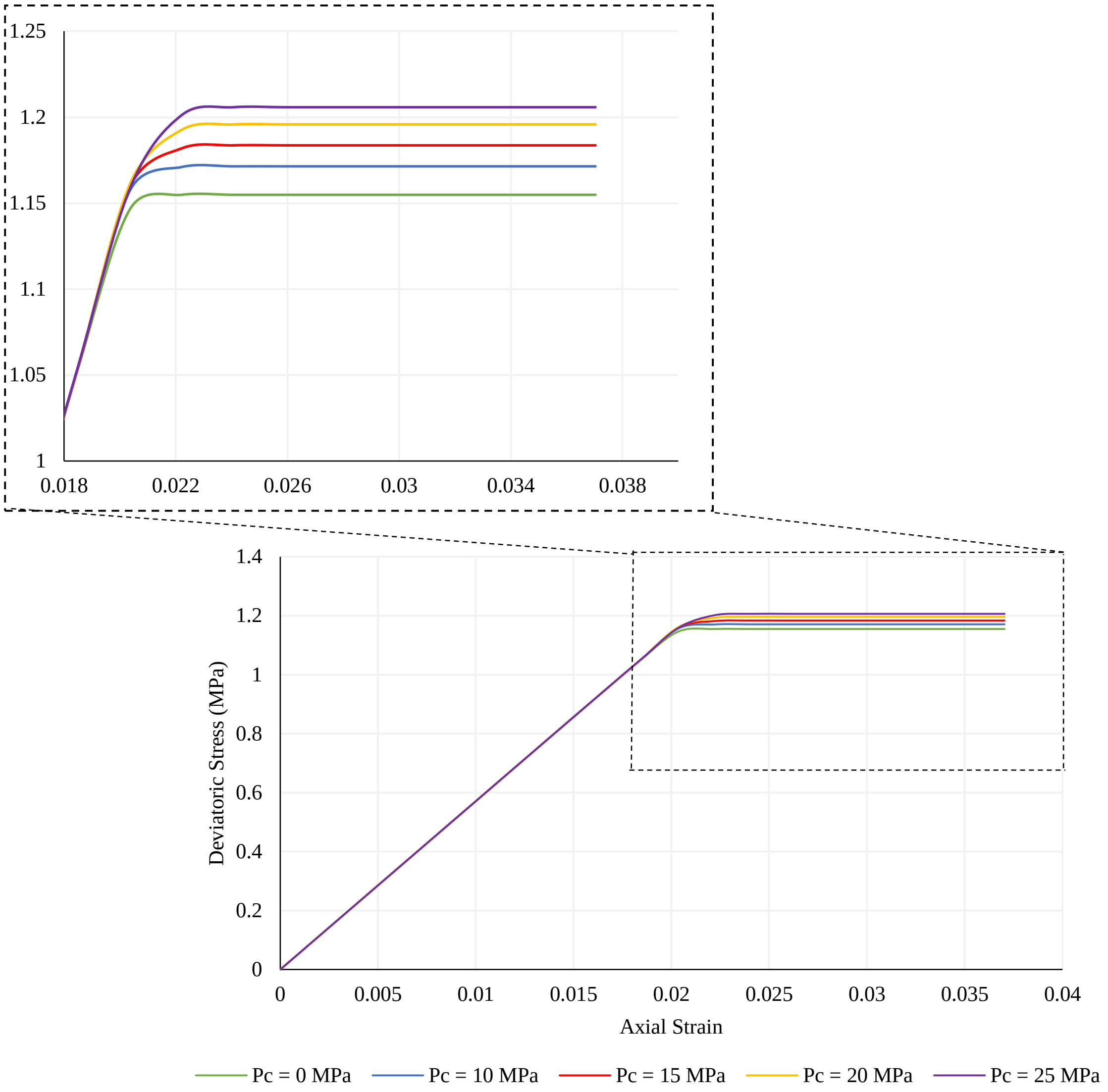

Deviatoric stress increment

From 0 to 10 MPa – 1.38%

From 10 to 15 MPa – 1.29%

From 15 to 20 MPa – 1.27%

From 20 to 25 MPa – 1.26%

Figure 7.16. Deviatoric stress variation of brown coal for 4 MPa CO_2 saturation

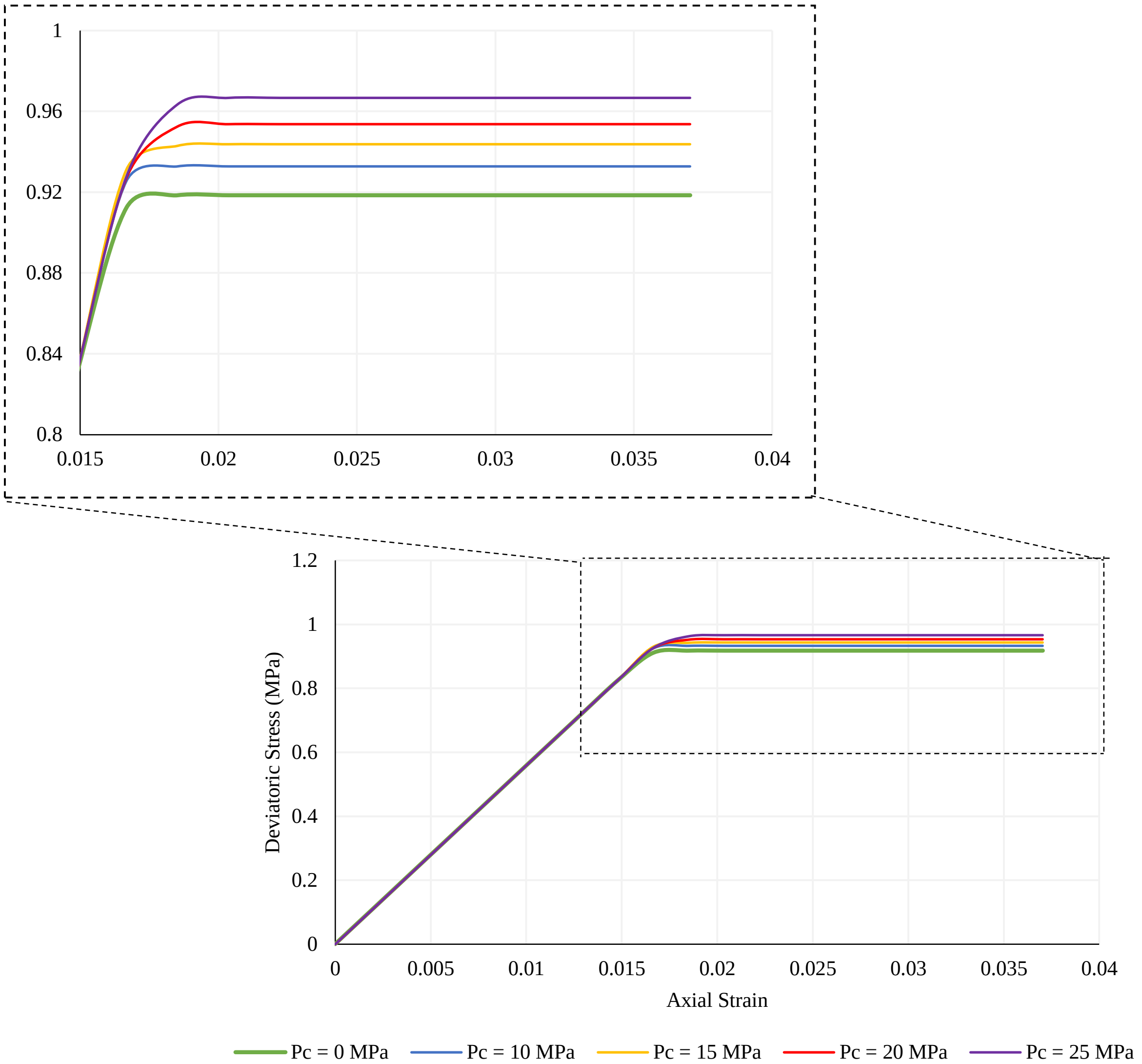

Deviatoric stress increment

From 0 to 10 MPa – 1.14%

From 10 to 15 MPa – 1.05%

From 15 to 20 MPa – 1.02%

From 20 to 25 MPa – 1.01%

Figure 7.17. Deviatoric stress variation of brown coal for 8 MPa CO_2 saturation

Similar to the observations of the unsaturated brown coal samples, 4 MPa and 8 MPa CO_2 saturated samples also show a reduction in deviatoric stress increment with increasing confining stress. However, compared to the observed deviatoric stress increment values under unsaturated conditions, the deviatoric stress increments for CO_2 saturated samples are comparatively low. For instance, from 10 to 15 MPa (lower confinements) confining pressure increase causes a deviatoric stress increment of 3.4 % in unsaturated coal, while it is 1.29 % and 1.05 % for 4 MPa (sub-critical) and 8 MPa (super-critical) CO_2 saturated coal specimens respectively (refer to Figure 7.16 and 7.17). Furthermore, 20 to 25 MPa (higher confinements) confinement increase exhibits a 3 % increase in deviatoric stress for unsaturated samples and for 4 MPa (sub-critical) and 8 MPa (super-critical) CO_2 saturated samples, it shows only 1.26 % and 1.01 % increment, respectively (refer to Figures 7.16 and 7.17). As observed in the experimental results (Ranathunga et al., 2016c), CO_2 saturation causes the coal mass strength to be reduced due to the matrix re-arrangement which occurs with CO_2 adsorption into the coal matrix and is higher at higher CO_2 saturation pressures. Hence, it can be concluded that the possible increment of deviatoric stress is lower for the coal mass already weakened by CO_2 adsorption. Therefore, brown coal's mechanical behaviour with different in situ stresses under various CO_2 saturation pressures is discussed further in the following sections.

a. Variation of deviatoric stress with different stress conditions

The effect of in-situ stresses on potential deviatoric stress application to the coal mass at failure for a given CO_2 saturation pressure was considered next. As mentioned previously, here deviatoric stress at failure ($\sigma_{dev,failure}$, refer to Eq. [7.12]) was compared instead of failure strength ($\sigma_{z,failure}$, refer to Eq. [7.10]), because this stress increment at failure can provide a general overview of the mechanical behaviour of the coal specimen due to the influence of CO_2 sorption under different in situ stresses in the field (Wang et al. 2013).

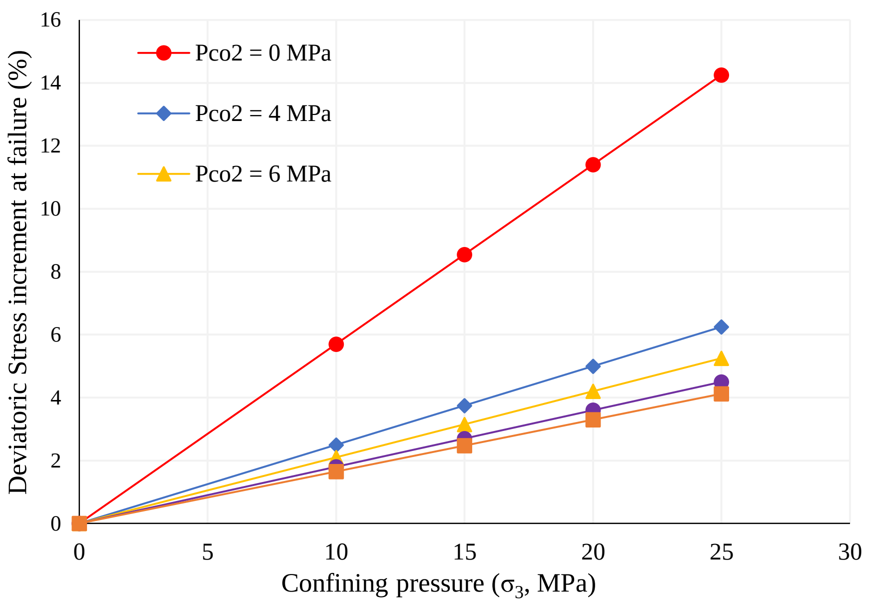

Figure 7.18. Variation of deviatoric stress at failure with confinement compared to unconfined conditions for different CO_2 saturation pressures

Figure 7.18 shows the deviatoric stress increments of coal specimens at failure under different in-situ stresses compared to unconfined conditions. As observed in Figures 7.15, 7.16 and 7.17, $\sigma_{dev,failure}$ increases with increasing confining pressures, regardless of the CO_2 saturation condition. For example, for 4 MPa sub-critical CO_2 saturation, $\sigma_{dev,failure}$ is increased by around 2.5% upon application of 10 MPa confinement and by around 5.1% upon application of around 20 MPa confinement. Similarly, for 8 MPa CO_2 saturation, there are around 1.82% and 3.6% increments in $\sigma_{dev,failure}$ upon increase of confining stress to 10 and 20 MPa, respectively. Apparently, doubling of confinement causes the deviatoric stress increment to double, regardless of the CO_2 saturation pressure condition. This shows that the potentially applicable deviatoric stress condition in a deep coal seam is proportional to the depth of the seam, regardless of the CO_2 pressure in the seam. This significant influence on coal seam depth or confining stress on seam strength is because coal is subject to mechanical strengthening with increasing effective stresses due to shrinkage of the pore structure (refer to Eq. [7.4]).

However, as mentioned earlier, this deviatoric stress increment reduces with increasing CO_2 saturation pressure (see Figure 7.18). For example, under 15 MPa confinement, $\sigma_{dev,failure}$ increment is around 3.75% and 2.7% for 4 and 8 MPa CO_2 saturation pressures, respectively. This is possibly due to the fact that coal has a much weaker structure at higher CO_2 saturation pressures due to the associated greater adsorption potential and coal matrix swelling (Perera et al., 2013), which eventually minimises the increment of deviatoric stress (Barton, 2013; Singh, 1986).

The effect of CO_2 saturation pressure on the effective plastic strain of brown coal was considered next, in order to understand the alteration of coal deformation characteristics upon CO_2 saturation under various conditions. Here, the term “effective plastic strain” indicates the unrecoverable portion of the true strain beyond the yield limit. The variations of effective plastic strain of brown coal specimens treated under 0 and 4 MPa CO_2 saturation pressure at different confinement levels are shown in Figure 7.19. Here, the 3-D plot of effective plastic strain was produced by the revolution of the 2-D axisymmetric data set about the axis of symmetry. According to Figure 7.19, under higher confining pressures, a major portion of the sample exhibits plastic deformation characteristics, whereas at lower confining pressures, only a smaller portion of the sample experiences plastic deformation characteristics. Compared to the unconfined coal sample, the region of volumetric contraction is clearly greater in confined coal samples, resulting in an extended peak stress-strain response. Wang et al. (2013) concluded that, at lower confinement levels, coal failure dominates with micro- and macro-cracks, whereas at higher confining stresses, failure is mostly related to larger strain values with few macro-cracks. Therefore, the restrained action provided by lateral confinement at higher confining stresses increases the mechanical strength and ductility characteristics of coal, offering increased mechanical integrity.

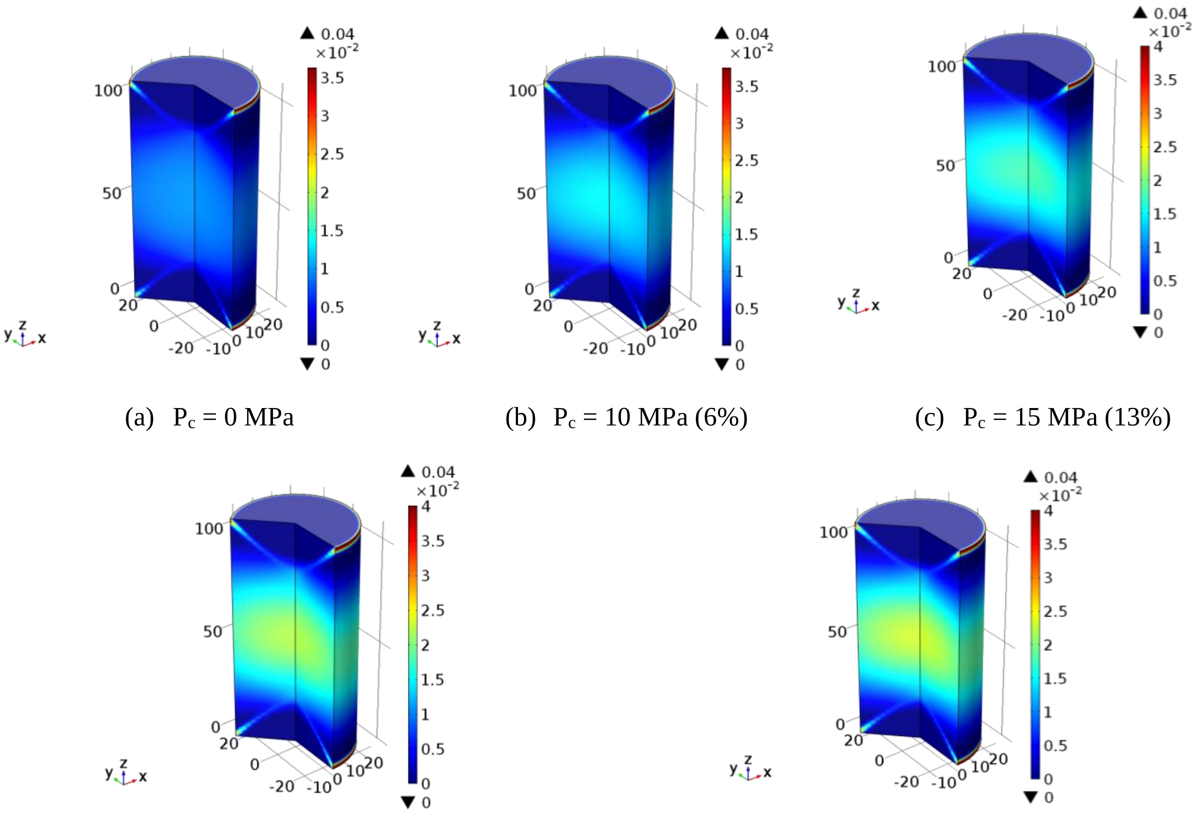

(a) P_c = 0 MPa (b) P_c = 10 MPa (6%) (c) P_c = 15 MPa (13%)

(d) P_c = 20 MPa (22%) (e) P_c = 25 MPa (29%)

Figure 7.19. Effective plastic strain variation of brown coal samples under different confinements with 4 MPa CO_2 saturation (The values in the brackets denote the percentage of the volume of plastic deformation)

b. Variation of deviatoric stress with different CO_2 saturation pressures

As discussed in the previous section, CO_2 adsorption into brown coal causes enhanced ductility characteristics and reduced deviatoric stress increments. Hence, in this section, further attention is paid to the variations of deviatoric stress induced by CO_2 adsorption. Figure 7.20 shows how the CO_2 saturation causes deviatoric stress (at failure) reduction in coal with different saturation pressures and confining pressure conditions. Ranathunga et al. (2016a) observed a reduction in uniaxial strength with increasing CO_2 pressure for reconstituted brown coal and a similar reduction was observed by Ranathunga et al. (2016b) for natural brown coal under 10 MPa confining stress conditions. As expected, the $\sigma_{dev,failure}$ reduction is increased with increasing injection pressure (see Figure 7.20), exhibiting the influence of CO_2 adsorption on coal strength. For example, there are around 32.82 % and 47.17 % reductions in $\sigma_{dev,failure}$ with increasing CO_2 saturation pressure from 0 to 4 MPa (sub-critical) and from 0 to 8 MPa (super-critical) at 10 MPa confining pressure (refer to Figure 7.20), and the deviatoric stress reduction caused by super-critical CO_2 is much higher. According to Gibbs (1878) and Griffith (1921), the adsorption of more chemically potent gas into any material with replacing any existing adsorbent in it reduces the surface energy of the material, weakening its strength characteristics. In addition, the induced coal matrix swelling also contributes to strength reduction in coal by reducing its mass density (Bae and Bhatia, 2006). This greater adsorptive potential of super-critical CO_2 therefore causes greater strength reduction, as is evident in Figure 7.20.

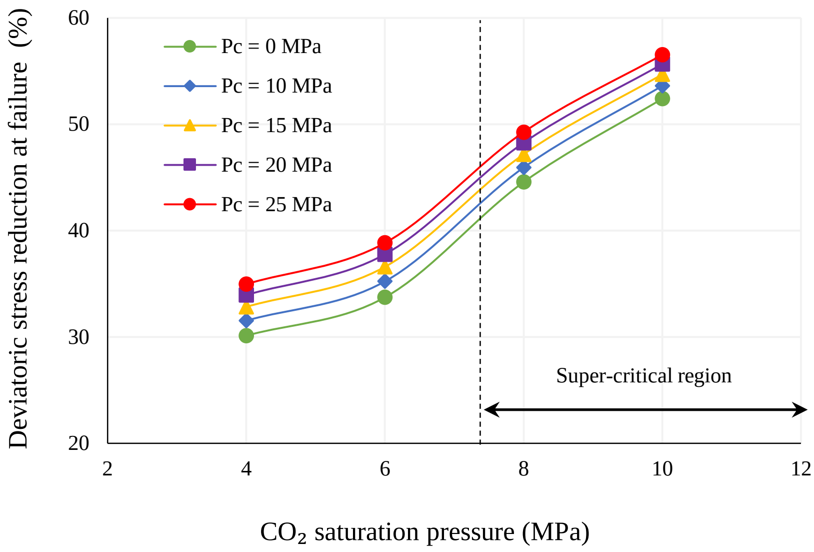

Figure 7.20. Overall variation of deviatoric stress with CO_2 saturation pressures for different confinements compared to unsaturated CO_2 condition

However, this deviatoric stress reduction due to CO_2 adsorption decreases with increasing confinement (see Figure 7.19). For example, 4 MPa sub-critical CO_2 saturation causes around 1.6 % deviatoric stress increase with increasing confining stress from 0 MPa to 10 MPa and around 4.7 % for a 15 MPa to 20 MPa confinement increment. Further, 8 MPa super-critical CO_2 saturated samples exhibit around 1.13 % and 3.4 % deviatoric stress increments with increasing confining stress from 0 MPa to 10 MPa and 15 MPa to 20 MPa, respectively. This is consistent with the findings of Ranathunga et al. (2016b), who showed a lower reduction in coal strength upon CO_2 saturation when confinement was raised from 0 to 10 MPa. For example, Ranathunga et al. (2016b) observed around 10.17% (6 MPa CO_2 pressure) and 12.16% (8 MPa CO_2 pressure) strength reductions in brown coal under 10 MPa confinement, while the samples tested without any confinement exhibited around 21.25% (6 MPa CO_2 pressure) and 57.50% (8 MPa CO_2 pressure) reductions (Ranathunga et al., 2016a), respectively. As explained by Ranathunga et al. (2016b), the reason may be both mechanical confinement and the reduction of CO_2 adsorption (Hol et al., 2011) with enhanced effective stress conditions in the tri-axial stress environment. Overall, this suggests that coal seams located at greater depths are subject to less swelling for these reasons, which is favourable for the ECBM process.

As described previously, the reduction of CO_2 saturation-induced deviatoric stress reduction with increasing confining stress can be confirmed by conducting plastic strain analysis. Therefore, it would be interesting to investigate the behaviour of effective plastic strain variation for different CO_2 saturation pressures, and this was studied next. Figure 7.21 shows the effective plastic strain variation of brown coal treated by different CO_2 saturation pressures at 10 MPa confining stresses.

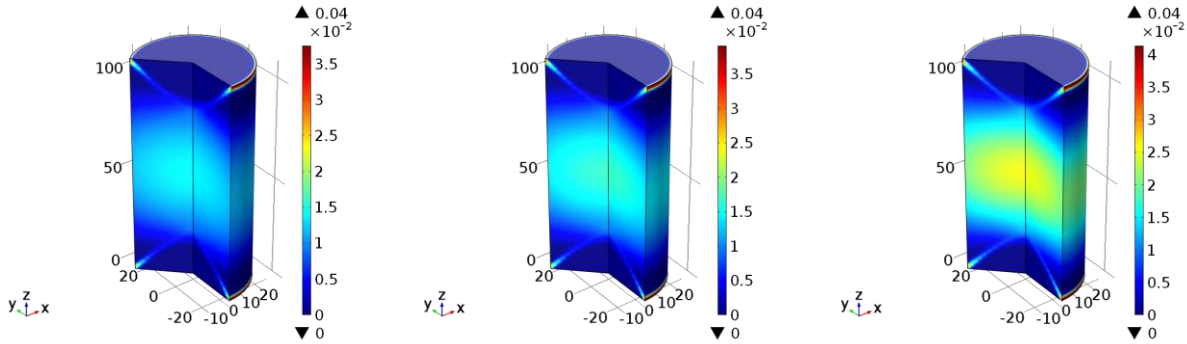

(a) P_{co2} = 0 MPa (b) P_{co2} = 4 MPa (9%) (c) P_{co2} = 6 MPa (23%)

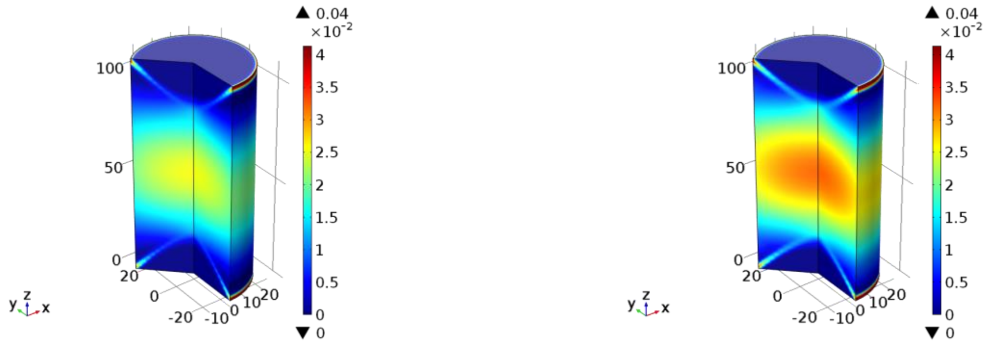

(d) P_{co2} = 8 MPa (34%) (e) P_{co2} = 10 MPa (42%)

Figure 7.21. Effective plastic strain variation of brown coal samples at 10 MPa confinement under various CO_2 saturations (The values in the brackets denote the percentage of the volume of plastic deformation)

Win relation to the effect of CO_2 saturation on plastic deformation, the portion of the brown coal sample that experiences plastic deformation increases with increasing CO_2 saturation pressure. The CO_2 adsorption-induced plasticisation effect (Karacan, 2007) is the main reason for these observed variations in plastic deformation. This plasticisation occurs due to the associated segmental mobility enhancement which occurs in the polymer structure upon CO_2 adsorption, which creates a softening effect in coal mass, weakening the coal mass polymer structure. Hence, expansion of the coal mass free volume with polymer structural rearrangement upon CO_2 adsorption (Larsen et al., 1997) leads to enhancement of its ductile characteristics, as observed in Figure 7.21.

7.3.4 Implications for field applications

According to the results of the present study, coal strength increases with increasing effective confining pressure. Here, the effective confining stress is the difference between the applied confining pressure and the CO_2 pore pressure. This implies that coal seams located at shallow depths with higher CO_2 pressures have the largest potential to fail easily. The mechanical strengthening which occurs due to the application of in-situ stresses is a common fact for any type of rock, including CO_2 treated coal. The important fact is that this mechanical strengthening effect in coal is not sufficient to fully overcome CO_2 adsorption-induced coal matrix strength reduction.

In addition, high in-situ stresses have the capability to provide greater mechanical integrity to the coal seam with greater lateral restraints and enhanced ductile characteristics. At the same time, higher CO_2 adsorption also causes greater ductility characteristics in coal. According to the model results, higher in-situ stresses and higher CO_2 saturations collectively cause a larger portion of the coal mass to become less brittle, which is a disadvantage for production-enhancement techniques such as hydro-fracturing. Hence, even though greater CO_2 injections can sequestrate more CO_2 in deep coal seams, attention must be paid to the expected coal mass mechanical behaviours for the long-term safety of the process.

According to the results of this study, CO_2 adsorption weakens the coal mass in two main ways: (1) the reduction of effective confining stress by increased pore pressure (see Figure 7.18), and (2) the reduction of the surface energy required for fracture propagation by the adsorption of highly chemically-potent CO_2 (Figure 7.20) (Ranathunga et al., 2016b). The degree of weakening caused by the first mechanism depends on the rate of CO_2 flow through fractures and the adsorption rate. The second mechanism depends on the gas composition, pressure and content, as these determine the amount of surface energy that can be released by CO_2 adsorption. Hence, these possible factors need to be considered for the effective field- scale application of CO_2 sequestration.

7.3.5 Conclusions and suggestions for future research

7.3.5.1 Conclusions

A numerical study was conducted to understand the mechanical behaviour of brown coal treated with different CO_2 saturation pressures (4, 6, 8 and 10 MPa) under tri-axial stress conditions using reconstituted coal to remove the effect of coal heterogeneity. The model developed using COMSOL was first verified using experimental uniaxial compressive strength results and the model was then extended to predict the tri-axial behaviour for different CO_2 saturation pressures under various confining pressures (10 to 25 MPa). The following conclusions can be drawn based on the outcomes of this study:

- At a given CO_2 saturation pressure, the resulting failure strength increases as the confining stress increases, due to the associated closure of pore voids and the enhancement of coal mass density. However, this increment is reduced for higher confining pressures due to the suppression of the potential for dilation under higher confinements.
- This strength increment with increasing confining pressure is applicable to any CO_2 saturation condition in coal. Interestingly, this deviatoric stress increment (at failure) is reduced with increasing CO_2 saturation pressure, due to the associated ductility enhancement in coal.
- The deviatoric stress reduction (at failure) increases with increasing injection pressure, because the associated reduction in CO_2 adsorption and swelling under high effective stress conditions in the tri-axial stress environment cause lower strength reduction under higher in situ stresses.
- For a given CO_2 saturation pressure, the percentage volume of brown coal undergoing plastic deformation increases with increasing confinement, due to the associated enhancements in the ductility and mechanical integrity of the coal. On the other hand, at a given confining pressure, the percentage volume of brown coal undergoing plastic deformation increases with increasing CO_2 saturation pressure, due to the associated polymerisation of the coal.

7.3.5.2 Suggestions for future research

- On the whole, brown coal provides comparatively lower mechanical strength reduction upon CO_2 adsorption at higher confinements, which is favourable for ECBM and CO_2 sequestration in deep coal seams. However, the CO_2 sequestration process is a long-term procedure and hence it is necessary to focus on how the observed mechanical strength alterations vary with time.
- Further, the increased ductility characteristics of coal under higher CO_2 pressures and confinements is unfavourable for some production enhancement techniques such as hydro-fracturing. Therefore, it would be worthwhile to conduct an in-depth study to determine optimal CO_2 injection conditions in deep coal seams for enhanced CO_2 storage while producing a suitable environment for production-enhancement techniques.

- As stated by Hooper et al. (2005), potential CO_2-ECBM sites in Victoria exist at depths of around 400 to 800 m. Therefore, for the present numerical study, CO_2 pressures were considered only up to 10 MPa (a 10 MPa CO_2 pressure represents a depth of approximately 1000 m (Oldenburg, 2006)) and in situ stresses up to 25 MPa (25 MPa in situ stress represents a depth of approximately 900 m). However, these conditions may vary for other coal types, especially higher rank coals. By changing the input mechanical properties, different types of coal can be modelled using a similar method.
- For the present study, the post-failure behaviour of the coal specimens was not modelled due to the limitations in the available experimental data required for model validation. Future studies are therefore necessary to understand the post-failure behaviour of coal samples after CO_2 sequestration to obtain better insights into coal mass mechanical behaviour.

7.3.6 References

Bae, J.S., Bhatia, S.K., (2006). High-Pressure Adsorption of Methane and Carbon Dioxide on Coal. *Energ Fuel* 20, 2599-2607.

Barton, N., (2013). Shear strength criteria for rock, rock joints, rockfill and rock masses: Problems and some solutions. *Journal of Rock Mechanics and Geotechnical Engineering* 5, 249-261.

Botnen, L.S., Fisher, D.W., Dobroskok, A.A., Bratton, T.R., H. Greaves, K., Robert McLendon, T., Steiner, G., Sorensen, J.A., Steadman, E.N., Harju, J.A., (2009). Field Test of CO_2 Injection and Storage in Lignite Coal Seam in North Dakota. *Energy Procedia* 1, 2013-2019.

Gentzis, T., Deisman, N., Chalaturnyk, R.J., (2007). Geomechanical properties and permeability of coals from the Foothills and Mountain regions of western Canada. *International Journal of Coal Geology* 69, 153-164.

Gibbs, J.W., (1878). On the equilibrium of heterogeneous substances. *American Journal of Science*, 441-458.

Griffith, A.A., (1921). The Phenomena of Rupture and Flow in Solids. Philosophical Transactions of the Royal Society of London. Series A, Containing Papers of a Mathematical or Physical Character 221, 163-198.

Hoek, E., Brown, E.T., (1980). Empirical strength criterion for rock masses. *Journal of Geotechnical and Geoenvironmental Engineering* 34(8), 1165 - 1186.

Hoek, E., (1983). Strength of jointed rock masses. *Geotechnique* 33, 187-223.

Hol, S., Peach, C.J., Spiers, C.J., (2011). Applied stress reduces the CO_2 sorption capacity of coal. *International Journal of Coal Geology* 85, 128-142.

Holzbecher, E., (2005). FEMLAB® Performance on 2D Porous Media Variable Density Benchmarks, Proceedings of FEMLAB Konferenz, pp. 203-208.

Hooper, B., Murray, L., Gibson-Poole, C. (2005). Latrobe Valley CO_2 Storage Assessment, Cooperative Research Centre for Greenhouse Gas Technologies, Canberra. CO2CRC Publication No. RPT05-0108.

Jaeger, J.C., Cook, N.G., Zimmerman, R., (2009). *Fundamentals of rock mechanics*. John Wiley & Sons, Methuen, London, p 87-91.

Jasinge, D., (2010). An investigation of the effect of carbon dioxide sequestration on the behaviour of brown coal (*PhD thesis*). Monash University, Melbourne, Australia.

[http://arrow.monash.edu.au/vital/access/manager/Repository/monash:63624]

Karacan, C.Ö., (2007). Swelling-induced volumetric strains internal to a stressed coal associated with CO_2 sorption. *International Journal of Coal Geology* 72, 209-220.

Larsen, J.W., Flowers, R.A., Hall, P.J., Carlson, G., (1997). Structural rearrangement of strained coals. *Energ Fuel* 11, 998-1002.

Liu, G., Smirnov, A.V., (2009). Carbon sequestration in coal-beds with structural deformation effects. *Energy Conversion and Management* 50, 1586-1594.

Masoudian, M.S., Airey, D.W., El-Zein, A., (2014). Experimental investigations on the effect of CO2 on mechanics of coal. *International Journal of Coal Geology* 128–129, 12-23.

Oldenburg, C.M., (2006). Geologic carbon sequestration: CO_2 transport in depleted gas reservoirs, *Gas Transport in Porous Media*. Springer, pp. 419-426.

Pan, Z., Connell, L.D., Camilleri, M., (2010). Laboratory characterisation of coal reservoir permeability for primary and enhanced coalbed methane recovery. *International Journal of Coal Geology* 82, 252-261.

Pekot, L., Reeves, S., (2002). Modelling coal matrix shrinkage and differential swelling with CO_2 injection for enhanced coalbed methane recovery and carbon sequestration applications. Topical Report, Contract No. DE-FC26-00NT40924, US DOE, Washington, DC (November 2002).

Perera, M.S.A., Ranjith, P.G., Choi, S.-K., Bouazza, A., (2013a). A parametric study of coal mass and cap rock behaviour and carbon dioxide flow during and after carbon dioxide injection. *Fuel* 106, 129-138.

Perera, M.S.A., Ranjith, P.G., Viete, D.R., (2013b). Effects of gaseous and super-critical carbon dioxide saturation on the mechanical properties of bituminous coal from the Southern Sydney Basin. *Applied Energy* 110, 73-81.

Perera, M.S.A., Ranjith, P.G., Ranathunga, A.S., Koay, A., Zhao, J., Choi, S., (2015). Optimization of enhanced coal-bed methane recovery using numerical simulation. *Journal of Geophysics and Engineering* 12, 90. DOI: http://dx.doi.org/10.1088/1742-2132/12/1/90.

Ranathunga, A.S., Perera, M.S.A., Ranjith, P.G., Bui, H., (2016a). Super-critical CO_2 saturation-induced mechanical property alterations in low rank coal: An experimental study. *The Journal of Supercritical Fluid*s 109, 134-140.

Ranathunga, A.S., Perera, M.S.A., Ranjith, P.G., (2016b). Influence of CO_2 adsorption on the strength and elastic modulus of low rank Australian coal under confining pressure. *International Journal of Coal Geology* 167, 148-156.

Ranathunga, A.S., Perera, M.S.A., Ranjith, P.G., Haque, R.T., (2016c). An experimental study on behaviour of reconstituted low rank coal under different fluid saturations, ISRM International Symposium and EUROCK 2016, Cappadocia, Turkey, Paper ID 166.

Singh, S., 1986. Brittleness and the mechanical winning of coal. Mining Science and Technology 3, 173-180.

Wang, S., Elsworth, D., Liu, J., (2013). Mechanical behaviour of methane infiltrated coal: the roles of gas desorption, stress level and loading rate. *Rock Mechanics and Rock Engineering* 46, 945-958.

White, C.M., Smith, D.H., Jones, K.L., Goodman, A.L., Jikich, S.A., LaCount, R.B., DuBose, S.B., Ozdemir, E., Morsi, B.I., Schroeder, K.T., (2005). Sequestration of Carbon Dioxide in Coal with Enhanced Coalbed Methane Recovery: A Review. *Energ Fuel* 19, 659-724.

Zhou, L., Feng, Q., Chen, Z., Liu, J., (2012). Modelling and upscaling of binary gas coal interactions in CO_2 enhanced coalbed methane recovery. *Procedia Environmental Sciences* 12, 926-939.

7.4 Chapter summary

The main objective of this chapter was to investigate the influence of CO_2 adsorption on the mechanical properties of brown coal using reconstituted coal samples to mitigate the effect of the heterogeneity of coal. Various meso-scale experimental and numerical studies were conducted to observe the effect of different effective factors on coal mass strength with CO_2-ECBM and the major findings of these studies are summarised below.

- **Section 7.2 - *How to overcome the effect of coal heterogeneity on the mechanical property variations in coal induced by different fluid saturations?***

Reconstituted low rank coal samples were prepared using Victorian brown coal powder with similar mechanical properties to natural coal. After examining the effect of different saturation conditions on the mechanical properties of the RC samples, it was found that both RC and natural brown coal samples behave similarly under CO_2, water and N_2 saturation. However, the strength reduction observed in the RC coal samples upon CO_2 saturation is considerably smaller than the strength reductions observed in natural brown coal. This is related to the natural cleat system in natural coal which acts as a locus for CO_2 movement, resulting in greater structural alterations.

- **Section 7.3 - *How do effective factors affect coal mass strength properties? A meso-scale numerical study using reconstituted coal.***

A laboratory-scale numerical model was developed using the experimental results of Section 4.4 to simulate the mechanical behaviour of CO_2-saturated coal mass under in-situ stress conditions. First, the COMSOL Multiphysics numerical simulator was used to simulate the uniaxial experimental results, and then to model the tri-axial behaviour of coal saturated under different CO_2 phases and pressures (4 to 10 MPa). Based on the modelling results, confining pressure adds strength to the CO_2 treated coal mass with pore shrinkage and lower CO_2 adsorption capacities at higher effective stresses. Notably, the model indicates a decline of the influence of CO_2 adsorption on reservoir strength with increasing reservoir depth. On the other hand, the volume of brown coal subjected to plastic deformation increases with increases in situ stresses and CO_2 saturation pressures contributing to the more ductile nature of the reservoir rock.

Part 4: Chapter 8 - Investigation of carbon dioxide injection-induced methane recovery enhancement

Part 4: Investigation of carbon dioxide injection-induced methane recovery enhancement

Although enhanced coal-bed methane (ECBM) recovery is a potential coal bed methane production enhancement technique, this method has been tested only on high rank coal. According to recent studies in USA and Australia, there are several potential CO_2-ECBM sites where low rank coal seams exist. Therefore, it is important to investigate the applicability of CO_2 sequestration-induced methane enhancement in low rank coal and this is the subject of this chapter. In addition, the effectiveness of this ECBM process is greatly dependent on the seam and injecting gas properties, and the development of knowledge of optimum reservoir conditions and injecting gas properties is essential. This is the subject of the next part of this chapter. The findings of the studies are presented in this section of the thesis as follows.

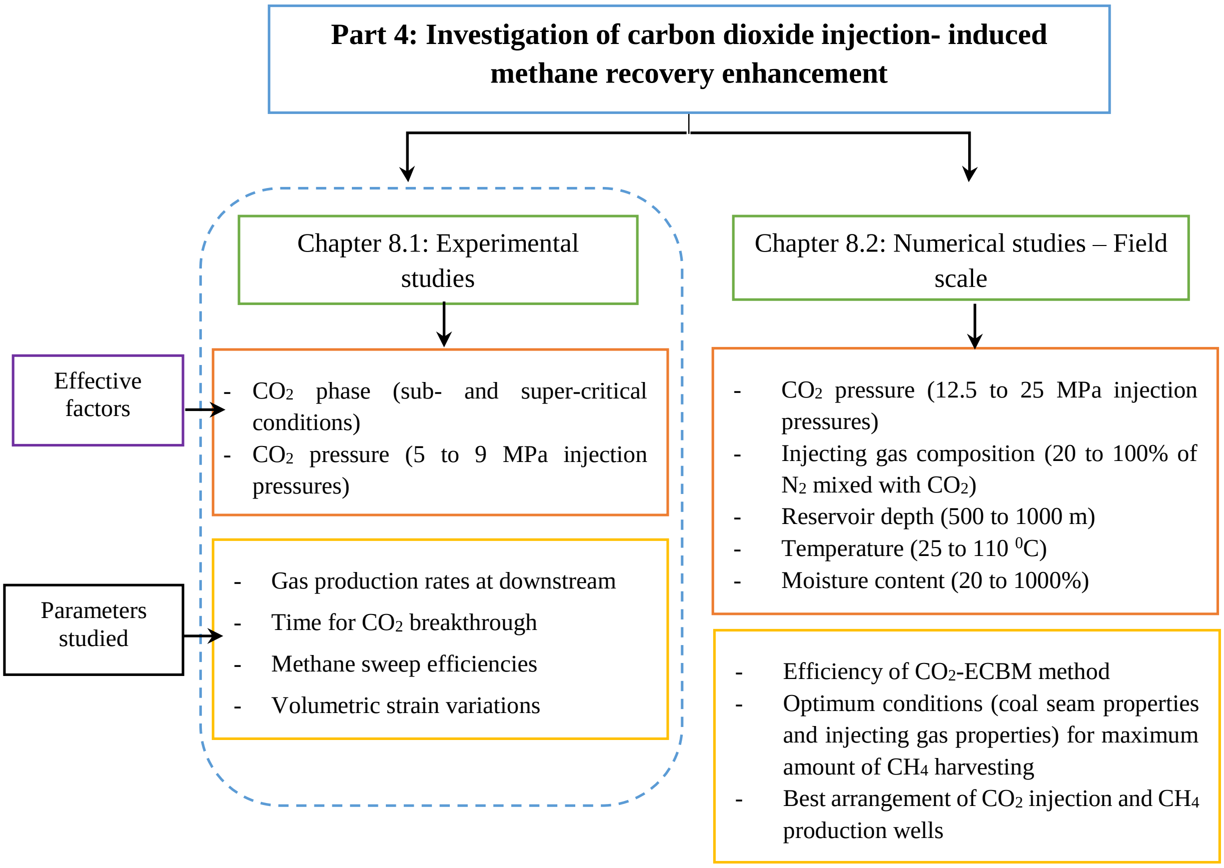

PART 4 - CHAPTER 8

Investigation of carbon dioxide sequestration-induced methane recovery enhancement

Publications in Chapter 8

Chapter 8 includes one publication. Details of the publication are as follows:

Ranathunga, A.S., Perera, M.S.A., Ranjith, P.G., Wei, C.H., 2017. An experimental investigation of applicability of CO_2-enhanced coal bed methane recovery to low rank coal. *Fuel* 189, 391-399.

Declaration for Thesis Chapter 8.2

In the case of Chapter 8.2, the nature and extent of my contribution to the work was the following:

Nature of contribution	Extent of contribution (%)
Initiation, key ideas, experimental work, data analysis and writing up	85

The following co-authors contributed to the work. If co-authors are students at Monash University, the extent of their contribution in percentage terms must be stated:

Name	Nature of contribution	Extent of contribution (%) for student co-authors only
Perera MSA	Key ideas, reviewing and editing the manuscript	N/A
Ranjith PG	Key ideas, reviewing and editing the manuscript	N/A
Wei CH	Reviewing and editing the manuscript	N/A

The undersigned hereby certify that the above declaration correctly reflects the nature and extent of the candidate's and co-authors' contributions to this work*.

Candidate's signature	[redacted]	**Date** 25/01/2017
Main Supervisor's signature	[redacted]	**Date** 25/01/2017

*Note: Where the responsible author is not the candidate's main supervisor, the main supervisor should consult with the responsible author to agree on the respective contributions of the authors.

8. Investigation of carbon dioxide injection-induced methane recovery enhancement

8.1 Overview

CO_2 sequestration in deep unmineable coal seams with the simultaneous recovery of natural coal bed methane (CBM) or coal seam gas (CSG) is an appealing way of addressing the rise in atmospheric concentrations of anthropogenic CO_2. This technology has the potential to off-set the costs of capture, compression, transportation and storage of CO_2 by producing a comparatively eco-friendly fuel, CBM. Of the other options for the possible storage of CO_2, deep unmineable coal seams are more convenient sinks because they are widespread and exist in many of the same areas as large coal-fired power plants. Further, around 98% of CO_2 is in its adsorbed phase of the coal micropores which enables the stable storage of CO_2 for a geologically significant period. The higher affinity of CO_2 to desorb methane from the coal matrix has drawn more attention to enhanced CH_4 recovery from deep coal beds.

- **Section 8.2** – ***Applicability of CO_2 enhanced coal bed methane recovery technique to low rank coal***

To date, several studies have been conducted experimentally and numerically at a laboratory and field scale to investigate the potential of CO_2 to increase methane recovery. However, in these experimental studies, the primary focus has been on high rank coal rather than low rank due to the unlikely existence of low rank coal beds at potential locations for CO_2 storage. However, as discussed in Chapter 2, several researchers have highlighted potential low rank coal beds for CO_2 sequestration. Hence, it is important to conduct experiments on low rank coal as a prospective catalyst for CO_2-ECBM. This is therefore the subject of this section.

This section of the chapter is the following publication:

Ranathunga AS, Perera MSA, Ranjith PG, Wei CH (2017). An experimental investigation of applicability of the CO_2 enhanced coal bed methane recovery technique to low rank coal. *Fuel*, 189, 391-399.

- **Section 8.3** – ***Optimization of CO_2-enhanced coal bed methane recovery***

As stated in the research literature (refer to Chapter 2) and highlighted in Parts 2 and 3, the effectiveness of the CO_2-ECBM process is greatly dependent on the properties of the coal seam and the injecting gas. Therefore, it is important to investigate the optimum reservoir and injecting gas properties to harvest the greatest amount of CBM by sequestrating large amounts of CO_2. Numerical modelling tools can be used to reduce the complexity, cost and extensive time associated with laboratory and field experiments. Section 8.3 presents a numerical study conducted to optimize enhanced methane recovery using CO_2 for a typical low rank coal seam.

8.2 Applicability of CO_2 enhanced coal bed methane recovery technique to low rank coal

According to the findings reported in Parts 2 and 3, CO_2 adsorption has comparatively less influence on low rank coal in terms of strength and permeability reduction compared to high rank coal. Hence, it is interesting to investigate how low rank coal behaves during CO_2 injection-induced coal bed methane recovery enhancement and its applicability to this process. A series of CO_2 core flooding tests was carried out on methane-saturated meso-scale Victorian brown coal specimens. Different CO_2 injection pressures were selected, representing both sub- and super-critical CO_2, to observe how methane enhancement varies with CO_2 phase condition. The concentration of methane and the flow rates of the gas produced at downstream were monitored to quantify the CO_2 breakthrough and methane sweep efficiencies. As stated in Part 2, CO_2 adsorption-induced coal matrix swelling can considerably reduce the permeability of coal, which is one of the main drawbacks of this process. Further, desorption of methane from the coal matrix causes the coal sample to shrink. Hence, it is interesting to observe the variation of sample volumetric strain for each test condition to identify the coal sample behaviour during the CO_2-ECBM process. This study was conducted next.

This section of the chapter is the following publication:

Ranathunga AS, Perera MSA, Ranjith PG, Wei CH (2017). An experimental investigation of applicability of CO_2 enhanced coal bed methane recovery technique to low rank coal. *Fuel,* 189, 391-399.

Fuel 189 (2017) 391–399

Contents lists available at ScienceDirect

Fuel

journal homepage: www.elsevier.com/locate/fuel

Full Length Article

An experimental investigation of applicability of CO_2 enhanced coal bed methane recovery to low rank coal

A.S. Ranathunga [a], M.S.A. Perera [a,b,*], P.G. Ranjith [a], C.H. Wei [c]

[a] Deep Earth Energy Laboratory, Department of Civil Engineering, Monash University, Building 60, Melbourne, Victoria 3800, Australia
[b] Department of Infrastructure Engineering, The University of Melbourne, Building 176, Melbourne, Victoria 3010, Australia
[c] School of Resource and Civil Engineering, North-eastern University, Shenyang, China

ARTICLE INFO

Article history:
Received 18 August 2016
Received in revised form 25 October 2016
Accepted 26 October 2016
Available online 2 November 2016

Keywords:
Brown coal
CH_4 recovery
CO_2-ECBM
Core-flooding test
Sweep efficiency

ABSTRACT

Previous studies have shown that carbon dioxide (CO_2) injection can enhance CH_4 production (CO_2-ECBM) compared to traditionally-used methods, mainly due to the higher adsorptive capability of CO_2 in coal, which desorbs the CH_4 with higher sweep efficiency. Many studies have been conducted to date on the CO_2-ECBM technique for high rank coals. However, there have been very few studies on low rank coal. Therefore, this study uses Victorian brown coal samples to investigate the CO_2-ECBM potential of low rank coal. A series of CO_2 core flooding tests was conducted on CH_4 saturated meso-scale brown coal samples for various CO_2 injection conditions, phases and pressures.

According to the experimental findings, compared to natural recovery, CO_2 flooding enhances CH_4 production by creating higher production rates, and higher CO_2 pressures can drive the CH_4 towards the production end with almost 100% sweep efficiency. Furthermore, the rapid CO_2 breakthroughs observed under higher CO_2 pressures are found to be significant for super-critical CO_2. Tests results show that the superior competence of super-critical CO_2 in CH_4 recovery is independent of coal rank or maturity. However, the greater volumetric strain created by higher CO_2 pressures may, have a negative influence on long-term gas productivity with the reduction of flow ability through the seam.

8.2.1. Introduction

The discovery of new energy sources has become crucial with the rising consumption caused by the ever-increasing population. The present world energy demand is basically fulfilled by oil (35.7%), natural gas (25.6%), coal (19.3%), nuclear (9.9%), biofuels and waste (5.5%), hydro-power (2.3%) and others (geothermal, solar, wind, heat etc. 1.7%) [1]. In the last few decades, much attention has been given to natural gas production as a replacement for oil and coal to overcome the environmental issues caused by them. As a result, a 35% increase in natural gas production was seen from 1973 to 2014, with 32% and 15% reductions in oil and coal energy production [1]. Coal seam gas (CSG) or coal bed methane (CBM) is a natural gas, which provides around 6–9% of the current natural gas production [2]. CSG is formed during the coalification process and is trapped in the coal matrix. CSG consists mainly of methane (CH_4) (more than 90%) and is used as a low emission alternative for energy production.

The CSG adsorbed in coal seams is extracted primarily using the reservoir pressure depletion method of reducing the partial pressure of the species adsorbed into the coal mass, which eventually reverses the physical adsorption potential [3]. However, this method is not sufficiently efficient for economically-viable CSG production, as it can only extract around 50% of the gas-in-place [4] Further, the production of extensive amounts of saline water from coal seams (around 17,000 gallons/day) and the related environmental issues are a major concern with this method [5]. Therefore, several CSG production-enhancement techniques have been implemented in the field to mitigate reduced CSG production and the possible environmental impacts.

Fracturing of coal seams is a technique which is widely used for CSG flow enhancement in the field. However, the presence of active aquifers adjacent to the coal seam creates risks in using this technique and it is not economical for thin coal seams [6]. Enhanced coal bed methane (ECBM) recovery is being trialled for effective and economical production of CSG. ECBM recovery is accomplished by either inert gas stripping or displacement desorption methods [7,8] using nitrogen (N_2), carbon dioxide (CO_2), flue gas, compressor gas and other industrial off gasses as recovery agents [9].

* Corresponding author at: Department of Infrastructure Engineering, The University of Melbourne, Building 176, Melbourne, Victoria 3010, Australia.

E-mail address: samintha.perera@unimelb.edu.au (M.S.A. Perera).

http://dx.doi.org/10.1016/j.fuel.2016.10.116

- *Inert gas stripping:* The introduction of a low adsorbing gas at a constant pressure leads to the reduction of the partial pressure and results in enhanced CSG production [7]. N_2 is a low adsorbing agent and N_2-ECBM can recover up to 90% of gas-in-place [10].
- *Displacement desorption:* The CSG adsorbed in the coal mass is recovered by injecting a gas with higher adsorption capacity [8]. The higher affinity of CO_2 to the coal mass than pre-adsorbed CH_4 warrants the greater use of CO_2 for ECBM recovery. Generally, it is assumed that at least 2 mol of CH_4 are adsorbed into the coal matrix for every 1 mol of CH_4 desorbed [9].

Of these two methods, displacement desorption using CO_2 has attracted attention due to the advantages of this method. The most important benefit is the ability to stably store large amounts of anthropogenic CO_2 in deep coal seams, because more than 95% of the CO_2 is in its adsorbed phase in coal seams [9]. The larger surface area in coal seams provides the potential to store substantial amounts of CO_2 in the coal seams (around 11.2 gigatons of CO_2 in the combined Bowen and Sydney basins) [9]. Hence, the adoption of the CO_2-ECBM technique will help to reduce global warming. However, previous studies have found some disadvantages of the CO_2-ECBM technique due to the associated physical and chemical changes which occur in the seam upon CO_2 adsorption. *Coal matrix swelling* is the main drawback, in which large strains are developed between the adsorbed CO_2 layer and the surface of the pore walls in the coal matrix during CO_2 adsorption. This matrix swelling causes reduced pore spaces by rearranging the matrix, which eventually causes a reduction of flow-ability [11–19] and coal mass strength [20–24]. Field CO_2-ECBM studies [9,25–27] have experienced the reduction of CO_2 injectivity upon coal matrix swelling within the first 6 months to 2 years of CO_2 injection. Hence, further research is needed to investigate CSG recovery by CO_2 sequestration. To date, many studies have been conducted on the CO_2-ECBM process and associated issues. Table 1 summarises some of the core-flooding experimental studies conducted on methane recovery by CO_2 sequestration using intact samples.

According to Table 1, it is evident that the use of CO_2 increases CH_4 production with a sweep efficiency greater than 90%. Furthermore, compared to CO_2, N_2 has an early breakthrough and interestingly, N_2 permits a moderate increase in permeability, unlike CO_2 which causes a reduction [28]. In addition, the sweep efficiency of flue gas (a mixture of CO_2 and N_2) is much lower than that of CO_2. Nevertheless, the higher the percentage of CO_2 in flue gas, the greater the CH_4 recovery [29]. Several researchers have conducted CO_2-ECBM studies using wet coal and found that the moisture present in a coal mass disrupts the CO_2/CH_4 exchange (see Table 1).

Potential coal seams for CO_2-ECBM are located at great depths, at which CO_2 is in its super-critical state due to the higher pressures and temperatures [9]. Wolf et al. [30] conducted several CO_2/CH_4 experiments on high rank coal, considering different phase effects of CO_2 (gas/liquid/super-critical). These researchers used a constant CO_2 injection rate under varying pore pressures to achieve the different phase conditions of CO_2. According to their findings, the CH_4 sweep efficiencies for both gaseous (52%) and liquid phase (48%) CO_2 are similar (see Table 1). In the case of super-critical CO_2, although a similar behaviour to liquid CO_2 may initially be seen, after an apparent breakthrough, super-critical CO_2 exhibits an improved exchange with CH_4 with higher sweep efficiencies [30].

However, almost all the CO_2-ECBM studies have been conducted on high rank coal specimens, due to the existence at unmineable depths and higher concentrations of CH_4-in-place. To date, much less attention has been given to CO_2/CH_4 exchange in brown coal, in particular Australian brown coal. The unlikely existence of brown coal in deep geological formations where geo-sequestration is considered workable is the main concern. According to Garduno et al. [36], the Jackson, Yegua and Wilcox formation in Texas has deep lignite formations (800–3800 ft from the standard sea level (SSL)) with CO_2-ECBM potential, and Hernandez et al. [37] stated that the close proximity of many CO_2 point sources near these potential Texas low rank coals generates attractive economic conditions. Further, recent surveys conducted by the Cooperative Research Centre for Greenhouse Gas Technologies (CO2CRC) have confirmed the presence of brown coal seams at unmineable depths (400–800 m), which can be used for the purpose of geo-sequestration in the offshore Gippsland Basin, in Victoria, Australia [13,38]. The main objective of this study is therefore to investigate the potential of the enhanced recovery of CH_4 in the presence of CO_2 in brown coal.

8.2.2. Experimental methodology

8.2.2.1. Samples used

Core-flooding experiments were conducted using brown coal samples from the Hazelwood coal mine, located at Morwell in South Gippsland, Victoria, Australia. Fig. 1(a) gives the energy dispersive X-ray spectroscopy (EDS) elements composition of the brown coal samples used for the study. Victorian brown coal has various pore structures with a wide range of sizes, comprising macro-pores (>50 nm in diameter), meso-pores (2–50 nm), micro-pores (0.4–2 nm) and sub micro-pores (<0.4 nm). The smaller pores are accountable for the large surface areas of Victorian brown coal (often exceeding 200 m^2/g) while larger pores contribute to the pore volume and porosity [39]. The experimental sorption data and the corresponding best fit Langmuir sorption isotherms for CO_2 and CH_4 (at 40 °C temperature) are shown in Fig. 1 (b) for the Victorian brown coal samples used (here both the samples used by Jasinge et al. [13] and the present work have almost similar chemical and microscopical properties). For the present study, samples of 38 mm in diameter and 80 mm in height were used, which were obtained from the same coal block. Dry samples were used for the experiments to avoid the effect of moisture and they were vacuumed to remove the residual gases present in the samples.

8.2.2.2. Experimental procedure

a. Core flooding tests for CH_4

Fig. 2 shows a schematic diagram of the experimental set-up used for the core-flooding tests. A detailed explanation of the set-up can be found in Ranjith and Perera [40]. The set-up consists of a tri-axial cell, which was used to apply the pressures and temperatures at reservoir conditions. For the current study, 11 MPa confining pressure was used under a constant temperature of 40 °C. Here, 11 MPa confining pressure was selected to represent a coal seam at a depth of around 400 m. First the specimen was pressurised with CH_4 (5 MPa) until the sample reached equilibrium. Next, the downstream flow rate was observed to find the CH_4 production under natural conditions without any injection at upstream. The CH_4 displacement tests were then started by injecting CO_2 at a constant pressure after equilibrating with CH_4. The test was continued until a steady state was achieved in upstream and downstream. The downstream flow was measured using a milli-gas counter and the downstream gas concentration was confirmed using a CO_2/CH_4 infrared gas sensor. This procedure was continued for all other CO_2 flooding tests (6, 7, 8 and 9 MPa) to observe the CO_2/CH_4 exchange patterns in brown coal. Here, 5, 6 and 7 MPa

Table 1
Previous experimental studies on CO_2-ECBM.

Sample information		Test conditions	Key findings	Reference
Basin Coal rank Sample size	Pricetown mine, West Virginia Not given 8.89 cm (dia.) or 9.555 cm (dia.) with varying lengths (5.08–10.16 cm) stacked up to 29.21 cm (approx.)	– Single-state CO_2 injection with CO_2 pressures from 0.34 MPa to 1.41 MPa – Multi-cycle CO_2 injection using CO_2 pressures 0.34 MPa and 0.7 MPa	– Recovery efficiency was increased from 36% to 132% when CO_2 pressure was increased from 0.34 to 1.41 MPa – Cyclic CO_2 injection is capable of completely removing adsorbed CH_4 and significant quantities of CO_2 remain adsorbed after cyclic injection. (e.g. around 98% and 90% injected CO_2 remained after 0.34 MPa and 0.7 MPa cyclic CO_2 injection, respectively)	Fulton et al. [31]
Basin Coal rank Sample size	Pricetown mine, West Virginia Not given 8.89 cm (dia.) or 9.555 cm (dia.) with varying lengths (5.08–10.16 cm) stacked up to 29.21 cm (approx.)	– Single-state CO_2 injection with CO_2 pressures from 1.38 MPa to 5.52 MPa and multi-cycle CO_2 injection using CO_2 pressure of 5.56 MPa for all the process pressures – Flue gas injection with pressures from 1.34 to 5.56 MPa using 9 injection cycles	– Around 30% of gas-in-place is produced by the primary method and this value may increase slightly for deeper coal seams – 3.45–5.56 MPa CO_2 injection could completely desorb all the gas-in-place by cyclic injection and would be a safer way to demethanate coal seams before mining – None of the N_2 was adsorbed by the coal in the presence of CO_2 and the recovery of CH_4 was comparatively reduced during flue gas injection (e.g. the sweep efficiency for CO_2 injection is around 90% while that for flue gas injection is 57% where total injection pressure is 5.56 MPa)	Reznik et al. [32]
Basin Coal rank Sample size	Beringen coal mines in Belgium and Anlage Westfalen mine in German R_{max} of coal specimens: Beringen coal – 0.78% German coal – 1.15% 72 mm diameter and 250 mm in length	– Five different test conditions were adopted: • Dry coal + CO_2 gas • Water wet coal + CO_2 gas • Dry coal + CO_2 liquid • Water wet coal + CO_2 liquid • Water wet coal + CO_2 super-critical	– Dry coal has a higher sweep efficiency than wet coal – Both gas and liquid phase CO_2 injection show similar CH_4 sweep efficiencies – Initially both liquid and super-critical CO_2 act similarly, then after an apparent breakthrough (around 92% in volume) it slowly improves in replacement of water and CH_4 – Super-critical CO_2 can achieve higher sweep efficiencies	Wolf et al. [30]
Basin Coal rank Sample size	Powder River basin, USA Not given 42.5 mm diameter and 250 mm in length	– Adsorption/desorption isotherms for CO_2, CH_4 and N_2 – Five CH_4 displacement tests at 4.14 MPa pressure: • 100% N_2 • 100% CO_2 • 85/15% CO_2/N_2 • 46/54% CO_2/N_2 • 24/76% CO_2/N_2	– Adsorption capacity is 1:1/3:1/7 for CO_2:CH_4:N_2 respectively – CO_2 breakthrough time is large due to the piston-like flow through the coal mass – N_2 shows a more displaced front by advancing rapidly	Jessen et al. [33]
Basin Coal rank Sample size	Beringen coal mines in Belgium, the Silezia coalfield in Poland and the Tupton coalfields in UK R_{max} of coal specimens: Beringen coal – 0.78% Silezia coal – 0.68% Tupton coal – 0.53% 69.5 and 75 mm diameter and 178.3–334 mm in length	– Effect of differential swelling on fracture porosity and permeability of coal for 4.3–22.85 MPa mean pore pressures of wet and dry coal specimens using CO_2 and flue gas (CO_2 – 1, 50 and 90%)	– Moisture in the coal mass obstructs the CO_2/CH_4 exchange process – Sweep efficiencies of the experiments with flue gas were less compared to CO_2 flooding for similar conditions – The higher the CO_2 percentage in the flue gas the greater the sweep efficiency	Mazumder and Wolf [29]
Basin Coal rank Sample size	Bowen basin, Australia High rank 60.6 mm diameter and 114 mm in length	– Binary experiments CH_4/N_2 for 2 and 10 MPa – Ternary experiments CH_4/(90% N_2 + 10% CO_2) for 2 and 10 MPa	– Earlier N_2 breakthrough compared to CH_4, hence N_2 displacing CH_4 sweep efficiency is lower than CH_4 displacing N_2	Connell et al. [34]
Basin Coal rank Sample size	Duanshi coal mine, China High rank 37.8 mm in diameter and 76.8 mm in length	– Binary experiments CH_4/N_2 and CH_4/CO_2 – 3.6 MPa back-pressure under 9.7 MPa confining pressure used to saturate samples with CH_4 – A water rate of 1.152×10^{-4} m^3/day was used to inject CO_2 and N_2 into the coal specimen	– Compared to CO_2, N_2 breaks through earlier – The compositional adsorption amounts for N_2-ECBM are better than those for CO_2-ECBM – N_2 injection causes a moderate increase in coal permeability, while CO_2 injection causes significant permeability reduction	Zhou et al. [28]
Basin Coal rank Sample size	Bowen basin and Hunter Valley basin, Australia High rank Bowen basin sample: 60.6 mm in diameter and 114 mm in length Hunter Valley basin sample: 60.85 mm in diameter and 126.3 mm in length	– Binary experiments CH_4/CO_2 for 4 and 10 MPa	– Permeability is increased when CO_2 displaces CH_4 – The sweep efficiency is almost 100% for CO_2 displacing CH_4 and is less when CH_4 displaces CO_2	Sander et al. [35]

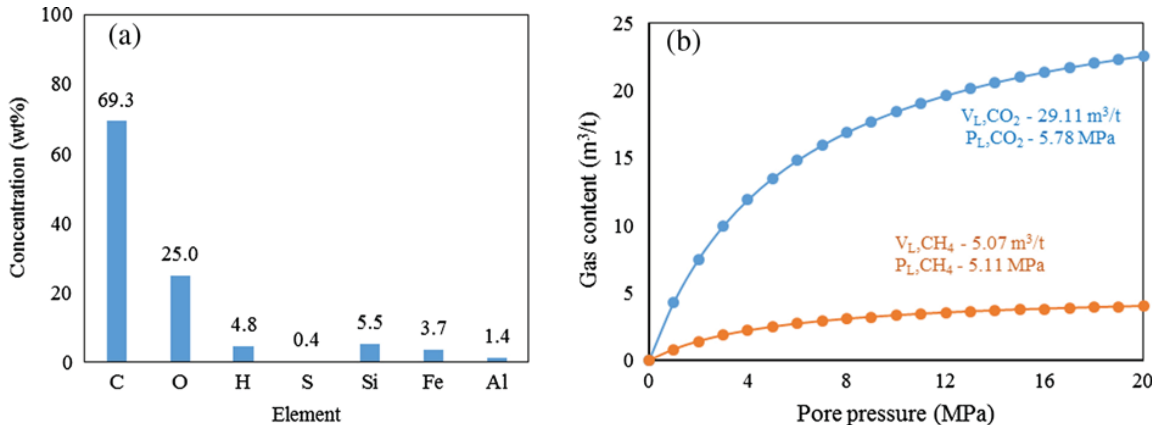

Fig. 1. (a) EDS analysis and (b) best fit Langmuir isotherms for CO_2 and CH_4 [13] for brown coal samples used.

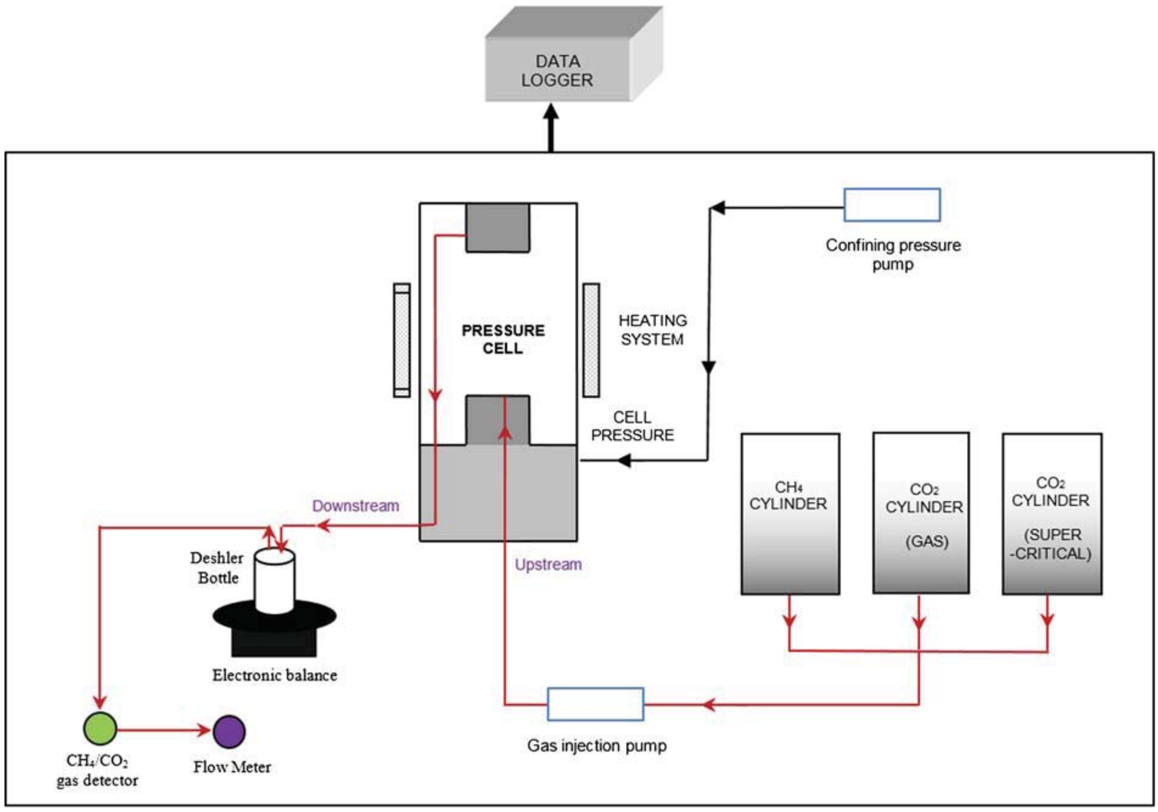

Fig. 2. Schematic diagram of the experimental set-up used for core flooding tests.

CO_2 flood represent gaseous CO_2 and 8 and 9 MPa CO_2 flood represent super-critical CO_2 (greater than critical pressure 7.38 MPa and temperature 31.8 °C of CO_2) (see Fig. 3).

b. Measuring coal mass volumetric changes

During the complete test sequence, the volumetric strain of the coal sample was recorded using an advanced data acquisition system at 1 s intervals to quantify the CO_2 adsorption-induced coal matrix swelling and CH_4 desorption-induced coal matrix shrinkage of the brown coal specimen. The volumetric strain was calculated considering the volume change of the syringe pump (see Eq. (1)) used to apply confining pressure. When the sample is subjected to swelling, the excess oil volume inside the cell is pumped out into the syringe pump, increasing the existing pump oil volume, while oil is pumped out to the cell from the syringe pump when the sample is shrunk, reducing the oil volume of the pump. Eq. (1) was used to calculate the volumetric strain of the coal specimen during various injection conditions:

$$\text{Volumetric strain of the sample } (S_v) = \left(\frac{\pm \Delta V_x}{V_{initial}}\right) \times 100\%; \quad \Delta V_x = V_{initial} - V_t \tag{1}$$

where $V_{initial}$ is the initial pump volume during the respective test condition, V_t is the pump volume at time, t and ΔV_x is the oil volume

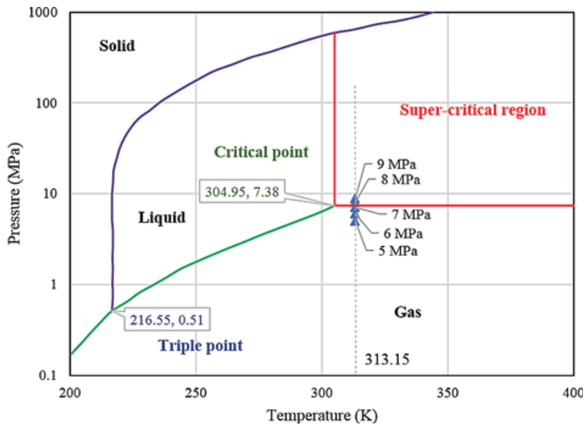

Fig. 3. CO_2 phase diagram (triangular bullet points denote the pressures used for the present study).

change (pumped in or out of the syringe pump). For the strain calculation, initial pump volume ($V_{initial}$) was taken only after the pump oil volume became stable after the application of confining pressure (upon completion of sample shrinkage due to confining pressure) and the CH_4 saturation. Hence, the volumetric strain values obtained from this Eq. (1) were only due to the sample volume changes caused by the adsorption or desorption of gases.

8.2.3. Results and discussion

A series of CO_2 flooding tests was conducted, representing different CO_2 phase conditions (gas and super-critical) to observe the CH_4 displacement of brown coal, and the results obtained are discussed in the following sections.

8.2.3.1. CH_4 displacement with CO_2 flood

a. Gas production from the coal matrix

The experimental flow rates obtained for natural CH_4 displacement under different CO_2 floods are presented in Fig. 4. According to the figure, CH_4 desorbs at a comparatively very slow rate during natural recovery, and the production rate becomes steady at 0.0008 m^3/d after around 13.5 days. In contrast, CO_2 flooding enhances the CH_4 displacement from the coal matrix and higher CO_2 injection pressures facilitate higher CH_4 production. For example, 0.0019 m^3/d and 0.0025 m^3/d steady production rates were obtained for 5 MPa CO_2 flood within 3.4 days and for 8 MPa CO_2 within 2.1 days. This increment is more than twice the natural steady production rate for 5 MPa sub-critical CO_2 injection, and more than three times the natural production rate for 8 MPa super-critical CO_2. Further, each CO_2 injection causes an increasing gas outflow gradient of around 0.0007 (5 MPa), 0.0009 (6 MPa), 0.0011 (7 MPa), 0.0014 (8 MPa) and 0.0019 (9 MPa) over time, before reaching the steady state (see Fig. 4). The larger CO_2 volume entering the coal mass at higher injection pressures is the reason for this higher gas production rate. Similar behaviour has been witnessed by Sander et al. [35] for high rank coal and these researchers observed around 0.003 and 0.008 gas outflow increasing gradients at 4 and 10 MPa CO_2 injection pressures over time, respectively. Interestingly, this increment is higher for super-critical CO_2 flooding compared to gaseous CO_2 flooding. Around 20% increase in gas outflow was observed from 5 to 6 MPa gaseous CO_2 injection, while that for 8–9 MPa was around 40%. The higher adsorption potential of super-critical CO_2 with its inherent greater viscosities and densities compared to gaseous CO_2 [23] may be the reason for these improved gas production rates at higher injection pressures, by displacing larger amounts of CH_4 from coal matrix. The greater penetration ability of super-critical CO_2 compared to liquid CO_2 due to reduced viscosity characteristics may offer greater CH_4 replacement potential for tiny pores.

The CO_2 injection rates at upstream during gas production are detailed in Table 2. According to the table, all the CO_2 floods have higher injection rates at the start and reduce to a constant injection rate over time. This initial injection rate and the constant injection rates increase with increasing injection pressure. It should be noted that, during this study, CO_2 injection pressure was kept constant and hence the inflow rates were varied accordingly to obtain the prescribed pressures. These enhanced injection rates also contributed to the observed increased gas production rates with increasing CO_2 injection pressures. Similar results were observed by Sander et al. [35] for high rank coal which observed an injection rate of 0.009 m^3/d which became constant at 0.0055 m^3/d for 4 MPa CO_2 flow and 0.025 m^3/d injection rate, which reached to a constant at 0.013 m^3/d for 10 MPa CO_2 flow. Therefore, these observed injection pressure variations are common for any coal type.

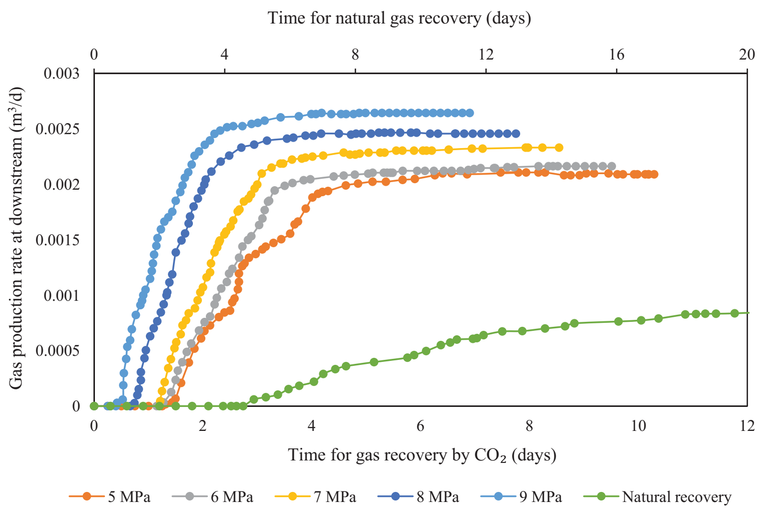

Fig. 4. Observed gas production rate at downstream with natural recovery and CO_2-enhanced methane recovery.

Table 2
CO_2 injection rates at upstream for different CO_2 floods.

CO_2 injection pressure (MPa)	Initial injection rate (m^3/d)	Constant injection rate (m^3/d)
5	0.0046	0.0019
6	0.0055	0.0020
7	0.0061	0.0022
8	0.0073	0.0025
9	0.0082	0.0028

b. CO_2 breakthrough during CH_4/CO_2 exchange

The time taken for CO_2 breakthrough varies with different CO_2 injections (see Fig. 5), and for 5, 6, 7, 8 and 9 MPa CO_2 injection pressures, it took around 1.25, 1.19, 1.10, 0.65 and 0.4 days, respectively for CO_2 breakthroughs to occur. As explained previously, a larger volume of CO_2 entering the coal mass at higher injection pressures may act as a driving force to adsorbed gases in the coal matrix for quicker displacement, and greater super-critical CO_2 penetration ability into pores may further enhance the effect. Similar results have been observed for high rank coal by Sander et al. [35], who found that it took around 0.8 and 0.5 days for 4 and 10 MPa CO_2 floods, respectively to have a CO_2 breakthrough. Interestingly, these breakthrough times for super-critical CO_2 are lower than those for gaseous CO_2. As mentioned before, only 0.4 days were required for 9 MPa CO_2 flood to break through the coal matrix, while it took around 1.25 days for 5 MPa gaseous CO_2. As explained before, the enhanced ability of super-critical CO_2 to adsorb into the coal matrix [11] caused this shorter breakthrough time with super-critical CO_2 flood. Therefore, higher CO_2 injections can break through rapidly and desorb CH_4 from the coal mass. Hence, super-critical CO_2 floods can facilitate higher CH_4 production rates in field conditions for any coal rank. However, this quicker CO_2 breakthrough at high injection pressures can result in early CO_2 outflow at downstream with CH_4 production. Therefore, in the course of this study, the downstream gas composition was observed and recorded to determine the CO_2 flow along the specimen during CH_4/CO_2 exchange.

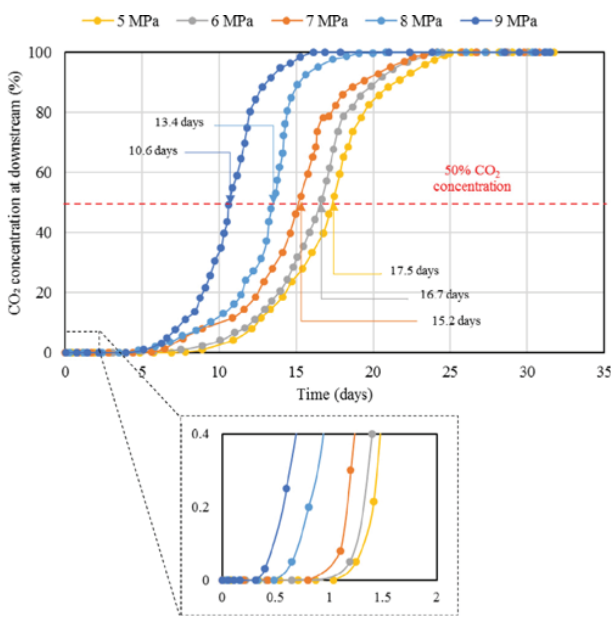

Fig. 5. CO_2 concentration of produced gas at downstream for different CO_2 floods.

Fig. 5 shows the CO_2 concentration (in percentages) at downstream for different CO_2 floods. As shown in the figure, the CO_2 concentration vary in an "S" over time. At first the concentration remained 0% for few days and then it progressively started to increase up to 7–15 days and then gradually became 100% at the end. Although this pattern is similar for all the CO_2 floods, the time before CO_2 is observed at downstream is less for higher injection pressures. For example, the times taken for CO_2 production under 5 and 9 MPa injection pressure are around 8 and 3.5 days, respectively. According to the results, the times taken to have 50% CO_2 in the gas produced under 5 and 9 MPa injections pressures are around 17.5 and 10.6 days, respectively. According to previous sections, higher CO_2 injection pressures have greater capability to break through the coal matrix by releasing CH_4 at higher production rates (see Fig. 4). Hence, early CO_2 release at the downstream can be witnessed and is higher for super-critical CO_2. This observation is important for field-scale projects, as super-critical CO_2 can break through the coal matrix easily and quickly while driving more CH_4 molecules towards the production end. Further, this behaviour of super-critical CO_2 leads to a larger transition zone from CH_4 saturated to CO_2 saturated coal mass under field conditions.

8.2.3.2.Methane sweep efficiency

Next, the mass balance of each core flooding test was calculated by using the cumulative inflow and outflow measurements and the results are presented in Table 3. As stated in the table, the natural recovery of CH_4 could only afford for a 46% sweep efficiency while CO_2 flood has a higher efficiency of desorbing CH_4 from coal mass with an average of 97% sweep efficiency. Further, this sweep efficiency is higher for super-critical CO_2 injection than for gaseous CO_2 flow. For example, around 93% efficiency was observed for 5 MPa CO_2 flood while it was 100% for 9 MPa CO_2 injection. This sweep efficiency value further confirms the higher affinity of super-critical CO_2 to adsorb into the coal mass by desorbing the pre-adsorbed CH_4 from the coal matrix.

Similar results have been observed by Sander et al. [35] for high rank coal (dry), which showed a 99.2% efficiency for 4 MPa CO_2 flood displacing CH_4 and 100% efficiency for 10 MPa CO_2 flood displacing CH_4. Moreover, Wolf et al. [30] used water-saturated high rank coal samples to investigate the effect of CO_2 phase on CH_4 recovery. They injected CO_2 at a constant flow rate of 9.4E−6 mol/h for each test and with varying pore pressure to obtain different phases of CO_2. According to their results, gaseous CO_2 flood through water wet coal has around 26% sweep efficiency, where super-critical CO_2 flood has an efficiency of around 40%. Hence, both gaseous and super-critical CO_2 desorb CH_4 in dry coal at higher sweep efficiencies. The adsorptive nature of super-critical CO_2 may result in this greater sweep efficiency compared to gaseous CO_2 and this is common for any coal type according to this study. Coal with moisture also exhibits a similar behaviour to dry coal; however, it has comparatively much lower efficiency in displacing CH_4. This is because the hydrophilicity of coal obstructs the CO_2 entrance into the matrix pores; hence CO_2 need to remove both water and CH_4 from the pores for adsorption, which leads to lower sweep efficiencies [30,41].

8.2.3.3. Brown coal volumetric deformation with CO_2 adsorption and CH_4 desorption

The flow ability along the coal specimen is varied by the CH_4 desorption and CO_2 adsorption processes, because CH_4 desorption from the coal matrix causes the coal matrix to shrink while CO_2 adsorption into the coal matrix causes it to swell. Hence, it is important to identify how the variable sorption affects gas produc-

Table 3
Calculated mass balance for CH_4/CO_2 core flooding tests.

CO_2 injection pressure (MPa)	Initial gas content in the coal sample (m^3/t)		Final gas content in the coal sample (m^3/t)		Sweep efficiency (%)
	CH_4	CO_2	CH_4	CO_2	
–	2.8	–	1.5	–	46.4
5	2.9	0.0	0.2	13.5	93.1
6	2.8	0.0	0.1	14.8	96.4
7	2.9	0.0	0.1	15.9	96.6
8	2.7	0.0	0.0	16.9	100.0
9	2.8	0.0	0.0	17.7	100.0

tion from the coal mass. Fig. 6 illustrates the gas production variation with the measured volumetric strain of the specimen. Natural recovery of gas causes a gradual increment in volumetric shrinkage over time, and the trend is similar to the gas production trend (see Fig. 6(a)). When an already adsorbed gas is removed from the pores, the specimen may undergo shrinkage [29,34,35,42], and this observation explains the effect of CH_4 desorption from the coal matrix. At the end of gas production, it shows around 0.84% volumetric strain reduction.

In relation to the CO_2 flood, all the CO_2 injections show a similar behaviour of volumetric strain, shrinkage at the beginning followed by coal mass swelling. The coal specimen does not start to swell immediately upon CO_2 injection, as it takes some time to develop considerable swelling upon CO_2 adsorption. However,

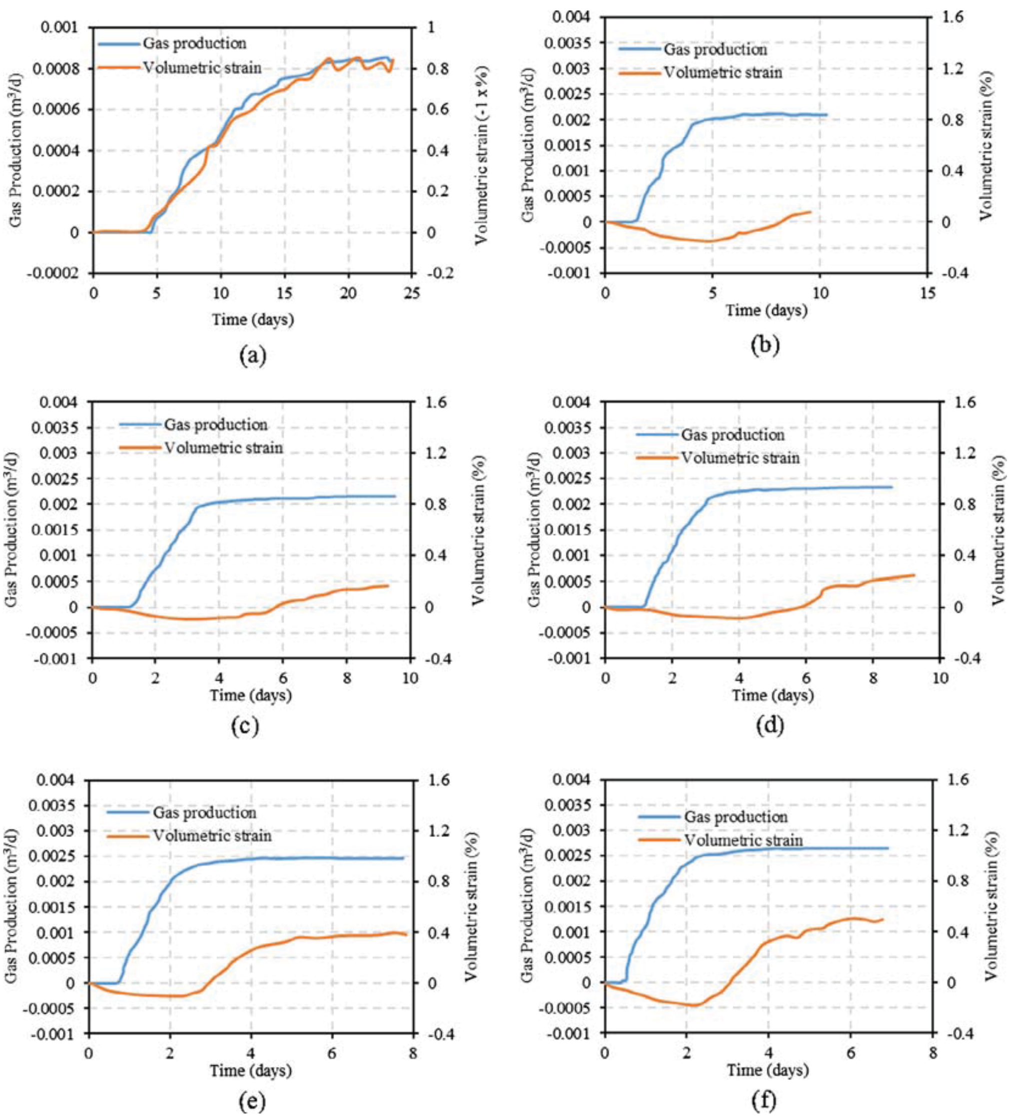

Fig. 6. Gas production variation with volumetric strain for (a) natural production, (b) 5 MPa, (c) 6 MPa, (d) 7 MPa, (e) 8 MPa and (f) 9 MPa CO_2 floods (note: negative strains are shrinkage and positive strains are swelling).

the methane desorption starts as soon as CO_2 reaches the matrix, shrinking the coal mass. Table 4 further demonstrates the volumetric strain behaviour during CO_2 injection. According to the table, volumetric strain with gas production is increased with increasing CO_2 injection pressure, meaning that the swelling increases with increasing CO_2 injection pressure. As Day et al., [11] have shown, coal matrix swelling in coal upon CO_2 exposure is greater at elevated pressures. A similar concept applies in the CO_2-ECBM experiments: for example, compared to 5 MPa CO_2 (gaseous), 9 MPa CO_2 (super-critical) flood caused a swelling increment of more than 500%. Similar results were observed for high rank coal by Mazumder and Wolf [29], who found around 0.0017 and 0.0035 linear strain increment (swelling) for gaseous to super-critical CO_2 flood while injecting CO_2 at a constant rate of 0.7 ml/h.

In addition, the minimum volumetric strain or maximum shrinkage also increases with increasing CO_2 injection pressure. From 5 to 9 MPa CO_2 injection, around 125% increment in shrinkage was observed. Interestingly, the time taken for the sample to initiate swelling is reduced with injection pressure and this reduction is higher at higher injection pressures. For example, around 62% of time reduction is observed when the CO_2 flood is raised from 5 to 9 MPa. The reason for these behaviours can be explained by considering Fig. 6(b)–(f). As depicted in the figures, gas production rate is increased with increasing injection pressure. Hence, higher CH_4 removal rate in the coal mass causes the sample volume reduction to be accelerated, with the associated desorption of CH_4 causing larger shrinkage. Next, the high pressure CO_2 molecules with higher adsorption capacity start to penetrate through the coal pores, leading to sample volume increment.

8.2.4. Implications for field-scale projects and recommendations for future research

The present study was conducted to investigate the possibility of using CO_2-ECBM in low rank coal. According to the results, CO_2 greatly enhances CH_4 production, which is greater at higher injection pressures, particularly in its super-critical state. As suitable coal seams for CO_2-ECBM favour super-critical CO_2 at their respective depths, the greater potential of super-critical CO_2 for augmenting CH_4 recovery is beneficial. Furthermore, higher CO_2 pressures are quicker in exchanging CH_4 to CO_2 and this behaviour of super-critical CO_2 leads to a larger transition zone from CH_4 saturated to CO_2 saturated coal mass under field conditions, which will drive the recovered CH_4 to the production wells. At the same time, this super-critical CO_2 causes higher coal mass swelling with CH_4 production. As explained in Section 8.2.1, this swelling reduces the flow ability of coal, which eventually disrupts both CO_2 injec-tion and CH_4 production. Therefore, N_2 has been used by several researchers and in field projects in a mixture with CO_2 to enhance gas recovery. N_2 is a comparatively less adsorbent gas than CO_2 which acts as a swelling recovery agent [9,43] while reducing the partial pressure of the coal reservoir for higher production of CH_4 while storing a larger amount of CO_2. Several studies have been conducted using flue gas for CH_4 recovery for high rank coal and few studies have been conducted using low rank coal. Hence, it is recommended to perform studies using flue gas to enhance CH_4 recovery for low rank coal.

In addition, the presence of water results in higher reductions in sweep efficiency for both gaseous and super-critical CO_2 floods (refer to Section 8.2.3.2). Generally, coal becomes more hydrophilic with decreasing rank and carbon content, and with increasing oxygen-containing groups [41]. Victorian brown coal is a low rank coal with a lower carbon content (69%, see Fig. 1(a)) and has around 55–60% moisture content [24]. Therefore, it is vital to study the effect of moisture on CH_4/CO_2 exchange in brown coal for a bet-ter understanding of the potential of coal as a catalyst for CO_2-ECBM projects, particularly for low rank coal like brown coal.

The current study was conducted on a meso-scale specimen 38 mm in diameter and 80 mm long). To better relate CO_2 adsorption and CH_4 recovery, larger scale (macro- and reservoir-scale) studies are essential. The findings of this investigation can be used as a platform to implement reservoir-scale studies to determine the effect of various effective factors, such as higher CO_2 pressures, different depths and different temperatures, and to extend knowledge about CO_2-ECBM recovery in low rank coal.

Table 4
Volumetric strain behaviour during CO_2 flood.

CO_2 injection pressure (MPa)	Time taken for the sample to start swelling, *a* (days)	Minimum volumetric strain (shrinkage) (%)	Volumetric strain at the end of gas production (%)
5	8.2	−0.08	0.08
6	6.1	−0.10	0.16
7	5.4	−0.11	0.24
8	3.3	−0.13	0.39
9	3.1	−0.18	0.51

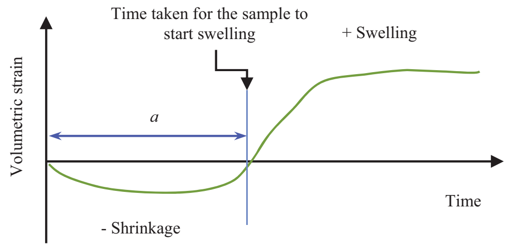

8.2.5. Conclusions

The applicability of CO_2-ECBM to low rank coal was investigated in this study using low rank Victorian brown coal (dry), and the following major conclusions can be drawn:

- Compared to natural recovery, CO_2 flooding can significantly enhance coal sema CH_4 production.
- Higher CO_2 inflows can drive the CH_4 competently towards the production end with almost 100% sweep efficiency with rapid CO_2 breakthrough, and the effect is much greater for super-critical CO_2. This creates a larger transition zone from a CH_4 saturated to a CO_2 saturated coal mass in the field, which more easily drives the recovered CH_4 towards the production wells.
- The effectiveness of super-critical CO_2 in CH_4 recovery is independent of coal seam maturity or rank.
- However, the greater coal matrix swelling which occurs in coal under higher CO_2 injection pressures may negatively affect long-term gas production through the reduction of the seam's flow ability.

8.2.6. Acknowledgements

The authors acknowledge the use of facilities in the Monash Centre of Electron Microscopy (MCEM) and the funding provided by the Australian Research Council (DE130100124).

8.2.7. References

[1] International Energy Agency (IEA). Key World Energy Statistics, Paris. (<https://www.iea.org/publications/freepublications/publication/KeyWorld_Statistics_2015.pdf>); 2015, p. 5–9.
[2] Energy Information Administration (EIA). Annual energy outlook 2015. Washington, USA: Energy Information Administration; 2015. p. 13–5. http://www.eia.gov/forecasts/aeo/pdf/0383(2015).pdf.

[3] Metcalfe R, Yee D, Seidle J, Puri R. Review of research efforts in coalbed methane recovery, Society of Petroleum Engineers (SPE) Asia-Pacific Conference. In: Society of Petroleum Engineers (SPE) Asia-Pacific Conference, Perth, Australia, 1991. p. 727–40.
[4] Gale J, Freund P. Coal-bed methane enhancement with CO_2 sequestration: worldwide potential. Environ Geosci 2001;8:210–7.
[5] Williams J, Stubbs T, Milligan A. An analysis of coal seam gas production and natural resource management in Australia. A report prepared for the Australian Council of Environmental Deans and Directors by John Williams Scientific Services Pty Ltd, Canberra, Australia. <https://aie.org.au/AIE/Documents/Oil_Gas_121114.pdf>; 2012.
[6] Ranathunga AS, Perera MSA, Ranjith PG. Deep coal seams as a greener energy source: a review. J Geophys Eng 2014;11:1–17.
[7] Ruthven DM. Principles of adsorption and adsorption processes. NY, USA: John Wiley & Sons; 1984. p. 336–75.
[8] Yang RT. Gas separation by adsorption processes. MA, USA: Butterworth Publishers; 2013. p. 141–93.
[9] White CM, Smith DH, Jones KL, Goodman AL, Jikich SA, LaCount RB, et al. Sequestration of carbon dioxide in coal with enhanced coalbed methane recovery: a review. Energy Fuels 2005;19:659–724.
[10] Puri R, Yee D, Buxton TS, Majahan O. Method of increasing the permeability of a coal seam. U.S. Patent No. 5,014,788; 1991.
[11] Day S, Fry R, Sakurovs R. Swelling of Australian coals in supercritical CO_2. Int J Coal Geol 2008;74:41–52.
[12] Durucan S, Shi JQ. Improving the CO_2 well injectivity and enhanced coalbed methane production performance in coal seams. Int J Coal Geol 2009;77:214–21.
[13] Jasinge D. An investigation of the effect of carbon dioxide sequestration on the behaviour of brown coal (PhD thesis). Melbourne, Australia: Monash University; 2010.
[14] Liu J, Chen Z, Elsworth D, Miao X, Mao X. Evaluation of stress-controlled coal swelling processes. Int J Coal Geol 2010;83:446–55.
[15] Pan Z, Connell LD, Camilleri M. Laboratory characterisation of coal reservoir permeability for primary and enhanced coalbed methane recovery. Int J Coal Geol 2010;2:252–61.
[16] Perera MSA, Ranjith PG, Airey DW, Choi SK. Sub- and super-critical carbon dioxide flow behavior in naturally fractured black coal: an experimental study. Fuel 2011;90:3390–7.
[17] Siriwardane H, Haljasmaa I, McLendon R, Irdi G, Soong Y, Bromhal G. Influence of carbon dioxide on coal permeability determined by pressure transient methods. Int J Coal Geol 2009;77:109–18.
[18] Vishal V, Singh TN. A laboratory investigation of permeability of coal to supercritical CO_2. Geotech Geol Eng 2015;33:1009–16.
[19] Ranathunga AS, Perera MSA, Ranjith PG, Ju Y, Vishal V, De Silva PNK. A macro-scale experimental study of sub-and super-critical CO_2 flow behaviour in Victorian brown coal. Fuel 2015;158:864–73.
[20] Aziz NI, Ming-Li W. The effect of sorbed gas on the strength of coal – an experimental study. Geotech Geol Eng 1999;17:387–402.
[21] Czapliński A, Hołda S. Changes in mechanical properties of coal due to sorption of carbon dioxide vapour. Fuel 1982;61:1281–2.
[22] Lama R. Errors in gas content measurements in underground sampling of coal using cores. In: International symposium-cum-workshop on management and control of high gas emissions and outbursts in underground coal mines, Wollongong, Australia, 1995. p. 557–67.
[23] Perera MSA, Ranathunga AS, Ranjith PG. Effect of coal rank on various fluid saturations creating mechanical property alterations using Australian coals. Energies 2016;9:440.
[24] Ranathunga AS, Perera MSA, Ranjith PG, Bui H. Super-critical CO_2 saturation-induced mechanical property alterations in low rank coal: an experimental study. J Supercrit Fluids 2016;109:134–40.
[25] Fujioka M, Yamaguchi S, Nako M. CO_2-ECBM field tests in the Ishikari coal basin of Japan. Int J Coal Geol 2010;82:287–98.
[26] Reeves S. Geological sequestration of CO_2 in deep, unmineable coalbeds: an integrated research and commercial-scale field demonstration project. In: SPE annual technical conference and exhibition, New Orleans, LA; 2001, paper no. 71749.
[27] Reeves S, Oudinot A. The Allison unit CO_2-ECBM Pilot–a reservoir and economic analysis. In: International coalbed methane symposium, Tuscaloosa, AL; 2005, paper no 0522.
[28] Zhou F, Hussain F, Cinar Y. Injecting pure N_2 and CO_2 to coal for enhanced coalbed methane: experimental observations and numerical simulation. Int J Coal Geol 2013;116:53–62.
[29] Mazumder S, Wolf KH. Differential swelling and permeability change of coal in response to CO_2 injection for ECBM. Int J Coal Geol 2008;74:123–38.
[30] Wolf K, Barzandji OH, Bruining H, Ephraim R. CO_2 injection in and CH4 production from coal seams: laboratory experiments and image analysis for simulations. In: las Actas de la 1a Conferencia Nacional sobre Captación de Carbono, Washington, DC; 2001, CD-ROM, DOE/NETL-2001/1144. p. 1–13.
[31] Fulton PF, Parente CA, Rogers BA, Shah N, Reznik A. A laboratory investigation of enhanced recovery of methane from coal by carbon dioxide injection. In: SPE unconventional gas recovery symposium, Pittsburgh, Pennsylvania; 1980, Paper ID SPE-8930-MS.
[32] Reznik AA, Singh PK, Foley WL. An analysis of the effect of CO_2 injection on the recovery of in-situ methane from bituminous coal: an experimental simulation. Soc Petrol Eng J 1984;24:521–8.
[33] Jessen K, Tang GQ, Kovscek AR. Laboratory and simulation investigation of enhanced coalbed methane recovery by gas injection. Transp Porous Media 2008;73:141–59.
[34] Connell L, Sander R, Pan Z, Camilleri M, Heryanto D. History matching of enhanced coal bed methane laboratory core flood tests. Int J Coal Geol 2011;87:128–38.
[35] Sander R, Connell LD, Pan Z, Camilleri M, Heryanto D, Lupton N. Core flooding experiments of CO_2 enhanced coalbed methane recovery. Int J Coal Geol 2014;131:113–25.
[36] Garduno JL, Morand H, Saugier L, Ayers Jr W, McVay DA. CO_2 sequestration potential of Texas low-rank coals. In: Society of petroleum engineers (SPE) annual technical conference and exhibition, Denver, Colorado, 2003, paper no 84154.
[37] Hernandez G, Bello RO, McVay DA, Ayers WB, Rushing JA, Ruhl SK, et al. Evaluation of the technical and economic feasibility of CO_2 sequestration and enhanced coalbed methane recovery in Texas low-rank coals. In: Society of Petroleum Engineers (SPE) gas technology symposium, Calgary, Alberta, Canada, 2006, paper no 100584.
[38] Hooper B, Murray L, Gibson-Poole C. Latrobe valley CO_2 storage assessment. Canberra: Cooperative Research Centre for Greenhouse Gas Technologies; 2005. CO2CRC Publication No. RPT05-0108.
[39] Li CZ. Advances in the science of Victorian brown coal. Oxford, UK: Elsevier; 2004. p. 11–84.
[40] Ranjith PG, Perera MSA. A new triaxial apparatus to study the mechanical and fluid flow aspects of carbon dioxide sequestration in geological formations. Fuel 2011;90:2751–9.
[41] Arif M, Barifcani A, Lebedev M, Iglauer S. CO_2-wettability of low to high rank coal seams: implications for carbon sequestration and enhanced methane recovery. Fuel 2016;181:680–9.
[42] Gorucu FB, Jikich SA, Bromhal GS, Sams WN, Ertekin T, Smith DH. Matrix shrinkage and swelling effects on economics of enhanced coalbed methane production and CO_2 sequestration in coal. In: SPE Eastern Regional Meeting, Morgantown, West Virginia; 2005, Paper ID SPE-97963-MS.
[43] Perera MSA, Ranjith PG, Ranathunga AS, Koay AYJ, Zhao J, Choi SK. Optimization of enhanced coal-bed methane recovery using numerical simulation. J Geophys Eng 2015;12:90.

8.3 Optimization of CO_2-enhanced coal bed methane recovery

8.3.1 Overview

As discussed in Section 8.2, the methane production enhancement ability of CO_2 from deep coal beds is highly dependent on the properties of the coal seam and the injecting gas. Hence, identification of the optimum conditions of these properties to optimize methane recovery is crucial. Although some experimental, numerical and field studies have been conducted on the CO_2-ECBM process, to date none has considered the influences of all the possible primary factors affecting this process, and it has therefore been difficult to obtain comprehensive knowledge of the subject specially on low rank coal. Hence, in this section, an effort is made to determine the most favourable conditions for CO_2-ECBM by developing a 3-D numerical model using the COMET 3 numerical simulator. First, the CO_2 ECBM process and the primary pressure depletion technique (removal of water from the coal seam) is compared to confirm the ability of CO_2 to improve methane production. Next, factors affecting the CO_2-ECBM process during CO_2-ECBM are reported as follows:

- Effect of coal seam properties
    - Temperature (25, 40, 60, 80 and 100 ^{0}C)
    - Moisture content (20, 50, 60, 70, 80, 90 and 100%)
    - Depth of injection (400, 500, 600, 700 and 800 m)

- Effect of injecting gas properties
    - CO_2 injection pressure (6, 8, 10, 12, 14, 16 and 18 MPa)
    - Injecting gas composition (20, 40, 60, 80 and 100% of N_2 mixed with CO_2)

The arrangement of CO_2 injection wells and the methane production wells is also important for the optimisation of the CO_2-ECBM process. Therefore, the influence of CO_2 injection well arrangement, methane production well arrangement and the distance between the injection well and production well are examined to determine the optimum conditions to recover a maximum amount of methane from a selected coal seam.

8.3.2 Introduction

The traditional CBM recovery technique involves the reduction of overall pressure in the coal seam by dewatering, either by pumping or mining. However, according to recent scientific findings, this CBM recovery process can be greatly enhanced through the injection of gases, such as carbon dioxide (CO_2) or nitrogen (N_2), into the coal bed (Fujioka et al 1995; White et al 2005; Perera et al., 2012a; Vishal et al 2013a), which is commonly known as enhanced coal-bed methane (ECBM) recovery. In the CO_2 injection-enhanced ECBM process (CO_2-ECBM), when CO_2 is injected into a coal seam, it displaces the CBM due to its higher affinity with coal. This has the added advantage of sequestering carbon dioxide in the coal bed, which reduces the amount of net carbon emissions, making methane extracted using ECBM recovery techniques one of the greenest sources of energy. In Australia, carbon was initially priced at AUD $23/ton (Maimone, 2011), which would considerably enhance the economic viability of ECBM, coupled with increasing gas prices. With regard to the N_2-ECBM technique, according to Reeves (2001) the injection of N_2 into the coal seam causes the CBM production rate to significantly increase. This is mainly due to the non-adsorptive nature of N_2, which causes it to remain as free gas in the fracture space, resulting in the creation of an imbalance between sorbed and free gas phases inside the coal mass and reduction of the CH_4 partial pressure. This process causes the CBM to be released from the adsorbed phase and to move into the free gas phase, which enhances methane production from the coal seam (Reeves, 2001; Perera et al., 2012b).

Although the CO_2-ECBM and N_2-ECBM recovery processes have the ability to enhance methane production from coal seams, they also have limitations. ECBM is a relatively new technology with relatively few commercial wells to date. Some of the pilot projects include the ARC (Reeves, 2003; Reeves and Odinot, 2004), RECOPOL (Pagnier et al., 2006), and MOVECBM (Wageningen and Cuesta, 2005) projects. In these projects, ECBM has been used to extract more methane in conventional CBM wells only after the rate of methane production has dropped significantly, because ECBM recovery has many associated economic risks. Drilling wells to deep coal seams is a very expensive process, and therefore production and field-scale testing have become quite expensive (Ranjith et al., 2013). This has caused less investment in ventures in which there is significant risk of a limited return on investment. The major cost parameters for the process include CO_2 and N_2 injection costs, processing and implementation costs, transportation expenses and the market value of the methane produced. In order to have an economical ECBM process, the value of the gas produced should exceed the production cost plus the cost of transporting the gas, minus the cost of taxes or CO_2 credits (Reeves, 2003). Therefore, ECBM recovery projects can be made more economical by using existing facilities, such as converting production wells for injection and using time-tested technological approaches, such as the organization of injection wells and production wells. However, such optimum recovery scenarios have not been fully studied to date, although such techniques are important for the economic aspect of projects in terms of harvesting an optimum amount of methane with the minimum capital cost. According to Reeves (2003), the lack of knowledge related to the ECBM process has also crucially affected ECBM implementation in the field, and according to Pini et al. (2006), it is necessary to conduct a broader range of scientific research studies to overcome this issue.

The injection of CO_2 into deep coal seams causes significant alterations to their chemico-physical structure, and the coal matrix swelling effect created by injecting CO_2 is significant (White et al., 2005). This can start as soon as 1 h after CO_2 injection, causing the seam's permeability to be significantly reduced, and resulting in unpredictable CO_2 injectivity and CH_4 productivity of coal seams (Perera et al., 2011a; Perera et al., 2011b; Perera et al., 2011c; Perera and Ranjith 2012; Vishal et al., 2013b; Vishal et al., 2013c). According to Perera et al (2011c), this swelling process is heavily dependent on the CO_2 phase condition, and super-critical CO_2 adsorption-induced swelling is up to two times greater than sub-critical CO_2 adsorption-induced swelling. Therefore, the injection of CO_2 into the coal seam, particularly under the super-critical conditions which exist below certain depths, greatly reduces flow ability through the coal mass by closing the pore space, consequently creating greater tortuosity for CO_2 movement and resulting in reduced coal mass permeability (Viete and Ranjith 2006; Perera et al., 2011; Perera et al., 2012a). In addition, existing safety rules in underground coal mines limit the amount of CO_2 permitted in them; the maximum percentage of CO_2 in a coal mine should be around 3% of the mine's air volume. Therefore, there is a risk associated with the injection of CO_2 into coal seams during the CO_2-ECBM process that may cause the coal seam to be unmineable forever (Sarmah, 2011). However, the significant contribution of the CO_2-ECBM process to the mitigation of atmospheric CO_2 levels through CO_2 sequestration also needs to be considered from the environmental protection perspective (Perera et al., 2011d). Therefore, performance evaluation of the process under various conditions (different injection gas and seam properties) is very important for the optimization of the CO_2-ECBM process.

In the N_2-ECBM technique, the existence of free N_2 in the seam causes quicker N_2 breakthroughs in the gas produced, which greatly reduces the benefits offered by the process when the higher gas treatment costs are taken into account (Reeves, 2001). For instance, specialized equipment is required to separate the N_2 from the product gas stream (a mixture of N_2 and CH_4 (Mazzotti et al., 2009)), which is quite expensive. This has been observed in both the Tiffany N_2-

ECBM unit in the San Juan basin and the Alberta ECBM project (Reeves and Odinot, 2004; Gunter, 2009). However, according to current research, there is a significantly higher production potential for the N_2-ECBM process compared to the CO_2-ECBM process (Perera and Ranjith, 2012), which also needs to be considered. Therefore, it is clearly necessary to find the optimum technique for the ECBM process with maximum productivity and minimum risk and environmental impact. Some studies have shown the advantages of flue gas (87% N_2 + 13% CO_2) injection compared to pure CO_2 or N_2 injection (Reeves and Schoeling, 2000), because the injection of a mixture of N_2 + CO_2 offers higher methane productivity with an earlier response compared to pure CO_2 injection, and it sequestrates similar amounts of CO_2 due to the higher injection rate. In addition, N_2 has some potential to recover CO_2 injection-induced swelling (Jasinge et al., 2011; Perera et al., 2012b; Perera et al., 2013a; Vishal et al 2013a), which also results in the greater injectivity of the N_2/CO_2 mixture compared to pure CO_2. Although the use of flue gas seems to be the optimum way to harvest commercially-viable amounts of CBM in an environmentally-friendly way, the injection of a CO_2/N_2 mixture at a predetermined ratio possibly offers a better solution.

However, to date few studies have been conducted on the N_2 + CO_2-ECBM technique. According to the experimental study conducted by Parakh (2007), the injection of a 45% N_2 + 55% CO_2 gas mixture causes an initially high rate of production, due to the N_2 and the rate gradually becoming slower due to the CO_2. Fieldwork in the Fenn Big Valley basin in Alberta, Canada (Gunter, 2009; Wong et al., 2000) involved the injection of different proportions of N_2/CO_2 (0% N_2, 53% N_2, 87% N_2 and 100% N_2) into the 1–4 mD low permeable Mannville reservoir using two injection wells. This project illustrates that the injection of a mixture of N_2 + CO_2 may help reduce the problems associated with CO_2 injection-induced coal swelling and early breakthrough with N_2 injection, and that flue gas injection avoids the high costs associated with the pure N_2/CO_2 capture process. However, it is necessary to conduct a comprehensive study to fully understand the process and find the best CO_2/N_2 composition to achieve optimum productivity and safety advantages related to the ECBM process. The results will be important for ECBM recovery field projects worldwide.

In addition, as ECBM recovery is an expensive and time-consuming process, it is necessary to establish appropriate numerical models to find the optimum method to recover a maximum amount of CH_4 from a selected coal seam. Of the many field-scale simulators available to simulate gas flow in underground reservoirs, including TOUGH 2 (Carneiro, 2009), COMSOL (Liu and Smirnov, 2009; Perera et al., 2013b), FEMLAB (Holzbecher, 2005) and COMET 3 (Perera et al., 2012a; Perera et al., 2012b; Perera et al., 2012c; Vishal et al 2012; Vishal et al., 2013d; Vishal et al., 2015), COMET 3 has been identified as one of the most appropriate and user-friendly numerical modelling tools for deep coal seams (Perera et al., 2012b). Therefore, the main objective of this study is to conduct a comprehensive numerical modelling study using COMET 3 software to investigate optimization measures for the ECBM process.

Although some experimental, numerical and field studies have been conducted on the ECBM process and production-enhancement techniques, none has considered the influences of all the possible primary factors affecting the process, and it has therefore been difficult to obtain comprehensive knowledge of the subject. This study therefore offers a comprehensive platform for the study of all possible major ECBM process-enhancing techniques.

8.3.2.1 Governing equations used

Mass conservation equations (Eqs. [8.1] and [8.2]) were used to simulate the CH_4, CO_2, N_2 and water flows in the deep coal seam (Sawyer et al., 1990; Perera et al., 2011d; Perera et al., 2012b; Ranjith et al., 2013):

$$\nabla.\left[b_g M_g(\nabla p + \gamma \nabla Z) + R_{sw} b_w M_w (\nabla p_w + \gamma_w \nabla Z)\right]_f + q_m + q_g = \left(\frac{d}{dt}\right)\left(\emptyset b_g S_g + R_{sw} \emptyset b_w S_w\right)_f \quad [8.1]$$

$$\nabla.\left[b_w M_w (\nabla p_w + \gamma_w \nabla Z)\right]_f + q_w = \left(\frac{d}{dt}\right)\left(\emptyset b_w S_w\right)_f \quad [8.2]$$

where, b_n (n=g or w) is the gas or water bulking factor, γ_n (n=g or w) is the gas or water gradient, R_{sw} is the gas solubility in water, ϕ is the fracture porosity, Z is the elevation, q_g is the gas flow rate, q_w is the water flow rate, q_m is the matrix gas flow rate, M_n (n=g(gas) or w (water)) = kk_m/μ_m, is the phase mobility (k-permeability, k_m-matrix permeability, μ_n-phase viscosity), S_n (n=g or w) is the gas or water saturation and P_n (n=g or w) is the gas or water pressure. Using the extended Langmuir model (Arri et al., 1992) gas adsorption was calculated (Eq. [8.3]).

$$C_i(P_i) = \frac{V_{Li} P_i}{P_{Li}\left[1 + \sum_{j=1}^{3}\left(\frac{P}{P_L}\right)_j\right]}, \; i = 1,2 \quad [8.3]$$

where, V_{Li} is the Langmuir volume, P_{Li} is the Langmuir pressure, P_i is the partial pressure of the gas component, $C_i(P_i)$ is the adsorbed gas concentration at P_i and P is the total pressure. Gas flow through the matrix is modelled using Fick's law of diffusion (Eq. [8.4]).

$$q_{mi} = \left(\frac{V_m}{\tau_i}\right)\left[C_i - C_i(P_i)\right], i = 1,2 \quad [8.4]$$

where, q_{mi} is the gas component flow, V_m is the bulk volume of the matrix element, τ_i is the sorption time and C_i is the average matrix gas concentration of gas component i.

The corresponding permeability variations in the coal matrix and fracture system were simulated using the Advanced Resources International (ARI) model (Eq. [8.5] and Eq. [8.6]):

$$\varphi = \varphi_i[1 + c_P(P - P_i)] - c_m(1 - \varphi_i)\left(\frac{\Delta P_i}{\Delta C_i}\right)(C - C_i) \quad [8.5]$$

$$\frac{k}{k_i} = \left(\frac{\varphi}{\varphi_i}\right)^n \quad [8.6]$$

where, c_p is the pore volume compressibility, c_m is the matrix shrinkage compressibility, φ is the coal mass porosity, φ_i is the initial coal mass porosity, P is the reservoir pressure, P_i is the initial reservoir pressure, C is the reservoir concentration, C_i is the initial reservoir concentration, k is the reservoir permeability and k_i is the initial reservoir permeability.

8.3.2.2 Model development

A 500 m × 500 m × 50 m unmineable coal seam (similar properties to those of the Victorian brown coal samples used for the current study) lying 800 m below the surface was considered for the model development, and gas production and injection were carried out at opposite corners of the coal seam, as shown in Figure 8.1. Table 8.1 shows the model parameters used. First, ordinary methane (CH_4) production capacity from the coal bed was examined without using any enhancement technique such as water production or CO_2/N_2 injection, and CH_4 production during 50 years (long-term) of production was simulated and examined.

The production rate was then accelerated by pumping out formation water at 25 m^3/day rate for 5 years. At this stage, the production well was used as a water pumping well to reduce the pressure inside the coal seam. Water production was terminated after 5 years and the well was then used to produce methane from the pressure-reduced coal seam for the remaining 45 years. In all of these cases, the injection well was kept shut when it was in operation.

After the first 5 years, the CO_2-ECBM technique was examined by injecting CO_2 into the coal seam at 10 and 18 MPa injection pressure for 45 years. Effective factors for the CO_2-ECBM process were then examined to identify possible ECBM process optimization measures. The effect of CO_2 injection pressure was first examined by changing the CO_2 injection pressure (6, 8, 10, 12, 14, 16 and 18 MPa) and the formation temperature effect was then examined by changing the coal seam temperature (25, 40, 60, 80 and 100 °C) for methane production for 50 years. In the latter case, CO_2 injection pressure and bed moisture content were maintained at 18 MPa and 60%, respectively. The effect of coal seam moisture content on enhanced methane production was then examined by changing the coal seam moisture content (20, 50, 60, 70, 90 and 100%), maintaining the CO_2 injection pressure at 18 MPa and the coal bed temperature at 60 °C. The effect of coal seam depth on CH_4 production was examined by changing the coal seam depth (400, 500, 600, 700, and 800 m) while maintaining the CO_2 injection pressure at 18 MPa, coal bed moisture content at 60% and temperature at 60 °C. During the study, maximum CO_2 injection pressure was set to 18 MPa considering the depth of 800 m (~ 20 MPa confining pressure).

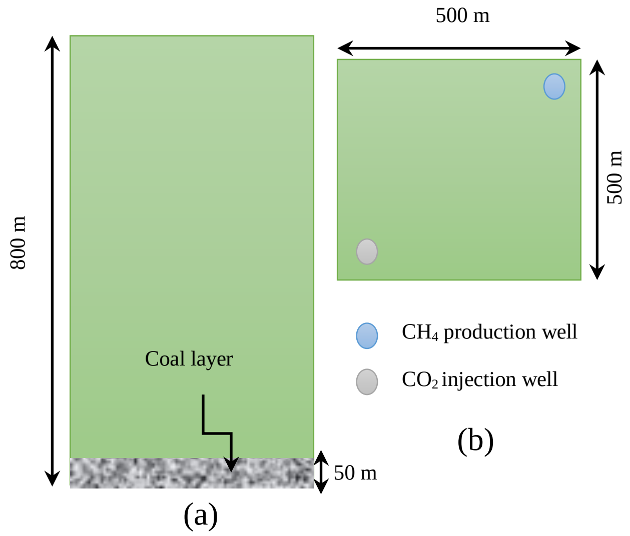

Figure 8.1. Block dimensions used for reservoir simulation (a) Cross-section and (b) Plan view

After investigating the effects of primary effective factors on the ECBM process, the ability of N_2 gas to enhance ECBM production was examined by mixing the injecting CO_2 with various percentages of N_2 (20, 40, 60, 80 and 100%). In this case, a 20% N_2 + 80% CO_2 gas mixture was first considered as the injection gas and the corresponding CH_4 production enhancement was examined. The N_2 percentage in the injecting gas was then gradually increased to 80% and the corresponding CBM production enhancements were examined.

After an analysis of the effects of injection gas and coal seam properties on CH_4 production, the potential for ECBM process optimization was examined by changing the production and injection well arrangements. In this case, pure CO_2 injection-enhanced CH_4 production was considered by maintaining the CO_2 injection pressure at 18 MPa, the coal seam depth at 800 m, the moisture content at 90% and the temperature at 60 °C. The effect of the CO_2 injection well arrangement was first examined by changing the number of injection wells (1, 2, 3 and 4) and the influence of the production well arrangement on CH_4 production was then examined by changing the number of production wells (1, 2, 3 and 4).

Table 8.1. Model Parameters

Model parameter	Value	Reference
Reservoir temperature (°C)	60	Suggate (1974)
Coal seam initial permeability (mD)	2	De Silva (2013)
Coal seam moisture content (%)	60	Jasinge et al. (2011)
Coal seam porosity	0.41	Jasinge et al. (2011)
Langmuir volume for CH_4 (m^3/t)	5.07	Refer to Chapter 3
Langmuir pressure for CH_4 (MPa)	5.11	Refer to Chapter 3
Langmuir volume for CO_2 (m^3/t)	29.11	Refer to Chapter 3
Langmuir pressure for CO_2 (MPa)	5.78	Refer to Chapter 3
Langmuir volume for N_2 (m^3/t)	3.29	Refer to Chapter 3
Langmuir pressure for N_2 (MPa)	6.16	Refer to Chapter 3
Exponent of pressure dependent permeability (n)	3.0	Pekot and Reeves (2002)
Differential matrix swelling factor of CO_2	1.5	Pekot and Reeves (2002)
Pore volume compressibility (kPa^{-1})	2.96×10^{-5}	Jasinge et al. (2011)
Matrix shrinkage compressibility (kPa^{-1})	1.21×10^{-5}	Jasinge et al. (2011)
Initial pore pressure	$P_o=h\times\rho_w\times g$*	-
Initial gas content in the coal seam (%)	100 % CH_4	Connell et al. (2011)
Relative permeability variation	Cooray formula (Akin, 2001), residual water and gas contents are 0.05 and 0.01 (cm^3/cm^3)	

* h is the depth, ρ_w is the water density and g is the gravitational acceleration

8.3.3 Results and discussion

8.3.3.1 Comparison of CBM production enhancements through water removal and CO_2 injection (CO_2-ECBM)

As described in the model development section, two main techniques were used to accelerate CH_4 desorption: coal seam pore pressure depletion by water removal, and the injection of a higher adsorption capacity gas, CO_2. Figure 8.2 compares the effects of each technique on CH_4 production. The figure exhibits significant CBM production enhancement through water removal, because removal of water from the coal seam reduces the pore pressure inside it, which enhances the CH_4 desorption rate (Fujioka et al., 1995). This can be easily examined in Figure 8.3(a), which shows that the removal of water at 25 m^3/day rate for 5 years causes the coal seam mean pore pressure to be reduced by around 21%, which in turn causes the CH_4 adsorbed under high pressure to be released from the coal matrix, which can subsequently be captured. However, according to Figure 8.2, CBM production enhancement created by the CO_2-ECBM technique seems to be much more productive compared to the enhancement through water removal, if an appropriate injection pressure is maintained (Fujioka et al., 1995). Interestingly, according to Figure 8.2, simply injecting CO_2 into the coal seam does not enhance CBM production and it is necessary to maintain an appropriate injection pressure to recover an optimum amount of CBM. For example, for the coal seam under consideration, 10 MPa injection pressure creates negligible CBM production enhancement and it is necessary to have a higher injection pressure to cause significant CBM production enhancement (Figure 8.2). This can be clearly seen in Figure 8.3, according to which, at around 10 MPa CO_2 injection pressure, the reservoir has a fairly low permeability value (1.3 mD), which is less than the original permeability of the coal seam (2 mD). This is because the use of CO_2 injection causes pore pressure development to occur in the coal seam, which prevents methane release from the coal mass unless an adequate flow rate is maintained. The coal seam under consideration is at a depth of 800 m and pore pressure at such a depth is close to 8 MPa (Oldenburg, 2006). Apparently, 10 MPa injection pressure is insufficient to maintain an adequate flow rate through the medium. According to Figure 8.3, the CO_2 permeability inside the coal seam increases with a rise in injection pressure (Figure 8.3(b)), even though the pore pressure inside the seam increases accordingly (Figure 8.3(a)). This is because, although there is a pore pressure development with CO_2 injection, the pushing force for the injected CO_2 increases with the increasing injection pressure. This results in a higher flow rate and a higher rate of production at higher injection pressures, because both coal permeability and adsorption processes are dependent on injecting gas properties, such as pressure and phase. According to Figure 8.3, the injection pressure should be greater than 12 MPa for the coal seam to have permeability enhancement.

This finding confirms the need for an appropriate numerical model to decide the required CO_2 injection pressure for field-scale CO_2-ECBM projects to achieve maximum production enhancement.

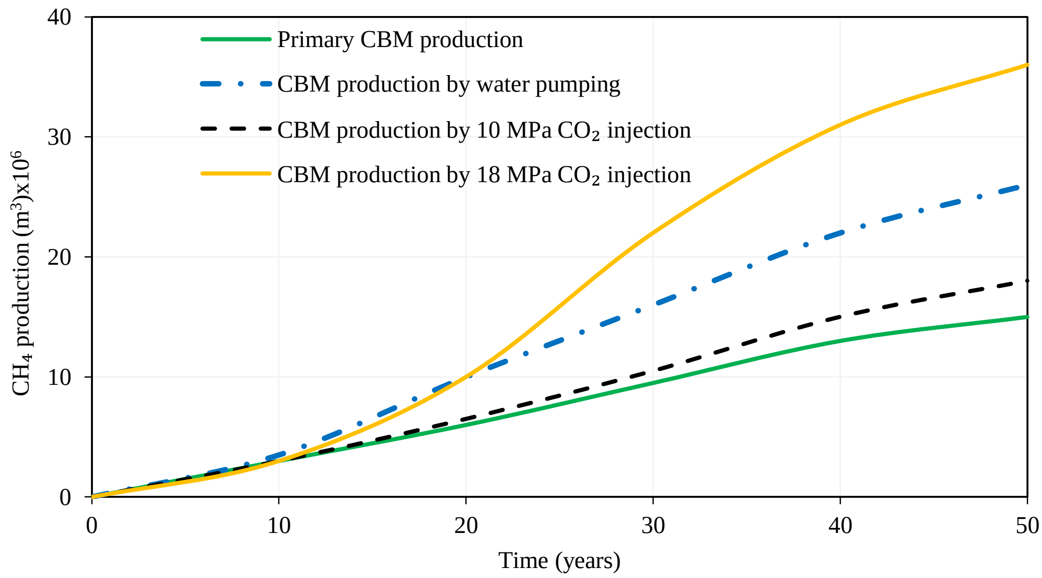

Figure 8.2. Comparison of CBM production enhancement techniques

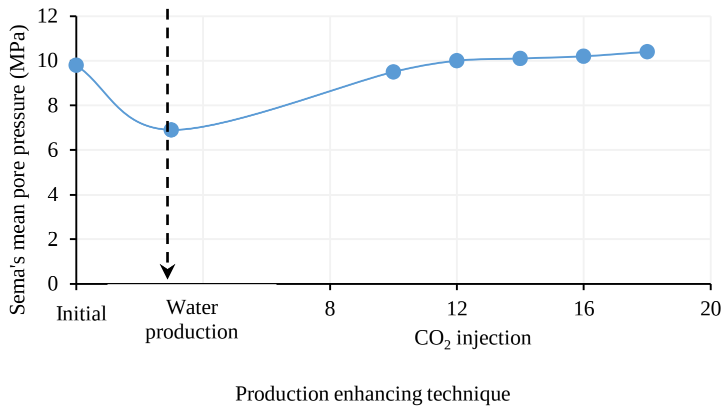

(a) Seam pore pressure

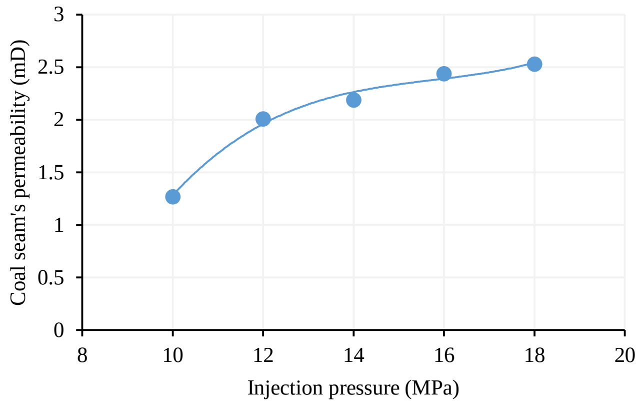

(b) Permeability near the injection point

Figure 8.3. Variation of seam pore pressure and permeability near the injection point under water removal and CO_2 injection

8.3.3.2 Factors affecting the CO_2-ECBM process

The applicability of the CO_2-ECBM process in any coal seam is mainly governed by the seam's permeability and its adsorption process. In turn, these largely depend on the properties of the injecting gas and the coal seam's chemico-physical properties, such as injecting gas pressure, phase and composition and coal seam depth, temperature, bed moisture content and rank.

a) *Effect of coal seam properties*

- Temperature

The effect of temperature on the CO_2-ECBM process was first considered for 50 years of production time by changing the temperature to 25, 40, 60, 80 and 100 ^{o}C while maintaining the CO_2 injection pressure at 18 MPa and coal seam moisture content at 60% (Figure 8.4). According to the figure, an increase of temperature from 25 to 60 ^{o}C causes CH_4 production to be enhanced by around 19%, and a further increase of temperature up to 100 °C causes it to decline by around 39%. The initial CH_4 production enhancement may be due to the fact that the increase of temperature from 25 to 60 °C causes the CO_2 phase condition inside the coal seam to change from sub- to super-critical. According to Perera et al., (2011c), super-critical CO_2 has greater sorption capacity in coal than sub-critical CO_2. Therefore, this greater sorption capacity may cause higher CH_4 desorption from the coal seam, resulting in higher CH_4 production. This can be confirmed by observing the coal seam porosity and permeability alterations close to the CO_2 injection point during the CO_2-ECBM process (Figure 8.5). According to this figure, coal seam porosity continuously decreases with increasing temperature, probably due to the thermal expansion of the coal matrix with the increasing temperature, which reduces the pore space.

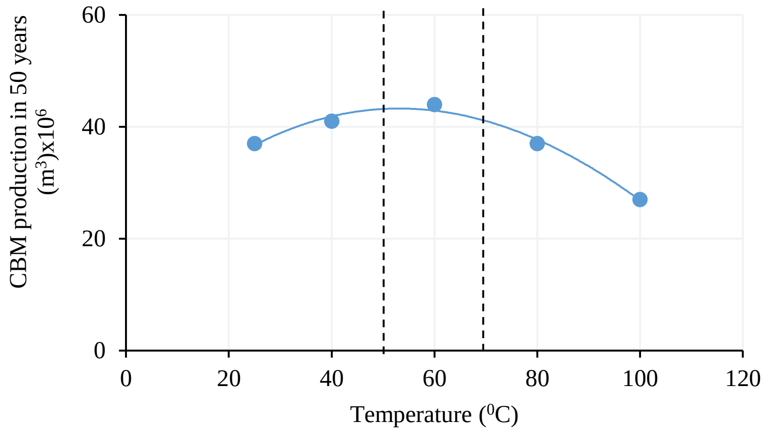

Figure 8.4. The effect of temperature on coal seam-enhanced CH_4 production

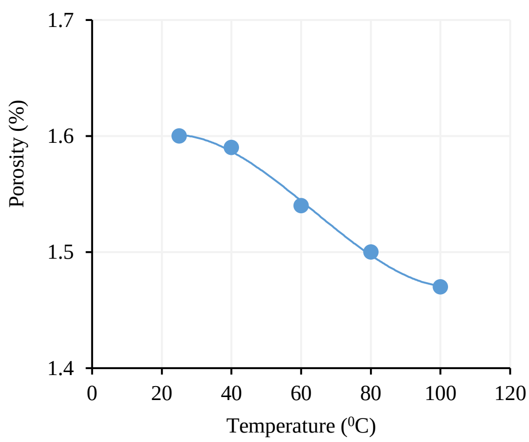

(a) Seam porosity

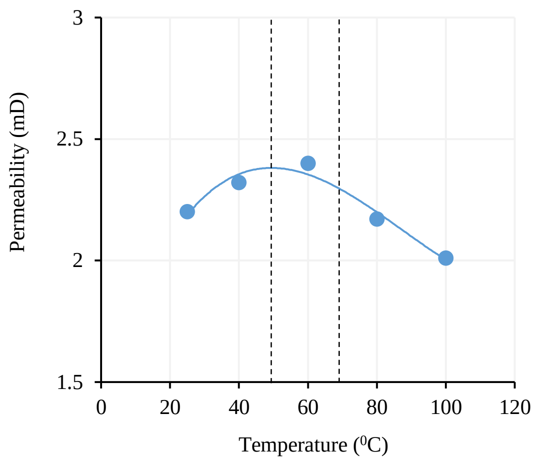

(b) Permeability

Figure 8.5. Variations of (a) seam porosity and (b) permeability with temperature

However, if the seam permeability is considered (Figure 8.5(b)), a similar pattern with gas production can be seen (Figure 8.4), where an increase of temperature from 25 to 60 ^oC causes the permeability to be enhanced, and a further increase of temperature up to 100 ^oC causes it to decline. The former permeability increment with increasing temperature from 25 to 60 ^oC is possibly related to the CO_2 phase transmission creating production enhancement and the latter permeability reduction with increasing temperature mainly relates to the previously mentioned temperature increment creating seam porosity reduction, which occurs due to the thermal expansion of the coal matrix. In addition, kinetic energy enhancement in the injecting CO_2 molecules with increasing temperature may also have a significant influence on permeability reduction, as the kinetic energy of the CO_2 molecules increases with increasing temperature (Perera et al., 2012a; Skawinski et al., 1991), which reduces the CO_2 adsorption rate into coal and, consequently reduces CH_4 production.

- Moisture content

The effect of coal seam moisture content on enhanced CH_4 production was then considered for 50 years of production by changing the moisture content to 20%, 50%, 60%, 70%, 80%, 90% and 100%, when CO_2 injection pressure was 18 MPa and coal seam temperature was 60 ^oC (Figure 8.6). According to Figure 8.6, up to around 70% moisture content, enhanced coal-bed CH_4 production decreases with increasing moisture content, and the increase of moisture content from 20 to 70% causes the enhanced methane production to be reduced by 7.5%. This is due to the fact that the amount of CO_2 that can be injected into the coal seam is highly dependent on the available pore space. The presence of water causes the coal mass pore space available for CO_2 and CH_4 movement to be significantly reduced (Skawinski et al 1991), resulting in a reduction in CO_2 adsorption capacity and CH_4 production capacity from the coal seam. This was confirmed by checking the coal seam porosity and permeability alterations which occurred with changes in moisture content (Figure 8.7). According to Figure 8.7 (a), increasing the moisture content from 20 to 70% causes the coal seam porosity to be significantly reduced due to the pore space occupied by the increased water molecules. This pore space reduction increases the tortuosity for gas molecules, resulting in reduced permeability in the coal seam (Figure 8.7(b)). This affects the CO_2 movement inside the coal seam and eventually delays the CO_2 adsorption process into the coal matrix, which consequently reduces the CH_4 production.

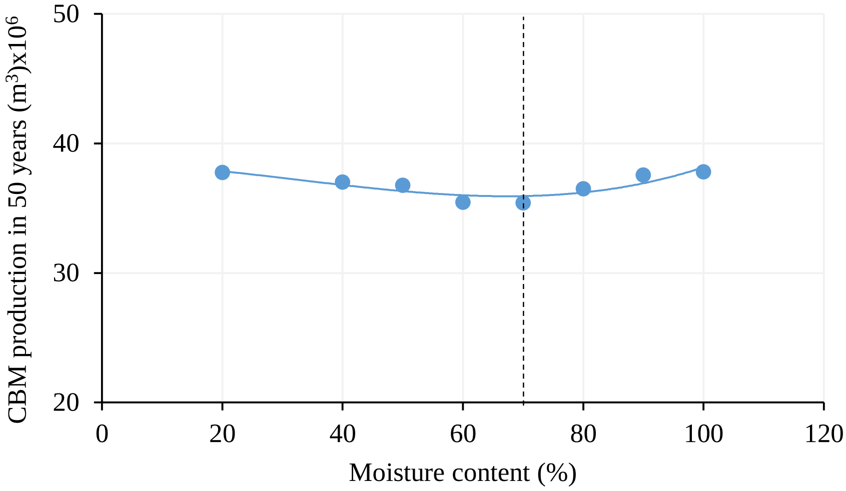

Figure 8.6. The effect of bed moisture content on coal seam enhanced CH_4 production

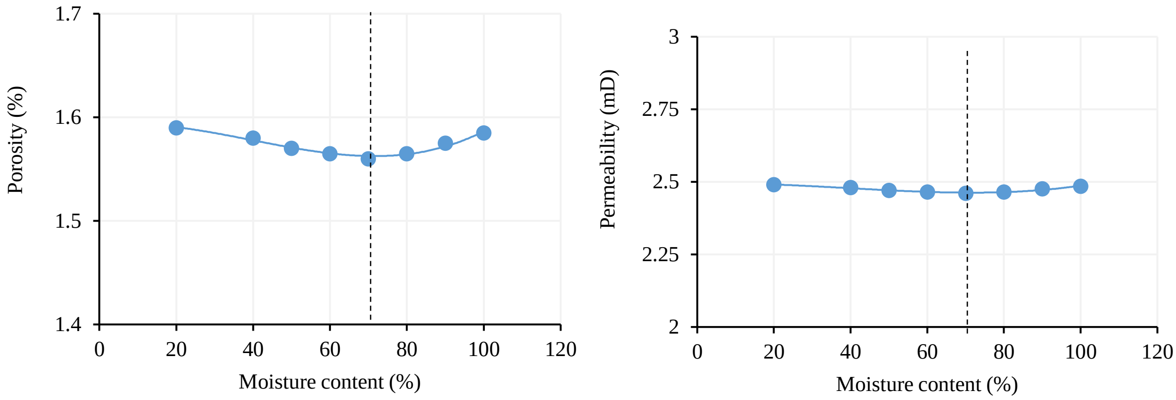

(a) Seam porosity

(b) Permeability

Figure 8.7. Variations of seam porosity and permeability with moisture content

The effect of bed moisture content was then considered for higher moisture contents (70% to 100 %), and according to Figure 8.7, both seam porosity and permeability remained stable after around 70 % bed moisture content. According to the studies of Anderson et al (1956), before reaching the critical moisture content, the water molecules occupy some of the adsorption sites in any porous medium, and after the saturation point, the excess water stays in the free state and does not affect the gas sorption capacity. This is believed to be the reason for the observed stable porosity and-permeability and consequently the gas production after 70% moisture content.

➢ Depth

The effect of depth on total CH_4 production was then examined by changing the depth to 400, 500, 600, 700 and 800m, while maintaining the coal seam temperature, moisture content and injection pressure at 60 ^{0}C, 90% and 18 MPa, respectively. The results are shown in Figure 8.8. As shown in the figure, coal seam CH_4 production reduces with increasing depth, and an increase of depth from 400 m to 800 m (100%) causes the CH_4 production to be reduced by around 58%. According to Perera et al. (2012), an increase in coal seam depth causes a large increase in the in-situ stress acting on the coal seam from the surrounding rock mass. This increases the effective stress applied on the coal mass, which increases the tortuosity for gas movement inside the coal seam and reduces the pore space available in the coal seam for CO_2 adsorption and CH_4 desorption, resulting in the reduction in CH_4 production rates.

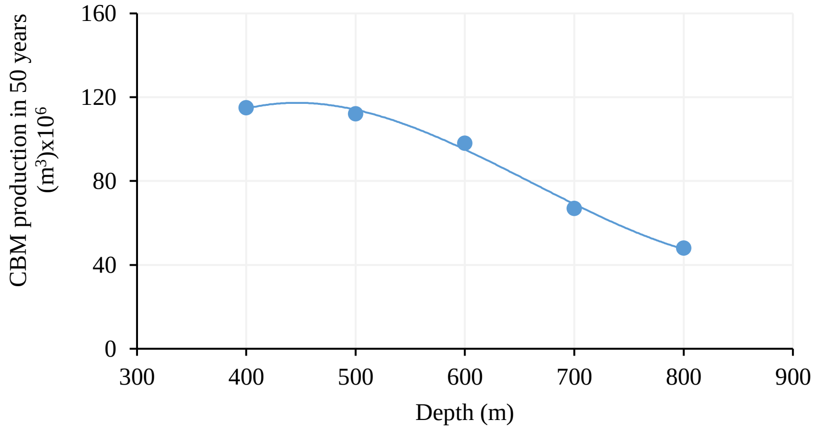

Figure 8.8. The effect of coal seam depth on enhanced CH_4 production

This was demonstrated by checking the seam porosity and permeability behaviours at each depth increment, and the results are shown in Figure 9. According to Figure 9, both seam porosity and permeability exhibit similar reduction trends with increasing depth, which implies pore space reduction with increasing depth, and the permeability reduction is due to the tortuosity increment under reduced pore space conditions. This delays the CO_2 movement inside the coal seam and eventually reduces CO_2 adsorption into the seam, resulting in reduced CH_4 desorption. In addition, the reduction of pore space itself affects the CO_2 adsorption and methane desorption processes in the coal seam.

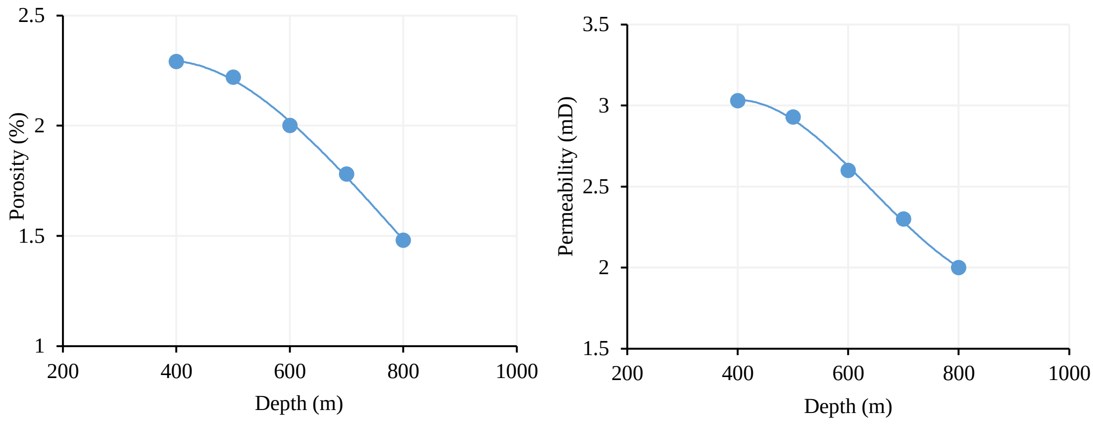

(a) Seam porosity

(b) Permeability

Figure 8.9. Variations of seam porosity and permeability with seam depth

b) Effect of injecting gas properties

➢ Injection pressure

The effect of CO_2 injection pressure on enhanced CH_4 production was then examined by changing the CO_2 injection pressure (6, 8, 10, 12, 14, 16 and 18 MPa). In order to maintain the injection pressure as a variable in the analysis, all other variables inserted in the model were treated as constants: temperature (60 ^{0}C), moisture content (90%), and depth (800 m). According to Figure 8.10, coal seam methane production increases with increasing CO_2 injection pressure, and the increase of injection pressure from 6 to 18 MPa (200%) causes the coal seam's CH_4 production to increase by around 150%. This is due to the fact that increased injection pressure produces a greater CO_2 adsorption capacity in the coal seam, which enhances the CH_4 desorption rate (Bae and Bhatia 2006). However, after 16 MPa CO_2 injection, CBM production shows a lower increment. Similar behaviour can be seen for the seam porosity and the permeability (near the injection point) (refer to Figure 8.11), which exhibit a gradual increase up to 16 MPa and a lower increment after 16 MPa CO_2 injection. This increasing trend of coal seam porosity with increasing CO_2 injection pressure is probably due to pore space expansion with the effective stress reduction created by the increased injection pressure up to 16 MPa. After 16 MPa CO_2 injection, the pore space expansion may have restricted with the coal matrix swelling due to CO_2 adsorption. This indicates that, at higher CO_2 pore pressures, the effective stress reduction-induced pore expansion is undermined by the sorption-induced strain. Further, the seam permeability enhancement under increased injection pressure enhances CO_2 flow ability through the seam (Figure 8.11 (b)) and the corresponding CO_2 adsorption process into the coal matrix, which consequently enhances the methane production.

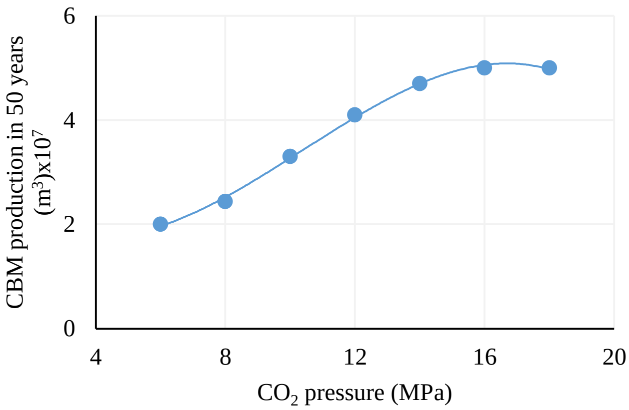

Figure 8.10. The effect of CO_2 injection pressure on enhanced CH_4 production

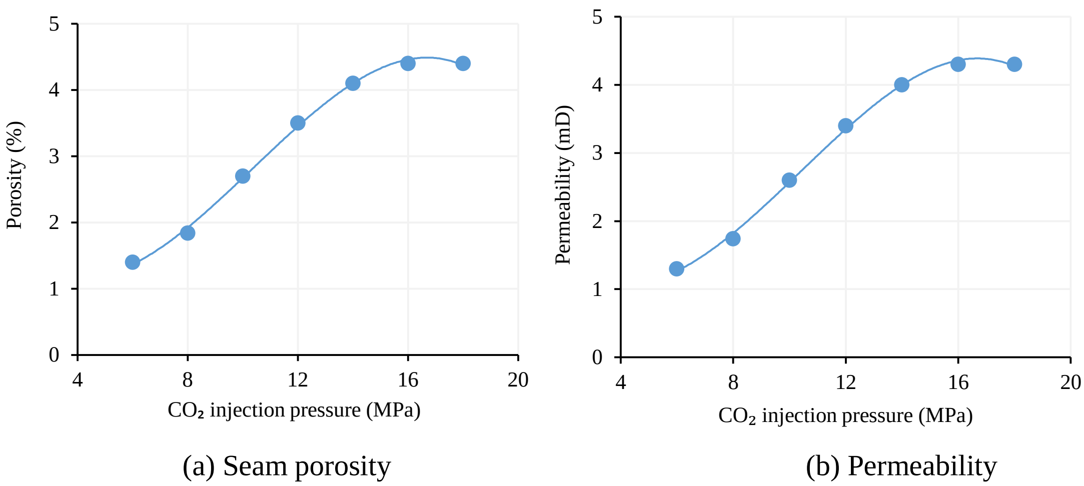

Figure 8.11. Variations of seam porosity and permeability with CO_2 injection pressure

However, it should be noted that too high injection pressures may cause hydraulic fractures to be created in the coal seam, resulting in back-migration of injecting CO_2 into the atmosphere. Hawkes et al (2005) showed that the most critical orientation for the opening of fractures is in a plane normal to the minimum in-situ stress component (σ_3), and therefore, fracture formation may occur once the pore pressure (P_u) exceeds σ_3. This phenomenon can be used to identify fracture formations in the coal seam. Fracture pore pressure was directly taken from the COMET 3 simulator and it was assumed that the third principal stress at 800m is equal to the gravitational stress, σ_g=h×ρ_r×g, where h is the depth (800 m), ρ_r is the rock density (2.5 g/cm^{-3}) and g is the gravitational acceleration (9.8 m^2/s) (Ranjith et al., 2013; Sheory, 1994), which is equal to 19.6 MPa. Therefore, for safety reasons, the maximum safe CO_2 injection pressure was selected as 18 MPa for the modeled coal seam and this pressure is used in the remaining sections.

Now, if the effects of all the considered factors affecting methane production are compared, 100% increment in injection pressure (from 6 to 12 MPa), depth (400 m to 800 m), temperature (25 to 50 ^{o}C) and moisture content (20% to 40%) cause the enhanced coal seam CH_4 production to be changed by around 89%, 58%, 19% and 3.1% respectively. It is therefore clear that CO_2 injection pressure is the most influential factor for the CO_2-ECBM process. In contrast, the least influence is created by the bed moisture content. Temperature and depth appear to have moderate influence on methane production during the CO_2-ECBM process. However, it should be noted that under actual conditions in deep coal seams, these parameters are inter-connected. For example, when the seam is deeper, moisture content reduces and temperature increases. The combined effect can be effectively identified by having a detailed understanding of each individual factor.

- Injecting gas composition

The next stage of the study examined the effect of injection gas composition on CBM production, and the gas composition was changed by adding N_2 to the injecting CO_2. The added N_2 percentage was changed (20%, 40%, 60%, 80% and 100%) and the corresponding CH_4 production was examined, while maintaining the temperature, moisture content and injection pressure at 60 ^{0}C, 90% and 18 MPa, respectively. The risk associated with the N_2 in the injecting gas was then examined by checking the leakage of CO_2 and N_2 from the production well during the 50 years' production period, because mixing any other gas (CO_2/N_2) with the CH_4 produced involves large costs to clean the gas produced. This step was therefore used to identify the best N_2 percentage in the injection gas to enhance CH_4 production with minimal contaminant gas.

Figure 8.12 shows how CH_4 production is enhanced by the injection of N_2+CO_2 gas into the coal seam. According to Figure 8.12, a clear enhancement of methane production can be observed with the addition of N_2 to the injecting CO_2 and this enhancement appears to increase with increasing percentage of N_2 in the injecting gas. For example, increasing the percentage of N_2 in the injecting gas from 20 to 80% causes the CH_4 production to be increased by around 160%, which is significant (Figure 8.13). This was expected, because N_2 remains as free gas in the fracture space, which creates an imbalance between the sorbed and free gas phases and eventually reduces the partial pressure for CH_4, resulting in the release of additional amounts of CH_4 from the coal mass (Reeves, 2003). Although CO_2 adsorption also creates a significant increase in methane production through the replacement of methane with CO_2, the process takes a significant time compared to the production enhnacement, which occurrs due to the pressure imbalance created by N_2 between the sorbed and free gas phases. Therefore, in short-term production, the influence of N_2 is much greater and production is proportionally increased with the increasing N_2 percentage in the injecting gas.

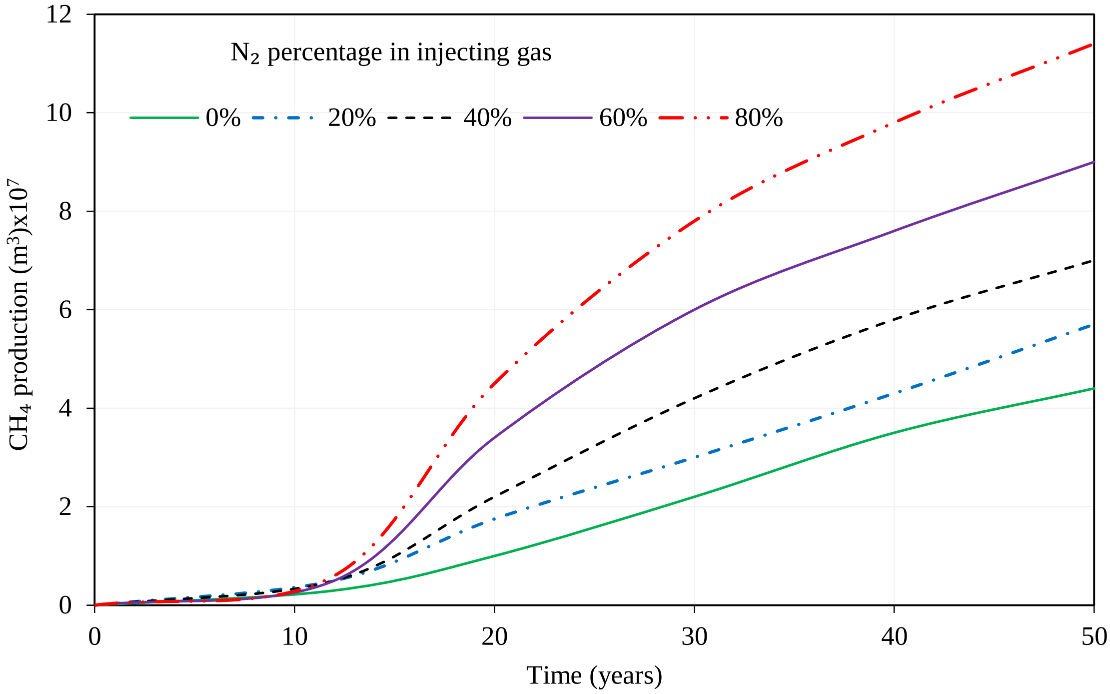

Figure 8.12. CH_4 production enhancement with N_2 + CO_2 injection

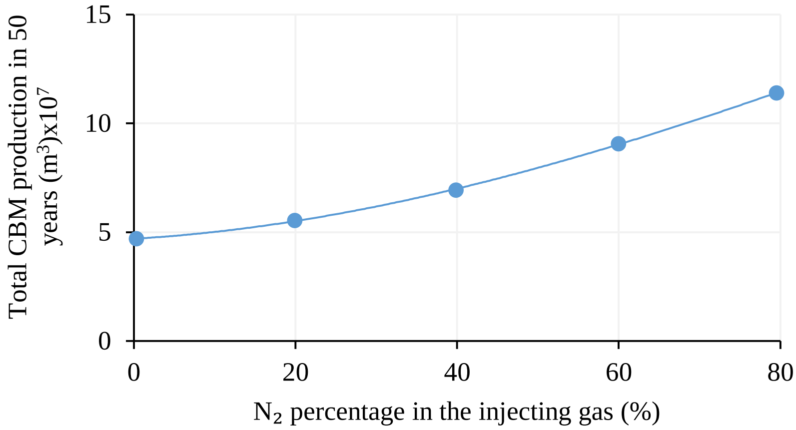

Figure 8.13. CH_4 production enhancement with N_2% in injecting gas

Figure 8.14 shows how coal seam porosity and permeability vary by increasing the N_2 percentage in the injecting gas and according to the figure, there is a significant pore space increment with increasing N_2%, probably as a result of the release of CH_4 molecules from the existing pore space (Figure 8.14(a)). In addition, seam permeability also seems to increase greatly with increasing percentage of N_2 in the injecting gas, and this is the governing factor for the CO_2 movement inside the seam, and consequently for the observed enhanced methane production.

Figure 8.15 compares the CO_2, N_2 and CH_4 present in the coal seam after 50 years of 80% CO_2+20% N_2 injection. According to the figure, a large amount of CO_2 remains in the coal matrix after the injection period, probably due to the replacement of existing methane with CO_2 through sorption (Figure 8.15(a)). This is confirmed by Figure 8.15(c), which shows negligible amounts of CH_4 in the coal seam close to the CO_2 injection well. It may need more time for this remaining CO_2 to diffuse to a greater distance and produce the remaining CH_4 from the seam. In relation to the amount of N_2 remaining in the coal seam after this 50 years' period, Figure 8.15(b) shows only a very small amount of N_2 remains in the coal matrix after the injection period, and the proportion of CO_2 to N_2 in the coal matrix is much less than the 5:1 proportion injected. This is because injecting N_2 largely stays as a free gas in the coal seam, and therefore has a greater tendency to be released from the coal seam with the gas being produced, resulting in lower volumes of N_2 remaining in the coal seam after the production process. This confirms the minor influence of the N_2 in the injection gas on post-injection gas production. Figure 8.16 compares the CO_2, N_2 and CH_4 present in the coal seam after 50 years of 20% CO_2+80% N_2 injection. According to the figure, although there is a 1:5 proportion of CO_2:N_2 in the injecting gas, the N_2 remaining in the seam after 50 years injection is much less than the CO_2. This again proves that N_2 has a greater tendency to be released from the coal seam with the gas being produced and therefore has a minor influence on post-injection gas production from the seam. This post-injection gas production seems to be mainly governed by the existing CO_2 in the seam. However, when Figures 8.15 and 8.16 are compared, in can be clearly seen that a lower amount of methane gas exists in the coal seam due to 20% CO_2+80% N_2 injection compared to the 80% CO_2+20% N_2 injection. This exhibits the greater degree of gas production enhancement created by N_2 during the injection period.

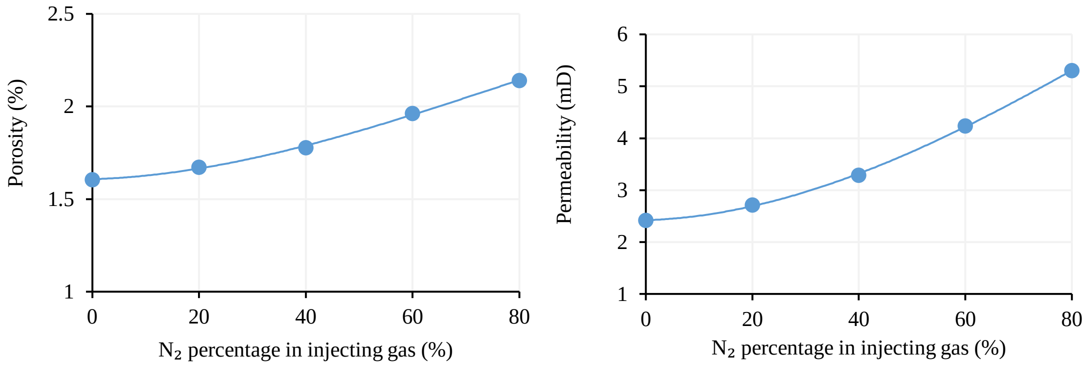

(a) Seam porosity (b) Permeability

Figure 8.14. Variations of seam porosity and permeability with N_2 percentage in the injecting gas

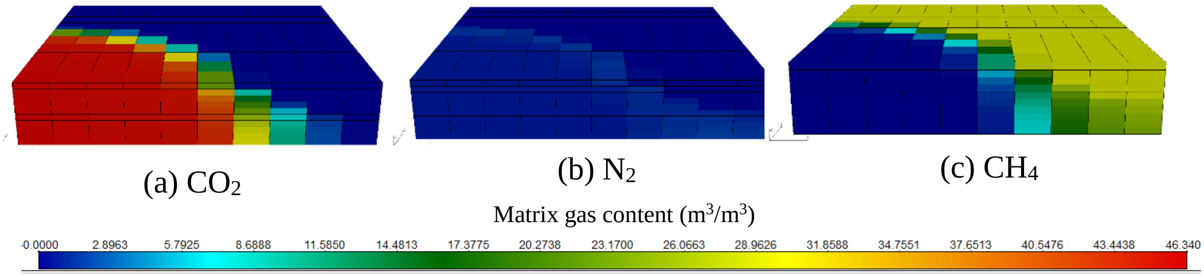

Figure 8.15. CO_2, N_2 and CH_4 in the coal seam after 50 years of 80% CO_2+20% N_2 injection

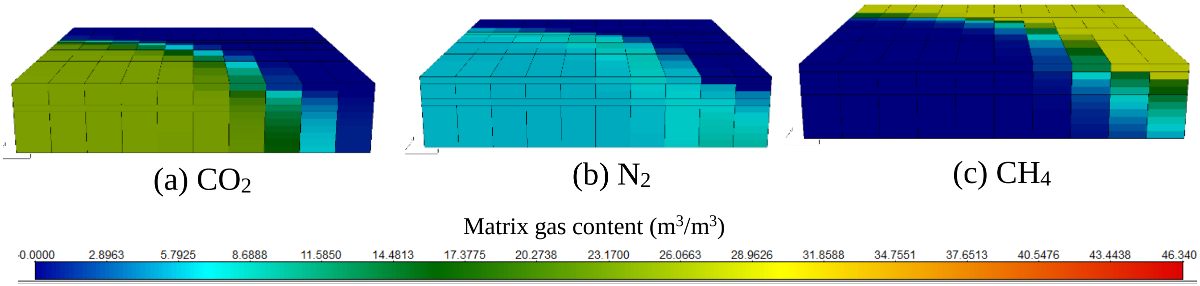

Figure 8.16. CO_2, N_2 and CH_4 in the coal seam after 50 years of 20% CO_2+80% N_2 injection

However, since N_2 is basically present as a free gas in the coal mass, there is a high risk associated with the leaking of injected N_2 with the produced gas via the CH_4 production well. Therefore, this was checked in the next stage of the study. According to Figure 8.17, N_2 starts to leak through the production well sometime after the N_2+CO_2 injection and the leakage rate increases with increasing N_2 percentage in the injecting gas. On the other hand, according to Figure 8.18, the injection of a N_2+CO_2 mixture also has a significant influence on CO_2 breakthroughs in the gas being produced, although the leakage initiates a long time after the N_2 leakage initiation and the leakage amount is more than a thousand times smaller than that of N_2. According to Figure 8.19, increasing the N_2 percentage in the injecting gas from 20 to 80 % causes the total N_2 and CO_2 leakage during 50 years of production to increase by around 490% and 95%, respectively, which implies that changing the N_2 percentage more than 5 times significantly affects N_2 leakage compared to that of CO_2. This implies that N_2 leakage should be a more important consideration when deciding the N_2 percentage in the injecting gas in field projects.

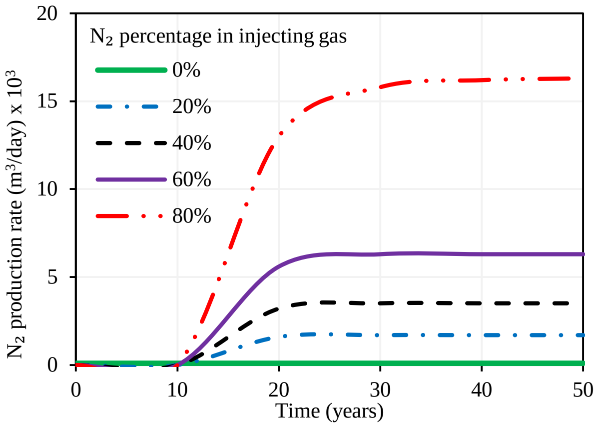

(a) N_2 production rate

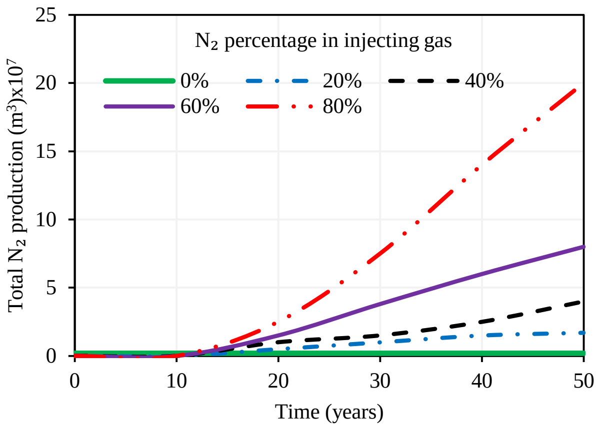

(b) Cumulative N_2 production

Figure 8.17. N_2 production rate and cumulative N_2 production through the production well

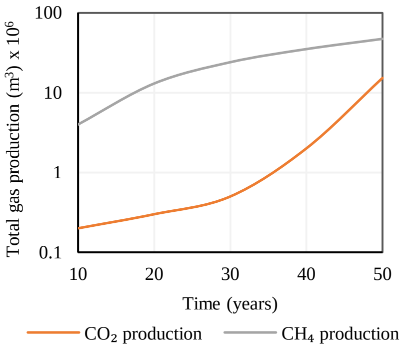

(a) 0% N_2 + 100% CO_2

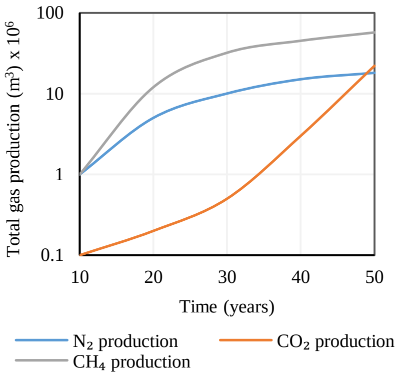

(b) 20% N_2 + 80% CO_2

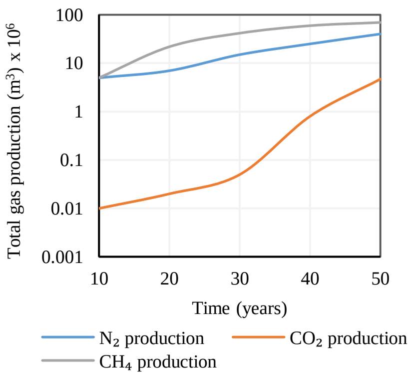

(c) 40% N_2 + 60% CO_2

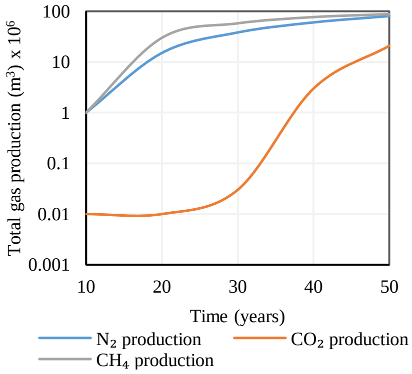

(d) 60% N_2 + 40% CO_2

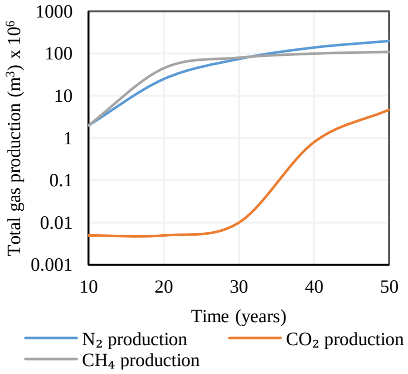

(d) 80% N_2 + 20% CO_2

Figure 8.18. Comparison of N_2 and CO_2 leakages and CH_4 production enhancement due to the N_2 + CO_2 injection into the coal seam with varying percentages of N_2

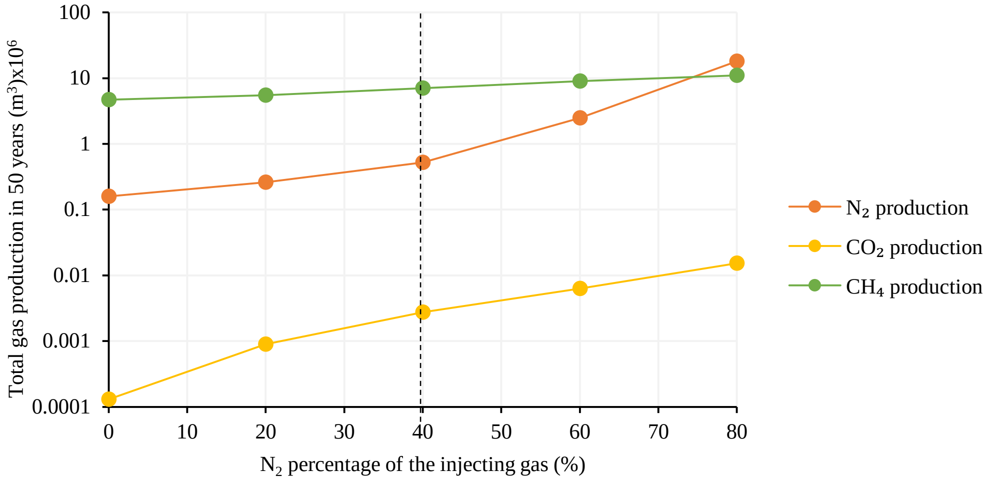

Figure 8.19. Comparison of effect of percentage of N_2 in the injecting gas on N_2 and CO_2 leakage

Therefore, it is very important to decide the best combination of N_2 and CO_2 in the injecting gas to minimize the risks associated with the ECBM process while maximizing CH_4 production. According to Figure 8.19, the addition of more than 60% N_2 in the injecting gas seems to create vary rapid N_2 and CO_2 leakage rates. Therefore, the injecting gas should contain less than 60% N_2 to ensure safe methane recovery enhancement. If the effect of the N_2 percentage in the injecting gas on the methane production enhancement is then considered, according to Figure 8.18, more than 40% N_2 in the injecting gas causes the production of greater amounts of N_2 than CH_4. Therefore, the desired N_2 percentage in the injecting gas should be less than or equal to 40%. Now, if Figure 8.18 is considered, increasing the N_2 percentage in the injecting gas from 0 to 20%, 20 to 40 %, 40 to 60% and 60 to 80% causes CH_4 production to be enhanced by around 16.5%, 19.5%, 21.4% and 21.7%, respectively. Therefore, at least 40% N_2 in the injecting gas is required to enhance methane production by a significant amount. Therefore, considering the effect of both CO_2/N_2 leakage and CH_4 production enhancement, 40% N_2 +60% CO_2 is the best injecting gas combination for an effective CO_2+N_2-ECBM process to safely enhance methane recovery from the selected coal seam.

8.3.3.3 Influence of production and injection well arrangement on enhanced coal seam production

Gas injection wells and water and methane production wells play a vital role in the ECBM process, and therefore have a significant influence on process optimization. This was considered in the next stage of the study, by changing the well arrangement while maintaining the other influencing factors at constant values (temperature, moisture content depth and injection pressure were 60 ^{0}C, 90%, 800 m and 18 MPa, respectively).

a) CO_2 injection well arrangement

The effect of CO_2 injection well arrangement on the optimization of the ECBM process was first considered. One CO_2 injection well was first used and the number of injection wells was then increased up to four, as shown in Figure 8.20 and the corresponding variation in CH_4 production was examined. As expected, increasing the number of injection wells from one to three causes the CH_4 production to be greatly enhanced (155%) (Figures 8.21 and 8.22). This was expected, as increasing the injection well allows more CO_2 to be injected into the coal seam, which enhances the CH_4 production process by replacing existing methane with the injecting CO_2.

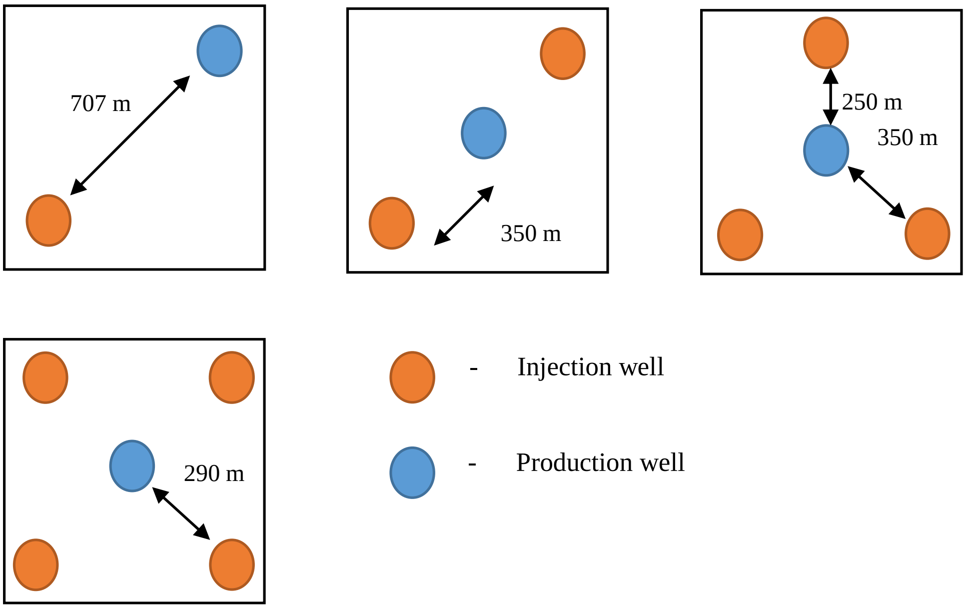

Figure 8.20. Different injection well patterns considered for the analysis

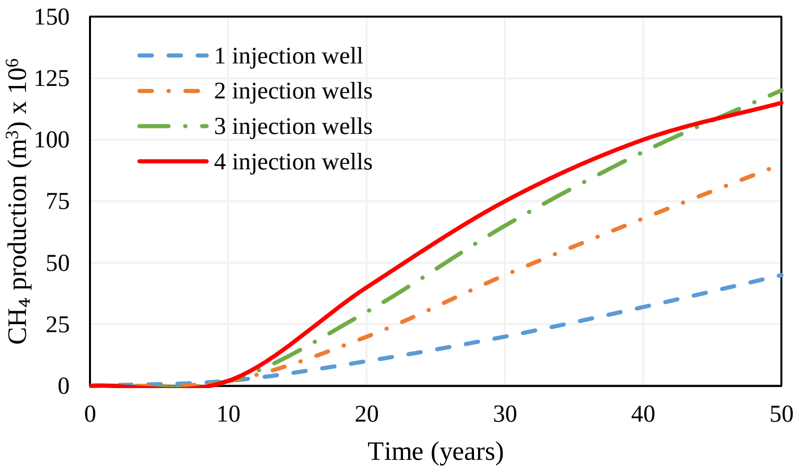

Figure 8.21. CH_4 production with time for different numbers of injection wells

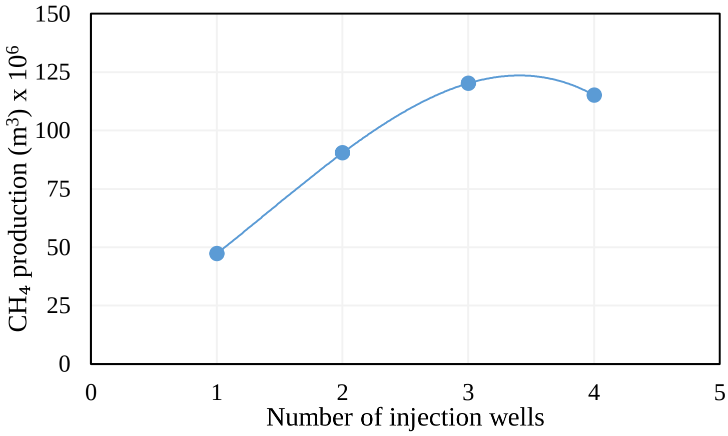

Figure 8.22. Change of CH_4 production with number of injection wells.

However, according to Figures 8.21 and 8.22, the addition of more than three injection wells causes a reduction in CH_4 production. In order to identify the possible reasons for this, pressure development inside the coal seam under each well condition was examined and the results are shown in Figure 8.23. According to the figure, coal seam pore pressure greatly increases with the increasing number of injection wells. This is because the distance between the injecting points is reduced with increased numbers of injecting wells, resulting in the pressure contours produced by each CO_2 injecting well meeting each other within a shorter time, which causes the build-up of unnecessary pore pressure inside the coal seam. This negatively influences CH_4 release from the coal matrix and consequently the CH_4 production capacity. The methane available in the coal seam after the injection period was examined for each well condition (see Figure 8.24). According to the figure, the configuration of three injection wells has the lowest amount of methane present in the coal seam after 50 years compared to other configurations. This further confirms the minor contribution to long-term CBM production by adding a fourth injection well to the system (refer to Figure 8.24(d)). When all of these facts are considered, it is clear that the addition of the fourth well to the seam does not make any significant contribution to methane production, instead it reduces overall production by creating unnecessary pressure in the coal seam, which must be removed to enable optimum gas production from the seam. This finding indicates the importance of numerical models to estimate the performance of injection wells, to facilitate the selection of the optimum number of injection wells for ECBM. This is very important for the economic aspects of the project.

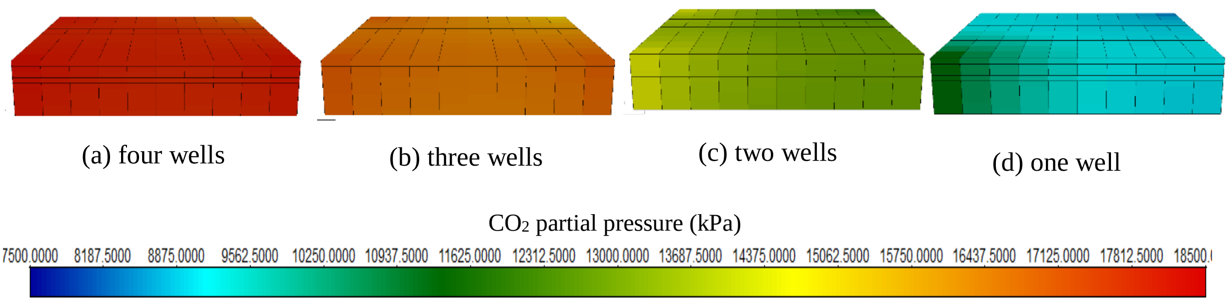

Figure 8.23. CO_2 pressure developed after 50 years of CO_2 injection using one to four injection well conditions

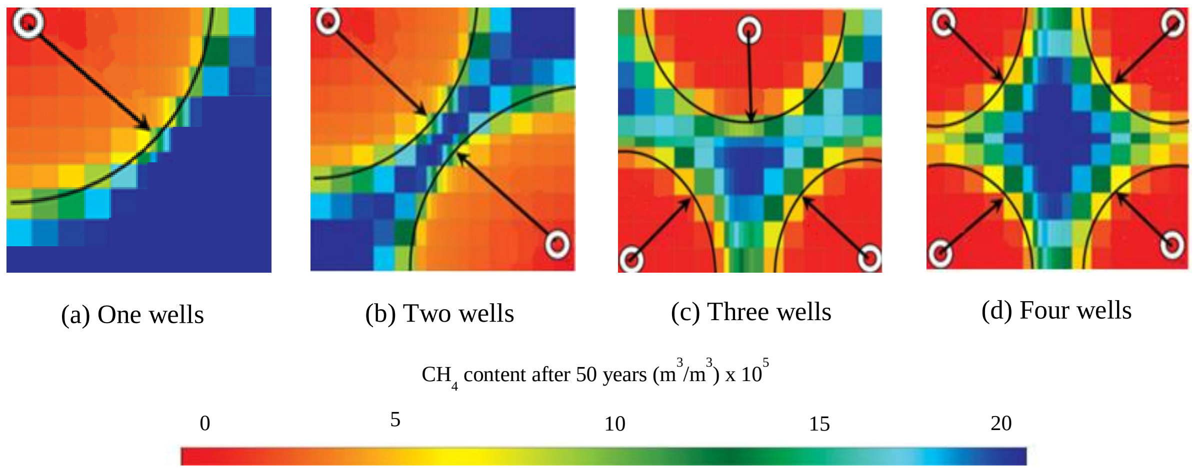

Figure 8.24. CH_4 available in the coal seam after 50 years of CO_2 injection using one to four injection well conditions

In addition, too many injection wells cause the distance between the injection and production wells to be reduced, resulting in the mixing of injecting CO_2 with the CH_4 produced. According to Oldenburg (2006), mixing these two gases also contributes to the development of additional pore pressure inside the seam, which causes additional production depletion.

b) CH_4 production well arrangement

The effect of production well arrangement was then considered, and the results are shown in Figure 8.25. One production well was used first and the number of production wells was then increased up to four and the corresponding variation in CH_4 production was examined (Figures 8.26 and 8.27). According to Figures 8.26 and 8.27(b), an increase in the number of production wells has an insignificant impact on long-term (50 years) CH_4 production, with less than 10% change from one to four wells. However, according to Figure 8.27(a), in the case of short-term CH_4 production (10 years), there is a significant increase in CH_4 production due to an increment in production. For example, an increase of production wells from one to two results in around a 145% increase in 10-

year total CH_4 production, and an increase from one to four results in around a 450% increase in 10-year total CH_4 production. It is most probable that more production wells open more points to the atmosphere, which reduces the average distance that methane has to travel to reach the well. This increases the rate of production and leads to a greater amount of methane being produced in the short term. However, in the long term the methane would have more than enough time to travel to wells placed farther away and hence there would be little difference between having one well or four wells. This may be the reason for the significant short-term increase in coal seam CH_4 production and the negligible variation in long-term CH_4 production with an increased number of production wells.

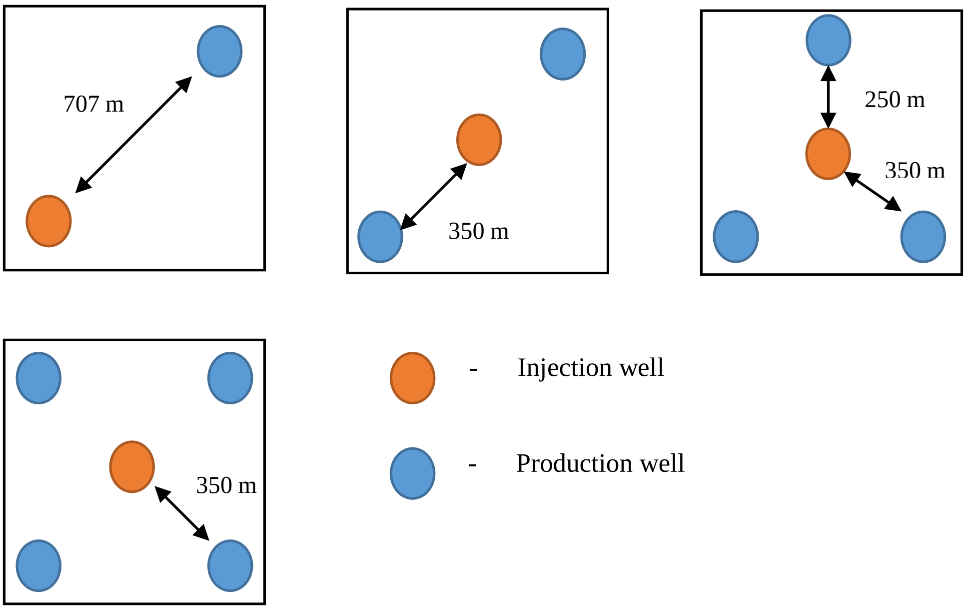

Figure 8.25. Different production well patterns considered for the analysis

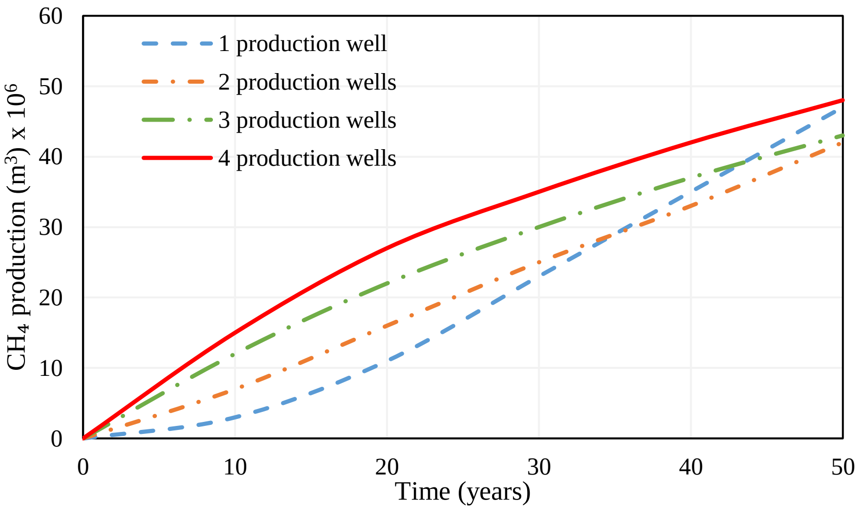

Figure 8.26. CH_4 production with time for different numbers of production wells

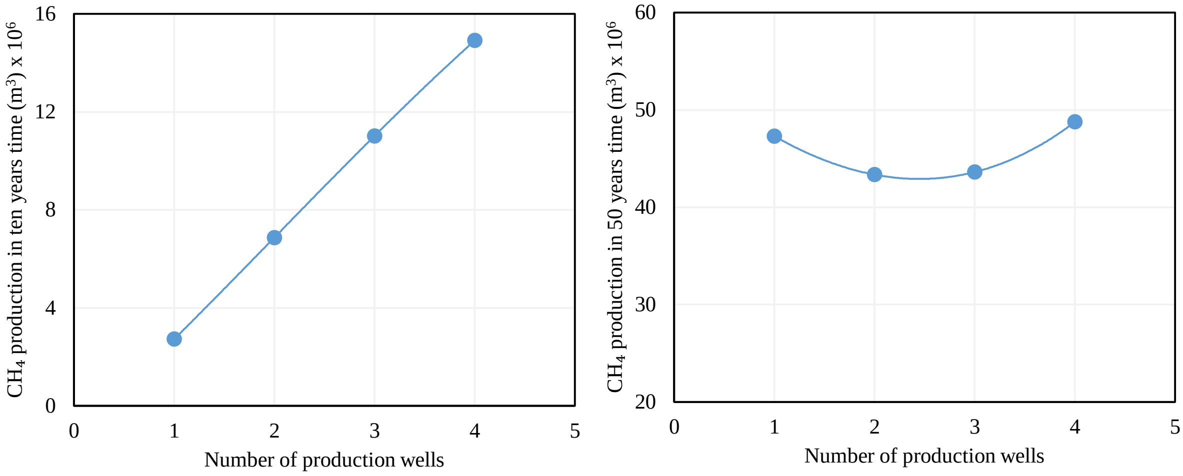

(a) After 10 years

(b) After 50 years

Figure 8.27. Change of CH_4 production in ten years and fifty years with number of production wells

In field situations, the short-term benefits of having extra production wells must be balanced against the costs of drilling in order to obtain the optimum number of production wells. This requires the use of an accurate numerical model.

c) Distance between the injection and production well

According to Sections 8.3.4.3(a) and (b), the distance between the CO_2 injecting well and the CH_4 production well (Figure 8.28) plays an important role in the optimization of the ECBM process, and this was therefore examined in the next stage of the study. In this case, the distance between the two wells was gradually changed (71 m, 142 m, 250 m, 350 m and 707 m) while maintaining the other factors as constants (temperature, moisture content, depth and injection pressure were 60 ^{0}C, 90%, 800 m and 18 MPa). According to Figure 8.29, the total CH_4 production increases by increasing the distance between the injecting and production wells, which is related to the combined influence of two different processes: (1) a close spacing between the injecting and production wells causes much CO_2 to be injected near the production well that greatly swells the coal matrix around the production well, resulting in reduced permeability, and (2) mixing of a small amount of CH_4 with CO_2 causes the CO_2 density to be greatly increased, which creates additional pore pressure development in the coal seam (Oldenburg 2006).

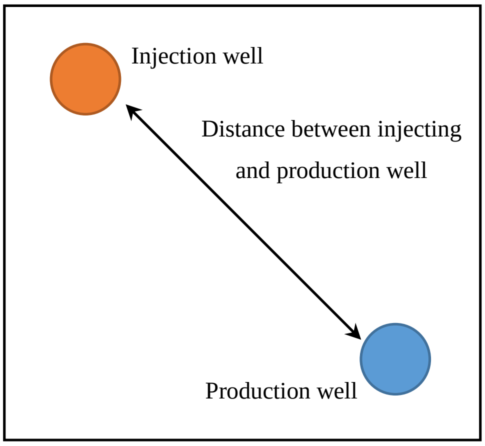

Figure 8.28. Distance between injecting and producing wells

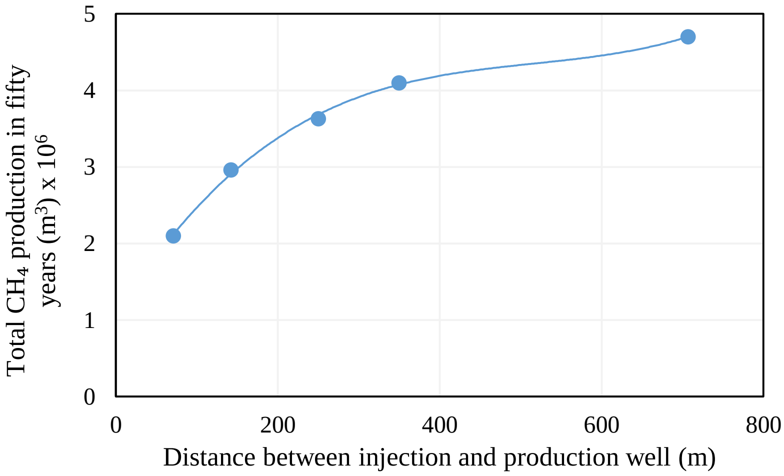

Figure 8.29. The effect of changing the distance between injecting well and production well on enhanced CH_4 production

Overall, all of these observations indicate the importance of an appropriate numerical model to estimate the optimum distance between the wells to recover the maximum amount of CO_2 from a selected coal seam during the CO_2-ECBM process.

8.3.4 Conclusions

The optimization of the enhanced coal bed methane (CBM) recovery process requires numerical modelling tools to reduce the complexity, cost and extensive time associated with laboratory and field experiments. Although some experimental, numerical and field studies have been conducted on the ECBM process and production enhancement techniques, to date none of them has considered the influences of all the possible primary effective factors on the process. As a result, it has been difficult to obtain a comprehensive knowledge of the subject. A 3-D numerical model was therefore developed using the COMET 3 numerical modelling tool to simulate 50 years of CH_4 production from a 800 m deep 500 m × 500 m × 50 m coal seam. All the possible major CBM production enhancement techniques were tested: changes of seam properties and injection gas properties, water removal, CO_2 injection, $CO_2 + N_2$ gas mixture injection, and change of injection and production well arrangement. According to the results the following major conclusions can be drawn:

- Although the CO_2-ECBM technique has greater ability to enhance CBM production than the traditional water removal process, it is necessary to maintain appropriate injection practices to obtain optimum gas production. For example, for the coal seam under consideration, the injection of CO_2 at 10 MPa pressure did not have a significant influence on CBM production, because CO_2 injection under that pressure fails to maintain an adequate flow rate through the coal seam due to insufficient pushing force created by the pressure gap between the injecting CO_2 and the coal seam.
- Coal seam properties have considerable influences on the CO_2-ECBM process, and ECBM production generally reduces with increasing seam temperature for two main reasons: a) thermal expansion occurs in the coal matrix with increasing temperature, which reduces the pore space and seam permeability, and therefore CO_2 adsorption and methane recovery potential, and 2) kinetic energy enhancement in the injecting CO_2 molecules with increasing temperature reduces the CO_2 adsorption rate into coal. However, changing the CO_2 phase condition from sub- to super-critical with increasing temperature may create a contradictory temperature influence on ECBM production due to the higher sorption capacity of super-critical CO_2. Regarding the bed moisture content effect, ECBM production decreases with increasing moisture content up to the critical moisture content of the seam, due to the porosity reduction created by the occupying water molecules. However, further increase of bed moisture content does not have any significant influence on ECBM production, because after the critical point, the excess water stays in a free state and does not affect the seam porosity or gas sorption capacity. Regarding the influence of seam depth on ECBM production, ECBM production greatly reduces with increasing depth, due to the increased effective stress acting on the coal, which reduces the pore space and consequently increases the tortuosity for gas movement inside the coal seam. In turn, both reduce the CO_2 adsorption capacity and consequently the CBM production.
- In addition to the seam properties, injecting CO_2 properties also significantly affect the performance of the ECBM process, and CO_2 injection pressure and composition are critical. Regarding the injection pressure effect, ECBM production exponentially increases with increasing CO_2 injection pressure, due to the expanded pore space and enhanced CO_2

adsorption capacity at increased CO_2 injection pressures. Interestingly, injection pressure plays the dominant role in the CO_2-ECBM process compared to the other factors. For example, in the selected seam, 100% increment in injection pressure, depth, temperature and moisture content cause ECBM production to be changed by around 88%, 58%, 19% and 3.1%, respectively. However, increasing the injection pressure should be done in a well-controlled manner to avoid any significant fracture formation in the seam that may lead to CO_2 leakage. Regarding the influence of injecting gas composition, the addition of N_2 to the injecting gas has considerable potential to enhance the ECBM process, and this enhancement greatly increases with increasing N_2% in the injecting gas. For example, for the considered seam, increasing the proportion of N_2% from 20 to 80% causes ECBM production to be increased by around 160%. This is because ECBM production enhancement caused by N_2 creating an imbalance between sorbed and free gas phases is quicker than the ECBM production enhancement caused by CO_2 through adsorption. Therefore, in short-term production, during the injection period, the influence of N_2 is greater. However, post-injection gas production is mainly governed by the existing CO_2 in the coal seam, because after the injection period only a small amount of N_2 remains in the seam. It is very important to decide the best combination of N_2 and CO_2 in the injecting gas to minimize the risks associated with the ECBM process (mainly the leakage of injecting CO_2 and N_2 with the gas produced, which causes large purifying costs) while maximizing CH_4 production. For the considered seam, 40% N_2 +60% CO_2 is the best injecting gas combination when both CO_2/N_2 leakage and CH_4 production enhancement are considered.

- The number of injection and production wells and their arrangement have a significant influence on the enhancement of ECBM production. Although ECBM production can be significantly increased by increasing the number of CO_2 injection wells, too many wells may cause it to be reduced. This is because having too close wells causes the pressure contours produced by each well to coincide, which may cause unnecessary pore pressure development inside the coal seam. For example, for the considered coal seam, the addition of more than three injection wells causes the production to be reduced instead of enhanced. The reason is that the fourth well has limited ability to spread the injected CO_2 into the coal seam, due to the pressure development in the surrounding areas caused by the other injection wells, which acts as a barrier to CO_2 movement. Under such conditions, creating additional pressure through this fourth well limits the CO_2 spreading ability of the other wells, which negatively influences the ECBM process. Regarding the influence of production wells on the ECBM process, increasing the number of production wells does not have a significant influence on long-term CH_4 production (50 years in the selected coal seam), although it has a great impact on short-term

ECBM production (10 years in the selected coal seam). This is because, with an increased number of production wells, the methane needs to travel shorter distances to reach the production wells, which increases the rate of production in the short term. In the long term, the methane has sufficient time to reach even far wells. Therefore, the influence of the number of wells is insignificant. Considering these findings, the following injection and production well arrangement (refer to Figure 8.30) is proposed for maximum methane production after 50 years' time.

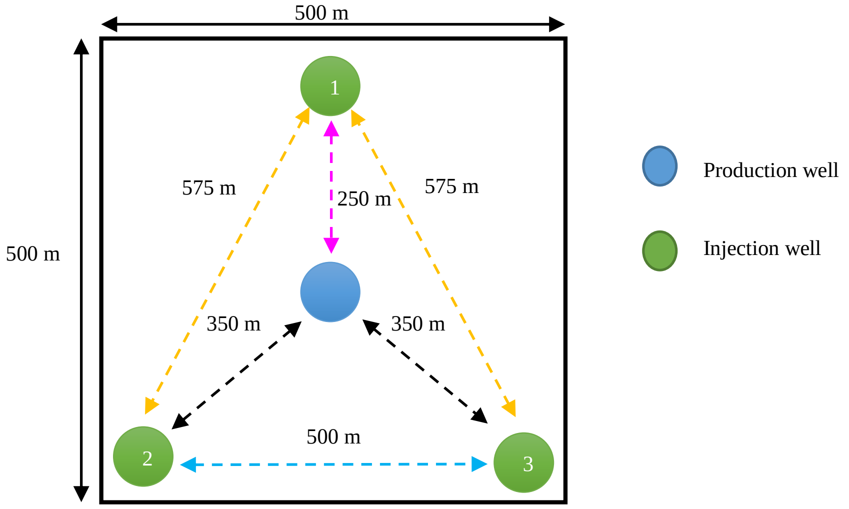

Figure 8.30. Proposed well arrangement for the maximum amount of CBM production under the optimum effective factors: temperature - 60 ^{0}C, moisture content – 90%, depth – 800 m and injection pressure - 18 MPa

8.3.5 References

Akin, S., (2001). Estimation of fracture relative permeabilities from unsteady state corefloods. *J Petrol Sci Eng* 30, 1-14.

Anderson, R.B., Hall, W.K,, Lecky, J.A., Stein, K.C., (1956). Sorption studies on American coals. *The Journal of Physical Chemistry* 60, 1548-1558.

Bae, J.S., Bhatia, S.K., (2006). High-pressure adsorption of methane and carbon dioxide on coal. *Energy & Fuels* 20, 2599-2607.

Balan, H.O., Gumrah, F., (2009). Assessment of shrinkage-swelling influences in coal seams using rank-dependent physical coal properties. *International Journal of Coal Geology* 77, 203-213.

Carneiro, J., (2009). Numerical simulations on the influence of matrix diffusion to carbon sequestration in double porosity fissured aquifers. *International Journal of Greenhouse Gas Control* 3, 431-443.

Connell, L.D., Sander, R., Pan, Z., Camilleri, M., Heryanto, D., (2011). History matching of enhanced coal bed methane laboratory core flood tests. *International Journal of Coal Geology* 87, 128-38.

De Silva, P.N.K., (2013). A study of CO_2 storage capacity in sedimentary rocks (*PhD thesis*). Monash University, Melbourne, Australia.

[http://arrow.monash.edu.au/hdl/1959.1/915653]

Fujioka, Y., Takeuchi, K., Ozaki, M., Shindo, Y., Komiyama, H., (1995). Stability of liquid CO_2 in seawater at high pressures. *International Journal of Energy Research* 19, 659-665.

Gunter, W.D., (2009). Coal bed methane, a fossil fuel resource with the potential for zero greenhouse gas emissions-the Alberta, Canada program 1996 -2009: A Summary, Alberta Research Council, Alberta.

Hawkes, C.D., Bachu, S., Haug, K., Thompson, A., (2005). Analysis of in-situ stress regime in the Alberta basin, Canada, for performance assessment of CO_2 geological sequestration sites, Fourth Annual Conference on Carbon Capture and Sequestration, Virginia, Paper ID 258.

Holzbecher, E., (2005). FEMLAB performance on 2D porous media variable density benchmarks. FEMLAB Conference, Frankfurt, Germany, pp. 1–6.

Jasinge, D., Ranjith, P.G., Choi, S.K., (2011). Effects of effective stress changes on permeability of Latrobe Valley brown coal. *Fuel* 90, 1292-1300.

Liu, G., Smirnov, A., (2009). Carbon sequestration in coal-beds with structural deformation effects. *Energy Conversion and Management* 50, 1586-1594.

Maimone, L., (2011). Carbon Pricing Implications for Australian Businesses. Price Waterhouse Coopers, Sydney, Australia.

Mazzotti, M., Pini, R., Storti, G., (2009). Enhanced coalbed methane recovery. *The Journal of Supercritical Fluids* 47, 619-627.

Oldenburg, C.M., (2006). Geologic carbon sequestration: CO_2 transport in depleted gas reservoirs, *Gas Transport in Porous Media,* Ho, C.K., Webb, S.W. (Eds.), Springer, Netherland, Chapter 26, pp 419-425.

Pagnier, H., van Bergen, F., Krzystolik, P., (2006). Reduction of CO_2 emission by means of CO_2 storage in coal seams in the Silesian coal basin of Poland, TNO-RECOPOL, final report, Delft.

Parakh, S., (2007). Experimental investigation of enhanced coal bed methane recovery (*MSc thesis*), Stanford University, CA, USA.

Pekot, L.J., Reeves, S.R., (2002). Modeling coal shrinkage and differential swelling with CO_2 injection for enhanced coal bed methane recovery and carbon sequestration application, Advanced Resources International, Houston, TX, pp.1-20.

Perera, M.S.A., Ranjith, P.G., Choi, S.K., Bouazza, A., Kodikara, J., Airey, D., (2010) A review of coal properties pertinent to carbon dioxide sequestration in coal seams: With special reference to Victorian brown coals. *Environmental Earth Sciences* 64, 223-235.

Perera, M.S.A., Ranjith, P.G., Peter, M., (2011a). Effects of saturation medium and pressure on strength parameters of Latrobe Valley brown coal: Carbon dioxide, water and nitrogen saturations. *Energy* 36, 6941–6947.

Perera, M.S.A., Ranjith, P.G., Choi, S.K., Airey, D., (2011b). Sub-and super-critical carbon dioxide flow behavior in naturally fractured black coal: An experimental study. *J Fuel* 90, 3390–3397.

Perera, M.S.A., Ranjith, P.G., Choi, S.K., Airey, D., (2011c). The effects of sub-critical and super-critical carbon dioxide adsorption-induced coal matrix swelling on the permeability of naturally fractured black coal. *Energy* 36, 6442–6450.

Perera, M.S.A., Ranjith, P.G., Choi, S.K., Airey, D., (2011d). Numerical simulation of gas flow through porous sandstone and its experimental validation. *Fuel* 90, 547-554.

Perera, M.S.A., Ranjith, P.G., Choi, S.K., Bouazza, A., Kodikara, J., (2011e). Effects of seam conditions, injection pressure and gas composition on CO_2 sequestration in coal, at Geo-Hung International Conference, USA. DOI: http://dx.doi.org/10.1061/47628(407)32].

Perera, M.S.A., Ranjith, P.G., (2012). Carbon dioxide sequestration effects on coal's hydro-mechanical properties: A review. *International Journal of Energy Research* 36, 1015-1031.

Perera, M.S.A., Ranjith, P.G., Viete, D.R., Choi, S.K., (2012a). Parameters influencing the flow performance of natural cleat systems in deep coal seams experiencing carbon dioxide injection and sequestration. *International Journal of Coal Geology* 104, 96-106.

Perera, M.S.A., Ranjith, P.G., Viete, D.R., Choi, S.K., Bouazza, A., (2012b). Effect of well arrangement on carbon dioxide sequestration process in deep un-mineable coal seams: A numerical study. *International Journal of Coal Preparation and Utilization* 32, 211-24.

Perera, M.S.A., Ranjith, P.G., Choi, S.K., Airey, D., (2012c). Investigation of Temperature Effect on Permeability of Naturally Fractured Black Coal: An Experimental and Numerical Study. *Fuel* 94, 596–605.

Perera, M.S.A., Ranjith, P.G., Choi, S.K., Airey, D., Weniger, P., (2012d). Estimation of gas adsorption capacity in coal: a review and an analytical study. *International Journal of Coal Preparation and Utilization* 32, 25-55.

Perera, M., Ranjith, P., Choi, S.K., (2013a). Coal cleat permeability for gas movement under triaxial, non-zero lateral strain condition: A theoretical and experimental study. *Fuel* 109, 389-399.

Perera, M., Ranjith, P., Choi, S.K., Bouazza, A., (2013b). A parametric study of coal mass and cap rock behaviour and carbon dioxide flow during and after carbon dioxide injection. *Fuel* 106, 129-138.

Pini, R., Ottiger, S., Burlini, L., Storti, G., Mazzotti, M., (2006). Experimental study of CO_2 adsorption on coal and other adsorbents aimed at ECBM recovery, 4-PBAST, Tianjin, China.

Ranjith, P.G., Perera, M.S.A., (2012). Effects of cleat performance on strength reduction of coal in CO_2 sequestration. *Energy* 45, 1069-75.

Ranjith, P.G., Perera, M.S.A., Khan, E., (2013). A study of safe CO_2 storage capacity in saline aquifers: A numerical study . *International Journal of Energy Research* 37, 189-199.

Reeves, S., (2001). Geological sequestration of CO_2 in deep, un-mineable coal beds: An integrated research and commercial-scale field demonstration project. Annual Technical Conference and Exhibition, New Orleans, LA, Paper ID SPE-71749-MS.

Reeves, S., (2003). Enhanced coalbed methane recovery, Advanced Resources International, Houston, TX [http://www.adv-res.com/pdf/Reeves%20DL%20Presentation.pdf].

Reeves, S., Schoeling, L., (2000). Geological sequestration of CO_2 in coal seams: Reservoir mechanisms, field performance, and economics, 5th International Conference on Green House Gas Control Technologies, Cairns, USA, pp. 593–598.

Reeves, S., Odinot, A., (2004). The Tiffany unit N_2 - ECBM pilot: A reservoir modeling study: Technical Report, Advance Resource International, Houston, TX [https://www.osti.gov/scitech/biblio/923257].

Sarmah, R., (2011). Coal bed methane:A strategic overview. Report. Ranko Energy Projects, Mumbai.

Sawyer, W.K., Paul, G.W., Schraufnagel, R.A., (1990). Development and application of a 3D coalbed simulator. CIM/SPE Annual technical meeting, Calgary, Document ID: PETSOC-90-119.

Sheory, P.R., (1994). A theory for in situ stresses in isotropic and transversely isotropic rock. *Int. J. Rock Mech. Min. Sci. & Geomech. Abstr*, 31, 23-34.

Skawinski, R., Zolcinska, J., Dyrga, L., (1991). Experimental investigations of the permeability in gas flow in coal with various water content. *Archives of Mining Sciences*, 36, 227-238.

Suggate, R., (1974). Coal ranks in relation to depth and temperature in Australian and New Zealand oil and gas wells. *New Zealand Journal of Geology and Geophysics* 17, 149-167.

Viete, D.R., Ranjith, P.G., (2006). The effect of CO_2 on the geomechanical and permeability behaviour of brown coal: Implications for coal seam CO_2 sequestration. *International Journal of Coal Geology* 66, 204-216.

Vishal, V., Singh, T.N., Ranjith, P.G., (2012). Carbon capture and storage in Indian coal seams, *Carbon Management Technology Conference*, Orlando, FL, Paper ID: CMTC-151614-MS.

Vishal, V., Ranjith, P.G., Singh, T.N., (2013a). CO_2 permeability of Indian bituminous coals: Implications for carbon sequestration. *International Journal of Coal Geology* 105, 36-47.

Vishal, V., Ranjith, P.G., Singh, T.N., (2013b). Geomechanical attributes of reconstituted Indian coals under carbon dioxide saturation. *Rock Mechanics for Resources, Energy and Environment*, Hofmann, M., Klinkenberg, R., (Eds.) CRC Press, London, UK, pp. 171-173.

Vishal, V., Ranjith, P., Pradhan, S., Singh, T., (2013c). Permeability of sub-critical carbon dioxide in naturally fractured Indian bituminous coal at a range of down-hole stress conditions. *Engineering Geology* 167, 148-156.

Vishal, V., Singh, L., Pradhan, S., Singh, T., Ranjith, P.G., (2013d). Numerical modeling of Gondwana coal seams in India as coalbed methane reservoirs substituted for carbon dioxide sequestration. *Energy* 49, 384-394.

Vishal, V., Singh, T.N., Ranjith, P.G., (2015) Influence of sorption time in CO_2-ECBM process in Indian coals using coupled numerical simulation. *Fuel*, 139, 51-8.

Wageningen, W.F.C., Cuesta, P.T., (2005) Determination of change in permeability of coal by bottom hole pressure survey and fall-off test, *Reduction of CO_2 Emission by Means of CO_2 Storage in Coal Seams in the Silesian Coal Basin of Poland Workshop*, Szczyrk, Poland.

Wang, Y., (2012) Reservoir characterization based on seismic spectral variations. *Geophysics*, 77, 89-95.

White, C.M., Smith, D.H., Jones, K.L., Goodman, A.L., Jikich, S.A., LaCount, R.B., DuBose, S.B., Ozdemir, E., Morsi, B.I., Chroeder, K.T., (2005) Sequestration of carbon dioxide in coal with enhanced coalbed methane recovery: A review. *Energy & Fuels*, 19, 659-724.

Wong, S., Gunter, W.D., Law, D., Mavor, M.J., (2000) Economics of flue gas injection and CO_2 sequestration in coalbed methane reservoirs. *International Conference on GHG Control Technologies*, Cairns, Australia, pp. 543–548.

8.4 Chapter summary

The main objective of this chapter was to investigate the CO_2 enhanced coal bed methane recovery technique, paying attention to the applicability of this technique for low rank coal and optimizing the effective factors (seam properties and injecting properties) for maximum methane recovery. The major findings of the experiments and the numerical study are summarised below.

- **Section 8.2** – ***Applicability of CO_2 enhanced coal bed methane recovery technique to low rank coal***

CO_2 injection can significantly enhance methane production compared to natural recovery and higher CO_2 pressures can obtain a 100% sweep efficiency in low rank coal. Super-critical CO_2 takes a shorter time for CO_2 breakthrough, which indicates quicker exchange of methane to CO_2 that drives the recovered methane easily towards the production wells in the field scale. Interestingly, this effectiveness of super-critical CO_2 in CH_4 recovery is common for any coal type. However, this quicker breakthrough of CO_2 causes swelling to start in short time periods after CO_2 injection, which may result in lower permabilities with time. This warrants more attention.

- **Section 8.3** – ***Optimization of CO_2-enhanced coal bed methane recovery***

The CO_2-ECBM technique has a greater capability to recover methane compared to traditional recovery methods when the appropriate injection conditions are practised. Coal seam properties have a great influence on methane recovery by CO_2 injection. For example, methane production is reduced with higher reservoir temperature and the maximum methane production after 50 years was achieved at 60 ^{0}C. Further, the gas production was reduced by up to 90% (critical moisture content) of moisture content and then remained stable for higher moisture contents. The reduced CO_2 adsorption capacity and lower permabilities at higher effective stress have a negative effect on methane production at higher depths, which warrants the use of flow enhancement techniques (such as hydro fracturing) to achieve targeted methane production. In relation to injecting gas properties, an exponential increment of methane production with increasing CO_2 injection pressure was observed for fifty years of injection. However, the use of very high CO_2 injection pressures can create fractures in the coal bed, resulting in leakage of injected CO_2. Comparing these effective factors on methane production, CO_2 injection pressure is the most influential factor for the CO_2-ECBM technique, while moisture content has the least influence and other properties (temperature and depth) moderately affect methane production.

The imbalance created by N_2 molecules between sorbed and free gas is capable of increasing methane recovery, and hence, the higher the N_2 percentage, the higher the methane production. However, N_2 has a greater influence on short-term methane production, while CO_2 governs the long-term production, as only a few N_2 molecules will remain in the coal matrix due to the quicker breakthrough of N_2. Therefore, 40% N_2 + 60% CO_2 is the best injection composition to optimise methane production.

For the considered coal seam, the use of three injection wells produced the maximum results and a greater number of wells reduces production, due to the limitation of CO_2 spreading in the coal bed with the surrounding injection wells. A greater number of production wells improves methane production in the short term and it is limited in the long term. This is because of the shorter travel distance for methane with a large number of production wells in the short term and in the long term, methane has sufficient time to reach even the most distant wells.

Part 5: Chapter 9 - Conclusions and Suggestions for future research

PART 5 - CHAPTER 9

Conclusions and suggestions for future research

9. Conclusions and suggestions for future research

9.1 Conclusions

The main aim of this thesis was to identify ideal injection strategies in order to determine the optimum conditions to harvest methane (CH_4) from deep coal seams while storing maximum amounts of CO_2. Experimental (85% of the thesis), numerical (10% of the thesis) and analytical (5% of the thesis) modelling studies were conducted to achieve the above main objective and this thesis reports them in a structured manner. This thesis comprises five major parts, of which three are dedicated to the presentation of the major outcomes of the thesis, while the other two parts provide the introduction, literature review and conclusions. These parts contain chapters devised to meet specific objectives to achieve the main goal of this thesis. The major conclusions drawn from each relevant part are presented in the following sub-sections.

9.1.1 Conclusions drawn from completion of objective 1: Coal mass flow behaviour during CO_2 sequestration

Several meso-scale and macro-scale flow experiments were conducted to observe coal mass flow behaviour during CO_2 sequestration in low-rank brown coal obtained from the Gippsland basin, Victoria, Australia. Micro-scale studies were also incorporated to gain better insights into the flow patterns observed. The test conditions were varied according to the different effective factors identified in the literature review. The test conditions included different injecting gas properties (different gasses – CO_2 and N_2, and phase and pressure of CO_2) and coal mass properties (depth and temperature). The permeability and swelling behaviour were studied under these different test conditions to determine the expected reservoir behaviours with CO_2 sequestration. Experimental, analytical and numerical studies were carried out to fulfil the objectives and the following major conclusions were drawn:

- In comparison to N_2 permeability (a more inert gas than CO_2), CO_2 permeation causes clear permeability variations in both low and high rank coal, because the uniform cellular-like micro-pore structure with relatively large pores alters significantly with CO_2 adsorption, which negatively affects the coal mass flow performance. Further, super-critical CO_2 (the phase condition of CO_2 which is likely to be available at the depths suitable for CO_2-ECBM) has much lower permeability than sub-critical CO_2, and this influence of CO_2 phase condition increases with increasing rank. This reduces the expected CO_2 injectivity into deep coal seams and eventually the methane production, warranting the use of flow enhancement techniques (e.g. hydro-fracturing).
- Permeability is reduced with increasing depth for both CO_2 and N_2 permeation due to the higher effective stress application and this is common for any coal type. However, this flow

reduction due to depth is less for high rank coal. Interestingly, the influence of depth on permeability reduces with the phase transition from sub- to super-critical in any type of coal, which is beneficial for the application of CO_2-ECBM in deep coal seams.

- CO_2 permeability decreases with higher injecting pressures at low temperatures (25 ^{0}C), whereas permeability increases when the temperature is increased to 40 ^{0}C for any coal type. However, further increase of temperature reduces the adsorption capacity of CO_2 due to the higher kinetic energy, and the expansion of coal mass reduces the porosity. This requires attention when using high temperature-prone coal seams for CO_2 sequestration.
- N_2 exhibits comparatively inert behaviour in coal, producing negligible swelling, regardless of pore pressure and reservoir depth. However, the partial pressure depletion created by N_2 in the coal mass has the ability to recover CO_2 adsorption-induced swelled areas in coal, and this ability is much greater for high rank coal. If N_2 flooding is carried out for a sufficiently long period under low effective stress conditions, the recovery of CO_2 adsorption-induced swelled areas is also increased. Hence, the use of alternative N_2 injection or N_2 and CO_2 co-injection is beneficial in field applications of CO_2-ECBM to enhance CO_2 injectivity.
- A new descriptive analytical model is proposed for coal matrix swelling with gas adsorption using the effective factors by modifying the existing D-R model. The proposed equation can estimate coal mass swelling due to various gas adsorptions in different coals with an accuracy of around ±1% and hence can be used as a descriptive analytical model to estimate swelling. However, the equation was developed for a range of coals with a fixed carbon content of >75% and hence, provides a better fit of data for this range.
- The laboratory-scale COMSOL model can predict the experimental results for macro-scale coal specimens reasonably well, and according to the extended model results, for a given axial load, CO_2 concentration increases with the increase in injection pressure, due to the increase in net advective CO_2 flux with the increase in injection pressure. Furthermore, greater amounts of CO_2 can be sequestrated in coal seams even at higher depths and higher CO_2 pressures despite the flow reduction observed if sufficient time is allowed for CO_2 permeation.

9.1.2 Conclusions drawn from completion of objective 2: Coal mass strength behaviour during CO_2 sequestration

Several meso-scale strength tests were conducted to observe the coal mass mechanical property variations during CO_2 sequestration in low rank brown coal coupled with micro-scale studies using SEM and X-ray CT, acoustic emission systems and ARAMIS optical photogrammetry system to obtain a better perception of the observed strength variations. The test conditions were varied according to the different effective factors similar to flow experiments including different fluid saturations, different durations of CO_2 saturation, the depth effect, the rank effect and the effect of heterogeneity of coal. Experimental and numerical studies were carried out to fulfil the objectives and the following major conclusions were drawn:

- Both sub- and super-critical CO_2 adsorption cause brown coal's mechanical properties to be significantly reduced and in comparison, super-critical CO_2 adsorption causes significantly greater mechanical property alterations than sub-critical CO_2 for any coal type. Further, CO_2 saturation in any coal type causes early stages of fracture development and the effect is greater for super-critical CO_2 adsorption. This is not favourable for the long-term integrity of the CO_2-ECBM process, as it may increase the risk of back-migration of injected CO_2 into the atmosphere.
- Similar to the permeability variations, high rank coal is subjected to greater strength reductions than low rank coal. Hence, more attention should be paid to the use of low rank coal seams (at suitable depths) for CO_2 sequestration.
- CO_2 adsorption-induced coal matrix alterations are largely completed with the initial interaction with CO_2, but considerable further coal matrix re-arrangement may occur at a slower rate.
- Similar to CO_2, water also causes a significant strength reduction in coal regardless of rank. Interestingly, these reductions are higher for high rank coal same as CO_2 saturations (around 25% higher). Further, both water and CO_2 saturations produce a less dense and altered pore structure for both low and high rank coals.
- N_2 saturation slightly enhances coal strength, regardless of rank, and this increment increases with increasing N_2 saturation pressure. Further, low rank coals with greater free moisture content are subjected to higher strength increments (2 to 4% higher) than low moisture high rank coal with N_2 saturation.
- Coal mass exposed to CO_2 behaves similarly even under confinement, however the reductions in strength parameters are much lower compared to unconfined environments. In addition, the strength and stiffness reductions with the application of confinement can be represented by a Langmuir-type equation.
- Although coal is highly heterogeneous in nature, the behaviour under different effective conditions (different fluid types and coal seam properties) is similar. However, the arrangement of the natural cleat structure is highly influential on the variation of the magnitudes of strength and permeability.
- The laboratory-scale COMSOL model can predict the experimental results for meso-scale reconstituted coal specimens reasonably well, and according to the extended model results, confining pressure adds a surplus strength to the CO_2 treated coal mass with pore shrinkage and lower CO_2 adsorption capacities at higher effective stresses. Hence, deep coal seams have

less risk of CO_2 leakage into the atmosphere. Notably, the volume of coal subjected to plastic deformation is higher at higher CO_2 pore pressures-saturated deeper coal seams contributing a more ductile nature for the reservoir rock.

9.1.3 Conclusions drawn from completion of objective 3: The optimum conditions to recover CH_4 while storing maximum amounts of CO_2 in deep coal seams

Firstly, the applicability of low rank coal seams as potential CO_2-ECBM sites was experimentally tested using Victorian brown coal. Different CO_2 pressures (sub- and super-critical) were injected into CH_4 saturated samples under confinement to observe the CH_4 production and CO_2 adsorption capacities. According to the experimental results:

- CO_2 injection can significantly enhance methane production compared to natural recovery, and higher CO_2 pressures can obtain a 100% sweep efficiency in low rank coal.
- Super-critical CO_2 takes a shorter time for CO_2 breakthrough, which indicates quicker exchange of methane for CO_2 that will drive the recovered methane easily towards the production wells in the field. Interestingly, this effectiveness of super-critical CO_2 in CH_4 recovery is common for any coal type.
- The coal sample does not start to swell upon the start of CO_2 injection and it takes some time until the sorptive exchange of CH_4 with CO_2, whereas the time taken to start swelling is decreased at higher injection pressures. This may negatively affect long-term gas production, due to the permeability reduction associated with the greater coal matrix swelling. This warrants more attention.

Next, a detailed numerical study was carried out using a 3-D field-scale model built using the COMET3 numerical simulator to investigate optimum injection scenarios and seam conditions to optimize the CO_2-ECBM process in a low rank coal seam (500×500×50 m Victorian brown coal seam at a depth of 800 m). The arrangement of injection and production wells was also considered. The following major conclusions were drawn from this numerical study:

- Methane production is reduced with higher reservoir temperature and the maximum methane production after 50 years was achieved at a range of 50 - 70 ^{0}C.
- Gas production reduced up to 70% (critical moisture content) of moisture content and then remained stable for higher moisture contents. Hence, coal seams with very low moisture contents (<<<critical moisture content) or coal seams with very high moisture content (>>> critical moisture content) will produce higher amount of methane.
- Methane production rates are reduced at greater depths due to the reduced CO_2 adsorption capacity and lower permeabilities with higher effective stress applications. This warrants the use of flow enhancement techniques (such as hydro fracturing) to achieve targeted methane production.

- In relation to injecting gas properties, a gradual increment of methane production with increasing CO_2 injection pressure was observed up to 16 MPa. However, the CBM production increment is reduced with higher CO_2 injection, as the sorption-induced strain of the coal mass restricts the pore spaces for CO_2 sequestration.
- A comparison of the collective effect of these factors on methane production, revealed that CO_2 injection pressure is the most influential factor for the CO_2-ECBM technique, while moisture content has the least influence and other properties (temperature and depth) moderately affect methane production.
- The injection of N_2 creates a reduction of partial pressure and hence an increment in methane recovery, and the higher the N_2 percentage, the higher the methane production. However, N_2 has a greater influence on short-term methane production while CO_2 governs the long-term production. Therefore, 40% N_2 + 60% CO_2 is the best injection composition to optimise methane production.
- For the considered coal seam, the use of three injection wells produced the maximum results and a higher number of wells reduces production due to the limitation of CO_2 spreading in the coal bed with the surrounding injection wells.
- A greater number of production wells improves methane production in the short term, although it becomes limited in the long term. This is because the travel distance for methane with a large number of production wells in shorter in the short term and in the long term, methane has sufficient time to reach even the most distant wells.

9.2 Key findings from the research

This research has been conducted to investigate the long-term safe storage of CO_2 in deep coal seams with enhanced methane recovery. Table 9.1 presents the key findings of the present research which has addressed a significant gap in the research area and made a contribution to knowledge.

Table 9.1. Key findings of the research

Objective 1	***Coal mass flow behaviour during CO_2 sequestration***			
Effective factor	**Observation for permeability of coal**		**Rank effect**	
	Conditions	*Influence**	*Low rank coal*	*High rank coal*
CO_2 phase and pressure	Increasing pressure	Negative (10 – 65%)	Lower	Higher
Depth	Increasing depth	Negative (45 – 80%)	Higher	Lower
Temperature	Lower temperatures (<40^0C)	Negative (1 – 9%)	-	-

CO_2 storage	Increasing effective stress	Negative (15 – 50%)	-	-
	Increasing CO_2 injection time	Positive (5 – 30%)	-	-
N_2 induced swelling recovery	Increasing N_2 pressure	Positive (1 – 20%)	Lower	Higher
	Increasing time of N_2 flooding	Positive (1 – 18%)	-	-
Objective 2	***Coal mass mechanical behaviour during CO_2 sequestration***			
Effective factor	**Observation for strength of coal**		**Rank effect**	
	Conditions	*Influence*	*Low rank coal*	*High rank coal*
CO_2 phase and pressure	Increasing pressure	Negative (15 – 70%)	Lower	Higher
Depth	Increasing depth	Positive (5 – 45%)	Higher	Lower
Different fluid types	Water	Negative (15 – 40%)	Lower	Higher
	N_2	Positive (2 - 8%)	Higher	Lower
Objective 3	***The optimum conditions to recover CH_4 while storing maximum amount of CO_2 in deep coal seams*** **1. Applicability of CO_2 enhanced coal bed methane recovery to low rank coal**			
Effective factor	**Observation for CH_4 recovery potential**			
	Condition		*Influence*	
Sweep efficiency	Increasing CO_2 pressure		Positive (~40%)	
	2. Optimization of CO_2-enhanced coal bed methane recovery			
Effective factor	**Observation for CH_4 recovery potential after 50 years**	**Optimum conditions for maximum CH_4 recovery for a typical low rank coal seam (500x500x50m) at a depth range of 800 m**		
Increasing CO_2 pressure		≤ 18 MPa Note: Should be less than the reservoir pressure for safe CO_2 injection pressure		
- Lower pore pressures	Positive (35 - 50%)			
- Higher pore pressures	Positive (~5%)			
Temperature	Negative (~40%)	50 – 70 ^{0}C		
Moisture content	Positive (~13%)	<20% or >70%		
Injecting gas composition				

- Higher % of N_2 and lower % of CO_2	Positive (>15%)	40%	To reduce the N_2 leakage and to store more CO_2
Higher no of injection wells	Negative	3	
Higher no of production wells			
- Short term	Positive	~ 1 or 2	
- Long term	Negative		
Greater distance between the injection and production well			
- Short term	Negative	~ 350 m onwards	
- Long term	Positive		

*Here negative means a reduction and positive means an increment of the considered coal parameters (permeability, strength or CH_4 recovery)

9.3 Suggestions for future research

The following sections highlight suggestions for future research based on the present research work.

9.3.1 Studies of flow behaviour

- Similar to CO_2 permeability, an understanding of CH_4 permeability is also essential for a better understanding of CH_4 production from coal seams. Therefore, future research is needed on methane permeation under various pressures for different rank coals.
- All the flow studies in the present research were conducted after removing the moisture from the samples. However, future flow studies are needed for samples with moisture to replicate actual field conditions.
- In the present study, the macro-scale tests were conducted using reconstituted samples due to the inability to obtain large blocks of low-strength brown coal. Therefore, it is proposed to conduct permeability tests on natural macro-scale samples, the results of which would help to determine the effect of the heterogeneous nature of coal on coal permeability, which is the actual nature of coal in natural coal seams.
- The analytical model proposed in the study does not contain the effect of depth on coal swelling due to the lack of experimental data for different coal types with various gas adsorptions. Therefore, it is suggested to conduct experiments and modify the proposed model to include a term for the effect of depth.
- It was observed that N_2 can recover CO_2 adsorption-induced swelling in coal and the field-scale numerical study showed CH_4 recovery enhancement with the co-injection of CO_2 and N_2.

There have been several experimental studies on CO_2 and N_2 co-injection for permeability enhancement in high rank coals, but studies on low rank coals are lacking. Therefore, it is proposed to conduct experimental studies on low rank coal regarding flow enhancement by CO_2 and N_2 co-injection.

9.3.2 Studies of strength behaviour

- Methane is one of the major components in coal seam gas that plays an important role in the overall mechanical response of the coal mass. Hence, to understand the overall influence of coal seam gas on coal's mechanical properties, future research is needed on methane saturation under various pressures for different ranks of coal.
- It is recommended to conduct further research on coal mass mechanical behaviour under different confinements for different saturation conditions, to represent the real case scenarios existing in the field.
- The water saturation effect of the present study was conducted under atmospheric pressure conditions due to the unavailability of the necessary laboratory facilities. However, it is essential to investigate the water saturation effect under different pressure conditions, so that it can be clearly compared with the different pressure effects of N_2 and CO_2.
- As found in the present study, coal mass mechanical behaviour under various saturations varies with different coal types. However, the results of this study need to be generalized by testing samples of various ranks of coal taken from different coal basins around the world. Future experimentation is therefore recommended using a wide range of coal specimens taken from different basins in the world with diverse cleat structures and mineral compositions, in order to obtain better insight into the observed strength variations.
- Generally, coal seams are saturated with saline water and hence there is a need to conduct studies regarding the effect of salinity on coal strength and CO_2 saturation-induced coal mass strength variations.

9.3.3 Studies of methane recovery

- It is proposed to conduct experiments using low rank coal on the potential of CH_4 recovery enhancement by CO_2 injection with different effective factors such as different depths, temperatures and moisture contents to confirm the use of low rank coal seams for CO_2-ECBM.
- The optimum conditions for CO_2-ECBM proposed in the present study with various effective factors also depend on the cost of implementation and the continuation of the projects and benefits of the project with CH_4 recovery. Therefore, it is essential to combine the physical factors and the cost-benefit factors in a more efficient and long-term CO_2-ECBM project. This is proposed for future research.